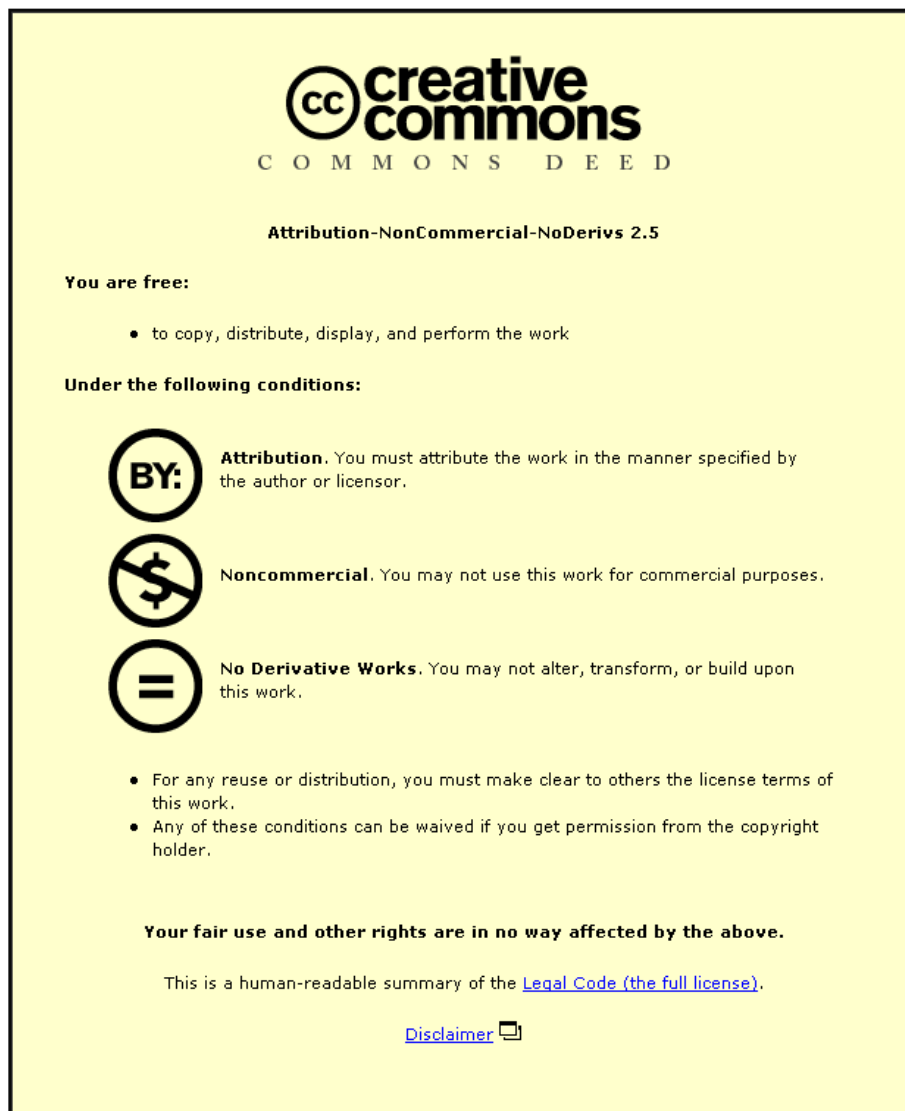


This item is held in Loughborough University's Institutional Repository (<https://dspace.lboro.ac.uk/>) and was harvested from the British Library's EThOS service (<http://www.ethos.bl.uk/>). It is made available under the following Creative Commons Licence conditions.



For the full text of this licence, please go to:
<http://creativecommons.org/licenses/by-nc-nd/2.5/>

**HIGH SPEED SELECTIVE JET ELECTRODEPOSITION OF GOLD AND GOLD
ALLOYS USING SINGLE CIRCULAR JETS**

by

C.E. BOCKING FIMF, Grad.IMF (Poly. South Bank)

A Doctoral Thesis

**Submitted in fulfilment of the requirements
for the award of the degree of Doctor of Philosophy
of the Loughborough University of Technology**

**Supervisor: Dr D.R. Gabe
Institute of Polymer and Materials Engineering
Loughborough University of Technology**

© by C. Bocking 1994

ABSTRACT

High Speed Selective Jet Electrodeposition (HSSJE) is a process in which metals and alloys may be electrodeposited at high rates and in a selective fashion without the need for masking. The method consists of directing a high velocity non-submerged jet of electrolyte at the surface to be plated and passing a current between the nozzle and the substrate. Due to the nature of the flow and the current distribution within the jet, deposition takes place at high rates but only in the impingement and immediately surrounding region. This technique has seen little commercial exploitation and only a small number of papers on the subject. These were concerned with developing mathematical models for the system. The purpose of this work was to examine the structural, morphological and metallurgical characteristics of both gold and gold alloy electrodeposits produced under varied conditions of high electrolyte flow using small geometry ($< 1\text{mm}$) nozzles. By relating factors such as electrolyte velocity, current density, temperature and metal ion concentration etc to the morphology of the deposits produced, an understanding of the limiting conditions for maximum deposition rates was ascertained. Results obtained from deposits produced by HSSJE were compared to those made under more conventional conditions. As well as examining the deposits, attempts were made to gain information on the electrochemical factors controlling deposition. These factors, such as mass transfer characteristics, required the production of polarisation curves identifying the limiting current densities of the system under study. Some potential applications of the technique are also discussed.

ACKNOWLEDGEMENTS

The author would like to thank the following people for the invaluable contribution to the work carried out in the experimental phase of this Thesis. First, Dr David Gabe, my Academic Supervisor, who originally suggested that I undertake this Thesis and without whom, it would never have been written. Also, my colleagues at the Hirst Research Centre. Dr Brian Cameron, my Group Leader and Mr Ian Christie, Laboratory Manager of the Materials Science Laboratory as well as my Industrial Supervisor, for the freedom given to me in the pursuit of the aims of the BRITE programme from which this work was derived. In addition, I would like to thank Dr Brian Cameron for carrying out the wear testing of connectors in this study. Mr Alan Vale, for the chemical analysis of the electrolytes and deposits produced. Mr Ian Gunter for the computer control program that controlled the jet plating equipment as well as advice and back-up on the electronic control systems used. Mr Colin Dineen, who operated the X-Ray Diffraction equipment and provided enormous expertise in the analysis and interpretation of the results. Mr David Prichard who produced some of the Scanning Electron Micrographs shown here. Mr Chris Fisher for the many varied, interesting and most useful discussions that we had in trying to fathom the complexities of the electrochemistry of the system.

At Loughborough University my thanks go to Mr Frank Page, who produced some stunning and prize winning Scanning Electron Micrographs of the more visually interesting deposits. Additionally, Dr Geoff Wilcox for the assistance he provided concerning conventional electrochemical procedures.

Finally, I would like to thank my wife Sue and children Laura and Lewis for their patience during the writing of this Thesis.

The experimental work described in this thesis was taken from a BRITE (Basic Research in Industrial Technology) programme No. RI1B-304, "The improvement in the control and attainment of high speed electrodeposition processes". It was undertaken with partners Centro Sviluppo Materiali, GEC-Marconi Hirst Research Centre and the Loughborough University of Technology. The work on HSSJE was carried out solely at the Hirst Research Centre by the author except where stated above. The other partners worked on different aspects of high speed deposition. As such, the programme was predetermined prior to its commencement. For this reason, certain avenues of interest could not be pursued due to the need to obtain definite milestones within pre-determined time periods.

Table of Contents

CHAPTER 1 INTRODUCTION	1
1.1 GENERAL BACKGROUND	1
1.2 SCOPE OF THIS STUDY	4
CHAPTER 2 GOLD ELECTRODEPOSITION	6
2.1 GOLD PLATING IN THE ELECTRONICS INDUSTRY	6
2.2 ELECTROLYTE TYPES.	8
2.2.1 Alkaline cyanide electrolytes.	8
2.2.2 Acid gold electrolytes	9
2.2.2.1 Pure acid golds	9
2.2.2.2 Alloy acid golds	10
2.2.3 Structural characteristics of gold deposits.	12
2.2.4 The influence of pulsed current on gold electrodeposition.	13
CHAPTER 3 SELECTIVE PLATING TECHNIQUES	15
3.1 DIELECTRIC MASKING	15
3.1.1 Solvent based lacquers	16
3.1.2 Thick film inks	17
3.1.3 Photo-resists	17
3.1.3.1 Photoresist chemistry	18
3.1.3.1.1 Positive working resists	18
3.1.3.1.2 Negative working resists	20
3.1.3.2 Outline of Printed Circuit Board Production Methods	21
3.1.4 Pre-formed masks	23
3.1.5 Controlled depth immersion	25
3.2 BRUSH PLATING	25
3.3 ANODE PLACEMENT AND GEOMETRY	27
3.4 AUTOCATALYTIC (ELECTROLESS) DEPOSITION	29
CHAPTER 4 HIGH SPEED ELECTRODEPOSITION PROCESSES	30
4.1 THEORETICAL ASPECTS	30
4.1.1 Transport mechanisms and the diffusion layer.	30
4.1.2 Realistic limiting current densities	32
4.2 MEASUREMENT OF THE LIMITING CURRENT DENSITY	32
4.2.1 Limiting current density measurement methods.	33
4.2.1.1 Galvanodynamic methods.	34
4.2.1.2 Potentiodynamic methods.	34
4.2.1.3 Convective control methods.	35
4.3 PRODUCTION PROCESSES	36
CHAPTER 5 ELECTROCRYSTALLISATION AND MORPHOLOGY	39
5.1 SOME FUNDAMENTAL ASPECTS OF ELECTROCRYSTALLISATION	39
5.1.1 Electrocrystallisation at low current densities.	42
5.1.2 Electrocrystallisation at high current densities.	43
5.1.3 Mechanisms of surface irregularity amplification.	44
5.1.4 Stability theories for roughness development.	45
5.1.5 Theories of needle, dendritic, dense branching morphology (DBM) and fractal growth.	46
CHAPTER 6 HIGH SPEED JET ELECTRODEPOSITION	53
6.1 CHARACTERISTICS OF FLUID FLOW WITHIN JETS	53
6.1.1 Flow within the free jet region	54
6.1.2 Flow within the impingement region	54
6.1.3 Flow within the wall jet.	55
6.2 MASS TRANSFER CHARACTERISTICS OF IMPINGING JETS	55

6.2.1 Mass transfer in submerged jets.	55
6.2.2 Mass transfer in the non-submerged jet	56
CHAPTER 7 EXPERIMENTAL STUDIES OF HIGH SPEED SELECTIVE JET ELECTRODEPOSITION	63
7.1. EQUIPMENT USED IN THIS STUDY.	63
7.1.1. Computer controlled X-Y drive system	63
7.1.1.1 The nozzle and substrate mount.	64
7.1.1.2 The pump system.	65
7.1.1.3 The X-Y Table	65
7.1.1.4 Motion control system.	66
7.1.1.5 The plating current power supply.	66
7.1.1.6 The computer and control program	67
7.1.2 Additional equipment	68
7.2 EQUIPMENT AND METHODS USED FOR DEPOSIT EVALUATION ..	68
7.2.1 Deposit Morphology	68
7.2.2 Deposit thickness	69
7.2.3 Deposit structure	69
7.2.4 Deposit hardness	74
7.2.5 Chemical analysis.	74
7.2.6 Types of substrate used.	74
7.3 METHODS USED FOR THE PRODUCTION OF EVALUATION SAMPLES.	75
7.3.1 Pure gold deposits.	75
7.3.1.1 Electrolyte composition	76
7.3.1.2 Experimental method	76
7.3.2 Gold alloy deposits	77
7.3.2.1 Initial trials for electrolyte selection.	78
7.3.2.2 Optimising the gold/nickel electrolyte.	78
7.3.2.3 Experimental method.	79
7.4 MASS TRANSFER STUDIES.	80
7.4.1 Principles of SCPV and SVPA.	80
7.4.2 The working electrode/reference electrode assembly.	81
7.4.3 The equipment used.	83
7.4.4 Experimental technique.	83
CHAPTER 8 RESULTS	85
8.1 PURE GOLD DEPOSITS.	85
8.1.1 The effect of nozzle to substrate distance.	85
8.1.2 The effect of current density.	86
8.1.2.1 General observations	86
8.1.2.2 Deposit topography.	88
8.1.2.3 Deposition rate	94
8.1.2.4 Cathodic current efficiency	94
8.1.2.5 Hardness of deposits	95
8.1.2.6 Selectivity of the deposit	96
8.1.2.7 Crystal structure and residual strain.	97
8.1.3 The effect of electrolyte velocity	101
8.1.4 Temperature effects.	101
8.1.5 The influence of the gold concentration.	101
8.1.6 The effect of pH	102
8.1.7 The role of electrolyte conductivity.	102
8.1.8 The influence of nozzle size.	103
8.1.8.1 Increased nozzle size.	103
8.1.8.2 Decreased nozzle size.	103
8.1.9 Pure gold deposition using pulsed current.	104
8.1.9.1 Variation of the average current density.	106
8.1.9.2 Variation of the on-time.	106
8.1.9.3 The effect of increasing the duty cycle.	106

8.1.9.4 The influence of pulsed deposition on selectivity.	106
8.1.10 Examination of the limiting factors controlling maximum deposition rates.	107
8.1.10.1 Mass transfer studies.	107
8.1.10.1.1 Sampled Voltage Pulse Amperometry.	108
8.1.10.1.2 Sampled Current Pulse Voltametry.	109
8.2 GOLD ALLOY DEPOSITS.	111
8.2.1 The influence of deposition parameters for the Ronovel N electrolyte with no nickel.	112
8.2.2 The effect of the addition of nickel to the basic Ronovel N electrolyte. ..	113
8.2.2.1 Relationship between nickel in the deposit, nickel in the electrolyte and current density.	113
8.2.2.2 Deposit topography.	115
8.2.2.3 Deposition rate.	116
8.2.2.4 Current efficiency.	117
8.2.2.5 Hardness of the deposits.	117
8.2.2.6 Selectivity of the deposits.	120
8.2.2.7 Crystal structure.	122
8.2.3 Sampled current pulse voltammetry of the Ronovel N electrolyte.	131
CHAPTER 9 THE APPLICATIONS OF HIGH SPEED SELECTIVE JET ELECTRODEPOSITION	132
9.1 APPLICATIONS WITHIN THE ELECTRONICS INDUSTRY.	132
9.1.1 The direct writing of Microwave Integrated Circuit Substrates (MICS).	132
9.1.2 The selective plating of reel to reel components.	133
9.1.3 Bump plating.	134
9.1.4 The direct writing of etch resist for printed circuit boards.	134
9.2 DEMONSTRATIONS OF THE USE OF HSSJE	135
9.2.1 Microwave circuit test samples - 50 ohm lines.	135
9.2.2 The plating of connectors with alloy gold.	136
9.2.3 Thermocompression bonding properties of HSSJE pure gold.	137
9.2.4 The direct writing of printed circuit boards.	137
CHAPTER 10 ANALYSIS AND DISCUSSION	139
10.1 GENERAL	139
10.2 MASS TRANSFER MEASUREMENTS	140
10.3 THE INFLUENCE OF DEPOSITION CONDITIONS	146
10.3.1. Nozzle to substrate distance.	146
10.3.2. Current density.	146
10.3.3. Electrolyte velocity.	149
10.3.4. Temperature.	149
10.3.5. Electrolyte composition	150
10.3.6. The influence of nozzle size.	151
10.3.7. The effects of pulsed current.	153
10.4 SOME PHYSICAL AND STRUCTURAL PROPERTIES OF PURE GOLD HSSJE DEPOSITS	153
10.5 SOME PHYSICAL AND STRUCTURAL PROPERTIES OF GOLD ALLOY HSSJE DEPOSITS	155
10.6 FLUID FLOW AND ITS INTERACTION WITH THE DEPOSIT	157
10.6.1 Interaction of the flow below the maximum useful current density	158
10.6.2 Interaction of the flow above the maximum useful current density.	161
10.6.2.1 Nodular deposits.	161
10.6.2.2 Needle-type deposits	161
10.6.2.3 Field oriented jet core structures.	163
10.7 THE GROWTH OF NODULAR DEPOSITS.	164
10.7.1. Inhibition versus diffusion mechanisms	165
10.8. SUMMARY OF FACTORS CONTROLLING THE MAXIMUM DEPOSITION RATE.	167

REFERENCES..... 169
PHOTOGRAPHS 1-39..... 174
TABLES 1-27..... 198

NOMENCLATURE

A	Amps
α'	Lattice parameter, Å
a	Constant as defined in equation (21)
α_r	Specific area, cm ² cm ⁻³
c	Concentration, mol cm ⁻³
c°	Concentration in the bulk electrolyte, mol cm ⁻³
c_0	Concentration at the electrode surface, mol cm ⁻³
C	Coulombs, A sec ⁻¹ .
C_f	Local coefficient of friction defined as $\frac{\tau_w}{\rho U_x^2/2}$
d	diameter of the nozzle, cm
d'	Radial distance from centre of impingement zone, cm
D	Diffusion coefficient, mol cm ² sec ⁻¹
D_{eff}	The effective crystallite size uncorrected for faulting, Å
D_{true}	True crystallite size, Å
E	Electrical potential, volts
F	Faraday's constant, 96,480 C
g	Hydrodynamic constant sec ⁻¹
H	Distance of the nozzle from the substrate, cm
i	Current density, A cm ⁻²
i_L	Limiting current density, A cm ⁻²
i_0	Exchange current density, A cm ⁻²
J_D	Diffusion flux, mol cm ² sec ⁻¹
k	Local mass transfer coefficient, cm sec ⁻¹
K	Mass transfer coefficient, cm sec ⁻¹
K_L	Mass transfer coefficient at the limiting current density, cm sec ⁻¹
l	Litres
l	Order of reflection, as in hkl
M	Molar
n	Number of electrons involved in an electrochemical reaction.
r	nozzle radius, cm
r'	radius of cathode, cm
R	Gas constant, 8.314 Joules K ⁻¹ mol ⁻¹
R	Dimensionless distance ratio, d'/r
Re	Reynolds number defined as Ud/ν
Re_x	Local Reynolds number defined as $U_x d'/\nu$

Sc	Schmidt number defined as ν/D
Sh	Sherwood number defined as Kd/D
Sh_x	Local Sherwood number defined as kd'/D
t	Time, seconds
t'	Transport number
t_{∞}	Time to achieve steady state condition, seconds
T	Temperature, °Kelvin
U	Average fluid velocity at the nozzle exit, cm sec ⁻¹
U_x	Average local velocity over the impinged surface, cm sec ⁻¹
x	Cartesian coordinate
y	Cartesian coordinate
z	Cartesian coordinate

Greek letters

α	Stacking fault probability, dimensionless
β'	Twin fault probability, dimensionless
β	Symmetry factor, often taken as 0.5
δ	Diffusion layer thickness, cm
η	Overpotential, volts
θ	Bragg angle, degrees
κ	Specific conductivity
ν	Kinematic viscosity, cm ² sec ⁻¹
μ'	Viscosity, g cm ⁻¹ sec
ρ	Density, g cm ⁻³
τ	Time to the steady state during a transient current pulse, seconds
τ_w	Local wall shear stress, N cm ⁻²
ω	Angular velocity, radians sec ⁻¹

Superscripts

b	Power of Re as defined in equation (22)
e'	Power of H/d
c	Power of Sc as defined in equation (22)

Note: In the graphs presented in this Thesis, the terms A/cm sq and kg/mm sq are used. This is due to limitations in the graph plotting software. The sq in these terms should be read as "squared" and represent, for example A cm⁻².

CHAPTER 1 INTRODUCTION

1.1 GENERAL BACKGROUND

Selective electrodeposition is a process whereby metals are electrodeposited in discrete areas of a substrate, precisely where that metal is required for functional or decorative purposes. It is widely practised in both the electronics and engineering industries. There are many reasons why a metal is deposited selectively. It may be necessary to alter the surface properties of the substrate metal in a particular area in order to confer wear resistance, hardness, electrical conductivity, solderability or weldability and in some cases, to provide a local form of corrosion resistance. In addition, with certain expensive materials such as gold, a considerable cost saving can be achieved by plating the minimum quantity of metal just where it is needed.

Examples of selectively plated metals in the engineering industry can be seen in the re-building of worn components such as drive shafts, bearing surfaces, crankshafts and piston sleeves. As part of a manufacturing process, bearings are usually plated with the bearing material on the wear surface only. Chromium is often plated selectively onto piston sleeves to confer wear resistance.

The electronics industry makes great use of selective plating. The printed circuit board (PCB) industry uses selectively plated metals to act as etch resists. These metals are plated onto regions where tracks etc are required so that when the rest of the copper clad board is etched away, the tracks remain. Electrical connectors are usually plated with a gold alloy to confer wear resistance and low electrical resistance. In order to minimise costs, only the region where contact is made is plated with the gold. Another example is where components that cannot easily be soldered are given a tin or tin alloy coating to confer solderability. To minimise the spread of solder, these components are plated selectively.

Many techniques are available to produce selective electrodeposition and these are detailed in subsequent Chapters. However, as with any process, they have their advantages and disadvantages. Most require the use of some form of dielectric mask to provide the edge definition which can lead to cost penalties. Those that do not use masking are generally of poor definition but tend to be lower cost processes compared with masking systems. Therefore there is a trade-off. Recently, a technique has been developed that offers some promise in overcoming the limitations of existing processes. This method will be referred to as High Speed Selective Jet Electrodeposition.

High Speed Selective Jet Electrodeposition (HSSJE) is an electrodeposition technique whereby metals are electrodeposited in a selective manner without the need for masking. The principle is that a non-submersed, free standing electrolyte jet impinges, at a high velocity, onto a substrate and with the application of a suitable potential, deposition occurs within the impingement region and to a minor extent, the immediately surrounding region. Due to the resistive nature of the electrolyte and the properties of the hydrodynamic flow surrounding the impingement region, the spread of the deposit is limited. Figure 1. shows a schematic view of the electrolyte jet and its interaction with the substrate. It is a combined schematic based on the work of two authors.^{1, 2.}

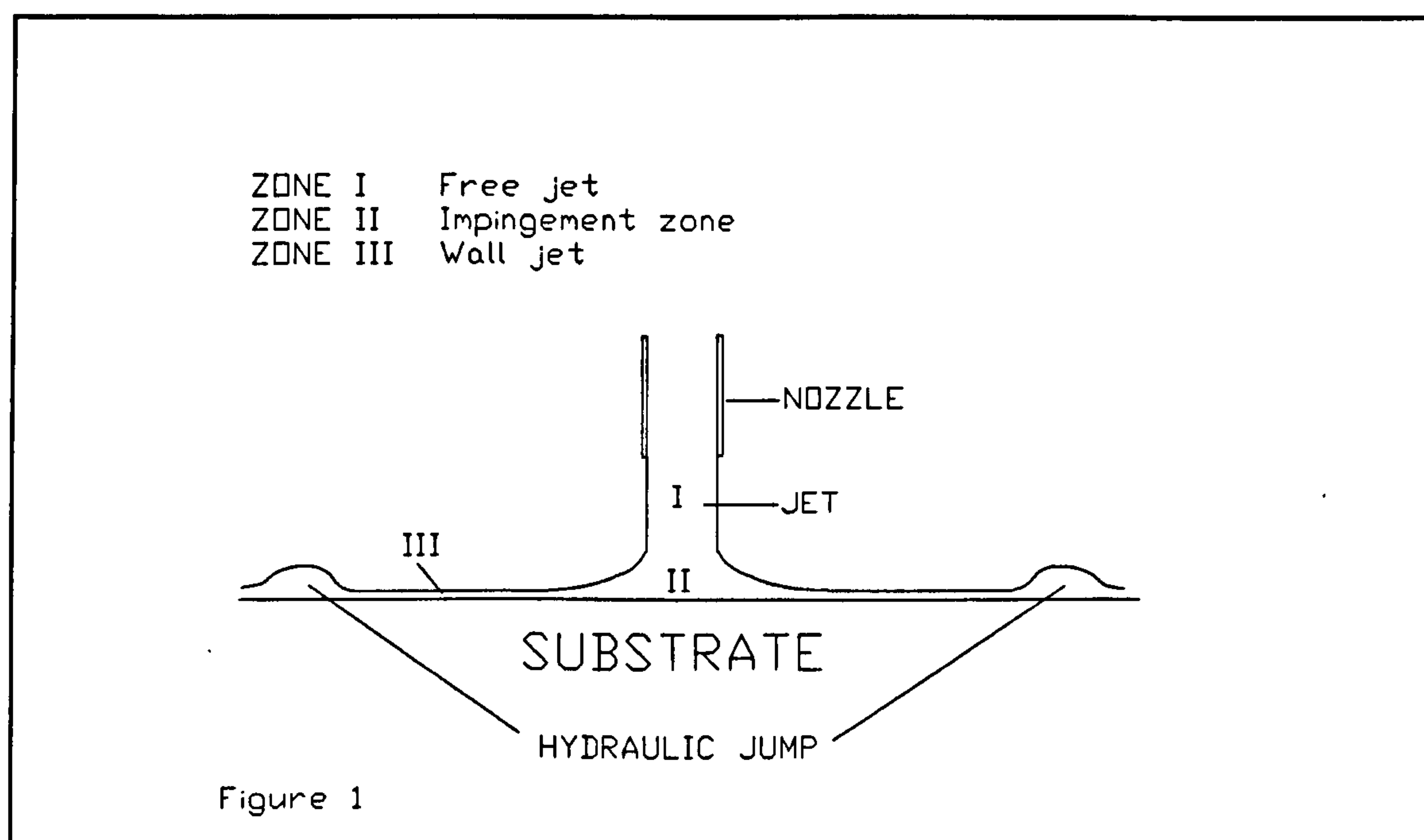


Figure 1. Schematic of the electrolyte jet interaction with a substrate

Region I is the free jet region where flow continues in a similar fashion to that within the tube of the nozzle. Region II is known as the stagnation region. Close to the point of impingement, the flow changes speed and direction from that of the free jet to that of region III, which is known as the wall jet (after Glauert³). Finally, there occurs what is known as the hydraulic jump where the wall jet increases thickness and the flow momentum changes. Further description of the flow will be given in Chapter 6.

Most electrochemical processes benefit from agitation of the electrolyte. This is because the reaction rates of these processes are often governed by the rate of mass transfer of the active species from the bulk of the electrolyte to the surface. In the case of electrodeposition, the active species

is the metal ion. The maximum current density obtainable is therefore controlled by the situation where the concentration of metal ions at the surface approaches zero. In other words, as soon as a metal ion reaches the surface, it is discharged. This situation is known as the limiting current density, i_L . The limiting current density is given by;

$$i_L = -\frac{nFDc_b}{\delta(1-t')} \quad (1)$$

It can be seen that the thickness of the diffusion layer δ has a strong influence on the limiting current density. The thinner this layer is, the higher the limiting current. Migration under the electric field is accounted for by $(1 - t')$. The magnitude of its influence is dependent on the total number of charge carriers. If there is an excess of indifferent charge carriers, ie a supporting electrolyte, then this term will be insignificant. Electrolyte agitation reduces the thickness of the diffusion layer, the stronger the agitation, the thinner the layer and the higher the maximum current density will be. By using a high electrolyte jetting rate, the interfacial agitation will be high and the diffusion layer thickness will be low. It is very difficult to measure the thickness of the diffusion layer directly but it can be measured indirectly by means of either a mass transfer coefficient, K_L , defined as

$$K_L = \frac{i_L}{nFc} \quad (2)$$

or by the Sherwood number, Sh , the dimensionless mass transfer coefficient;

$$Sh = K_L \frac{d}{D} \quad (3)$$

In the electrodeposition of metals, the limiting current density cannot usually be achieved without the deposit quality deteriorating before this is reached. This deterioration takes the form of dendritic, nodular or powdery growth. It has been reported^{4, 5, 6, 7, 8} that this deterioration commences at a ratio of i/i_L of between 0.4 and 0.9 for many of the common plating electrolytes. However, little is known about the effects of very high electrolyte velocities on the ratio of i/i_L or the metallurgical structure of deposits produced under these conditions.

1.2 SCOPE OF THIS STUDY

The purpose of this work was to examine the structural, morphological and metallurgical characteristics of both gold and gold alloy deposits produced under varied conditions of high electrolyte flow using small geometry ($< 1\text{mm}$) nozzles with a constant current DC supply. By relating factors such as electrolyte velocity, current density, temperature and metal ion concentration etc to the morphology of the deposits produced, an understanding of the limiting conditions for maximum deposition rates could be ascertained. Properties of deposits produced by HSSJE were compared to those from deposits produced under more conventional conditions. As well as examining the deposits, attempts were made to gain information on the electrochemical factors controlling deposition. These factors, such as mass transfer characteristics, required the production of polarisation curves to identify the limiting current densities of the system under study. Whilst such information can be obtained using "ideal" redox couples or dilute electrolytes using conditions of rapid electrolyte agitation, it was necessary to establish this information for the systems under study to be effective. Such information is difficult to obtain for relatively concentrated and agitated electrolytes using even well defined measurement systems such as the rotating disc electrode. For this reason, more conventional techniques were modified and used in an attempt to obtain this information. In order to confirm the effectiveness of these modified methods, trials were additionally carried out using a dilute copper sulphate electrolyte.

After optimum deposits had been produced using DC, further trials were carried out to observe the effectiveness of pulsed current in improving the deposition rate and/or the quality of such deposits.

A number of different acid and neutral gold electrolytes were used in this study. Pure gold deposits were produced from acid cyanide/citrate and cyanide/phosphate electrolytes. In the case of the gold alloys, several commercial electrolytes were briefly examined for their effectiveness under jet conditions and the most promising was chosen for further study.

Once the conditions for maximum deposition rates had been established, sample components were prepared for some evaluation trials. The results of these trials are reported separately in Chapter 9.

Because the technique of HSSJE encompasses many different disciplines and aspects of the electrodeposition process, it is necessary to review a wide range of subject areas to provide a starting point for the current work. Therefore, Chapters 2 to 6 examine the various aspects relevant

to this process. Chapter 2 details gold electrodeposition, the electrolytes used and the electrochemistry of the process. Chapter 3 examines the current methods of selective electrodeposition. Chapter 4 deals with the mass transport mechanisms as applicable to high speed deposition processes. Chapter 5 looks at electrocrystallisation and morphology and how the structure of the deposit is related to the deposition conditions. Chapter 6 reviews the current knowledge of jet deposition theory and examines the characteristics of fluid flow within jets. Chapters 7 onward describe the experimental research work carried out for this thesis.

A number of papers have already been published on work connected with this Thesis and these have been added as an Addendum.

CHAPTER 2 GOLD ELECTRODEPOSITION

The unique properties of gold are highly desirable in many spheres of life. Its chemical and aesthetic properties have meant that gold has acquired a special position in society. The most famous of these are a function of the surface - its colour as well as its resistance to corrosion and tarnishing. In many respects, thin layers deposited onto base metals can function in the same way as if the whole article was made of gold. Applying gold onto base metals has its roots in antiquity, with gold leaf being applied ornamentally as far back as Egyptian times. In the 18th and 19th centuries, gold was deposited onto metal items by the application of a gold/mercury amalgam, the mercury subsequently being evaporated off. However, it did not escape the attention of those involved that the life of a gilder was not a long one as mercury poisoning took its toll. The first record of the *electroplating* of gold was in 1802 by Luigi V. Brugnatelli,⁹ a colleague of Alessandro Volta. His work was not widely publicised though. Volta was invited with Brugnatelli to the French Academy of Sciences to discuss their work. Unfortunately, when Volta introduced him to Napoleon, the Academy President, as "the great Italian chemist, Brugnatelli", Napoleon insulted him by saying "there are no great Italian chemists".¹⁰ With this, Brugnatelli returned to Pavia and published his work there, which was not widely seen. It was not until 1840 that Henry and George Richard Elkington patented¹¹ the forerunner of the modern gold electroplating solution, based on gold potassium cyanide. From 1845 the process was commercially available and was popular up to the end of the Victorian period. During this time, many grand objets d'art were gold plated. In Russia gold plating was carried out on a very large scale. For example, the bases and capitals of the interior columns of St Isaac's cathedral in St Petersburg were gold plated, using 280 kg of gold. However, because of a poor understanding of the chemistry of the process, success depending on "black book" recipes known only to a few, it fell into disrepute. Thereafter, gold plating was largely relegated to the production of inexpensive novelties or trinkets until its re-emergence as part of the electronics industry in the early 1940's.

2.1 GOLD PLATING IN THE ELECTRONICS INDUSTRY

With the advent of the electronics industry, a special interest in the technology emerged. Gold became popular because of its inert nature, its high electrical conductivity and low contact resistance. The modern electronics industry is one of the largest users of gold plating. In 1990 in Europe alone, it has been estimated¹² that 13,482 kg of gold was deposited out of a total electronics usage

of 18,097 kg. For the same year, the world electronics consumption of gold was 142,800 kg.¹³. This would indicate that approximately 110,000 kg was electroplated with a value of just over \$1.3 billion.

Within the electronics industry, the two major scale applications of gold are for electrical connectors and printed circuit boards. It is estimated that in 1990, 6,869 kg was plated onto connectors whilst 2,440 kg was deposited onto printed circuit boards in Europe. The satisfactory performance of a connector is crucial to the overall performance of any piece of electrical equipment. It has to have a low contact resistance, as well as good corrosion and wear resistance. This latter property is necessary because connectors are frequently mated and un-mated during the course of the equipment lifetime. Many specifications require a connector to remain functional through up to 500 insertion/withdrawal cycles. In order to achieve this wear resistance, small quantities (approximately 0.1 - 1.0 % by weight) of a transition group metal, such as nickel or cobalt, are co-deposited with the gold. This increases the hardness from about 80 Hv (Vickers Pyramidal Hardness) for pure gold up to about 150 Hv with very little increase in the contact resistance.

Printed circuit boards (PCB's) are plated with gold in order to suppress corrosion of the underlying copper and to improve solderability. Many boards still use gold plated edge connectors. These are areas at one end of the board that act as connecting pads that can be mated with external connectors. They are plated with the gold alloy to confer wear resistance. With the advent of microwave communications systems, gold has been the preferred metal to use for the production of the specialised circuit boards needed for high frequency applications. The glass reinforced plastic that is used for conventional PCB's has been replaced by either sintered alumina, quartz or PTFE based materials for these applications. These are metallised using sputtering techniques and the tracks are built up using a combination of photolithography and electroplated gold. The remaining metallisation is then removed.

Gold plating is particularly important in space applications. The unique properties of gold, especially its high infra red reflectivity and tarnish resistance in terrestrial atmospheres, make it invaluable for thermal radiation control. In addition, gold resists sublimation in the high vacuum of space. This phenomenon can lead to short circuits in electronic equipment if other "electronic metals" are used, due to vaporisation and condensation of the metal.

Beside these applications, gold is plated onto semiconductor lead frames for the purposes of bonding gold wire interconnects from the chip to the frame. Because gold is ductile, soft and when pure, readily forms cold welds, components can easily be joined by thermo-compression bonding. Die attachment is facilitated by the use of gold plating, again due to its tarnish resistance. There

are numerous minor electronics applications of gold plating that cannot be mentioned here which together ensure that electronics is the second largest fabrication consumer of gold next to the jewellery trade.

2.2 ELECTROLYTE TYPES.

Gold, being a noble metal, requires only a very small overpotential for reduction from the ionic to the metallic state. Therefore, in electrolytes containing free metal ions, immersion deposits readily form. In addition, electrodeposits from such an electrolyte are coarse grained and tend to form nodules and dendrites. It is therefore essential that the gold ions are complexed in order to reduce this effect. There are only 2 suitable complexes of gold for general commercial use. The cyanide complex is produced in the form of potassium gold cyanide, KAu(CN)_2 . In the case of the sulphite complex, the gold is in the form of sodium gold sulphite, $\text{NaAu(SO}_3\text{)}$. However, the cyanide complex may be used in a number of different electrolytes over a wide pH range.

2.2.1 Alkaline cyanide electrolytes.

Alkaline cyanide electrolytes use the gold potassium cyanide together with excess potassium cyanide at a pH in excess of 12. A typical formulation is shown below;

Au as KAu(CN)_2	4-12 g l ⁻¹
Potassium cyanide	30 g l ⁻¹
Potassium orthophosphate	30 g l ⁻¹
Potassium carbonate	30 g l ⁻¹
pH	> 12
Temperature	50 - 65 °C
Current density	1 -8 mA cm ⁻²

The free cyanide is usually maintained at above 15 g l⁻¹. Due to their alkaline nature, these electrolytes have rarely been used in the electronics industry particularly in the gold plating of PCB's. As a result of the increased requirement for such applications during the 1950's, acid to neutral electrolytes based on gold potassium cyanide were developed.

2.2.2 Acid gold electrolytes

2.2.2.1 Pure acid golds

In 1959, Ehrhardt¹⁴ found that potassium dicyanaurate was stable in acid media down to a pH of 3.0. Subsequently, a number of formulations were developed based on a carboxylic acid/carboxylic salt mixtures with potassium dicyanaurate. The first electrolytes employed citric acid and sodium citrate and operated at a pH between 3.0 and 5.0. The citrate mixture was present to buffer the electrolyte. In addition, citrate was found to be capable of complexing transition metals such as nickel, cobalt and iron. This allowed the electrolyte to be used for both pure gold deposits as well as alloy deposits. Because of this ability, it is important that when depositing pure gold from such an electrolyte that stronger complexing agents be added so that codeposition with impurity transition metals is avoided. Ammonium citrates are used in modern formulations of this type of electrolyte thus eliminating the possibility of contaminating electronic devices with sodium, which could be deleterious to the device performance.

A typical pure acid gold is shown below;

Au as $\text{KAu}(\text{CN})_2$	8.0 g l ⁻¹
Citric acid	40 g l ⁻¹
Ammonium citrate	40 g l ⁻¹
EDTA	1 - 2 g l ⁻¹
pH	3.0 - 6.0
Temperature	25 - 30 °C
Current density	5 - 10 mA cm ⁻²

With the development of transistors and integrated circuits the need for gold plating the device packages grew. The acid electrolytes were not very suitable for the barrel plating applications that these devices required and thus neutral electrolytes were developed. The acid electrolytes were subject to metallic contamination and were able to co-deposit the contaminants. Nobel and Thomson¹⁵ demonstrated the superiority of neutral electrolytes in a study of the barrel plating of transistor headers. Subsequently, numerous proprietary formulations were developed, based on mixtures of phosphates and citrates, phosphate only and pyrophosphates. To reduce the danger of co-deposition, complexing agents such as organic phosphonic acid derivatives were used. Many of these electrolytes used various addition agents such as organic thio compounds as well as trivalent

arsenic to act as grain refiners and brighteners. Due to the wide variety of formulations for neutral electrolytes, there is no "typical" formulation and the reader is referred to the literature for further information.^{16, 17, 18.}

In the early 1970's, it was discovered that the additive free acid and neutral baths worked quite well when freshly made up but on use and with ageing, the deposit quality deteriorated, giving rise to brownish deposits. Reinheimer^{19.} was one of the first to discover that the reason for this was that freshly made electrolytes often contained small quantities of lead as a contaminant. As the bath was used, so the lead was removed by co-deposition. It was only when more lead was added that the quality of the deposit was returned. The addition of lead at a level of about 0.5 ppm was patented by him. At about the same time, it was found that thallium and arsenic were also effective brighteners. McIntyre and Peck^{20.} carried out a study on the depolarising effect of heavy metal ions including arsenic, lead, thallium bismuth and mercury. They demonstrated that lead and thallium depolarised the gold electrode. The proposed mechanism was of adsorption of the trace metal followed by an electrochemical displacement reaction between the adsorbed metal and $\text{Au}(\text{CN})_2^-$. This displacement was thought to modify the crystallisation of gold allowing well formed fine crystals with a strong preferred orientation. This resulted in a bright appearance. However, they discovered no depolarisation effects with arsenic. Eisenman^{21.} examined the kinetics of the reduction of dicyanaurate both with and without lead. He explained that the effect of lead was to lower the activation energy of the electron transfer which gave rise to the accelerated establishment of a preferred orientation. Rao and Weil^{22.} and more recently Dinan and Cheh^{23.} studied the effects of arsenic additions to gold electrolytes. Rao and Weil thought that arsenic adsorbed onto the gold and acted as nucleation sites but at the same time inhibited the lateral growth of the gold crystals. As a consequence, the grain size was considerably reduced and this was responsible for the brightening effect. Dinan and Cheh examined the effect of arsenic on the hardness of gold. They concluded that arsenic additions led to an increase of hardness and that this was due to the incorporation of the trace metal in the deposit.

One disadvantage of using these trace metals as brightening agents has been due to their incorporation into the deposit and their subsequent influence on the performance of the gold. It was been shown^{24, 25.} that both the thermocompression and ultrasonic bondability was reduced in the presence of such incorporated additives, particularly when the gold was deposited at high current densities. These workers concluded that low additive concentrations and low current densities should be used for such applications.

2.2.2.2 Alloy acid golds

At the same time as Ehrhardt's disclosure, Rinker^{26.} independently discovered the acid stability of potassium dicyanaurate. He also found that by introducing suitably complexed base metals, the

deposits produced were much harder. With as little as 0.1 % base metal incorporation, the hardness of the gold deposit could be doubled. As well as increasing the hardness, the wear resistance of the deposit was drastically improved. Complexing agents such as EDTA (ethylenediamine tetraacetic acid (disodium salt) and NTA (Nitro triacetic acid) were necessary to facilitate the slow release of the metal for codeposition. Without some form of additional complexing, the base metals are in fact more noble than the complexed gold ions and will deposit preferentially. Thus an alloy would be deposited with a high base metal content for very low concentrations of base metal in the electrolyte. Modern formulations make use of a wider range of carboxylic acid buffers and often, phosphates or phosphonates are used.

A typical acid hard gold formulation is described below that uses nickel as the alloying element. The tetraethylene pentamine is used to complex the nickel in this case.

Au as $\text{KAu}(\text{CN})_2$	4.0 g l ⁻¹
Citric acid	120 g l ⁻¹
Tetraethylene pentamine	20 g l ⁻¹
Nickel (as nickel citrate)	2.5 g l ⁻¹
pH	4.0
Temperature	40 °C
Current density	20 mA cm ⁻²

The most widely used and studied hard gold is one that uses cobalt as an additive. In this case, the bath formulations are similar to the above but the cobalt is added as the EDTA complex. There have been many studies carried out on the mechanism of hardening and wear resistance properties of this electrolyte. The addition of cobalt has been shown to increase the hardness from a value of 80 -100 kg mm⁻² to 150 - 200 kg mm⁻². It was thought that the hardness increase was brought about by a significant reduction in the grain size. Lo *et al*²⁷. concluded that the hardness was a result of the reduction in the grain size from about 2 µm down to 20 -30 nm. Eisenmann,²¹ in his study of the kinetics of the reduction of gold concluded that the cobalt increased the activation energy of the electron transfer reaction and gave rise to a high nucleation rate leading to a small crystallite size. However, a high hardness alone does not account for the good wear resistance of the cobalt and nickel hardened golds. Koch *et al*²⁸. developed an additive free hard gold that exhibited a similar hardness to these deposits. However, it was shown that the sliding wear resistance of the additive free deposits was not as good as those containing cobalt in the absence of a suitable lubricant. Munier²⁹. found an organic material co-deposited with the cobalt gold and described it as a "polymer". It was thought for some time that this was responsible for both the increased wear resistance of these deposits as well as the slightly increased contact resistance associated with them.

However, there were many studies carried out subsequently and in one of them,³⁰ it was concluded that the "polymer" discovered by Munier was in fact cobalt II hexacyanocobaltate III, $\text{Co}_3[\text{Co}(\text{CN})_6]_2 \cdot x\text{H}_2\text{O}$. By using extraction with mercury instead of aqua regia as Munier had, it was found that potassium cobalticyanide, $\text{K}_3\text{Co}(\text{CN})_6$ was co-deposited. Of this, only 25 % of the cobalt was in this state, the rest being in the form of metallic cobalt. In addition, only 21 % of the carbon and 41 % of the potassium could be attributed to the $\text{K}_3\text{Co}(\text{CN})_6$. The rest was later found to be from incorporated AuCN. Later studies by Antler³¹ showed that in addition to high hardness, good wear resistance required a low ductility. Another study by DeDoncker *et al*³² showed that good wear resistance could only be obtained if the deposit contained at least 0.08 wt % of the cobalt complex together with between 0.06 - 0.2 wt % of metallic cobalt. If the complexed cobalt was below this value, then the wear resistance was poor. High levels of cobalt in the electrolyte tended to suppress the co-deposition of the complex leading to high metallic cobalt contents. This resulted in abrasive wear characteristics.

The use of cobalt as an additive has a major disadvantage when used for high speed deposition.³³ The CoII is readily oxidised to the inert CoIII complex, $\text{Co}(\text{CN})_6^{3-}$ at the anode. However, nickel does not suffer from this problem.

There are many reviews of gold electrodeposition technology in the literature and further information can be obtained from them.^{10,33,34}

2.2.3 Structural characteristics of gold deposits.

The structure of any metal deposit is highly dependent on the deposition conditions, the electrolyte formulation, the temperature and the substrate. The substrate exercises its influence during the early stages of deposition and ceases to exert a significant influence once the thickness of the deposit has exceeded about 5 μm . A number of studies have been carried out on the initial stages of deposition of gold.^{35, 36} It was found in these studies that the greatest influence on deposit structure was due to the lattice mismatch between the gold and the substrate. The current density was found to have little influence on the initial stages of deposition. However, additives in the electrolyte were found to significantly influence the structure and the coverage. Lin *et al*³⁷ examined the crystal structure, using Transmission Electron Microscopy (TEM), of thicker deposits from a citrate electrolyte both with and without additives over a current density range of 4 to 12 mA cm^{-2} . They found that the deposits grew mainly as the (111) planes, this trend being greater at lower temperatures and higher current densities. The next major plane was the (311), the growth of which was suppressed by increasing the current density. Certain surfactant additives were found to suppress the growth of the (111) planes allowing the emergence of a (220) and (311) structure.

The changes in the preferred orientation were reflected in the change of morphology. The deposits with a preferred (111) orientation exhibited a plate-like structure whilst those with the (220) and (311) orientations showed what was described as a "shell-like" morphology.

Wakabayashi²⁵ reported that the presence of lead or thallium favoured the growth of the (311) planes whilst the addition of arsenic leads to a (111) preferred orientation. They also reported that in the absence of additives, the (111) plane was predominant.

DeBonte *et al*³⁸ described the influence of current density on the structure of both the additive free hard gold and a cobalt hardened gold. In the case of the additive free hard gold, low current densities favoured a mixed (200) and (311) texture, the deposits having what they term as a polyhedral morphology. With increasing current density, a (111) texture became predominant, associated with a fine grained structure. With increasing current density, the deposits adopted a mixed (200) and (211) texture which showed as a lenticular or plate-like morphology. Before the onset of burning, a slightly nodular structure was observed that exhibited a (200) texture. In the case of the cobalt hardened gold, the structure at low current densities was a mixed (220) and (311) texture. With increasing current density, this became a (111) preferred orientation.

Antler³⁹ reported a (311) major preferred orientation for a pure acid gold using XRD. In addition, he reported a (111) preferred orientation for a nickel hardened alloy gold. The electrolyte nickel content was 0.15 %. However, for cobalt hardened gold, he reported an un-oriented deposit.

2.2.4 The influence of pulsed current on gold electrodeposition.

It has long been known that the use of either pulsed current or pulsed voltage can influence deposit characteristics. Reduced porosity, smaller grain size, improved distribution and higher deposition rates have all been claimed as benefits to the use of pulsed deposition. The use of pulsed current on pure gold electrolytes was first studied by Cheh.⁴⁰ He found that although the instantaneous applied current, i_p , could be considerably higher than under DC conditions, the overall plating rate was generally lower. He concluded that the main advantage to the use of pulsed current was not in increasing the deposition rate but the ability to increase the rate of nucleation, leading to a finer grain structure and a reduced porosity. Rehrig⁴¹ confirmed this by finding that at high peak current densities and duty cycles less than 50%, the grain diameter was inversely proportional to the peak current and the duration of the pulse. This effect has been observed in other investigations.⁴²

It has been pointed out⁴² that using very high peak current densities can lead to grain refinement and thus greater deposition rates than under DC conditions. However the rate can never exceed the DC limiting current density. Therefore, whilst peak current densities can approach the peak limiting current densities with no degradation of deposit quality, the average limiting current density cannot be surpassed without deposit deterioration. This means that for such high peak current densities, there has to be an appropriate off-time to allow recovery of the metal ions in the diffusion layer so that the average limiting current density is not exceeded. One advantage of using high peak current densities is that a thin, pulsating diffusion layer is produced adjacent to the substrate. If this layer is small compared to surface irregularities, then both the peaks and the troughs of the irregularity are equally accessible to diffusion. Such a situation reduces the tendency of peaks to be magnified by excessive growth as would be the case under DC conditions where a thicker diffusion layer inevitably forms. This will be discussed further in Chapter 5. As a consequence, by using very short, high peak current pulses, such a tertiary distribution is achieved and the micro-distribution of the deposit is improved. Such an improvement in the microthrowing power has been shown by Andricacos *et al*⁴³ using a citrate gold electrolyte. They deposited gold onto a rotating disc electrode with a small groove on it. They found that the microthrowing power was significantly better using pulsed current of short duration than under DC conditions. The most important criteria for such a current regime to be successful is that the peak current density must be such that deposition occurs under diffusion control. Another important condition for adequate tertiary current distribution is that the mass transport rate should not vary across the electrode surface. Such a condition is rarely achieved under DC conditions but can easily be achieved with pulse plating.

One disadvantage of relying on tertiary current distribution to smooth deposits lies in their susceptibility to hydrodynamic effects. If the pulsating diffusion layer is disturbed by turbulent flow conditions, the microthrowing power may be affected due to an uneven accessibility to diffusion occurring.

As was mentioned previously, the use of very high peak current densities does require long off-times. It has been shown by Puippe⁴² that the off-time can significantly influence the quality of the deposit. Working at average current densities well below the limiting current density, he found that increasing the off-time during pulsed gold deposition from a citrate bath led to an increase in the grain size. He used a peak pulse current density of 100 mA cm^{-2} . With an off-time of 9 ms a smooth deposit was obtained. Increasing the off time to 99 ms led to an increase in surface texturing. He claimed that this was due to grain growth during the off-time.

CHAPTER 3 SELECTIVE PLATING TECHNIQUES

Selective electrodeposition has been practised since the early days of electroplating in one form or another. There are numerous ways of depositing metals just where they are required. The main objective is to prevent either the electrolyte from coming into contact with areas where the plating is not required or to direct the electric field in such a way that plating only occurs within the field. Turner⁴⁴ divided these techniques into 5 main categories.

1. Dielectric masking
2. Brush plating
3. Jet or gelled electrolyte plating
4. Anode placement and geometry
5. Electroless plating

Each of these categories will be discussed in greater depth, with the emphasis on currently used methods. Jet plating will be covered in Chapter 6 and will not be discussed here. Gelled electrolyte plating consists of placing a gelled electrolyte onto the surface to be plated where deposition is required. It is a rarely used technique and will not be discussed further.

3.1 DIELECTRIC MASKING

Dielectric masking encompasses a great range of different techniques. The principle is that some non-conducting material (a dielectric) is placed in intimate contact with the substrate leaving only those areas requiring plating exposed to the electrolyte. After plating, the dielectric is removed leaving the component selectively plated. There are three main sub-categories of this method, solvent based organic polymers, pre-formed masks and controlled depth immersion. This latter category makes use of the fact that the air above the level of the plating electrolyte makes a good dielectric.

3.1.1 Solvent based lacquers

Prior to the development of solvent based systems, masking was generally carried out with waxes, especially bees wax. This was melted and applied whilst molten by means of dipping or brushing. However, it was not really suitable for high definition due to its rapidly changing viscosity as it cooled leading to poor flow during brushing. With more demanding needs, the industry turned its attention to solvent based systems.

This category probably has the most widespread use for general selective plating. Many different systems have been used depending on the application. For general use on items of complex shape, lacquers are widely used. These consist of a resin type material, or a cellulose, either natural or synthesized that are dissolved in a solvent, usually a ketone, that can be applied either by dipping, spraying or brushing. The type of resin or polymer used is very dependent on the plating conditions and very often, lacquers are tailored for highly alkaline or highly acidic plating electrolytes.

The geometry of the item dictates the method of application. Whilst dipping and spraying are highly effective at covering large areas, delineating the area to be exposed can be difficult. The use of masking tapes of various kinds which are removed after coating with the lacquer often leaves a weakened edge and the electrolyte can often creep under the lacquer allowing deposition or even corrosion to occur there. Painting by hand is often the only way to ensure a good edge but this does rely on operator skill and the definition is often poor. Despite these difficulties, this method, in combination with masking tape that remains on the item defining the edges, is still the most common method used in the plating industry for complex geometry items. Adhesion of the lacquers may be enhanced by a low temperature heat treatment but this is probably due to shrinkage of the film as the remains of the solvent are removed. However, despite the use of plasticisers in the formulations, these coatings tend to be brittle and can easily fracture or become detached if any stresses are introduced into the component eg. thermal cycling, flexing when jigging etc.

Another type of solvent based material that has found increasing popularity is that based on a soluble rubber or latex. This material, which uses toluene or xylene as the solvent has certain advantages over the former products. After the solvent has dried, the coating retains a high degree of flexibility. This gives it a greater resistance to the thermal cycling that occurs during transfer from hot solutions to cold rinses. Being flexible, thin section components can readily be handled after the application of the film. This type of masking is frequently used for electroless nickel as high temperatures are used in this process. The disadvantage with this method is that the film is slow to dissolve in the solvents that are used to remove it after plating.

3.1.2 Thick film inks

In the early days of printed circuit production, screen printed inks were used to define the tracks prior to etching. Originally, these inks were similar to the lacquers mentioned previously, being based on cellulose. The method of application, screen printing, allowed thick films of a high definition to be produced. As these films dried rapidly by solvent evaporation, the definition obtained was fairly good. However, the flammability and toxic nature of the solvents led to the development of resin based inks that were able to be force dried and baked to give a very tough, acid resistant film. They were removed using chlorinated solvents or in some cases, aqueous caustic solutions. However, the early types were not suitable for plating due to leaching of organic material into the plating electrolyte. Also, they were limited to acidic solutions. Modern formulations have generally overcome these problems and are often used in the PCB industry.⁴⁵ In particular, high viscosity, UV cured inks based on acrylic or vinyl are commonplace for many commercial applications.

The screen printing method of application is a stencil printing technique which uses a circuit pattern defined on the woven mesh of a screen fabric. The fabric can be made from silk, polyester, nylon or stainless steel. The ink is forced through open areas of the screen mesh not protected by the stencil, onto the copper clad board by a squeegee wiped across the surface of the screen. The process is popular because of its relatively low cost and reasonably good definition. However, it has a lower limit of line spacing of about 0.3 mm.

Thick film inks may also be used for general masking of items to be selectively plated although they are expensive compared to air curing lacquers.

3.1.3 Photo-resists

Photoresists are organic materials that can be applied to surfaces by a variety of methods to form a chemically resistant, polymeric layer. They have unique properties in that after application, the chemical resistance of the layers may be modified by ultra-violet light. By the use of light blocking masks, the chemical activity of the areas exposed to the U.V. radiation can be altered. Photoresists may be classified into two main groups, namely positive and negative working. The positive working resist, when applied, forms a hard chemically resistant layer. When this is exposed to UV light, the polymer becomes soluble in the chemicals used for developing solutions. In the case of negative resists, polymerisation occurs when exposed to UV light, forming a more chemically resistant layer. Photoresists are used mainly in the PCB and microelectronics industries as the flat geometry of the circuit boards and silicon wafers respectively are suited to the application methods.

Photoresists may be further classified into two sub-divisions based on the methods of application. Liquid photoresists, as the name suggests, are supplied with the photo-polymer dissolved in an organic solvent. They are applied to the substrates by means of spraying, dipping, roller coating or spinning. After application, they are cured in an oven to remove the solvent and harden the film. The dried film thickness has to be low (2.5 to 8.0 μm) for adequate penetration of the UV light. Negative working liquid resists are usually developed in chlorinated solvents. The main disadvantages of these types of resist include their sensitivity to pin-holes in the mask that is used. This can lead to spots of resist remaining on areas requiring plating leading to broken tracks. In addition, these resists tend to plug the through holes in the board and are difficult to develop and remove. Controlling the resist thickness is another problem with the liquid resists. Positive working liquid resists overcome the difficulties mentioned above with the exception of the control of the film thickness.

The second sub-division is the dry-film resist. Dry film resists consist of a thick (17 to 75 μm) photo-polymer layer sandwiched between Mylar and polyolefin films. These films allow the resists to be wound into rolls in lengths of up to 300 metres without the photo-polymer sticking to itself. It is applied to the copper clad board by a hot roller process, the polyolefin film being removed automatically prior to rolling. The Mylar film remains in contact with the resist up to the developing stage, preventing the photo-polymer from damage. These resists can be developed in a number of ways. Some are designed for solvent stripping whilst others use aqueous or mixtures of aqueous and solvent developers. The advantages of the dry film resist include its relative ease of processing and being thicker than the liquid resists, they prevent the subsequent plating from "mushrooming" over the resist layer.

3.1.3.1 Photoresist chemistry

The chemistry of photoresists is a vast subject with a great number of formulations and mechanisms of operation. It is beyond the scope of this thesis to detail these systems. A detailed description of photoresist chemistry is given in the work by Allen⁴⁶ and the reader is referred to this. However, some typical photoresist chemistry will be described to convey the general chemical principles at work.

3.1.3.1.1 Positive working resists

The photochemical reactions involved in the case of positive resists are such that the UV radiation produces a cleavage of the polymer so that the molecular weight (MW) of the polymer film is significantly reduced, in some cases down to the original monomer. Because low molecular weight substances possess a greater solubility than the higher MW polymer, exposed regions may

be removed with a suitable solvent or developer. Typical of the more modern liquid positive resist systems are based on the photochemistry of diazonaphthoquinone sulphonate esters (NDS) in a cresol-formaldehyde condensation polymer binder (novolac). With exposure to near UV radiation (360–440 nm), the NDS forms a ketene intermediate which reacts with residual water in the film to form an indene carboxylic acid with the elimination of nitrogen. However, in the absence of water in the film, the ketene reacts with the phenolic -OH groups on the novolac to form pendant ester linkages. As the resist is formulated with sufficient water in the film, the former reaction is the most prevalent.

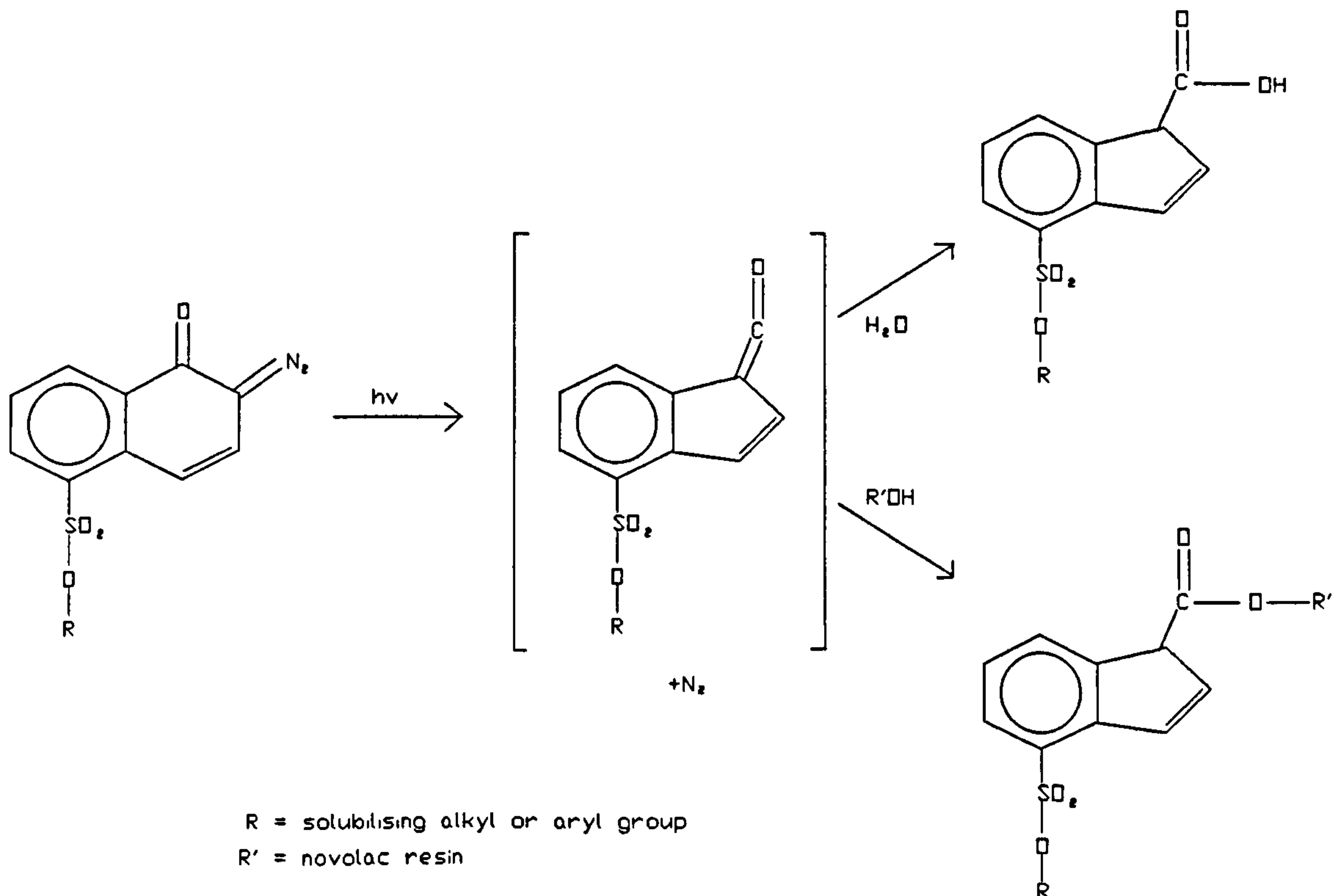


Figure 2. The chemical reactions involved in the exposure to UV radiation on the NDS/Novolac photoresist system

Figure 2 shows the reaction mechanisms involved. In the initial applied state, the NDS acts as a dissolution inhibitor for the novolac binder due to its hydrophobic nature. The indene carboxylic acid formed by the photolysis reaction is hydrophilic and therefore acts as a dissolution accelerator for the polymer film and thus allows the removal of exposed areas. After development, the resist image is normally baked at a temperature of 130 °C to "harden" it. At this temperature, the NDS decomposes to the ketene. As the polymer dehydrates, the ketene reacts primarily with the phenolic groups inducing crosslinking of the polymer, making it more chemically resistant to subsequent processing.

3.1.3.1.2 Negative working resists

Negative working resists are based upon the fact that the dissolution rate for a polymer decreases as the molecular weight increases. Ultimately, a fully cross linked polymer is insoluble in any solvent. As a consequence, cross-linking high molecular weight linear polymers reduce the susceptibility to dissolution. Alternatively, suitable monomers may be polymerised to create a cross linked network. There are three basic methods used to create insoluble resist structures. Photodimerization, photocrosslinking and photoinitiated polymerisation (free radical) are the mechanisms used to produce resistant polymeric layers.

Photodimerization is a process by which two linear polymer chains may be cross linked together. The simplest resist using this mechanism is polyvinyl cinnamate, made by the esterification of polyvinyl alcohol with cinnamoyl chloride. Upon irradiation, the cinnamate groups from two chains can dimerize to form a truxillate as in Figure 3.

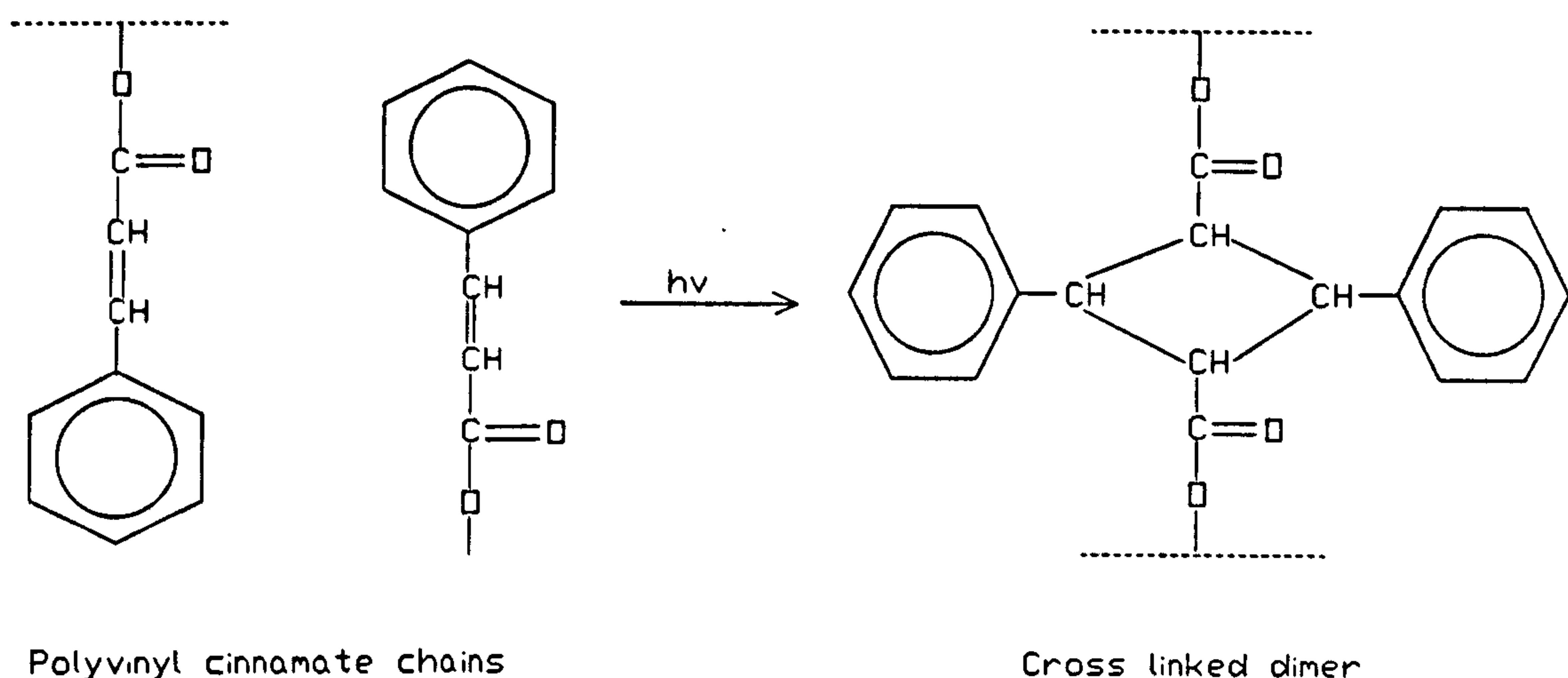


Figure 3. The chemical reactions involved in the photodimerisation of polyvinyl cinnamate.

A typical example of photocrosslinking can be seen in resists composed of cyclized polyisoprene (CPI). Crosslinking is achieved by incorporating a bis(azide) photoactive compound in the resist. Irradiation of an azide creates the highly reactive nitrene which can react with the CPI. As a bi-functional azide is used, two polymer chains can be linked leading ultimately to a cross linked network. Figure 4 shows the types of reactions that can occur in the crosslinking mechanism.

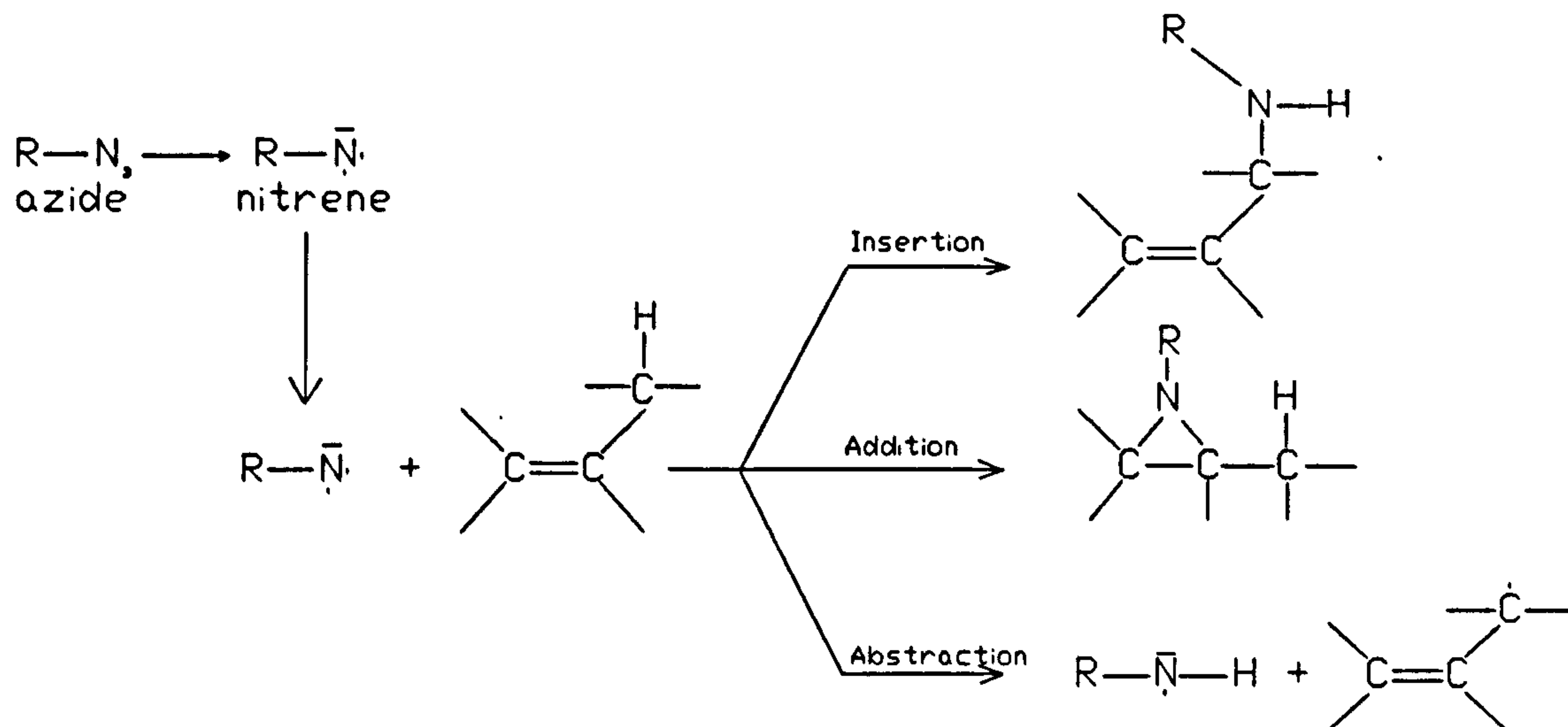


Figure 4. The chemical reactions involved in the photo-crosslinking of cyclized polyisoprene using a bis(azide) photoactive compound.

Photoinitiated polymerisation works by the inclusion of a photoactive compound in a monomer base. Irradiation of the photoactive compound creates free radicals that can polymerise the monomer. A typical example of this is the polymerisation of vinyl monomers using alkyl ethers of benzoin. The radiation cleaves the C-C α bond of the benzoin ether creating the free radicals that lead to the polymerisation of the monomer.

3.1.3.2 Outline of Printed Circuit Board Production Methods

Detailed information on the production of PCB's is available in the literature but the most comprehensive treatise can be found in the work edited by Coombes.⁴⁶ However, a brief outline of the current production methods is given here.

PCB production can be categorised into two processes, the subtractive and the additive. The subtractive method makes use of a positive resist image to protect the underlying copper whilst the unprotected copper is etched away. The resist image can be produced by either a positive or negative photoresist system. The former makes use of a positive mask (black circuit lines) whilst the latter requires a negative photo-mask (clear circuit lines). Whilst this is not a selective plating process, it constitutes a large proportion of commercial quality circuit boards produced. It is also the favoured choice for the production of prototype boards.

The additive process is further sub divided into three different classes, print, plate and etch, panel plating and pattern plating. Print, plate and etch consists of defining the tracks etc by means of a positive image mask and a negative photoresist. The unexposed resist is removed in the development leaving the copper exposed in the track regions. After suitable cleaning, the copper is plated with a appropriate metal etch resist such as tin, tin-lead, nickel or gold. After plating, the resist is removed and the unwanted copper is etched away leaving the tracks.

If double sided boards with plated through hole connections are required the panel plating method may be used in conjunction with print, plate and etch. Through-hole-plating is a technique used where high component densities are required. This allows interconnections between either side of the board, avoiding track cross-over. It consists of drilling the appropriate holes in the copper clad boards prior to processing. In order to plate the non-conducting holes, it is necessary to sensitise the them by producing an adsorbed layer of palladium on the hole walls. The board is placed in an electroless copper solution and the palladium acts as a catalyst to initiate the deposition of copper onto the walls of the hole. A thickness of between 2 to 5 μm is applied and this is followed by electroplated copper to produce a plating thickness of 25 μm within the hole. This may require a copper thickness of up to 40 μm on the copper cladding. The print, plate and etch plating method as described above is then used to define the features. However, this method of panel followed by print, plate and etch plating has significant disadvantages. Circuit features less than 0.4 mm cannot be produced with this technique. This is because of the total thickness of unwanted copper to be etched is very high and this leads to undercutting of the tracks beneath the etch resist. This reduction can be as much as 0.2 mm and slivers of etch resist metal can break away leading to subsequent short circuits. Where tin or solder is used as the etch resist, this problem can be eliminated by fusing with hot oil or infra-red heating.

The pattern plating process is the most widely used manufacturing process to produce plated-through-hole PCB's. It is suitable for fine feature geometries as there is less undercut involved. The manufacturing route is the same as that for panel plating up to the application of the electroless copper. However, after the electroless copper, the photoresist is applied and the image produced as in the print, plate and etch method. Copper is then electroplated onto the exposed areas and into the holes, followed by the etch resist metal. After the removal of the resist, the unwanted copper is etched away. With this method, there is much less copper to etch and therefore, less undercutting occurs to the tracks. Dry film resists are very applicable to this route as their thickness is of the same order as that of the plated copper and etch resist combined.

The masks used for the production of PCB's are critical to the final product. These can be generated in a number of ways. For prototyping, a mask of the final size may be drawn directly onto a Mylar sheet but with obvious limitations to accuracy and tolerances. The artwork for production purposes is often produced manually using large scale layouts with master to final size

ratios of up to 10:1. These are then reduced in size using specialised and expensive cameras. More modern techniques produce artwork automatically to the final size using precision x-y plotters from computer generated designs.

The level of automation that can be applied to the large scale production of PCB's means that large numbers of boards can be produced at a relatively low cost. However, the costs of producing high precision, fine geometry ($< 0.3\text{mm}$) one-off boards can be very high considering the generation of the artwork constitutes a large proportion of the overall cost. In the case of greater geometry lines, the use of laser printers or plotters to directly generate the artwork has now become the main route for the production of such prototype circuitry.

3.1.4 Pre-formed masks

Pre-formed masks are used mainly in the field of the continuous selective plating of strip or pressed strip. Most electrical connectors are produced from phosphor bronze or beryllium copper strip which has been punched to form the shape of the connector. These then require a nickel deposit followed by hard gold plating on the mating faces to provide necessary wear and contact resistance properties. Another type of continuous strip, the lead frame, is produced this way. These are manufactured from either Kovar or stainless steel. Lead frames are used to connect integrated circuits (IC's) from the inside of their hermetically sealed dual-in-line package (DIL) to the outside world, ie the circuit board. This requires soft gold to be plated at the internal ends of the lead to facilitate thermo-compression bonding of gold wires between the frame and the IC. In both cases, the gold is only required in discrete areas of the strip. By the use of selective plating, many tons⁴⁷ of gold have been saved. One of the earliest gold reductions was brought about by the use of controlled depth immersion. This will be discussed in the next section.

The use of selective plating of continuous strip became popular in the early '70s. In 1975, Heiestad⁴⁸ described a variety of selective strip plating equipment that he was involved in developing. These included anode geometry control (shielding), stationary mask striping, tip plating, moving mask stripe plating and mask spot plating. The anode geometry method is described in section 3.3. Stripe plating is a process in which a stripe of metal or metals is plated onto a continuous strip of metal ribbon. The stationary mask method made use of a rubber lipped longitudinal slot placed within the plating cell. The moving strip was passed over this slot and was tensioned against it to obtain a solution seal. The electrolyte was pumped at high velocity through the slot and onto the strip. In this way, stripes of 2mm width with a tolerance of $\pm 0.13\text{ mm}$ could be achieved. Current densities of up to 600 mA cm^{-2} were used for the gold plating. The moving mask stripe plating was achieved by means of synchronising the mask and the strip as it was moved through the plating bath. A split ring and rubber belt combination was used for the mask. However,

its plating speed was limited by poor anode positioning and the use of relatively low current densities of between 50 and 100 mA cm⁻² were used. The process did have the advantage of allowing the plating of pre-punched strip lead frames. Mask spot plating was achieved by using a wheel mask constructed from G10 fibreglass with appropriate holes for delineating the deposit. This had problems with speed and registration but showed the principle of operation very well. Strip speeds for the various processes were described and speeds range from 2 m min⁻¹ for intermittent wheel spot platers up to 12m min⁻¹. for continuous lead frames, both receiving 50 u in. of gold.

At the same time, Texas Instruments⁴⁹. reported the use of a spot plater for plating nickel and gold onto continuous contact strip. A Teflon mask incorporating a platinised tantalum mesh anode was used. No mention was made on whether the mask was stationary or moving or of the strip speed used.

Menzies⁵⁰. described reel-to-reel plating in 1978. The two techniques mentioned were controlled depth immersion and stripe plating, similar to that described previously. At the same time, Rehrig⁵¹. described a step and repeat spot plating unit for the plating of lead frame bond pads in which the spot plating was carried out using a mask that opened and closed in a clamshell manner. The mask was constructed from silicone rubber.

Hain *et al*⁵². reviewed selective plating techniques. These included controlled depth immersion, fixed masks and moving masks as well what was termed as fluid flow masking. This was a method equivalent to HSSJE. They commented on the various advantages and limitations of the methods, noting that fixed mask systems can create problems of distortion and slow strip speeds due to friction between the mask and the strip.

In 1982, Turner⁵³. described the latest techniques for the selective plating of connectors with gold. He described how high agitation rates and high metal ion concentrations enabled high processing speeds to be achieved. Current densities in the gold bath were in the region of 250 mA cm⁻². He claimed that a combination of dielectric masking and fluid flow masking (jetting in air) was the most successful technique for high speed continuous strip plating. Details of how this was obtained were not given in this reference.

A more recent review of the selective plating of precious metals for connectors has been given by Wingenfeld.⁵⁴ He stated that the moving mask system in conjunction with jetting of the electrolyte is the most widely used selective plating system. A wide range of configurations are described for many connector configurations.

3.1.5 Controlled depth immersion

Controlled depth immersion is a relatively simple selective plating technique. The continuous strip is fed into a plating electrolyte vertically and at a controlled depth. The immersed region therefore gets plated whilst the remainder does not. The solution level is maintained by means of a weir at each end of the plating tank. The electrolyte is pumped into the tank from a reservoir to provide a rapid flow past the work allowing high current densities to be used. Hain *et al*⁵² described the advantages of the system as being simple and versatile but listed the disadvantages of surface turbulence and capillary action reducing the selectivity. As a consequence, the feed-through rates have to be low. Also, as many components such as connectors require plating on one face only, as the whole of the immersed component is plated, there is a considerable wastage of gold.

3.2 BRUSH PLATING

Brush plating is a generic term that covers a range of techniques used for selective deposition by means an anode, covered by an absorbent material soaked in a plating electrolyte and rubbed across the cathodic surface being plated. Its origins probably date back to the early days of electroplating. For many years, it was common practice, particularly in the decorative plating industry, to use this method for touching up defective electroplate. In those days, a piece of anode material wrapped in a rag was used. This was soaked in the plating electrolyte and the "tampon" was connected to a power supply and rubbed across the defective area. The history and development of brush plating has been extensively reviewed by Rubinstein.^{55, 56, 57} The problem with using conventional electrolytes and anode materials is that deposition rates and deposit quality are very poor. Modern systems use specially developed high metal concentration electrolytes. The metals are usually in the form of an organo-metallic complex as this allows high metal ion concentrations to remain soluble. A high conductivity is also a requirement of the system.

Special insoluble anodes are used. These are usually made from high purity graphite although small anodes are made from a platinum/iridium alloy. Soluble anodes are unacceptable as at the high current densities employed, polarisation rapidly occurs leading to a significant drop in current density. The anodes can be specially shaped to conform to the job in hand. The process usually generates a significant quantity of heat so the anode is modular in design. It consists of a metal cored, plastic handle fitted with aluminium cooling fins. The graphite or platinum alloy anode is fitted to the metal insert at the cooling fin end and electrical connection is made at the other end. The work-piece is connected to the negative terminal of a high voltage, high current power supply. The usual rating for such a supply is 30V/30A although higher power/voltage models are used for

certain applications. The anode is wrapped with cotton batting of a long fibre variety. To reduce wear on the batting, it is sleeved with surgical tubing made from Dacron. Polypropylene wool is sometimes used as an alternative.

The tampon or stylus as it is generally called, is dipped into the plating electrolyte and rubbed across the surface to be plated in a circular motion, with frequent replenishments of electrolyte. For cylindrical shaped items, these may be attached to a slowly rotating lathe or turning head and the stylus held in steady contact with the work-piece. In these applications, the electrolyte may be fed directly to the stylus by means of a small pump. In this way, the process can be made semi-automatic.

Control of the thickness is based on precise amp-minute meters. Due to the varying current, which depends on the volume of electrolyte in the stylus, the distance of the anode from the cathode etc, the use of ammeters is not recommended. It is usual to apply a voltage within a range specific to the electrolyte and monitor the current/time integral.

There are many advantages claimed for the brush plating technique. Refractory metals and difficult to plate metals such as aluminium are easily plated with this method. It is claimed⁵⁶ that the adhesion is superior to conventional methods although the mechanism by which this occurs has not been made apparent. It is also claimed that the hydrogen embrittlement of high tensile steels is eliminated by the use of brush plating. In particular, the deposition of cadmium onto high strength steels does not require a subsequent de-embrittlement heat treatment. This is confirmed by the fact that U.S. Air Force has approved the process without the de-embrittlement heat treatment.

Rubenstein^{56,58} lists a very wide range of applications for the brush plating process. These range from aircraft engine components through to flexible waveguides, with any deposit that can be conventionally deposited. Some of the more common uses are in the repair of damaged or worn components. These can be built up with an electrodeposit by means of brush plating and then re-ground. In many instances, this may not even be necessary. Plating rates are very high. For example, gold deposits at up to $1.7 \mu\text{m sec}^{-1}$, whilst silver can be deposited at up to $2.5 \mu\text{m sec}^{-1}$. Deposit quality is very good because the high current densities employed produce deposits with a very fine grain size.

Selectivity is achieved because only those areas that come into contact with the electrolyte are plated. This has many advantages. Components that are too large to fit into conventional plating tanks can be selectively plated in the functional areas. For engine components, the entire engine may not need to be stripped down to expose the worn region that needs re-plating. If an area

requires a sharp cut off, conventional masking methods can be applied. Because there is no immersion in the electrolyte, these conventional masking systems remain in place much better than if immersed.

Wingenfeld⁵⁴. recently reported the use of the brush technique for the selective plating of continuous reel electrical connectors. He described two kinds of brush, the moving brush and the stationary brush. The moving brush⁵⁸. consists of a cylinder, wrapped in an absorbent material, partially dipped into the electrolyte. The cylinder, which is made from platinised titanium, is used as the anode. This slowly rotates and the connector strip passes along the cylinder with only the area requiring plating in contact with it. In this way, selective plating is achieved. Plating rates of up to 6 $\mu\text{m}/\text{min}$. of gold can be achieved with this method. This technique is becoming less popular as connector sizes become smaller and the area of contact reduces, the required degree of selectivity can no longer be achieved. It has been replaced by the stationary brush.⁵⁹. The brush is a V shaped hollow platinised titanium block covered with an absorbent material. The angle of the V is such that the point has a contact area of about 0.8mm. The electrolyte is pumped at low pressure into the block. A series of holes allows the material to become wetted by the electrolyte by capillary action. The components are then passed along the V of the block and where they touch, electrolyte gently oozes out at a slow but constant rate. The block is mounted onto an adjustment platform that allows the position and the angle of tilt of the block to be set. By tilting the block, larger areas may be plated. Plating rates of between 5-6 $\mu\text{m}/\text{min}$. are obtained with this method.

In general, the brush plating method has many advantages compared with conventional masking methods. High deposition rates are obtainable, deposition can be carried out *in situ* and many difficult to plate metals present few problems with adhesion. However, there are a few disadvantages. The selectivity of the process is not very good especially in the absence of additional masking methods. The operation is dependent on the skill of the operator, except where automation is used.

3.3 ANODE PLACEMENT AND GEOMETRY

Selective plating can be achieved by the judicious use of anode design and geometry of the plating cell. In order to understand how this can be achieved, it is necessary to understand how metal distribution and current distribution are related. In the absence of any surface overpotential (either activation or concentration) primary current distribution applies. During electrodeposition this situation can never occur although concentration polarisation can be effectively eliminated. There will always be some activation polarisation but in the case of certain systems that exhibit very fast electrode reactions ie copper sulphate this is minimal. However, if the electrolyte resistance is much higher than the activation resistance, primary current distribution will occur.

In this case, the current distribution on a cathode will depend largely on the distance between it and the anode as well as the electrolyte resistance. The closer the electrodes, the more even will be the deposit.

Secondary current distribution occurs if the cathode experiences significant overpotentials. Concentration polarisation usually gives rise to secondary electrode reactions such as hydrogen evolution. Therefore, in regions where the concentration polarisation is highest, local high current density areas, the deposition rate is reduced. This causes the metal distribution to deviate from that expected under primary current distribution.

Because of these factors, it can be seen that by reducing the distance between the anode and cathode, using an electrolyte that allows fast electrode reactions, reducing the electrolyte resistance and eliminating concentration polarisation, electrodeposits can be produced selectively by means of small, shaped anodes. Landau⁶⁰ patented such a system for the electrodeposition of precious metals onto plug connectors. The plating cell made use of an anode that conformed to the shape of the area to be plated on the connector comb. The anode was placed adjacent to the comb, with a narrow gap between them. In this way, the current flux was concentrated on the part of the comb where plating was required. To eliminate concentration polarisation, the electrolyte was pumped past the electrodes at a rate of several hundred cm sec⁻¹. Current densities in the region of 200 mA cm⁻² were used. It was found that the metal distribution closely matched the primary current distribution.

An improvement on this design was made by Bacon *et al*⁶¹, who made use of a focused anode cell. In this method, the anode was not placed close to the cathode but at some distance from it. The current flux was focused on the required area by means of a dielectric slot, which was part of the cell. In this way, a virtual conforming anode existed at the same point as would a real conforming anode. This design had the advantage that the anode no longer presented an obstacle to the electrolyte flow, thus reducing the pressure drop and the uniformity of the deposit no longer depended on the exact spacing between the comb and the conforming anode, which was critical in the former design.

The use of close proximity anodes has been studied in conjunction with pulse plating.^{62, 63, 64} Because the high instantaneous current densities produced by pulse plating favour primary current distribution, improvements in selectivity were obtained.

3.4 AUTOCATALYTIC (ELECTROLESS) DEPOSITION

Autocatalytic or electroless plating can be made selective on non-conducting substrates such as PCB's or MICS if the catalyst that initiates the deposition is put onto the surface selectively. There have been a number of recent developments in the printed circuit industry that use this method. Cook⁶⁵ reported a novel approach to selective metallisation of through hole PCB's. The drilled board is conditioned in an atmosphere of sulphur trioxide, produced from oleum. The conditioning process leaves functional chemical sites of SO_3H on the board. Subsequent to this, a photoresist layer is applied and exposed through a mask in the usual way. The board is then processed through a palladium activator and the regions exposed through the resist reduce the palladium. The boards are then processed through a highly stable electroless nickel bath to metallise the exposed regions and the board is finished in the usual way.

CHAPTER 4 HIGH SPEED ELECTRODEPOSITION PROCESSES

The previous chapter described the various methods used to obtain selective deposition. Many of the techniques mentioned also made use of high speed plating techniques. This chapter describes the theory and methodology of high speed deposition for both selective and non-selective plating.

4.1 THEORETICAL ASPECTS

For many processes that require large volumes of components or bare metals to be plated, there is an obvious commercial advantage to produce these as quickly as possible. In order to do this, high current densities need to be applied. However, the current density cannot be raised above a certain limit. To understand why, we need to know the mechanisms that control the rate of deposition and how these mechanisms can be manipulated to the advantage of the plater.

4.1.1 Transport mechanisms and the diffusion layer.

For a metal to be deposited from an electrolyte, metal ions need to be present at the cathode surface to accept electrons and become incorporated into the growing surface. During deposition, metal ions are consumed at the interface. These are replaced by metal ions arriving at the surface by means of diffusion, migration and convection. Convection results from the movement of the bulk electrolyte by stirring etc. Migration occurs as the result of the electric field on the charged ions. For example, Cu^{2+} ions having a positive charge will migrate under the influence of the electric field to the cathode. However, a complexed anion such as the cyanoaurate anion, $\text{Au}(\text{CN})_2^-$, will migrate to the anode. The influence of migration can be affected by the quantity of other charged species in the electrolyte that do not take part in the electrode reaction, as each charged species is responsible for carrying a portion of the current. In the presence of a large excess of charge carriers other than the electroactive species of interest, the influence of migration on each individual electroactive ion is minimised. Diffusion is a process that occurs by means of a random walk process. Diffusion of ions is a continuous process in the bulk electrolyte but the net distance travelled is zero.⁶⁶ However, at the interface during deposition, metal ions are being removed leaving a lower concentration close to the interface compared to the bulk solution. These are replaced by diffusion because a concentration gradient has been set up. Ions outside the interface region will tend to diffuse to the lower concentration region at the interface under the influence of the concentration gradient.

The region over which this directional diffusion occurs is known as the diffusion layer. The thickness of the diffusion layer is very dependent on the prevailing hydrodynamic conditions within the bulk of the electrolyte, the convection. In unstirred solutions, the diffusion layer thickness can reach 0.05 cm whereas under conditions of high electrolyte flow, it can be as low as 0.002 cm. The diffusion flux J_D is related to the current density. It can be found using Ficks law of diffusion and if migration is ignored

$$\frac{i}{nF} = J_D = -D \left(\frac{dc}{dx} \right)_{x=0} \quad (4)$$

This can be put in terms of the concentration at the interface by

$$\frac{i}{nF} = J_D = -D \frac{(c_b - c_0)}{\delta} \quad (5)$$

On solving for i we obtain

$$-i = \frac{nFD(c_b - c_0)}{\delta} \quad (6)$$

If the current density is raised sufficiently, diffusion will not be able to re-supply the ions and the concentration at the interface will drop to zero. This represents the limit of current density that can be applied under any set of hydrodynamic conditions.

$$i_L = -\frac{nFDc_b}{\delta} \quad (7)$$

Also, the diffusion coefficient is temperature dependent as can be seen from

$$\frac{D\mu'}{T} = \text{constant} \quad (8)$$

It can be seen from equation (7) that the magnitude of the limiting current density is controlled by the thickness of the diffusion layer, the concentration of metal ions and because the diffusion coefficient is related to temperature by equation (8), the temperature. The thinner the diffusion layer and the greater the metal ion concentration, the higher the value of i_L . There is a certain limit to the metal ion concentration that can be used. This is dictated by the solubility of that particular ion. However, the thickness of the diffusion layer is dependent on the degree of agitation of the bulk electrolyte.

It follows that for high speed electrodeposition, high metal ion concentrations in conjunction with high rates of agitation and high temperatures should be used.

4.1.2 Realistic limiting current densities

Despite the fact that the limiting current density is the absolute limit on the deposition rate for a particular set of conditions, it has been found by a number of workers^{4,5,6,7,8} that the deposit quality begins to deteriorate at some value below i_L . This deterioration is apparent by the formation of either dendritic growth or nodular powdery deposits. It is, therefore, important to ascertain the fraction of the limiting current density at which deposits begin to deteriorate rather than the limiting current density itself. This deterioration is certainly related to the i_0 value, with high exchange current density systems exhibiting degradation at a lower ratio of i/i_L . It would seem logical that if the diffusion layer thickness could be reduced without affecting the critical ratio of i/i_L then higher deposition rates could be obtained from any particular electrolyte.

4.2 MEASUREMENT OF THE LIMITING CURRENT DENSITY

Information on the mass transfer characteristics of any system can only be obtained if the magnitude of the limiting current density, i_L , is known. This can be made by direct measurement of the relationship between the overpotential and the current density or by measurement of the thickness of the diffusion layer. This latter technique is difficult to achieve although there have been some successful attempts.⁶⁷

4.2.1 Limiting current density measurement methods.

Measurement of i_L for any electrode reaction requires that the surface concentration of the reacting species at the electrode is reduced to as close to zero as possible. By plotting the relationship between the overpotential, η and the log of current density, $\log i_L$, the limiting current condition can be seen as a plateau where the current density remains almost constant with increasing η . These plots may be obtained by applying increments of either current or overpotential and measuring the resultant change in the uncontrolled variable. Figure 5 shows an ideal polarisation curve. The limiting current density is clearly visible. The increase in current at the end of the plateau is due to a consecutive electrochemical reduction process such as hydrogen evolution. However, such an ideal plateau is difficult to obtain in practice for a number of reasons.⁶⁸ Firstly, the surface area of the electrode increases during deposition due to the formation of rough deposits in the region of i_L . This effectively changes the true current density. Secondly, if competing electrochemical reactions occur simultaneously with deposition, such as hydrogen evolution, then the partial metal deposition current is masked by the current due to the secondary reaction. Thirdly, at very high rates of mass transfer, such as is found under conditions of high electrolyte agitation, the size of the limiting current plateau is reduced or disappears. A similar effect is seen with high metal ion concentrations in the electrolyte. Both these phenomenon are due to the onset of the consecutive reaction at overpotentials in the region of i_L as under these circumstances, i_L occurs at a much higher value of η . Finally, the rate of change in the perturbation applied has a strong influence on the appearance of the plateau. Too fast an increment can lead to non-steady state effects occurring which do not allow a steady state diffusion layer to be established.

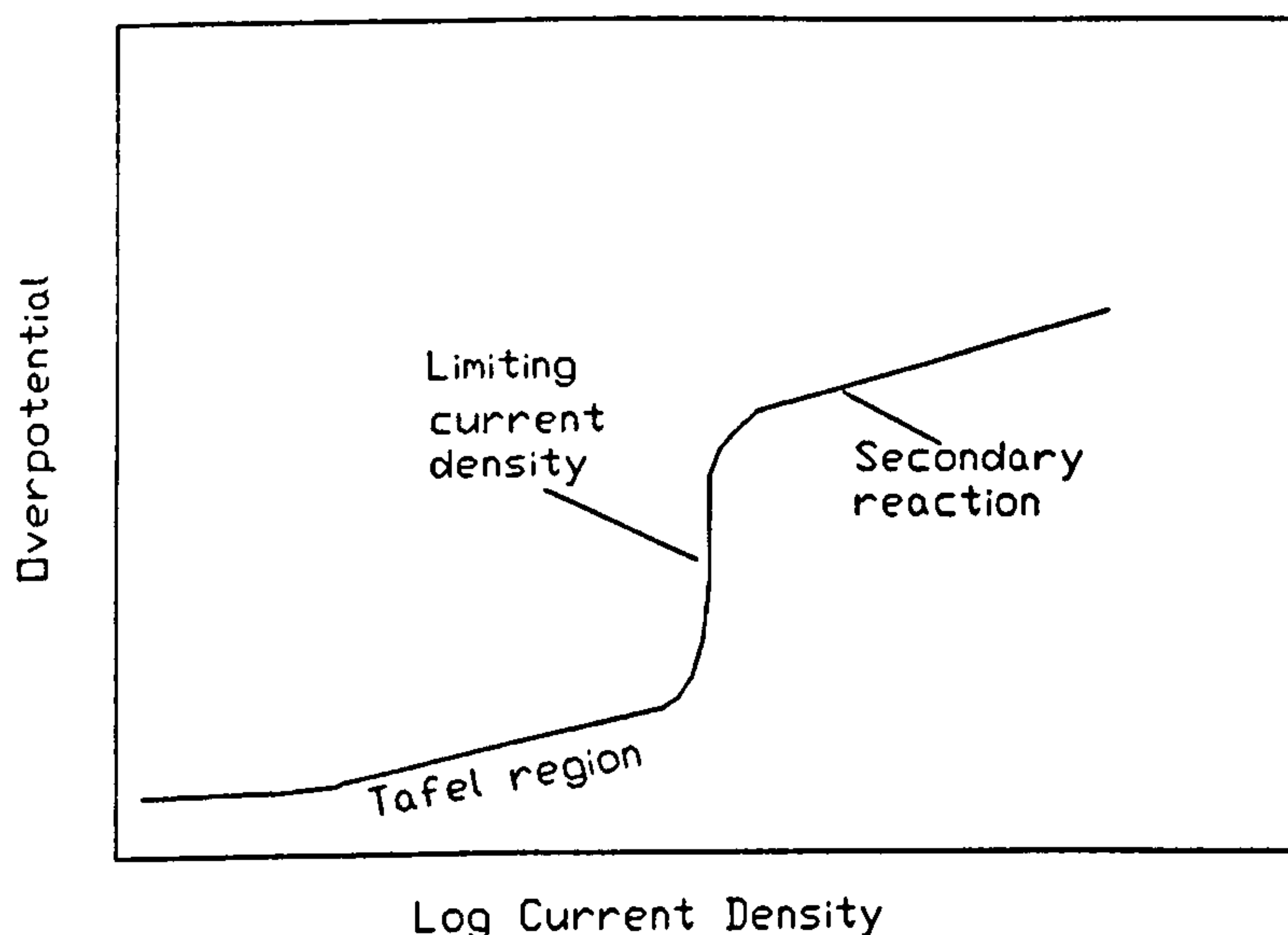


Figure 5. A typical polarisation curve showing the limiting current density.

In addition, it is important when measuring i_L that the effects of migration are reduced. The contribution to the value of i_L of migration can be seen as the $(1 - t)$ term in equation (1). This influence can be significantly reduced if an excess of a supporting electrolyte is added, which will then carry the major portion of the current. Such an electrolytic material should not influence or be involved in the cathodic reaction of interest. Despite these difficulties, there are a number of basic techniques that can be used to obtain the necessary data to construct such a polarisation curve.⁶⁸

4.2.1.1 Galvanodynamic methods.

The simplest approach to obtaining i_L is by applying a controlled, incrementing current and measuring the overpotential with a reference electrode and high impedance voltage measuring device. The current may be incremented in steps or continuously. The success of this method is dependent on the conditions of measurement as well as the species being examined. For the system to attain a steady state in terms of zero surface concentration, C_0 , a finite time is required. Hickman⁶⁹ reported that under free convection conditions, a time of 8 minutes or more was needed in order to obtain reproducible values of i_L . Selman *et al*⁶⁸ found that using the rotating disc electrode (RDE), steady state currents required a minimum time of

$$t_{ss} = \frac{i_L}{di/dt} \geq 60 Sc^{1/3} \omega^{-1} \quad (9)$$

This was found to be three times as high as for the equivalent time using the potentiodynamic method (see below). However, despite this, it is often preferable to use the galvanodynamic method for metal deposition reactions as there is less roughening of the deposit close to i_L than with other methods.⁶⁸

4.2.1.2 Potentiodynamic methods.

In the case of the potentiodynamic method, the potential of the working electrode is altered either step-wise or continuously with respect to a reference electrode. The potential difference between the working electrode and the reference electrode is maintained by means of a potentiostat. The current flowing through the cell is recorded and plotted as before. Once again, it is essential that a steady state diffusion condition is attained for each value of applied potential before the current is recorded. However, it has been found that the minimum times to reach steady state are about 1/3 of the equivalent galvanodynamic method.⁶⁸ However, as the current density initially

risks more rapidly during a potential ramp compared to a current ramp, this can lead to excess surface roughening of the electrode with the potentiodynamic method. As a result, excessively high limiting current densities can be measured.

Related to the potentiodynamic method is the potential step technique.⁷⁰ This method involves separately establishing the approximate potential, E_L , at which i_L is found, by a potentiodynamic sweep. This is followed by plotting the current-time relationship at potentials below, at and above this arbitrary value of E_L . The value of E_L used for the potential step analysis is that at which the smallest variation in current magnitude is observed. Then, a potential step of magnitude E_L is applied to the electrode and the current measured over a period of time. The steady state current measured by this method is the value of i_L . This method is claimed to have the advantage of being less sensitive to surface roughness of the working electrode.

4.2.1.3 Convective control methods.

This method can be used if forced convection is involved. A constant current density is applied under high convective velocity conditions. The velocity is then reduced in controlled manner until a steep rise in potential is observed. This rise indicates that the limiting current density has been reached for the associated convective velocity. This method is particularly suited to electrolytes with low conductivities as the ohmic drop under the conditions of measurement is constant.

There are several other methods which include minor variations on the aforementioned themes but their use is limited to specific situations. Once the limiting current density for any particular electrode geometry/hydrodynamic situation has been established, it is relatively easy to characterise the mass transfer properties of that system in terms of the Sherwood number by equations (2) and (3)

When measuring limiting current densities, the problem of deposit growth can be serious. This is especially so in convective systems that allow the rapid deposition of metals. In order to establish the mass transfer characteristics of such a system in terms of the hydrodynamic flow, use is often made of a redox couple. A frequently used redox couple is the alkaline ferricyanide/ferrocyanide electrolyte. Ferricyanide is reduced to ferrocyanide, with the advantage of the system exhibiting a large limiting current plateau. Such systems have been used extensively in establishing the relationships between fluid flow and mass transfer in jet electrolysis.

4.3 PRODUCTION PROCESSES

Whilst there has been a large quantity of work produced through high speed deposition plants, relatively little has been published on the plating conditions and deposit morphology. This is presumably because of the commercial confidentiality of such processes. In 1982, Safranek⁷¹ reviewed the latest developments in the high speed plating of chromium, copper, nickel, zinc, gold and silver. He reported that the first commercial uses of the technique occurred in the early 1940's when thin layers of tin were deposited onto continuous steel strip at current densities of up to 0.5 A cm^{-2} . This was achieved by passing the steel strip at high speed (1.2 m sec^{-1}) through the electrolyte. Since then the process has been used for the high speed zinc plating of steel strip and wire. However, the application was limited until the 1970's, when suitable pumps capable of continuous high speed movement of electrolytes were developed. He concluded that generally, high temperatures, high turbulent flow rates (in excess of 1.2 m sec^{-1}) and high metal ion concentrations were needed to achieve high deposition rates. He reported rates of deposition as high as $120 \mu\text{m min}^{-1}$ for thin coatings of gold and $180 \mu\text{m min}^{-1}$ for silver. For tin and zinc, rates as high as $140 \mu\text{m min}^{-1}$ and $80 \mu\text{m min}^{-1}$ respectively were achieved.

Apart from the plating of steel strip and wire, the most important application of high speed deposition has been within the electronics industry. As mentioned in the previous section, gold is used extensively within this industry. The most common applications of gold are for the plating of electrical connectors, lead frames, PCB edge connectors and transistor headers. Other applications include the deposition of gold spots or bumps for the bonding of gold connector wires to integrated circuits. Sewell⁷² reported the reel-to-reel selective pure gold plating of lead frames at high electrolyte velocity using a mechanical mask and electrolyte jetting. Current densities of up to 0.6 A cm^{-2} were used with electrolyte velocities of up to 1 m sec^{-1} . The current efficiencies were measured for differing concentrations of gold. It was found that although high deposition rates could be achieved with efficiencies rising to 100%, the deposit quality deteriorated as the efficiency approached the maximum. This maximum occurred at current densities of around 0.12 A cm^{-2} with a 24 g l^{-1} metal ion concentration. Above this value, the deposit appearance changed from a yellow, fine crystalline to a rougher, brown colour. The later deposits showed poor eutectic die attach and wire welding properties. Plating rates for a 24 g l^{-1} gold citrate electrolyte were reported to be $6 \mu\text{m min}^{-1}$. The most significant factors in the high speed deposition of gold were found to be the flow rate, composition and temperature.

In contrast to the previous author, Dorey *et al*⁷³ who examined gold deposits produced in a similar way, but using fluid flow masking (see Chapter 5), concluded that for thermocompression bonding, a gold with a distinctly "foxy brown" colour was optimum. Both a citrate based electrolyte with 22 g l^{-1} Au and a proprietary electrolyte with 126 g l^{-1} Au were used. The hardness of the optimum deposit was between 137 to 200 Knoop. Flow rates of up to 39 cm sec^{-1} were used although

the optimum was found to be 13 cm/sec using a current density of between 0.58 to 0.86 A cm⁻². Scanning Electron Micrography (SEM) revealed that the "foxy brown" appearance was due to a high degree of nodulation. This was not surprising considering the relatively low flow rates employed.

The aforementioned work was an extension of the results of Rehrig.⁵¹ He described the deposit characteristics and morphology using both DC and an asymmetric waveform using high rates of electrolyte flow in a spot plating unit. Unfortunately, the electrolyte velocity was not mentioned. Gold concentrations of between 30 and 40 g l⁻¹ were used. The influence of the nickel undercoat was also included in the assessment. He claimed that DC current was unsuitable for good bondability at current densities in excess of 300 mA cm⁻². A wide range of deposition conditions were examined using an asymmetric AC waveform, with a peak cathodic current density of between 1.0 A cm⁻² and 3.0 A cm⁻². The AC frequency was tested between 60 and 500Hz. Anodic peak current densities were examined between 0 and 0.4 A cm⁻². It was found that it was essential to use an anodic current for good bondability. Using an anodic current density component of 0.25 A cm⁻², all bonds were satisfactory. The morphology of such a deposit showed a significant grain surface projection, whereas with no anodic cycle, smooth deposits were produced. He found that a certain degree of surface micro-roughness was necessary for good bondability. The peak cathodic current density also influenced the grain structure and bondability. At current densities of 3.0 A cm⁻² the surface roughness was high but the deposit was powdery and lacked adhesion. He concluded that the most important factor in obtaining good bondability was the presence and magnitude anodic current offset and the pH of the nickel plating solution used for the undercoat. If this was too low then poor adhesion of the gold occurred. The frequency of the AC waveform did not have a significant influence on the bondability.

Endicott and Casey⁷⁴ examined the high speed plating of gold using dilute electrolytes for the reel-to-reel plating of lead frames. A gold concentration of 10 g l⁻¹ was used. The plating cell employed a moving mask for selectivity. The strip speed was optimised at 18.3 m min⁻¹. Electrolyte was pumped through the mask but no details of the relative strip to electrolyte velocity was given. It was found that a 1 µm deposit could be achieved at this strip speed using a current density of 0.8 A cm⁻². The deposits produced were relatively smooth and nodule free and were able to sustain a consistently high performance for thermocompression wire and die bonding.

It is interesting to note the different performances of the systems used by the previous authors. Whilst a micro-rough surface was found to be optimum for some, the opposite was true for others. Rehrig⁵¹ noted that for good die attach performance, a soft gold (less than 152 kg mm⁻²) was required. Dorey⁷³ also found that his optimum gold was also soft (< 124 Knoop). In both cases, the gold was considerably micro-roughened with Dorey's being brown and Rehrig's being matt gold. Endicott did not carry out micro-hardness measurements but it must be assumed that the

deposit was soft enough to form a thermo-compression bond. The real difference in the performance of the different methods is likely to reside in the electrolyte flow rate which was not clearly defined. As flow rate affects the thickness of the diffusion layer and thus the ratio of i/i_L , then this could be the reason for the differences.

It is quite evident that high speed deposition processes are required for rapid through-put of materials. Processes are available that give quite high rates of deposition (about $1 \mu\text{m sec}^{-1}$ for gold) but it is still possible to increase this further by optimising electrolytes and flow rates for particular applications.

CHAPTER 5 ELECTROCRYSTALLISATION AND MORPHOLOGY

It was mentioned in section 4.1.2. that deposit quality deteriorates at some value of current density below the limiting current density. This degradation takes the form of rough, nodular, dendritic or powdery deposits. It is obvious that the mechanism of growth goes through changes as the current density is increased and these changes are related to the rate of mass transport of metal ions to the growing surface. However, the mass transport limitation is not necessarily the only influencing factor. Electrodeposits are produced by a mechanism known as electrocrystallisation. An understanding of the mechanisms of electrocrystallisation is needed in order to establish how the various morphological structures observed at high current densities are produced.

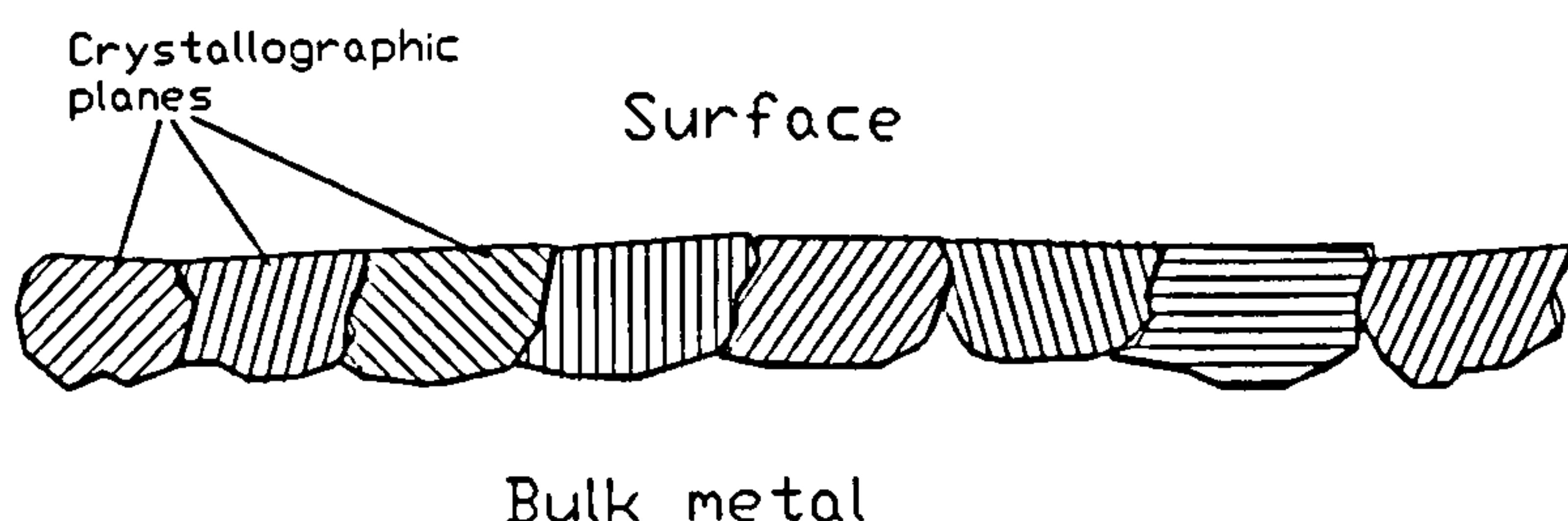


Figure 6. A schematic representation of the surface of a metal showing the random exposure of crystal planes at the surface.

5.1 SOME FUNDAMENTAL ASPECTS OF ELECTROCRYSTALLISATION

Electrodeposits are crystalline in nature as are the metals onto which they are deposited. The nature of the substrate can exert a significant influence on the way in which electrocrystallisation proceeds. All metal surfaces, no matter how apparently flat, are uneven. Most metals consist of randomly orientated crystallites with grain boundaries separating them. If any crystal plane other than a close-packed plane faces the solution, it will present a series of stepped crystal planes or edges. There will also be kink sites, dislocations and vacancies which are present in most metals.

A schematic representation of the surface can be seen in figure 6. This is true even for *single* crystals. This provides a depositing metal ion with many different locations in which to join the lattice. How it does so is dependent on the conditions at the interface at the time of deposition.

Having established growth sites, the deposit will then grow in a fashion that is highly dependent on the prevailing conditions such as current density, ionic form, temperature, nature of the metal deposit etc. It is well known that electrodeposits can follow many different growth habits ranging from compact epitaxial to single crystal needle types. The first comprehensive attempt to classify these structures was made by Fischer.^{75, 76} His classification was based on observations made with the optical microscope. He concluded that there were six main forms of growth, with a number of subdivisions of these types.

1. Field oriented isolation type (FI)
2. Basis-oriented reproduction type (BR)
3. Twinned transition type (T)
4. Field oriented texture type (FT)
5. Non-oriented dispersion type (NT)
6. Rhythmic lamellar type (RL)

Fischer concluded that all these different growth forms were the result of differing degrees of inhibition of the growth surface by foreign substances. These substances could be organic molecules deliberately added to modify structures or impurities. In addition, anions could act as inhibitors as could the products of the reduction process. The list above is ordered with increasing degree of inhibition.

Field oriented isolation types are generally referred to as dendrites, whiskers or needles. According to Fischer, these form as a result of low or no inhibition at the surface in conjunction with low metal ion content and high current densities.

Basis oriented reproduction types refer to epitaxial or pseudomorphic growths. These are produced at low overpotentials or current density in the absence of inhibitors. This type of deposit is produced mainly from simple salt electrolytes.

The twinned transition type occurs in the presence of moderate levels of inhibitor. It is characterised by a high degree of twin crystal formation centred around what is termed re-entrant grooves.

Field oriented texture types occur when a considerable area of the surface is covered by inhibitor molecules. This leads to two dimensional nucleation with a subsequent outgrowth forming layers. Lateral blocking by the inhibitor molecules prevents merging with adjacent crystallites. This leads to a structure consisting of numerous fine fibres oriented in the direction of the field and are associated with a strong preferred crystallographic orientation.

Non oriented dispersion types are associated with considerable inhibition and consequently deposition proceeds under conditions of high overpotential. The deposits consist of fine grained, equiaxed crystallites, typically 100 to 500 Å and do not show any preferred orientation.

The rhythmic lamellar type is associated with relatively high levels of inhibition and manifests itself as a lamellar or layered structure parallel to the surface. This structure is thought to form as a result of periodic fluctuations in the degree of inhibition as the deposit grows. It is believed that the effects of the reduction reactions occurring at the interface cause a fluctuation in the adsorption of the inhibitor or that the inhibitor is generated as a consequence of the reduction process. In the latter case, a new layer forms only after a minimum concentration of inhibitor has been formed. During the production of such structures, periodic variations of the overpotential may be observed.

These classifications provide a good guide-line to deposit structures although there are some structures not included such as the rounded mound and nodular structures observed with deposits produced at relatively high current densities. Such structures are often observed in deposits formed under strongly diffusion controlled conditions. In addition, they have also been observed with cobalt hardened gold electrodeposits. It has now been accepted that although the Fischer model is quite satisfactory as a general theory, it does not explain the many individual anomalies that may be observed when studying individual systems. An example of this is in the case of hard gold deposits.

Nakahara⁷⁷ studied the "rounded mound" structure of cobalt hardened gold. He found that uniformly distributed mounds were visible even at low thicknesses and have diameters of the same order as the thickness of the deposit. These mounds were found to increase in size as the deposit thickened and ultimately impinged on one another. Transmission Electron Microscopy (TEM) revealed that the deposits consisted of fine, uniform grains 200-300 Å in diameter. In addition, the grains had a preferred orientation of 111 normal to the surface. According to the Fischer classification, such grains should not possess any preferred orientation. Nakahara went on to observe that the texture had a spread of about 15° that corresponded to that extended by the profile of the mound. He inferred from this that the surface of the mound was bounded by 111 close packed planes onto which further growth occurred. Transmission Electron Microscopy also showed clear evidence of the incorporation of a high density of non-metallic inclusions. He concluded that these inclusions, presumably the potassium cobalticyanide mentioned in Section 2.2.2, inhibited

lateral diffusion during deposition and hence there is an amplification of random small protuberances formed in the initial layers. He went on to suggest that adsorption of inhibiting molecules on the top surface caused continuous nucleation and is responsible for the small crystallite size.

Such rounded mounds are observed under certain conditions of Physical Vapour Deposition (PVD). Sheppard and Nakahara⁷⁸ observed that under conditions of low surface temperature, PVD deposits show a similar structure. Under low surface temperature conditions, the rate of surface diffusion is very low. This is analogous to the electrodeposition situation where adsorbed molecules inhibit surface diffusion. Under the Fischer classification, such a deposit should be a Field Oriented Texture (FT) type. However, the deposit does not possess all the criteria used for the description of FT types, particularly the small grain size, and therefore the classification shows its limitations.

Another of the limitations of the Fischer scheme is its reliance on the inhibition process alone with no reference to the interaction of the growing interface with either the diffusion layer or the hydrodynamic boundary layer that exists in convected electrolytes. As a consequence, more elaborate theories have been developed to account for such interactions.

5.1.1 Electrocrystallisation at low current densities.

Bockris and Razumney⁷⁹ have been influential in establishing some of the theories of electrocrystallisation. They proposed that at low current densities or more particularly, low overpotentials, the following mechanism prevailed. The hydrated metal ion in the Outer Helmholtz Plane under the influence of the electric field approaches the metal surface where it lands on a crystal plane. However, the hydration sheath is still attached but is distorted due to the presence of the plane. Before it can be incorporated into the crystal lattice, it has to lose its hydration sheath and be electronated. It is likely that partial electronation occurs at this stage as in this form, an adion, it has less than the full ionic charge of an ion in solution. In order to lose its remaining water molecules, the adion diffuses to a step where some water molecules are replaced by co-ordinating metal atoms at the step. The adion then diffuses along the step to a kink site where further co-ordinating metal atoms replace the water molecules until the adion becomes fully co-ordinated and incorporated in the lattice. In the case of complexed ions, a similar growth mechanism occurs except that the ligands of the complex are lost instead of the hydration sheath. Further adions are incorporated and growth continues. Dislocations are particularly important to this mechanism of growth and the perpetuation of growth is adequately covered in the work of Bockris and Razumney and will not be detailed here. The rate determining step of such growth mechanisms is often the surface diffusion of the adions, up to overpotentials of 10mV. Such a growth mechanism is often termed epitaxial or pseudomorphic as it closely continues the underlying structure of the substrate.

5.1.2 Electrocrystallisation at high current densities.

With increasing overpotential and therefore increasing current density, growth proceeds by 2 dimensional nucleation, with groups of adions incorporating together at step sites. Charge transfer (activation control) now becomes the rate determining step and this tends to control the manner in which the deposit grows.⁸⁰ The steps sweep across the surface and form well-faceted crystallographic structures. With increasing overpotential, diffusion of metal ions from the solution begins to influence the mode of growth. When the concentration overpotential is comparable to the activation overpotential, deposition is under mixed activation and mass transfer control. Because of the high surface concentration and high overpotentials, adions have sufficient kinetic energy to form nuclei on the crystal planes, forming a fine grained structure which is no longer epitaxial. This mode of growth continues with increasing overpotential and current density until at some overpotential determined by the ratio of i/i_L , activation control is lost and mass transfer becomes the rate controlling step. Deposit growth then becomes increasingly nodular. West⁸⁰ has defined the critical current density ratio in terms of the exchange current density, i_0

$$\frac{RT}{nF} \ln \left\{ 1 - \left(\frac{i}{i_L} \right)_{crit} \right\} = x \left\{ - \frac{RT}{(1-\beta)nF} \right\} \ln \left(\frac{i}{i_0} \right)_{crit} \quad (10)$$

thus giving

$$\left(\frac{i}{i_L} \right)_{crit} = 1 - \left(\frac{i_0}{i} \right)^{x/(1-\beta)} \quad (11)$$

where x in this case is an empirical constant. These equations indicate that $(i/i_L)_{crit}$ is small for large values of i_0 . This is supported by experimental evidence that nodular growth occurs for i/i_L values of 0.9 for iron and nickel ($i_0 = 2 \times 10^{-9}$) but for copper, i/i_L is about 0.4 ($i_0 = 4 \times 10^{-5}$)⁸¹. Growth now proceeds through 3 dimensional nucleation, in which nuclei form and grow not only in the radial direction but also in the axial direction, ie perpendicular to the surface. This mode of growth is responsible for the increasing nodulation of deposits as $(i/i_L)_{crit}$ is exceeded. With increasing overpotential, a number of unique growths may be observed, such as dendrites, needles and tip splitting branches (also known as dense branched morphology, DBM).

High speed deposition is concerned with obtaining compact, high quality deposits at as high a current density as possible. It is therefore necessary to examine in greater detail the way in which

morphological changes occur as $(i/i_L)_{crit}$ is approached. In this way, it may be possible to understand the way in which deposit deterioration occurs and may lead to a means of increasing the rate of deposition whilst maintaining the quality of the deposit.

5.1.3 Mechanisms of surface irregularity amplification.

Electrodeposits formed at "conventional" current densities are generally smooth and compact. However, as the current density is increased, surface roughening is observed to increase. There have been many studies on the mechanism of surface roughening. Gabe and Robinson⁸² examined the formation of powder and dendrites in copper deposition using a rotating cylinder electrode. They found that the incidence of dendritic or powder deposition was related to the transition between charge transfer to mass transfer control. They estimated that the critical ratio, i/i_L , for copper was 0.4. Ibl⁸³ reviewed the subject of powder formation by electrodeposition and its relation to mass transfer. He concluded that powder formation (an extreme form of nodulation) occurs when i_L is reached. He also concluded that roughness development was attributable to instability of the deposit surface under diffusion limiting conditions. Instability here means the selective growth of surface perturbations, leading to roughening. As explained above, under conditions of diffusion control, 3 dimensional nucleation occurs which can lead to nodule formation. It has been shown by Kindler *et al*⁸⁴ that for copper, at current densities substantially below i_L , a large number of nodules can form. These nodules appeared to be large faceted crystals, overgrown with a fine microcrystalline structure. They claim that the fine structure deposits preferentially on the large crystals, leading to nodule formation. The number of large crystals also increases with increasing current density. Therefore, surface perturbations are common below i_L . Degrez and Winand⁸⁵ studied the deposition of copper at high rates using a high speed flow channel. Under these controlled mass transfer conditions, they concluded that roughening of deposits was the result of 3 dimensional nucleation, the onset of which was proportional to the combined kinetic and concentration overpotentials. Despic and Popov⁸⁶ have also identified the factors that enhance powder formation. These are a decreased concentration of depositing ions, an overall increase in the concentration of the electrolyte (supporting electrolyte), an increase in the viscosity, a decrease in the temperature and a reduction in the electrolyte velocity. All these factors result in a lowering of the limiting current density.

Bockris *et al*⁶⁶ have presented a simplified explanation for instability occurring under diffusion control in the presence of surface perturbations. Figure 7 shows a schematic diagram of the interfacial region with a single surface perturbation, the height of which is considerably less than the diffusion layer thickness. If deposition proceeds under diffusion control and a linear diffusion gradient is assumed (not strictly true), then the diffusion current will be given by

$$i = -DnF \frac{c_b - c_0}{\delta} \quad (12)$$

As the thickness of δ_{peak} is less than that of δ_{surf} , i_{peak} will be greater than i_{surf} due to both field and diffusion distance effects. Therefore, the peak will increase in height. In addition, the electric field becomes concentrated at a perturbation further increasing its rate of growth. This implies that any slight surface perturbation will always lead to a rough deposit. It is obvious from practical observations that this is not always the case and there are other factors at work that can lead to stabilisation of the surface. Therefore there have been many attempts to analyse all the factors responsible for surface roughening and put these into a stability theory.

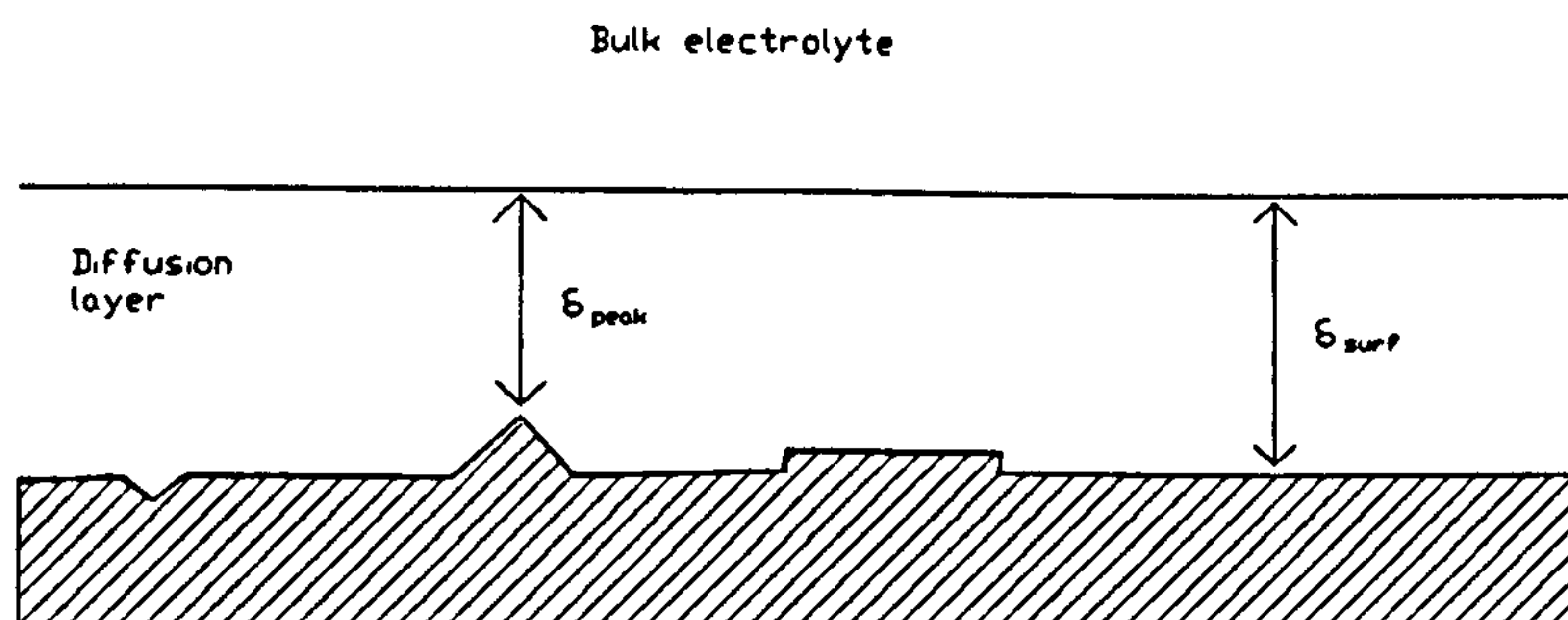


Figure 7. A diagram showing how the thickness of the diffusion layer is lower above a surface perturbation provided the perturbation is small.

5.1.4 Stability theories for roughness development.

Most of the stability theories for electro-growth have been developed based on the analogous situation of crystal growth during solidification from the melt. The analogy of electro-growth with solidification is a reasonable one. During solidification, the driving forces controlling crystal growth are heat diffusion away from the growing crystal (equivalent to diffusion of metal ions to the surface) and the degree of undercooling (the equivalent to overpotential). Mullins and Sekerka⁸⁷ postulated a stability theory for a planar surface during the solidification of a binary alloy by calculating the time dependence of the amplitude of a sinusoidal perturbation of small amplitude

introduced to the plane. They also addressed the morphological stability of a particle growing by diffusion or heat flow.⁸⁸ Their conclusion was that although a surface perturbation will be amplified and thus be unstable, stability could be achieved by the effects of the surface tension of the crystallites, termed capillarity, providing the curvature of the perturbation was sufficiently small. Aogaki⁸⁹ extended this theory to the formation of electrodeposited metal powders. Landau and Shyu⁹⁰ applied the theory to the development of surface roughness. This was further extended by Barkey *et al.*^{91, 92} The previous theories were claimed to be deficient as they did not take account of the ohmic overpotential. They concluded that the morphological stability of the electrode surface is controlled by the electric field, the fraction of the limiting current and the surface energy. However, the model developed by Barkey *et al* did not correctly predict the magnitude of protrusion spacing and were half that found by experiment.

Chen and Jorne⁹³ included a damping factor to account for the degree of influence a perturbation has on the diffusion layer thickness. They claimed that if the perturbation is very small compared to the thickness of δ , then the diffusion layer boundary would be unaffected and could be taken as being flat. This was not taken into account in the previous treatments. They went on to develop a mathematical treatment and formulated a stability theory which agreed with experimental evidence. They showed that the surface tension was the only stabilising factor in the system. Without the influence of the surface tension, the perturbations would always grow with time. They pointed out that the surface concentration of adions influences the stability by affecting the surface tension. In the case of a zero surface concentration, the surface tension loses its stabilising effect and all the surface perturbations will tend to grow. Instability is also encouraged by the magnitude of the concentration gradient at the surface with large concentration gradients encouraging the growth of increasingly smaller perturbations. In addition, increasing the metal ion concentration and reducing the thickness of the diffusion layer both encouraged instability. This, in effect, is the same as increasing the concentration gradient

5.1.5 Theories of needle, dendritic, dense branching morphology (DBM) and fractal growth.

Deposits produced above the critical ratio of i/i_L not only produce rough nodular deposits. Under certain conditions of electro-growth, needles, dendrites, tip splitting dense branching morphologies and fractal structures have been observed. Figure 8 shows schematic diagrams of these morphological structures produced by electrodeposition in a 2 dimensional Hele-Shaw cell (See later). Whilst these structures have been produced in a two dimensional cell, they share many characteristics with those produced in the more conventional three dimensional systems. In the case of a needle growth, this is characterised by a number of thin needle-like crystals with parabolic tips exhibiting little or no lateral growth habit. This should not be confused with whisker formation, which are caused by the interaction of foreign molecules with a growing surface.⁷⁵ A dendrite is

essentially a needle growth with lateral side arms growing at specific angles to the main growth direction. Further lateral growths are often observed on these side arms. The DBM structure is characterised by its lack of crystalline regularity although the DBM also differs from a dendritic structure in terms of its tip splitting habit. They also exhibit a regular growth front, with all the leading tips in the same spatial position relative to the electric field. Fractal growths are characterised by their irregular growth fronts. Each of these structures may be produced electrochemically but they are also observed in solidification from melts, precipitation from supersaturated solutions and amorphous annealing. This would indicate that there are common causal principles to these growths irrespective of the nature of the growth medium.

The earliest theories of dendritic and needle growth are attributed to Barton and Bockris⁹⁴. They proposed that dendritic growth proceeded from a surface perturbation by means of mass transfer control. They started with the growth of a macrospiral (the growth of a spiral dislocation) that has a very small tip radius ($r \sim 10^{-6}$ cm). Under these conditions, diffusion to the tip is controlled by spherical diffusion as opposed to planar diffusion. The current density at the tip is given by $DnFc_b/r$ instead of $DnFc_b/\delta$. Since $r \ll \delta$, the limiting current density is much higher on the tip. They also argued that because of the high step and kink density, the tip has a higher exchange current density and the activation overpotential would be much less than on the surrounding planar surface. This leads to an accelerated growth of the tip which subsequently develops into a needle. The important factors relating to the initiation of needle and dendritic growth have been identified as being two critical overpotentials, the first being required to initiate the growth of the screw dislocations and the second to produce diffusion controlled conditions at a rate necessary to produce the tip radius suitable for spherical diffusion.⁹⁵ An initiation period was identified in which these changes occurred. Critical overpotentials for both dendrite and powder formation were identified for copper and cadmium by Popov *et al.*^{96, 97, 98} using the Barton-Bockris theory. Whilst the theory is able to explain the growth of needles, there still remained the question of the instability of the needle growth to branching. It also treated the dendrites as individual with no reference to the influence that other protrusions had on their neighbours.

Despic and Popov⁸⁶ commented in their review of transport controlled mechanisms that as twinning is frequently observed in dendrites, the regular angled sidearms may be due to growth from twin sites. Twin sites represent low energy sites for lateral growth and as such enjoy an enhanced growth rate. This would account for unique angles observed any particular metal as the angle is controlled by the properties of the crystal twin. However, they were unable to offer a reason for the regular spacing of the sidearms on the dendrite.

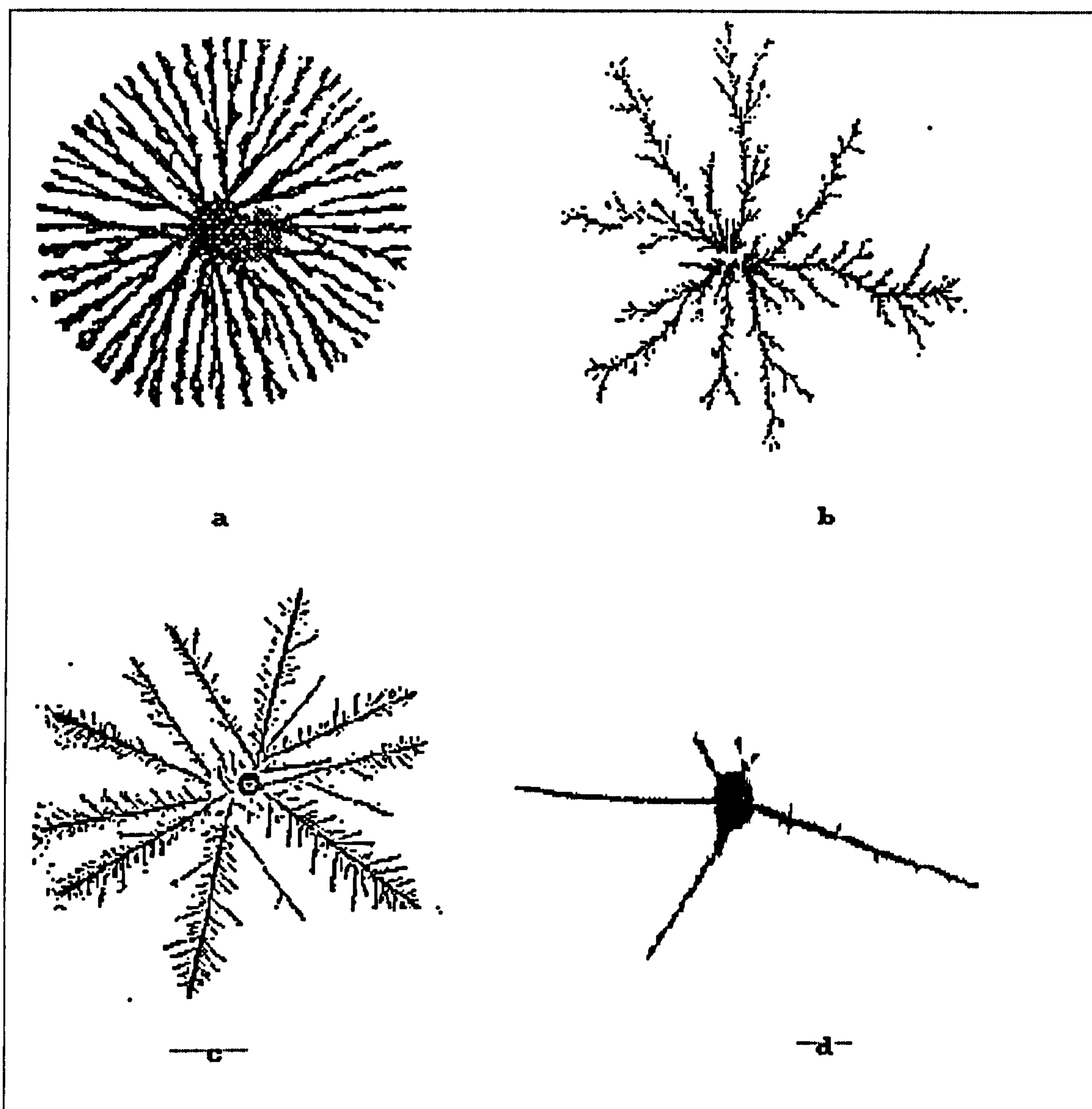


Figure 8. Typical morphological structures produced by electrodeposition in a Hele-Shaw cell. (a) A dense branching morphology structure (DBM), (b) a fractal or diffusion limited aggregate (DLA) structure, (c) a dendritic structure, (d) a needle structure.

One important distinguishing feature of a dendrite is the long range crystalline order present. It has been suggested¹⁰³ that a stacked plane structure provides the necessary anisotropy that stabilises the growth of a dendrite and prevents it forming similar but disordered fractal or tip splitting structure.

Dense Branching Morphology structures occur if the influence of anisotropy is reduced by other external factors. This type of morphology is characterised by the formation of irregular branching structures that undergo random tip splitting. However, there is generally a long range order in that they follow a regular growth front. Barkey⁹⁹ has examined the differences between this type of morphology and dendritic structures by examining Schlieren photographs during the growth of both dendrites and DBM structures. These photographs highlight density differences in liquids allowing the shape of the mass transfer boundary layers to be seen. He concluded that it is the shape of the mass transfer boundary layer that selects the development of either a dendrite or a DBM structure. In the case of a dendrite, the boundary layer resembles a shock wave with the tip of the dendrite being close to the boundary layer. In the case of the DBM, the boundary layer was observed advancing some distance ahead of the tip splitting branches. He went on to conjecture that in the case of the DBM, a hydrodynamic instability is set up due to the fast growth of the tip and the interaction of the less viscous boundary layer and the bulk. This creates a gradient stress across the liquid interfaces that sets up a dynamic surface tension. It is this surface tension that stabilises the growth front and prevents random variations in the growth velocity of different branches. Thus, a continuous, regular growth front is preserved. The tip splitting results from the growth of a surface perturbation via a Mullins-Serkerka type instability between the fluid layers. In the event of a significant protrusion, growth occurs of that protrusion resulting in tip splitting. This type of morphology is rarely seen under conventional conditions of electrodeposition but may be realised under conditions of high overpotential and low metal ion concentration.

Fractal structures have been likened to Diffusion Limited Aggregates (DLA) observed in other systems such as smoke particle aggregation. These are characterised by a non-uniform growth front and a lack of symmetry. In addition, they have been shown to possess no long range ordering. Such structures occur if the surface tension effects seen in DBM are reduced. As a consequence, the Mullins-Serkerka instability predominates allowing surface perturbations to grow unchecked and at random. This results in a random structure that has been found to possess a fractal Hausdorf

dimension". One other important property of fractal objects is what is known as scale invariance. These objects are invariant under a transformation which replaces a small part by a bigger part, that is, under a change in scale of the object.

Recent work has been carried out on the morphology selection mechanisms of dendritic and allied growth by means of two dimensional electrodeposition cells known as Hele-Shaw cells.^{99, 100, 101, 102, 103.} The cell consists of 2 sheets of plexi-glass separated by a narrow gap of about 0.001-0.01 cm which contains the electrolyte. A ring anode is set around the edge of the plates and a small hole is supplied in the top plate for the insertion of the cathode. The cathodes used vary but are usually copper wire. By applying a suitable potential across the cell, a variety of two dimensional dendritic and fractal structures may be grown. The type of structure is highly dependent on the nature of the electrolyte and the growth conditions. It has been found that for true dendritic growth, crystalline anisotropy must be influential. If the influence of anisotropy is reduced, then DBM and fractal growths predominate. The conditions controlling the type of structure produced can be summarised by figures 9a and b.^{101,100.}

The differences in the morphological diagrams presented above are presumably due, in part, to differences in interpretation of the types of structure observed and partly on slight differences in experimental set-ups. Additionally, it has been noted that there is a considerable region of overlap between morphology transitions.

The work by Ben-Jacob and others (see references above) has been primarily to correlate the formation of similar patterns over a wide range of physical and organic systems that have much in common. Such diverse patterns as that of a snowflake to the structure of a coral reef or the formation of electrodeposits, both fractal and dendritic, to the formation of aggregations of soot particles are believed to be subject to unifying underlying principles. It is now recognized that such structures are the result of the interplay between microscopic interfacial dynamics, such as diffusion, and macroscopic forms under highly non-equilibrium conditions.

*The Hausdorff dimension, also termed the fractal dimension D can be derived as follows. The density correlation function $c(r)$ of a fractal may be defined as the average density of an object at distance r from a point on the object and is an measure of the average environment of an individual particle making up the object. The term $c(r)$ reflects the scale invariance and it may be shown that the only way in which c may vary is as a power law in r . Any other function would have an intrinsic scale. The term c may be written in the following form:

$$c(r) = kr^{-(d-D)}$$

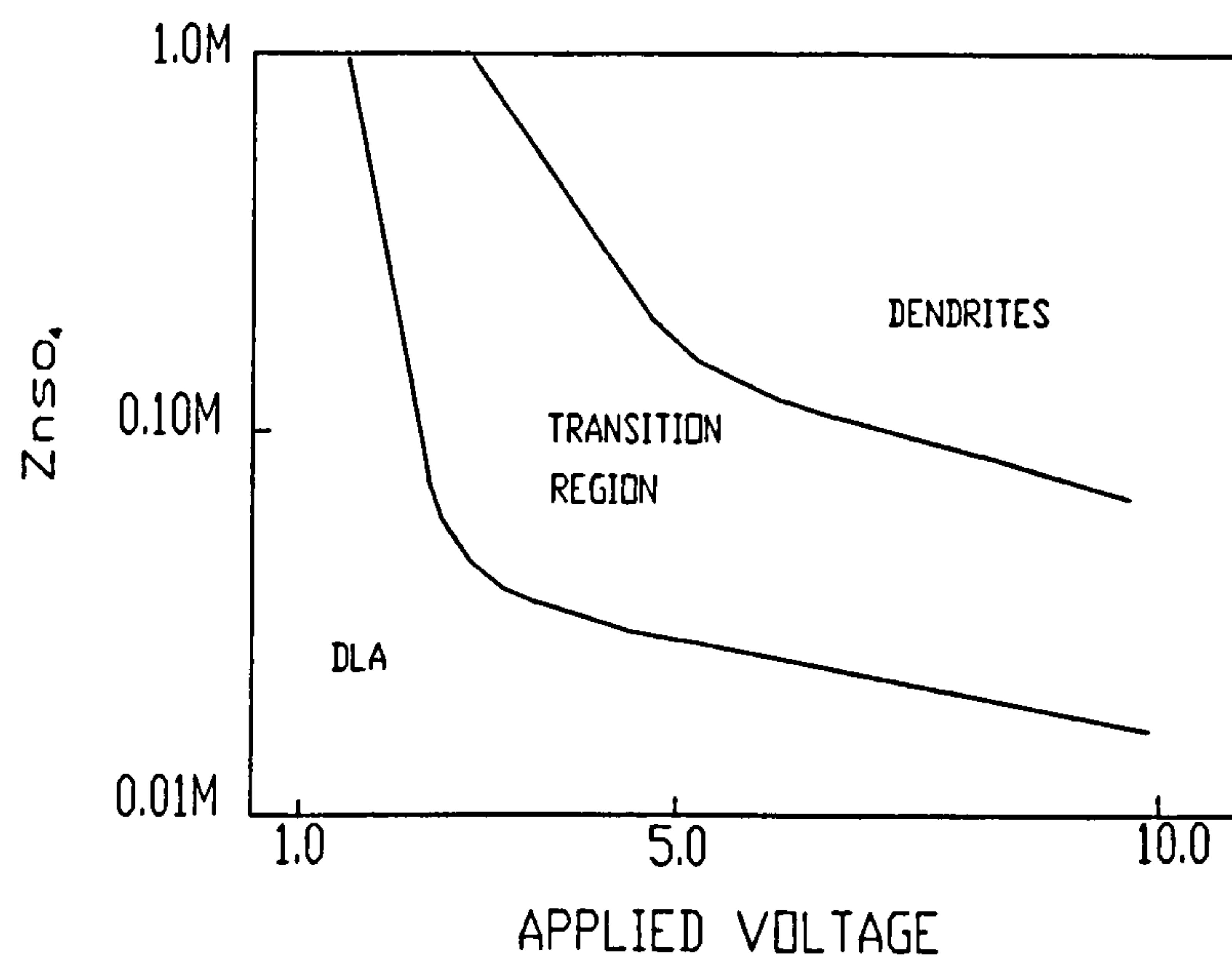
Here, k is a constant and the exponent is written in terms of the dimension of space, d and D is the fractal or Hausdorff dimension. Now, $c(r)$ is a decreasing function of r as the average density decreases as the object becomes larger. Consider how the mass of an object, M , scales with the mean radius, R . We can estimate this by multiplying a typical density from the above equation, by the volume:

$$M(R) = KR^{d-D}R^d = KR^D$$

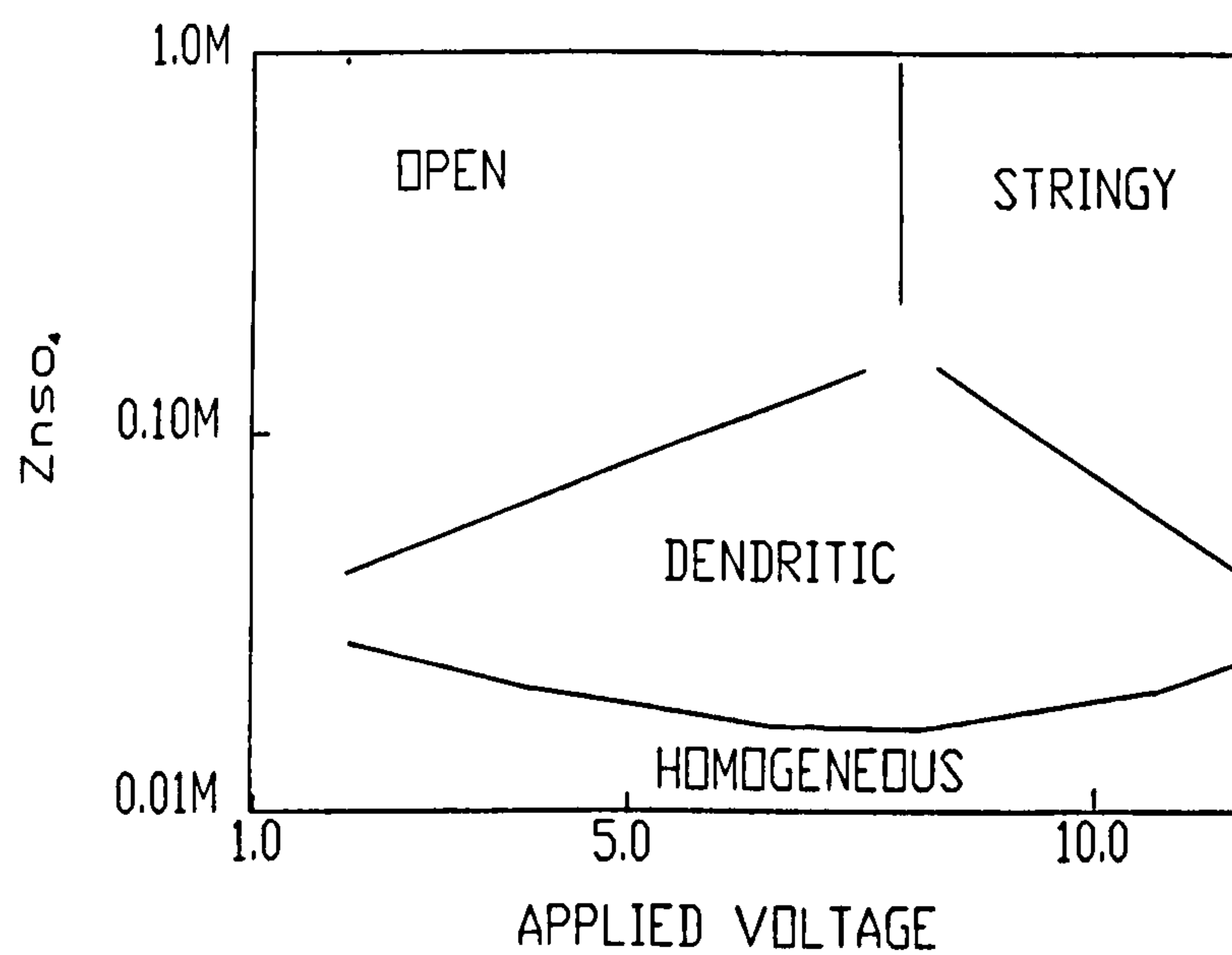
The term K is another constant. It may now be apparent why D is called a dimension. For simple objects, D coincides with the usual notion of dimension. But for fractals, D is not an integer. Therefore, if an object can be shown to possess a non-integer Hausdorff dimension, it can truly be called a fractal.

For a quantitative description of this interaction between the microscopic and macroscopic forces that dictate morphology selection, the reader is referred to reference 103. However, a brief qualitative description will be given here. Under conditions of non-equilibrium growth, such as the formation of a snowflake or the growth of a dendrite, the initial stable solid phase will propagate into an unstable or metastable phase. In the case of the snowflake, a collection of solid stable nuclei propagates into the unstable supersaturated water vapour phase. In the case of the dendrite, it propagates into an electrolyte that is in a highly non-equilibrium state ie a moving tip into a continuously changing diffusion and hydrodynamic layer. The rate of growth of the stable phase is limited in both cases by a diffusion process. As a result, the kinetics of the diffusion process determine the macroscopic approach of the solid phase to equilibrium. In doing so, the system is driven towards the formation of irregular or dendritic shapes. The exact form of the resultant shape will depend on such things as surface tension, surface kinetics and anisotropy. and these are determined by the exact conditions of growth and the nature of the growing material. Together with diffusion kinetics, these microscopic forces determine the macroscopic approach towards equilibrium and influence the structures on many length scales.

The reason for investigating such non-equilibrium crystallisation modes is that under conditions of jet electrodeposition, the interface is far from equilibrium due to the high overpotentials applied. As such, it is to be expected that such structures are likely to occur close to the upper deposition limit during jet deposition. This is indeed observed and will be discussed later.



(a)



(b)

Figure 9 (a) Morphological diagram of zinc deposits from the Hele-Shaw cell (After Grier et al¹⁰¹.
(b) Morphological diagram of zinc deposits from the Hele-Shaw cell (After Sawada et al¹⁰⁰.)

CHAPTER 6 HIGH SPEED JET ELECTRODEPOSITION

There have been relatively few papers published on the subject of high speed jet deposition. Of these, deposit morphology has not been given serious consideration. The emphasis in these papers has been on establishing mathematical models for the mass transfer characteristics of jet deposition. Of these, a high proportion deal with a submerged jet,^{1,104, 105, 106, 107}. Although under certain conditions, these mass transfer results are applicable to the un-submerged jet.^{2,108} There have been a number of papers published concerning the use of jets in electrochemical machining but these are of little consequence to this study and will not be referred to. The earliest published work on jet electrodeposition was by Zarb.¹⁰⁹ He described a system that made use of multiple jets in order to produce selective gold deposits on lead frames. No masking was used. He claimed that deposition rates of 2 μm in 15 seconds could be achieved using a pure gold electrolyte.

In 1974, Fletcher,¹¹⁰ describing an invention of G.D. Oliver, filed a Patent on behalf of NASA describing a selective plating method using a pressurised jet of electrolyte. The jet could be moved under computer control. By means of a video digitising system, information on a pattern could be introduced into the control system. The jet was scanned, raster fashion, across the substrate and the current was applied at the appropriate times in accordance with the control pattern. In this way, a plated pattern could be written, much in the same way as a dot-matrix printer produces a picture. No other publication by Oliver has been found and therefore few details of the process and the morphology of the deposits produced are available.

Before examining the mathematical models for the mass transfer within jets, it is essential understand the nature of the hydrodynamics of such a system.

6.1 CHARACTERISTICS OF FLUID FLOW WITHIN JETS

Many studies have been carried out on the flow characteristics of submerged and un-submerged jets. The flow patterns created within both systems are very complicated. The Navier-Stokes equations* that could describe the flow are difficult to solve for the whole system. Therefore, many

*The Navier-Stokes equations represent the equations of motion for a Newtonian fluid of a constant density and viscosity. It relates the motion in a unit volume of fluid in terms of the x,y and z cartesian co-ordinates. The derivation of the equation is beyond the scope of this work. However, it is given here in vector terms

$$\frac{\partial \mathbf{v}}{\partial t} + \mathbf{v} \cdot \nabla \mathbf{v} = -\frac{1}{\rho} \nabla p + \nu \nabla^2 \mathbf{v} + \mathbf{g}$$

A fuller description may be found in References 123 and 124, together with the equation written in rectangular co-ordinates.

workers have divided the flow into four distinct regions as can be seen in figure 1. These regions are termed 1) The free jet region, 2) The impingement region, 3) The wall jet region, 4) The hydraulic jump. The hydraulic jump is unique to non-submerged jets. Whilst there are considerable differences between the flow mechanisms, it has been shown that when the nozzle is within a specific distance from the surface, then conditions of flow are similar for both the submerged and un-submerged jets within the impingement region. The wall jet characteristics, however are significantly different due to interaction between the surrounding medium.

6.1.1 Flow within the free jet region

The free jet is the region between the nozzle and the impingement zone prior to any interaction with the target surface. Schlichting¹¹¹. studied the free jet within the submerged jet system using boundary layer equations. He found that a jet will become completely turbulent at a short distance from the discharge point as the emerging jet becomes partly mixed with the surrounding fluid at rest. Consequently, the mass flow decreases in the direction of flow and the jet spreads out with a reduction in velocity. However, the total momentum remains the same. Studies of non-submerged jets¹¹². have shown that the velocity remains nearly constant close to the nozzle exit. However, as in the case of the submerged jet, at some distance from the nozzle, turbulence occurs due to a varying velocity profile within the jet. The velocity profile becomes bell shaped with the maximum velocity occurring on the jet centre line. This is a result of entrainment of the surrounding air and the flow breaks up. Squire¹¹³. discussed the theoretical solution to the Navier-Stokes equation for laminar flow in a free jet.

6.1.2 Flow within the impingement region

As the free jet approaches the surface, the axial centre line velocity decreases rapidly to zero at what is termed the stagnation point. Within this flow zone, the axial velocity is transformed to a radial velocity. The exact solution to the Navier-Stokes equation was found by Schlichting.¹¹¹. The stagnation zone is, in effect, a region in which a static boundary layer develops, the thickness of which is dependent on the prevailing flow conditions. The transition point between the stagnation region and the wall jet has been calculated by Dawson¹¹⁴. to be $r/d' = 4$. However, as will be seen below, this value depends on the value of H/d .

6.1.3 Flow within the wall jet.

The wall jet region has been extensively studied^{3,115, 116} as it is observed in other flow situations. The equivalent of wall jets can be found in laminar flow in pipes, channel flow and flow across a plate. At the edge of the stagnation region, flow accelerates rapidly in the radial direction in the form of a thin layer. As the fluid spreads, a boundary layer develops adjacent to the surface. The flow adopts a Blasius type flat plate profile*. The boundary layer increases in thickness with radial position. Outside this boundary layer, flow is uniform and unaffected by viscous stresses.

In an un-submerged jet, there comes a point, dependent on the original axial velocity, at which the thickness of the boundary layer approaches the total thickness of the wall jet. This is known as the transition region. The whole flow is subsequently subject to viscous forces and can be described using a similarity solution². Due to the viscous effects from the plate, the bulk velocity gradually becomes retarded. When the thrust of the pressure of the flow is equal to the rate at which momentum is destroyed, a hydraulic jump occurs in order to conserve momentum. In effect, a standing wave is created. Flow beyond the jump region then continues undisturbed.

6.2 MASS TRANSFER CHARACTERISTICS OF IMPINGING JETS

Mass transfer characteristics have been developed by both mathematical modelling and tested by experiment. Both submerged and un-submerged systems have been evaluated. Much work has been carried out using the analogous system of heat transfer. Whilst the general behaviour of submerged jets are very different from that of non-submerged systems, under certain conditions, behaviour within the impingement region is very similar. Therefore, some of the characteristics of the submerged system will be reviewed.

6.2.1 Mass transfer in submerged jets.

Mass transfer and heat transfer are analogous in their behaviour. As such, work carried out using heat transfer models and experiments are applicable to mass transfer. Work undertaken by Gardon and Akfirat¹¹⁶ measuring heat transfer with air jets has shown that at large nozzle to surface distances, the heat transfer decreased in a monotonic manner from the stagnation point. However, at small H/d , a local maximum in heat transfer was observed at $d'/d = 0.5$.

*The Blasius flat plate boundary layer profile is found in a number of hydrodynamic situations. In particular, when flow accelerates along a flat plate, a boundary layer develops, commencing at the start of the plate and increases with distance along the plate. The thickness that the layer attains is a function of the flow rate, the viscosity and the friction induced by the wall. Nakoryakov² has described the analysis of mass transfer in this region.

Mass transfer in a submerged jet system was also shown to be highly dependent on the distance between the nozzle and the impingement surface. Giralt¹¹⁷ and Scholtz¹¹⁸ have explained that with large nozzle to surface distances ie $H/d \geq 8.0$, the flow in the free jet has a fully developed bell-shaped profile. As a consequence of this, the acceleration of the wall jet commences at the stagnation point and mass transfer is greatest at the stagnation point. At smaller values of H/d , the jet still retains much of the flow characteristics of the nozzle. Providing the flow within the nozzle is uniform to begin with, then this profile is retained. Consequently, the acceleration of radial flow commences at a position corresponding with $d'/d = 0.5$. This is the position at which the boundary layer is thinnest and the mass transfer highest. In between these values of H/d , the mass transfer is relatively constant. Other experiments and theoretical calculations using controlled flow conditions¹¹⁹ have shown that with uniform flow distribution, the position corresponding to $d'/d = 0.5$ exhibits the greatest mass transfer. With a parabolic flow profile, this position corresponds to $d'/d = 0.1$.¹¹⁸ Mass transfer within the impingement region has been studied by Chin and Tsang.¹⁰⁵ Using disc electrodes of various radii, they measured the mass transfer using the limiting current method. They found that the average limiting current density remained constant up to $d'/d = 0.5$ for laminar jet flow. However, under conditions of turbulent flow, this value increased to 1.0. These phenomenon may be explained in terms of fluid acceleration. The fluid velocity of the wall jet along the substrate may be derived from inviscid theory¹ as

$$\begin{aligned}
 U_x &= 1.161 \frac{d'}{r} \quad \text{for } H/d = 0.25 \quad \text{for non-uniform flow} \\
 U_x &= 0.4516 \frac{d'}{r} \quad \text{for } H/d = 1.0 \quad \text{for uniform flow}
 \end{aligned} \tag{13}$$

The acceleration with increasing distance from the stagnation point for a non-uniform jet is twice that of the uniform jet. With a reduction in H/d , the passage of the fluid is restricted, leading to an enhanced pressure differential between the stagnation point and ambient. Consequently, the fluid acceleration is increased leading to a maximum outside the stagnation point. At intermediate values of H/d , no maxima are observed. It may be concluded, therefore, that the mass transfer characteristics of the system are dependant on the impinging fluid profile, which depends on the value of H/d . However, under conditions of turbulent flow, uniform mass transfer may be observed up to 1 nozzle diameter providing H/d is not too great or too small.

6.2.2 Mass transfer in the non-submerged jet

Mass transfer data is generally presented in the form of the Chilton-Colburn analogy, originally developed for heat transfer studies. The general form for the equation is given by

$$Sh_x = Re_x Sc^{1/3} (C_f/2) \quad (14)$$

Chin and Hsueh¹²⁰ used this equation to derive a form that is applicable to the non-submerged impinging jet geometry. Local friction coefficients were obtained from the work by Nakoryakov *et al.*

(i) in the impingement region

$$C_f = 0.662 \nu^{1/2} U^{3/2} x / U_x^2 (d/2)^{3/2} \quad (15)$$

(ii) in the boundary layer and wall jet regime

$$C_f = 0.579 \nu^{1/2} U^{3/2} x / U_x^2 (d/2)^{1/2} \quad (16)$$

Additionally, it has been shown that the radial velocity component have the following forms

(i) in the impingement region¹¹¹.

$$U_x = gd' \quad (17)$$

(ii) in the boundary layer region¹²⁰.

$$U_x = U \quad (18)$$

By substituting equations (15) (16) (17) and (18) into the Chilton-Colburn equation and averaging the local mass transfer coefficients over the electrode surface, a set of correlations for the average Sherwood number can be calculated as

(i) for the impingement region

$$Sh = (0.936/\alpha^*) Re^{1/2} Sc^{1/3} \quad (19)$$

(ii) for the boundary layer region

$$Sh = 0.767 Re^{1/2} Sc^{1/3} (r'/d)^{-1/2} \quad (20)$$

The parameter α^* is a dimensionless hydrodynamic constant defined as ad/U , which is a function of the dimensionless nozzle height, H/d .

Most mass transfer characteristics are defined by such an equation as that derived above and take the general form of

$$Sh = a Re^b Sc^c f(H/d) \quad (21)$$

The derivation of this equation can be found in the excellent Chapter by Ibl and Dossenbach¹²³. The value for c is generally accepted to be $1/3$. The mass transfer characteristics are different for the impingement region compared to the wall jet region. For the former, it has been found by Giralt and Scholtz that the value of b is 0.5 for the submerged jet. The value of a is dependent on the velocity profile and the degree of turbulence but is generally between 0.5 and 1 . For the wall jet, b has been determined as 0.75 and is inversely proportional to the radial distance, d' . The functional relationship between the mass transfer coefficient and the nozzle to substrate distance is generally expressed as a power relationship

$$f(H/d) = (H/d)^{-e'} \quad (22)$$

Values for e' vary. Chin and Tsang found a value of -0.054 and -0.057 for the submerged laminar and turbulent jet flow respectively. However, in a later study, Chin and Hsueh found that for $0.5 < H/d < 5.0$, a value of -0.09 was appropriate.

The basic mathematical model for the non-submerged jet has been determined by Alkire and Chen as applicable to electrodeposition systems. They modelled the current and potential distribution along a cathode surface in a high speed jet plating cell. The model was based on the limiting current measurement of mass transfer using the reduction of ferricyanide in an alkaline solution. They went on to study copper deposition from an acid sulphate electrolyte both with and without a ferric/ferrous redox couple added. The reader is referred to this reference for a detailed description of the derivation of the model. They found that in the impingement region, correlated in dimensionless form, gave the following relationship over the range $3000 < Re < 60000$

$$Sh = 21.03 Re^{0.448} \quad (23)$$

This, they claimed, agreed to within 10% of a semi-empirical correlation derived by Chin and Tsang for a turbulent submerged jet. In this work the H/d was maintained at a value of 2.0. This ensured that the mass transfer characteristics in the impingement region were essentially the same as for a submerged jet. For the wall jet region, they found the following relationship

$$Sh_x = 0.572 Re_x^{0.5} Sc^{0.33} \quad (24)$$

Nakoryakov *et al* also derived a relationship for the wall jet based on theoretical predictions of

$$Sh = 0.59 Re^{0.5} Sc^{0.33} \quad (25)$$

after converting to the Sherwood number dimensionless notation.

Alkire and Chen, based on both their theoretical and experimental studies, went on to establish certain behavioural properties of the jet system. From their experiments using the redox system, they established to within 15% of theoretical calculations the following;

1. Low currents led to high selectivity but a low plating rate whilst high currents give high plating rates but low selectivity. Here selectivity is defined as

$$S = \frac{\text{metal deposition in impingement region}}{\text{total metal deposition rate}}$$

They claimed that the reason for this was that at low currents, the behaviour was controlled by potential distribution and that as the impingement region was closest to the anode, the reaction in the impingement region was favoured. At high currents, the limiting current was achieved and the system was controlled by mass transport.

2. The electrolyte conductivity influenced the behaviour. Electrolytes with a reduced conductivity led to an improved selectivity at low applied currents but at high currents had no influence.
3. Increasing the reactant concentration led to a significant increase in selectivity at large currents as the system was mass transport limited in the impingement region but not in the wall jet. At lower currents, the system was dominated by charge transfer and ohmic resistance effects. Increasing the concentration led to an increased exchange current density, causing a reduction in charge transfer resistance compared to the ohmic resistance and thus moderately improved selectivity.
4. Increasing the jet velocity improved the selectivity at large currents because the impingement region operated at a higher fraction of the limiting current than the rest of the surface. Increases in the rate of agitation thus favours reactions in the impingement region and enhances selectivity. However, at low currents, as the kinetic and ohmic parameters controlled the behaviour, no change in the selectivity was observed.

Whilst they found good agreement between the experimental results and the theoretical calculations, errors were found under conditions that gave high selectivities ie high flow rates, high reactant concentrations and low conductivity. They put this down to errors in the one dimensional simplification they used for the theoretical calculations and had underestimated the reaction rates. These errors predicted a higher selectivity than were actually observed.

In the case of copper deposition from the acid sulphate electrolyte, the calculations included a factor to take into account hydrogen evolution that occurred at high current densities. In this case, the selectivity behaviour was quite different. Not enough data was given for the copper system to enable as complete an analysis as for the ferricyanide but essentially, low applied currents exhibited poor selectivity which increased with increasing applied current eventually levelling to a constant

value. The reason for this was believed to be the difference in the exchange current densities of the two systems. During their studies, a dimensionless notation was derived to assist in the mathematical modeling of the system including a term ξ . This was defined as

$$\xi = \frac{rFa_r d^2 i_0}{\kappa RT} \quad (26)$$

where a_r is the specific surface area and is a volume component of the electrolyte involved in the reaction. Its derivation is given in reference (1) but is not important to this discussion. The important aspect is the inclusion of the ratio of exchange current density to the conductivity i_0/κ . This played an important role in the selectivity achieved. This ratio could be interpreted as a ratio of ohmic potential losses to charge transfer overpotential. If this value was greater than unity, the current distribution would be highly non-uniform and thus selectivity would be high. By way of illustration, three values of ξ were plotted as selectivity vs total applied current for high rates of flow. These values were 10^{-4} , 10^{-1} and 10^1 . Of these, the intermediate value exhibited the poorest selectivity. At low currents, a large value of ξ corresponded to ohmic control so that selectivity would be expected to be high due to non uniform current and potential distributions. Very small values of ξ correspond to charge transfer control and thus a more uniform potential distribution. However, the charge transfer overpotential must be very high in order to support the required current. Due to the exponential nature of the kinetic rate relationship (Butler-Volmer equation) modest potential variations can generate highly non-uniform current distributions. Therefore, for low currents, selectivity passes through a minimum as ξ is increased. For high currents, selectivity depends on mass transfer and is thus insensitive to variations in ξ .

Another term defined was Γ . This dimensionless term comprised

$$\Gamma = \frac{n^2 F^2 k c^b a_r d^2}{\kappa RT} \quad (27)$$

This term included the ratio kc/κ and could be interpreted as the ratio of mass transfer overpotential to ohmic potential. Such a term could be viewed as a dimensionless limiting current. If Γ had a value much greater than unity, then very high deposition rates could be achieved. The mathematical model predicted that very high deposition rates with good selectivity could be achieved if both Γ and ξ had values greater than 10.

In the case of copper deposition with a redox couple, the chosen system was more noble than the copper reduction. Therefore, at low current densities, the reduction of ferric to ferrous predominated. The current efficiency for copper deposition therefore increased with increasing current density. Thus, the current efficiency was highest in the impingement region. This led to a situation in which the selectivity was low at low currents increasing to a maximum with increasing applied current. At very high applied currents, the selectivity reduced as copper was deposited outside the impingement region. It was found that by using the redox couple, the maximum selectivity was increased twofold.

CHAPTER 7 EXPERIMENTAL STUDIES OF HIGH SPEED SELECTIVE JET ELECTRODEPOSITION

The following chapters describe the experimental work carried out to evaluate the properties of electrodeposits produced by the non-submerged jet plating method. As this technique would be of particular value within the electronics industry, the bulk of the studies concentrated on gold and gold/nickel alloys. However, some studies were carried out on copper and this is mentioned where applicable in order to support, or otherwise, findings from the gold deposition work.

7.1. EQUIPMENT USED IN THIS STUDY.

For the purposes of relating the deposition conditions to the deposits produced, a large number of deposit spots were produced over a wide range of current densities and flow conditions. To produce these, it was necessary to devise a step and repeat system that was able to move the nozzle relative to the substrate and switch the plating current on and off for the appropriate times. In addition, to demonstrate the applicability of the process for the purposes of selective plating, the equipment was required to move the nozzle at a desired speed whilst depositing the metal. It was decided that these requirements could best be provided by a motion control system managed by a microcomputer. Additional equipment was added to this for specific requirements during the course of the experimentation.

7.1.1. Computer controlled X-Y drive system

Figure 10 shows a schematic diagram of the computer controlled X-Y system designed for this study. Photograph 1 shows a photograph of the system, with the X-Y Table in place within a fume cupboard. This was necessary for safety reasons as some fine electrolyte spray was produced. An enclosed nozzle/substrate container was considered but this would have restricted access and observation during operation. However, a spray shield (not shown in the photograph) was included to collect any backspray that occurred. The individual components of the system are described below.

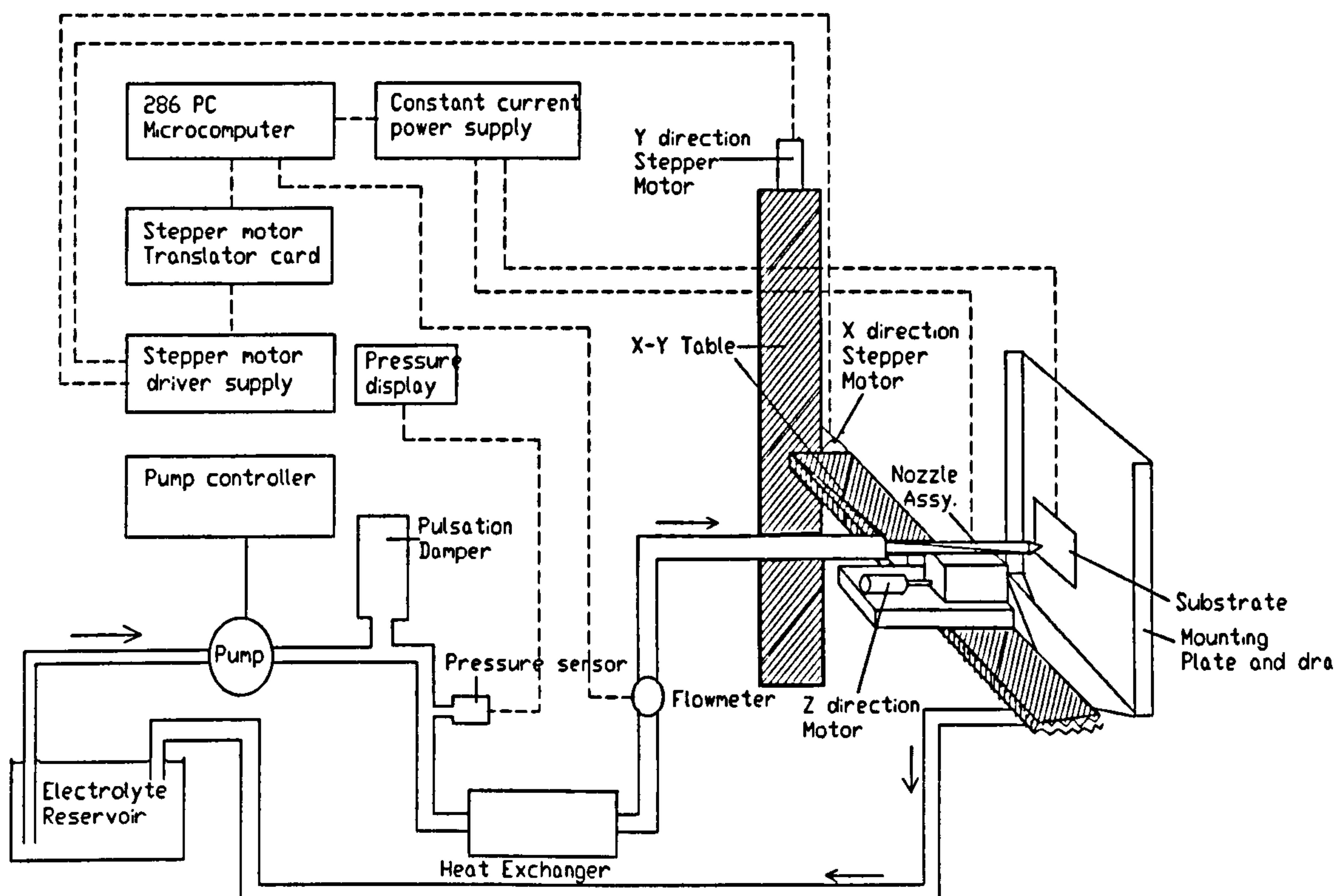


Figure 10. A schematic diagram of the computer controlled jet plating system.

7.1.1.1 The nozzle and substrate mount.

The nozzle used for the majority of the experiments consisted of a 2 cm long by 0.4 mm diameter platinum tube sealed into a 0.3 mm, high lead content soda glass tube. About 0.5 cm of the platinum tube was sealed into the glass. The exposed end was strengthened by casting an epoxy resin block around it and the end of the glass tube. After setting, the end of the strengthened tip was chamfered, ground and then polished. The internal diameter of the platinum tube was then checked for ovality and size using a microscope.

The nozzle assembly was then mounted onto a support block on the X-Y table. The support block was provided with a motorised Z direction control that allowed the nozzle to substrate distance to be adjusted.

The substrate was mounted on a perspex plate by means of point contact stainless steel spring clips. These also provided the electrical connection for the plating current. The plate was fixed onto a perspex housing that collected the electrolyte run-off and returned it to the reservoir.

7.1.1.2 The pump system.

The electrolyte was pumped through the nozzle using a Wallace and Tiernan diaphragm dosing pump, Model No. G 50V. It was capable of providing up to 70 L hour⁻¹ at pressures of up to 0.7 MPa continuous flow and 0.9 MPa maximum flow. The pump was provided with two control mechanisms, one being electronic and the other a mechanical handwheel controller. The flow could be controlled to within $\pm 2\%$ of the desired rate by means of these controllers. Diaphragm pumps produce a pulsed flow and therefore a pulsation damper was fitted. This was supplied by Flowguard and the chamber pressure was maintained at 0.44 MPa by an external nitrogen supply. At this pressure, flow pulsations were eliminated over the electrolyte pressure ranges used during the experimentation. A pressure relief valve was fitted and set to divert the flow at pressures exceeding 0.84 MPa.

An electronic pressure transducer model BT2025G1A, supplied by Sensortechncs was fitted downstream of the pulsation damper to monitor system pressure. The output was calibrated in terms of the electrolyte flow and provided a means of continuously monitoring the flow rate.

The electrolyte was passed through a heat exchanger placed upstream from the nozzle assembly. This consisted of a Quickfit glass condenser with a spiral internal tube. The outer jacket was supplied with hot water from a separate reservoir delivered by a peristaltic pump. The electrolyte temperature was monitored on emerging from the nozzle by a fine thermocouple wire placed 3 cm past the impingement point on the substrate mounting plate. Adjustment of the hot water flow provided suitable temperature control.

Immediately upstream from the nozzle, a Titan Enterprises flowmeter, model No.103 was fitted to give a direct measurement of the flow as a back-up to the pressure transducer. The computer provided the measurement output for this meter.

As each electrolyte used in this study had a different viscosity, it was necessary to calibrate the flow measuring devices for each one. This was carried out by measuring the volume of discharge over a range of pump settings and producing a calibration curve. The computer output from the flowmeter was then compensated for any differences, as was the output from the pressure transducer.

7.1.1.3 The X-Y Table

The X-Y table was custom built by Time and Motion. It consisted of a double screw vertical slide carrier to which was fitted a single screw horizontal slide carrier. Fixed onto the horizontal carrier was a mounting plate where the nozzle assembly was fitted. The unit was equipped with a

pair of home proximity sensors and end of travel cut-off switches. X and Y motion was provided by stepper motors. The unit was capable of $2.5\ \mu\text{m}/\text{step}$ and a repeatability of $\pm 2.5\ \mu\text{m}$ in half step mode.

7.1.1.4 Motion control system.

The stepper motors were controlled via the computer. Fitted to the computer was a PCL 738 stepper motor translator card. This converted motion information from the host computer to suitable signals for the stepper motor driver unit. This driver unit was built "in-house" based on the SGS-Thompson 296 and 298 stepper motor driver chips. A 40 volt, 4 Amp power supply powered the stepper motors via the driver. The driver was operated in half step mode to obtain the motion resolution described above. The nozzle could be moved either from the control program or directly from the computer keyboard.

7.1.1.5 The plating current power supply.

The plating current supply was designed and built in house. It was a constant current system which was capable of supplying up to 100 mA at voltages of up to 60 volts with a resolution of 0.01 mA. A constant current was generated by means of an operational amplifier controlling the magnitude of current supplied from a power transistor by means of an adjustable reference voltage. This reference voltage could be supplied either from the computer or by means of internal circuitry controlled by a potentiometer. The current could therefore be set either manually or automatically via the computer. When used in manual mode, a short circuit switch was used so that the appropriate current could be pre-set prior to deposition. It was also capable of supplying pulsed currents upwards of 0.01 msecs. duration from signals provided by an external pulse generator. This mode was used for all the pulse plating experiments. A schematic diagram of the pulse plating modification is shown in Figure 11. The reference voltage for the power supply was delivered by a pulse generator. The total plating period was controlled by triggering the pulse generator from the computer for the appropriate time. The applied current was measured via the voltage drop across a 1.0 K resistor in series with the cathodic supply by means of one channel of a storage oscilloscope. The magnitude of the peak pulse current could be set prior to plating by short circuiting the output and setting the current pulse via a DC input.

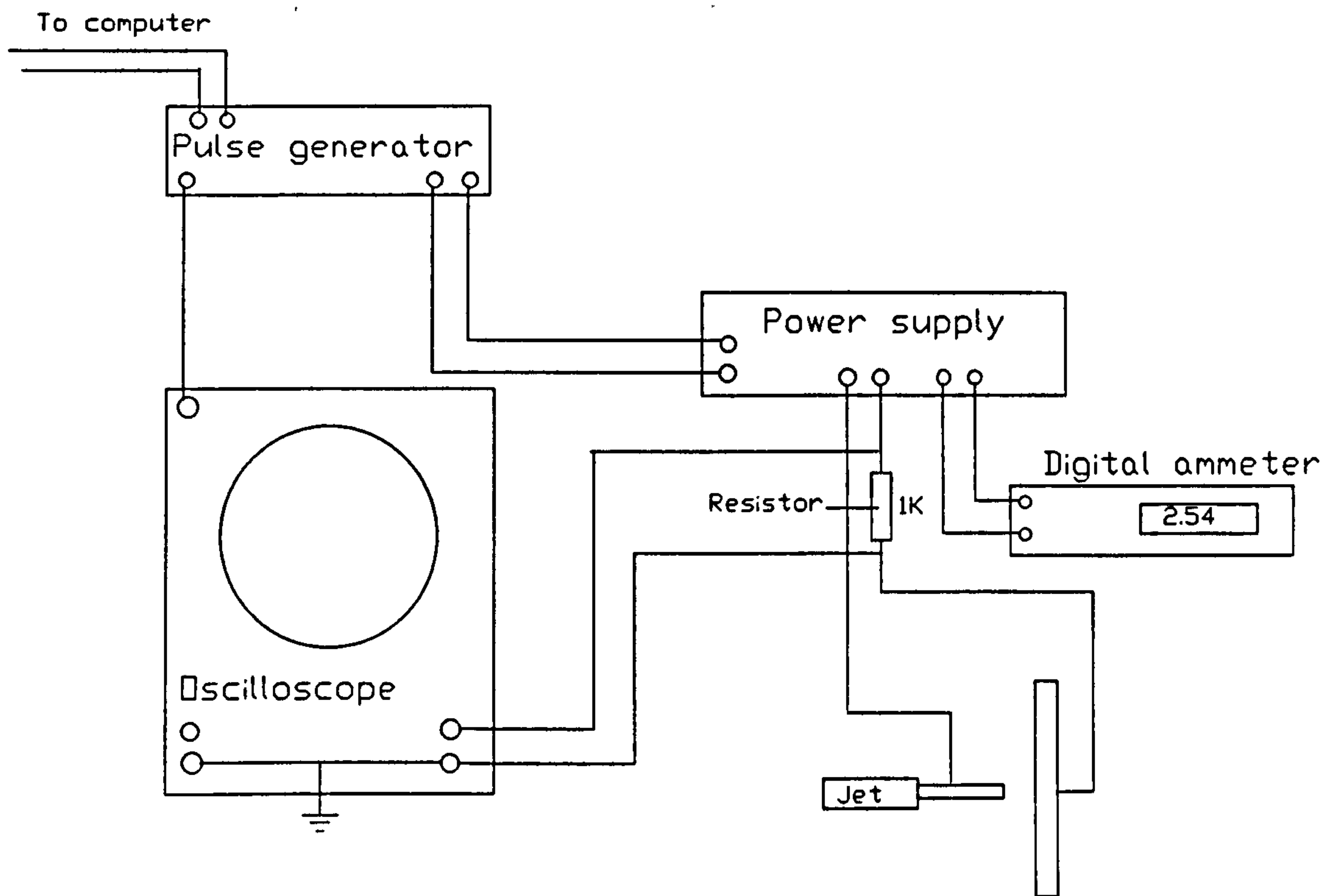


Figure 11. The modification to the power supply to enable pulsed current electrodeposition.

7.1.1.6 The computer and control program

The computer used was an IBM compatible 286 processor based system. The program used to control the jet plating unit was written "in house". It was designed with the following capabilities.

- 1) A Computer aided design (CAD) user interface that allowed the computer to be programmed to move the nozzle to appropriate places on the substrate and produce deposit spots of the required current and duration on a step and repeat basis. This interface could also be used to program the computer to move the nozzle on a continuous basis, allowing the jet to "directly write" the electrodeposit. Figure 12 shows such a design as it appeared on-screen
- 2) It allowed the currents and times of deposition to be set automatically.
- 3) It measured the flow rate of the electrolyte.
- 4) It allowed the importing and conversion of Hewlet Packard Graphics Language (HPGL) plotter files produced by other CAD packages to be used to drive the nozzle.

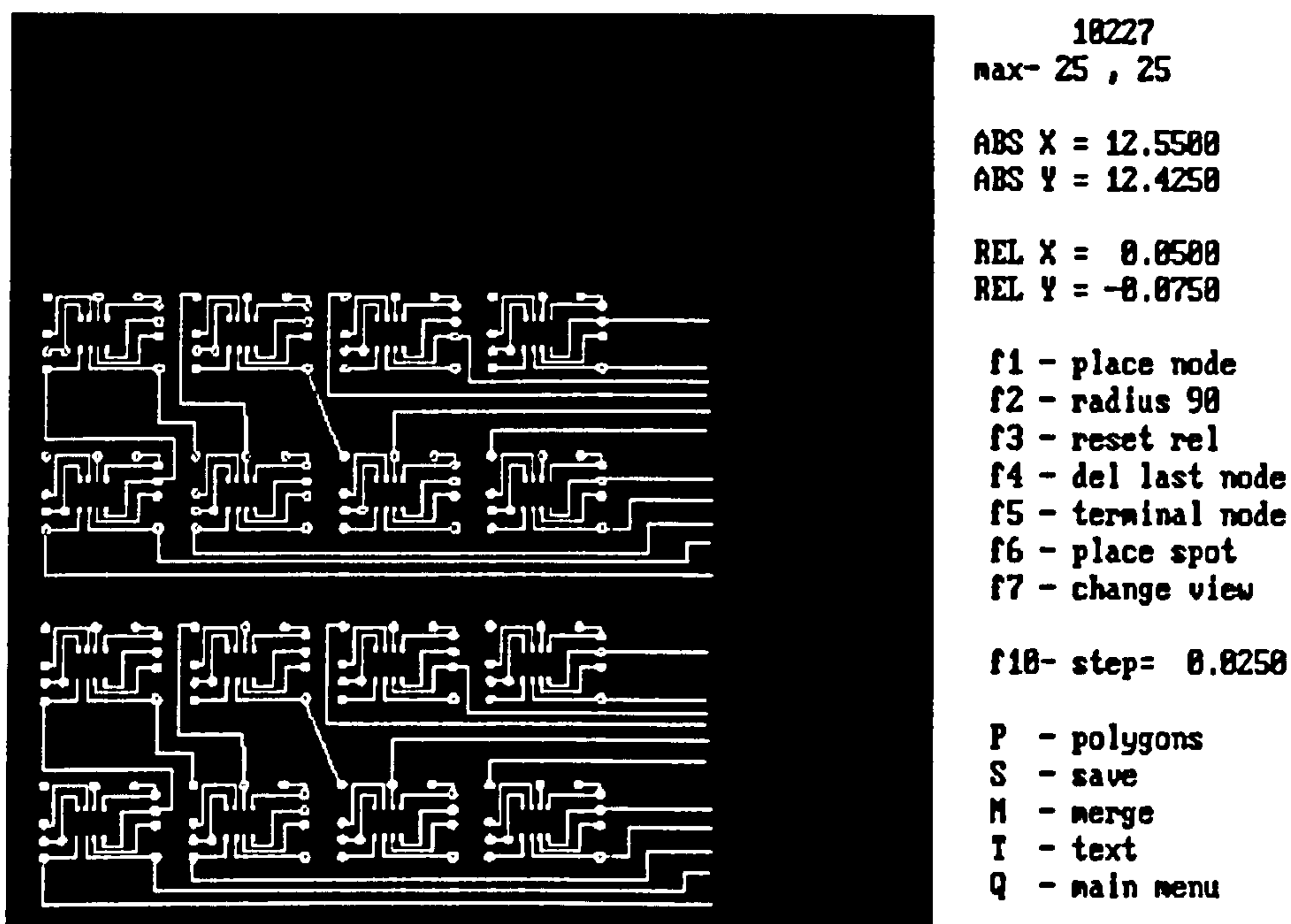


Figure 12. The computer "user interface" showing the CAD design screen.

7.1.2 Additional equipment

In order to carry out fundamental studies to establish mass transfer characteristics of the jetting system, it was necessary to establish the relationship between overpotential and current density. This required additional equipment in differing configurations. This will be described in Section 7.4.

7.2 EQUIPMENT AND METHODS USED FOR DEPOSIT EVALUATION

The deposits produced were evaluated for a variety of characteristics. The following techniques were used for these evaluations.

7.2.1 Deposit Morphology

All of the deposits produced were examined using an optical microscope. In addition, many were examined using either a Cambridge S350 or a Cambridge S150 Scanning Electron Microscope (SEM). Optical micrographs were prepared using an offset light source to create a slight shadow around surface features, thus highlighting them.

7.2.2 Deposit thickness

Deposit thickness was measured using either a Sloan Dektak II or a Sloan Dektak 3030 surface profilometer. A 5 μm stylus was used for all measurements. As the deposits were found to have a gaussian profile, the maximum thickness of the deposit at the centre of the spot was recorded. In addition, surface profiles were constructed by taking measurements at 100 μm intervals from the centre of the spot to the apparent point of extinction of the deposit profile. The reproducibility of measurement was obtained by taking 12 measurements of the same spot and obtaining the standard deviation of the average measured value. The thickness measurements obtained by this method were occasionally checked against a microsection through the centre of the spot to confirm accuracy.

7.2.3 Deposit structure

The internal structure of some of the deposits was evaluated using both standard metallographic microsection methods as well as by X-ray diffraction. Microsections were made from deposits produced on metal substrates. The substrate, with up to 6 spots in a row, were first overplated with about 20 μm of silver as a backing coating. These were then mounted in a clear acrylic resin and ground until the deposit spots were exposed. They were then polished until the centre of each of the spots was reached. The gold was then etched for 10 -15 seconds using Imastrip*, gold stripping solution at room temperature to reveal the crystallite and grain structure.

Glass substrates, 1.5 X 1.5 cm, metallised using sputtered coatings of chromium followed by gold (400 Å and 1000 Å respectively) were used to prepare samples for XRD examination. Samples of HSSJE gold alloy deposits for XRD examination were prepared over a current density range of between 3.0 and 16.0 A cm⁻² with differing quantities of nickel and/or addition agent (booster) in the deposit. In the case of HSSJE pure gold, samples were produced over a current density range of between 1.0 and 8.0 A cm⁻². The samples consisted of an array of 25 identically produced spots plated onto the substrates. Prior to XRD examination, the chromium/gold layers not covered by the deposited spots were stripped. The gold was removed using Imastrip followed by 20% hydrochloric acid to remove the chromium. As the metallised layers were extremely thin, the stripping operation left the HSSJE spots virtually unaffected. The centre-line thickness of the spots in the array was maintained above 15.0 μm and confirmed by measurement using a Dektak Surface Profilometer after the XRD examination had taken place.

*Imastrip, supplied by Enthone-OMI (UK)

For comparison, a series of control samples were prepared for XRD examination by conventional vat deposition methods. One set were produced from a Ronovel N electrolyte containing 1.7 g l⁻¹ nickel over the current density range 3.0 - 40 mA cm⁻². A further set of samples were produced over the same current density range from an Auronal MRN bath also containing 1.7 g l⁻¹ nickel, which is identical to the Ronovel N but contains no booster. These samples were used to study the influence of the booster. Pure gold samples were produced from a typical acid citrate electrolyte containing 0.06M gold, over a current density range of 1.0 to 20 mA cm⁻². These deposits covered the same total surface area of the substrate as that covered by the jet plated spot array.

The X-ray diffraction data was acquired using an Siemens D5000 X-ray Powder Diffractometer (Bragg-Brentano geometry) equipped with a diffracted beam monochromator ((CuK α)). Measurements of diffracted intensity were carried out over the 2 θ range 30° to 90°. Corrections to the angular positions and breadth of the diffraction peaks derived from the samples, required to compensate for various instrumental and physical effects were applied. To determine these corrections, each sample was dusted with a fine layer of powdered silicon (@ 1 μ m in size). The positions and Full Widths at Half Maximum (FWHM) intensity of the silicon peaks which bracketed those from the gold were used to calculate the appropriate corrections to position and width. Using the precisely known lattice parameter of silicon it was possible to interpolate a correction to the position of the gold peaks and thus calculate an accurate value for the lattice parameter for each line. The correction for line broadening was made by assuming Gaussian models for the observed profiles, instrumental and corrected diffraction profiles.

Data was derived from an analysis of the position, intensity and FWHM of the first five diffraction peaks recorded from the gold deposits. In the Bragg - Brentano geometry, the diffraction pattern originates only from those crystallographic planes which are essentially parallel to the surface of the sample. The 111, 200, 220 and 311 reflections are therefore derived from quite separate and distinct crystallites within the deposit. Only the 111 and 222 reflections are derived from the same crystallites. Considerable care therefore needs to be exercised in interpreting data from samples which do not exhibit a true crystallographic random orientation.

Lattice parameters were calculated from the angular positions of the first five lines (111, 200, 220, 311 and 222) in the diffraction pattern from each of the samples.

For the purposes of this Thesis, crystallite size will be defined as a single, coherent diffracting region. This is not always the same as the true crystallite size, D_{true} , as will be explained below, but is used for convenience. The full width at half maximum intensity of the K α_1 line corrected for instrumental broadening was used to calculate the crystallite size using the Scherrer equation.

$$B = \frac{(0.9\lambda)}{(t \cos \theta)} \quad (28)$$

where B = the broadening of the diffraction line measured at its half width maximum intensity (radians), t = diameter of the crystal particle λ = radiation wavelength and θ = angular position in degrees.

It was noted that the crystallite size values calculated from the broadening of the 111 reflections using the Scherrer equation were significantly greater than the values derived from the 222 reflections. The crystallite sizes calculated for the two planes should be the same; that they are not, suggests that the Scherrer model employed, which attributes all the intrinsic line broadening to crystallite size effects, is an over-simplification. On the basis of this information, samples were selected for a more detailed analysis in order to separate the contribution to the observed line broadening from crystallite size and strain (RMS) effects. This was undertaken using the method of Warren and Averbach.¹²¹ The successful application of this type of analysis requires as many unique orders of reflection as possible. However, for an FCC metal examined using copper radiation, the number of accessible reflections with multiple orders is just 2, the 111 (222) and the 200 (400). In this study, line overlap problems combined with low peak intensities ruled out the use of the h00 reflections so that only the 111 and the 222 peaks were used for the analysis.

In order to accomplish the analysis, a better defined instrumental line broadening standard was required. This was achieved by producing a pure gold powder and annealing it to the point where no further improvement in the resolution of the $k\alpha_1$ and $k\alpha_2$ lines could be achieved. It is particularly difficult to obtain a suitable gold powder commercially and anneal it in this way due to its tendency for grain growth and sintering. Therefore, a powder was specifically produced*. The observed diffraction lines were corrected for instrumental broadening by dividing the Fourier Transform of the diffraction lines derived from the sample by the Fourier Transform of the appropriate line from

*A 50 g l⁻¹ solution of gold chloride was produced by dissolving pure gold powder in aqua-regia and evaporating to near dryness. Concentrated hydrochloric acid was added and re-evaporated until all oxides of nitrogen were removed. The solution was then adjusted to the correct concentration using de-ionised water. It was necessary to produce gold grains with a size in the region of 10 μ m with a well ordered structure. This meant they had to be nucleated and grown very slowly. It had been shown that such a structure could be achieved by reducing the gold chloride using acetone at room temperature. A 100 ml sample of the gold chloride was placed on a magnetic stirrer at a temperature of 35°C and 30 ml of acetone was added. Stirring was continued for a period of 5 hours after which the sample was cooled to ambient and allowed to stand for a period 3 days. At the end of this period, a layer of gold powder was seen at the bottom of the beaker that had merged to form a thin film. A piece of this film was cleaned in de-ionised water and mounted on a glass slide so that the X-ray diffraction pattern from the film could be recorded. The resolution of the $k\alpha$ doublet was determined for the first five lines in the X-ray diffraction pattern from the film. The film was then subjected to a number of annealing operations at 350°C until no further improvement resolution of the doublets was obtained. The total time of annealing to obtain this condition was 5 hours.

the standard as described by Stokes.¹²² It was found necessary to subtract the signal derived from the blank glass substrates from that of the samples prior to calculating the transform, in order to obtain a level base line required for an accurate analysis.

The full application of this analysis yields the mean column length ($n_0 a_3$) and its distribution and the RMS strain and its distribution. The apparent cell size is a_3 and n_0 , the number of cells in the average column length, is determined by a linear extrapolation of the real part of the Fourier Transform of the (000) reflection.

The cell size (a_3) is determined by the angular range over which the diffraction profile is analysed and is given by:-

$$l - 1/2 = (2a_3/\lambda) \sin \theta_1 \quad (29)$$

$$l = (2a_3/\lambda) \sin \theta_0 \quad (30)$$

$$l + 1/2 = (2a_3/\lambda) \sin \theta_2 \quad (31)$$

where θ_1 and θ_2 are the start and end of the diffraction profile, θ_0 is the position of the peak, λ is the wavelength of the radiation employed and l is a reflection order as in hkl . In order to simplify the subsequent calculations, it is convenient to choose scan ranges so that a_3 is the same for all reflections used in the analysis. In this study, a cell size of $2.4 \times d_{111}$ was used.

Close and careful examination of the diffraction patterns from these samples showed both the 111 and 222 diffraction peaks overlapped with their nearest neighbours, the 200 and 311 peaks respectively. This was also true for the specially prepared reference gold sample used to determine instrumental broadening. In the present study, data was collected over an angular range of $\pm 10^\circ$, centred about the 111/200 and 311/222 lines.

In order to obtain adequate representation of the diffraction profiles in the "tails" of the peaks (where most of the crystallite size and strain information is contained) a variety of mathematical functions were fitted to the experimental data and the parameters for the best fits used to calculate model diffraction profiles. Pearson 7, Split Pearson 7 and three different pseudo Voigt (mixed Cauchy and Gaussian) type functions were employed in the modelling.

The modelled 111 and 222 diffraction profiles were calculated at 1024 data points over an angular range of 16 and 20° respectively. Fourier transforms were calculated using an FFT routine. The instrumental contribution to the diffraction data was removed by dividing the FT of the samples by the FT derived from the precipitated and annealed gold powder described above. The Fourier coefficients of the 000 reflection were calculated using the extrapolation procedures described by Warren and Averbach.¹²¹ This method enables the individual contributions of crystallite size and strain to line broadening to be evaluated. The contribution to broadening from crystallite size (column length) is independent of the order of reflection whilst that from strain is dependent on the order of reflection. Because of this, the two contributions may be resolved. The mean crystallite sizes were calculated by extrapolating the linear region of the real part of the 000 transform to obtain n_0 . The mean column lengths (crystallite size) and RMS strains are listed in Table 23.

In addition to crystallite size and RMS strain, layer sequence faults on the 111 plane may also contribute to line broadening. The contribution of stacking and twin faults to line broadening may be identified once the strain and size contributions have been established. The effective crystallite size, D_{eff} comprises for the (111) plane

$$\frac{1}{D_{eff}} = \frac{1}{D_{true}} + \left(\frac{1.5\alpha + \beta'}{\alpha'} \right) \frac{\sqrt{3}}{4} \quad (32)$$

where D_{true} is the true crystallite size, α is the stacking fault probability, β is the twin fault probability and α' is the lattice parameter. The stacking fault probability may be established by measuring any relative shift between the 111 and the 200 peaks. The probability may then be calculated. Twin fault probabilities may be calculated from any asymmetry of the diffraction peaks that have been reconstructed from the inverse Fourier transform produced during the Warren and Averbach analysis. However, it was not possible to accurately calculate the twin fault probabilities because the deposit was highly oriented in the 111 direction. Twin fault probabilities are usually calculated for the 100 (200) reflections. Due to the high degree of texture, the 200 signal was very weak and could not be used for the analysis. Table 23 also includes the stacking fault probabilities where these were significant.

Metallurgical Microsection was carried out on a number of samples in order to observe any resolvable micro-structures.

7.2.4 Deposit hardness

Where required, the deposit hardness was measured using a Matsuzawa Model DMH-2 fitted with a Vickers diamond indenter. The indenter was applied normal to the surface. It was established that using a 25 g mass on the indenter and a deposit thickness of at least 16 μm , the influence of the substrate was eliminated. For each set of conditions, 12 deposit spots were produced. A single hardness measurement was carried out at the centre of each spot and the results of the 12 measurements were averaged.

7.2.5 Chemical analysis.

Chemical analysis was primarily required for the establishing the nickel content of gold alloy deposits as well as maintaining the electrolytes at the required gold ion concentration. The nickel in solution was analysed by X-ray Fluorescence Spectroscopy (XRF), as was the gold. The nickel in the deposit was analysed by XRF calibrated using samples additionally analysed by Atomic Adsorbtion Spectroscopy (AA). Further details are given in 7.3.2.3

7.2.6 Types of substrate used.

During the early stages of this work, gold flashed, nickel plated copper strips 1 cm by 5 cm were used as cathodes. The strips were polished to a 6 μm diamond finish, cleaned and then plated with 10 - 15 μm of bright nickel. They were then given a gold flash of about 0.2 μm to prevent any immersion deposits forming by chemical replacement from the gold electrolytes. However, these proved to be unsuitable for two reasons. Firstly, it appeared that there was some variability in the substrate that led to variations in growth habit of the jet deposits under the same conditions. Whilst this was small, it was an undesirable property of the substrate. Secondly, the substrates were not sufficiently flat to allow accurate measurements of the thickness and width of the spots, particularly at low thicknesses. It was therefore decided that glass substrates, sputtered with 40 nm of chromium followed by 100 nm of gold would be used. The advantages of using this substrate were the improved flatness and the fact that thin sputtered gold layers tend to adopt a (111) preferred orientation and thus provide a more consistent crystallographic surface than the metal substrates.

For the analysis of nickel in gold, OFHC copper discs plated with 0.4 μm of pure gold were used.

7.3 METHODS USED FOR THE PRODUCTION OF EVALUATION SAMPLES.

The purpose of this work was to identify and optimise the conditions under which high quality gold and gold alloy deposits could be produced at maximum plating rates. To achieve this, a large number of deposit spots were produced under varying conditions of temperature, flow rate, electrolyte composition and current density. The exact conditions for each sample may be found in Tables 2 to 15. Pure gold deposits were used for the initial trials to establish the general governing principles of deposition under high speed jetting conditions. The conditions were then adjusted to allow the maximum deposition rates that allowed good quality deposits to be produced. This current density is referred to as the maximum useful current density. The optimised electrolyte was then used to produce samples for characterising the deposit. The principles established for pure gold were then applied where possible to the gold alloy system.

The value of the applied current densities quoted in this work were based on the cross sectional area of the nozzle exit and thus the impingement zone. However, it is known that deposition occurs outside the impingement zone and therefore this assumption is not strictly true. Unfortunately, there would appear to be no other way to define the current density under these conditions and therefore this assumption will be adopted. Under certain deposition conditions, it is clear that this assumption is incorrect but this will be discussed later.

7.3.1 Pure gold deposits.

It has been established in previous chapters that to obtain high quality electrodeposits at high plating rates, it is necessary to provide (a) high metal ion concentrations, (b) to provide high rates of agitation and (c) to operate at elevated temperatures. Using these principles, a matrix experiment was designed to establish the validity of these principles under jetting conditions. At the same time, the influence of these factors on the selectivity of the jetting process was examined. As such, the main criteria for evaluation of this set of samples was deposit morphology, plating rate and selectivity. The selectivity may be defined as the ratio of the thickness or mass of metal deposited in the impingement region to that deposited outside the impingement region. By plotting the thickness against R , where R is a dimensionless distance defined as the distance from the centre of the impingement region divided by nozzle radius, an indication of the comparative selectivity of the process can be seen.

It was only when the optimum conditions were established that other characteristics such as hardness etc were evaluated.

7.3.1.1 Electrolyte composition

Two types of electrolyte were chosen for this study, the citrate and the phosphate buffered cyanide gold. Table 1 gives full details of these electrolytes. Metal ion concentrations were varied between 0.041M up to 0.28M. The pH values were maintained at 6.1 for the citrate electrolytes and 7.1 for the phosphate electrolytes except where stated otherwise. The viscosity of each electrolyte was measured at temperatures at which samples were produced in accordance with BS188. (1977) using a calibrated Ostwald viscometer. The electrolyte conductivities were measured using a Phillips Conductivity meter using 0.1M KCl as a standard. The electrolyte was analysed after making up and after approximately 60 spots had been produced. Any deficiencies were corrected. Chelating agents such as EDTA was not added for this work to eliminate the possibility of any unwanted surface effects that may be experienced under high values of polarisation. Also, at the pH values used, little co-deposition of contaminant metals would be expected.

7.3.1.2 Experimental method

The experimental method was similar for all the evaluation samples. After the electrolyte under test had been loaded into the pump system the flowmeters and pressure transducer were calibrated. A freshly prepared substrate was clipped into the substrate holder. The flow rate and temperature were set for the current test conditions and the nozzle was aligned with the substrate. The appropriate program for the test conditions was loaded and the experiment was initiated. Each substrate was plated with up to 18 spots, each spot being produced at an increasing current density over the range 0.25 up to 8.0 A cm⁻². The time of deposition was adjusted to supply a total of 0.039 ± 0.0004 coulombs per spot. This was calculated to give a thickness of about 20 μm. Each series of spots were produced at electrolyte temperatures of 25°C, 40°C and 55°C ± 1 °C and over a wide range of Reynolds number.

As has been mentioned in Chapter 6, in order to maintain a constant pipe flow profile and therefore a constant mass transfer accessibility, the ratio of H/d had to be as low as possible. Initial trials using H/d = 1 indicated that the nozzle became engulfed with electrolyte due to contact between itself and the hydraulic jump of the electrolyte, particularly at low flow rates. This effectively produced a submerged jet. As it was necessary to compare deposits under differing flow conditions but constant H/d ratios the influence of H/d had to be established so that the lowest *practical* distance could be used. A series of samples were prepared using a current density of 3.0 A cm⁻², a Reynolds No. of 10,500 and a temperature of 40°C using the phosphate electrolyte. The H/d ratios were varied between 0.625 to 8.25 at 0.625 intervals. The appearance, maximum thickness and profile was recorded.

A further series of spots were prepared at a constant current density, velocity and temperature but with increasing deposition time to establish how the deposit varied with increasing thickness.

The effects of dissolved oxygen were examined by preparing a series of spots both before and after bubbling nitrogen through the electrolyte for 30 minutes to de-aerate the electrolyte.

The influence of pH was also examined when all other factors had been optimised. A series of samples were produced from the optimised citrate bath at pH values of 5.3 and 8.1.

The cathodic current efficiency was evaluated for an optimised electrolyte over a range of current densities. For current densities below 2.0 A cm^{-2} , a single spot plated for a long period of time was used whilst at current densities above this an array of 20 spots was used. The reason for the different methods was that at low current densities, because of the long plating times involved, there was some chemical attack of previously plated spots by the electrolyte run-off. Using a single spot reduced the likelihood of losses due to chemical attack.

The mass of deposit produced by either method was low (about 10 mg) and therefore the substrate was weighed 7 times both before and after plating and an average value taken. The cathodic current efficiency was calculated using Faraday's Laws by comparing the theoretical mass deposited for the number of coulombs passed to the actual mass measured and expressing the result as a percentage.

Using the optimised electrolyte, a further series of deposits were produced using nozzles of different diameters between 0.1 mm and 0.54 mm to establish whether the nozzle size influenced the deposition rate, structure etc.

To examine the influence of pulsed current, a series of deposit spots were produced over a wide range of on-time and duty cycles. The on-times ranged from 0.02 msecs. to 10.0 msecs. and duty cycles between 5.0 and 90%. The average current densities used were between 6.0 A cm^{-2} and 10.0 A cm^{-2} .

7.3.2 Gold alloy deposits

As has been previously mentioned, gold may be alloyed with small quantities of transition group metals thus altering the properties of the deposit. Nickel and cobalt are the preferred choices for this purpose although iron has been used. It was decided that it would be better to use an existing commercially available electrolyte designed for high speed operation as this would reduce the development time required for optimisation. There were disadvantages to this decision. The

composition of proprietary electrolytes is often a closely guarded secret and it was not possible to control all the compositional variables. However, despite this, three electrolytes were chosen to represent the three common alloy systems. The cobalt and nickel electrolytes were Ronovel CM and Ronovel N, supplied by Lea Ronal. The gold/iron electrolyte was the Auruna 7000 supplied by Degussa. A series of plating trials were carried out on all three electrolytes in order to establish which electrolyte was the most suitable for optimising for plating under high speed jetting conditions.

7.3.2.1 Initial trials for electrolyte selection.

Each of the electrolytes were made up with three different concentrations of gold, 0.05M, 0.076M and 0.1M. The recommended optimum quantity of the alloying metal was added to each of the electrolytes. The initial trials consisted of depositing a series of spots from each electrolyte at the highest velocity obtainable (approx. $Re. = 11,000$) over a current density range of between 3.0 and 10 A cm⁻². The resulting deposits were examined and the electrolyte giving the best deposit at the highest current density was chosen for optimisation. Results indicated that the Ronovel N was the most suitable and this electrolyte was used.

7.3.2.2 Optimising the gold/nickel electrolyte.

The criteria for obtaining an optimum gold/nickel alloy was based on several factors. The deposit had to contain the appropriate quantity of alloying constituent. It had to have a suitably high hardness, it had to have a similar morphology to conventional high speed gold alloy deposits and it had to be compatible with existing specifications. Finally it had to exhibit these qualities at the highest possible deposition rate. The optimum conditions of deposition for pure gold under jetting conditions were applied to the plating trials for this electrolyte. The variables that were adjusted were the concentration of nickel added to the electrolyte and the current density. In addition, this electrolyte made use of an organic addition agent to boost the maximum current density. Unfortunately, the recommended quantity was already added to the make-up solution as supplied. This meant that its concentration could not be reduced. However, it could be increased and this was included as a variable. The nickel content was varied over the concentration range of between 0.0085M and 0.05M (0.5 to 3.0 g l⁻¹). The standard addition agent concentration was increased from 60 ml l⁻¹ to 80 ml l⁻¹.

7.3.2.3 Experimental method.

As with the pure gold electrolyte, a series of deposited spots were produced for morphological as well as structural examination. Spots were deposited over the current density range of 0.25 to 16.0 A cm⁻². Because it was found that the overall deposition rate was significantly lower than that of the pure gold, the number of coulombs passed was increased to 0.07876 ± 0.0001 coulombs per spot. The deposits were produced at a temperature of 55 ± 1 °C and at a Reynolds number of about 11,000. The pH of the electrolyte was maintained at a value of 4.6 for all the experiments.

The cathode current efficiency was measured in the same way as with the pure gold deposits.

Chemical analysis of the nickel content of the deposits was carried out by X-ray Fluorescence Spectroscopy (XRF). For each concentration of nickel in the deposit, an array of 90 deposited spots was produced at current densities of 2.0, 4.0, 6.0, 8.0, 12.0 and 16.0 A cm⁻². An oxygen free high conductivity (OFHC) copper substrate was used, pre-plated with 0.4 µm of gold. A pure gold deposit array was used as a blank. The sample was placed in the XRF spectrometer with only the array exposed to the X-rays.

The XRF spectrometer was calibrated by measuring the nickel content of 6 array samples using AA analysis. The count rate from each of the samples was first determined using the XRF. In order to minimise errors, the substrate surrounding the array was cut off. The array and remaining substrate were then placed in 50% nitric acid to dissolve the substrate. This left a thin gold foil consisting of the 0.4 µm initial deposit with the array of spots on it. The foil was weighed to establish the total mass. Prior to plating the array, the thickness of the initial gold deposit was determined over the array deposition area using an X-ray 1000 XRF thickness measuring instrument. The mass of this initial deposit was calculated and subtracted from the total mass of the gold foil with the array. The foil plus the array was then dissolved in aqua-regia and analysed. The results of this analysis were then used to produce a calibration curve for the XRF and all subsequent samples were evaluated from this data. It should be noted that the nickel concentrations obtained by this method gave only the average nickel content of the deposited spots and did not give any indication of the distribution of nickel within the individual spots.

The methods used for structural analysis and hardness have been described in sections 7.2.3 and 7.2.4.

7.4 MASS TRANSFER STUDIES.

In order to examine the validity of the various Sherwood number to Reynolds number relationships that had been suggested by other workers, it was necessary to obtain mass transfer data for the gold system. Information concerning the mass transfer characteristics of the various electrolytes under jetting conditions was carried out by evaluating the current/overpotential relationships by plotting polarisation curves and determining where possible the value of i_L . It was immediately obvious that significant difficulties would be encountered using conventional voltage or current scans over the potential and current range of interest. This was because at such high current densities as those used in jetting, the deposit grew so rapidly that the effective surface area quickly changed due to crystalline growth. Initial experiments confirmed this. In addition, there was the difficulty of placing a reference electrode in such a position as to avoid interference with the electrolyte jet. These problems were overcome by using a specially designed working electrode/reference electrode assembly and by using two techniques which will be termed Sampled Current Pulse Voltammetry (SCPV) and Sampled Voltage Pulse Amperometry (SVPA). The validity of the technique was established by using a copper sulphate electrolyte, a well studied system, in the jet unit and identifying appropriate electrochemical factors from the polarisation curves obtained.

7.4.1 Principles of SCPV and SVPA.

Both of these novel techniques have been adapted from the method of sampled current voltammetry, which is the basis of polarography. Ordinarily, polarisation data is recorded as described in section 3.2. However, deposit growth did not allow such steady state measurements to be used. It was therefore necessary to minimise deposition times for each value of overpotential or current applied. As both SCPV and SVPA are essentially similar, the difference being the controlled variable, SCPV will be described. A short period, say 40 mseconds, single voltage pulse of small magnitude (50 or 100 mV) is applied to the working electrode. The current transient is recorded on a storage oscilloscope or similar recording device and the process is repeated with an increasing magnitude pulse over the desired potential range. A typical current transient is shown in Figure 13. As the potential is first applied, a large current flows. This consists of the double layer charging current. As the double layer becomes charged so there is an increase in the proportion of faradaic current as metal ions in the vicinity are discharged. However, these are rapidly consumed and the current falls. As a diffusion layer develops, the current gradually decreases further with increasing time as the diffusion layer thickens. By choosing a time period, τ , within the transient at which the current stabilises close to its minimum value, the current at τ is used for the polarisation curve. If the value of τ is too short, then the current will include the double layer charging current. If τ is too great, the current will be influenced by the effects of deposit growth. The ideal situation is

to choose a value of τ which corresponds to the point at which a steady state diffusion layer has formed. The value of τ will be dependent on the magnitude of the potential and the current flowing as this will influence the magnitude of the diffusion gradient. The greater the current, the faster the influence of diffusion. Also, at high overpotentials and currents, deposit growth becomes rapid and this influences the surface area of the electrode leading to enhanced currents.

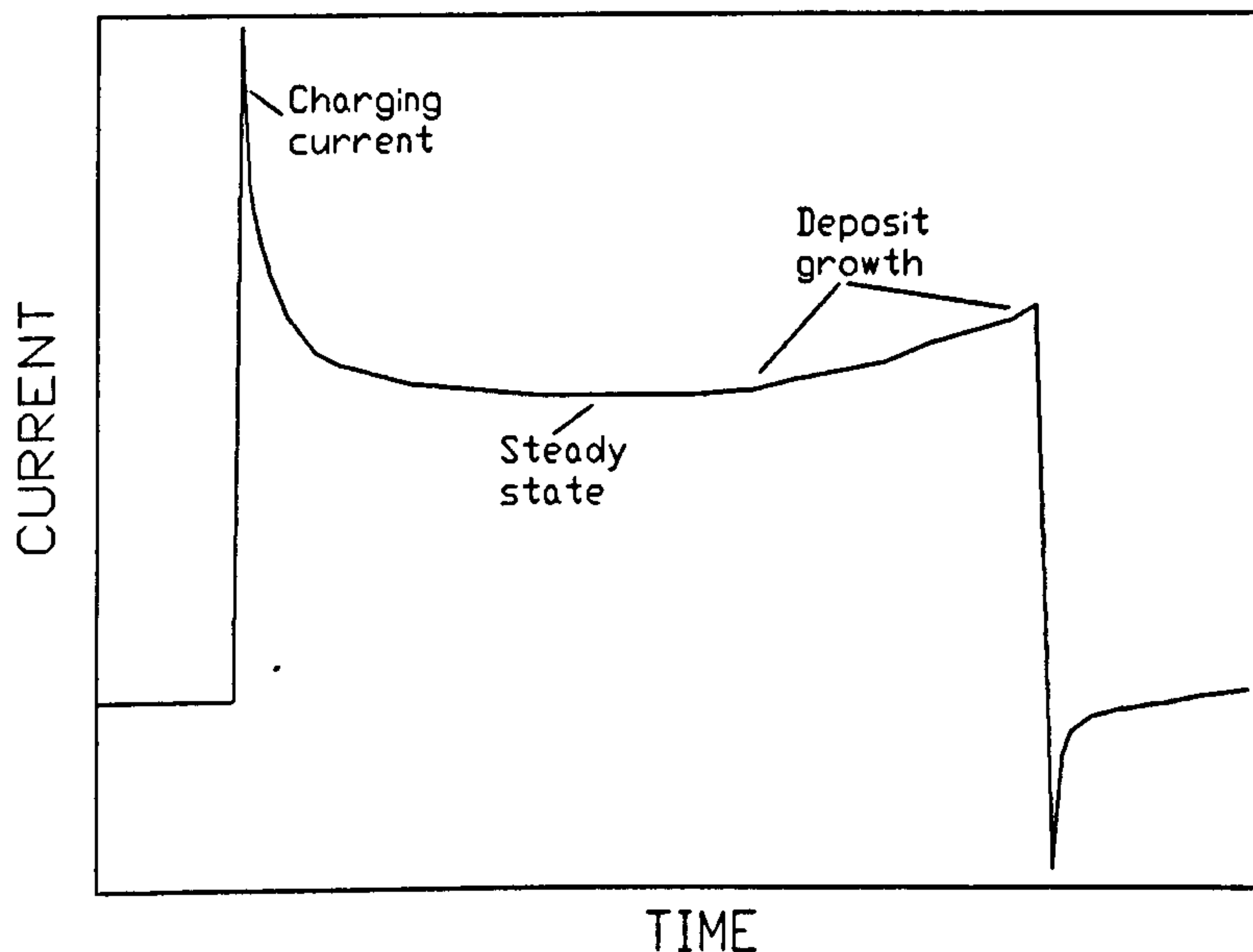


Figure 13. A typical current transient produced during a single pulse using the SCPV method. A relatively high overpotential has been chosen to show the effect of deposit growth.

Below the limiting current density, the metal ions are not completely consumed. They are however, lower than the bulk concentration of metal ions. At the limiting current density, the surface concentration of metal ions will be zero and further increases in potential will not lead to any further rise in current unless a secondary electrode reaction occurs. This technique should allow the identification of such parameters as the limiting current density i_L , the Tafel slope and the exchange current density.

7.4.2 The working electrode/reference electrode assembly.

In order to produce a valid current density/overpotential relationship, the surface area of the working electrode has to be known. As jetted deposits spread beyond the impingement region and the degree of spread has been found to be current density dependent, a fixed diameter conductive working electrode was fashioned. This consisted of an enamelled copper wire, the same diameter as the nozzle (0.4 mm) mounted vertically into an epoxy block. A gold wire reference electrode was mounted adjacent to the working electrode separated from it by a distance of approximately

0.1 mm. The face of the block where the electrodes emerged was polished flat to a mirror finish thus providing a pair of flush mounted electrodes. Several of these electrode pairs were mounted in the same block. A schematic diagram of the electrode block is shown in Figure 14. The advantage of this method of electrode arrangement was that the reference electrode did not interfere with the jet. The gold wire reference electrode was not ideal because the gold systems used in these trials were electrochemically irreversible. An ideal reference electrode should show complete reversibility with the ions in the electrolyte or there is the danger of some current flowing through it and influencing the results. This was offset by ensuring that the potentiostat had an extremely high input impedance.

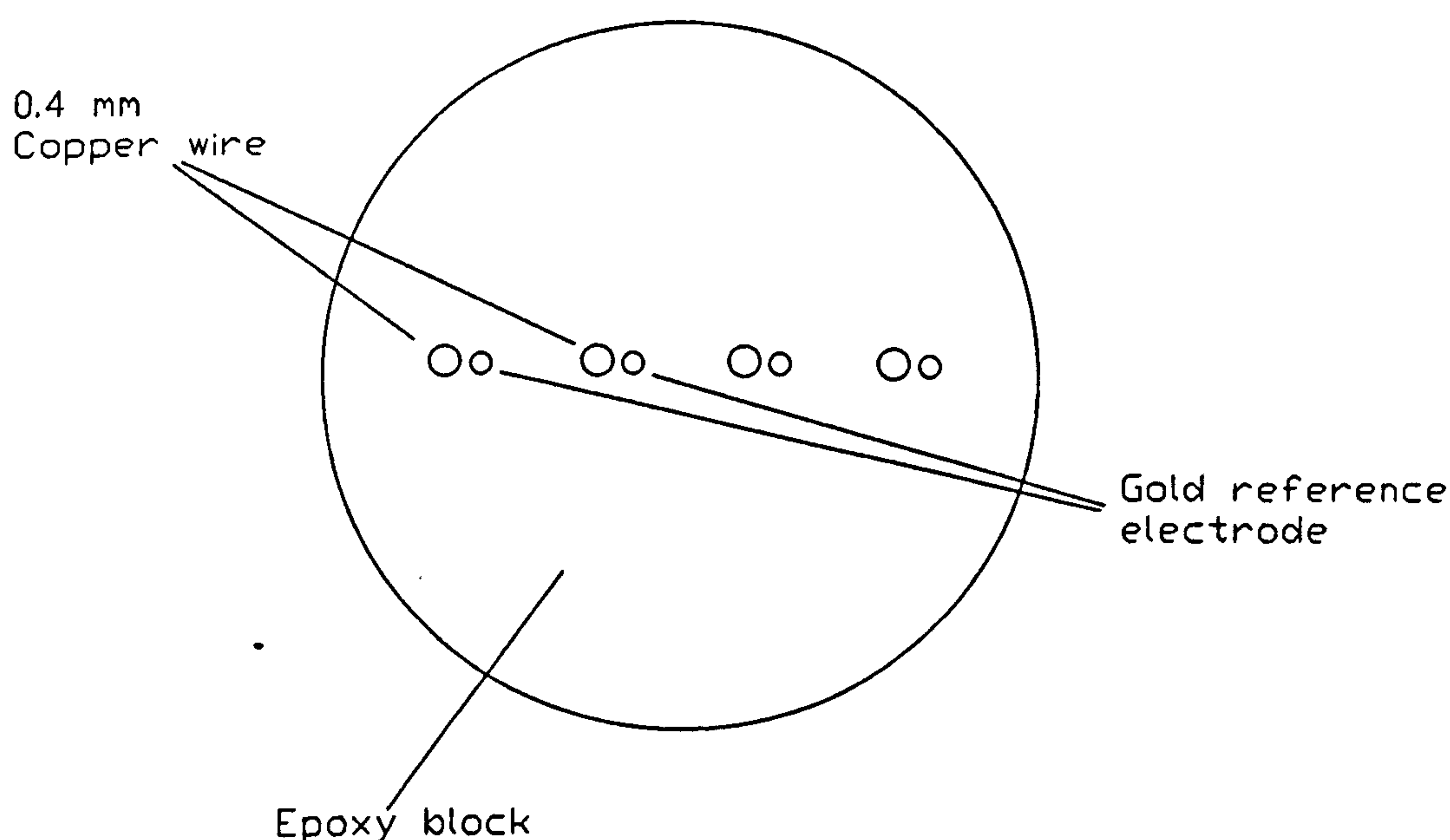


Figure 14. The electrode block used for polarisation measurements.

A further difficulty with this electrode arrangement was that of the IR drop between the working and the reference electrodes. Despite the close spacing between them, there was still an IR drop between them due to the low conductance of the thin radial wall jet. In order to compensate for this, the SVPA method was used. With this method, it was thought possible to measure the IR drop between the two electrodes by means of the magnitude of the initial potential rise of the voltage transient.

To allow the evaluation of the technique of SCPV, a copper electrolyte was used. A similar electrode system was used to that of the gold except that the reference electrode was a copper wire.

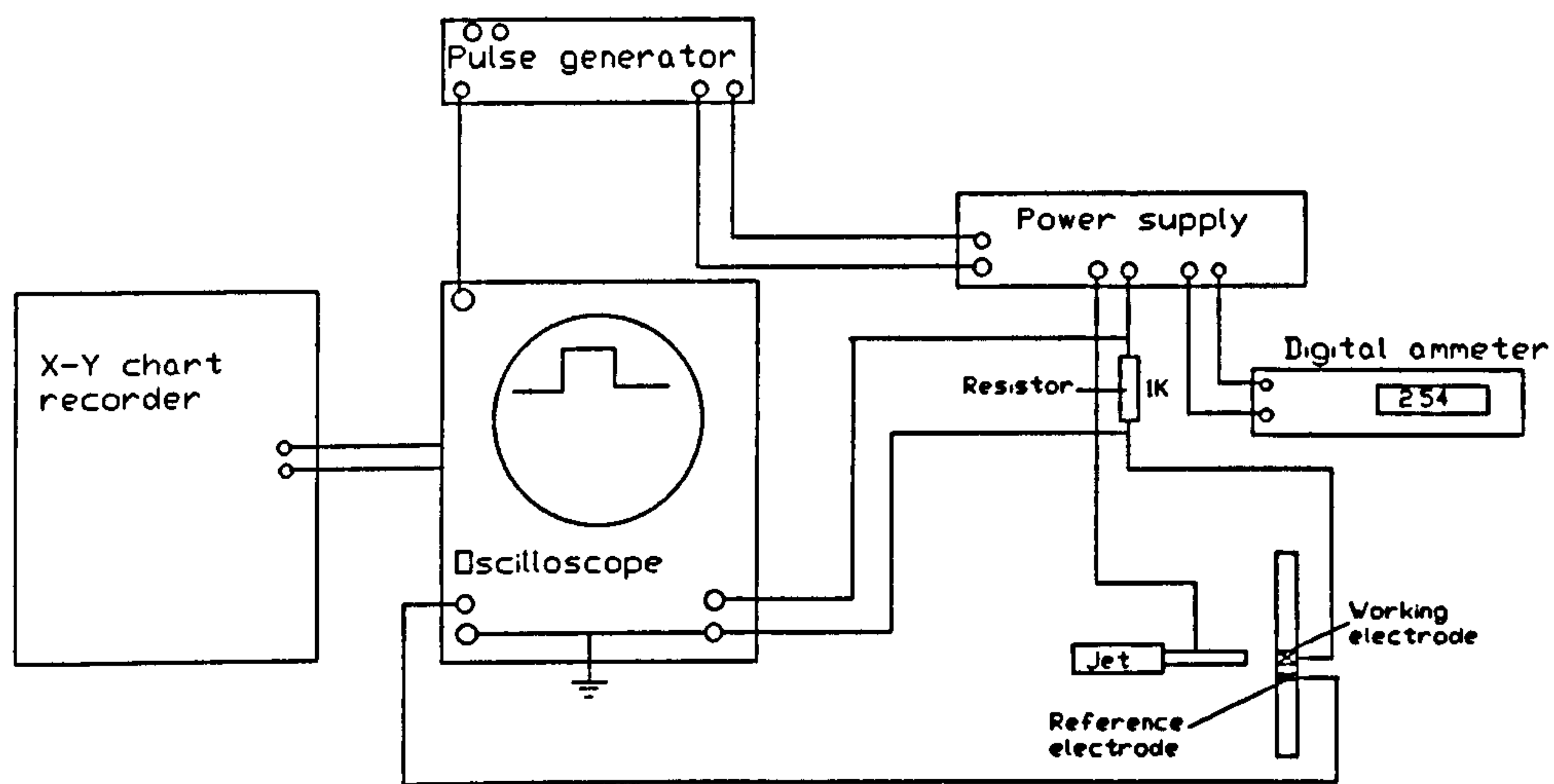
7.4.3 The equipment used.

A schematic diagram of the equipment used for these studies is shown in Figures 15 (a) and (b). Figure 15 (a) shows the SVPA system. It was similar to that used for pulse plating. In this case a single voltage pulse was supplied from the pulse generator to the power supply which then generated the current pulse. The current was recorded by the voltage drop across the 1.0 K resistor by one channel of the storage oscilloscope. The voltage difference between the working electrode and the reference electrode was recorded on the second channel of the oscilloscope. The magnitude of the current pulse could be pre-set by means of short circuiting the output. The recorded current and voltage pulse was then downloaded to a Bryants X-Y recorder for a permanent record of each pulse. At low applied currents, there were significant levels of 50 Hz noise on the potential signal. This was reduced by placing a 0.1 μ F capacitor across the output terminals of the power supply.

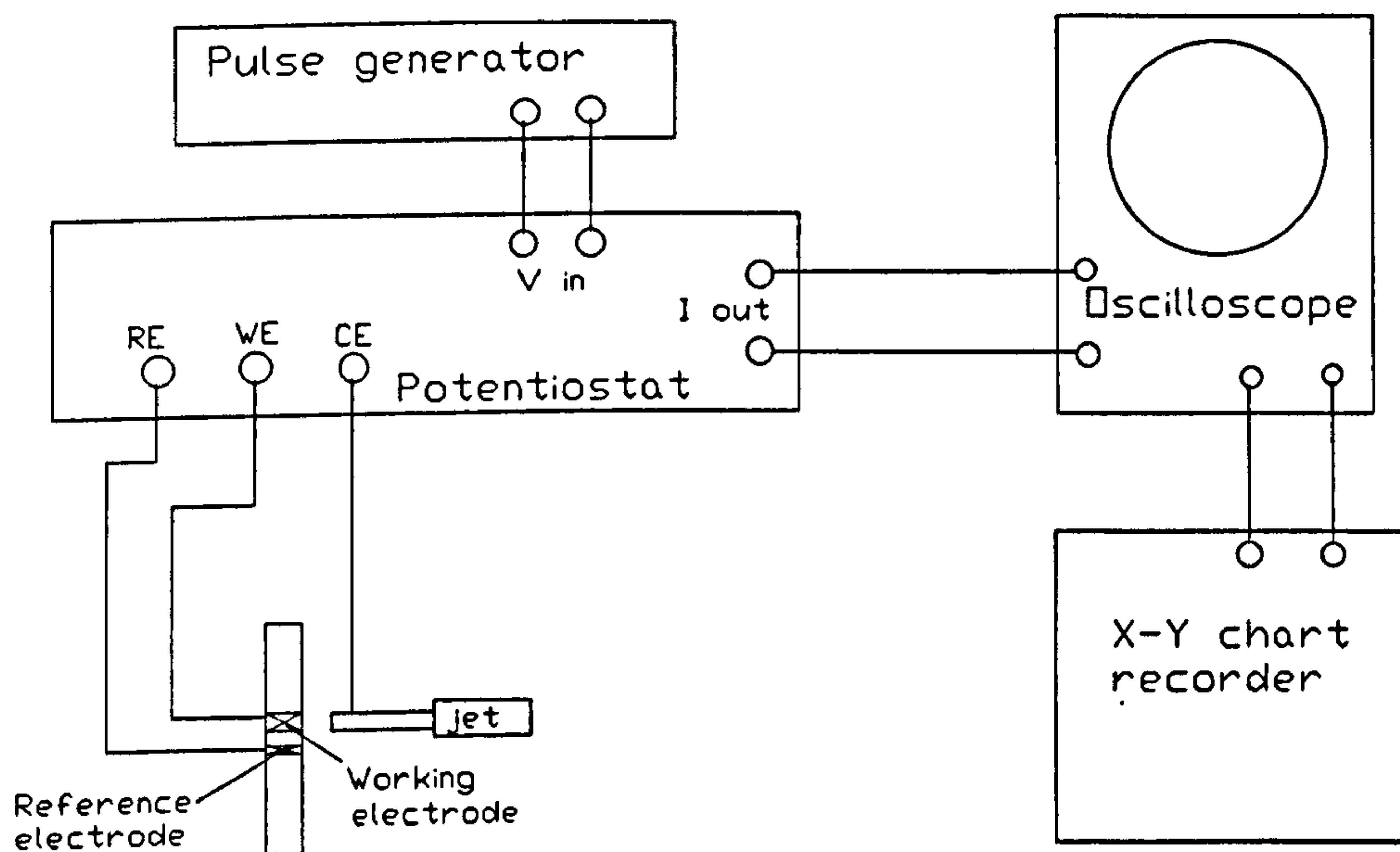
Figure 15 (b) shows the equipment used for the SCPV technique. A standard Wenking HP72 potentiostat was used in conjunction with a pulse generator. The current and applied potential was measured using a storage oscilloscope and downloaded to an X-Y recorder.

7.4.4 Experimental technique.

The method of obtaining polarisation data was similar for both the SCPV and SVPA techniques. The electrodes were first lightly abraded using 1200 grade emery paper. The jet was carefully aligned with the working electrode with a nozzle to electrode distance of 1 mm. A small current of about 0.03 mA was applied for 30 seconds to deposit a thin layer of gold onto the electrode. The current was switched off and the system maintained at the current free for 2 minutes to establish the rest potential. With the SCPV method, a potential pulse of between 50 and 100 mV was applied above the rest potential and the current recorded. The electrode was then abraded with 1200 grade emery paper to remove the gold. The process was repeated using 50 or 100 mV pulse increments above the previous level up to 4.0 volts. With the SVPA method, a single current pulse was used. The current density range used was between 0.04 A cm⁻² and 50 A cm⁻². The voltage obtained from each pulse was recorded. In addition, the potential jump was recorded as a measure of the IR drop between the working and reference electrodes.



(a)



(b)

Figure 15. (a) The equipment used during the SVPA experiments. (b) The equipment used during the SCPV experiments.

The results of this work will be presented mainly in the form of graphs and micrographs. Where relevant, the data collected is shown in the form of Tables towards the end of the Thesis.

8.1 PURE GOLD DEPOSITS.

Whilst both the citrate and phosphate buffered gold electrolytes had some different characteristics, particularly in the morphology of the deposits produced, the general principles of the influence of the deposition conditions hold for both types. They will therefore be treated together except where the differences are significant.

The electrodeposited gold spots produced by this jetting technique were generally gaussian in profile and were symmetrical depending on the current density and electrolyte flow rates used. However, at low flow rates and high current densities, the deposit quality deteriorated with the production of powdery, nodular or dendritic structures. These deposits no longer showed the gaussian profile. The influencing factors controlling the deposit structures and deposition rates under DC conditions are detailed in the following sections.

8.1.1 The effect of nozzle to substrate distance.

By varying the nozzle to substrate distance, or the H/d ratio, a number of effects were observed. At ratios in excess of 4.375, radial needle structures were seen towards the edge of the deposit. Photograph 2 shows such a structure. Below this value under the conditions used, no such forms were observed. Figure 16 shows the effect of the increasing H/d ratio on the selectivity of the deposits produced. It can be seen that at H/d below 1, the deposit showed a greater selectivity, with a greater proportion of gold being deposited within the impingement region. Between 1.25 and 4.375, the selectivity did not vary with the distance. At $H/d = 8.75$, the deposit selectivity was reduced. Whilst a greater selectivity could be achieved at H/d ratio's of below 1, the problem of nozzle interaction with the flow across the substrate precluded its general use. On the basis of this information, a H/d ratio of 1.25 or a distance of 1mm was used for all the trials with the 400 μm nozzle. With smaller nozzles, the effect of the electrolyte interaction with the nozzle became

increasingly influential as the hydraulic jump occurred much closer to the nozzle exit. By maintaining the H/d value between 1 and 4, a constant selectivity could be ensured even when using small diameter nozzles.

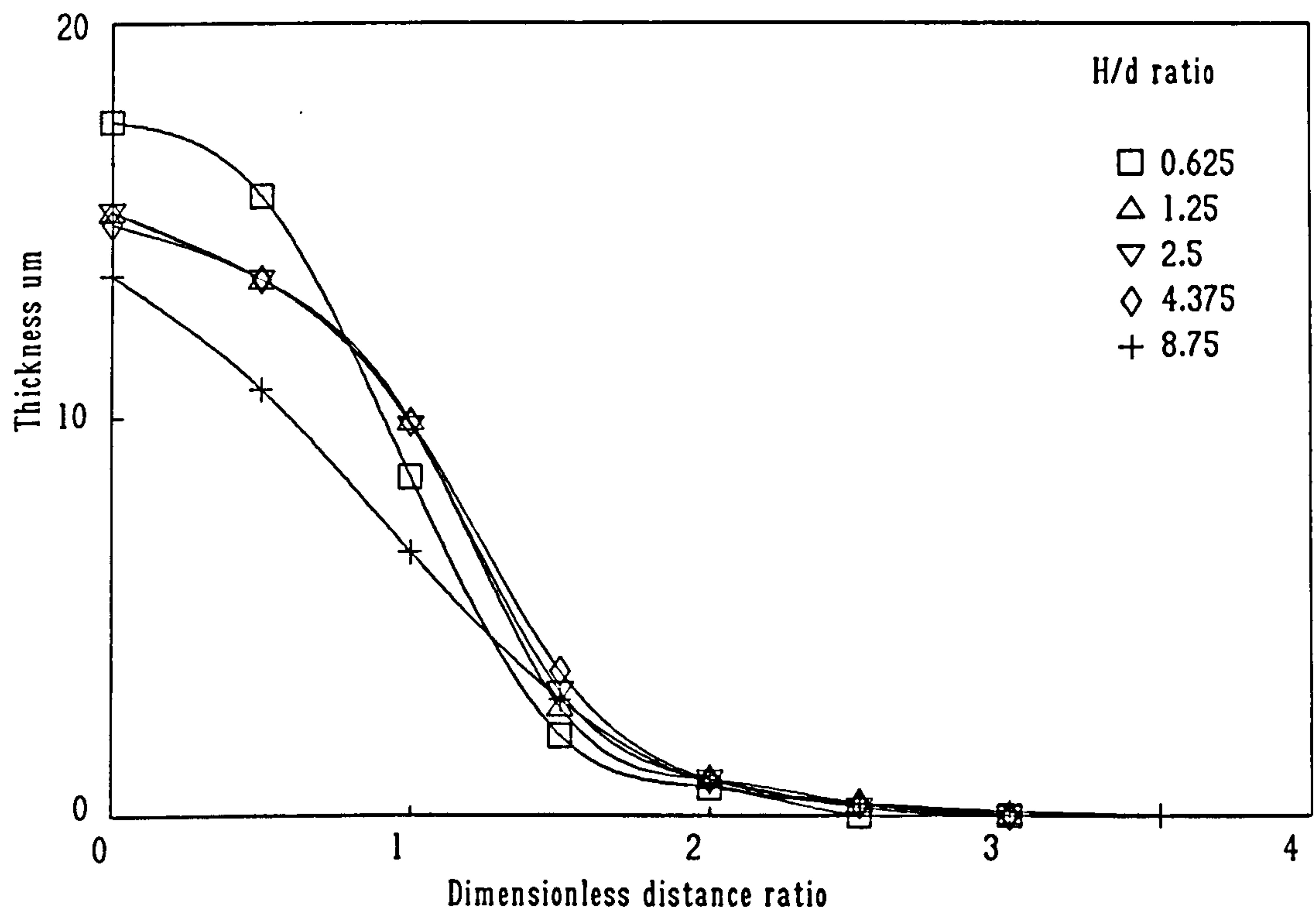


Figure 16. The effect of the H/d ratio for a 0.4mm nozzle on the selectivity of the deposit.

8.1.2 The effect of current density.

As would be expected, the magnitude of the current density influenced the deposit structure and morphology. It also had a significant influence on the selectivity, the current efficiency and the hardness.

8.1.2.1 General observations

At a current density of 0.25 A cm^{-2} , the deposit could not be measured within the impingement region using the Dektak as the deposit was thin leading to difficulty of differentiating the deposit from the background noise of the substrate. However, the existence of some deposition was visible up to a diameter of about 4 mm as a subtle colour change was observed in comparison to the rest

of the substrate. At a current density of 0.75 A cm^{-2} , a thin, sub-micron deposit could be measured in the impingement region but it was difficult to measure the overall spread as there was no clearly definable edge. However, the spread of the deposit was visible up to 8 mm in diameter. The sputtered glass slides used as substrates were found to be translucent when viewed with a strong backlight. Low current density deposits were produced on such a substrate and viewed under a low power microscope fitted with an eyepiece micrometer. Where deposition had occurred, the transmitted backlight disappeared and the spread of the deposit could be measured. Figure 17 shows a plot of the optically measured widths as a function of the current density. It can be seen that the deposit spread passes through a maxima at a current density of 0.75 A cm^{-2} but becomes constant at current densities above 3.0 A cm^{-2} .

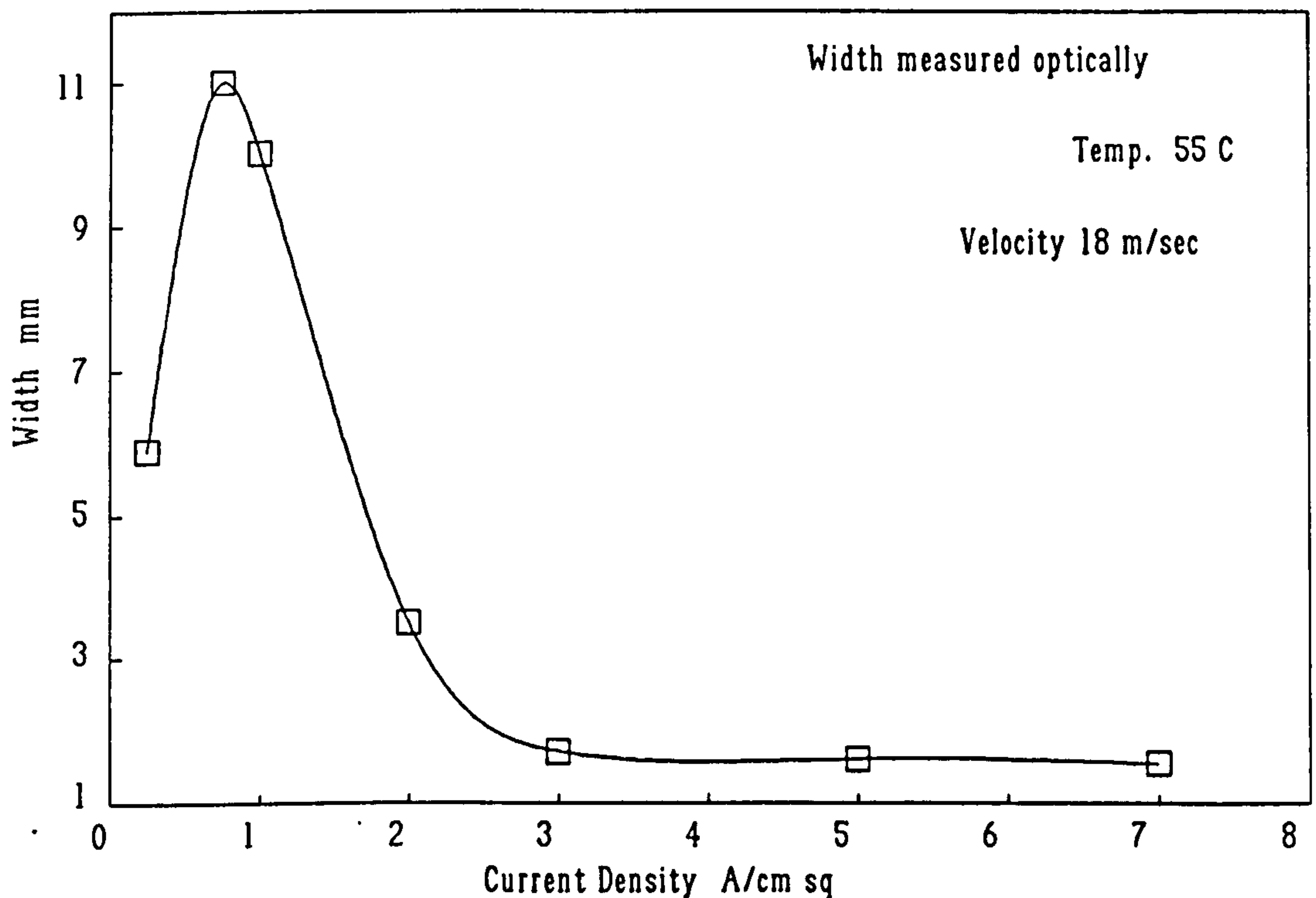


Figure 17. Current density vs deposit width measured optically showing the maximum spread of the deposit spots produced from a 0.17M citrate electrolyte.

It was also noted that although the number of coulombs passed per spot was constant, the thickness of the deposits increased with increasing current density. The reasons for this will be discussed at a later stage.

It was found that the presence of dissolved oxygen had the effect of reducing the deposition rate at current densities below 3.0 A cm^{-2} . With the dissolved oxygen removed by de-aeration, the deposition rates at these low current densities increased by up to 60%. In addition, the selectivity was reduced by around 30%.

8.1.2.2 Deposit topography.

Current density influenced the topography and morphology of the deposit significantly. The actual current densities at which topographical changes occurred depended strongly on the prevailing conditions of temperature, electrolyte velocity and metal ion concentration. However, a general pattern was observed. A typical example will be described where the flow conditions corresponded to a Reynolds No. of approximately 12,000 and a temperature of 55°C . At current densities below 1.0 A cm^{-2} , deposits were similar in appearance to those produced by conventional deposition. Photograph 3 shows such a structure. Increasing the current density led, initially, to a very smooth structure with few surface features. As the current density was increased above 4.0 A cm^{-2} , the deposit exhibited small, hemispherical features similar to those observed by Nakahara in hard gold deposits. These can be seen in Photograph 4. Above a current density of 6.0 A cm^{-2} , a nodular structure formed. Finally, at current densities in excess of 10 A cm^{-2} , a wide variety of dendrite-like structures formed, ranging from radial needles growing in the direction of the wall jet to non-directional organic-like growths. Ultimately, at very high current densities, growth became highly field orientated as the deposit grew along the free jet, producing tree-like structures. Typical examples of these can be seen in Photographs 5, 6, 7, 8 and 9. Reducing the flow rate and/or the temperature led to a reduction in the current density at which the morphological changes occurred.

Figures 18 to 23 show morphological/topological diagrams of the 0.041M and the 0.28M citrate gold deposits. These diagrams relate deposit structures as a function of current density, temperature and flow rate. These were used to identify trends with which to establish an optimum electrolyte composition and operating conditions. The phosphate electrolyte showed a similar behaviour except that the transition from smooth to nodular deposits occurred at a lower current density than the equivalent citrate electrolyte.

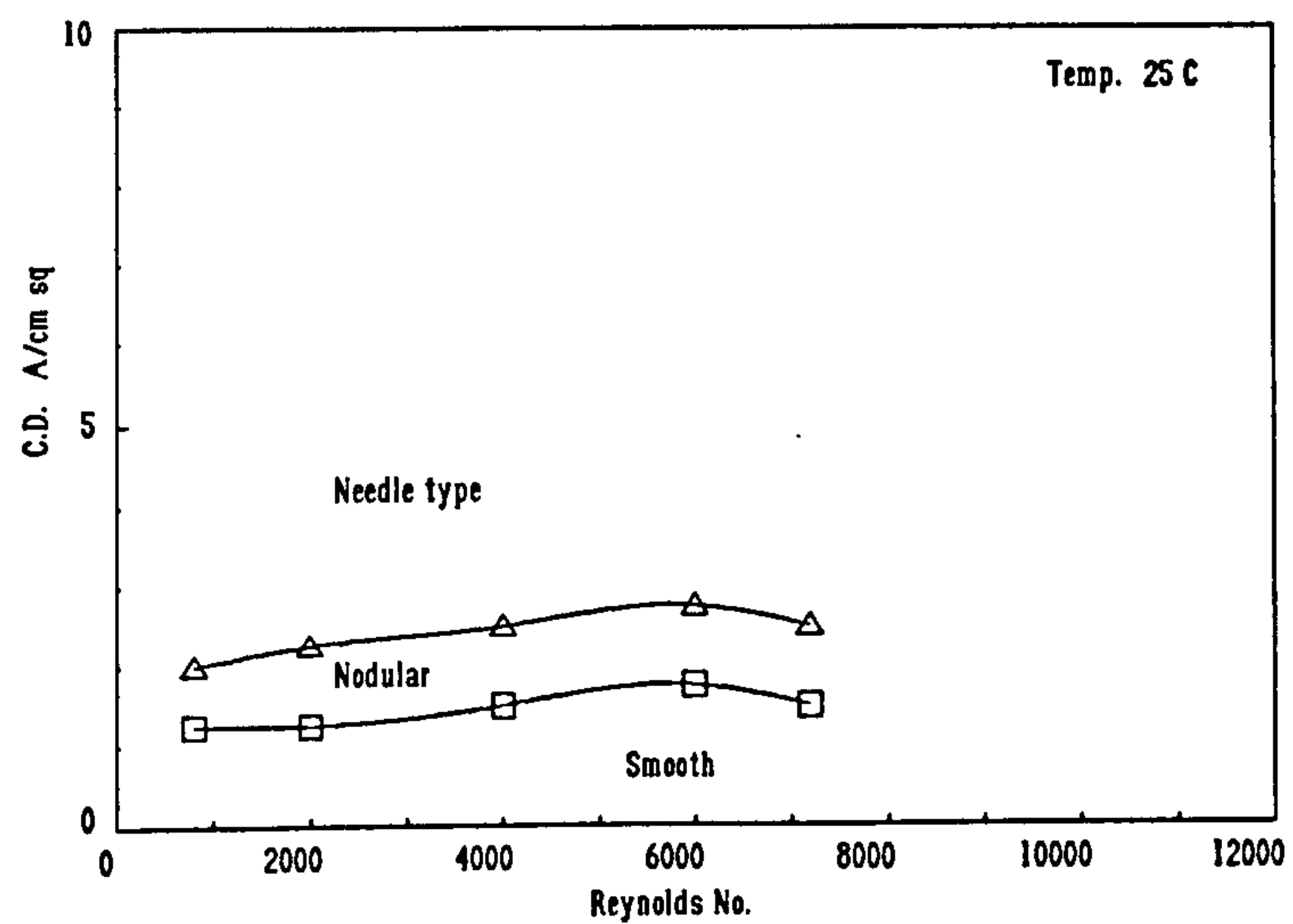


Figure 18. Morphological diagram for the 0.041M citrate gold at a temperature of 25°C.

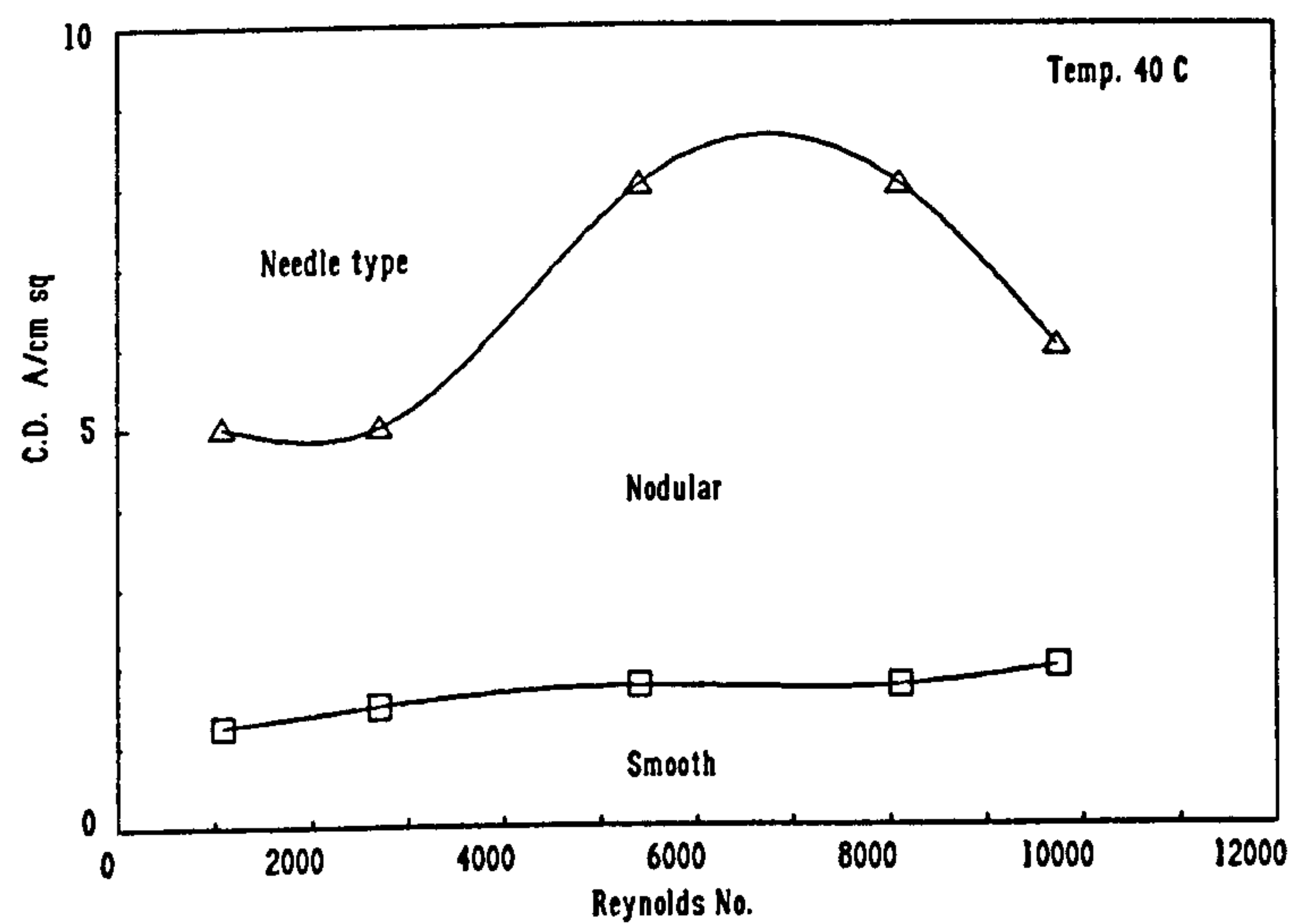


Figure 19. Morphological diagram for the 0.041M citrate gold at a temperature of 40°C.

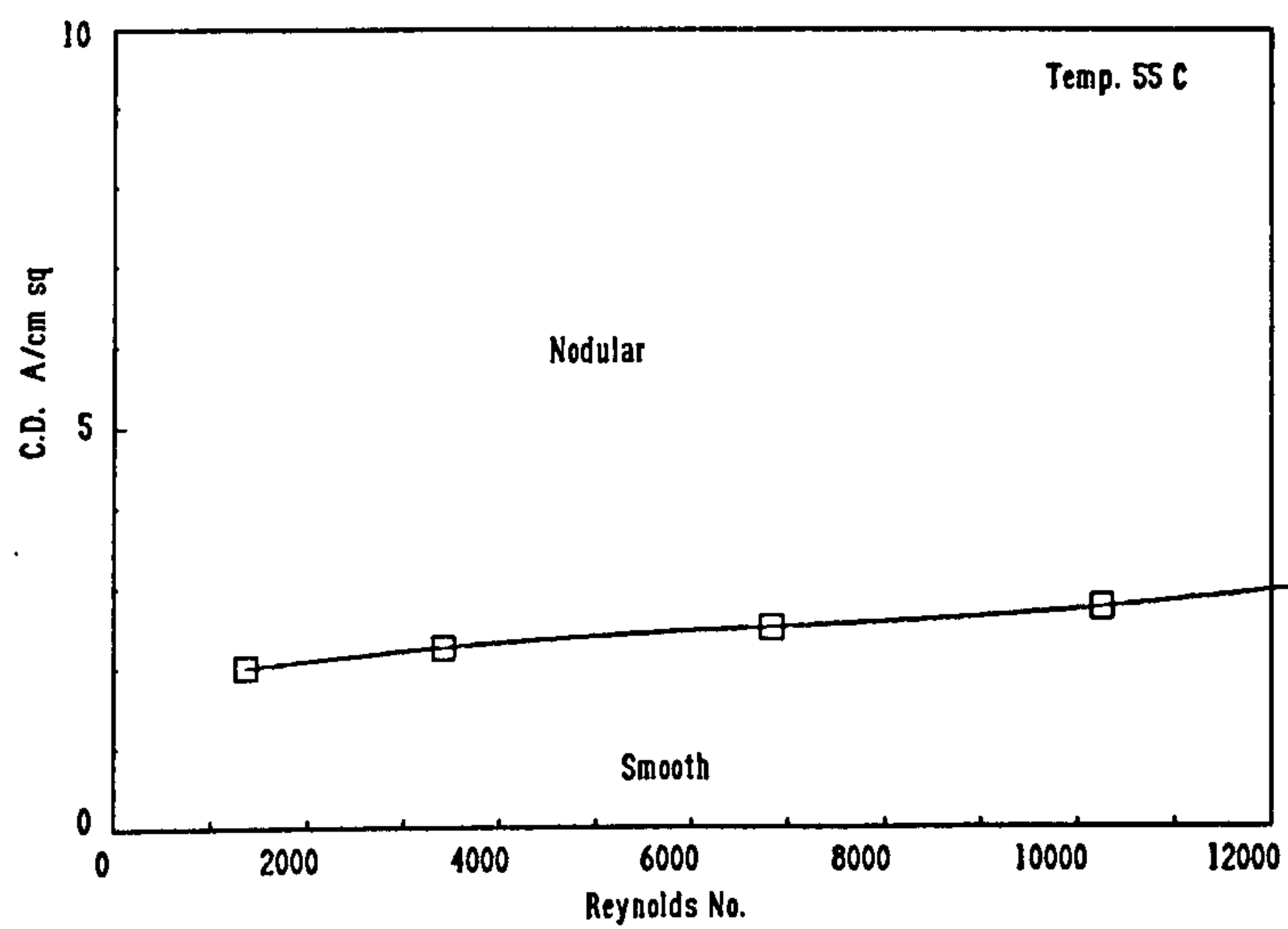


Figure 20. Morphological diagram for the 0.041M citrate gold at a temperature of 55°C.

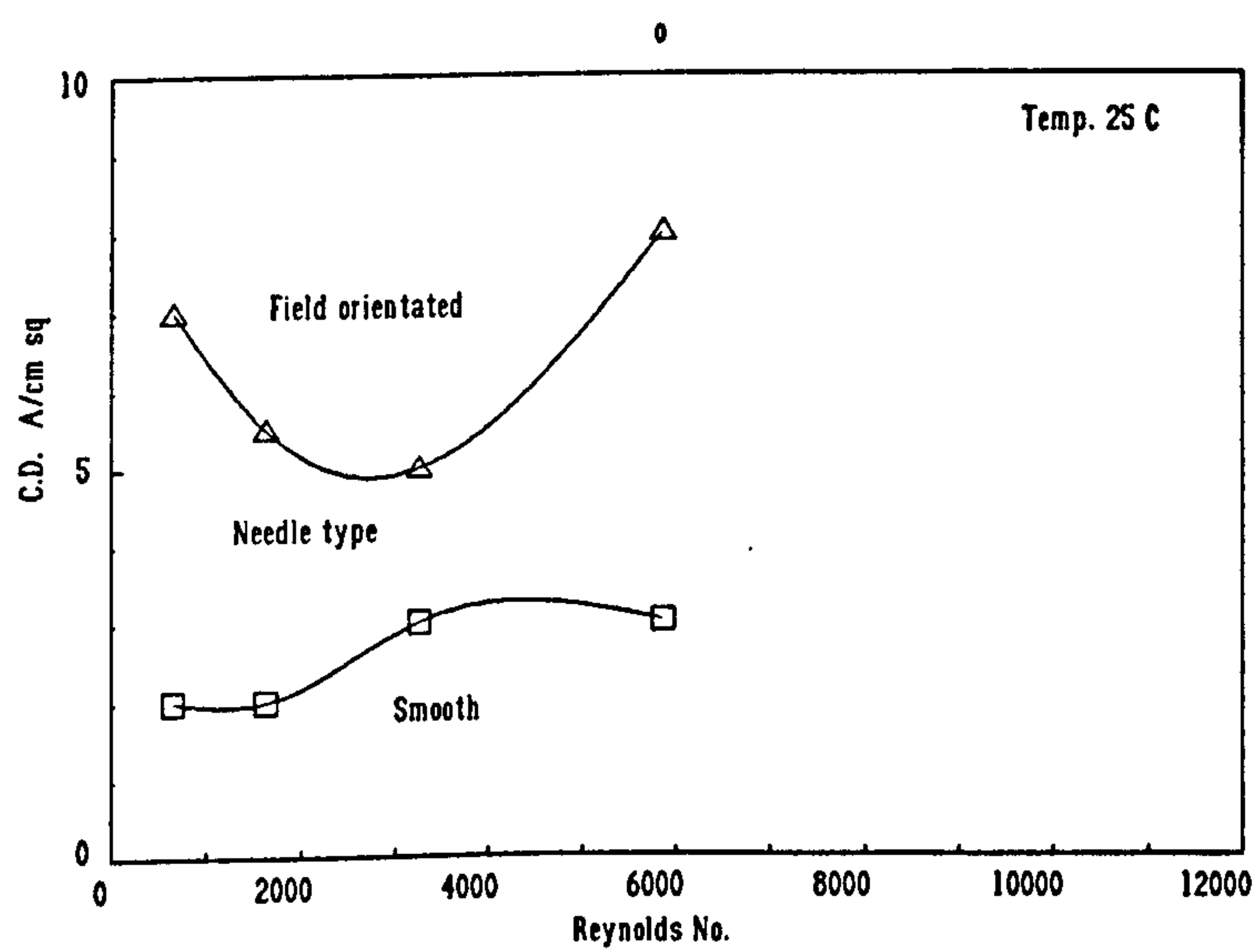


Figure 21 Morphological diagram for the 0.28M citrate gold at a temperature of 25°C.

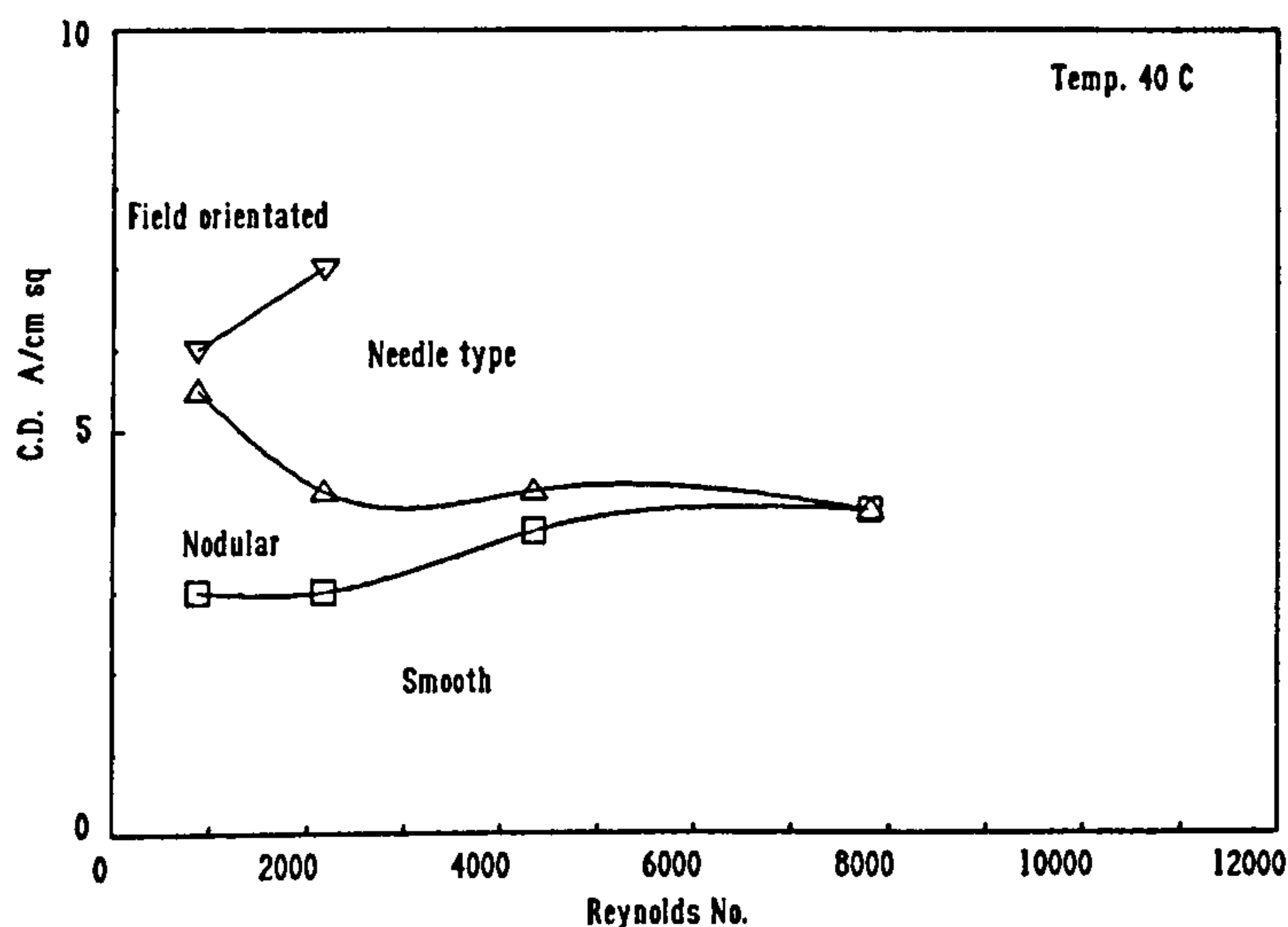


Figure 22. Morphological diagram for the 0.28M citrate gold at a temperature of 40°C.

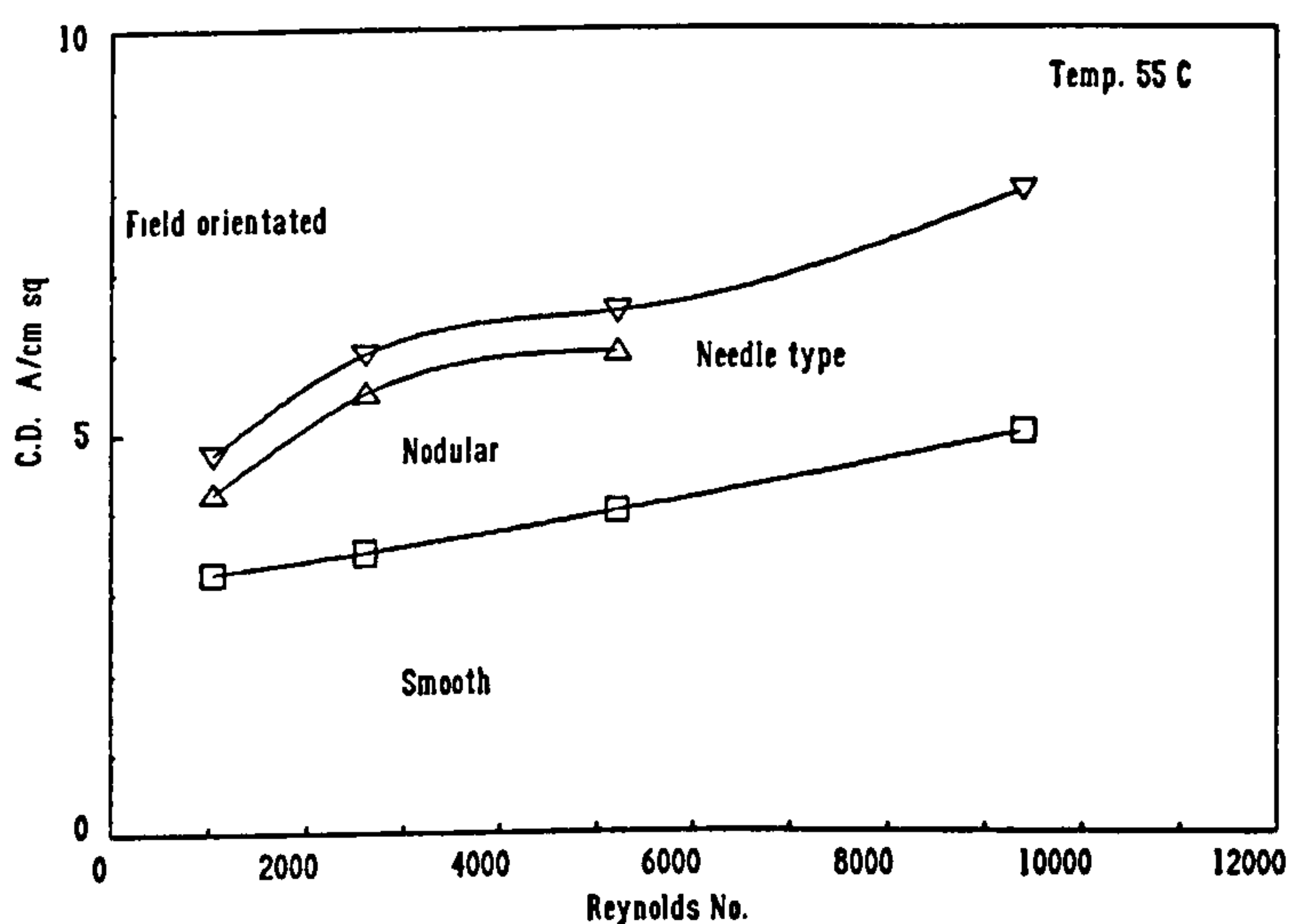


Figure 23. Morphological diagram for the 0.28M citrate gold at a temperature of 55°C.

Although these diagrams show a fixed transition point between structures, it should be noted that the transition was gradual. The transition lines were placed at positions where the deposit had adopted a definite structure type as evidenced by visual assessment using low power magnification. Where needle type structures are stated, the type of needle growth depended on the flow rate and temperature. High temperatures and low flow rates led to needles growing in both the radial and

axial direction. Such structures were difficult to distinguish between field oriented growth and the recorded structure depended on the relative magnitude of the axial and radial components. Low temperatures resulted in purely radial growth. High flow rates with low temperatures increased the thickness and regularity of the needles for the same applied current density. For the same low temperature and flow rate, increasing the current density led to a finer, more filamentary type of radial needle growth. In the case of field oriented growth, the structures observed depended largely on the applied current density. At high current densities, field oriented growths were nearly always preceded by needle growth.

From the above results, it was clear that the limiting factor to high speed deposition was the deterioration of the deposit by nodulation or dendritic growth of various kinds. In order to establish how such structures initiated and grew, a series of samples were prepared above the maximum useful current density for the prevailing deposition conditions. Each sample was prepared by incrementing the time of deposition slightly so that a picture could be built up of the mode of growth. Photographs 10(a) to (f) show a series of deposits produced at a current density of 7.0 A cm^{-2} at a Reynolds no. of 3335. Photographs 11 (a) to (d) show some of the same but at a higher magnification. These samples show the initiation and growth of nodular deposits.

After a deposition time of 0.8 seconds, the substrate was fully covered with small nuclei interspersed with small nodules about $3.5 \mu\text{m}$ in diameter (Photograph 10a). Close examination of this sample revealed that there were signs of nuclei inhibition surrounding the larger nodules (Photograph 11a). After 1.5 seconds, the nuclei had grown to a size of about $2.5 \mu\text{m}$ in diameter with the original larger nodules having grown to about $7.5 \mu\text{m}$ (Photographs 10 and 11 b). Most of these larger nodules were outside a $50 \mu\text{m}$ region, presumably the stagnation zone. It was also noticed that larger nodules grew on surface defects such as scratches. After 2.5 seconds, there were a greater number of larger nodules with a cluster of these appearing in the same $50 \mu\text{m}$ region. It could be seen that growth was occurring by means of 3 dimensional nucleation, the nodules taking on a cauliflower appearance (Photographs 10c and 11c). Deposits produced at a time of 3.5 seconds were now distinctly nodular over the entire impingement region with the fastest growth of nodules occurring outside the stagnation zone (Photographs 10d and 11 d). By 5 seconds, the nodules had attained about $25 \mu\text{m}$ in diameter (Photograph 10e). The growths in the stagnation zone had attained the same size as their neighbours but growth showed a more distinct 3-dimensional mechanism with numerous nuclei forming and growing on them. After 6 seconds, whilst all the nodules had grown slightly larger, the fastest growth occurred at the centre of the spot, with these nodules adopting a columnar axial habit. These central nodules displayed a distinct powdery texture (Photograph 10f). Some nodules towards the edge of the impingement region were obviously influenced by the radial flow of the electrolyte as it entered the wall jet and had adopted a slightly elongated shape, following the direction of the flow.

A second series of samples were used to identify the mode of growth of dendritic deposits. A current density of 10 A cm^{-2} was used at a Reynolds No. of 12078. Photographs 12 (a) to (f) show this series. The deposit produced at a time of 0.6 seconds showed a high coverage of nodules about $3 \mu\text{m}$ in diameter. In addition, as Photograph 12 (a) shows, there was a small, needle like structure about $30 \mu\text{m}$ long that had grown in the radial flow direction. Also visible were 2 larger nodules of about $7 \mu\text{m}$ in diameter, close to the edge of the impingement region. At a time of 1.5 seconds, most of the nodules had grown to about $7 \mu\text{m}$ although some were about $10 \mu\text{m}$. In addition, a multiple needle structure had grown from a particularly enlarged nodule (Photograph 12 b). With increasing times of deposition, several needle type structures had grown, all appearing to have emanated from a single, fast growing nodule. At a deposition time of 3.5 seconds, growth predominance changed from the radial direction to the axial direction of the free jet. These structures then grew along the jet core producing feathery needles in the direction of the flow (Photographs 12 (d), (e) and (f)). These structures were undoubtedly caused by the interaction of the deposit growth with the hydrodynamic flow of the free jet. This will be discussed further in Chapter 10.

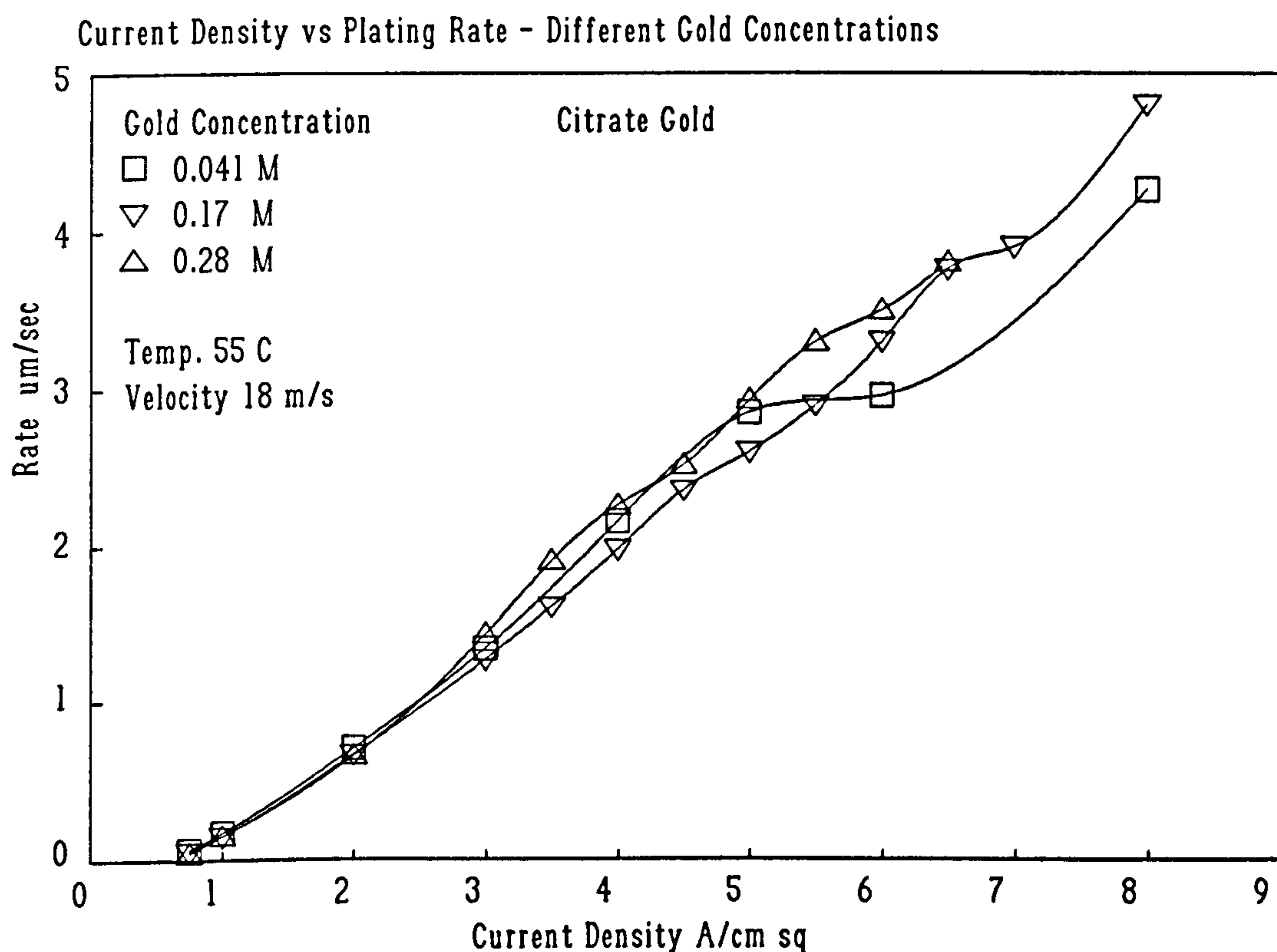


Figure 24. Current density vs plating rate for different gold concentrations, citrate electrolyte. The exit velocity corresponds to a Re. No. of 12,000.

8.1.2.3 Deposition rate

Figure 24 shows the effect of current density on the deposition rate for different concentrations of gold in the citrate electrolytes at a Reynolds No of 12,000. There are several points to note. Firstly, the rate bears a linear relationship with the current density at current densities between 1 and 5 A cm⁻². Above this upper value, the apparent rate varied, presumably due to the increasingly coarse deposits produced at these current densities. This led to non-representative thicknesses being measured due to void and porosity formation. Secondly, the rate curves do not pass through the origin of the graph, indicating that at low current densities, the rate no longer has the same linear relationship with current density. Similar results were observed with the phosphate electrolyte.

It was found that the maximum deposition rate allowing smooth, high quality deposits was obtained from a 0.17M citrate electrolyte at 55°C and a Reynolds No. of 12,000. The rate obtained from this electrolyte was 3.4 μm/second. Photograph 13 shows a deposit 18 μm thick produced under these conditions. By way of comparison, photograph 14 shows a deposit of the same thickness produced under conventional vat plating conditions. It can be seen that the conventional deposit has an angular structure whilst the sample produced by jetting is comparatively smooth with a surface consisting of small hemispherical mounds.

8.1.2.4 Cathodic current efficiency

The effect of the current density on the current efficiency was established only after the electrolyte had been optimised. Consequently, it will be noted that the pH had been increased to 8.1 compared to 6.0 as shown in Table 1. for this set of experiments (see section 8.4)

Figure 25 shows the relationship between the current density and the current efficiency of the 0.17M citrate electrolyte produced at 55°C and a Re. No. of 12,000. It can be seen that at current densities above 2.0 A cm⁻², the efficiency is in the region of 70%. Below 2.0 A cm⁻², the efficiency is reduced to 40% at a current density of 0.25 A cm⁻². Experiments carried out to remove dissolved oxygen in the electrolyte revealed that whilst oxygen, when present, was electrochemically reduced leading to a reduction in efficiency, this only accounted for about 10%, averaged over the entire current density range.

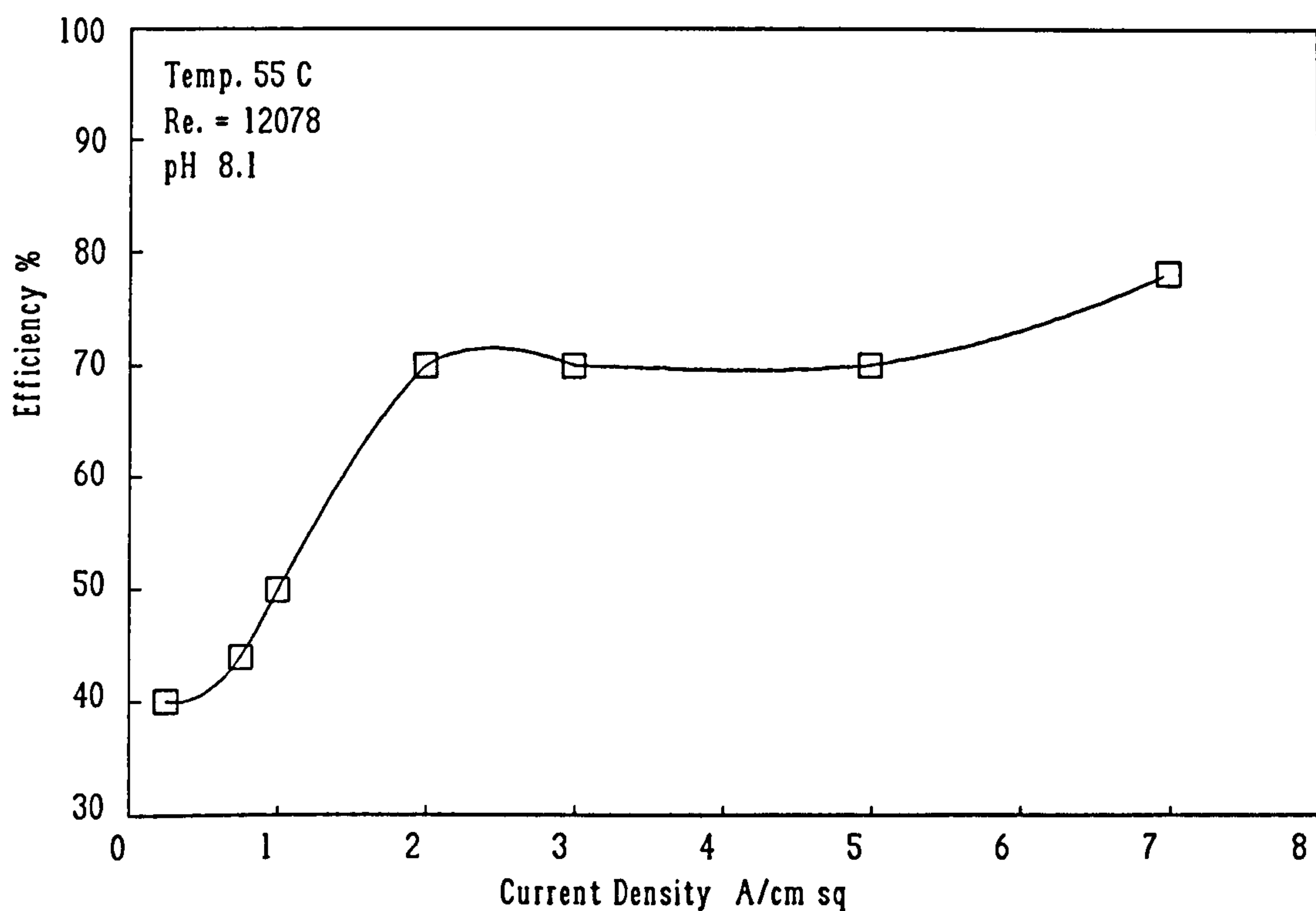


Figure 25. Current efficiency vs current density for the optimised 0.17M citrate gold electrolyte.

8.1.2.5 Hardness of deposits

Hardness measurements were carried out on deposits produced from the optimised citrate gold electrolyte. Figure 26 shows the relationship between the current density and the hardness of the deposit. It can be seen that the hardness increased with increasing current density, being in the region of 200 kg mm⁻² at the maximum useful current density of 6.0 A cm⁻². This value is approximately twice that of conventionally deposited pure gold. Even at the lower current densities, the hardness represents a significant increase over that obtained under conventional deposition conditions.

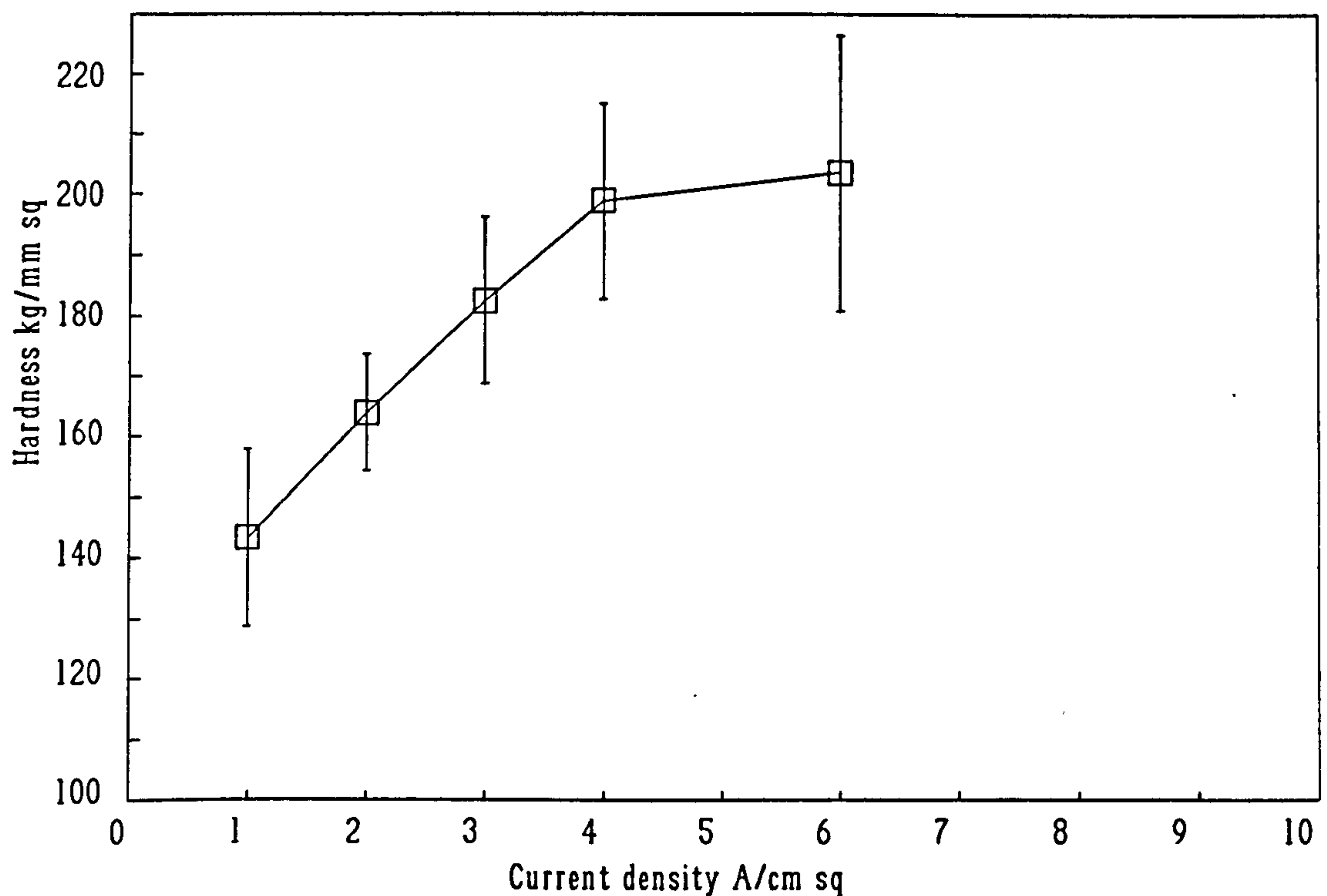


Figure 26. Hardness vs current density for the optimised 0.17M citrate gold electrolyte.

8.1.2.6 Selectivity of the deposit

Figure 27 shows a typical selectivity plot as measured with the Dektak. This shows deposits from the 0.17M citrate electrolyte produced at a constant temperature and velocity at different current densities. They are plots of thickness as a function of the dimensionless distance ratio (see 7.3.1). A dimensionless distance ratio of 1 represents the edge of the impingement region. This graph shows the limitations of the Dektak as a means of profile measurement. Comparison of this with Figure 16 shows that it was not possible to measure the maximum width of the deposits using the Dektak due to the asymptotic nature of the deposit spread. It was found that the limit of thickness determinations in the edge region of the Dektak were limited to approximately $0.15 \mu\text{m}$. This was due mainly to the variation in flatness of the substrates. However, this graph does show that within the measurement limitations of the instrument, no significant thickness of deposit greater than $0.15 \mu\text{m}$ was produced beyond a dimensionless ratio of between 3.0 and 3.5. As Figure 16 shows, the current density does influence the selectivity up to a current density of 3.0 A cm^{-2} , with an increase in the deposit spread from 0.25 A cm^{-2} up to a maximum at 1.0 A cm^{-2} after which it falls to a constant value. This value was close to that measured by the Dektak. It was found that other deposition conditions did not significantly influence the selectivity as a function of current density.

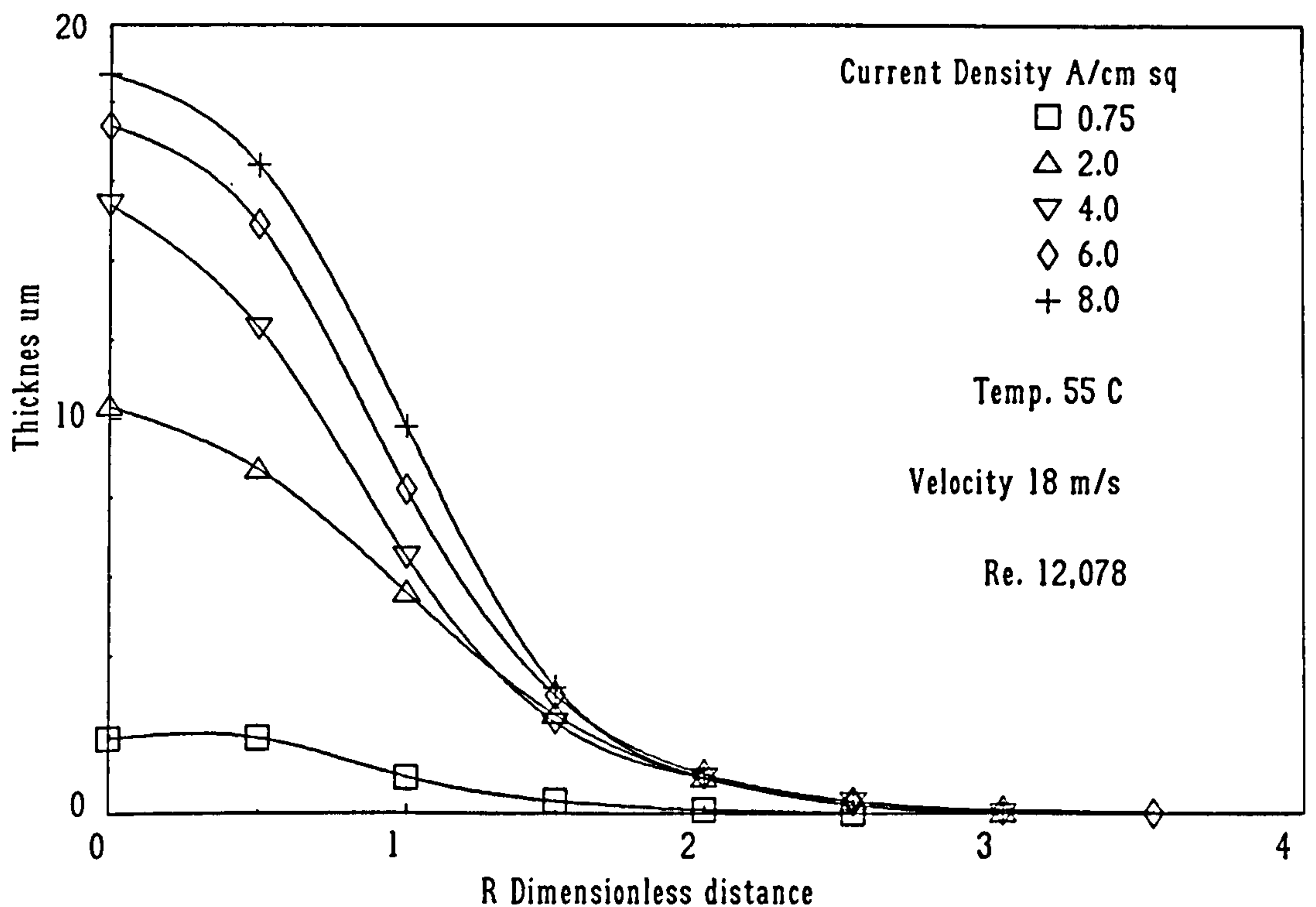


Figure 27. A typical selectivity plot showing selectivity as a function of current density measured using the Dektak.

8.1.2.7 Crystal structure and residual strain.

Examination of deposits produced from the optimised 0.17M citrate gold electrolyte using XRD enabled the lattice parameter, crystallite size and preferred orientation to be determined. Figure 28 shows the lattice parameters and orientation of the major first and second order reflections for a deposit produced under conventional conditions. The electrolyte was identical to the citrate electrolyte used in this study except that the gold concentration was 0.06M. The normal operating current density range for this electrolyte was between 3 and 7 mA cm⁻². The degree of preferred orientation has been expressed for each of the reflections as a percentage of the sum of those measured. In this way, the preferred orientation may be quantified. Because of the crystal structure of the deposit, there will always be a variation in the intensity of the various crystal planes. For example, in a FCC material, there are more 111 planes than 200 and therefore a material possessing a totally random orientation will show a greater 111 signal intensity. The intensity of the reflections for a totally randomly oriented sample have been calculated and are shown on the graph as parallel lines for each of the crystal planes measured.

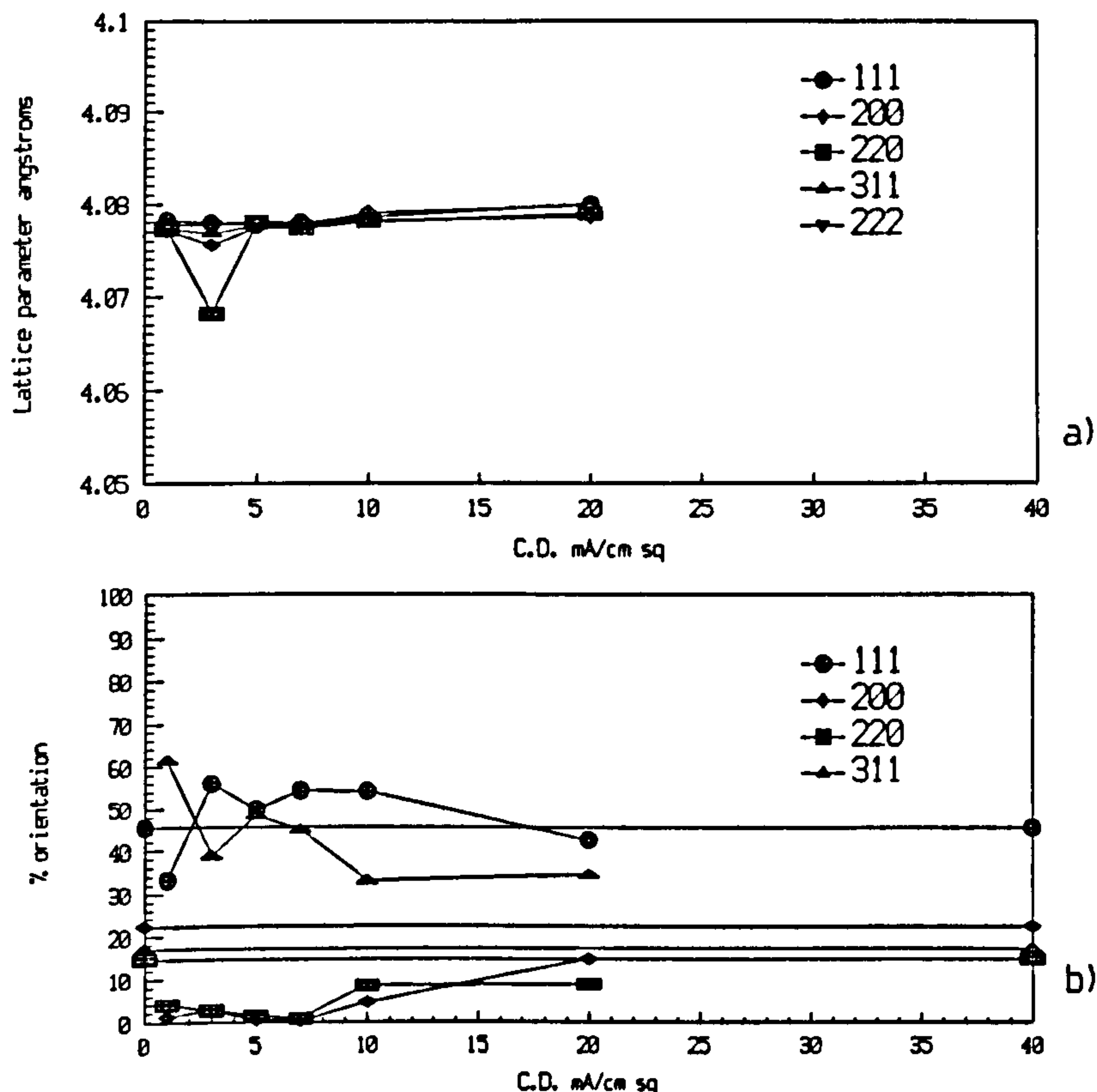


Figure 28. The relationship between current density and structural characteristics as determined by X-ray diffraction for a conventional pure gold deposit in terms of (a) Lattice parameter and (b) preferred orientation.

Analysis of the data from Figure 28(a) showed that all planes generally exhibited the same lattice parameter, although a slight increase was observed with increasing current density. The average lattice parameter of 4.077 was close to that of pure gold, which is generally accepted as being 4.0786 Å at 25°C. It is thought that the single point of the 220 plane that deviates from this is due to experimental error.

It was noted that, on calculating the crystallite size using the Scherrer method, a significant variation was observed, depending on the reflection. This was particularly evident at the higher current densities. An analysis of this is difficult as the line broadening observed has been assumed to be purely due to crystallite size and ignores the existence of strains and faults that may also contribute. Analysis of the 111 reflection using the Warren and Averbach method indicated that such an assumption was invalid as the crystallite size was found to be considerably greater (See Table 23). The actual crystallite size after correcting for strain was in the region of 0.23 µm. No evidence of faulting was observed.

Figure 28(b) shows the degree of preferred orientation of the deposit. It can be seen that by comparison with the expected ratios of the various planes (parallel lines) that there is a distinct 311 texture over the normal current density range of 1-7 mA cm⁻². Above this, the deposit tends towards a more random orientation.

The RMS strain of the conventional deposits was independent of current density over the range analysed and was comparatively low, calculated to be $\langle e^2 \rangle = 0.000035$.

The above measurements of a conventional deposit were necessary to compare and contrast with those produced under jetting conditions. Whilst a direct comparison cannot be made due to the orders of magnitude difference in the current densities applied, in terms of the morphological characteristics ie the structural changes that occurred with increasing current density, a comparison was considered to be valid. Figure 3 shows similar graphs for samples produced from the 0.17M citrate gold using a Re. No. of 12,000. The maximum current density under which useful deposits could be produced was found to be 6.0 A cm⁻². The lattice parameter of each of the crystallites was slightly smaller than the bulk value, with an average value in the region of 4.075 Å. However, at current densities below 2.0 A cm⁻², the lattice parameter exhibited a smaller size.

The crystallite size of the jetted sample calculated using the Scherrer equation was in the region of 200 Å for all but the 111 plane which showed a size of around 300 Å. It must be remembered that this method of estimating the crystallite size assumes all line broadening is attributable to grain size. The fact that the 222 planes were not the same as the 111 planes indicate that this assumption was incorrect. Further analysis of the line broadening revealed that this difference was due to residual strain, which over the current density range measured averaged $\langle e^2 \rangle = 0.0001275$. There was no evidence of either twin or stacking faults, except for a very low probability of $\alpha = 0.007$ at a low current density. The crystallite size of the 111 plane as determined by the Warren and Averbach method was found to be between 320 to 350 Å.

The preferred orientation of the jetted sample was found to be strongly 220 above a current density of 2.0 A cm⁻². Below this value, a 111 orientation predominated.

The RMS strain observed in these samples given in Table 23 was nearly an order of magnitude greater than for deposits produced under conventional conditions. There was, however, no clear relationship with current density.

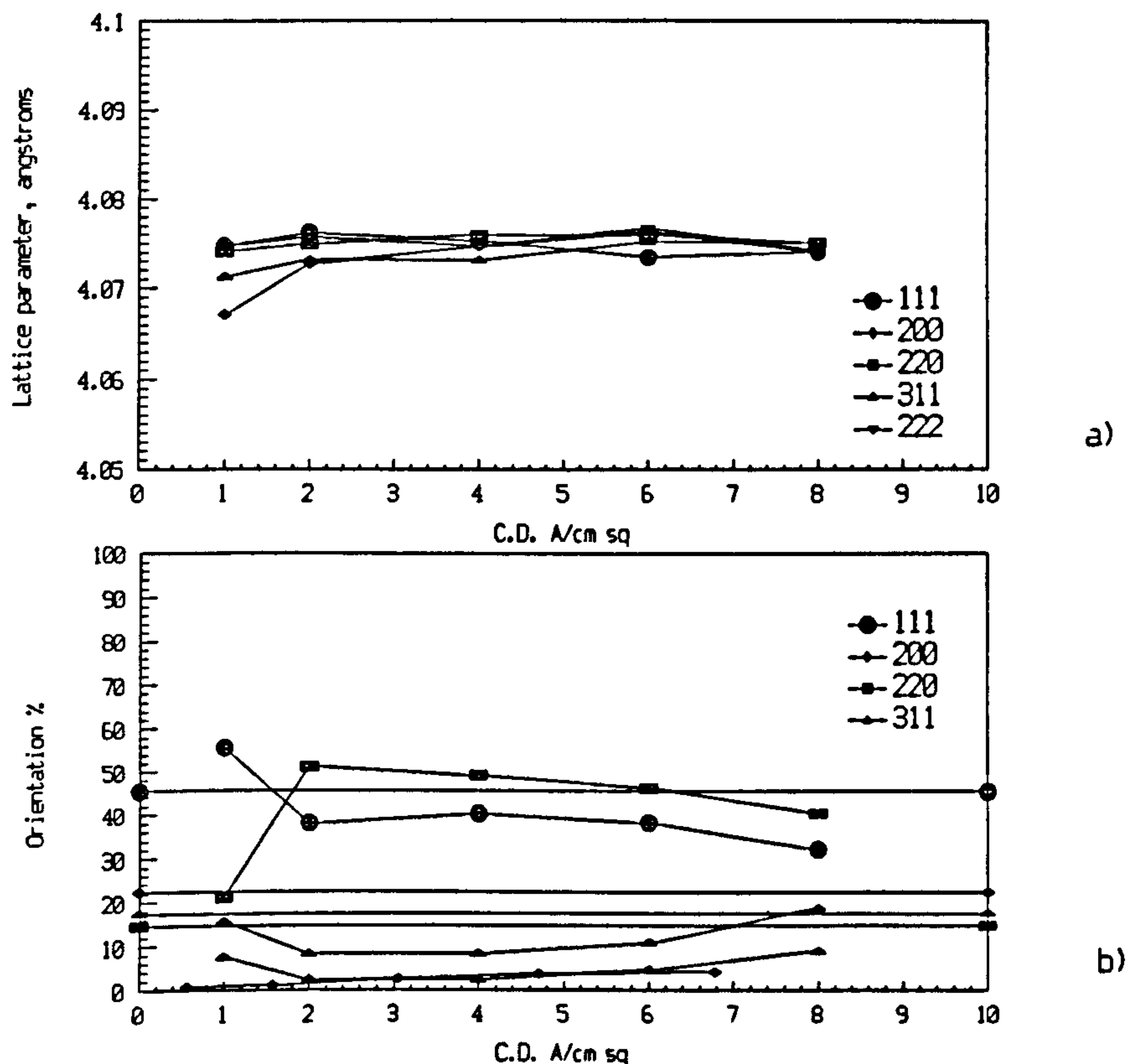


Figure 29. The relationship between current density and structural characteristics as determined by X-ray diffraction for a pure gold deposit produced by jetting in terms of (a) Lattice parameter and (b) preferred orientation. Reynolds No. = 12,000, Temp. = 55°C.

Polished and etched microsections of jetted samples can be seen in Photographs 15, 16, 17 and 18. These showed that there were few structural features apparent at current densities below 6.0 A cm⁻². Above this value, fan shaped, cell-like structures could be observed. These cells became apparent after a thickness of about 8 μ m had been achieved. Photograph 18 shows examples of these cells. Below 8 μ m, the cell structure was integral with the rest of the deposit but as the thickness increased, the cell "wall" exhibited a discontinuity. Extrapolation of the wall line showed a coinciding point close to the substrate surface. Topographically, these cells appear as nodules, increasing in size with increasing current density as well as deposit thickness. These structures clearly resemble the "rounded mounds" described by Nakahara⁷⁷, who studied the structure and morphology of gold alloy deposits. He concluded that such structures formed as a result of an inhibition process that forced a small crystallite size to be produced as well as forming the rounded mound structure.

8.1.3 The effect of electrolyte velocity

The velocity of the electrolyte played an important role in the morphology of the deposits produced. As the velocity was increased, so the deposit became smoother for any particular current density and temperature. This effect can be seen clearly in Photographs 19, 20 and 21. The overall influence of the Reynolds No. can be seen clearly in the morphological diagrams in figures 18 to 23. However, the deposits produced at a temperature of 25°C did not follow this trend particularly for the samples produced from the phosphate electrolyte. The citrate electrolyte exhibited a reduction in the value of the current densities at which smooth deposits were produced at high velocities at this temperature. The morphological diagrams also revealed that the velocity modified the growth behaviour of the deposits at current densities above those at which the deposit was no longer smooth. This was particularly evident at the higher metal ion concentrations.

The velocity did not appear to have any significant influence on the selectivity.

8.1.4 Temperature effects.

It can be seen from the morphological diagrams that for any particular current density and flow rate, the temperature generally increased the current density at which smooth deposits were obtained. For example, the transition between smooth and nodular deposits at a temperature of 25°C and a Reynolds No. of 6000 was in the region of 3.0 A cm⁻² for the 0.28M citrate electrolyte. At 40°C, this increased to about 3.8 A cm⁻² and at 55°C to 4.0 A cm⁻². The temperature also influenced the type of growth of deposits above this transition. The 0.28M citrate electrolyte produced a transition from smooth to needle type deposits at 25°C but at 55°C, the transition was from a smooth to a nodular structure. Similar effects could be seen for deposits produced from the other electrolytes used.

8.1.5 The influence of the gold concentration.

As the gold content of the electrolyte was increased, so the maximum useful current density and deposition rates increased. However, a maximum was reached in the region of 0.17M where increasing the concentration led to a slight reduction in the maximum useful current density. The maximum useful current densities and deposition rates achievable over the range of deposition conditions tested are listed in Table 24

From these results, it is evident that the type of supporting electrolyte, as well as its pH, has a significant influence on the maximum current density and plating rate.

8.1.6 The effect of pH

It was found that the deposit structures of the citrate electrolytes improved by increasing the pH to 8.1. This allowed a greater deposition rate to be achieved. Photographs 22, 23 and 24 show deposits from the 0.28M citrate electrolyte at pH values of 5.3, 6.1 and 8.1 respectively.

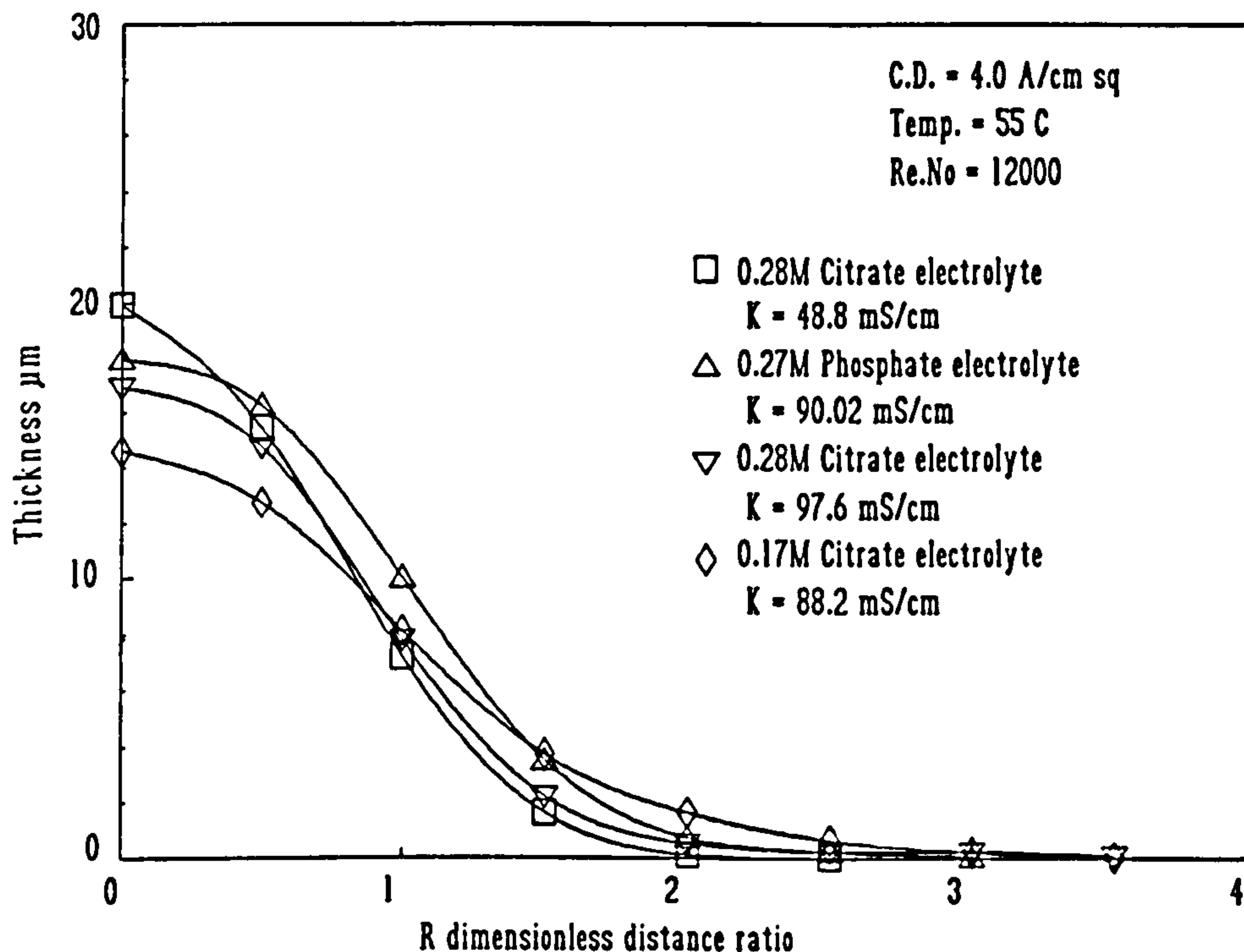


Figure 30. The effect of a reduced conductivity on the selectivity compared with equivalent higher conductivity electrolytes.

8.1.7 The role of electrolyte conductivity.

The low conductivity electrolyte in Table 1 was used to examine the effect of electrolyte conductivity. Figure 30 shows the effect of the reduced conductivity on the selectivity in comparison with equivalent electrolytes. Also shown is the lower concentration 0.17M citrate electrolyte. It can be seen that there is a noticeable improvement in the selectivity from the low conductivity electrolyte compared with the others. In particular, there is a 17% improvement over the equivalent

higher conductivity citrate electrolyte. However, the deposit quality deteriorated at a much lower current density of about 3.75 A cm^{-2} . Despite this, reasonably good deposits could be produced at a plating rate of $2.3 \text{ } \mu\text{m/second}$.

8.1.8 The influence of nozzle size.

The size of the nozzle has a marked influence on both the selectivity of the deposit as well as the maximum deposition rate obtainable. Two other nozzle diameters were briefly examined during this study, a $100 \text{ } \mu\text{m}$ and $540 \text{ } \mu\text{m}$.

8.1.8.1 Increased nozzle size.

Little work was carried out with the $540 \text{ } \mu\text{m}$ diameter nozzle. Results indicated that both the deposition rate and selectivity were similar to the $400 \text{ } \mu\text{m}$ nozzle.

8.1.8.2 Decreased nozzle size.

Using the $100 \text{ } \mu\text{m}$ nozzle, a Reynolds number of just 3233 could be obtained due to pressure limitations of the pump. Comparison of Figure 31 with Figure 27 shows that the deposition rate was reduced when compared to equivalent current densities using the $400 \text{ } \mu\text{m}$ nozzle. In addition, the selectivity was not as good. One important experimental factor may have been influential in the reduced selectivity. Due to the nozzle interfering with the flow at close proximities to the substrate, it was not possible to maintain an H/d ratio of 1.25 as in the experiments with the other nozzles. Instead, a H/d ratio of 10 had to be used. It was observed that selectivity becomes reduced with increasing H/d ratios (see Section 8.1.1.) and this probably accounts for this behaviour. No further experiments were carried out to verify this as using lower ratios would be impractical for commercial use. The deposition rate reduction is harder to account for in terms of experimental procedures and this will be discussed later.

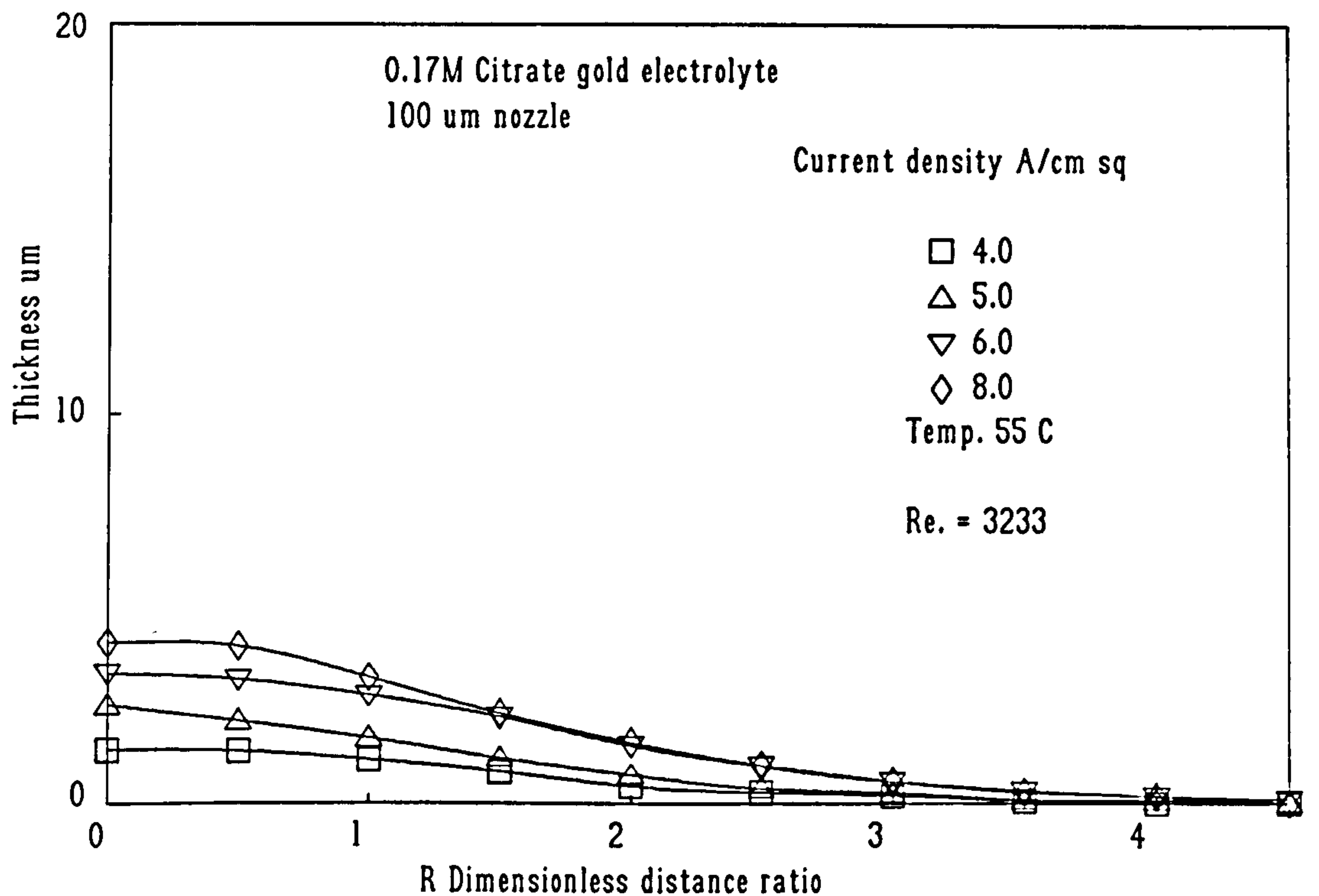


Figure 31. The selectivity of pure gold using a 100μm nozzle.

8.1.9 Pure gold deposition using pulsed current.

The application of pulsed current has been shown to improve deposit quality under conventional deposition conditions. Having established the factors that gave the highest deposition rates under DC conditions, the influence of pulsed current was established. The conditions of deposition are given in Tables 16 to 18. Examination of the deposits produced enabled a detailed morphological diagram to be produced for an average current density of 6.0 A cm⁻². This is shown in Figure 32. Figure 33 shows a morphological diagram of deposits produced at an average current density of 8.0 A cm⁻². However, this is less detailed due to the fewer samples produced at this current density. From figure 32, it can be seen that there were a wide variety of morphological structures produced. Typical structures can be seen in Photographs 25, 26, 27, 28 and 29. For both average current densities, it can be seen that there is a narrow region of both low duty cycle and short on-time at which smooth deposits were produced. None of the smooth deposits were as good as those produced by DC as can be seen in Photograph 28 with obvious gaps between the surface nodules. Deposits that did exhibit equally good structures as those deposited by DC were produced at lower deposition rates.

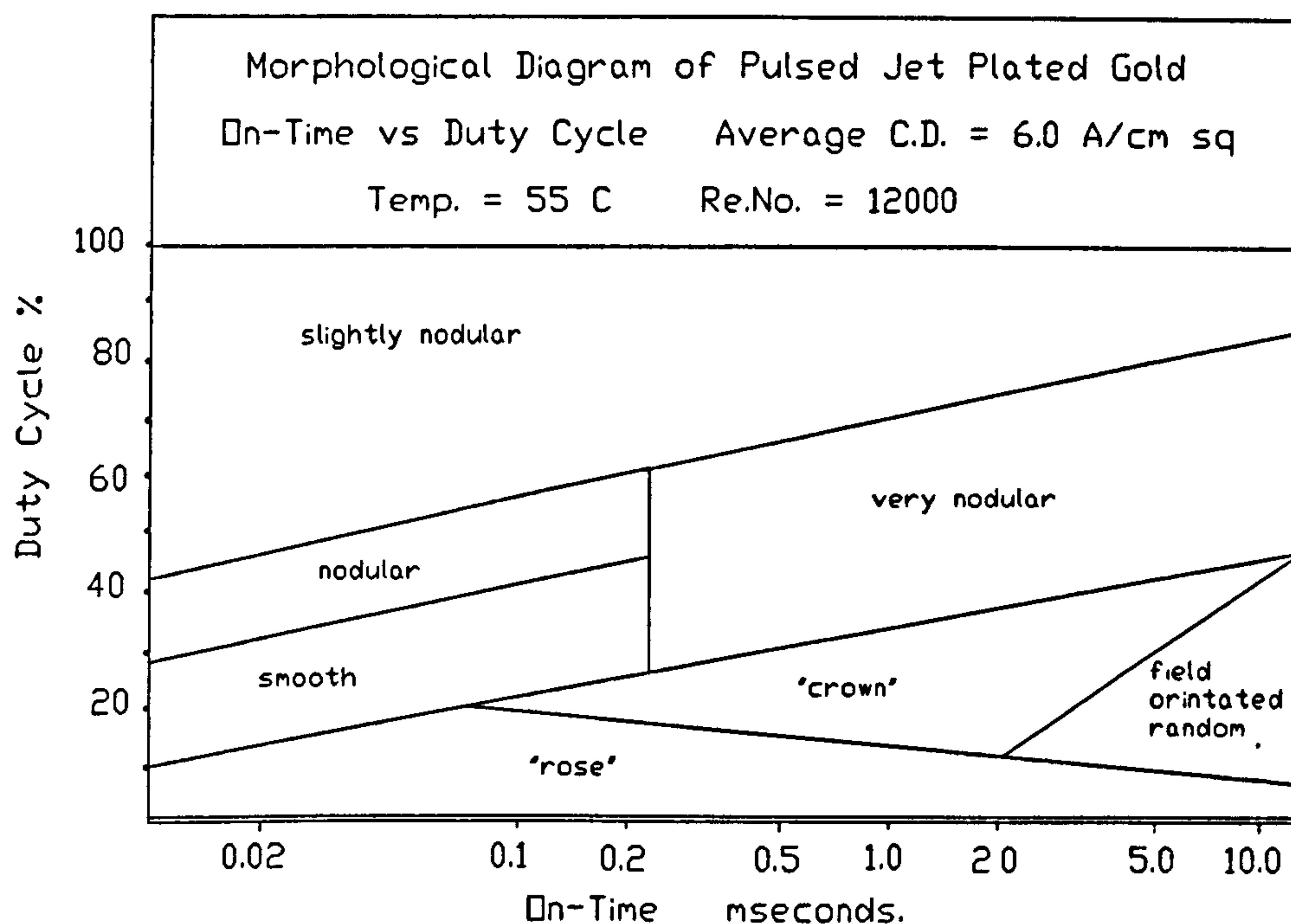


Figure 32. Morphological diagram of on-time vs duty cycle at an average current density of 6.0 A cm⁻².

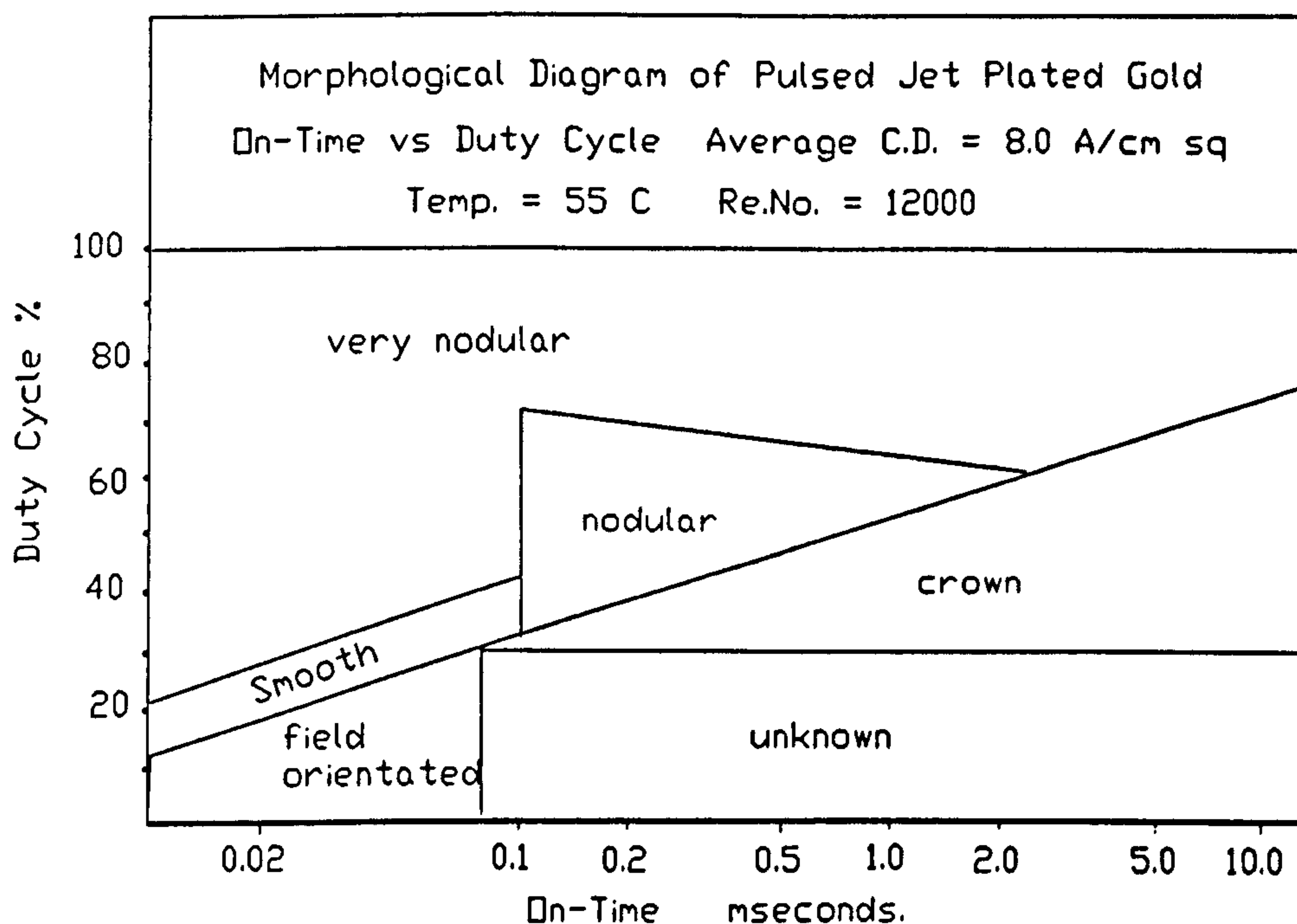


Figure 33. Morphological diagram of on-time vs duty cycle at an average current density of 8.0 A cm⁻².

8.1.9.1 Variation of the average current density.

Increasing the average current density led to a decrease in the size of the smooth window. An increase in the plating rate was also observed, up to a maximum of $5.5 \mu\text{m/sec.}$ at an average current density of 9.0 A cm^{-2} . Increasing the average current density further reduced the plating rate to less than $3.0 \mu\text{m/sec.}$ However, SEM examination revealed an even greater level of porosity. Examination of all the samples showed that a deposition rate of $3.5 \mu\text{m/sec.}$ could not be exceeded using pulsed current deposition without the introduction of inter-granular porosity. Overall, there was an increased tendency towards nodular and dendritic deposits with increasing average current density.

8.1.9.2 Variation of the on-time.

Increasing the on-time led to an increased number of nodules formed and an increase in the size of nodules. A increase in the rate of dendritic structure formation was also seen especially at duty cycles below 60%.

8.1.9.3 The effect of increasing the duty cycle.

Low duty cycles produced dendritic, needle like, crown shaped or rose shaped deposits, particularly with increasing on-times. High duty cycles tended to produce nodular deposits irrespective of the on-time. The most suitable duty cycles were between 20 and 40 %.

8.1.9.4 The influence of pulsed deposition on selectivity.

Figure 34 shows a selectivity plot comparing a DC and a pulse plated spot. The average current density of the pulse plated spot is the same as that used for the DC plated sample, that is 6.0 A cm^{-2} . It can be seen that there is an improvement in the selectivity in the pulse plated sample. The reason for this behaviour would seem to be that the peak pulse current densities were high. In this example, the peak current density was 30 A cm^{-2} . Under these conditions, the electric field intensity within the jet was much higher during the on-time than under DC conditions thus enhancing the primary current distribution. This led to less lateral deposition outside the impingement region.

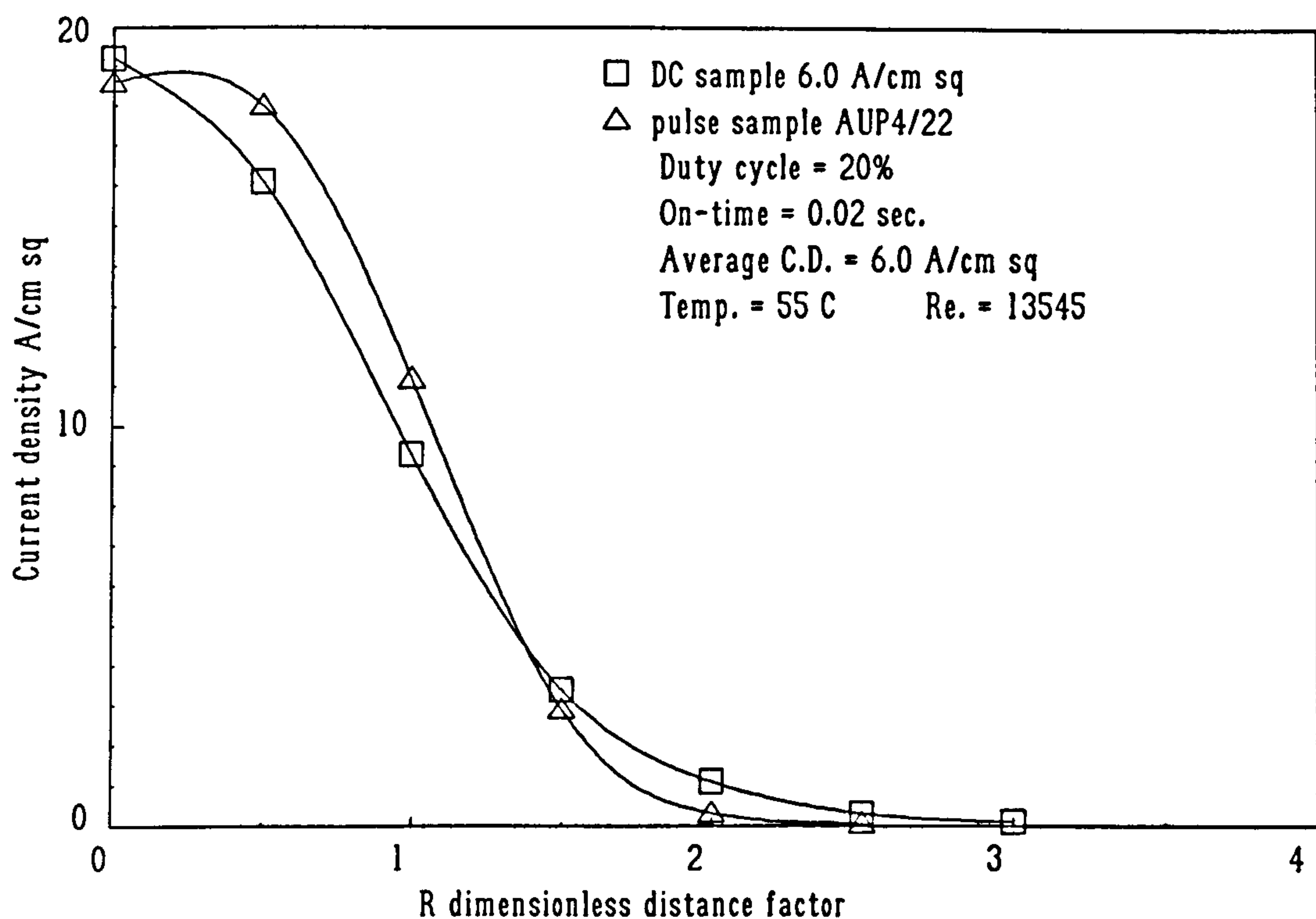


Figure 34. A selectivity plot comparing a pulsed current deposit with the equivalent DC deposit.

8.1.10 Examination of the limiting factors controlling maximum deposition rates.

Having established the electrolyte and the deposition conditions that gave the greatest plating rates together with deposits of acceptable quality and selectivity, the mechanisms by which the deposit deteriorated could be examined. These were established by means of both electrochemical and structural observations.

8.1.10.1 Mass transfer studies.

Because the limiting current density controls the maximum rate at which electrodeposits can be produced, polarisation curves were prepared to identify this value and the ratio of i/i_L at which jetted deposits began to deteriorate. As described in Section 7.4. two techniques were applied, Sampled Current Pulse Voltametry, SCPV and Sampled Voltage Pulse Amperometry, SVPA.

8.1.10.1.1 Sampled Voltage Pulse Amperometry.

This method was tried initially as it was simpler to set up and operate. In addition, as mentioned in Section 3.2.1.2. there was less likelihood of problems with surface roughening with galvanodynamic methods as with potentiodynamic methods. Figure 35 shows a polarisation curve of the 0.17M citrate gold system. No compensation for the IR drop between the reference and working electrode was used. It can be seen that there is no clear limiting current plateau. However, a large Tafel region is visible. The slope of the Tafel line was calculated to be -330 mV/decade. The maximum useful current density for these conditions was in the region of 3.0 A cm⁻². This lies beyond the Tafel area in what would appear to be a mixed activation/diffusion controlled region. At the high current density end, the slope of the curve alters. This could indicate the post limiting current region but there was no evidence to confirm this.

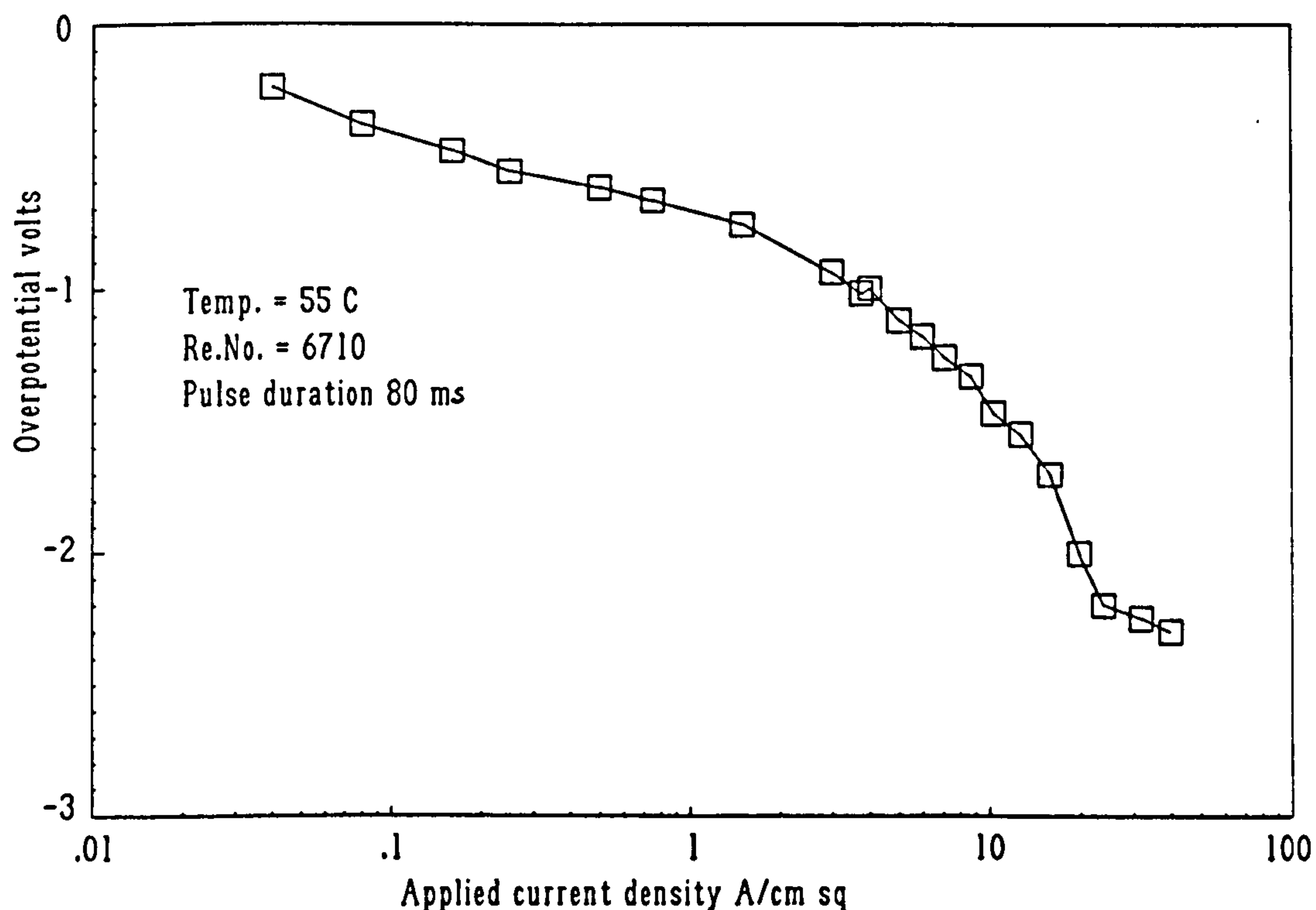


Figure 35. Polarisation curve for the 0.17M citrate gold electrolyte using SVPA

One problem with obtaining information using this technique was the influence of superimposed 50Hz noise on the signals, particularly at low applied current densities. The source was from surrounding equipment but despite efforts to shield and isolate the cell and sensing resistors this problem could not be eliminated.

8.1.10.1.2 Sampled Current Pulse Voltametry.

It was found that using SCPV, the noise problem encountered with the other technique could be reduced although not eliminated. This made signal measurements much easier. Figure 36 shows the polarisation curves for the 0.17M citrate gold electrolyte at three different values of Reynolds No.

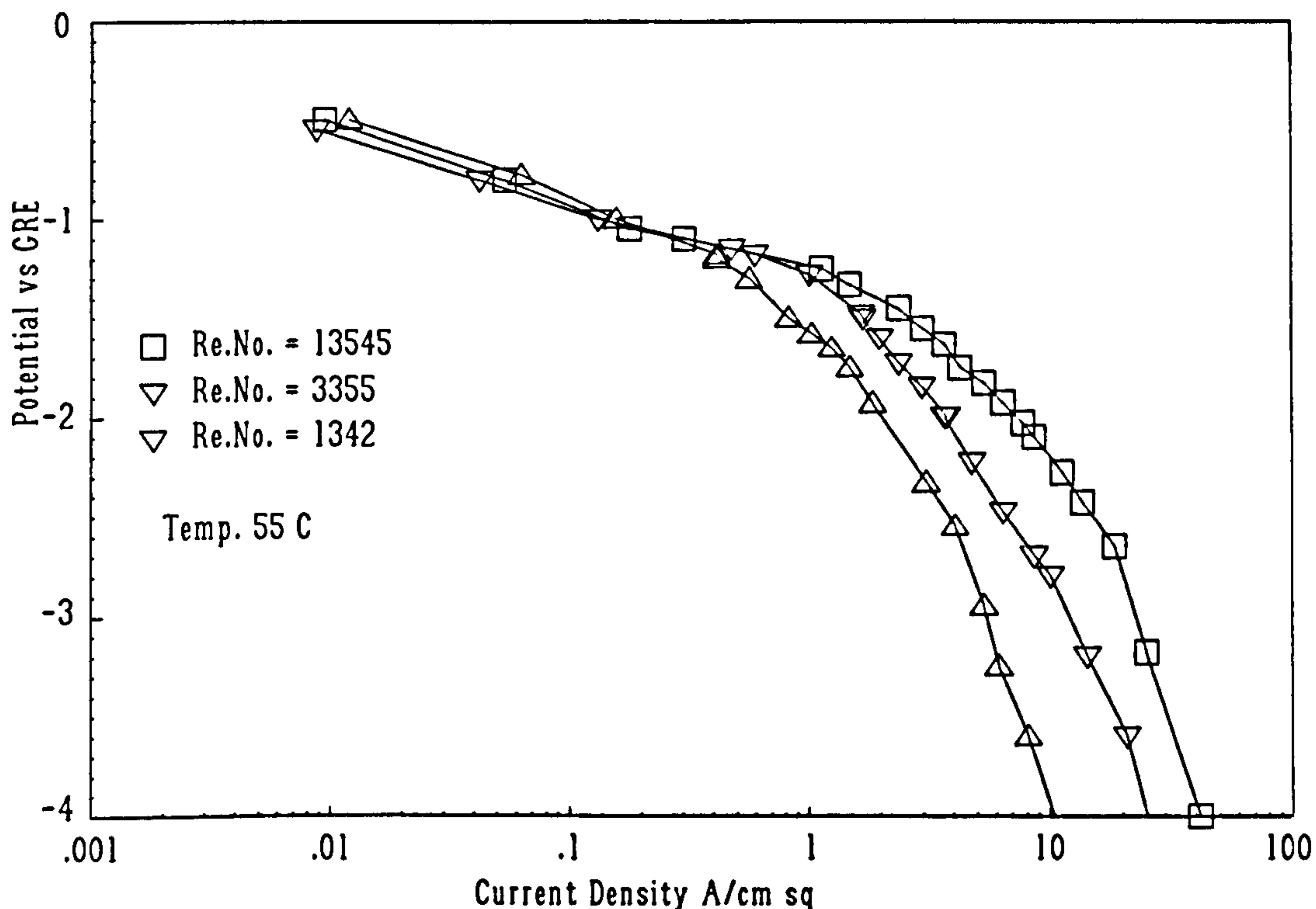


Figure 36. Polarisation curves for the 0.17M citrate gold electrolyte using SCPV.

Once again, no clearly defined limiting current density plateau could be seen. In order to establish if this was due to purely electrochemical factors or was a function of the measurement technique, the method was applied to a copper sulphate electrolyte. The electrolyte chosen was one that has been used previously¹²⁵ for mass transport studies. The formulation was 0.014M CuSO_4 with 1.5M H_2SO_4 as supporting electrolyte. The method was applied to this electrolyte and the polarisation curves produced as in Figure 37. With this electrolyte, it can be seen that a definite limiting current plateau can be seen for all three values of Reynolds No. The limiting current densities were found by calculating the mid-point between the lowest point on the plateau and the highest. These are listed below.

Reynolds No.

Limiting current density

1843

0.367 A cm⁻²

5252

0.470 A cm⁻²

7538

0.591 A cm⁻²

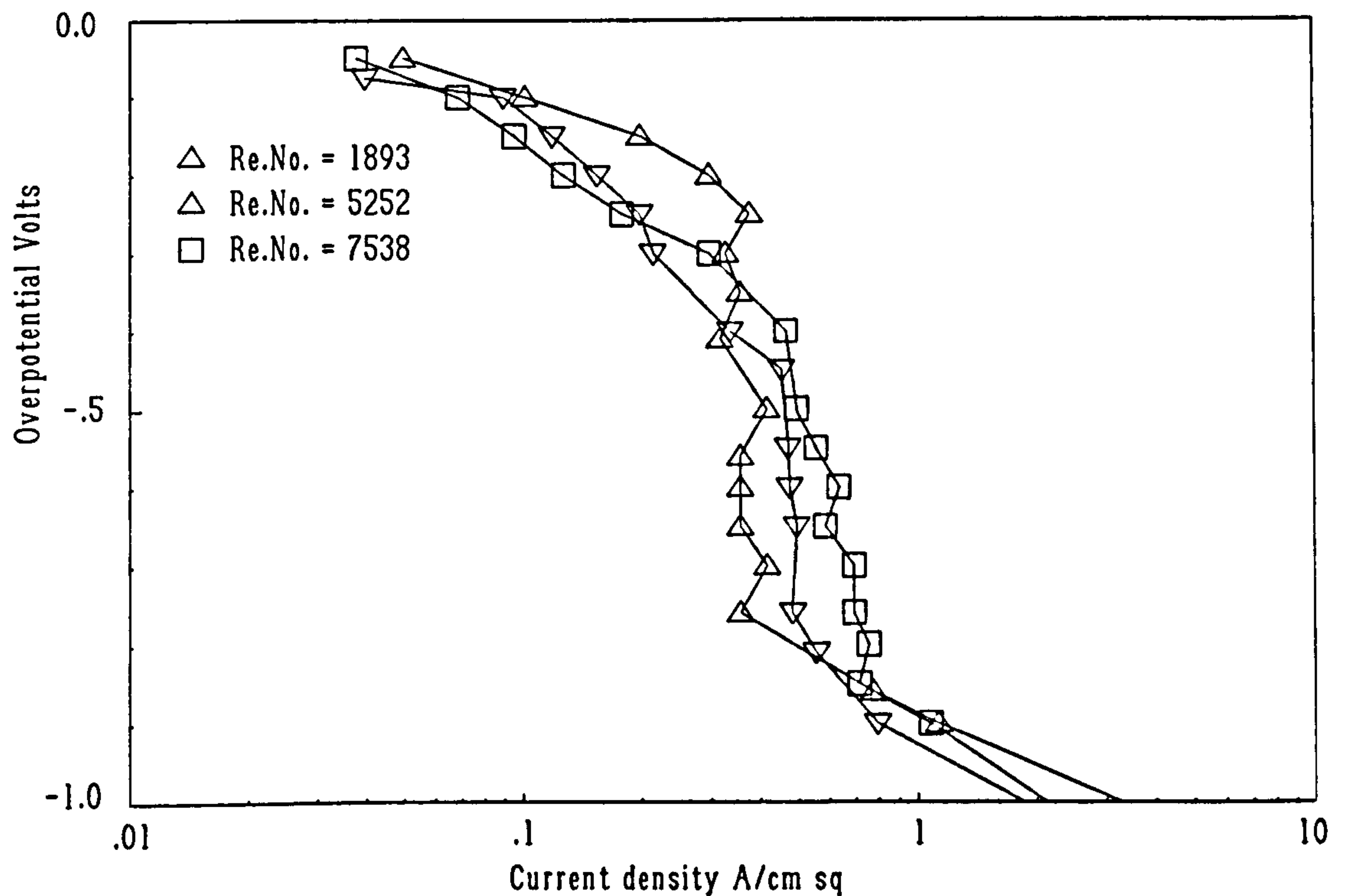


Figure 37. Polarisation curves for a 0.014M CuSO₄ electrolyte at 25°C using SCPV

It can be concluded that whilst the data points on these curves are subjected to some individual variations, they do appear to be valid and were repeatable to within a variance of better than 10%. It should be noted that although there appears to be a linear region prior to the limiting plateau, this is unlikely to be the Tafel region. Evidence for this is that the slope varied in a positive direction with increasing Reynolds No. between 1500 and 7000. The onset of turbulent flow occurred for this system in the region of 2000. This would indicate that this apparent linear region was in fact the mixed activation/diffusion controlled domain. In addition, as copper in a sulphate electrolyte is highly reversible, it has a low activation energy for deposition and a well defined Tafel region would not be expected.

The limiting current densities obtained were used to obtain the Sherwood number relationship with the Reynolds number. As the diameter of the cathode was the same as that of the nozzle, an impingement correlation was deemed most suitable for analysis. It was found that by using the correlation obtained by Alkire and Chen.¹⁰⁸

$$Sh = 21.03 Re^{0.448} \quad (29)$$

the data from the turbulent flow experiments agreed to 10% and 20% for $Re = 7000$ and $Re = 10800$. If it is considered that some deposit growth was experienced during the measurements, some variations could be expected. Additionally, if a complete, steady state equilibrium was not achieved, this would be expected to lead to higher values of limiting current densities.

Other workers who have attempted to measure limiting current densities for pure citrate gold electrolytes have also been unsuccessful. However, as described in Chapter 2, the addition of a few ppm of lead has been shown to interfere with the hydrogen evolution reaction and allow a limiting current plateau to be observed. However, the addition of lead to the electrolyte was not considered, as a limiting current density obtained by this method would not necessarily be applicable to the results obtained in the absence of lead. As has been described earlier, lead and other metallic gold additives can lead to poor gold wire bonding performance.

8.2 GOLD ALLOY DEPOSITS.

Having established the basic controlling factors with the pure gold electrolyte system, these factors were then applied to the production of alloy gold deposits. Three commercial electrolytes were chosen for initial studies, Ronovel N, containing nickel, Ronovel CM, containing cobalt and Auruna 7000, containing iron. Samples were prepared as described in Section 8.3.2.1. As was observed with the pure gold samples, all the electrolytes exhibited maximum deposition rates at the higher gold concentrations. The maximum useful plating rates and current densities found are listed in Table 25.

Whilst the Auruna 7000 solution gave the greatest deposition rate, examination of the deposits produced showed that at these high plating rates, the spots were fracturing the underlying glass substrate and exfoliating, indicating high levels of internal tensile stress. For this reason, Auruna 7000 was not used for further trials. In addition, whilst the cobalt and nickel alloy golds are generally accepted within existing specifications, the iron alloy golds are relatively new and would present a greater difficulty in gaining acceptance commercially. The Ronovel CM electrolyte

showed significant evidence of instability, with what appeared to be single gold cyanide precipitating on the container walls after several hours use in the jetting equipment. For these reasons, the Ronovel N electrolyte was chosen for further examination.

As Ronovel N was a proprietary electrolyte, the composition was not disclosed. However, it was known from the safety data supplied that the basic electrolyte was composed of an oxalic acid/alkali metal oxalate/phosphonate mixture. As supplied, the basic electrolyte also contained an addition agent referred to as "booster". This was a solution of nicotinamide with some oxalic acid. The purpose of this addition agent was claimed to allow operation at an increased current density and plating rate.

8.2.1 The influence of deposition parameters for the Ronovel N electrolyte with no nickel.

In order to establish the basic deposition parameters for this electrolyte, a series of trials were initiated using the basic electrolyte and a gold concentration of 20 g l⁻¹ but with no nickel added. As was found with the pure gold, the maximum useful current density was influenced by the electrolyte velocity. At a Reynolds No. of 1000, the maximum useful current density was found to be 2.0 A cm⁻², at a Reynolds No. of 2600 it was 3.5 A cm⁻², whilst at a Reynolds No. of 10,600 it was 4.25 A cm⁻². On the basis of these results, it was again evident that to obtain the highest deposition rates, high electrolyte velocities would be required. A temperature of 55°C was chosen for the remaining trials in accordance with the manufacturers recommendations. Tables 19 to 21 give full details of the conditions used.

The basic Ronovel N electrolyte containing no nickel but with 60 ml l⁻¹ "booster" produced semi-bright deposits. Optical examination revealed that the deposit topography exhibited a rounded mound appearance over a wide current density range, the size of the mounds increasing with increasing current density. The nodules were approximately twice the size of the equivalent thickness of pure gold deposited under identical jetting conditions. As with the pure gold samples, it was clear that surface features were amplified as the plating time and thus the thickness increased. Photograph 30 shows an optical micrograph of a 17.2 µm deposit from this electrolyte produced at a current density of 8.0 A cm⁻². Photograph 31 shows a microsection of a similar deposit but produced at a current density of 9.0 A cm⁻². It can be seen that unlike the pure gold electrolytes, the nodulation would seem to have commenced as deposition proceeded and not during the initial stages of growth. Above a current density of 9.0 A cm⁻², the nodule size was reduced but with an increase in the number of nodules.

Photograph 32 shows a typical microsection of a gold/nickel alloy produced from a Ronoval N electrolyte that contained nickel as well as booster. This particular sample contained 3.0 g l⁻¹ and 60 ml l⁻¹ booster. An "inverted cone" structure associated with one of the surface rounded mounds can clearly be seen. In the case of nickel containing deposits, the roots of the mounds originated at or near the substrate surface.

The deposition rate was considerably less than that of the pure gold for the equivalent current densities although higher current densities could be obtained without serious degradation of the deposit.

Increasing the booster concentration to 80 ml l⁻¹ reduced the plating rate by a further 20% with no observable improvement in the deposit topography.

8.2.2 The effect of the addition of nickel to the basic Ronoval N electrolyte.

The following additions of nickel additive were made to the basic electrolyte; 0.5 g l⁻¹, 0.7 g l⁻¹, 1.1 g l⁻¹, 1.5 g l⁻¹, 2.2 g l⁻¹, 2.5 g l⁻¹ and 3.0 g l⁻¹. With each increment, deposit spots were produced for topographical examination, nickel content of the deposit, hardness and XRD examination. Two sets of samples were produced. The first set were plated to a thickness of > 16 µm so that comparisons with pure gold could be made. In addition, thick deposits were required for the testing of the physical characteristics of the deposit. The second set were plated to a thickness of ≈ 2.5 µm, a more realistic value for use in production. These were produced from an electrolyte containing 1.9 g l⁻¹ nickel.

8.2.2.1 Relationship between nickel in the deposit, nickel in the electrolyte and current density.

Figure 38 shows the relationship between the nickel in the electrolyte and the nickel in the deposit over a range of current densities. A linear regression has been applied to the data presented. It can be seen that a linear relationship exists for all concentrations of nickel used. The error bars indicate the analytical error of ± 6% of the nickel in the deposit. A further ± 5% error, not shown on the graphs, represents the analytical error for nickel in solution.

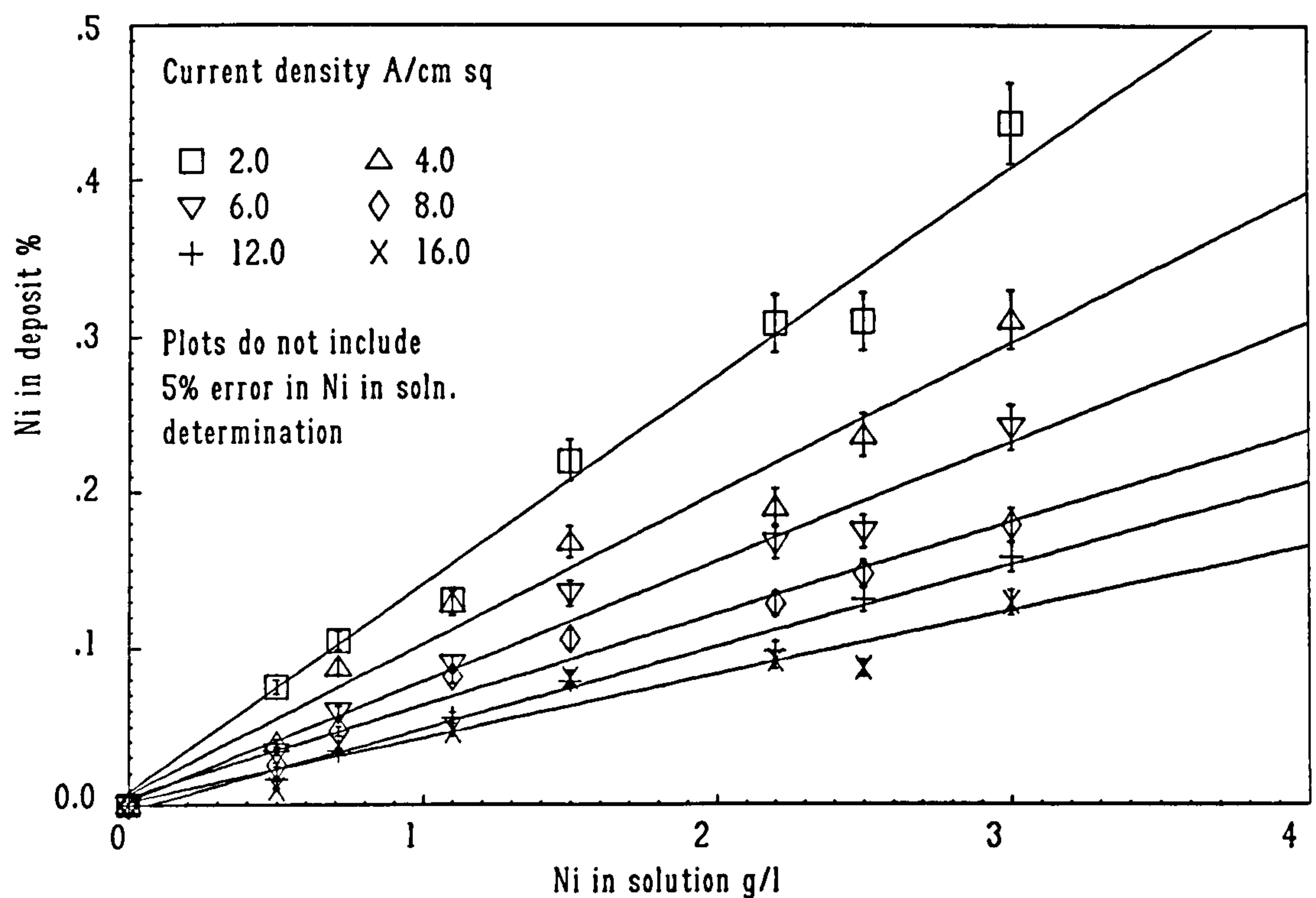


Figure 38. The relationship between the nickel in solution and the nickel in the deposit for different applied current densities

Figure 39 shows how the nickel in the deposit varied with the applied current density. A geometric regression analysis has been applied to the data to provide the best curve fit. Whilst this may be questionable for the lower concentrations of nickel in solution, its validity is quite clear at the higher values. There is no reason to believe, therefore, that such a relationship will be different for low values of nickel. The graph indicates that at low current densities, a greater quantity of nickel was incorporated in the deposit than at high current densities. This is understandable considering that the nickel in a citrate electrolyte is considerably more noble than gold unless it is strongly complexed.

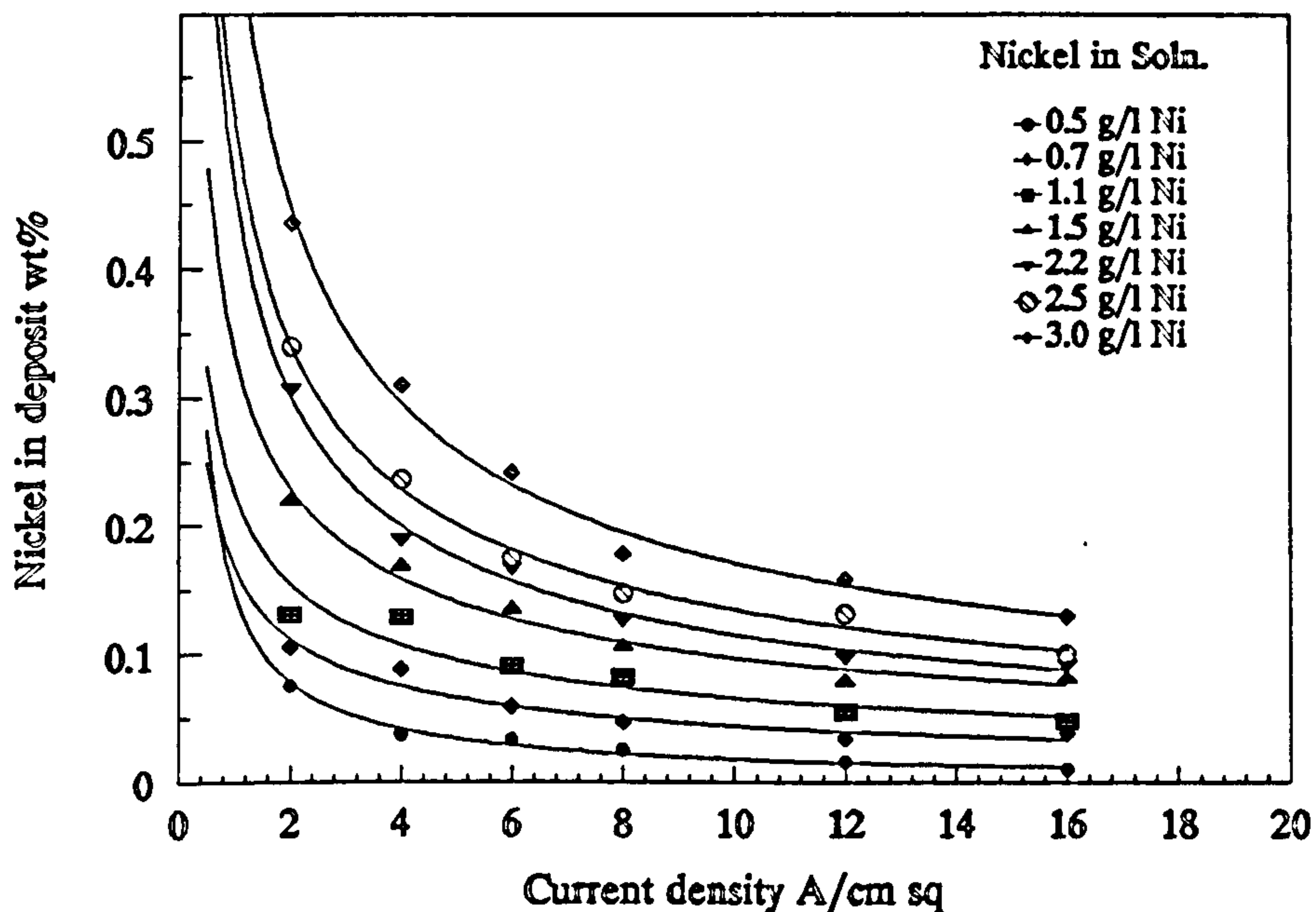


Figure 39. The relationship between the nickel in the deposit and current density for different concentrations of nickel in the electrolyte.

8.2.2.2 Deposit topography.

The addition of nickel significantly affected the surface topography particularly for thick deposits. Concentrations of nickel in solution greater than 0.7 g l^{-1} reduced the nodule size and smoothed the deposit when compared with those produced from electrolytes not containing nickel. An increase in the nickel content produced deposits with a marginal reduction in the size and frequency of surface features. Comparison between Photograph 30 and Photographs 33 and 34 show these effects clearly. However, the thicker samples showed evidence of high internal stresses at nickel concentrations of $> 2.2 \text{ g l}^{-1}$ as some of these showed signs of deposit cracking or fracturing of the glass substrate.

Photographs 35 and 36 show deposits about $2.5 \mu\text{m}$ thick. It can be seen that there are few surface features, with small nodules becoming apparent on those samples produce above a current density of 10.0 A cm^{-2} . By way of comparison, Photograph 37 shows a $2.5 \mu\text{m}$ thick gold/nickel deposit produced under conventional conditions.

8.2.2.3 Deposition rate.

Figure 40 shows the deposition rates obtained from electrolytes both with and without nickel. The samples with only 60 ml l⁻¹ booster and those containing nickel show roughly the same deposition rates and it may be concluded that the addition of nickel does not affect the deposition rate. Increasing the booster concentration in the absence of nickel does reduce the deposition rate significantly. Comparing Figure 40 with Figure 24, it can be seen that the presence of the booster reduced the deposition rate considerably.

It was found that a maximum deposition rate of 2.8 $\mu\text{m sec}^{-1}$ could be obtained from an electrolyte containing 60 ml l⁻¹ booster and ~ 2.0 g l⁻¹ nickel at a Reynolds No. of 10600 and a temperature of 55°C. These conditions also provided a similar hardness to those produced under conventional deposition conditions.

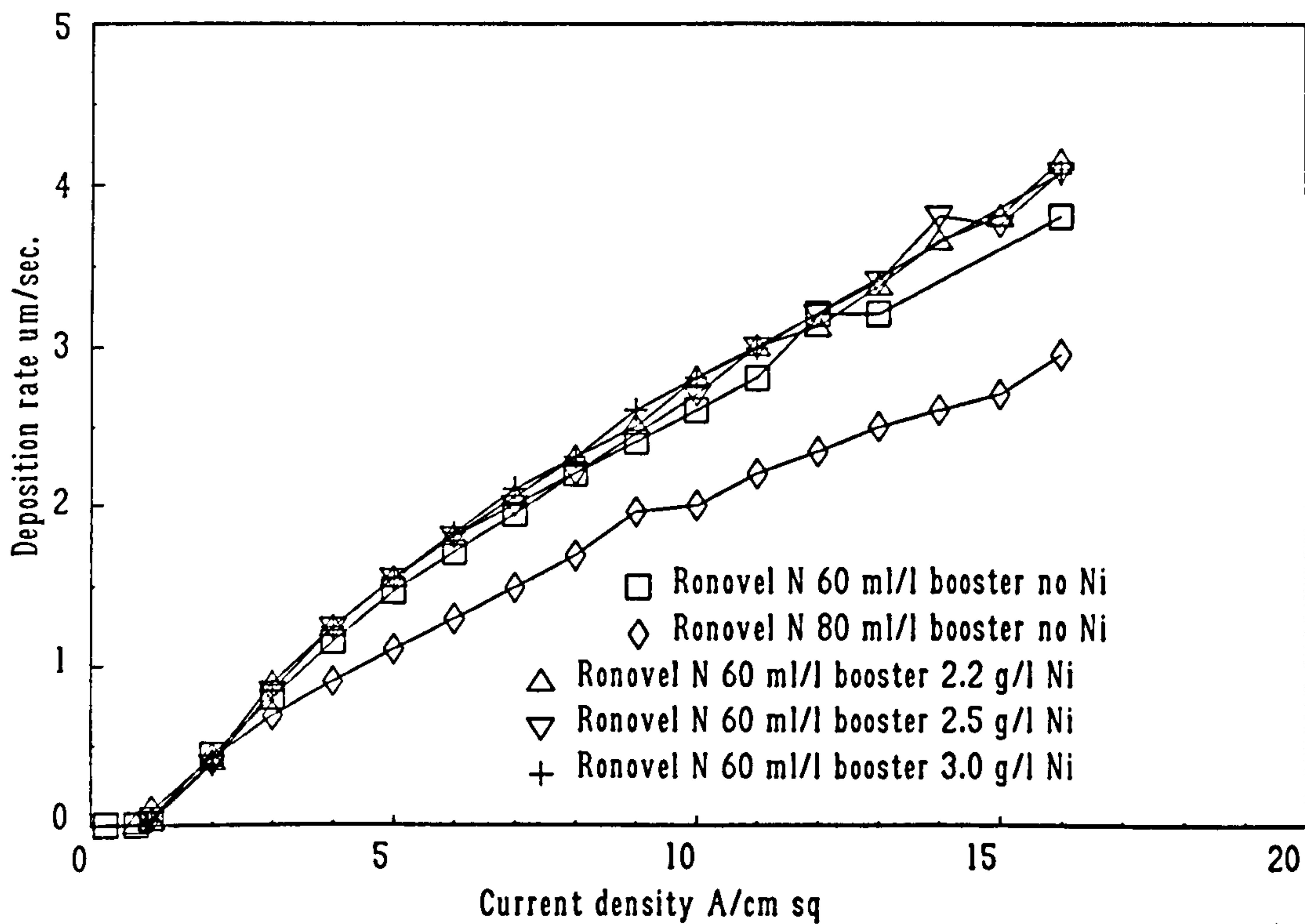


Figure 40. Current density vs deposition rate for various concentrations of nickel and booster in the Ronovel N electrolyte.

8.2.2.4 Current efficiency.

The current efficiency was measured for an electrolyte containing 1.9 g l^{-1} nickel and 60 ml l^{-1} booster. Figure 41 shows the relationship between the current density and the current efficiency. As with the pure gold, low current densities gave rise to low efficiencies in the region of 30%. At a current density of 3.0 A cm^{-2} , the maximum efficiency of about 60% was achieved after which it fell.

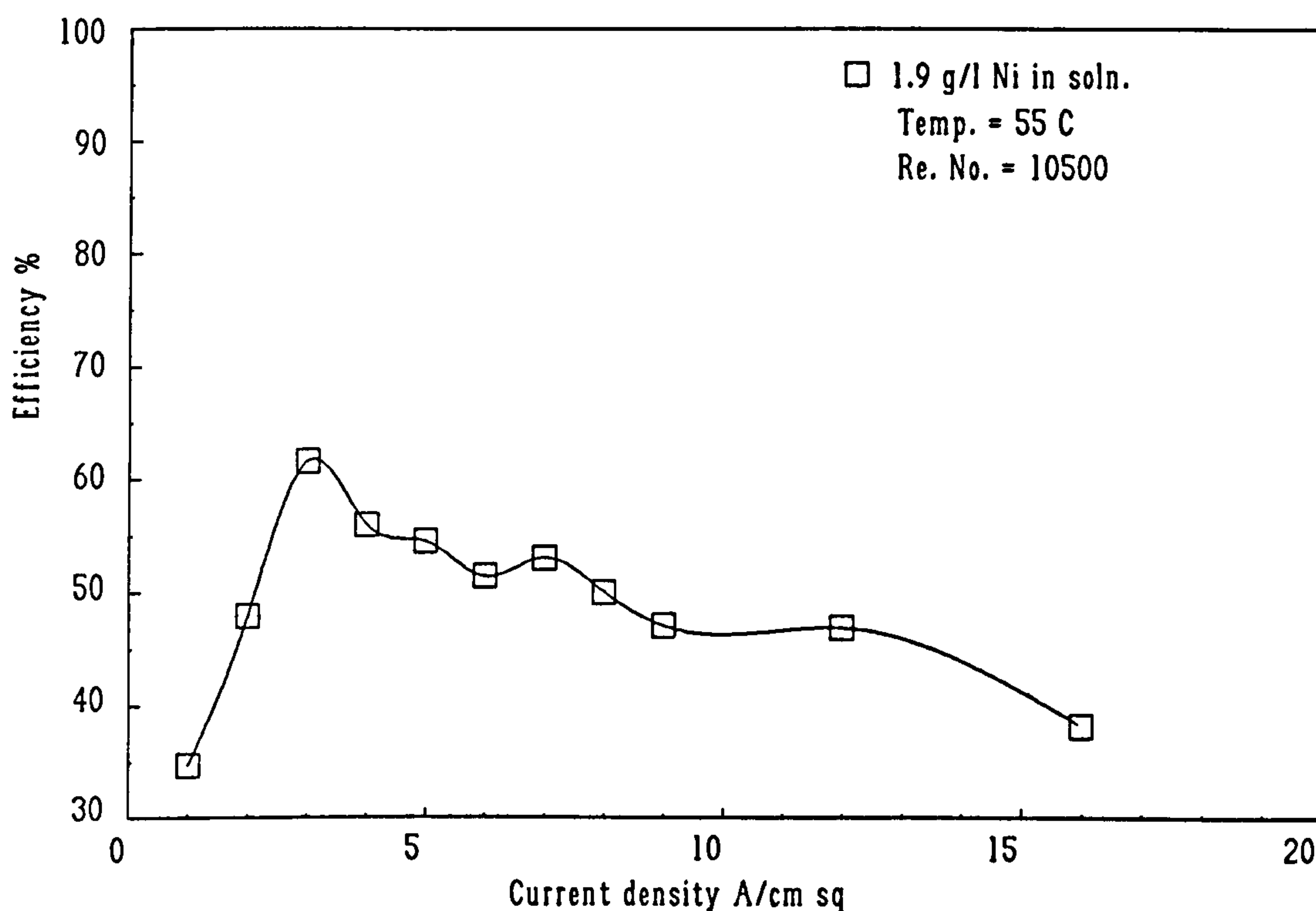


Figure 41. Current efficiency vs current density for the Ronovel N electrolyte containing 1.9 g l^{-1} Ni and 60 ml l^{-1} booster.

8.2.2.5 Hardness of the deposits.

Figure 42 shows the influence of nickel and booster on the hardness of the deposits at different current densities. The samples produced from the electrolyte containing 60 ml l^{-1} booster only were the hardest of all, being the equivalent hardness to pure gold deposits. An increase in the booster reduced the hardness of the deposits produced. Additions of nickel to the electrolyte containing 60 ml l^{-1} booster reduced the hardness proportionately. Referring to Figure 38 together with Figure

42, it is clear that at lower current densities, where the nickel in the deposit is greater, a lower hardness results. This is in conflict with the well known effect of the hardness increasing with the addition of nickel seen with conventional gold nickel alloys.

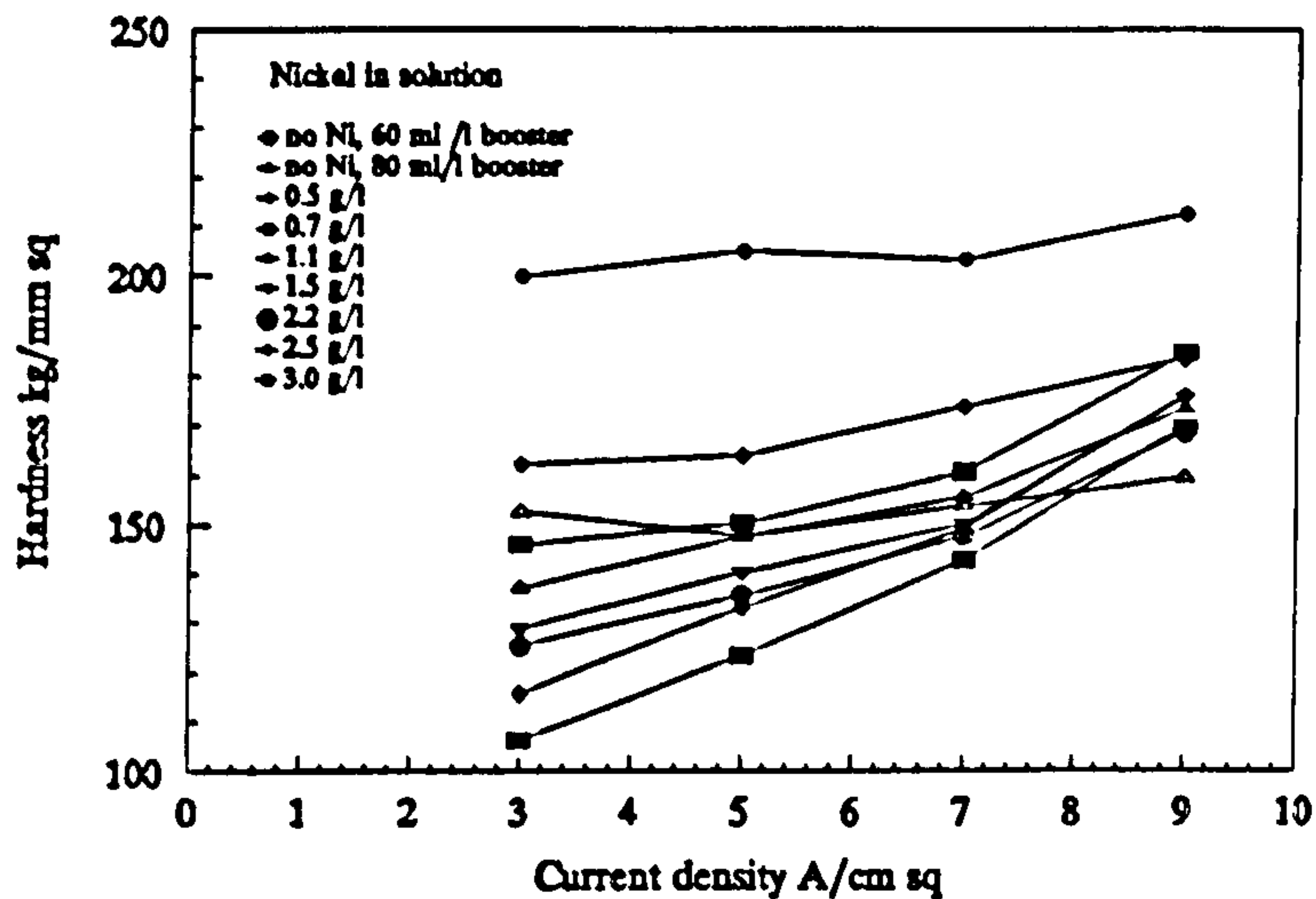


Figure 42. Deposit hardness vs current density for different concentrations of nickel in the electrolyte.

Figure 43 shows how the nickel in the deposit influenced the hardness when deposited at different current densities. It is evident from this graph that the quantity of nickel in the deposit was not the only factor affecting the hardness. Low nickel contents ($< 0.1\%$) showed roughly the same hardness values irrespective of the current density. This did not vary by much for samples produced at current densities below 5.0 A cm^{-2} . However, increased current densities exhibited different hardnesses for the same value of nickel in deposit. The relationship between the nickel in deposit, current density and hardness is summarised in Figure 44, which shows a 3-dimensional surface plot of each of the parameters.

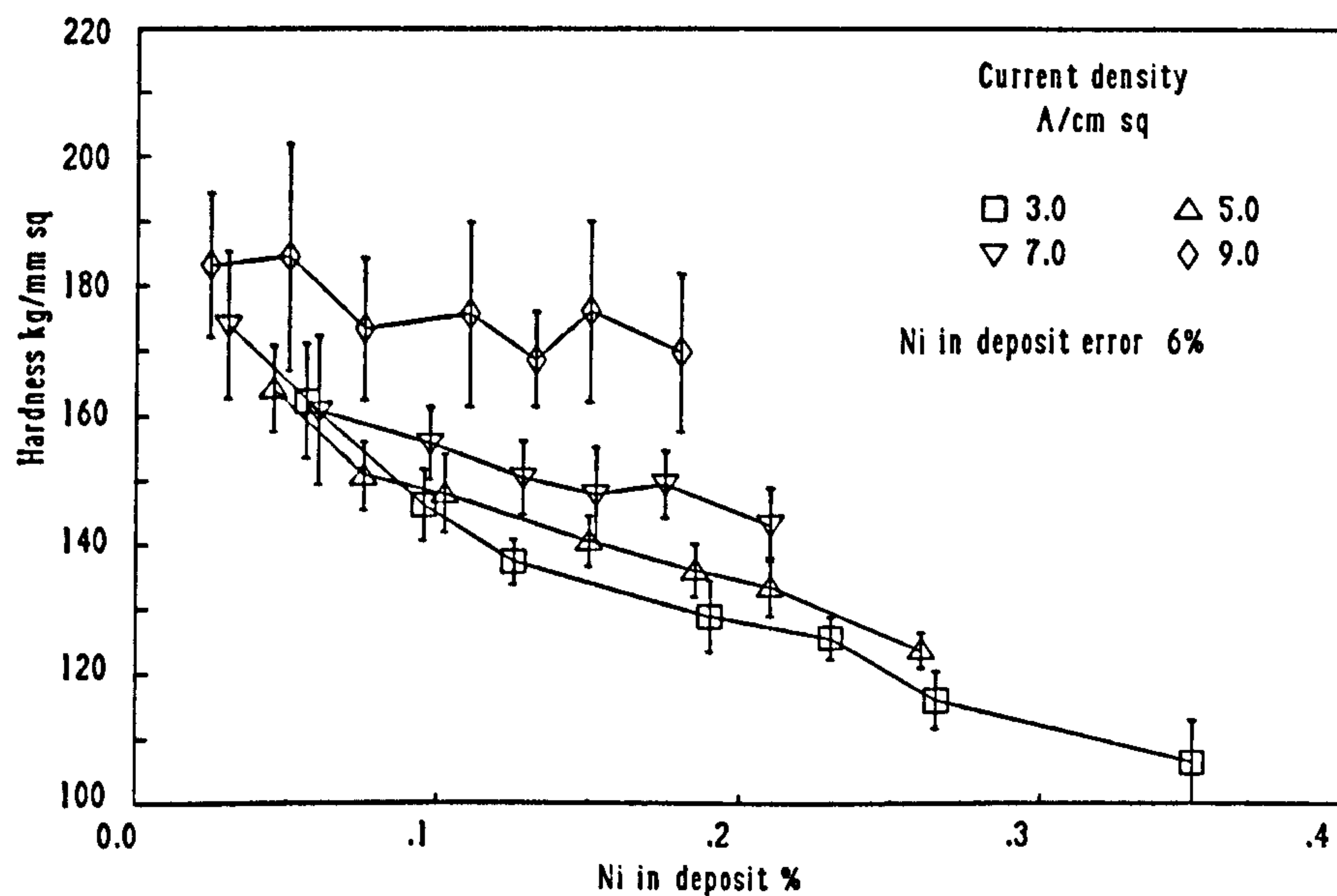


Figure 43. The relationship between nickel in the deposit and the hardness for different values of applied current density.

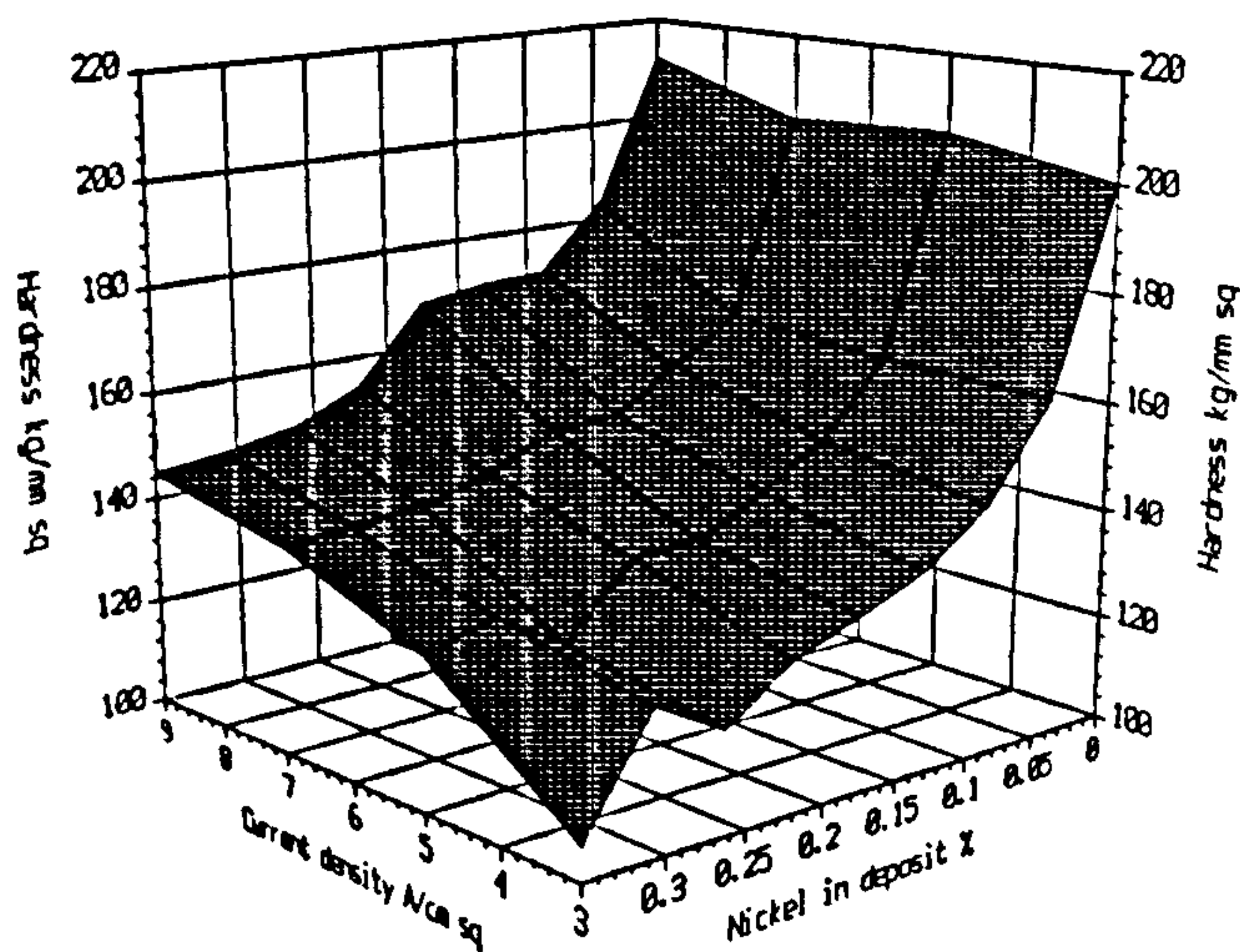


Figure 44. A 3-D surface plot summarising the relationship between current density, nickel in the deposit and hardness.

8.2.2.6 Selectivity of the deposits.

Figure 45 shows a selectivity plot of deposits from the Ronovel N electrolyte without nickel but containing 60 ml l⁻¹ of booster. It can be seen that the selectivity was not as good as the case of the pure gold deposits from the non-commercial electrolytes. In particular, there was a greater thickness of deposit in the wall jet region than was previously seen, especially at low current densities. With the addition of nickel, the situation was improved. Figure 46 shows the selectivity of deposits produced from the Ronovel N containing 1.5 g l⁻¹ nickel. With nickel, the selectivity approached that of pure gold.

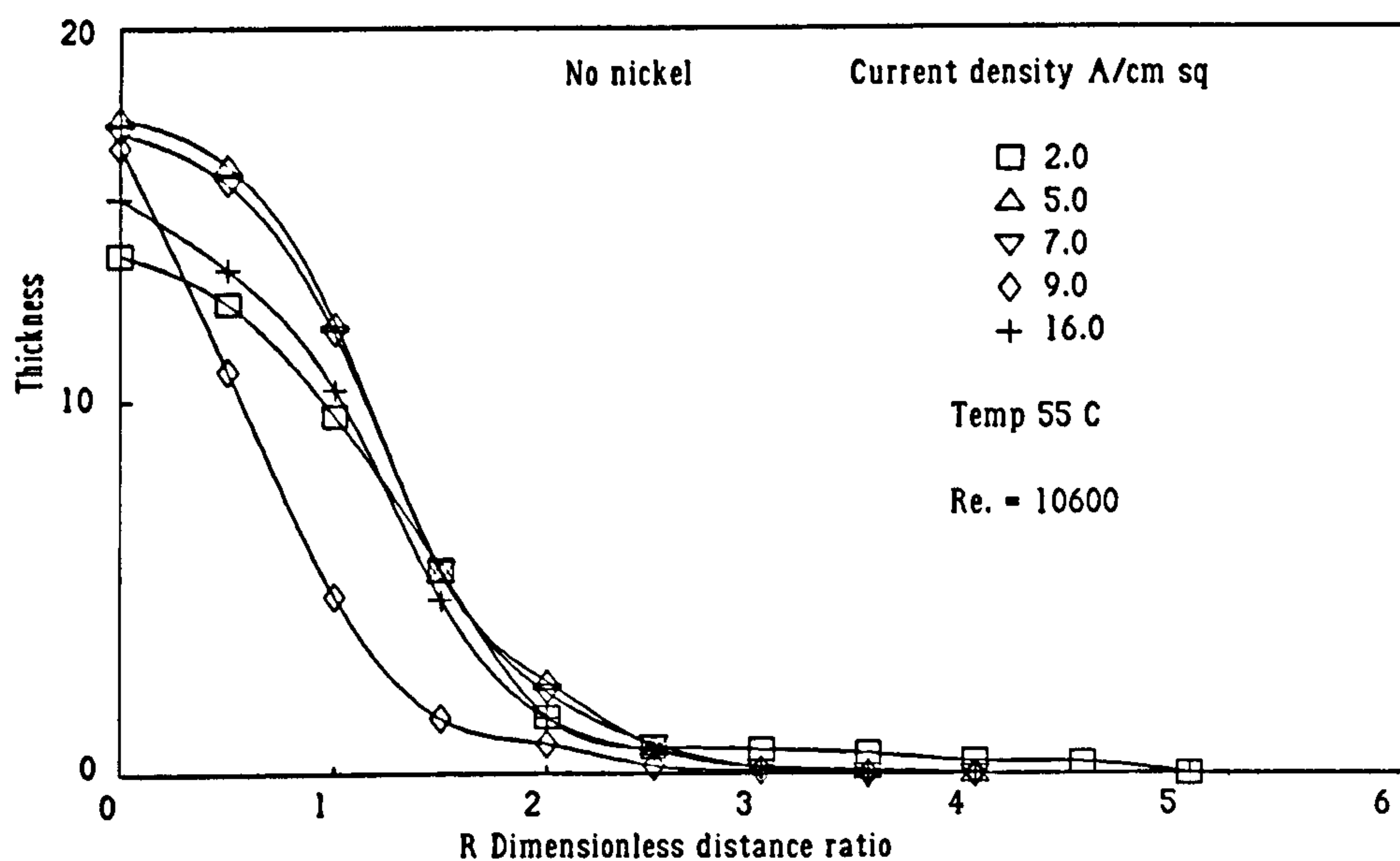


Figure 45. Selectivity of deposits from a Ronovel N electrolyte containing no nickel

An increase in the nickel concentration to 3.0 g l⁻¹ marginally worsened the selectivity with a slightly greater spread of a very thin deposit in the wall jet region as Figure 47 shows. However, at current densities below 2.0 A cm⁻², an interesting effect was observed. Figure 48 shows the selectivity of a gold/nickel deposit produced at a current density of 1.0 A cm⁻². It can clearly be seen that at a value of $R = 4$, there was an increase in the thickness, an effect not observed in the pure gold samples measured. This was presumably caused by a local increase in mass transfer, or it is a result of the variation in current efficiency with current density.

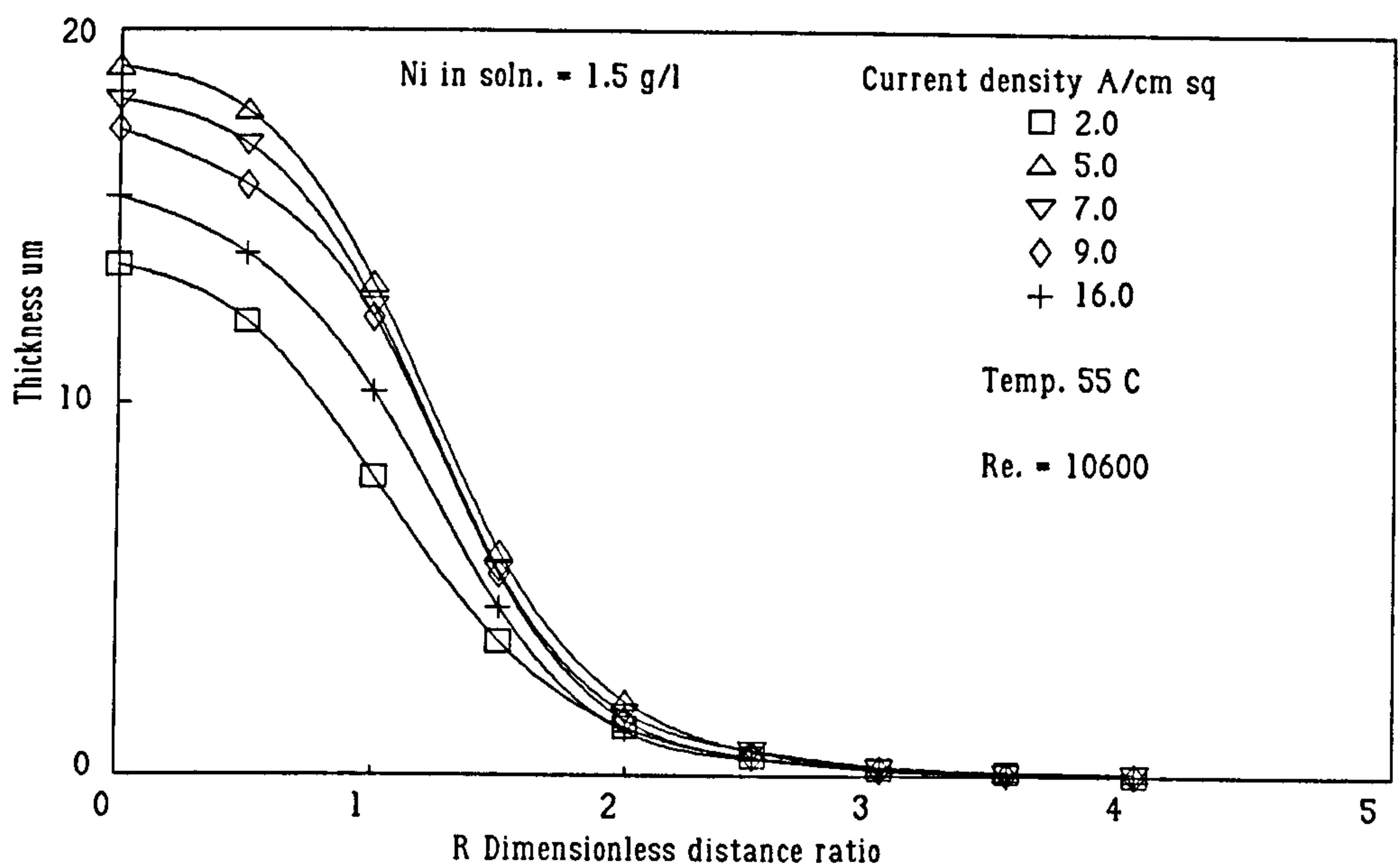


Figure 46. Selectivity of deposits from a Ronovel N electrolyte containing 1.5 g l⁻¹ nickel.

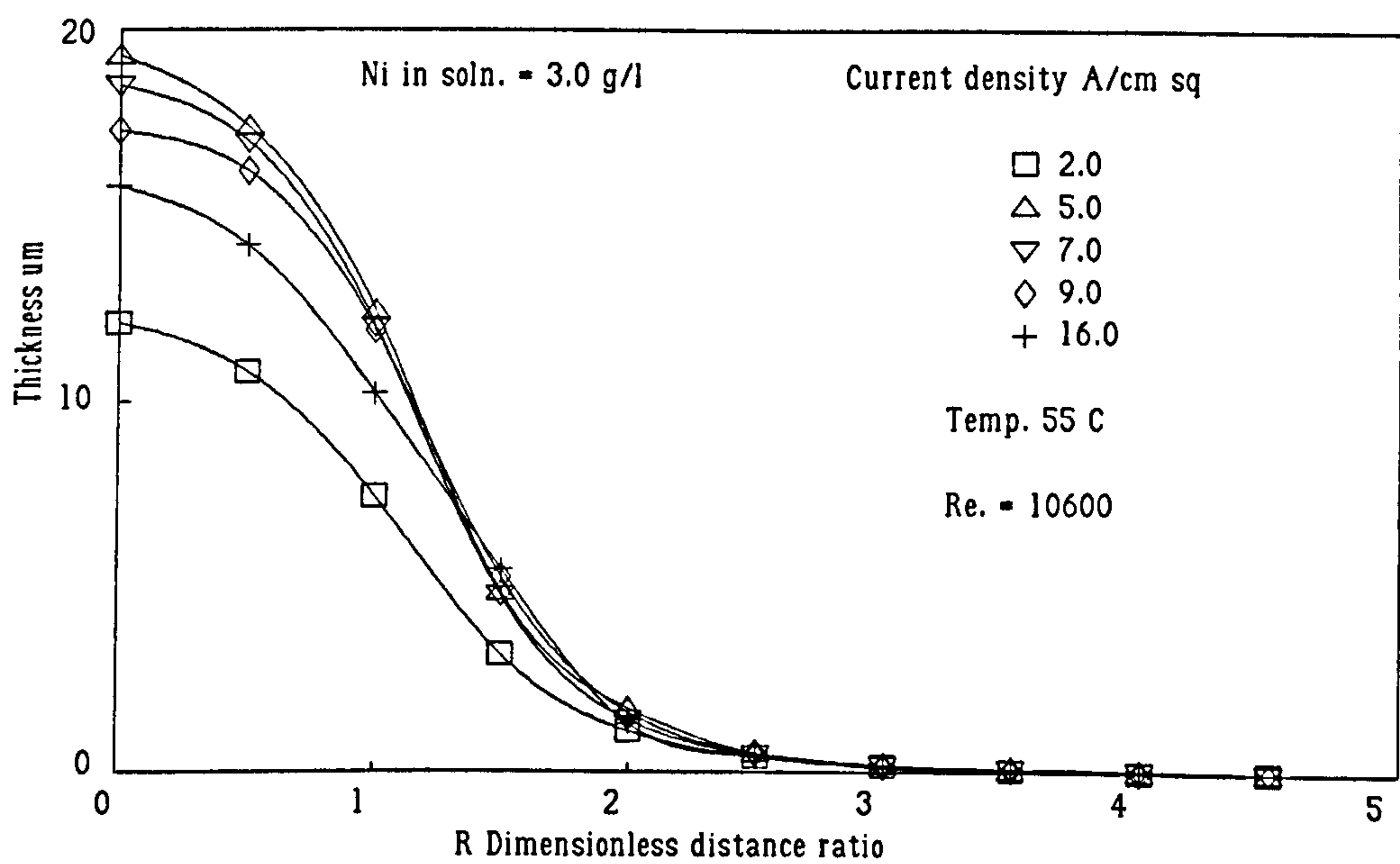


Figure 47. Selectivity of deposits from a Ronovel N electrolyte containing 3.0 g l⁻¹ nickel

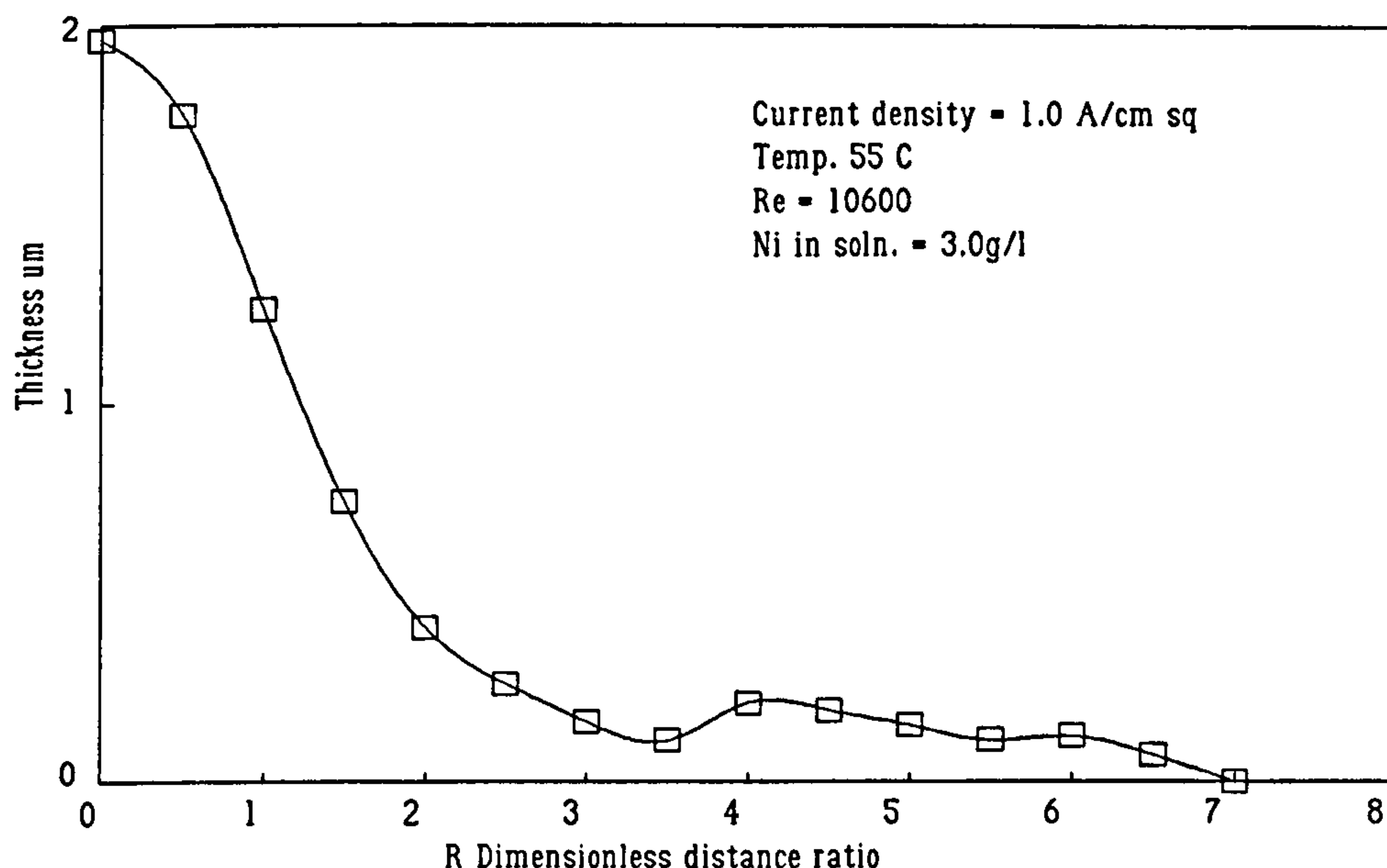


Figure 48. Selectivity of a deposit from a Ronovel N electrolyte containing 3.0 g l⁻¹ produced at 1.0 A cm⁻².

8.2.2.7 Crystal structure.

As with the pure gold, samples of gold nickel alloy were examined using XRD. In addition, a number of samples of gold nickel alloys were produced under conventional deposition conditions for comparison. Figure 49 shows the results obtained from these conventional deposits. In addition, a sample of a Ronovel N electrolyte not containing booster was obtained from the suppliers. Unfortunately, it came too late for the production of jetted samples but it was possible to observe the effects of the booster under conventional deposition conditions. These results can be seen in figure 50. Figures 51, 52, 53, and 54 show the results obtained from electrolytes containing 60 ml l⁻¹ booster only, 80 ml l⁻¹ booster only, 60 ml l⁻¹ booster and 1.9 g l⁻¹ nickel in solution and 60 ml l⁻¹ booster and 3.0 g l⁻¹ nickel in solution respectively.

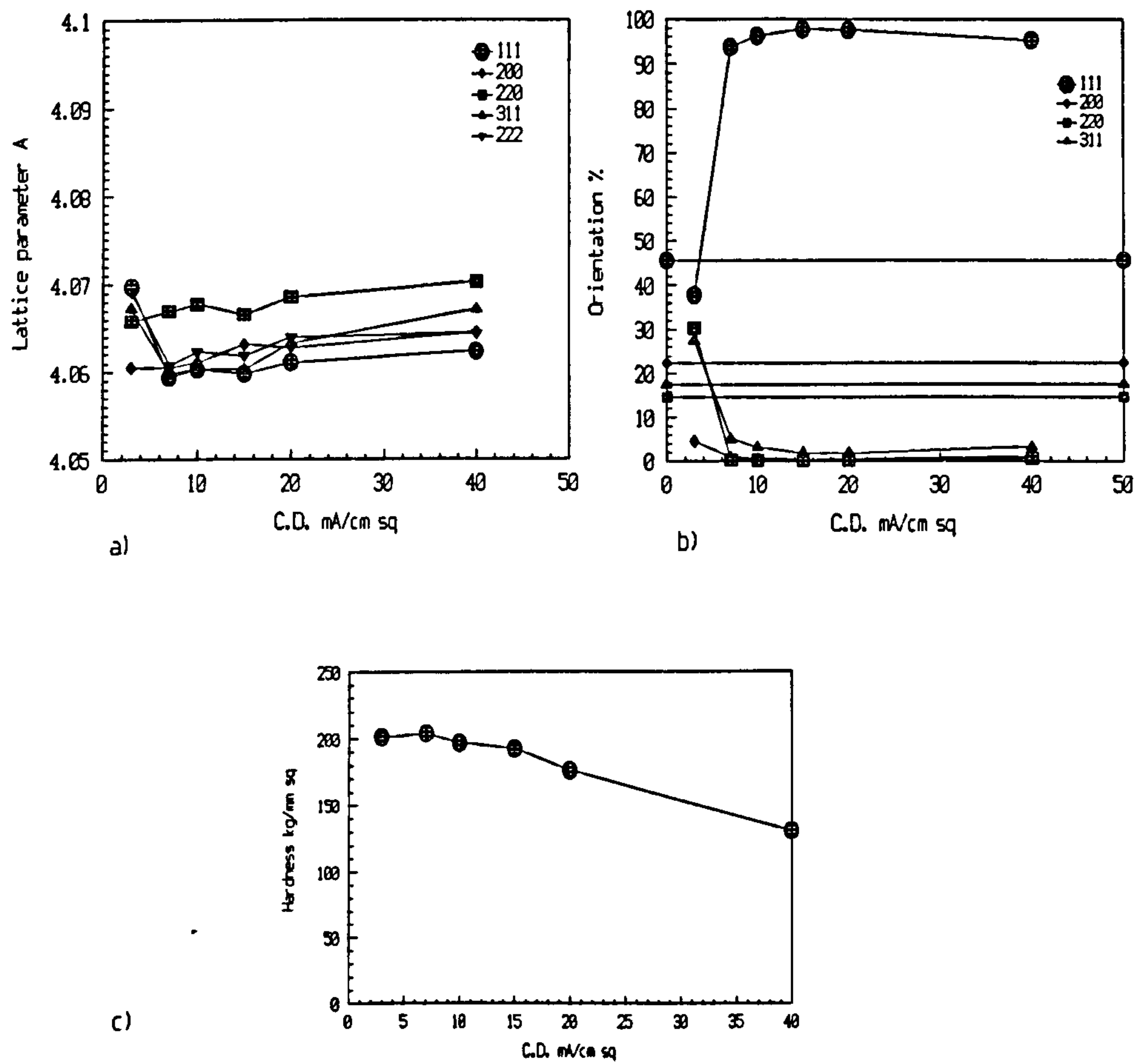


Figure 49. The relationship between current density and structural characteristics as determined by X-ray diffraction for a conventionally deposited gold nickel alloy from a Ronoval N electrolyte in terms of (a) lattice parameter (b) preferred orientation and (c) hardness.

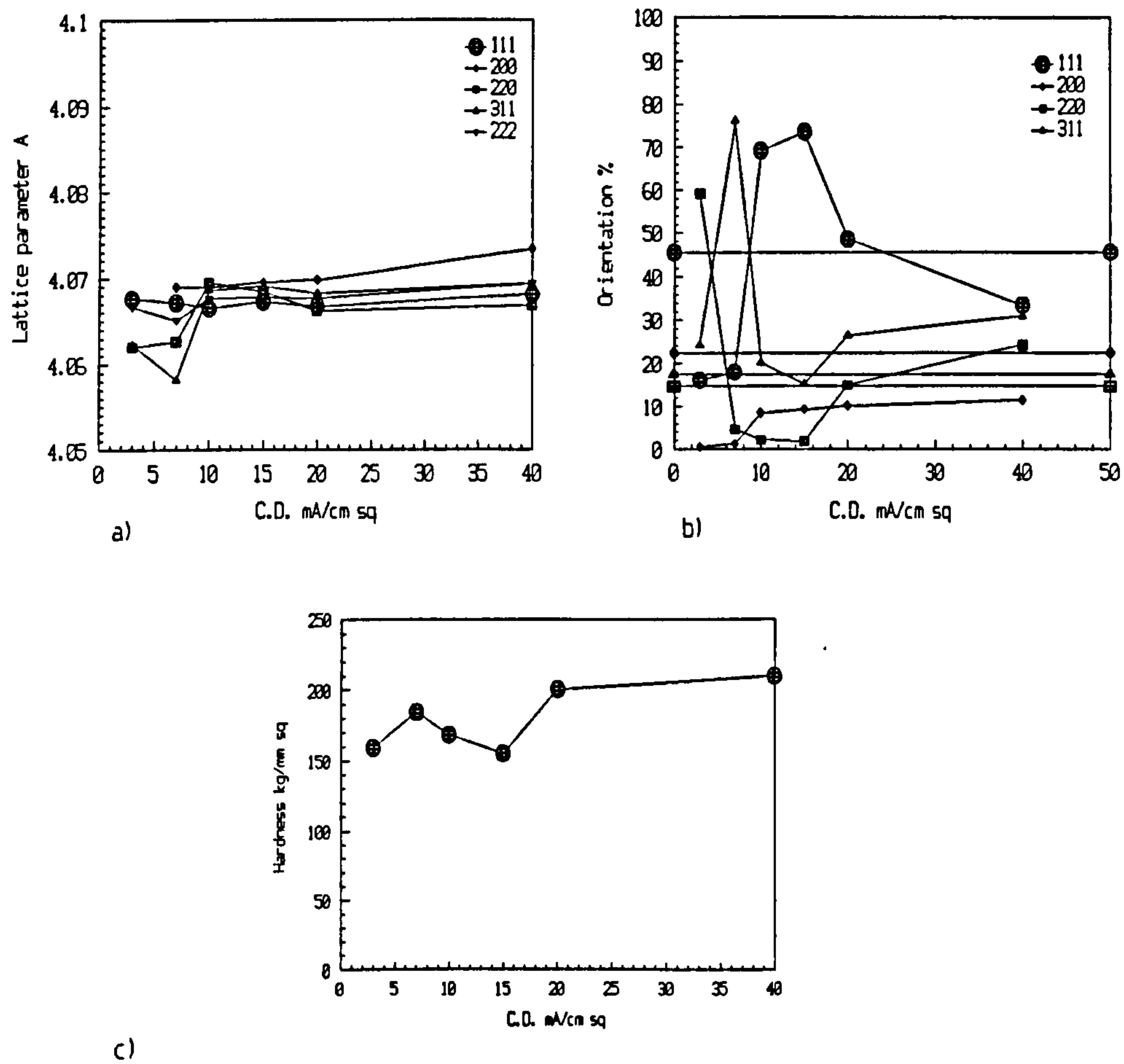


Figure 50. The relationship between current density and structural characteristics as determined by X-ray diffraction for a conventionally deposited gold nickel alloy without booster from an Auronal MRN electrolyte in terms of (a) lattice parameter (b) preferred orientation and (c) hardness.

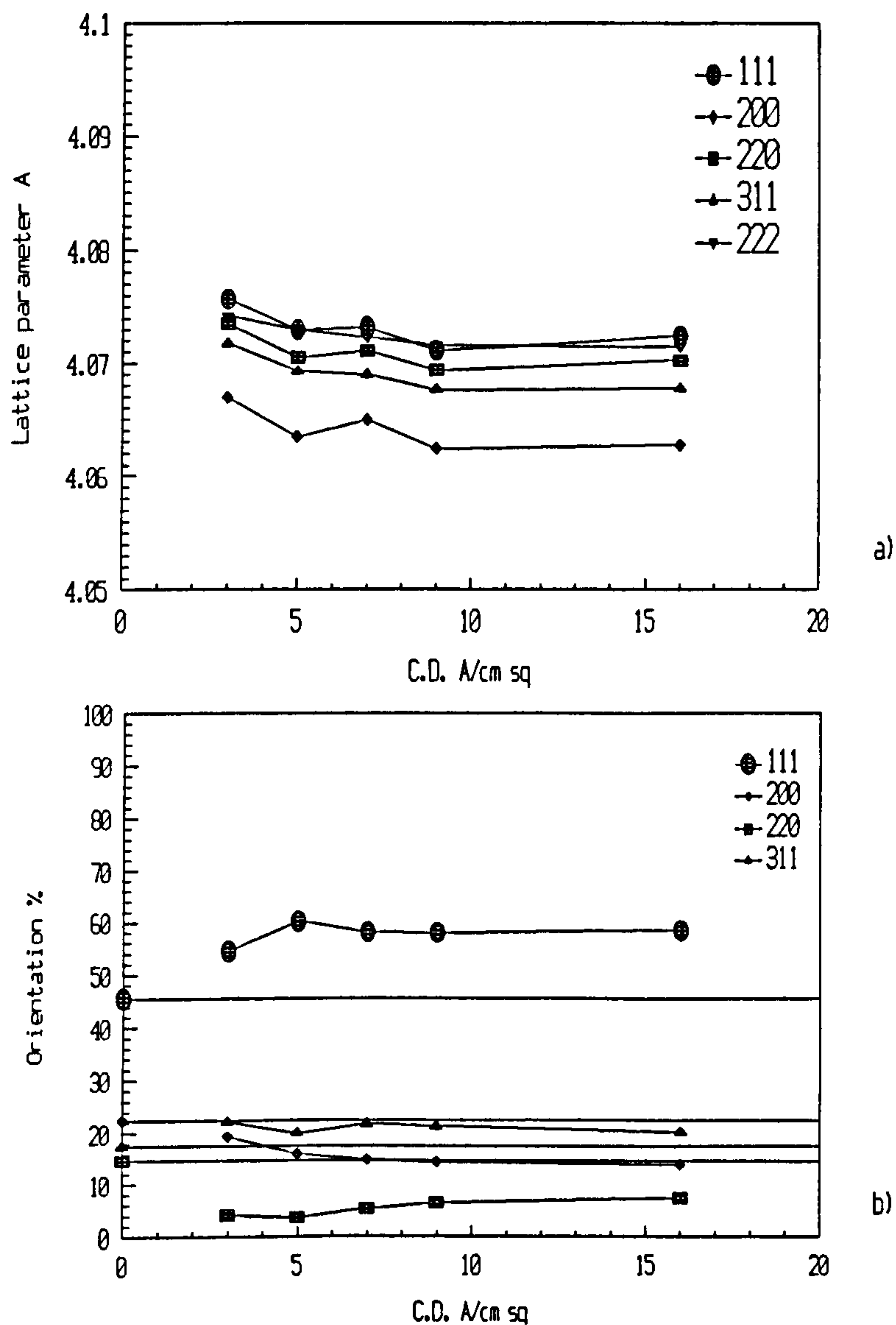


Figure 51. The relationship between current density and structural characteristics as determined by X-ray diffraction for jet deposited gold from an electrolyte containing 60 ml l⁻¹ booster in terms of (a) lattice parameter (b) preferred orientation.

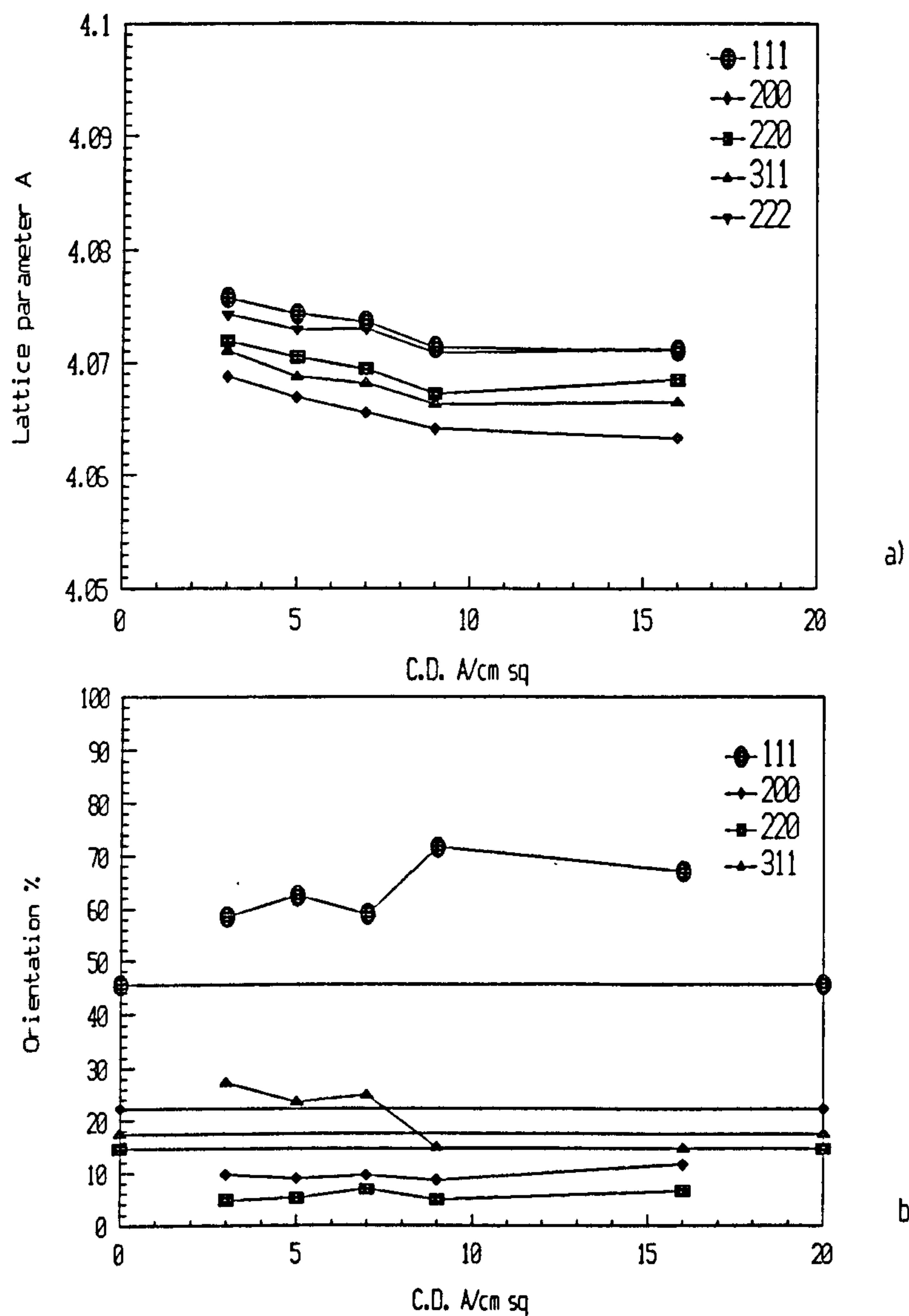


Figure 52. The relationship between current density and structural characteristics as determined by X-ray diffraction for jet deposited gold containing 80 ml l⁻¹ booster in terms of (a) lattice parameter (b) preferred orientation.

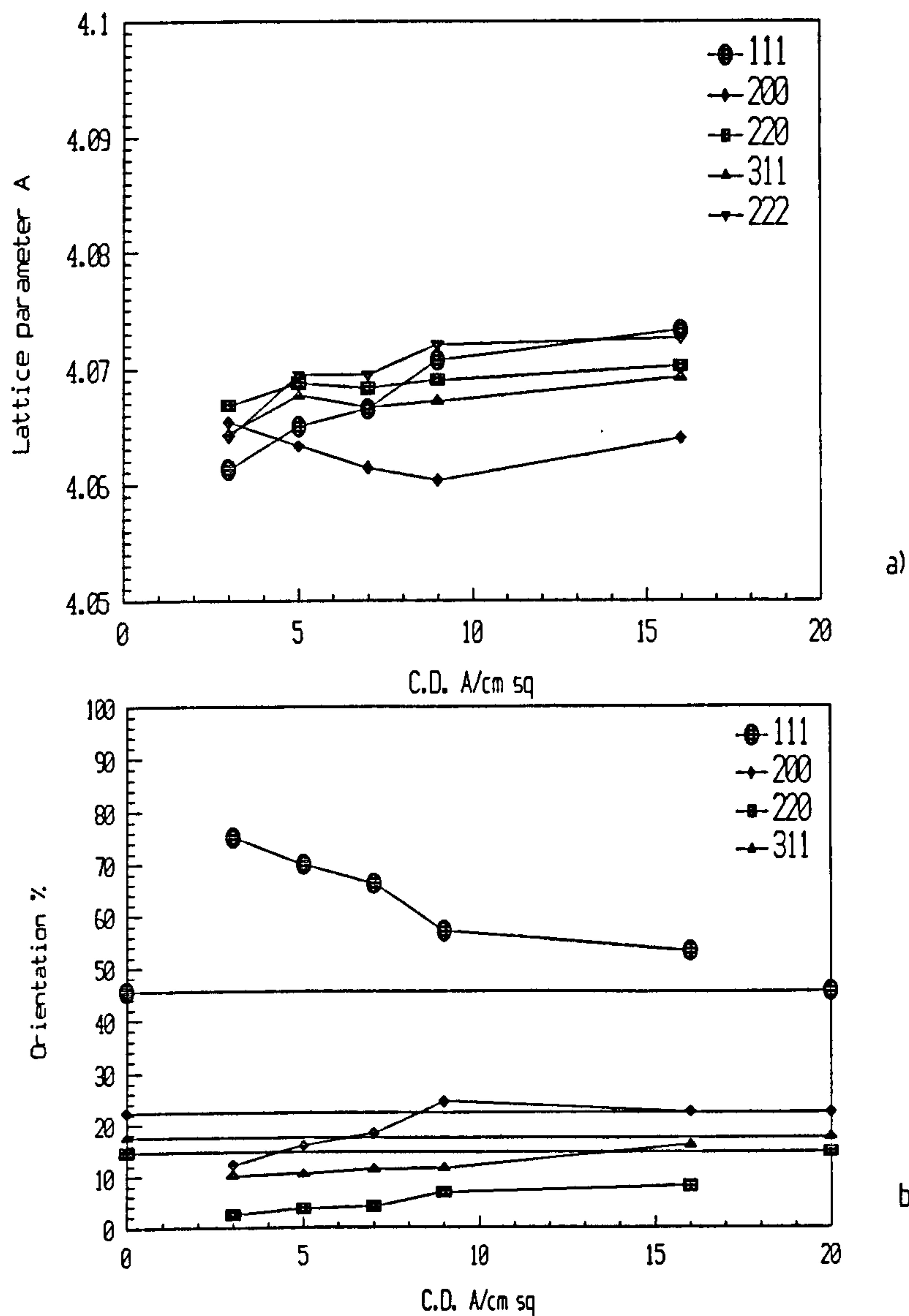


Figure 53. The relationship between current density and structural characteristics as determined by X-ray diffraction for jet deposited gold nickel alloy from an electrolyte containing 1.9 g l^{-1} nickel and 60 ml l^{-1} booster. (a) lattice parameter (b) preferred orientation.

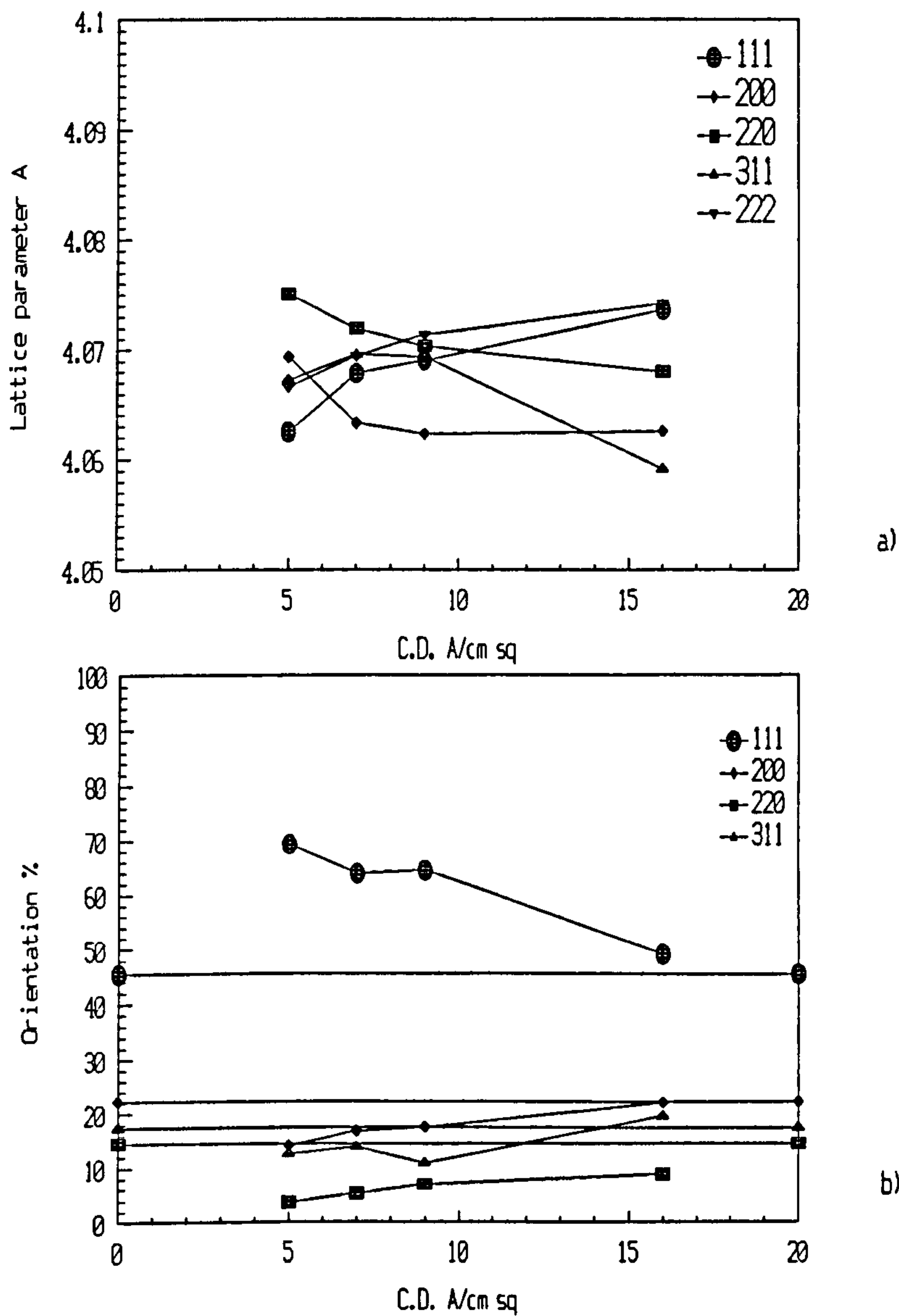


Figure 54. The relationship between current density and structural characteristics as determined by X-ray diffraction for jet deposited gold nickel alloy from an electrolyte containing 3.0 g l⁻¹ nickel and 60 ml l⁻¹ booster. (a) lattice parameter (b) preferred orientation.

The effect of the booster can be clearly established under conventional deposition conditions by comparing Figures 49 and 50. Figure 50(b) shows that in the case of the Auronal MRN, a distinct 111 texture is formed between 10 and 15 mA cm⁻², the normal operating range of this electrolyte. Indeed, below this range, the deposit appearance was matt. Above this range, the deposit showed signs of "burning" at the edges of the sample. Figure 49(b) shows that with the addition of the booster, the 111 texture was predominant above 5 mA cm⁻², with the apparent suppression of other growth directions. Pure gold, as has been seen earlier, possessed a distinct 311 texture under conventional deposition conditions. It would appear, therefore, that a 111 texture is one of the necessary conditions for the effective performance of a nickel hardened alloy gold. Hardness measurements showed that the deposits with the booster were 15% harder than those without, up to a current density of 15 mA cm⁻². It can also be seen that the booster reduced the effective lattice parameter compared to those deposits produced in its absence.

The lattice parameter of the conventional deposits without booster exhibited a mean lattice parameter $\sim 0.27\%$ less than that of annealed gold and remained essentially constant with current density. The values for all the planes were comparable within the overall accuracy of measurement. The lattice parameter of the conventional deposit containing booster was also lower than that of annealed gold, the mean value being $\sim 0.33\%$ less than that of pure gold and showed a small increasing linear dependence on current density. However the 220 planes were significantly larger and were comparable to those of the electrolyte without booster.

In both cases, the crystallite size of the 111 planes as determined by the Scherrer equation was greater than for the other measured planes. The calculated value for the 111 reflection was ~ 350 Å for deposits produced at the lower current densities, decreasing to ~ 200 Å with increased current density. The crystallite sizes calculated for the other planes measured were typically in the region of 100 Å. In the case of the samples produced from the electrolyte containing booster, closer analysis using the Warren and Averbach analysis revealed that a significant RMS strain contributed to this difference as can be seen from Table 23. In addition, a slight asymmetry of the reconstructed peaks suggested that some twin faulting was present but as explained earlier, no accurate measurements of their magnitude could be made.

Figures 51 and 52 show the data calculated from samples produced by jetting from electrolytes containing 60 ml l⁻¹ and 80 ml l⁻¹ booster respectively but no nickel. Figures 6(b) and 7(b) show the preferred orientation. It can be seen that with increasing current density, the 111 component of orientation rises rapidly to around 60% at the expense of the 220 component. The contributions from the 200 and 311 remained fairly constant and close to their values expected in a random sample. This is consistent with a 111 texture.

Figures 51(a) and 52(a) show the influence of the booster on the lattice parameter. There is a general trend of a reduction in the lattice parameter for all planes with increasing current density. It will be noted that the 200 plane exhibited a significantly smaller lattice parameter than the other planes. This would suggest that a distortion of the lattice was being created due to the incorporation of the booster (or breakdown product of it) within the 100 (200) planes.

As was observed in the previous samples, the 111 planes exhibited a larger apparent crystallite size than the others as determined using the Scherrer equation. For both concentrations of booster, the 111 plane was found to be in the region of 300 Å whilst that of the other measured planes was in the region of 150 Å. This may be attributed to both stacking faults as well as residual strain as can be seen from Table 23.

The presence of nickel reduced the lattice parameter of most of the planes examined to below 4.07 Å at low current densities, increasing to slightly above 4.07 Å. This latter value was about the same as that for the samples containing booster alone. Examination of Figures 53(a) and 54(a) revealed that the lattice parameter of the 200 plane fell with increasing current density, similar to that of the samples with booster alone. With relatively large concentrations of nickel in the electrolyte, the 311 and the 220 also exhibited reductions in the lattice parameter, particularly at high current densities.

The crystallite size of the 111 planes as determined by the Scherrer equation was in the region of 200 Å whilst that of the other planes was in the region of 100 Å. Again, further analysis revealed that both stacking faults and RMS strain contributed to this difference.

To summarise, both the booster and the nickel induced a 111 preferred orientation but it was clear that the booster exhibited the greater influence over a wide current density range. The evidence provided by the measurement of the lattice parameter indicated that the presence of both booster and nickel reduced these values to below the pure gold value, probably due to incorporation of the additives within the lattice. Indeed, the evidence indicated that certain planes incorporated a larger proportion of these materials. The true grain size for the 111 plane, after correction for residual strain and stacking faults, indicated that for all the jetted samples, a small crystallite size in the region of 200 to 300 Å was produced. The nickel had a slight influence in reducing the crystallite size further under jetting conditions. However, under conventional deposition conditions, it appeared to be the main cause of the reduction of crystallite size.

8.2.3 Sampled current pulse voltammetry of the Ronovel N electrolyte.

Polarisation curves were produced for the Ronovel N electrolyte both with and without nickel using SCVP. Figure 55 shows the results of this study. In the absence of nickel, but with 60 ml l⁻¹ booster, a well defined Tafel region was observed, the slope being -186mV/decade. Beyond the Tafel region, a small mixed activation/diffusion controlled region was observed which led into a small but well defined limiting current plateau at a current density of 3.6 A cm⁻². With the addition of 1.9 g l⁻¹ nickel, the shape changed considerably. At low overpotentials, a much steeper slope was observed leading to what appeared to be a small plateau at a current density of 0.078 A cm⁻². Beyond this, a more well defined Tafel region could be seen, with a slope of -290 mV/decade. However, the limiting current plateau seen in the absence of nickel had disappeared. The initial plateau that occurred on this curve is probably the limiting current density for nickel. These results will be discussed in Chapter 10.

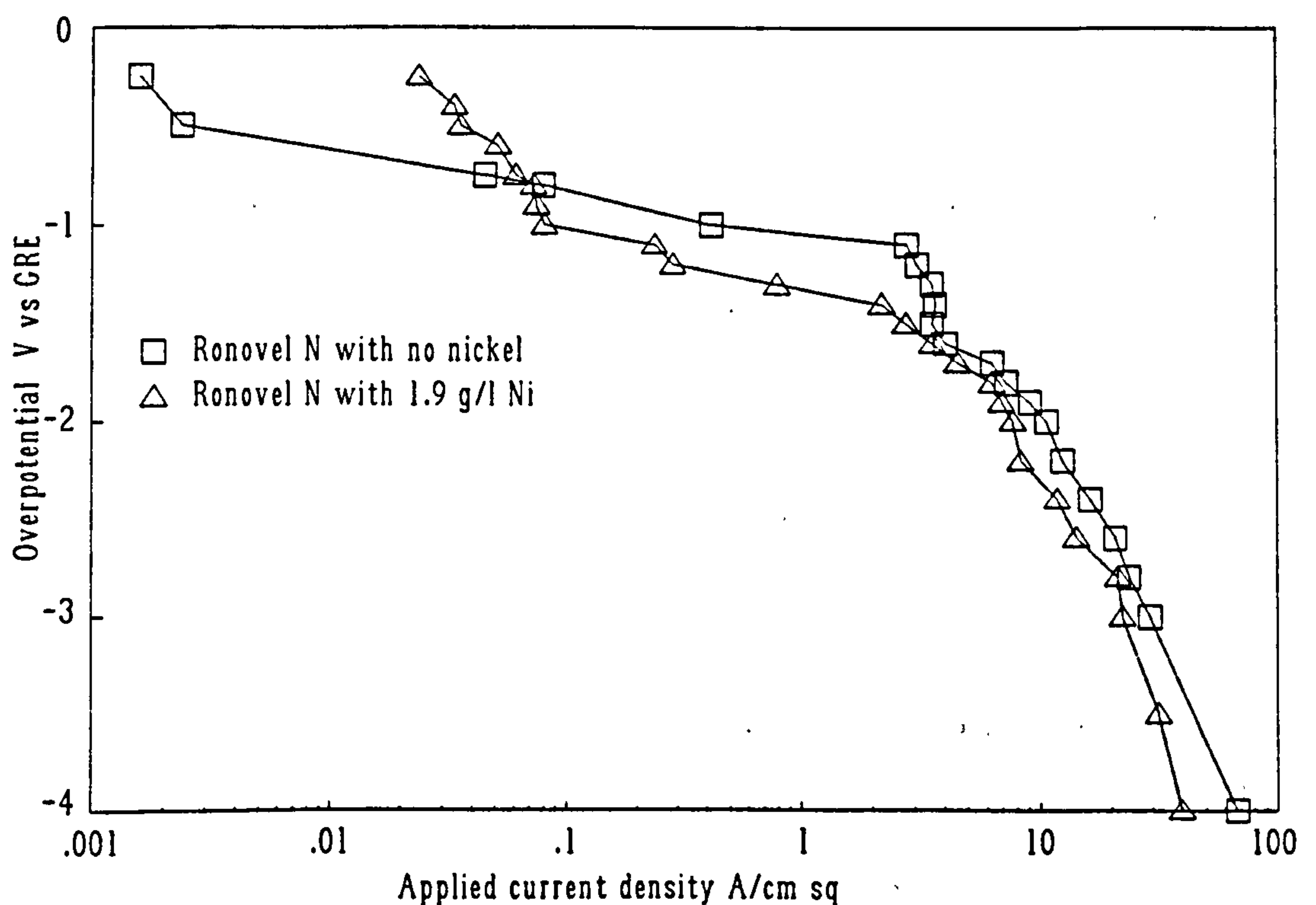


Figure 55. Polarisation curve of the Ronovel N electrolyte both with and without nickel using SCPV.

CHAPTER 9 THE APPLICATIONS OF HIGH SPEED SELECTIVE JET ELECTRODEPOSITION

There are a number of potential applications for which HSSJE would be suited. These are mainly in the electronics industry. With a suitable scale-up of the system, it could be adapted for engineering use, applying the principles outlined here to other metals. There are also areas within the decorative market that could also be exploited. The following Sections outline some of these applications in more detail.

9.1 APPLICATIONS WITHIN THE ELECTRONICS INDUSTRY.

There are 4 main areas of the electronics industry where such a process may be utilised.

9.1.1 The direct writing of Microwave Integrated Circuit Substrates (MICS).

MICS are used extensively throughout the Telecommunications and Defence industries for mounting active devices such as amplifiers, delay lines etc. The substrates can be made from sintered alumina, quartz or PTFE composites. These are metallised by sputtering a "keying" layer of chromium, followed by approximately 0.1 μm of gold. Circuit tracks are either defined by photoresist and gold plated through the defined lines. Alternatively, the whole substrate is plated with gold and the tracks defined by a print and etch process. Each process has its disadvantages. The additive process suffers from photoresist attack by the gold deposition process. This is due to the production of cyanide at the interface as a by-product of the deposition process. This effectively undercuts the edge of the resist leading to poor definition or a complete failure of the adhesion of the resist. There are a number of formulations that are claimed to overcome these problems, including a tin brightened gold (III) electrolyte that operates at a pH of 0.6*. However, the usefulness of such an electrolyte is doubtful for the microwave industry where very pure deposits are required. The subtractive process can produce very high definition tracks as the photoresist is applied at the etching stage and does not come into contact with the gold electrolyte. However, up to 80% of the electrodeposited gold is etched off, constituting a considerable re-processing cost. Consequently, these methods are expensive. Apart from the gold, the main cost lies in the production of suitable masks. These are produced in an enlarged form and require photo-reduction. However, by using the direct writing facility provided by HSSJE, the circuits can be written without the need

*Auruna 332, supplied by Degussa GMB.

for masking directly from the CAD designs. A sputtered or electroless plated layer is still required in order to make the insulator conductive. After the direct writing process, these thin metallised layers can then be removed by etching with virtually no attack on the written gold layer. Photograph 38 shows a simple ring oscillator produced by direct writing.

The propagation of microwave signals is not as good as that for a conventional track. It will be necessary to improve the selectivity of the process before it may be used on current design technology. However, there is an alternative approach. The reason that the propagation is poor is due to an impedance mismatch between the track, the substrate and the ground plane. By altering the thickness of the substrate to accommodate the impedance difference, the gaussian shape may not cause large losses. In fact, due to the absence of sharp corners, losses may be improved compared to conventional designs. Conventional tracks tend to radiate some of their signal from the corners of the track. Alternatively, by using the same thickness of substrate, the track could be widened to correct the problem. In both cases, the new track design would have to be mathematically modelled in order to modify overall design features. This may not be acceptable to many electronics engineers so it will be necessary to continue to research into methods of improving the selectivity.

9.1.2 The selective plating of reel to reel components.

Large quantities of strip or pressed strip components such as connectors and lead frames are currently being produced either by controlled depth immersion or by submerged jet deposition with the reel being held between either fixed or moveable rubber masks. With fixed mask systems, selective plating operates as a step and repeat process. This tends to limit the speed of throughput. Conversely, the moving mask system tends to lose accurate registration when run at high speeds. The use of resist materials allows both high throughput and very high definition but is limited to flat pressed strip. Additional facilities for application of the resist, exposure and developing increase the capital cost of such plant.

There has been a distinct trend over recent years to reduce the thickness of gold applied to commercial connectors. It is not uncommon to find gold thicknesses of about $0.15\ \mu\text{m}$ applied. Such low thicknesses are used where repeated mating of connectors is not envisaged in the intended application. Such systems are used particularly in the consumer goods market. As a consequence of this reduced thickness, very high deposition rates, in the order of up to $12\ \mu\text{m s}^{-1}$ can be achieved, leading to very high strip speeds. This is possible as very thin coatings have not had time to develop any pronounced structural features. However, for the military and aerospace market, such thin coatings are considered to be highly unacceptable, with minimum thicknesses of $2.5\ \mu\text{m}$ or above still being specified. It is to this market that the HSSJE process is aimed. The HSSJE system will

enable such components to be produced at very high production rates without the need for any form of masking. The size of the plant required and the volume of electrolyte will be considerably reduced, thus reducing the capital expenditure and reducing throughput times. Multiple jets may be used for extra speed or where more than one area requires selective plating. The use of such a small system will enable larger numbers of connectors to be produced in smaller floor areas. This should considerably reduce the cost and lead to higher specification products being available at currently commercial quality product prices.

As well as connectors, the gold plating of lead frames for the semiconductor industry is carried out on reel-to-reel systems. Whilst silver is replacing gold for a number of applications, the use of HSSJE could make gold more competitive as well as giving a high reliability product.

9.1.3 Bump plating.

Tape Automated Bonding is a technique that is acquiring importance in the electronics industry. The process consists of the production of lead frames on a metallised plastic strip, similar to a 35 mm photographic film. In order to connect the integrated circuits to the lead frames, ultrasonic bonding of gold or aluminium wires is used. To facilitate this, a gold bump is required at the end of each lead. There are a number of difficulties in using a photoresist technique for this. However, selective jetting can overcome many of these problems.

9.1.4 The direct writing of etch resist for printed circuit boards.

The use of electrodeposited metal etch resists has been described in Chapter 3. Using HSSJE it will be possible to directly write the tracks using a metal etch resist. Although such a system could not compete with the conventional high volume techniques in use today, it could well find an application in the area of PCB prototyping. Prototype PCB's are relatively expensive as they need one-off photo-tooling. By using the direct writing of metal etch resists, a board could be produced very rapidly directly from a computer aided design (CAD). By using the design as the pattern, the computer control system will enable the nozzle to be moved in relation to the board thus writing an etch resist pattern. The capital cost of such a system would be relatively low in comparison to other rapid PCB manufacturing systems such as Direct Laser Writing of photoresists. However, it would have the disadvantage of not being able to produce through hole boards. This may not be such a problem with a prototype as there are many existing processes that can provide through hole connections, either manually or automatically.

There are other applications more suited to metals other than gold but these will not be discussed here. The electrochemical and hydrodynamic considerations that apply to gold will most likely be applicable to other metals.

9.2 DEMONSTRATIONS OF THE USE OF HSSJE

A number of test samples showing demonstrations of the potential applications have been produced. Some of these samples have undergone initial trials with regard to their potential application. Others have been produced to demonstrate the possibilities for use for a particular application.

9.2.1 Microwave circuit test samples - 50 ohm lines.

If HSSJE is to be used for microwave circuit applications, it should be capable of transmitting the signal with minimal losses. There are two primary areas of signal loss. The first is radiation loss, due to sharp edges, corners etc that allow the signal to radiate from the conductor. In other words, it behaves as an aerial. The second is more complex and is due to impedance mis-matching. It is not proposed to describe in detail this problem but very briefly, there is an impedance mismatch if the thickness and width of the circuit track does not relate in a specific way to the thickness of the dielectric substrate and the ground plane on the reverse side. If there is a mis-match, the signal is projected back to the source, leading to a loss in signal strength or even damage to the transmitter.

There are a number of ways to assess transmission losses, the simplest being the construction of 50 ohm transmission lines of varying lengths. The signal losses can then be calculated from the response of each line. Four single circuit tracks were produced on 640 μm thick alumina substrates sputtered with chromium followed by gold. The opposite face of the substrate was plated with 10 μm of pure gold. The track face was plated with a single track using HSSJE pure gold to a centre-line thickness of 10 μm . The total track width was 640 μm . After depositing the track, the thin sputtered layer was removed using chemical etchants. The tracks were then tested for transmission properties. At the same time, 4 conventionally produced strip-lines were tested. The reference frequency was 10 GHz. It was found that the HSSJE gold exhibited a transmission loss of 0.06 dB/mm whereas the conventional line showed a loss of 0.01 dB/mm. The reason for the increased transmission loss was due mainly to the deposit profile. The gaussian shape led to an overall reduction in the total mass of gold within the track. Because of the reduced volume of gold in the transmission line, the impedance was increased. Measurements of the DC resistance suggested that the reduction in resistance was proportional to the reduction in the cross sectional area. As a consequence, it

would be necessary to improve the selectivity of the deposition process in order to produce microwave circuitry of an equivalent quality to those currently being produced. Alternatively, the impedance characteristics of the HSSJE deposits could be accommodated by a small redesign of the circuits based on the deposit profile and accommodating an increased thickness. It would be necessary to carefully assess the economics of such a process before it could be used for microwave circuitry.

9.2.2 The plating of connectors with alloy gold.

Some initial trials have been conducted on the wear properties of HSSJE gold nickel alloy deposits on connector components. Wear measurements were carried out using the GEC Contact Tester CTII. This is an instrument designed to allow the measurement of contact resistance against an adjustable contact force both prior to, during and after a pre-determined number of insertion-/withdrawal cycles. Actual pairs of contacts are mated rather than the pin and disc configuration which is commonly used; the test geometry is thus much more representative of the actual wear situation. The individual contact halves are clamped between gold plated jaws, one on each half of the test stage. One half of the test stage can be reciprocated. The other half of the test stage is provided with X-Y control for alignment of the contact halves. The Z adjustment controls the contact force between the pair. Photograph 39 shows the test stage. The instrument gives a true four point measurement of resistance by determining the voltage drop across the contact pair when a current of 25 milliamps is passed through the mated contacts. The force measurement system uses a stiff, bridge strain gauged load cell beam. Measurements were made at two loads, 55g and 100g. Contact resistance measurements were made after the initial set-up and then after 50, 100 and 200 insertion/withdrawals. The insertion/withdrawal rate was 40 cycles per minute. A number of contact pairs were measured at each condition and the contact resistance values presented were an average for each set of conditions.

The tests were carried out using male and female connectors plated with both HSSJE and conventional deposits, with thicknesses of 0.5 and 1.0 μm . The jetted samples were prepared at a current density of 5 A cm^{-2} , using a Ronoval N electrolyte containing 1.9 g l^{-1} nickel whilst the samples prepared under conventional plating conditions were plated at 15 mA cm^{-2} . The nickel concentration of this electrolyte was 1.7 g l^{-1} . For simplicity, the deposits were produced directly onto the copper substrates with no intermediate layer of nickel. Both male and female connectors were micro-sectioned to show the distribution of gold over the mating surfaces. It was found that the deposit thickness was constant over the desired area of contact.

After testing, the wear scars were examined using scanning electron microscopy with an energy dispersive X-ray analysis facility. Copper X-Ray maps were produced of the contact regions to determine the extent of the penetration of the gold layer.

The results of contact testing indicated that in the case of the jetted samples, higher contact loads gave rise to lower contact resistances whereas the conventional samples only showed this effect with the 1.0 μm deposit. The overall contact resistance for both types of deposit was within generally accepted limits, below 8.0 mOhms.

Examination of the wear scars after 200 cycles indicated that jetted 0.5 μm deposits showed little apparent wear with loads of 55g after 200 cycles, whereas the equivalent conventional deposits showed significant wear. However, at a thickness of 1.0 μm , the jetted samples showed severe wear with penetration of the coating, apparently abrasive in nature. The equivalent conventional deposits showed less wear although some coating penetration was apparent. No wear was observed for any of the samples after 50 cycles.

These results are very limited but they do indicate the potential for the use of HSSJE for the plating of connectors and further work will be undertaken to identify the optimum conditions for good wear properties.

9.2.3 Thermocompression bonding properties of HSSJE pure gold.

In order to establish the thermocompression bonding properties of jetted pure gold, an array of 20 deposit spots of 3.0 μm thickness were produced at a current density of 5.0 A cm^{-2} . Gold wire as used by the semiconductor industry was thermocompression bonded between adjacent spots. These were subjected to a tensile test by pulling at the wire loop formed, gradually increasing load until failure occurred. The bond areas were then examined using an optical microscope. Most of the failures, 85%, occurred by wire fracture, the remainder failed within the bond ball. No direct pull-offs were observed.

9.2.4 The direct writing of printed circuit boards.

The ability to move the jet in relation to the substrate allowed the jet to be used to directly write an etch resist pattern onto a copper clad fibre reinforced circuit board. To prevent an immersion deposit of gold forming on the copper and to minimise contamination of the gold, a 0.05 - 0.1 μm deposit of gold was plated onto the board prior to processing. The circuit pattern was imported into the computer that controlled the X-Y table in the form of an HPGL file, a common CAD

format. The tracks were written using pure gold at a linear tracking rate of 1.5 mm sec^{-1} and at a current density of 6.5 A cm^{-2} . It was found that a slightly higher current density could be used when tracking the jet without any degradation to the deposit. A deposit thickness of $3.5 \text{ }\mu\text{m}$ was measured. After completion, the thin background gold layer was chemically removed and the un-coated copper cladding was etched away using a 500 g l^{-1} ferric chloride solution at 60°C . Using a $400 \text{ }\mu\text{m}$ jet, a consistent track width of 0.9 mm was produced. Virtually no undercutting of the tracks were observed.

CHAPTER 10 ANALYSIS AND DISCUSSION

10.1 GENERAL

This work has been the first comprehensive study of deposit structures produced using the technique of High Speed Selective Jet Electrodeposition. It has been shown that both gold and gold alloys of an acceptable quality can be produced using this process at deposition rates significantly higher than have been achieved previously. In addition, these deposits attain a reproducible degree of selectivity without the need for masking. The factors that control the maximum rate of deposition as well as selectivity have generally been identified. The morphology and topography of the deposits have been studied and related to the deposition conditions. This Chapter attempts to correlate the results of the investigation into an overall mechanism of deposition and to relate, where possible, this mechanism to previously reported mathematical models of such systems.

One of the most important factors when attempting to deposit metals at very high deposition rates is the process by which deposit deterioration sets in. An understanding of such mechanisms is essential if the rate is to be increased further. Consequently, the method by which such deterioration occurs will be discussed in depth as a basis for any future studies that may be carried out on this technique.

In order for metals to be electrodeposited at high rates, it is necessary to ensure that an adequate supply of metal ions be provided to the substrate to replace those consumed by the deposition process. This means that all factors controlling such transport mechanisms will influence the maximum rate. These factors are the overall metal ion concentration, the degree of agitation, the temperature, the diffusion coefficient and the current density. Additional factors may also influence the overall rate. Competing electrochemical reactions such as hydrogen evolution or oxygen reduction may reduce or even halt the metal reduction process. Species other than those taking part in the reaction such as organic molecules, by-products generated during the deposition reaction or anions present in the electrolyte may all influence the maximum deposition rate by interfering with the process of electrocrystallisation by affecting the surface diffusion of adions. It is probably true to say that the most influential factor controlling the maximum deposition rate (in the absence of the aforementioned detrimental factors) is the rate of bulk electrolyte agitation. This factor controls the rate at which metal ions are re-supplied to the diffusion layer effectively becoming the rate determining step in any process that is under diffusion control. In the case of HSSJE, very high rates of electrolyte agitation are feasible. The maximum rates of deposition are obtained when flow rates are such that turbulent flow conditions exist. Such conditions strongly influence the thickness

of the hydrodynamic boundary layer adjacent to the diffusion layer. The maximum possible re-supply of metal ions will be achieved when this boundary layer is of the same magnitude as the diffusion layer. However, limits are set by the way in which the growing electrodeposit interacts with both the boundary and diffusion layers and this will be discussed in depth later.

It has also been shown that it is possible to deposit alloys in a controlled fashion. In the case of gold alloys, the situation is more complex as some of the co-deposited metal is incorporated in the form of an inorganic complex. However, it has been shown that in terms of the structure and physical properties of the deposit, high speed deposits retain a number of the characteristics observed in those produced under conventional conditions.

During the course of this study, a novel technique has been used in an attempt to establish the mass transfer characteristics of the gold deposition system. The validity of this technique and its applicability to other systems will be discussed.

10.2 MASS TRANSFER MEASUREMENTS

Mass transfer was measured in an attempt to characterise the gold system. Very little work has been carried out on the mass transfer characteristics of metal deposition using HSSJE. Most of the models available come from experiments carried out using the reduction of ferricyanide. However, as explained previously, during metal deposition at high rates, the growth of the deposit interferes with mass transfer measurement. Therefore, the methods of SCPV and SVPA were developed. For pure gold, no limiting current plateaux were observed. The data obtained from the Ronoval N electrolyte in the absence of nickel did exhibit a plateau whilst none was observed in the presence of nickel. In the case of copper, a limiting current plateau was also seen. The apparent limiting currents observed were used to calculate the Sherwood number in accordance with equation (3). This was used to compare with correlations obtained by Chin and Tsang,¹⁰⁵ Alkire and Chen¹⁰⁸ and Chin and Hsueh.¹²⁰ These are shown in Table 26.

From these figures it is clear that the limiting current plateaux did not exactly agree with the three correlations. However, for the laminar flow correlation given by Chin and Tsang, agreement was within +18%. For the turbulent flow conditions, agreement was between +20% and +25% for both the Chin and Tsang and Alkire and Chin correlations. It is thought that the poor correlation was due, in part, to the influence of deposit growth but the greatest contribution is most likely to be due to measurement taking place before a steady state condition had been achieved. In both cases, a higher limiting current density would be expected.

In the case of the pure gold mass transfer experiments, as no limiting current plateau could be seen, a graphical method consisting of extrapolating both the Tafel slope and the high overpotential region was used. Extrapolations were obtained using a linear regression process using the points that gave the highest correlation coefficient for each region. The point of intersection represents the limiting current density. Figures 56 to 59 show the extrapolations on the polarisation curves. It was decided to adopt the correlation derived by Alkire and Chin to compare the results for the gold as theirs was the more recent study. Table 27 shows the experimentally obtained limiting currents for both SCPV and SVPA methods together with the values calculated from the Alkire & Chin model.

This data shows a very close agreement with the correlation of Alkire and Chin. Based on these results it is possible to obtain some quantitative data on the thickness of the diffusion layer within the impingement region.

Analysis of the polarisation curve of the Ronoval N showed a similar agreement with that predicted using the model. Figure 59 shows the graphical assessment of the limiting current density. Table 27 shows this value together with that predicted by the Alkire & Chin model. It is interesting to note that the limiting current density plateau from the electrolyte without the nickel occurred at a value somewhat lower than the value obtained by the graphical method. As the latter method provided values in close agreement with the model, it would be reasonable to assume that the apparent limiting current plateaux obtained using SCPV should not be relied on and the graphical approach used where possible. The use of the graphical method is not possible, however, in situations where little or no Tafel region is apparent on the polarisation curve, as in the case of copper, as no clear extrapolation was possible.

The results of the mass transfer studies show that the techniques of both SCPV and SVPA are a suitable method of obtaining limiting current density values for HSSJE where metal deposition at high rates interferes with the conventional means of obtaining such data. However, it would appear that the method may not be as accurate in the case of highly reversible systems where no clear Tafel region is observed.

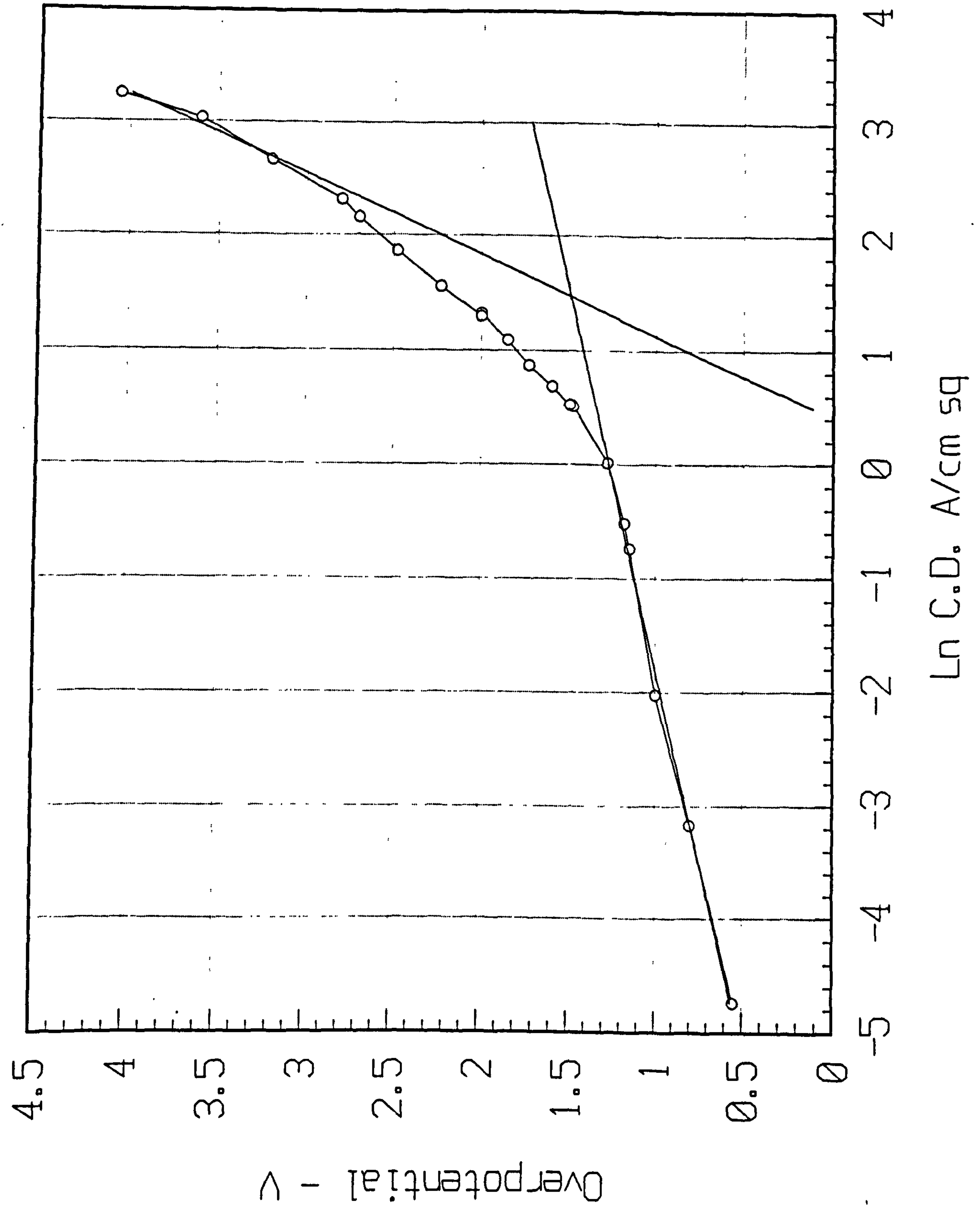


Figure 56. Graphical evaluation of the limiting current density for jetted pure gold at a Reynolds number of 3355 using data obtained by SCPV. $i_L = 4.41 \text{ A cm}^{-2}$.

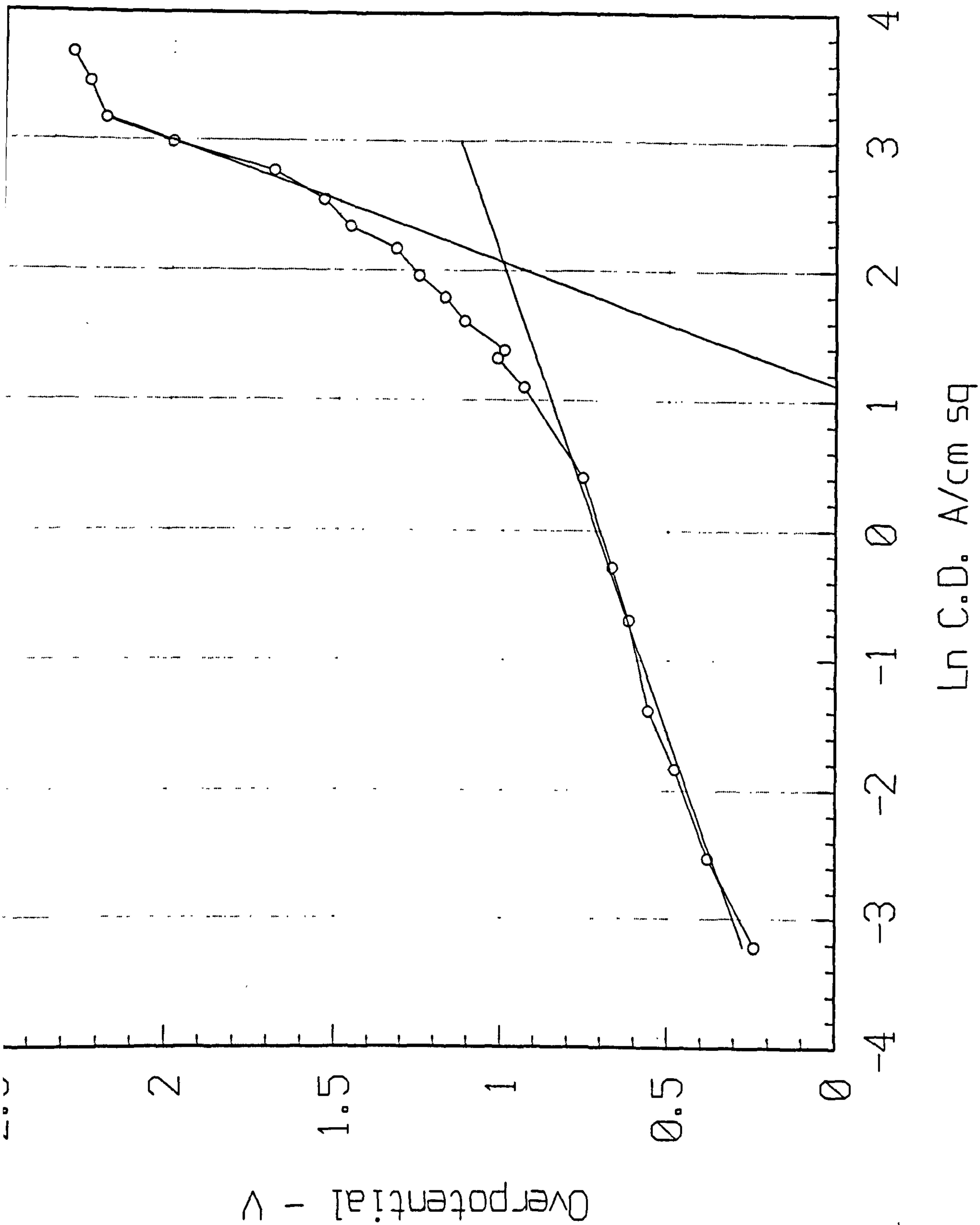


Figure 57. Graphical evaluation of the limiting current density for jetted pure gold at a Reynolds number of 6710 using data obtained by SVPA. $i_L = 6.3 \text{ A cm}^{-2}$.

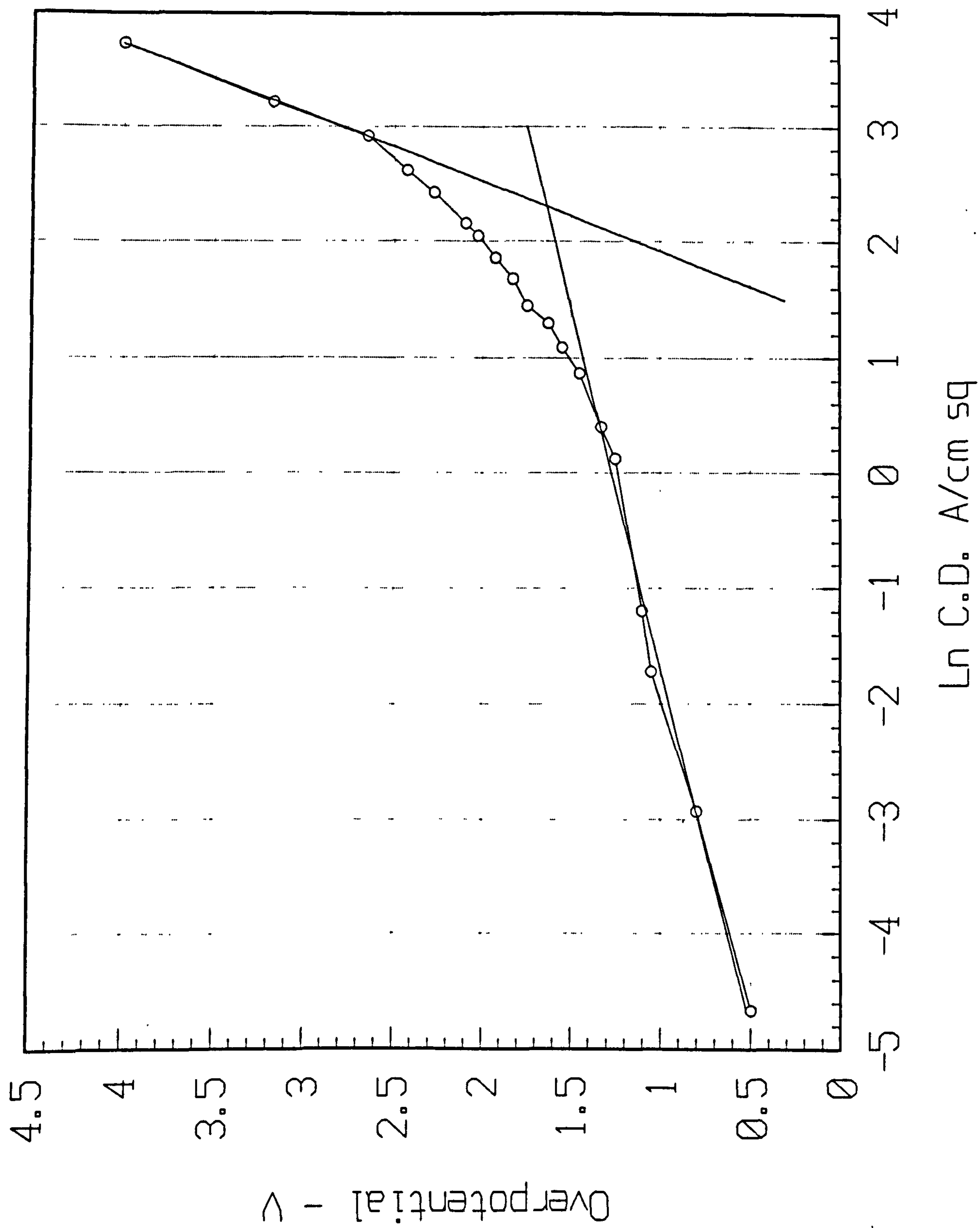


Figure 58. Graphical evaluation of the limiting current density for jetted pure gold at a Reynolds number of 13545 using data obtained by SCPV. $i_L = 9.97 \text{ A cm}^{-2}$.

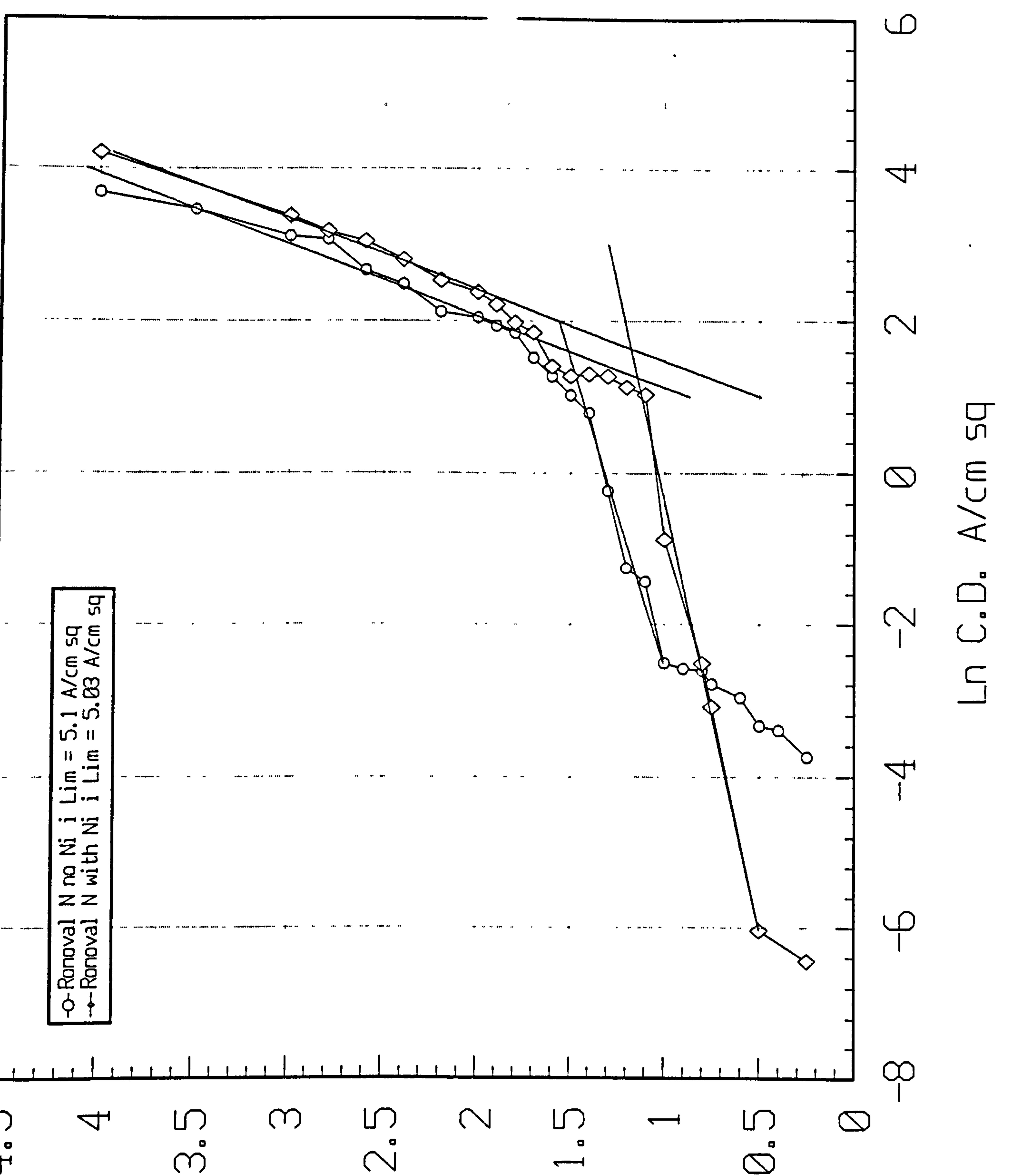


Figure 59. Graphical evaluation of the limiting current density for jetted gold from a Ronoval N electrolyte both with and without nickel at a Reynolds number of 10600 using data obtained by SCPV. Electrolyte nickel concentration = 1.9 g/l, limiting current density values are shown on the graph.

10.3 THE INFLUENCE OF DEPOSITION CONDITIONS

The factors that control the deposit quality have already been mentioned in Section 9.1. To summarise, these are the current density, temperature, metal ion concentration, flow rate and electrolyte composition. Additionally it has been shown that the nozzle to work-piece distance can influence the quality. These will now be discussed in more detail.

10.3.1. Nozzle to substrate distance.

The effects on the flow characteristics of the un-submerged jet with reference to the nozzle-to-substrate distance have been discussed in Chapter 6. The experiments carried out on the nozzle to substrate distance showed two effects. The first was that the selectivity was improved at H/d values of less than 1. This can be explained by the current distribution. When an anode is placed very close to a cathode, there is a tendency for a reduction in the effects of secondary current distribution. This will be pronounced if the IR drop between the anode and cathode is less than the total overpotential at the anode and cathode. Under these conditions, primary current distribution will predominate, which like Ohms Law, is based on geometrical factors. As a consequence, an increased rate of deposition will occur within the impingement region. The second effect observed was that at H/d values above 4, needle structures were observed at a distance of $\sim d' = 100 \mu\text{m}$ or $d'/d = 0.25$. The mechanism of the development of these structures is described in detail in Section 10.6.2.2. but essentially, under certain circumstances, needles form at the point at which the wall jet commences. This would suggest that at low values of H/d , the wall jet commences outside the impingement region ($d'/d \geq 1$) whereas at values of $H/d > 4$, the wall jet commences much closer to the jet centre-line. This is in general agreement with the findings of the studies on submerged jets (See Section 6.2.1). The exact value of d'/d will depend on the nozzle Reynolds number but it may be concluded that for un-submerged jet electrodeposition, the relationship between the value of H/d and the local mass transfer characteristics is similar to that of the submerged jet. Consequently, the H/d value must be kept at a value below 4 in order to avoid local variations in mass transfer, which can lead to undesirable deposit structures being formed.

10.3.2. Current density.

The current density influenced the deposit characteristics in many ways. The most obvious was the deterioration of the deposit above a certain current density for any particular set of deposition conditions. This is common to all electrodeposition systems. The maximum useful current density was found to be in the region of 6.0 A cm^{-2} for pure gold and 9.0 A cm^{-2} for alloy gold, giving deposition rates of $3.4 \mu\text{m/second}$ and $2.8 \mu\text{m/second}$ respectively. A discussion of the morphology of the deposit and its relationship to the current density will be given later. It will have been noted

that in the deposition of the samples, a constant number of coulombs was passed for each spot. However, it was found that the measured thickness of the deposit at the jet centre-line increased with increasing current density. Figure 60 shows a typical example of the behaviour of a pure gold deposit. There are a number of reasons for this. Figure 17 shows the spread of the deposit measured optically. It can be clearly seen that the diameter of the deposit was high between a current density of 0.25 and 3.0 A cm⁻² although not readily measurable using the Dektak. In addition, Figure 25 shows the current efficiency as a function of the current density. If these two effects are taken into consideration together, the behaviour observed in Figure 60 would be expected.

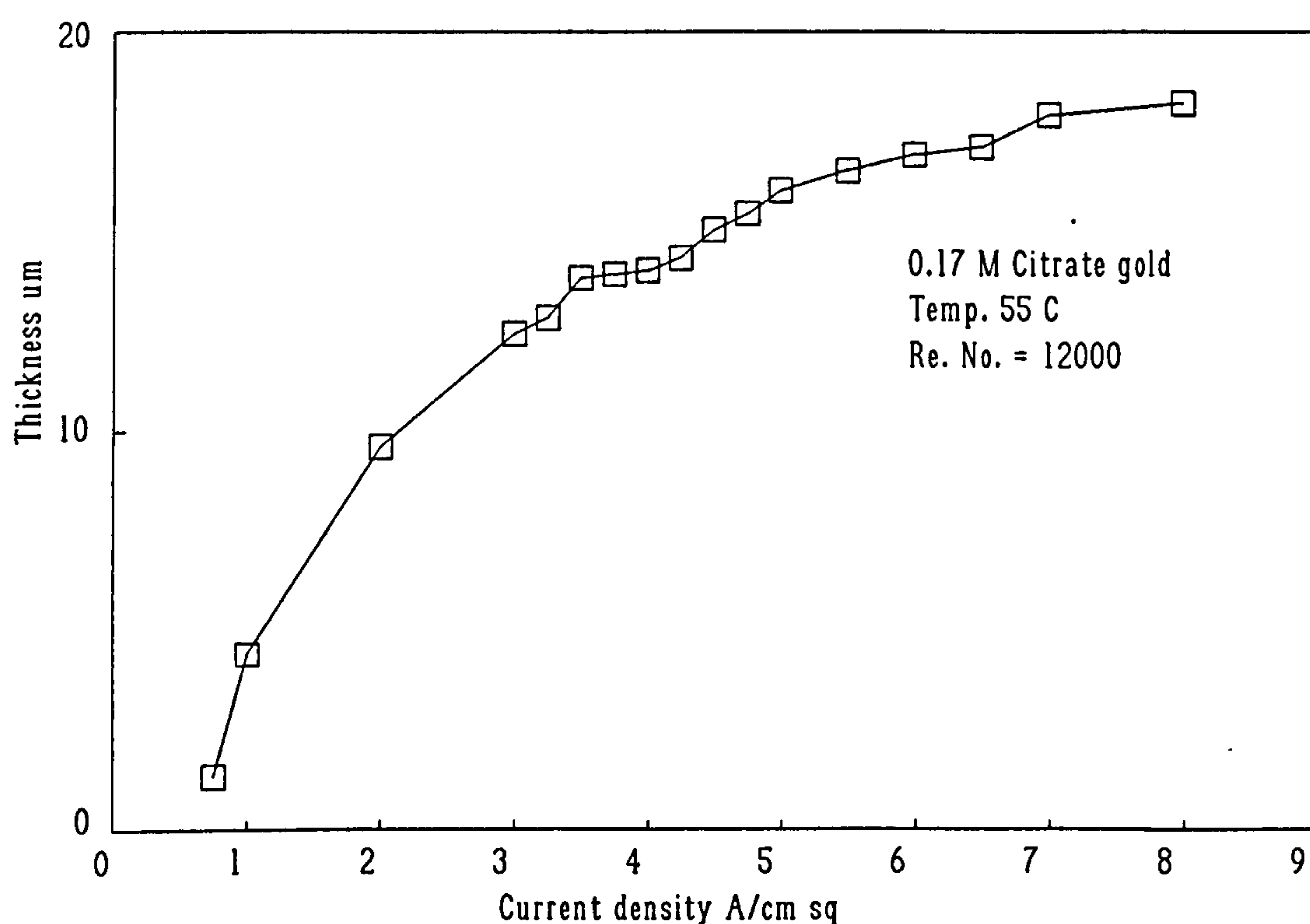


Figure 60. The relationship between the measured thickness at the jet centre-line and the current density for the 0.17M citrate gold.

A reduced current efficiency in the lower current density region, together with a decreased selectivity combined to reduce the overall measured thickness over the current density range of 0.25 to 3.0 A cm⁻². It can also be seen that between a current density of 3.0 and 4.5 A cm⁻² the thickness was almost constant. This may be expected as the efficiency and deposit width is constant over this range. The increase in thickness above 4.5 A cm⁻² roughly coincided with an increase in the current efficiency above a current density of 5.0 A cm⁻². The increase in the thickness was in the region of 10% between a current density of 4.5 and 6.0 A cm⁻². However, the efficiency and

deposit width remained constant over this range. This would indicate that a change in the density occurred either by micro-void or foreign matter incorporation into the deposit. It was not possible to measure the density of the deposits, although microsections did not show any signs of porosity up to a current density of 7.0 A cm^{-2} . Between a current density of 5.0 and 7.0, a relative increase in efficiency of 10% occurred. Over this range, an increase in thickness of 10% also occurred. This would explain the increase in thickness with increasing current density above 5.0 A cm^{-2} . Additionally, above a current density of 7.0 A cm^{-2} , the deposit became increasingly nodular, thus artificially increasing the apparent measured thickness.

It is interesting to note that the width of the deposit passed through a maximum at a current density of 0.75 A cm^{-2} and thereafter reduced. The model developed by Alkire and Chin, together with experimental results using a redox reaction indicates that low currents should lead to high selectivity. In the case of copper deposition, they found that the opposite was true, with high currents exhibiting better selectivity. This was similar to the deposition of pure gold. They attributed this behaviour to the difference in the exchange current densities of the copper and ferricyanide electrolytes. If the Alkire model was correct, then in the case of pure gold, the value of ξ (Equation 26) would have to be in the region of 10^{-1} and the system would be operating under conditions of mixed ohmic and charge transfer control. The polarisation data that closely corresponds to the deposition conditions used to generate Figure 17 can be seen in Figure 36. It can be seen that for a Reynolds number of 13545, a current density of $\sim 1.0 \text{ A cm}^{-2}$ signifies the onset of mixed charge transfer and mass transfer control. This does not agree with the Alkire/Chin prediction. However, it should be noted that the Alkire/Chin model was based on theoretical calculations and experimental conditions over a "nozzle current density" of between 0 and 100 mA cm^{-2} . This is at least an order of magnitude lower than the experimental values used in this work. Additionally, the reactive ion concentration was an order of magnitude lower than in this work. Consequently, this part of the model may not apply for the conditions used for the present study. The model and experimental data did show that at higher reactant concentrations, the selectivity was increased at higher currents. This was because the impingement region operated under mass transfer control. Under these conditions, an increase in the concentration improved the deposition rate within the impingement region compared to the wall jet and led to a significant increase in selectivity. The experimental results obtained in this study agree with such a prediction and therefore this part of the model was applicable to the conditions studied. Significant improvements in selectivity were observed at current densities in the mixed control region for the relatively higher metal ion concentrations used in this study. At current densities below 0.75 A cm^{-2} the selectivity increased and this agrees with the model for higher reactant concentrations at low current densities. The model predicts that a moderate improvement in selectivity would be observed as an increase in concentration increases the exchange current density reducing the charge transfer resistance compared to the ohmic resistance. Such an effect would be more appreciable at the commencement of the Tafel region, reducing as the current density was increased. This, then, explains the shape of the curve observed

in Figure 17 with the maxima coinciding with the end of the Tafel region and the start of the mixed charge transfer and mass transfer controlled region. Further discussion of the effects of current density on the selectivity will be given later when the deposit interaction with the fluid flow is discussed.

10.3.3. Electrolyte velocity.

As expected, the electrolyte velocity significantly influenced the deposit quality. The mechanisms by which the quality was altered was dependent on the interaction of the flow with the deposit as well as the influence of enhanced metal ion replacement at higher flow rates. These mechanisms will be discussed in Section 9.6. The Alkire/Chin model suggested that an increase in the velocity at large currents improved the selectivity because the impingement region operated at a higher fraction of the limiting current density compared to the rest of the surface. Therefore, an increase in the flow should favour the impingement region and improve selectivity. However, under the experimental conditions used in this study, no significant effect on the selectivity was observed with changes in velocity. This is difficult to explain, particularly for those deposits that were of good quality. It is possible that such behaviour did occur, particularly at current densities close to the limiting current density. However, such deposits were difficult to measure in terms of selectivity as deterioration of the deposit set in well before the limiting current was reached. A number of deposits exhibited an increase in nodulation towards the edge of the impingement region, indicating that the stagnation region was operating at a lower fraction of the limiting current density but measurements of deposit widths were difficult due to the roughness of such samples.

10.3.4. Temperature.

The temperature influenced the structure of the deposits in two ways. Firstly, an increase in temperature increased the diffusion coefficient and enhanced the rate of mass transfer. This led to an increase in the limiting current density and an increase in the maximum useful current density. Secondly, it influenced the flow characteristics by altering the viscosity. This led to a significant alteration in the interaction between the deposit and the electrolyte flow and this will be discussed in Section 9.6. The Alkire/Chin model did not include temperature effects and therefore a comparison cannot be made. The temperature did not significantly influence the selectivity of the deposits measured.

10.3.5. Electrolyte composition

The effect of the composition of the pure gold electrolyte will be considered separately from that of the alloy gold. It is clear from the results that an increase in the metal ion concentration markedly increased the maximum current density and deposition rates at which useful deposits could be produced. However, it was found that above a certain concentration of metal ion, this maximum current density did not increase further. For example, at a gold concentration of 0.17M, the maximum useful current density was found to be 5.5 A cm⁻² with a deposition rate of 2.9 μm/second at a pH of 6.1. However, increasing the concentration to 0.28M reduced the maximum current density to 5.0 A cm⁻² but with the same deposition rate. It is suggested that the reason for this behaviour lies in the stability of surface perturbations. As described in Section 5.1.5. instability of surface perturbations is controlled, in part, by the magnitude of the concentration gradient at the surface. Increasing the metal ion concentration allows the growth of smaller perturbations by increasing the magnitude of the concentration gradient for any fixed thickness of diffusion layer. Low metal ion concentrations allow the growth of perturbations as the condition of a low surface adion concentration (the condition required for instability) will occur at low current densities (low values if i_p). Increasing the metal ion concentration allows higher current densities to be achieved before the stabilising effect of surface concentration is lost. There will come a point at which an increase in the metal ion concentration will have a negative influence on stability of the growing surface as the magnitude of the concentration gradient is increased. Therefore, the maximum current density will be reduced. The fact that despite a reduction in the maximum useful current density for the 0.28M citrate gold was observed, the deposition rate was the same as for the lower concentration electrolyte would tend to confirm this theory. In both cases, the surface ion concentration would be the same at the point at which instability was observed.

Increasing the pH of the citrate electrolyte increased the maximum useful current density. This would be expected based on the stability theory. The citrate electrolyte operated at a pH of 6.0 has a lower current efficiency compared to that at a pH of 8.1. This is because the hydrogen ion concentration is lower in the latter case and the deposition potential of hydrogen is more negative than at lower pH values. Therefore, more surface adsorbtion sites will be available at higher pH values. This effectively allows a greater surface concentration and encourages stability.

The role of the supporting electrolyte is also influential in the maximum deposition rate. The phosphate electrolyte exhibited both a decreased maximum current density and deposition rate compared to the citrate. The reason for this is un-clear and further work will be required to establish this. It is possible that the supporting ions adsorb to differing degrees, with the phosphate ions adsorbing at a much higher level.

The electrolyte conductivity influenced the deposit in two ways. Firstly, a reduction in the conductivity of about 50% lowered the maximum useful current density to 3.75 A cm^{-2} and the deposition rate to $2.3 \mu\text{m/second}$. However, it improved the selectivity by about 17%. The reduction in conductivity was achieved by reducing the concentration of supporting electrolyte to an extremely low value. The Alkire/Chin model predicted that a reduction in the conductivity would improve the selectivity for low applied currents but at high currents no influence would be observed. It was found that over the current density range 0.25 to 8.0 A cm^{-2} , the selectivity was constant, with a maximum $R = 2.5$. The basis of the Alkire/Chin model was that at low currents, the system was dominated by charge transfer and ohmic resistance effects, with the wall jet region being greatly influenced by the ohmic resistance. At higher current densities, the system is controlled by mass transfer and conductivity should not influence the system. The results do not agree with the model. It is suggested that the improved selectivity arises by the following mechanism. In the wall jet, the ohmic drop will be a linear function of radial distance, assuming that there is no IR drop in the axial direction. This is a valid assumption as the electrolyte layer in the radial wall jet is exceedingly thin. Because of this, any significant reduction in the conductivity will increase the ohmic resistance in the radial direction. As a consequence, for any value of current density beyond the ohmic control region, a reduction of conductivity will reduce the potential at any particular radial position thus lowering the deposition rate at that point. In this way, the spread of the deposit will be reduced and the selectivity improved.

10.3.6. The influence of nozzle size.

It was not possible to obtain data for small nozzle sizes ($< 300 \mu\text{m}$) under identical conditions to those used for the bulk of the experiments in this study due to pressure limitations of the pump. Smaller nozzles required significantly higher pressures than could be obtained from the pump in order to attain similar Reynolds Numbers. However, the results indicated that the nozzle size influenced both the selectivity and the maximum useful current density. Using the $400 \mu\text{m}$ nozzle as a reference, increasing the nozzle size appeared to reduce both the maximum useful current density as well as the selectivity. The reduction in selectivity was presumably due to the overall increase in the conductance of the electrolyte in the wall jet. As the nozzle size was increased, so the overall thickness of the wall jet apparently increased. This increase in the wall jet thickness was observed but not measured.

The reduction in the maximum useful current density is not so easy to explain. There is insufficient evidence with which to describe the cause of this phenomenon. The effects of scaling need further study before a satisfactory explanation may be derived.

A reduction in the nozzle size led to a reduction in the deposition rate of around 80% as well as a reduction in the selectivity to $R = 4.5$. In order to ascertain why the deposition rate was reduced, it was necessary to establish the total mass of gold deposited from both the 100 μm and the 400 μm nozzle under similar conditions, except for the Reynolds number for reasons described above. Deposit half profiles, similar to the selectivity plots except using thickness vs d' were obtained from samples produced at a current density of 6.0 A cm^{-2} and a time of 5.7 seconds from both nozzles. It was assumed that there were no voids or inclusions that would reduce the deposit density. A polynomial regression curve fitting routine was applied to each profile to obtain the best fitting formula for each curve. The following data was obtained;

$$y = 17.39 + 6.316x - 32.21x^2 + 22.005x^3 - 5.905x^4 + 0.567x^5 \quad (30)$$

for the 400 μm nozzle and

$$y = 3.3 + 0.107x - 0.942x^2 + 0.264x^3 - 0.021x^4 \quad (31)$$

for the 100 μm nozzle.

These were integrated in two axial directions in order to find the volume of each deposit. If deposition conditions were identical for each deposit, the ratio of the volume to the number of coulombs passed should be very similar. It was found that for the deposit produced from the 400 μm nozzle, a ratio of 0.00156 was obtained. However, a ratio of 0.00108 was obtained for the deposit from the smaller nozzle, 30% lower than the larger nozzle. This is not as high as the deposition rate reduction of around 80% would suggest. The mass of the deposits were calculated, assuming a density of 19.3 g cm^{-3} . The theoretical mass of each deposit was calculated from Faraday's Law. The cathode current efficiency could be calculated from this data. It was found that for the larger nozzle, an efficiency of 76% was obtained. This compares very well with the measured efficiency for this current density of 74% (Figure 25). The efficiency calculated for the smaller nozzle was 53%. There are two possible reasons for the reduction in efficiency. The first is that the Reynolds number is considerably lower for the smaller nozzle and as the mass transport of gold ions is likely to be reduced as a result of this, then the efficiency will be reduced. The second reason involves the interpretation of the current density. Throughout the project, the current density has been given in terms of the nozzle diameter. This is not strictly valid as deposition occurs outside the impingement region. In the case of the smaller nozzle, the selectivity is worse than with the larger nozzle. As a consequence, the true current density would probably be lower than that taken. Evidence for this is the maximum useful current density for the 100 μm nozzle is

higher than for the larger nozzle, being 10.0 A cm^{-2} , despite operating at a much lower Reynolds number. It is likely that it is a combination of both possibilities that leads to the reduction in the deposition rate from small nozzles.

10.3.7. The effects of pulsed current.

The application of pulsed current did not improve the maximum current density as may have been expected. Under the conditions of deposition studied, there was a reduction in the maximum useful deposition rate for the equivalent deposit quality produced under DC conditions. The morphological diagrams shown in Figures 32 and 33 show that there was a narrow region of duty cycle and on-time from which smooth deposits could be produced. However, for the equivalent average current density at which the electrolyte produced the maximum useful deposition rate, 6.0 A cm^{-2} , the "smooth" deposits were actually slightly porous. The structures in the diagrams can be interpreted in terms of the peak current densities applied. At low duty cycles, and short on-times, the peak current density is very high. For example, at a duty cycle of 5% , an on-time of 0.1 msec. and an average current density of 6.0 A cm^{-2} , the peak current density was 120 A cm^{-2} . High peak current density gave rise to fractal type structures. This was not too surprising as such high momentary potentials will lead to the rapid growth of individual nuclei due to the predominance of primary current distribution experienced at high overpotentials. Additionally, the surface will experience an instantaneous reduction in surface concentration leading to instability. These two factors will lead to the rapid growth of perturbations in the direction of the electric field. At higher duty cycles, the peak current density was lower. This reduced the primary current distribution but would have maintained a high rate of nucleation. However, it is known that AuCN adsorbs on the surface and probably takes place during the off-time. This adsorption can inhibit the lateral growth of nuclei leading to growth by means of 3-dimensional nucleation. As a consequence of reduced lateral growth, the growing nuclei do not merge and therefore form a pseudo-nodular structure.

10.4 SOME PHYSICAL AND STRUCTURAL PROPERTIES OF PURE GOLD HSSJE DEPOSITS

Some of the more important physical and structural properties of pure gold deposits produced using HSSJE have been examined during the course of this experimental work. These properties have been compared to deposits produced under more conventional deposition conditions. Conventional pure gold deposits from a citrate electrolyte exhibit a grain size of around $0.2 \mu\text{m}$ (after accounting for strain and faulting) for the 111 planes and have hardness values of around 100 kg mm^{-2} . These deposits exhibit a strong 311 preferred orientation. Such a texture has been observed by other workers as described in Section 2.2.3. It was not possible to obtain data on the 311

crystallites as higher orders of reflection could not be obtained with this experimental method. However, examination of the lattice parameters would suggest that no stacking faults were present as they are all the same size. These samples exhibited the lowest RMS strain for the 111 planes of all the samples examined over the current density range analysed. The morphology of the deposits produced may be described as angular and crystalline.

When deposits are produced from the same electrolyte using HSSJE, both the structure and morphology are significantly altered. This is due both to intrinsic changes in the deposit structure due to the deposition conditions as well as the interaction with the electrolyte flow. The latter will be discussed in the following Sections. The intrinsic changes result from the very high rates of deposition. The grain size is considerably reduced to a value in the region of 200 Å, a tenfold reduction. Such a reduction is the most likely cause of the increase in the deposit hardness up to a value of around 200 kg mm⁻². The surface appearance was smooth and featureless, gradually developing smooth rounded mounds with increasing current density. This rounded mound morphology is similar to that developed in the case of alloyed golds. The mechanism of the growth of these structures is discussed in a subsequent Section.

A (220) preferred orientation develops which, as has been suggested by Lin *et al*³⁷ may be caused adsorbed species. A slight reduction in the lattice parameter is observed, which may be due to the incorporations of small quantities of foreign species. This would not be surprising at such high rates of deposition as the speed at which growth takes place can easily bury surface adsorbed species within the deposit. It is important to note that both the conventional and jetted pure gold deposits, the lattice parameter of each of the measured planes was self consistent. This would suggest that the deposit structure was fairly well ordered. No structural faults were detected, except for a very low probability at low current densities. This means that $D_{\text{eff}} = D$ and the true crystallite size is as in Table 23.

Some pure gold deposits were produced for trials of thermocompression bonding properties. The results of these trials indicate that despite the relatively high hardness of the gold, good bonds were achieved with wire breakage as the most frequent failure mechanism. Such results would suggest that the gold was relatively pure and that an adequate ductility was maintained despite the hardness. These results indicate that pure gold HSSJE deposits would not be suitable for wear resistant applications such as connectors despite the hardness being of the same order as alloy deposits. Failure would inevitably occur due to cold welding. However, this would allow pure gold deposits to be used for applications such as the selective deposition of lead frames where good bondability is required.

10.5 SOME PHYSICAL AND STRUCTURAL PROPERTIES OF GOLD ALLOY HSSJE DEPOSITS

In the case of the alloy gold, conventional deposits produced from the Ronovel N electrolyte exhibited RMS strains higher than the equivalent pure gold samples. However, no evidence of stacking faults was seen from studies of relative peak shifts. There was a slight asymmetry of the peaks. Unfortunately, the twin fault probability cannot be calculated from the 111 peak. Therefore, whilst it is known that twin faults existed within the deposit, their contribution could not be measured. It is therefore most likely that in this case $D_{\text{eff}} < D$. It is possible that a significant contribution to broadening is due to twin faulting. Nakahara⁷⁷ has studied transition metal hardened gold deposits produced under conventional deposition conditions, using the Transmission Electron Microscope (TEM) and observed similar topographic features as in this study, with the deposit surface exhibiting "rounded mounds" or small nodules. It was found that the rounded mounds observed exhibited a strong 111 orientation with a crystallite size of between 200 and 300 Å. It was concluded that such a structure formed as a result of inhibition of lateral growth by adsorbed species, presumably transition metal complexes. The same inhibiting molecules adsorbed on the top surface of the growing planes and caused continuous nucleation leading to the small crystallite size and high hardness. A high number of twins were observed within the structure. It is evident that gold nickel alloy deposits produced conventionally shared a number of morphological features with both jetted pure and alloy gold deposits but some significant differences were observed in the micro-structure.

In the case of the jetted samples, similar values of D_{eff} were observed for the conventional Ronovel N and jetted deposits containing only booster. The presence of nickel however led to a reduction of ~25% in this value. There appeared to be no direct dependence of D_{eff} on current density. It is generally accepted that increasing the current density in simple electrolyte systems leads to a reduction in crystallite size. These results would suggest that in the case of the conventional deposits, an inhibition process as envisaged by Nakahara was operative. The fact that a similar crystallite size was observed under jetting conditions suggests that inhibition processes were also responsible for the small crystallite size and not an influence of increased current density. The exact nature of this process is unclear and difficult to identify as there are a number of possible inhibiting species. These include AuCN, CN⁻, booster and transition metal cyanide complexes. It is most likely that there is an equilibrium between the adsorbates which alters depending on the prevailing concentration and deposition conditions. The structural properties are therefore altered, depending on the nature of the inhibiting species influencing the growth of the deposit.

One of the most significant differences in physical properties between the conventionally produced gold alloy deposits and those produced by jetting is the influence of nickel additions. Conventionally produced pure gold deposits exhibit a hardness in the region of 100 kg mm⁻², whilst

jetted pure gold deposits manifest a hardness of between 160 kg mm⁻² at low current densities and 200 kg mm⁻² at high current densities. Deposits produced from electrolytes containing booster exhibited a consistent hardness of around 200 kg mm⁻² over the current density range examined. When nickel was added to a conventional electrolyte as in the case of the Auronal MRN, the hardness increased from 100 kg mm⁻² to between 150 and 200 kg mm⁻². Similar hardness values were observed when nickel was added to the Ronovel N electrolyte containing only booster. In the case of the electrolyte containing only nickel, there was a tendency for an increasing deposit hardness with increasing current density. In the case of the electrolyte containing booster and nickel, the opposite trend was seen. The hardness of the nickel containing deposit produced using HSSJE, is reduced proportional to the quantity of *nickel added to the electrolyte*, from 200 kg mm⁻² down to as low as 110 kg mm⁻². There is no direct evidence to explain this behaviour as the jetted samples containing booster both with and without nickel exhibited similar structures in terms of RMS strain and stacking faults. The main difference was the reduction in the crystallite size in the case of the nickel containing sample. This alone was insufficient to account for the change in hardness as no current density dependence was seen in terms of the crystallite size. However, a linearly increasing current density dependence was observed in the lattice parameters. The nickel in the deposit reduces with increasing current density and there is an empirical linear relationship for alloys whose individual component structures are similar between the lattice parameter and the atomic percent of an alloy constituent (Vegards Law) This would imply that some of the nickel was being incorporated within the lattice in the form of metal atoms. It is known that when transition metals are added to a gold electrolyte, conventionally produced deposits incorporate the majority of the transition metal in the form of a cyano- complex. A change in the way in which the transition metal interacts with the deposit is the most likely explanation of the reduction in hardness observed. It is clear from Figures 39 and 43 that the change in the hardness is a function of the nickel in the electrolyte and not that in the deposit. This tends to confirm the inhibition mechanism as the main influence on the hardness changes observed.

The wear properties of gold alloy deposits produced by jetting have already been described in Chapter 9. It is further suggested that the change in the inhibition process is responsible for the difference in the wear characteristics observed between conventional and jetted deposits. It was found that jetted deposits showed some reduction in the wear resistance particularly with thicker coatings. There was also evidence that the wear mechanism was abrasive in nature. Such abrasive wear is not observed in gold alloy deposits produced from properly controlled electrolytes under conventional deposition conditions. DeDoncker and Vanhumbeek³² have suggested that in the case of gold cobalt alloys, the wear behaviour is strongly related to the proportion of cobalt present as metal to that present as a cobalt ion complex, with high values of the latter being required for good wear resistance. If the cobalt concentration in the electrolyte was too high, the incorporation of the complex within the deposit was suppressed leading to too high a value of metallic cobalt in the deposit. Such deposits exhibit abrasive wear behaviour. In addition, Antler³¹ has found that

in order to obtain good wear resistance, the deposit must have a low ductility as well as a high hardness. Such a combination would not be expected from a deposit in which the alloying constituent was present purely in the metallic phase. Nakahara⁷⁷ has suggested that it is the inhibition due to the nickel complex and its incorporation into the deposit that is responsible for the crystallographic structure observed in gold nickel alloys. It would seem to follow, therefore, that due to the high rates of deposition achieved in HSSJE, the inhibition process is changed, with much less of the nickel complex being incorporated into the deposit but as metal within the gold lattice. This would explain the reduction in the wear resistance observed by Bocking and Cameron.

10.6 FLUID FLOW AND ITS INTERACTION WITH THE DEPOSIT

In order to discuss the way in which the flow and the deposit interact, it is necessary to outline the established mechanisms by which the fluid jet interacts with an impinged surface. Let us consider the overall flow mechanisms operating during HSSJE. In the case of a non-submerged jet, the electrolyte emerges from the nozzle with a flow profile identical to that experienced within the nozzle tube. Providing the nozzle tube length is an order of magnitude greater than the nozzle diameter, then this flow regime will effectively be that existing within a tube. However, if H/d is greater than 1, then the flow is affected by the surrounding air, leading to a reduction in the flow at the edges. At very high H/d ratio's, this eventually leads to turbulent interaction and a break up of the flow structure. The influence that this has on deposition can be seen in the experiments conducted with large nozzle to substrate distances. Most of the work carried out during this study did not include such a regime and will only be considered where necessary. As the emerging free jet approaches the substrate, interaction with the later reduces the axial flow rate, with a consequent diversion of flow in the radial direction. This region is the stagnation zone, the size of which will depend on the flow rate of the free jet. Within this zone, a hydrodynamic boundary layer of almost constant thickness develops. The flow properties of this region are common to both the submerged and non-submerged jets. Towards the edge of the stagnation zone, the flow is redirected into the radial direction. Axial flow decelerates as radial flow accelerates. This flow has the characteristics of a wall jet and the region is termed the wall jet region. However, the behaviour of the wall jet depends on whether it is submerged or not. In the case of the submerged system, interaction occurs with the surrounding fluid and thus influences its behaviour. We will restrict our discussion to the non-submerged jet for the wall jet region. At the edge of the stagnation zone, a boundary layer starts to grow, having a Blasius type plate profile. Beyond the boundary layer, flow is uniform. With increasing radial distance, the thickness of the boundary layer increases until the fluid layer becomes a complete boundary layer, subject to viscous drag from the substrate. This is the transition region. When the viscous drag becomes sufficiently high, then the hydraulic jump occurs.

10.6.1 Interaction of the flow below the maximum useful current density

Most of the models for the impinging jet have been based on fluid thickness and limiting current measurements. The limiting current method makes use of a ferricyanide/ferrocyanide redox system. Such a system provides a very good means of establishing the mass transfer characteristics of the jet as it does not produce a solid product that would interfere with measurements. However, in electrodeposition, the product is a growing layer of metal. Figure 61 shows how a pure gold deposit grew with increasing time. The conditions of deposition were such that a smooth, featureless deposit was produced. The growth rate at the centre of the deposit showed a linear growth rate with time.

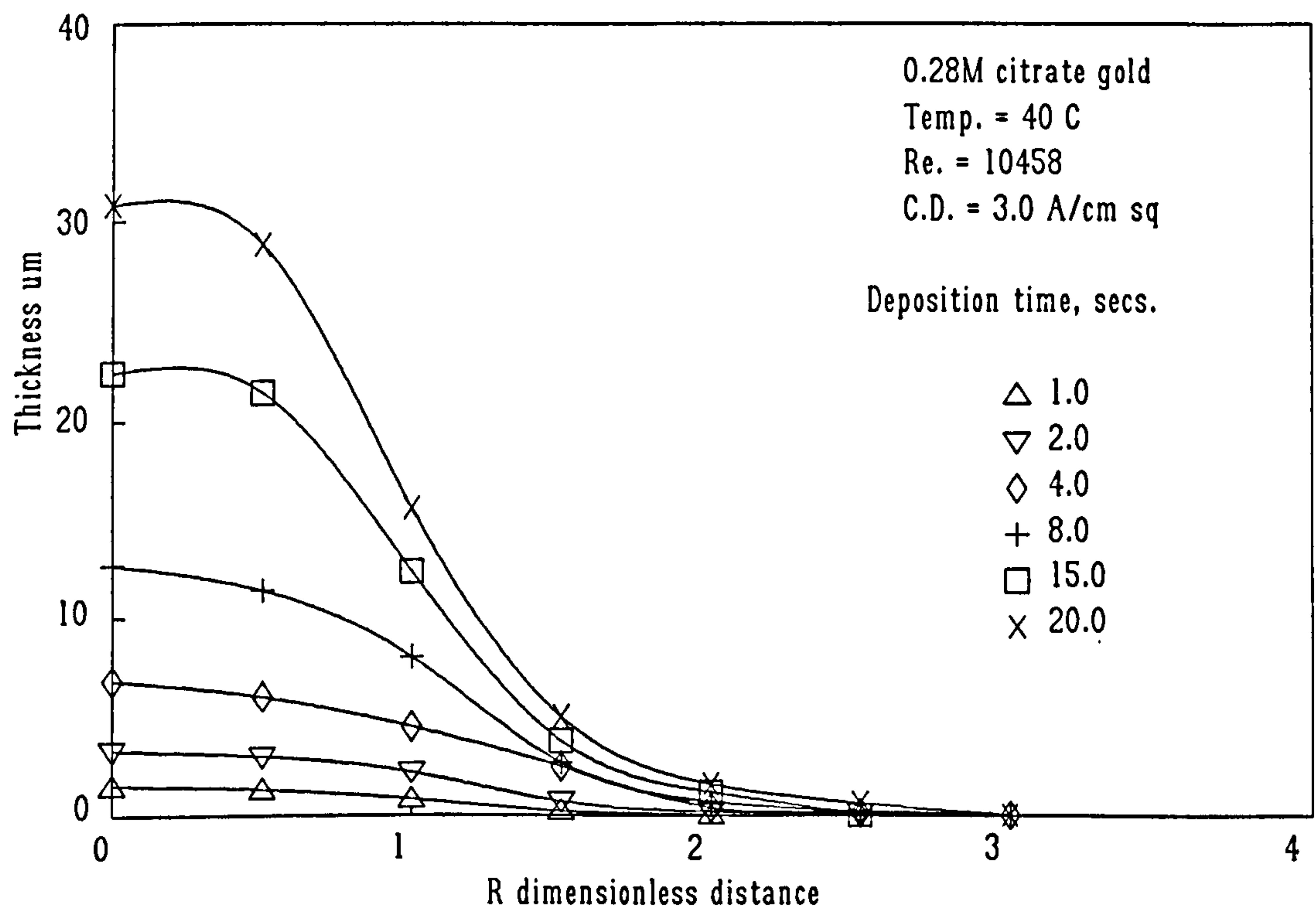


Figure 61. The effect of increasing deposition time on the selectivity. The data for $T = 0.5$ is not shown.

This would indicate that mass transfer was constant in the stagnation region. Also, at $R = 0.5$, the growth rate was also linear in its relationship with time. This position corresponds approximately to the edge of the stagnation zone. However, this relationship was not valid outside the impingement region. Figure 62 shows a plot of the ratio of the thickness at the jet centre-line to various values of R outside the impingement region. It can be seen that for deposition times above 8 seconds ie

when the characteristic "dome" shape has fully developed, the ratios are virtually constant. However, during the initial stages of growth, there is an acceleration in the rate of growth of the stagnation zone compared to the wall jet region, particularly at high values of R . It is proposed that there is a sudden increase in the rate of deposition in the stagnation zone due to an increase in the local current density at this point. This is because the distance between the deposit and the substrate has been reduced and because of the highly non-uniform current distribution within the jet, the electric field is enhanced. The deposit grows at an enhanced rate within the stagnation zone with respect to the wall jet region. This can be seen by the significant increase in the ratio at low deposition times.

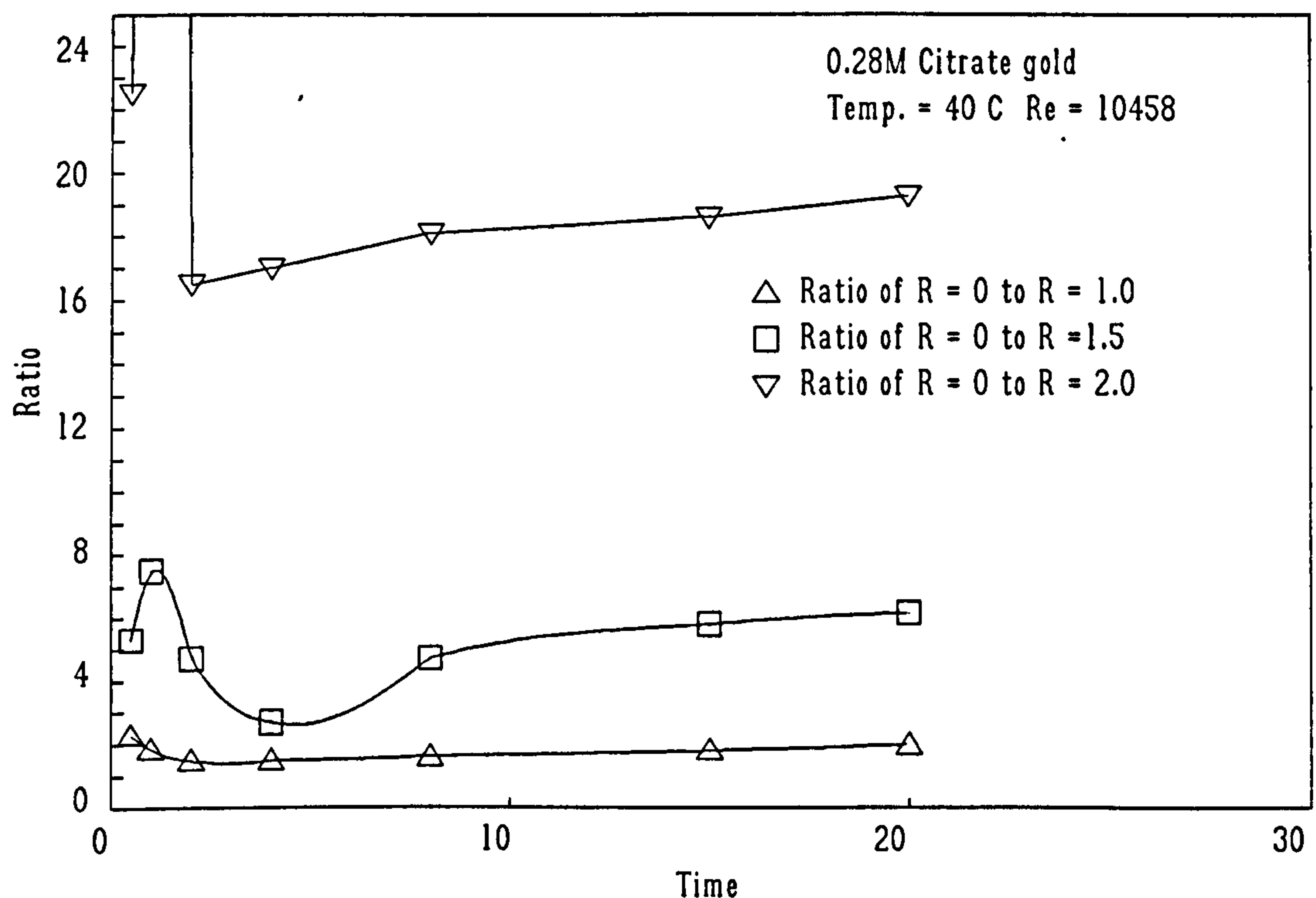


Figure 62. The effect of increasing time on the ratio of centre-line thickness to various values of R .

Additionally, due to this increase in current density, the wall jet operates at a lower current density at which the efficiency is lower. As the deposit grows, two things happen. First, the position at which the wall jet forms will be shifted away from the stagnation region as the flow is no longer normal to the substrate. In effect, the stagnation region becomes larger. Secondly, flow into the wall jet becomes accelerated, similar to the effects of an aerofoil. This increase in acceleration would have the effect of reducing the thickness of the boundary layer, which in turn would reduce

the thickness of the diffusion layer compared with a flat surface. Consequently, an enhanced current density over and above that previously experienced would prevail in the transition region between the impingement region and the displaced wall jet region. As a consequence, the efficiency would also improve. The evidence for this lies in the sudden reduction of the ratio as observed in the graph with increasing deposition time. As the deposit continues to grow, the growth rate in the wall jet region attains a comparable ratio to that in the impingement region, although there is a noticeable upward slope in these values. This would be expected as the deposit becomes increasingly "domed", further displacing the wall jet away from the stagnation region and increasing the local acceleration in the wall jet. Additional evidence for this mechanism can be seen in Figure 63. The data for this was taken from the study of the effect of nozzle to substrate distance. It can be seen that when the nozzle is very close to the substrate, a greater differential thickness occurred between the impingement region and the wall jet. This is because a narrow gap would emphasise the difference in current distribution between the two regions. Further evidence of the mechanisms operating would require a detailed study of flow rates and local mass transfer on hemispherical substrates of the same dimensions as the nozzle. This was beyond the scope of this work.

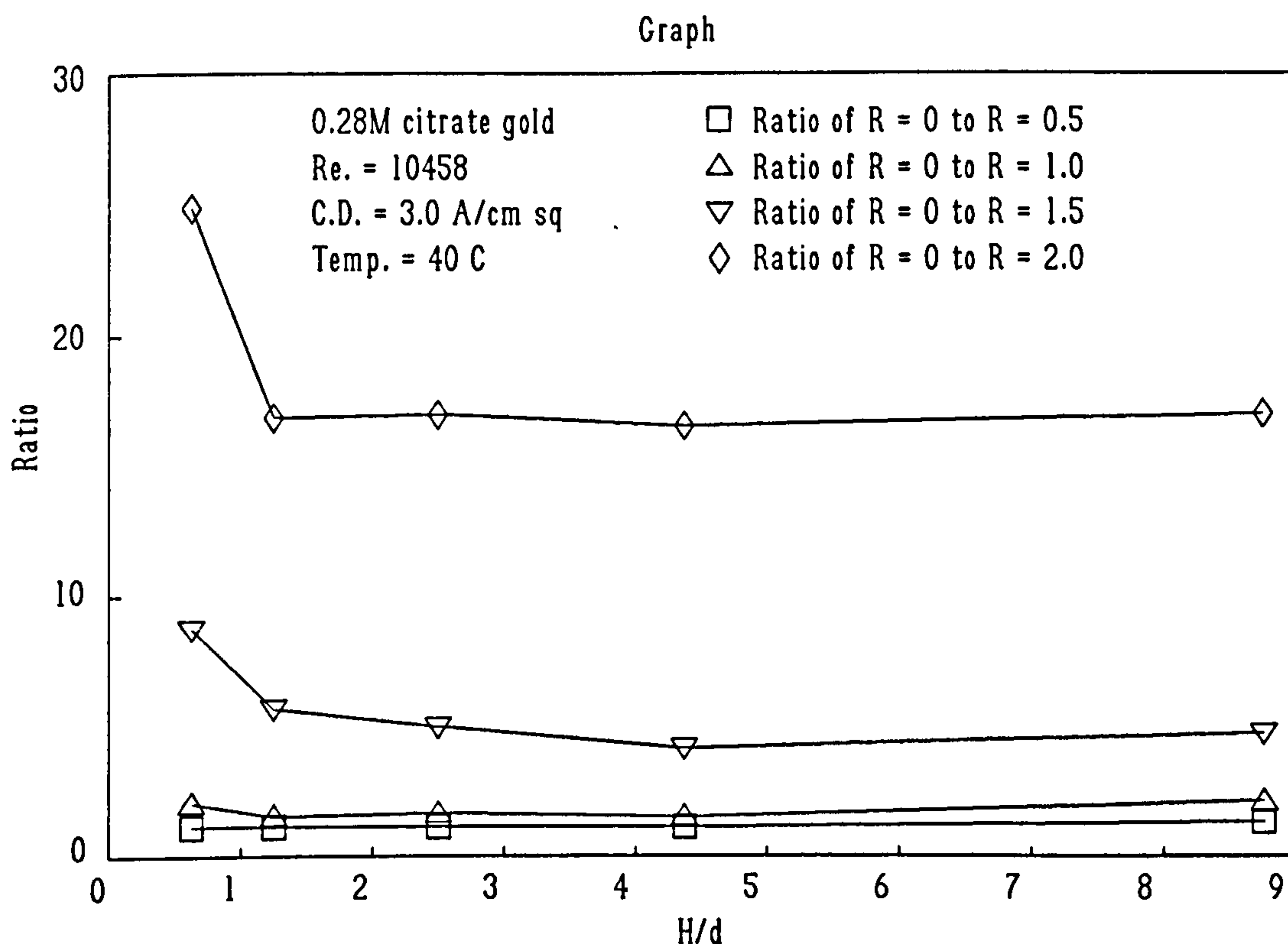


Figure 63. The effect of the nozzle to substrate distance on the ratio of the centre-line thickness to various values of R.

10.6.2 Interaction of the flow above the maximum useful current density.

As has been shown earlier, the deposits lose their featureless appearance under certain conditions of current density, flow or temperature. The deposits then take on a nodular, needle-like or dendritic character. The morphology diagrams show such transitions. There are many factors that influence these transitions and it is certain that the interaction of the flow with the deposit will depend on such factors as the interplay between temperature, current density, flow rate, nozzle to substrate distance and chemical composition of the electrolyte. Such complex interactions are difficult to evaluate but each individual growth structure will be discussed separately. It should be noted that in the case of the alloy golds, no structures other than nodular types were observed under the conditions examined. As a consequence, the discussion will be limited to that of pure gold.

10.6.2.1 Nodular deposits.

As the current density exceeds the maximum useful current density, the deposit growth habit changes from a relatively smooth surface, exhibiting small rounded mounds, to a true nodular structure. In fact, it would appear that the nodular structure is just a coarser version of the rounded mound. There is no fixed transition point, the mounds simply grow to greater dimensions for greater values of applied current density. The formation of nodules creates a different surface for the impinging electrolyte. Surface imperfections reach length scales of the diffusion and boundary layers and local interaction with these become likely. If the magnitude of the nodules does not exceed the thickness of either the diffusion layer or the boundary layer, then nodular growth will proceed unhindered. As with this type of growth, no direct interaction with the fluid flow occurs, this subject will be discussed in greater depth later.

10.6.2.2 Needle-type deposits

At low temperatures, an increase in current density leads, in most instances, from nodular deposits to the formation of needle-like forms. These structures form very rapidly under suitable conditions. At low current densities, they grow from the jet centre-line but at higher current densities, they commence from a certain distance from it. The exact position at which they grow is a function of the current density but would appear to be associated with the edge of the stagnation zone. Evidence for this is that for the same current density, the diameter of the needle free region reduces with increasing flow rate. They extend in a radial fashion from this region to a diameter of about 600 μm irrespective of the prevailing deposition conditions. The formation and number of needles produced tends to be a function of the flow rate and the temperature. Higher temperatures

with low flow rates lower the number of needles formed. Examination of deposits exhibiting needles in the process of formation has indicated that the tip radii are very small ($< 0.1 \mu\text{m}$). However, examination of tips that have reached their "maximum" length of around $225 \mu\text{m}$ show radii in the region of $1\text{-}2 \mu\text{m}$. This suggests a mechanism by which the needles grow and what limits their length. It is proposed that the needles grow by a mechanism of spherical diffusion. With low metal ion concentrations, increasing the current density rapidly leads to a nodular deposit formation due to ion depletion. Once the nodule size exceeds the thickness of the local boundary layer, needle structures form by creating a wake in the direction of the flow. This wake causes turbulent eddies that disturb the boundary layer leading to enhanced local agitation that allows a preferred growth in the direction of the flow within the wake. Once the growth tip attains the critical radius for needle growth, then growth proceeds via spherical diffusion in the direction of flow behind the eddy. Higher current densities promote the onset of needle growth by generating large nodules at increased distances from the centre-line. Additionally, an increase in the current density promotes the rapid growth of these nodules, leading to a greater number of needles to be formed.

The type of needle structure strongly depends on the prevailing temperature as described in Section 8.1.2.2. At low temperatures, flow rates and current densities, the needles are varied in size and shape. At high flow rates, there are a larger number of needles and they have a more regular size. Increasing the temperature leads to needles growing in both the radial and axial direction. At low flow rates under these conditions the needles grow mainly in the axial direction and form jet core structures, usually emanating from within the stagnation region. The form the needles take is highly dependent on their interaction with the boundary layer. It is suggested that the variance in size and shape of the needles seen at low flow rates and temperatures is due to the increased viscosity of the electrolyte when compared to higher temperatures. Due to the viscous nature of the flow, the eddies that form are damped and highly dependent on local conditions. This will lead to a variation in the shape and size of the needle. At high flow rates and low temperatures, the needles are of a more consistent size, due to the increased shear stresses within the flowing liquid. This leads to a less damped eddy formation beyond the protruding nodules and therefore a more regular growth habit. High temperatures also allow the eddies to proceed undamped due to the lower viscosity of the electrolyte. High flow rates increase the number of needles because of a greater interaction between the nodules and the thinner boundary layer. As well as radial growth, the needles thicken as they grow. It is this process that leads to the limit of radial growth. As the needles thicken, they effectively shield the growing tips and rob a greater proportion of the current. This shielding effectively reduces the overpotential at the growing tip and the critical overpotential for needle growth is reduced. In addition, it is likely that the metal ion concentration available to the tip is seriously reduced thus lowering the local limiting current density. Indeed, it has been observed that at low metal ion concentrations, considerable nodule growth occurs on the needles within the impingement region but this is not seen close to the needle tip. Henceforth, the tip no

longer grows in a radial direction. However, although no further increase in length occurs, some growth in the diameter of the needles may still take place. This would explain why fully formed needles have comparatively large tip diameters.

10.6.2.3 Field oriented jet core structures.

Some of the more unusual and beautiful growth patterns are observed at high current densities and medium to high temperatures. These are field oriented jet core structures. Photographs 9 and 12 show examples of such forms. It can be seen that they are varied in shape, and indeed, they are a small number of the variations on the general theme. However, there are two basic types of jet core growth. These are central growths, that extend into the central region of the free jet and edge growths. The latter grow along the outer edge of the free jet. The variations that occur to these basic shapes is largely due to local turbulences and electric field variations, each of which become markedly modified as the deposit grows. There is no clear distinction between these growths however as examples have been observed that obviously begin their growth as needles but then, after attaining a certain axial size, start to grow within the free jet. Other examples commence growth in the radial direction but is then diverted along either the edge of the free jet or along the centre-line. These structures are not true dendrites, as they possess no crystalline regularity. Some do have a regular growth front, resembling DBM structures. They tend to grow along the free jet edge as fern-like forms, growing from a single point but flattening and branching to form a cylindrical configuration. Multiple layers of these branches may be observed, resembling the petals of flowers. Others show just a single layer and resemble a crown.

One thing is common to this type of growth. In all cases, they appear to start at the edge of the stagnation zone. Those that grow along the jet centre-line do so from a point or points away from it. Photograph 12 shows the way in which a centre-line core structure forms. Initially, a nodular deposit forms. Then, at one or more points at some distance from the centre-line, a nodule penetrates the wall jet boundary layer and forms a radial needle. The most likely point at which this would occur is at the edge of the stagnation zone. At this point, the wall jet commences and the boundary layer is at its thinnest. This would account for the regular radial position of the needles observed in Photograph 12(c). Because of the high current density associated with these structures, the head of the needle experiences enhanced growth compared to the tails by virtue of ohmic influences. It grows rapidly and meets the electrolyte flowing in the axial direction. Here, it is subject to both a high electric field and a high flow rate and growth accelerates even further. It can be seen that in addition to growth towards the nozzle, secondary growths may be observed away from the nozzle as needles form in the direction of the flow. The mechanisms for the formation of these are similar to those described previously.

The mechanism of growth of the fern-like forms that grow along the edge of the free jet are not so clear. Examination of all the deposits would indicate that centre line forms tend to grow at lower values of Reynolds number, lower current densities and lower temperatures compared with the former. It is thought that the crown-like structures develop as a result of additional turbulence in the edges of the free jet due to the greater velocities but the exact mechanism would require further investigation.

One of the features of the deposits formed at high current densities is their lack of crystalline regularity. Many of the fern-like or crown-like forms resemble fractal structures whilst others resemble dense branched morphology (DBM) types. Generally, there would appear to be a regular growth front like that observed with DBM structures. However, closer examination reveals a significant number of irregular growths within them. Because of the highly non-equilibrium conditions of deposition, it is not surprising that a mixture of both may be present. The presence of a regularly growth front would suggest that these are DBM type forms. The method of growth suggested by Barkey (Section 5.1.5), in which a thick boundary layer exists at the growing tips, is unlikely under the high rates of flow experienced during growth. Tip splitting is certainly a feature but it is more likely that this occurs due to nucleation and growth on or close to the tips leading to secondary and multiple arms forming. This process is repeated creating a multi-branched growth. Stability of the growth front may be induced by means of the constancy of the impinging flow together with the effects of the electric field, which would also be constant across the jet. However, there are many examples in which certain branches grow at the expense of others leading to a non-uniform growth front. The most likely explanation is that all the structures are fractal diffusion limited aggregates (DLA) and that in some cases, regularity is produced due to the overall interaction of the flow and the electric field. Indeed, under these conditions of growth, the deposition is truly diffusion controlled.

10.7 THE GROWTH OF NODULAR DEPOSITS.

Whilst the fractal structures produced at very high current densities are an interesting field of study, they do not constitute a major limitation to the production of smooth deposits that possess useful properties. All the above phenomenon are preceded at lower current densities by the formation of nodular deposits. Smooth deposits have been shown to be produced at rates as high as 3.4 $\mu\text{m}/\text{second}$. However, if the current density is increased, then the deposit becomes increasingly nodular and therefore, for most applications, useless. It has been shown that smooth deposits of both gold and gold/nickel alloy, exhibit rounded mounds. Microsections have shown that these rounded mounds extend to a region close to the substrate. With increasing current densities, the rounded mounds grow in both radial size and height. At some current density, depending on the

prevailing conditions, the mounds become nodules, that is they no longer exhibit integrity with their neighbours. This is the true limiting condition to high speed jet deposits of gold. The mechanism by which these structures form will now be discussed.

10.7.1. Inhibition versus diffusion mechanisms

Nodular deposits are produced when diffusion controls the rate of reaction. They occur as a consequence of low surface adion (partially electronated ions) concentration, low rates of surface diffusion and are generally associated with 3-dimensional nucleation. In Chapter 5, the various mechanisms of surface amplification of irregularities were discussed. The main factor that controlled whether a perturbation would be amplified or not depended on it being stabilised by means of surface tension. The surface tension is controlled by the surface concentration of adions. At low adion concentrations, the stabilising influence of the surface concentration is lost and the perturbation will grow, forming a nodule. In the case of gold, rounded mounds (the early stages of nodule formation) are often observed when depositing thick alloy hardened gold deposits. Nakahara studied the formation of these rounded mounds. The mechanism for such a growth was suggested to be due to inhibition of lateral growth due to adsorbed species. However, as such growths are often seen under diffusion controlled deposition in other deposition systems, this may not be the only mechanism. If we consider the mechanisms of deposition of gold as described by Eisenmann,²¹ growth proceeds via an adsorbed AuCN species and CN^- is produced from this reaction. At high deposition rates, significant quantities of CN^- will be produced influencing the surface equilibrium. As adsorption is a relatively slow step, it is likely that only a low surface concentration of adsorbed AuCN can exist on the surface under these conditions and growth will thus proceed with a low adion concentration. The higher the current density, the lower the adion concentration. Stability theory suggests that as the surface concentration is lowered, the growth of increasingly smaller perturbations increases, as the surface concentration controls the surface tension of the growing crystallites. When the surface concentration becomes exceedingly small, stability is lost and smaller perturbations will grow increasingly larger to form extensive nodulation. The nodular deposits from pure HSSJE gold show evidence of 3-dimensional nucleation. This occurs when little surface diffusion occurs under conditions of high applied overpotentials. It is suggested that particularly in the case of pure gold, nodular deposits result when the AuCN is reduced as soon as it reaches the surface with little time for surface diffusion. Consequently, the high overpotential forces the immediate nucleation with near neighbours leading to a small perturbation. As the surface concentration is low, the perturbation grows due to instability and benefits from enhanced diffusion. This creates a situation where further growth occurs on the perturbation at the expense of the surroundings. Consequently, the perturbation grows from a single nuclei, or small group of nuclei, rapidly in the direction of the diffusion gradient and the electric field.

The typical inverted cone sectional profile of the nodule results because the radius of the growing perturbation is not small enough to benefit from spherical diffusion as a dendrite would. This is because 3-dimensional nucleation produces a cluster formation which is significantly larger than the growth of a spiral dislocation that leads to a dendrite. The cluster of crystallites will benefit from some diffusion in a lateral direction, leading to an increase in the diameter of the nodule as it grows. Additionally, as the nodule robs the diffusion layer of ions as it grows, it effectively inhibits the region surrounding it from further growth. This ultimately creates a growth that is not integrated with and proud of its immediate surroundings. The degree to which the nodule protrudes above its surroundings is dependent on all the factors that control its growth and is therefore predominant at high current densities. At lower current densities, more ions are available in the diffusion layer and thus can reach the regions adjacent to the nodule allowing them to grow as well. Consequently, at lower current densities, nodules may be incorporated within the deposit with only the tops showing. Such a situation would account for the rounded mound structure. It is clear from microsections that where rounded mounds are observed, they emanate from a single point on or close to the substrate and grow as individual entities but due to surrounding growth, are integrated within the deposit.

Whilst such a mechanism may operate in the absence of surface inhibition, it does not preclude the influence of inhibition on nodule growth. Indeed, inhibition of lateral growth could also lead to nodule formation by a slightly different route. In Nakahara's study of cobalt hardened gold, he found that the rounded mounds were evenly distributed with diameters of the same order as the thickness. Such regularity would not be expected based on the randomness of diffusion processes exclusively and indeed, nodular deposits of pure gold exhibit a wide range of sizes. Nakahara suggested that the reason for these mounds was the inhibition of lateral diffusion by non-metallic species. As a consequence, small perturbations were amplified in the axial direction. He also suggested that due to the adsorption of inhibiting molecules on the top surface of the mound, continuous nucleation occurred, in effect, 3-dimensional nucleation. This was responsible for the small grain size observed.

Both mechanisms are equally feasible in the formation of nodules. In the case of alloy golds, it is clear that even under conventional deposition conditions, a relatively small grain size is produced. This is usually as a result of surface inhibition and 3-dimensional nucleation, which is the way most brighteners work. In the case of pure gold deposited conventionally, the grain size is not unusually small, indicating that little or no inhibition is in operation. Under conditions of high speed deposition, the grain size is reduced to similar values as the alloy golds. It is well known that increasing the current density leads to a smaller grain size but in this case it is uncertain whether the reduction is due purely to this factor alone. The cyanide generated during deposition can readily

adsorb on a surface such as gold particularly as it is formed on the surface. Further studies are required to establish the actual mechanism of nodule formation, particularly with regards adsorption phenomenon.

10.8. SUMMARY OF FACTORS CONTROLLING THE MAXIMUM DEPOSITION RATE.

It is clear from the preceding results and discussion that the factors that control the maximum deposition rate during HSSJE are complex and highly interactive. Under conventional deposition conditions, the accepted ways of increasing the deposition rate such as increasing the metal ion concentration, increasing the rate of agitation, increasing the temperature and the use of additives are practical and valid. Under conditions of high speed deposition, such factors become totally dependent on each other. It is to be expected that when a system is pushed to its operating limit, small changes in the operating conditions can have a profound effect on the performance of that system. This has been shown to be the case for HSSJE. Jetting an electrolyte through an air gap has been shown to be capable of increasing the maximum deposition rates of gold by up to 3 fold for thick deposits ($> 10 \mu\text{m}$). Additionally, the method produces deposits selectively without the need for masking. However, it has been shown that for the conditions and electrolytes tested, this increase in deposition rates would appear to be the maximum achievable without a resultant degradation of deposit quality. Increasing the flow rate leads to an increase in deposition rates as the diffusion layer and hydrodynamic boundary layer thicknesses are reduced. However, increasing the flow rate leads to such a reduction in both that an interaction with the growing surface inevitably occurs. This interaction is predominant at very high current densities where a large diffusion gradient and low surface ion concentration exist. This leads to instability in the electrocrystallisation process allowing small surface perturbations to be amplified. As the diffusion layer is sub-micron, a small amplification rapidly grows and penetrates outwards and into and beyond the boundary layer and into the region of uninterrupted flow. Accelerated growth is then experienced in the direction of the flow leading to many beautiful but technologically worthless growths. Once the surface becomes unstable, the deposit is effectively destroyed. Despite the fact that, in the case of pure gold, the maximum useful current density is around 0.7 of the electrochemical limiting current density, it would not seem possible that a further increase could be achieved without the use of growth inhibiting additives. However, the use of such materials is often associated with an increase in polarisation and in the case of gold, a reduction of current efficiency would be probable. In addition, such materials often become incorporated into the deposit, which is likely to affect its functional performance.

The use of pulse plating has been examined as it can often improve deposit quality and smoothness. However, under the conditions examined, no further increase in deposition rates could be obtained. It is likely that the conditions at the interface did not allow the even establishment

of a pulsating diffusion layer that followed the micro-profile of the surface. As a consequence, tertiary current distribution was affected. A further factor was that even though equitable deposition rates to DC could be achieved, the deposits were more porous due to gaps between the mound structures. These almost certainly result from inhibition of the lateral faces during the off-time by species such as AuCN or CN. It is worth exploring other pulse regimes but there are these intrinsic problems to be overcome.

In the case of alloy golds, much higher current densities can be achieved but at the expense of a lower current efficiency due to the influence of the additives on the polarisation. Many applications of alloy hardened golds now require vanishingly small thicknesses to be applied, as in the commercial connector manufacturing industry. For this industry, it may well be possible to apply such thin coatings at rates an order of magnitude greater than shown in this study. However, for the majority of applications that require thicker coatings, such rates would be hard to obtain without the degradation of the deposit. On the basis of the evidence and the mechanisms proposed in this Thesis, it would seem that we have indeed reached the limit.

References

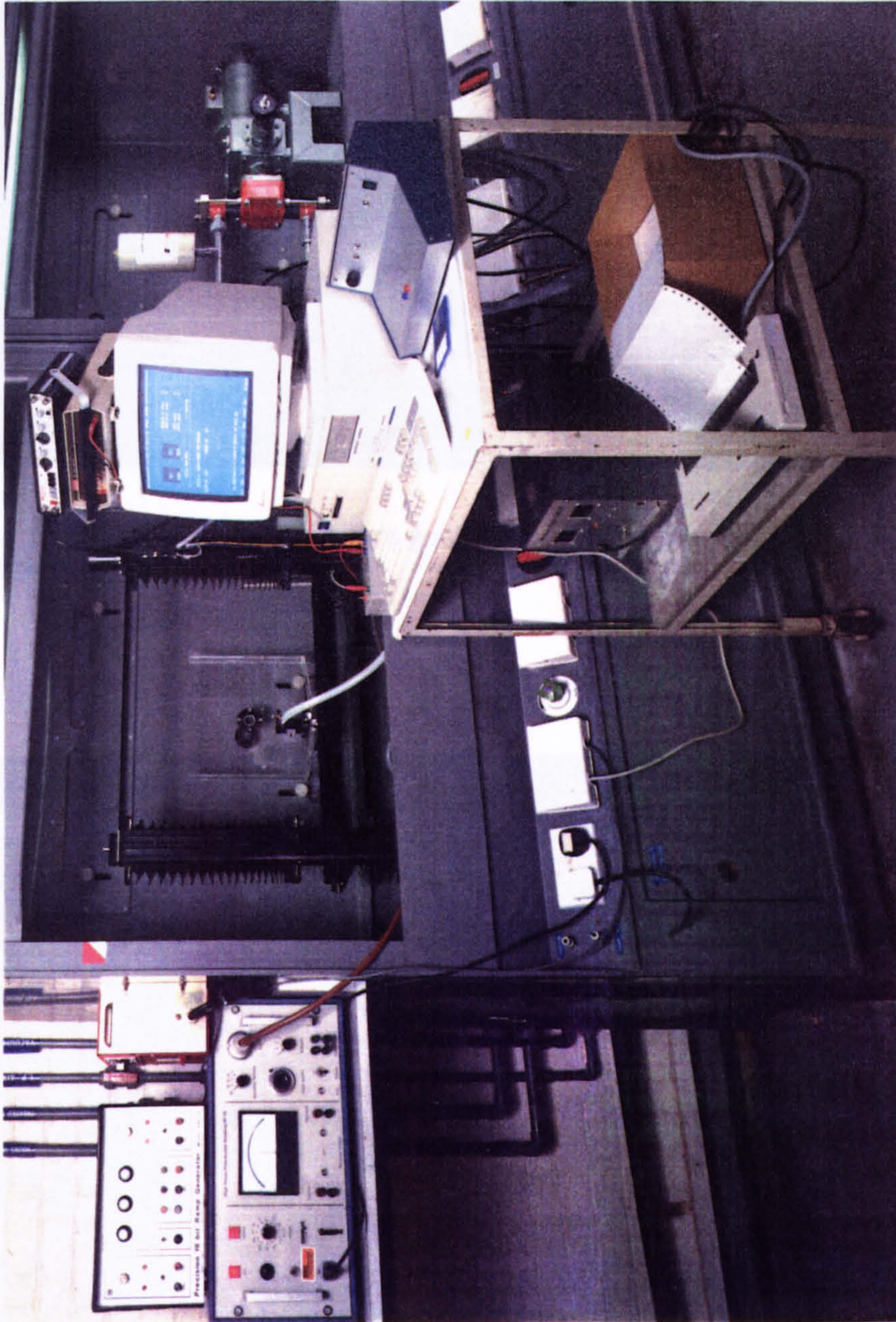
1. T.-J. Chen, Ph.D. Dissertation, University of Illinois at Urbana-Champaign, Illinois (1981)
2. V.E. Nakaoryakov, B.G. Pokusaev and E.N. Troyan, *Int. J. Heat Mass Transfer*, **21** 1175 (1978)
3. M.B. Glauert, *J. Fluid Mech.* **1**, 625 (1956)
4. D.R. Gabe, Asia-Pacific Interfinish Conf. 1990
5. D.J. Robinson and D.R. Gabe, *Trans. Inst. Met. Fin.* **48**, 35 (1970)
6. *Idem, Ibid.* **49**, 17 (1971)
7. E. Mehl, *Powder Met.* **1**, 33 (1958)
8. D.P. Barkey, R.H. Muller and C.W. Tobias, *J. Electrochem. Soc.* **136**, 8, 2199
9. L. Brugnattelli, *Ann. Chim. (Pavia)*, **21**, 148, 1802
10. F.H. Reid & W. Goldie (Ed), "Gold Plating Technology", Electrochemical Publications Ltd, Scotland, 1974
11. Elkington G.R & H., British Patent 8447, 1840
12. "The consumption of gold products by the West European Electronics and Electrical Industries, third quarter and whole year, 1991", C.G. Wedgewood Consultancy Service, London, December, 1991
13. "Gold 1991", Gold Field Mineral Services Ltd, London, 1991
14. R. A. Ehrhardt, *Proc. Am. Electropl. Soc.*, **47**, 78, 1960
15. F. Nobel, D.W. Thompson, *Plating*, **57**, 469, 1970
16. R. Zimmerman, R. Brennerman, British Pat. 1,275,386, 1972
17. R.W. Hodgson, A.H. Szudlowski, *Plating*, **57**, 693, 1970
18. B.D. Ostrow, F.I. Nobel, British Pat. 1,198,527, 1970
19. H.A. Reinheimer, U.S. Patent 3,833,487, 1974
20. J.D.E. McIntyre, W.F. Peck, *J. Electrochem. Soc.* **123**, 1800, 1976
21. E.T. Eisenman, *J. Electrochem. Soc.*, **125**, 717, 1978
22. S.T. Rao, R. Weil, *Metal Finish.* **57**, 97, 1979
23. T.E. Dinan, H.Y. Cheh, *J. Electrochem. Soc.*, **139**, 410, 1992
24. D.W. Endicot, H.K. James & F. Nobel, *Plating and Surf. Fin.*, **68**, 11, 58, 1981
25. S. Wakabayashi, A. Murata & N. Wakabayashi, *ibid*, **69**, (8), 63, 1982
26. E.C. Rinker & R. Duva, US Patent 2,905,601, 1959
27. C.C. Lo, J.A. Augis & M.R. Pinnel, *J. Appl. Phys.*, **50**, 6887, 1979
28. F.B. Koch, Y. Okinaka, C. Wolowodiuk & D.R. Blessington, *Plating and Surf. Fin.*, **67**, 50, 1980
29. G.B. Munier, *Plating and Surf. Fin.*, **56**, 1159, 1969

30. Y. Okinaka, F.B. Koch, C. Wolowodiuk & D.R. Blessington, J. Electrochem.Soc., 125, 1745, 1978
31. M. Antler, IEEE Trans. Components, Hybrids & Man. Tech., CHMT-4, 1, 15, 1981
32. R. DeDoncker & J. Vanhumbeek, Trans. Inst. Met. Fin., 62, 59, 1985
33. Y. Okinaka, East Report, Eugen G. Leuze Verlag, Saulgau, 1992
34. R.T. Page, Met. Fin. Journ. 19, 274 1973; *ibid*, 19, 338, 1973; *ibid*; 20, *ibid*,
35. K. Lin & R. Weil, J. Electrochem. Soc., 133, 690, 1986
36. S.T. Rao & T. Weil, J. Electrochem. Soc., 127, 1030, 1980
37. K-L. Lin, W-C. Liu, M.H.M. Lin & Y.W. Hu, J. Electrochem. Soc., 138, 3276, 1991
38. M. DeBonte, J.P.Celis, J.R. Roos & J. Vanhumbeek, East Report, Eugen G. Leuze Verlag, Saulgau, 1992
39. M. Antler, Plating, 54, 915, May 1967
40. H.Y.Cheh, J. Electrochem. Soc., 118, 551, 1971
41. D.L. Rehrig, H. Ledheiser & M.R. Notis, Plat. & Surf. Fin., 64, 40, (12), 1977
42. J-C. Puippe & F. Leaman (Ed), "Theory and Practice of Pulse Plating", American Electroplaters and Surface Finishers Society, Orlando, Florida, 1986
43. P.C. Andricacos & H.Y. Cheh, Plat. & Surf. Fin., 44, 9, 1977
44. D.R. Turner, Thin Solid Films, 95, 2, 143 (1982)
45. C.F. Coombes (Ed), "Printed Circuit Handbook", McGraw-Hill, 3rd Edition, New York,
46. N.S. Allen (Ed), "Photopolymerisation and photoimaging Science and Technology", Elsevier, London 1989
47. F.I. Nobel & R.T. Hill, American Electroplaters Society, 'Second Continuous Plating Seminar', 75, 1977
48. D. Heiestad, '8th Annual Connector Symposium', Cherry Hill, N.J. Electronic Computer Study Group, 337, 1975
49. "Texas instruments uses spot plating of gold to cut costs of keyboards", Plat. & Surf. Finish., 62, 9, 846, (1975)
50. G. Menzies, Electronic Prod., 38, May (1978)
51. D.L. Rehrig, Western Electric Eng., 48, April (1978)
52. W.R. Hain & L.W. Rudolf, Western Electric Eng., 91, April (1978)
53. D.R.Turner, Thin Solid Films, 95, 1443, (1982)
54. P. Wingenfeld, Proc. Connectors 91, 91 (1991)
55. M. Rubenstein, Plating, 59, 6, 540 (1972)
56. *Idem*, Electroplat. & Met. Finish. 29, 2, 12 (1976)
57. *Idem, Ibid*, 29, 3, 7 (1976)
58. U.S. Patent No. 4361470

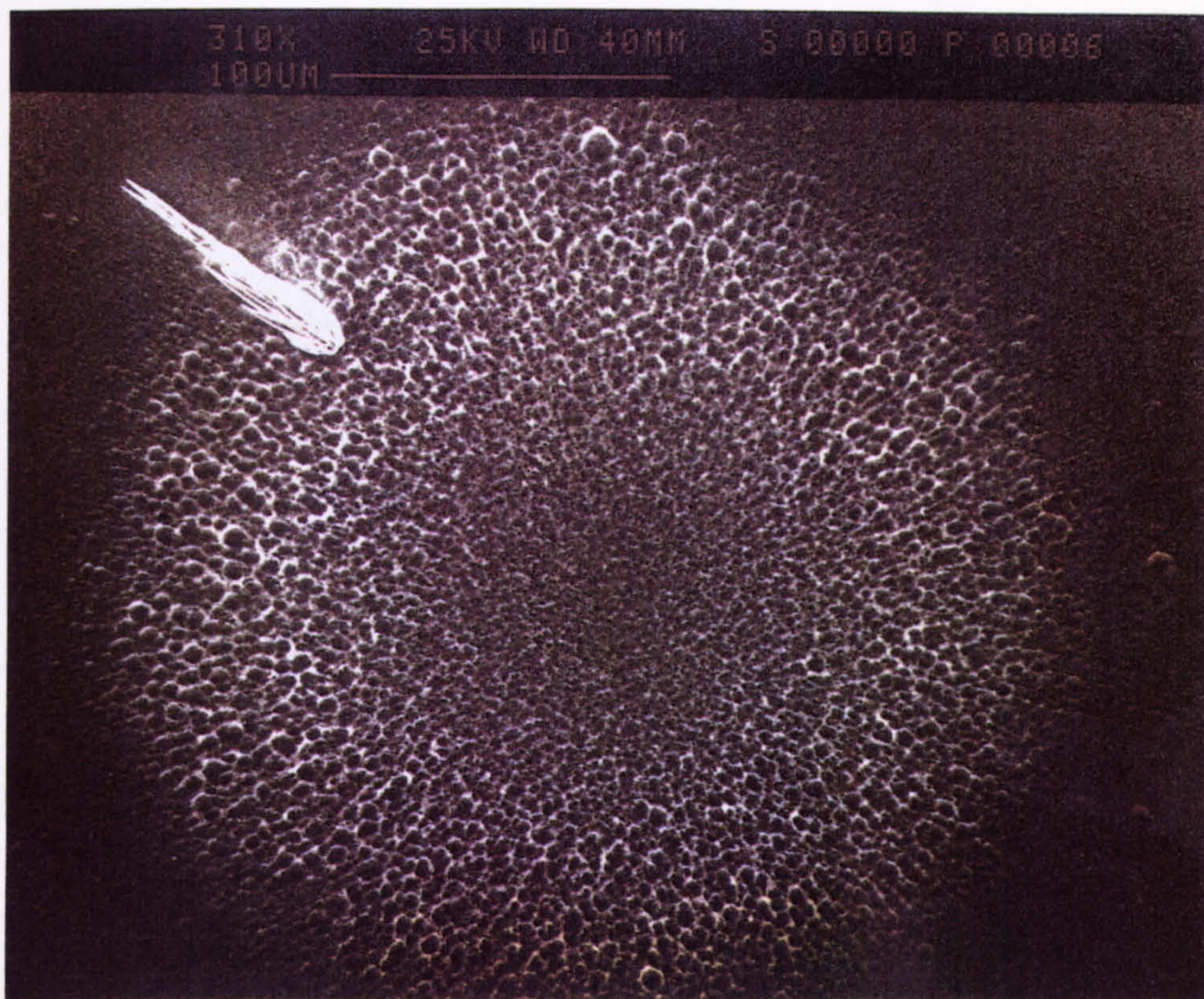
59. U.S. Patent No. 3730740
60. U.S. Patent No. 4001093
61. D. Bacon, U. Landau & R.L. Meek, Western Electric Eng. 19, April 1978
62. N.R.K. Vilambi & D-T. Chin, Plat. & Surf. Fin. 1, 67, 1988
63. D-T Chin, N.R.K. Vilambi & M.K. Sunkara, Plat. & Surf. Fin. 10, 74, 1989
64. D-T Chin & M.K. Sunkara, Plat. & Surf. Fin. 78, 2, 57, 1991
65. G. Cook, 59th International Conference on Surface Finishing, Torquay, April 1991
66. J. O'M. Bockris & A.K.N. Reddy, "Modern Electrochemistry Vol 1", Plenum Press, 1970
67. R.H. Muller, Adv. Electrochem. Electrochem. Eng. 9, 281, 1973
68. J.R. Selman & C.W. Tobias in "Advances in Chemical Engineering Vol 10", Ed. T.B. Drew, G.R. Cokelet, J.W. Hoopes & T. Vermeulen, P. 211 - 318, Academic Press, London, 1978
69. R.G. Hickman, PhD Thesis, Univ. of California, Berkley, 1963
70. D.R. Gabe & P.A. Mekanjuola, Proc. IChemE Symp. No. 98, Loughborough University, April 1986, P. 309
71. W.H. Safranek, Plat. Surf. Fin. 69, 3, 48 (1982)
72. B. Sewell, Trans. Inst. Met. Fin. 50, 121, (1972)
73. J.K.Dorey II, R. Haynes, R.E.Sinitski and R.E. Woods, Plat.& Surf. Fin. 67, 81 (May 1980)
74. D.W. Endicott and G.J. Casey Jr, *Ibid*, 67, 58 (March 1980)
75. H. Fischer, Z. Elektrochem., 54, 459, 1950
76. H. Fischer, Habil & H. F. Heiling, Trans. Inst. Met. Fin., 31, 90, 1954
77. S. Nakahara, Journ. Cryst. Growth, 75, 212, 1986
78. K.G. Sheppard & S. Nakahara, Process. of Advanc. Mat, 1, 27, 1991
79. J.O'M. Bockris, G. Razumney, "Fundamental Aspects of Electrocrystallisation", Plenum Press, New York, 1967
80. J.M. West, "Electrodeposition and Corrosion Processes", Von Nostrand Reinhold, London, 1970
81. R. Piontelli & G. Poli, Comite International de Thermodynamique et de Cinetique Electrochimiques, Second Meeting, Tamburino and Milan 1950, Butterworths, London, 1951
82. D.R. Gabe & D.J. Robinson, Trans. Inst. Met. Fin. 49, 17, 1971
83. N. Ibl, in "Advances in Electrochemistry and Electrochemical Engineering", P. Delahay & C.W. Tobias, Eds. Interscience Publishers Inc, New York, 1962
84. A. Kindler & C.W. Tobias, Abstract 413, p 679, The Electrochemical Society Extended Abstracts Vol 82-1, Montreal, Que, Canada, May 9-14, 1982
85. M. Degrez, R. Winnand, Electrochim. Acta, 29,365, 1984

86. A.R. Despic & K.I. Popov, "Modern Aspects of Electrochemistry Vol. 7", Plenum Press, London 1972
87. W.W Mullins & R.F. Sekerka, Journ. Appl. Phys. **35**, 2, 444, 1964
88. W.W Mullins & R.F. Sekerka, Journ. Appl. Phys. **34**, 2, 323, 1963
89. R. Aogaki & T. Makino, Electrochim. Acta, **26**, 1509, 1981
90. U. Landau & J. H. Shyu, Report EM-2937, Electric Power Research Institute, Palo Alto, Calif. 1983
91. D.P. Barkey, R.H. Muller & C.W. Tobias, J. Electrochem. Soc., **136**, 8, 2199, 1989
92. D.P. Barkey, R.H. Muller & C.W. Tobias, J. Electrochem. Soc., **136**, 8, 2207, 1989
93. C-P. Chen & J. Jorne, J. Electrochem. Soc., **138**, 11, 3305, 1991
94. J.L. Barton & J. O'M. Bockris, Proc. R. Soc. London, Ser. A, **268**, 485, 1962
95. J.W. Diggle, A.R. Despic & J.O'M. Bockris, J. Electrochem. Soc., **116**, 11, 1503, 1969
96. K.I. Popov, Lj.M. Djukic, M.G. Pavlovic & M.D. Maksimovic, J. Appl. Electrochem. **9**, 527, 1979
97. K.I. Popov, M.D. Maksimovic, D.T. Lukic & M.G. Pavlovic, *Ibid*, **10**, 299, 1980
98. K.I. Popov, M.D. Maksimovic, J.D. Trnjacev & M.G. Pavlovic, *Ibid*, **11**, 239, 1981
99. D. Barkey, J. Electrochem. Soc., **138**, 10, 2912, 1991
100. Y. Sawada, A Dougherty & J. P. Gollub, Phys. Rev. Letts, **56**, 12, 1260, 1986
101. D. Grier, E. Ben-Jacob, R. Clarke & L.M. Sander, Phys. Rev. Letts., **56**, 12, 1264, 1986
102. M. Matsushita, M. Sano, Y. Hayakawa, K. Honjo & Y. Sawada, Phys. Rev. Letts., **53**, 3, 286, 1984
103. E. Ben-Jacob & P. Garic, Nature, **343**, 523, Feb. 1990
104. F. Coeuret, Chem. Eng. Sci., **30**, 1257, 1975
105. D-T. Chin & C-H. Tsang, J. Electrochem. Soc., **125**, 9, 1461, 1978
106. A.A. Sonin, J. Electrochem. Soc, **130**, 7, 1501, 1983
107. D-T. Chin & M Agarwal, *ibid*, **138**, 9, 2643, 1991
108. R.C. Alkire & T-J. Chen, *ibid*, **129**, 11, 2424, 1982
109. G.A. Zarb, Proc. 8th Congress of the International Union for Electrodeposition and Surface Finishing, Basel, 5th - 9th September, 1972
110. U.S. Patent No. 3810829, J.C. Fletcher, NASA, May 1974
111. H. Schlichting, "Boundary Layer Theory", 4th Ed., McGraw-Hill, New York, 1960
112. T. Tanaka & E. Tanaka, Bull. JSME, **19**, 133, 792, 1976
113. H.B. Squire, Quart. J. Mech. App. Math., **4**, 3, 321, 1951
114. D.A. Dawson & O. Trass, Can. J. Chem. Eng., **44**, 121, 1966
115. E.J. Watson, J. Fluid Mech, **20**, 481, 1964
116. R. Gardon & J.C. Akfirat, Int. J. Heat Mass Transfer, **8**, 1261, 1965

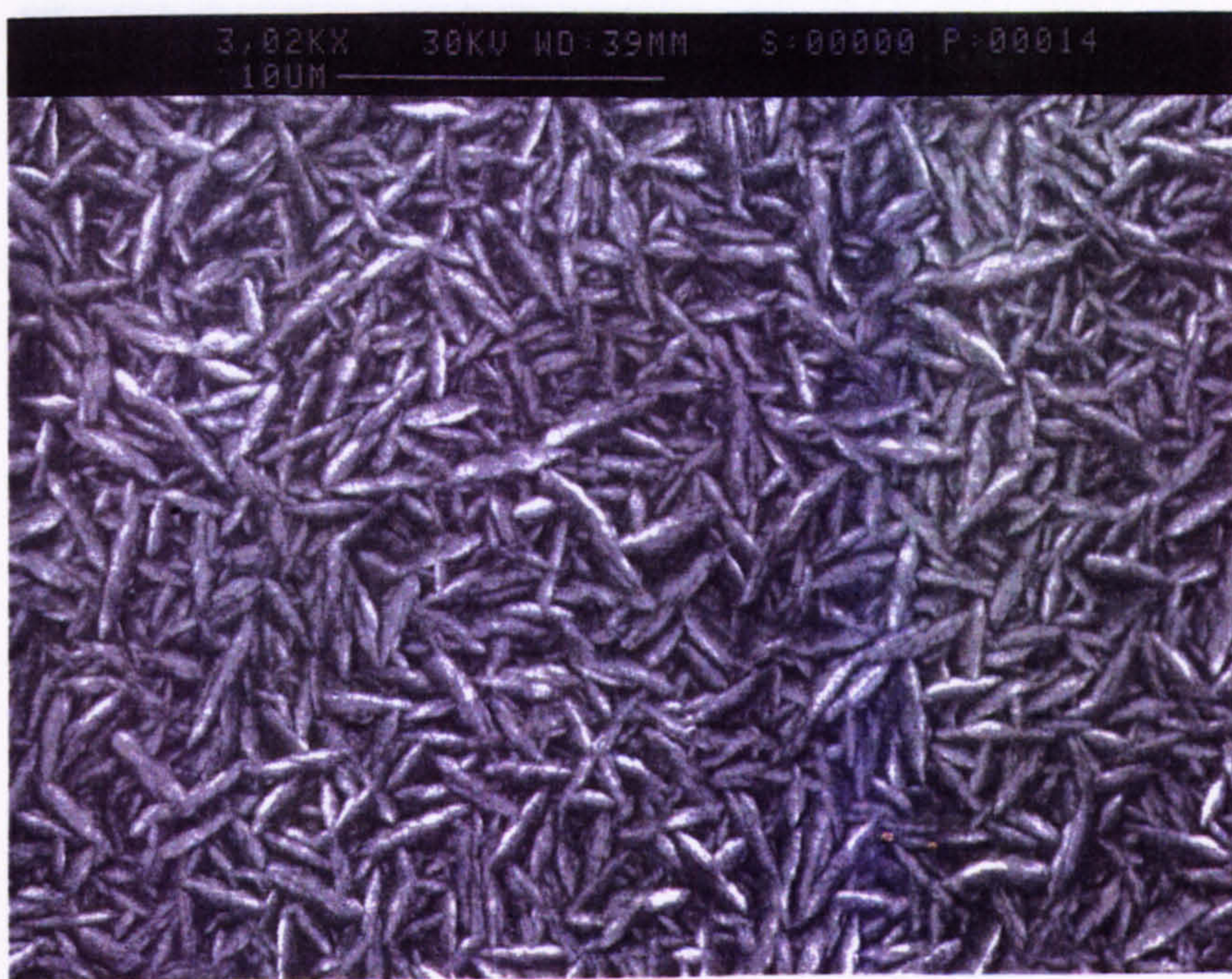
117. F. Giralt, C-J. Chin & O. Trass, *Ind. Eng. Chem. Fundam.*, **16**, 21, 1977
118. M.T. Scholtz & O. Trass, *AIChE J.*, **16**, 82, 1970
119. T. Strand, *Am. Inst. Aeron. Astronaut.*, Paper No. 62, 144, 1964
120. D-T. Chin and K-L. Hsueh, *Electrochim. Acta*, **31**, 561, 1986
121. B.E. Warren & B.L. Averbach, *Journ. Appl. Phys.*, **21**, 595, 1950; **23**, 497, 1952
122. A.R. Stokes, *Proc. Phys. Soc. (London)*, **B61**, 382, 1948
123. "Comprehensive Treatise of Electrochemistry Vol 6", Ed. E. Yeager, J. O'M Bockris and S. Sarangapani, Chapter 3 "Convective Mass Transport", N. Ibl & O. Dossenbach, Plenum Press (New York) 1983
124. J. Newman, "Electrochemical Systems", Prentice Hall, Engelwood Cliffs, N.J. 1973
125. F. Walsh, PhD Thesis, Loughborough University, Loughborough, 1982



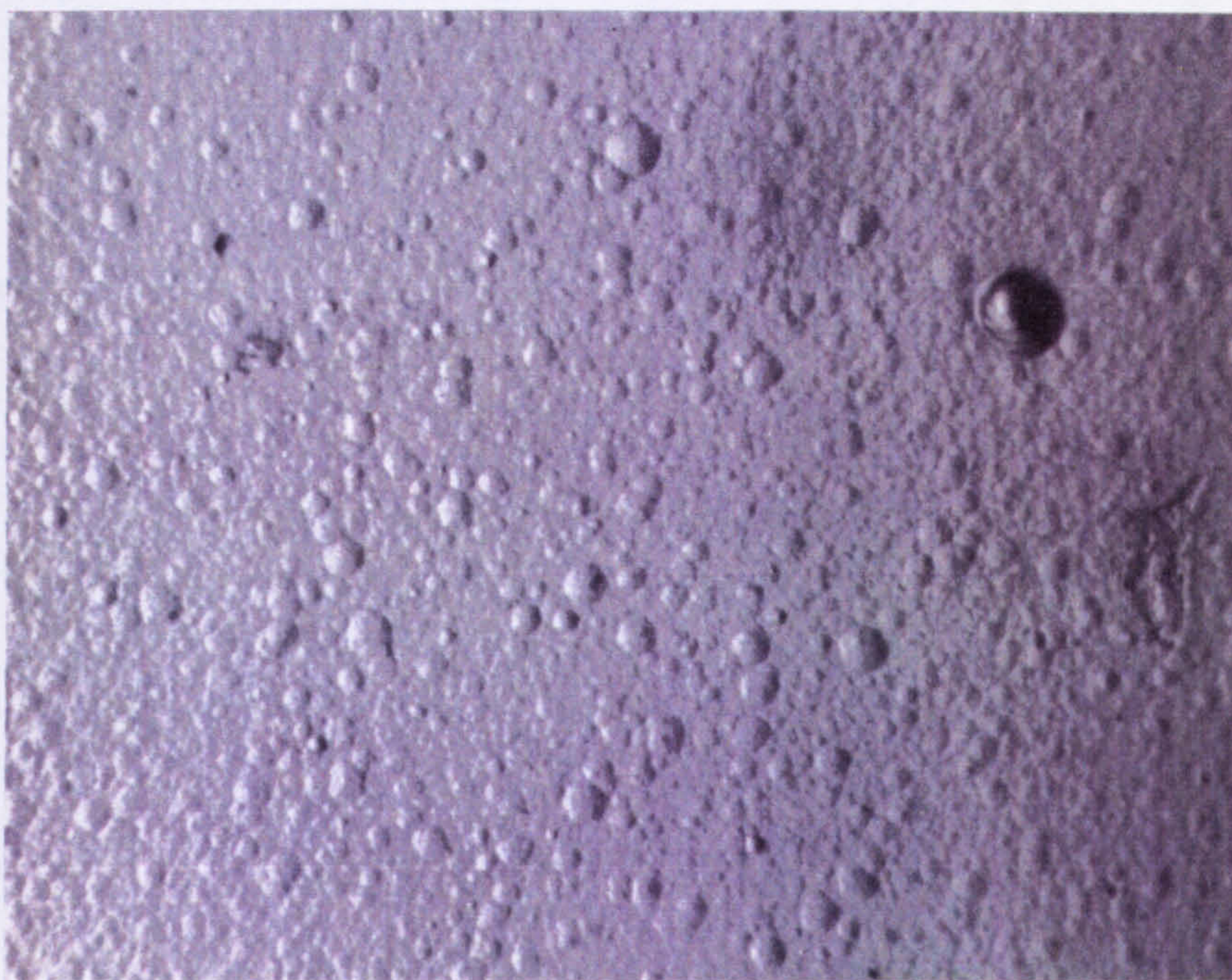
Photograph 1. The X-Y table (in the fume cupboard) with the control computer and ancillary equipment.



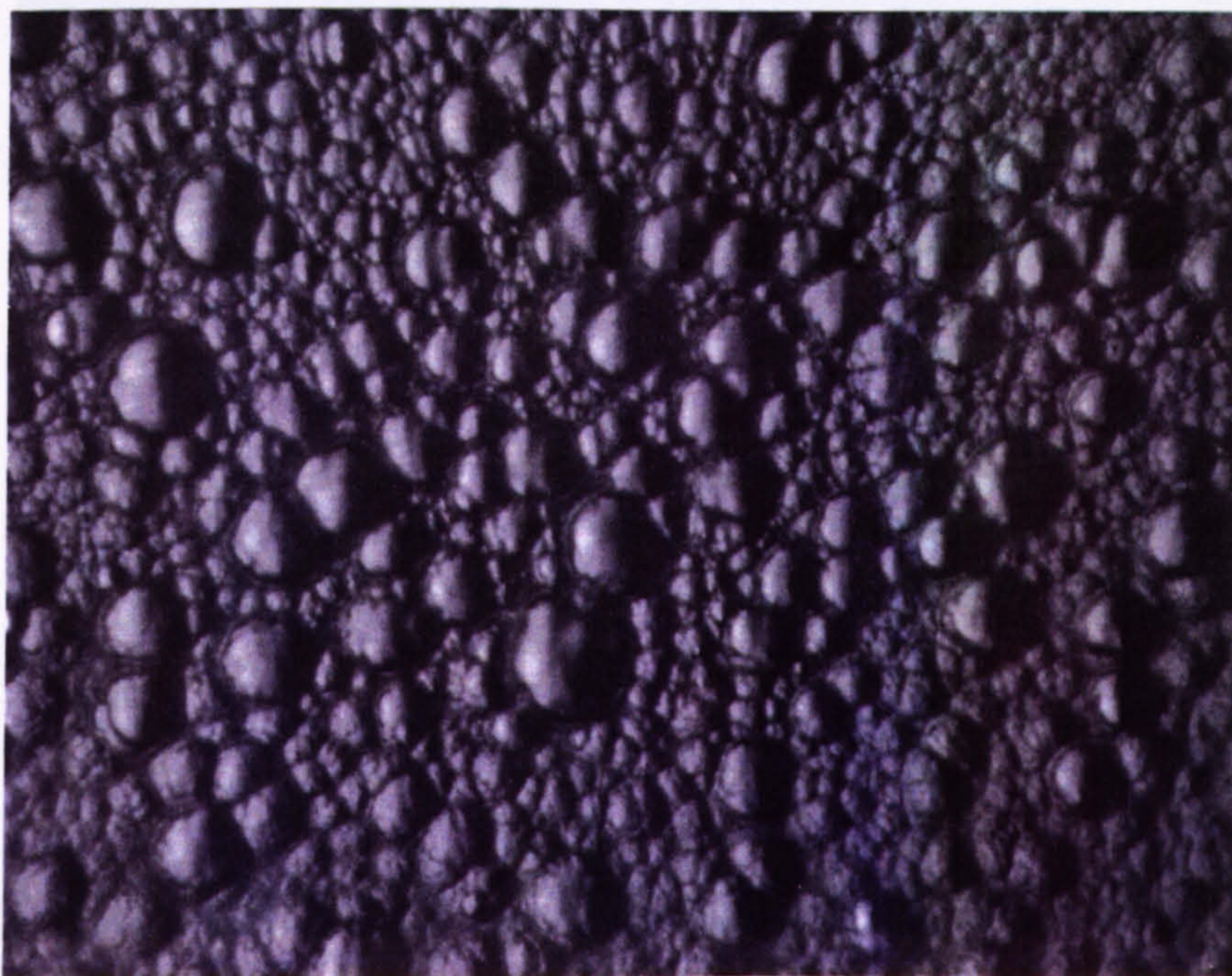
Photograph 2. SEM micrograph of a pure gold deposit produced using $H/d = 4.375$. 0.27M phosphate gold electrolyte.



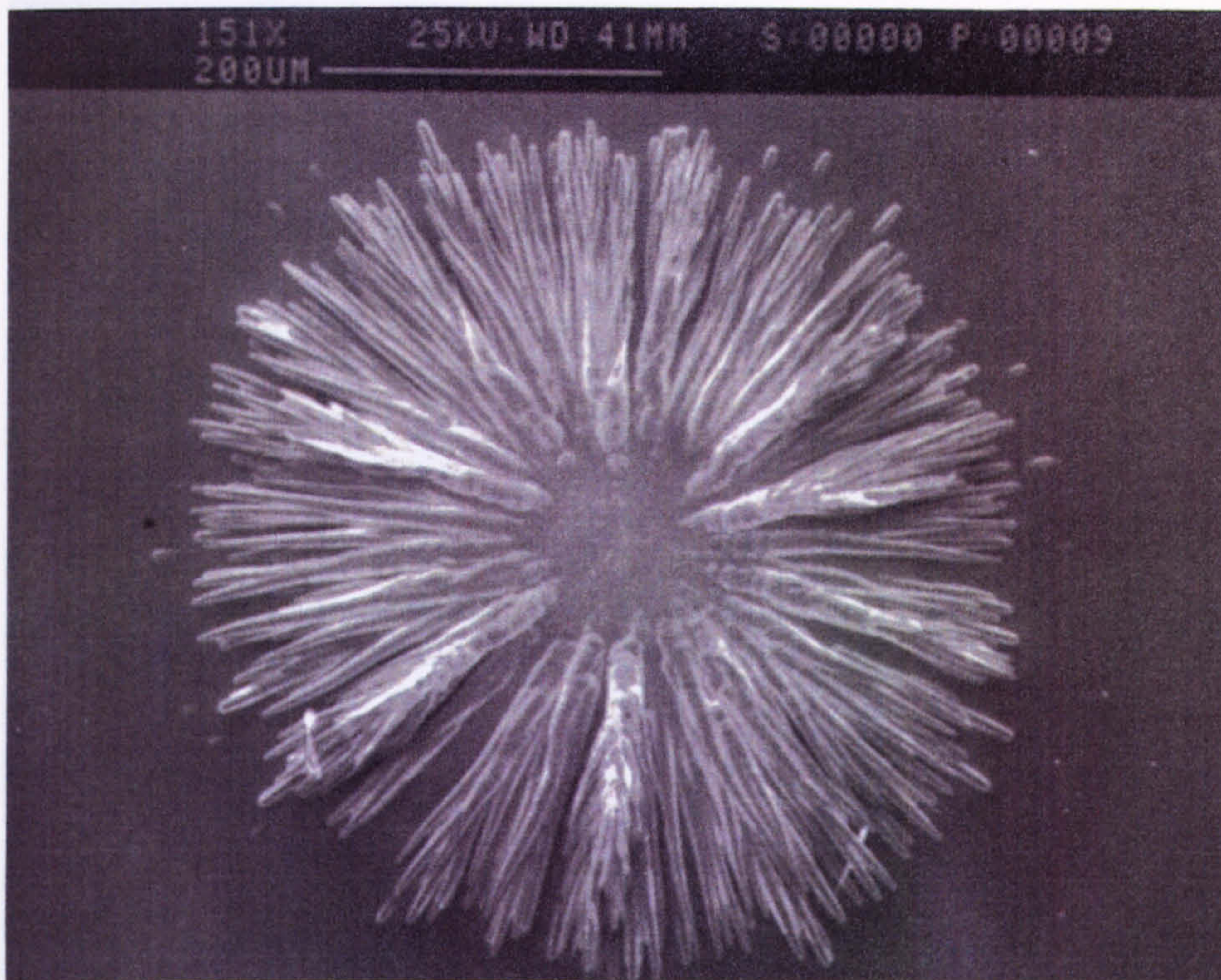
Photograph 3. SEM micrograph of a pure gold deposit produced at a current density of 0.75 A cm^{-2} , typical of a "dull" appearance. The topography is similar to that of a conventional deposit. 0.17M Citrate gold, 55°C



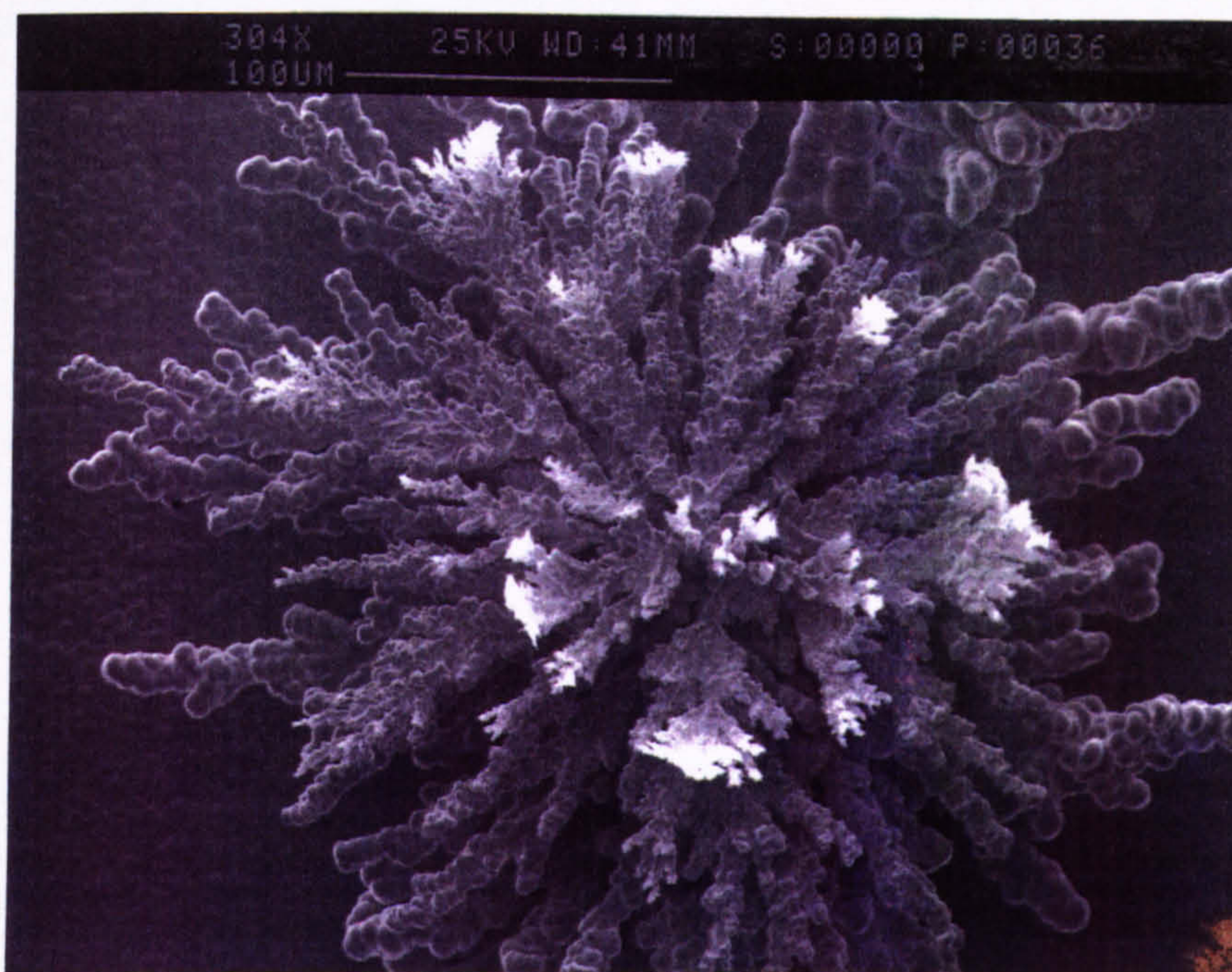
Photograph 4. Optical micrograph of a pure gold deposit produced at a current density of 4.75 A cm^{-2} showing a typical "rounded mound" appearance. 0.17M citrate gold, 55°C .



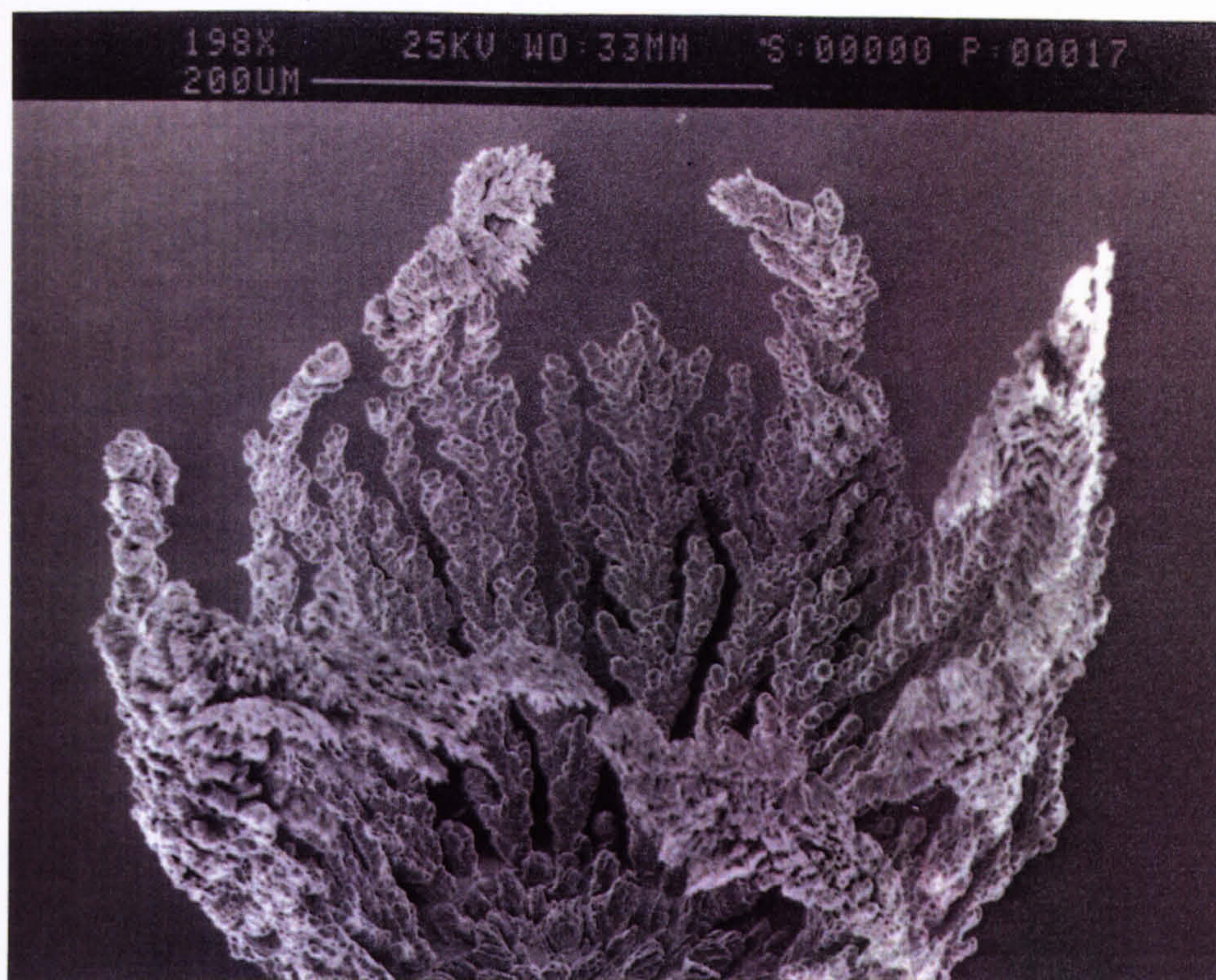
Photograph 5. Optical micrograph of a pure gold deposit produced at a current density of 7.0 A cm^{-2} showing a nodular structure. 0.17M citrate gold, 55°C



Photograph 6. SEM micrograph of a typical radial needle structure.



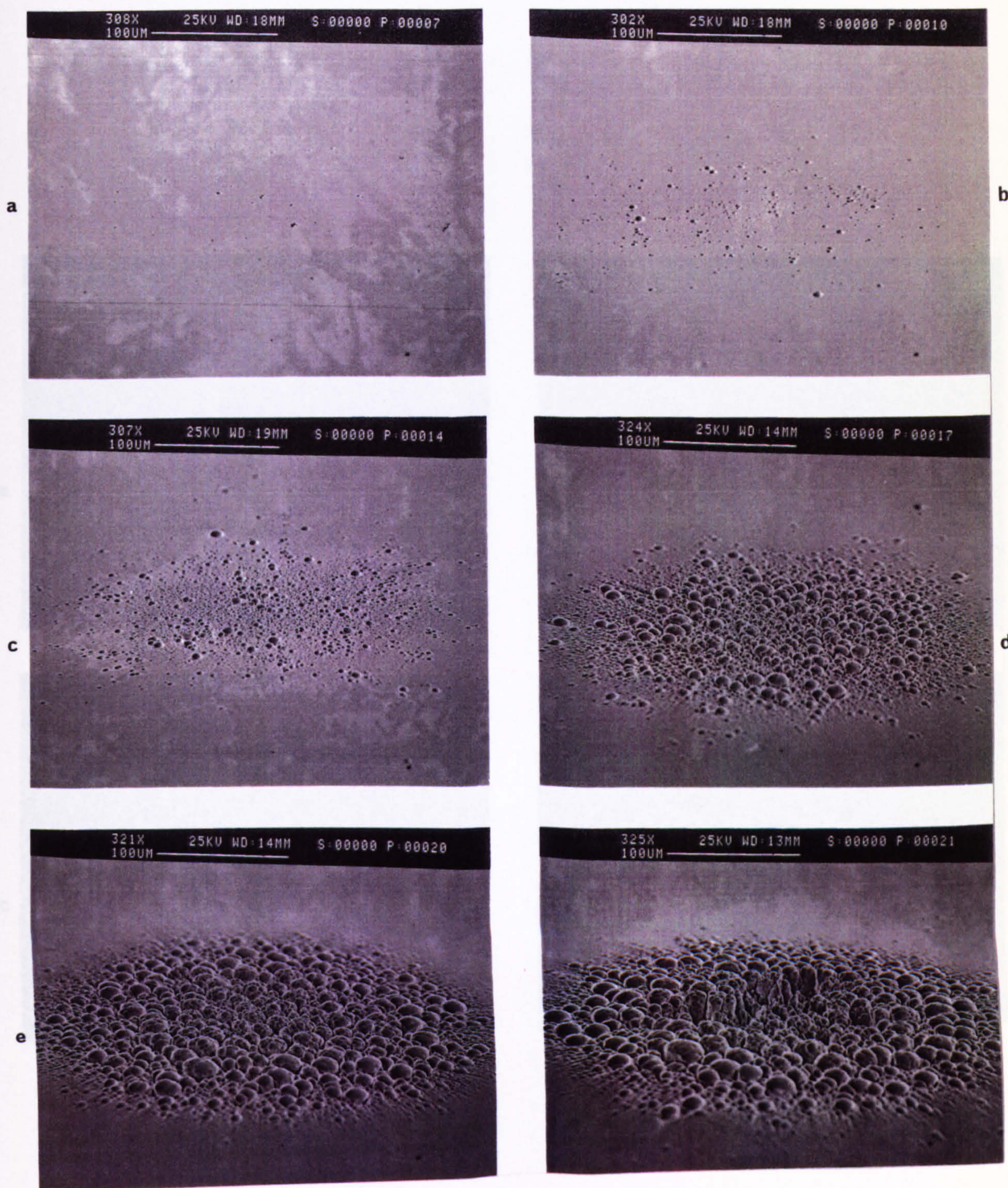
Photograph 7. SEM micrograph of a typical non-directional organic type of growth, classified as "severe needle" type.



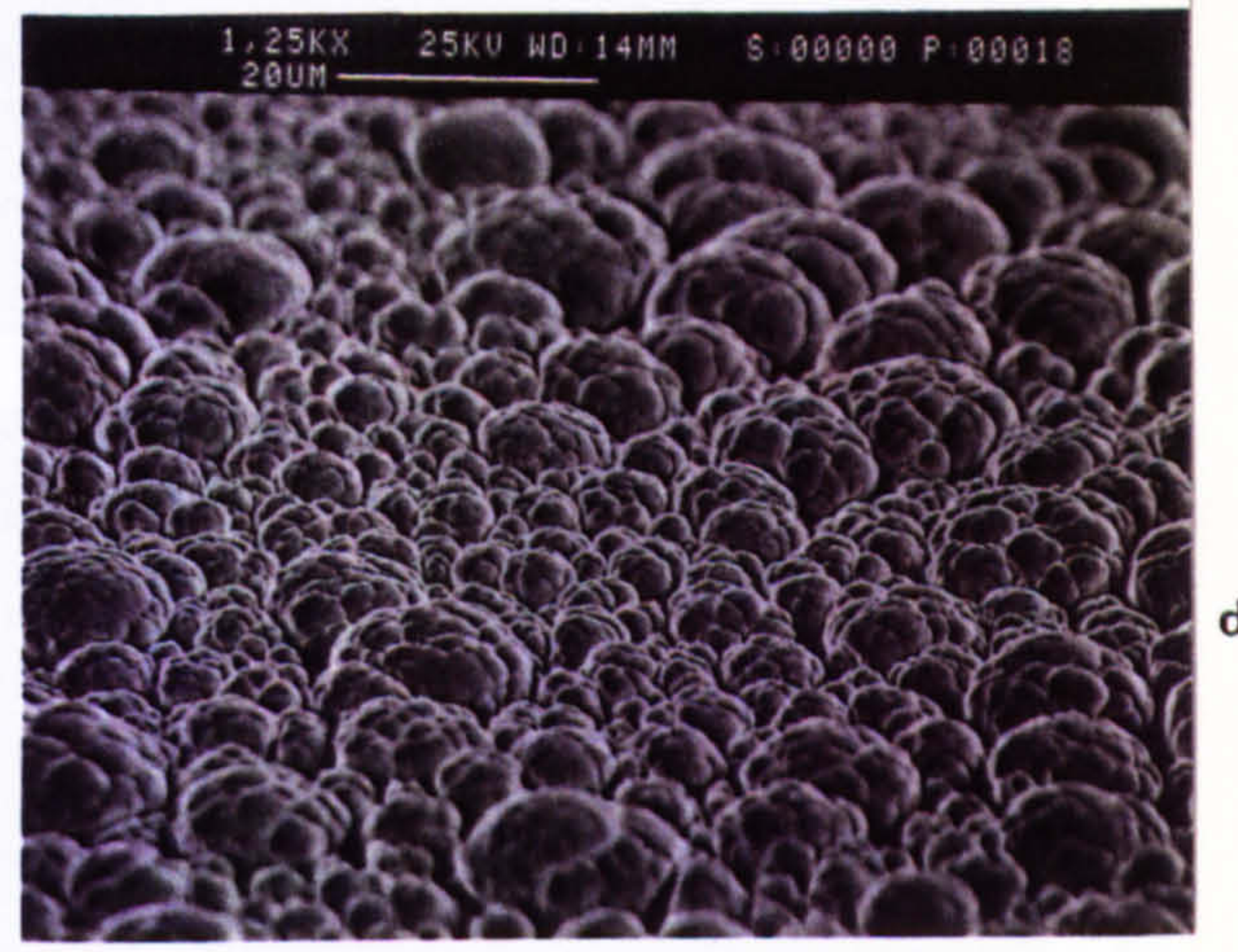
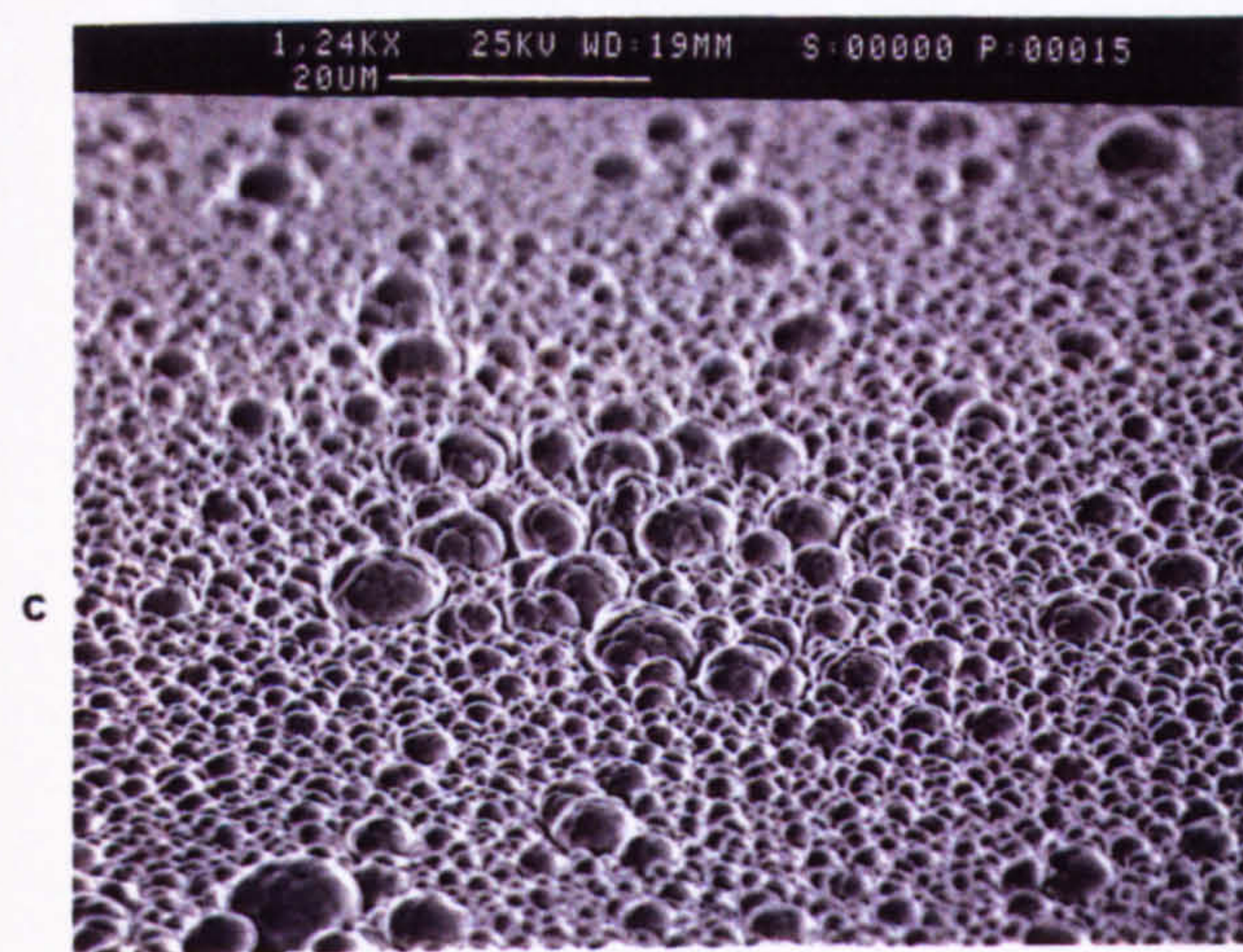
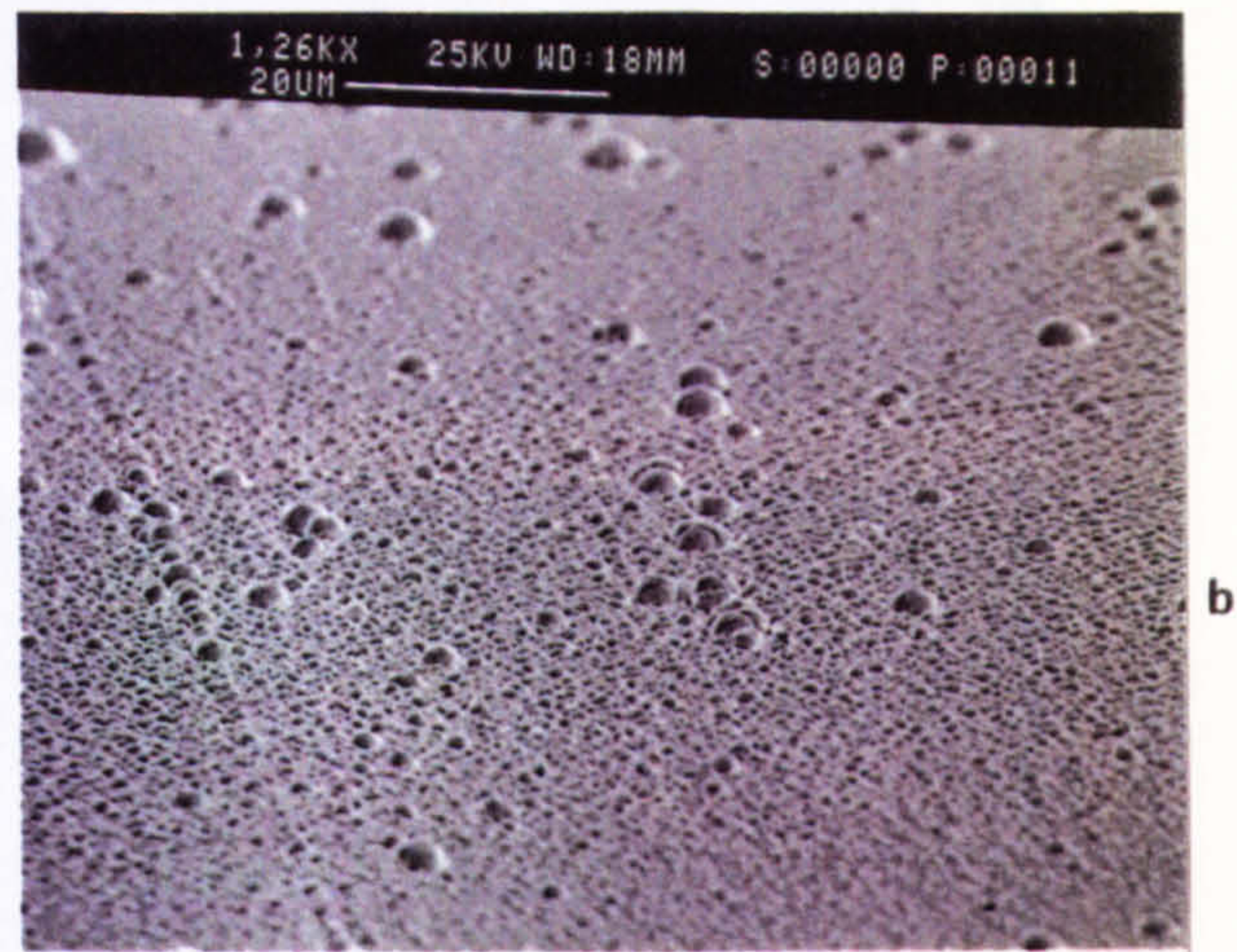
Photograph 8. SEM micrograph of a structure growing into the edge of the jet.



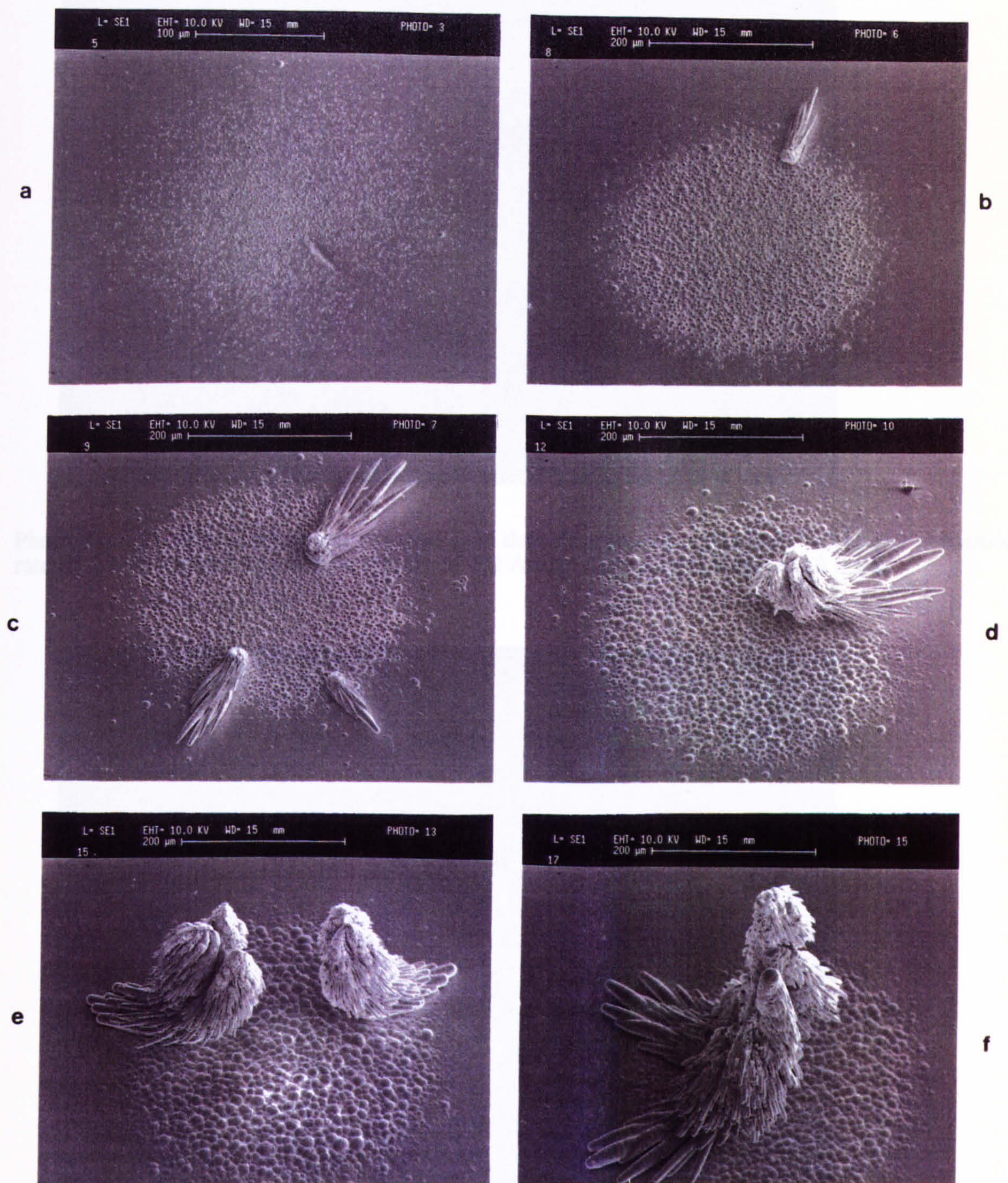
Photograph 9. SEM micrograph of a jet core structure. The colour has been added by computer enhancement.



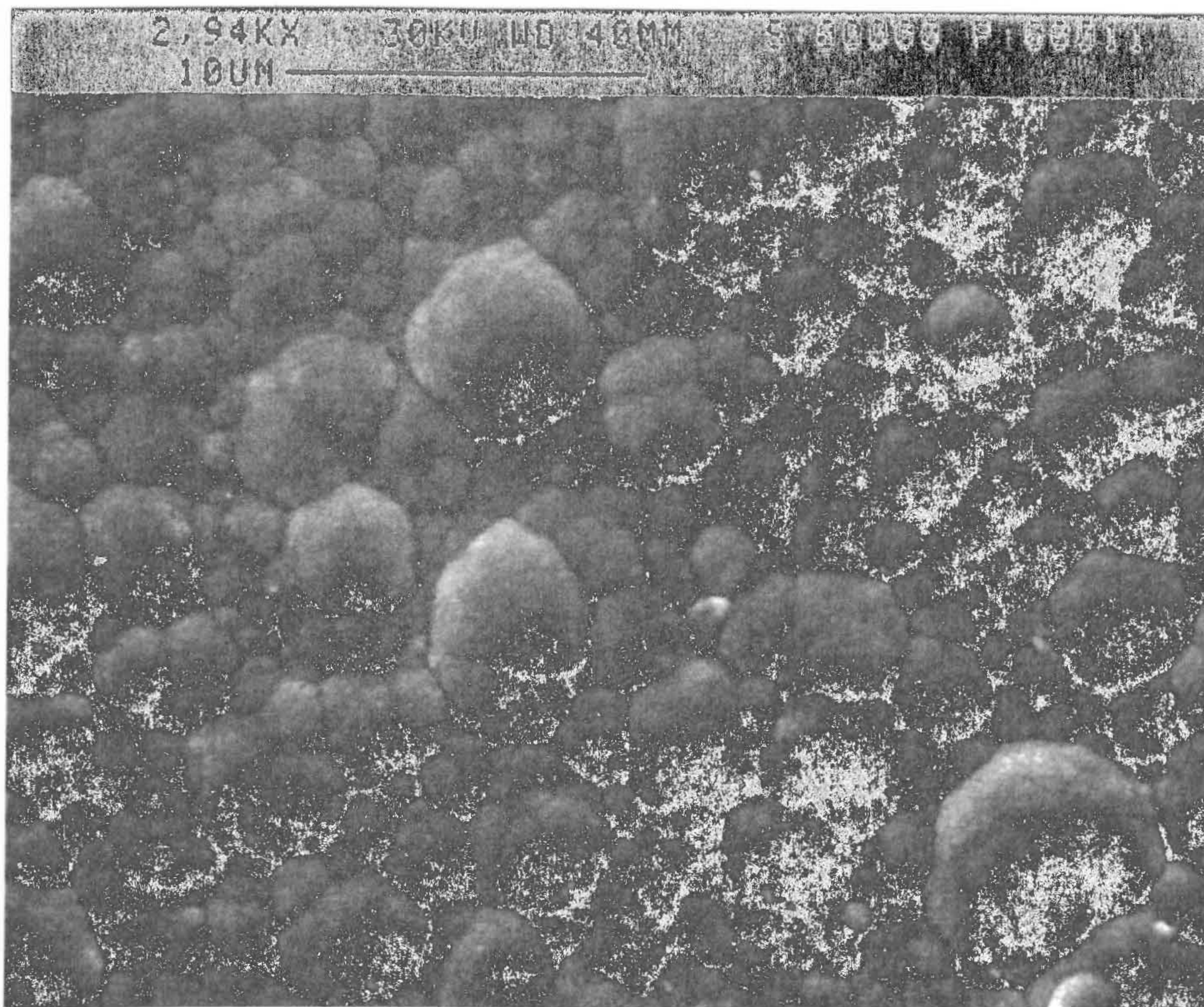
Photograph 10. SEM micrographs showing the growth of the deposit with increasing time. 0.17M citrate gold. Current density = 7.0 A cm^{-2} . Re. = 3335. (a) 0.8 secs. (b) 1.5 secs. (c) 2.5 secs. (d) 3.5 secs. (e) 5.0 secs. (f) 6.0 secs.



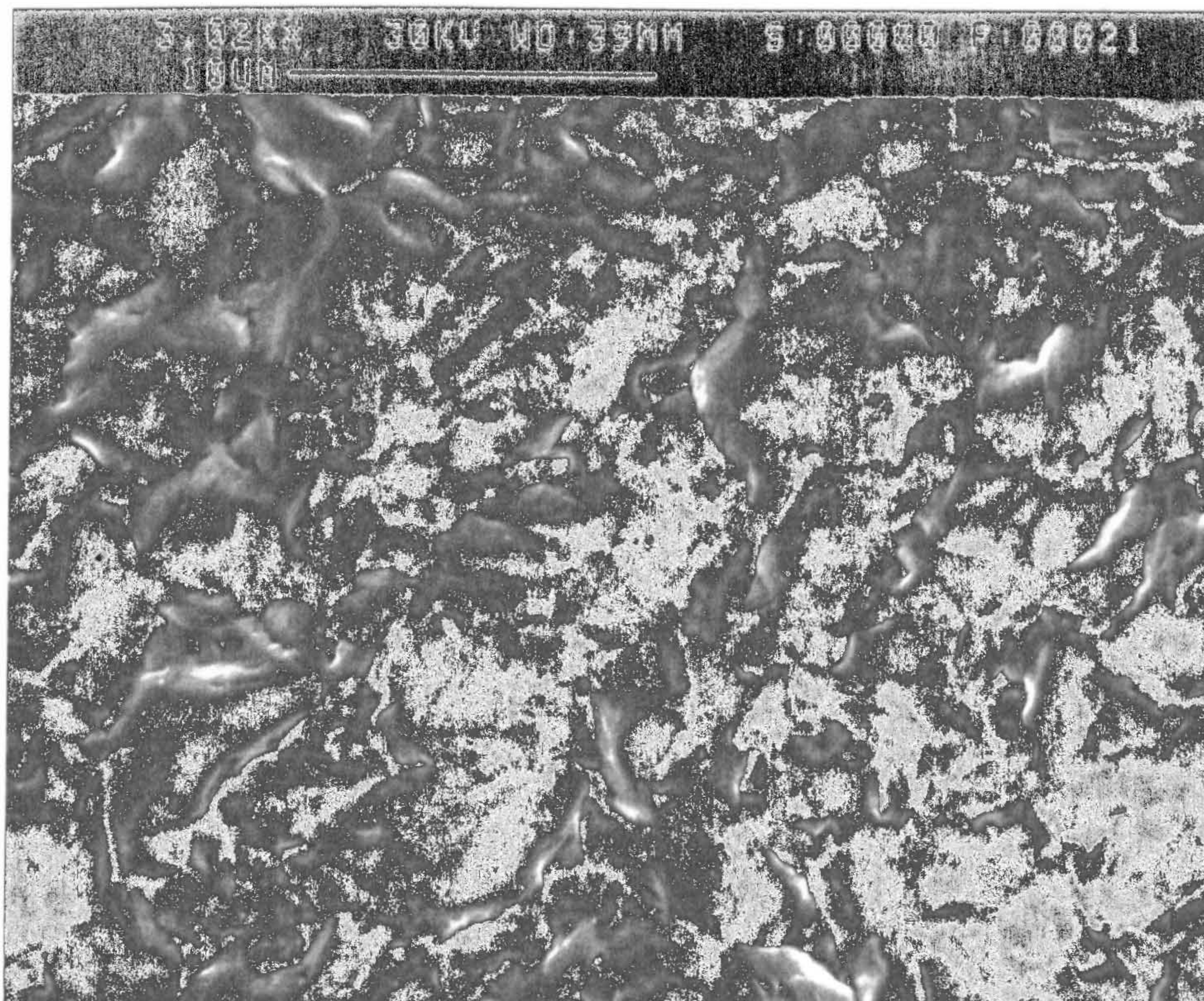
Photograph 11. SEM micrographs of some of the deposits shown in Photograph 10 but at higher magnification showing the effects of increasing deposition times. 0.17M citrate gold. Current density = 7.0 A cm^{-2} . Re. = 3335. (a) 0.8 secs. (b) 1.5 secs. (c) 2.5 secs. (d) 3.5 secs.



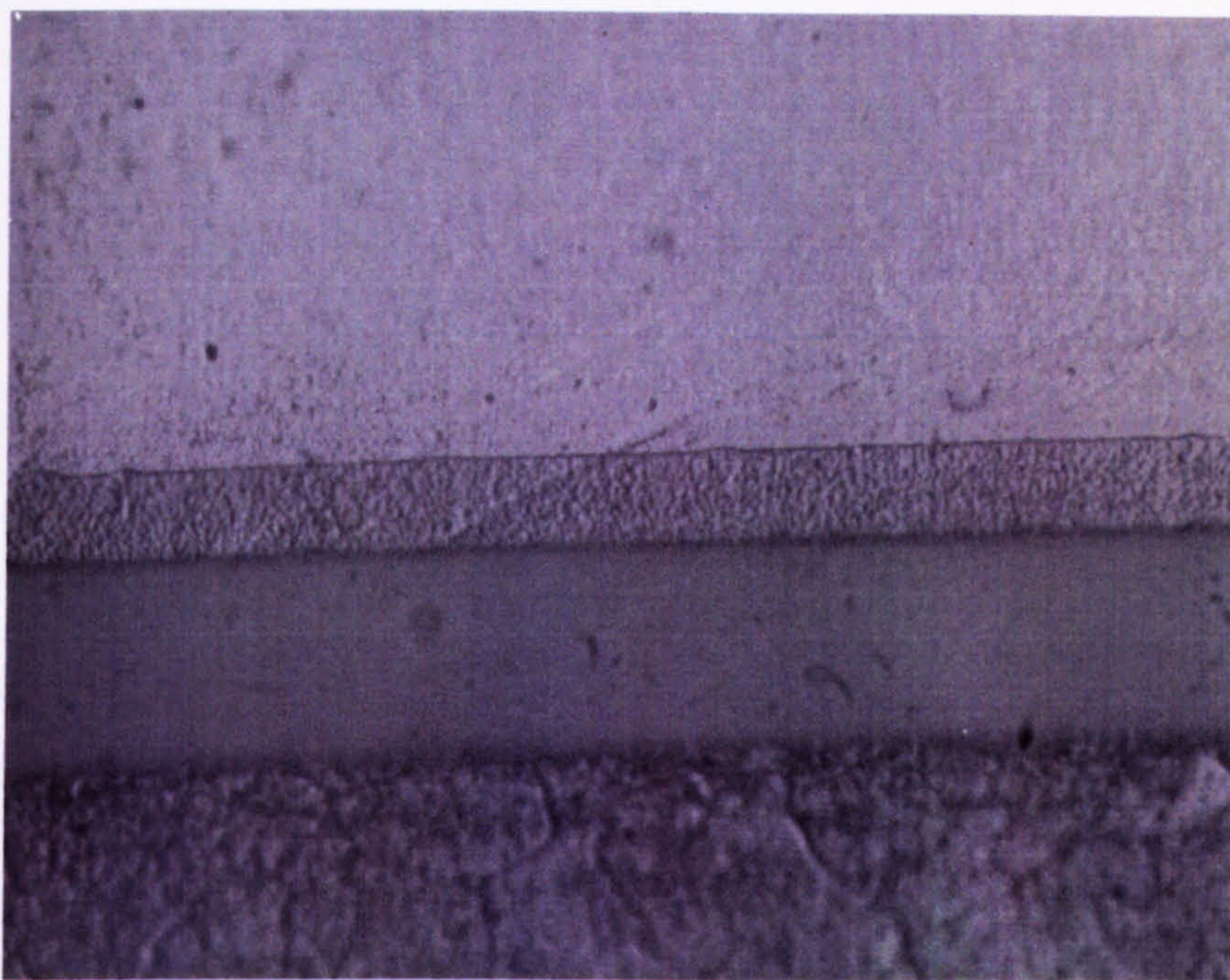
Photograph 12. SEM micrographs showing the growth of the deposit with increasing time at a current density at which jet core structures are produced. 0.17M citrate gold. Current density = 10.0 A cm⁻². Re. = 12078. (a) 0.6 secs. (b) 2.0 secs. (c) 2.0 secs. (d) 3.5 secs. (e) 6.0 secs. (f) 8.0 secs.



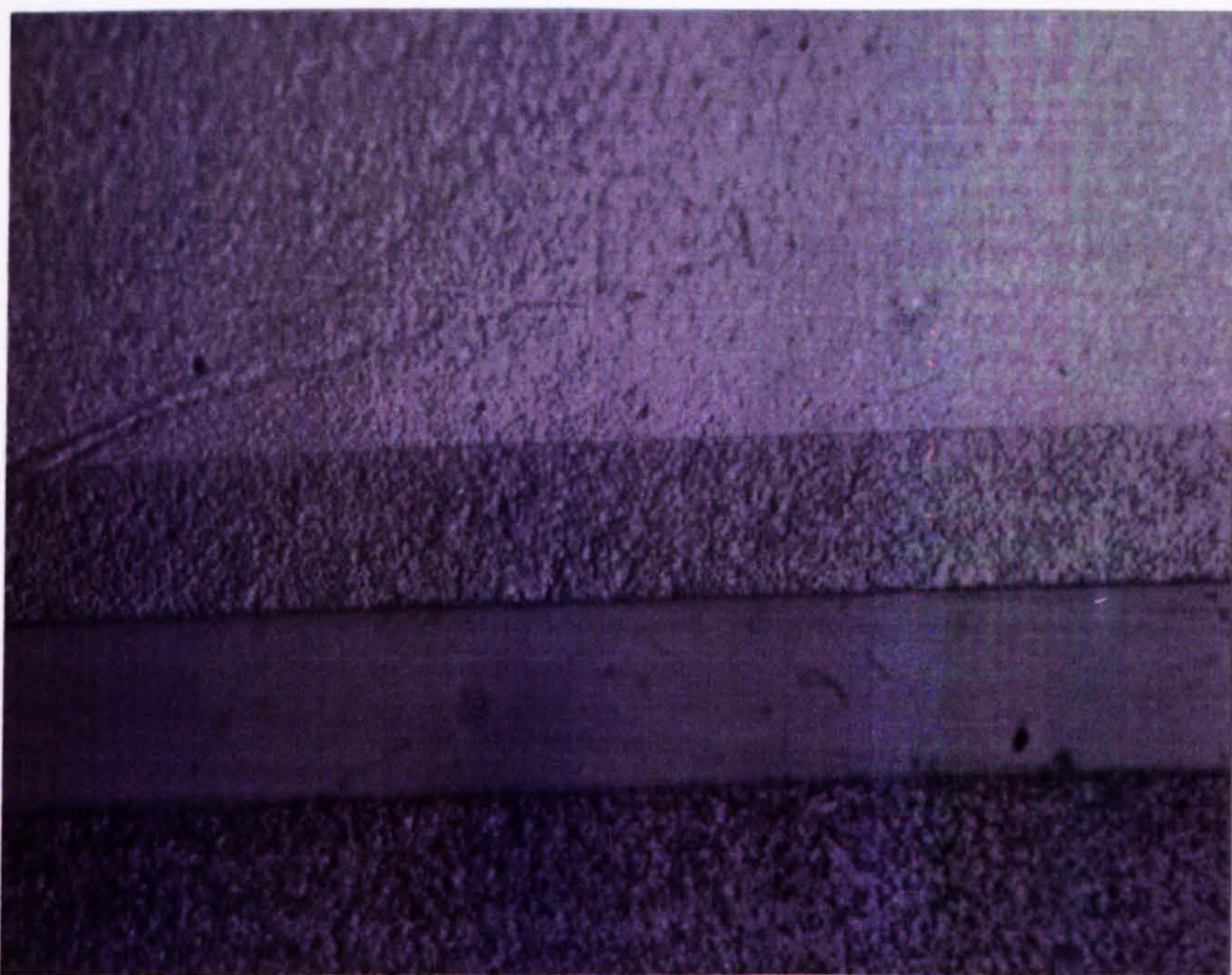
Photograph 13. SEM micrograph of a pure gold deposit produced at the maximum useful deposition rate of $3.4 \mu\text{m}/\text{second}$ at a current density of 6.0 A cm^{-2} . Deposit thickness = $18.0 \mu\text{m}$.



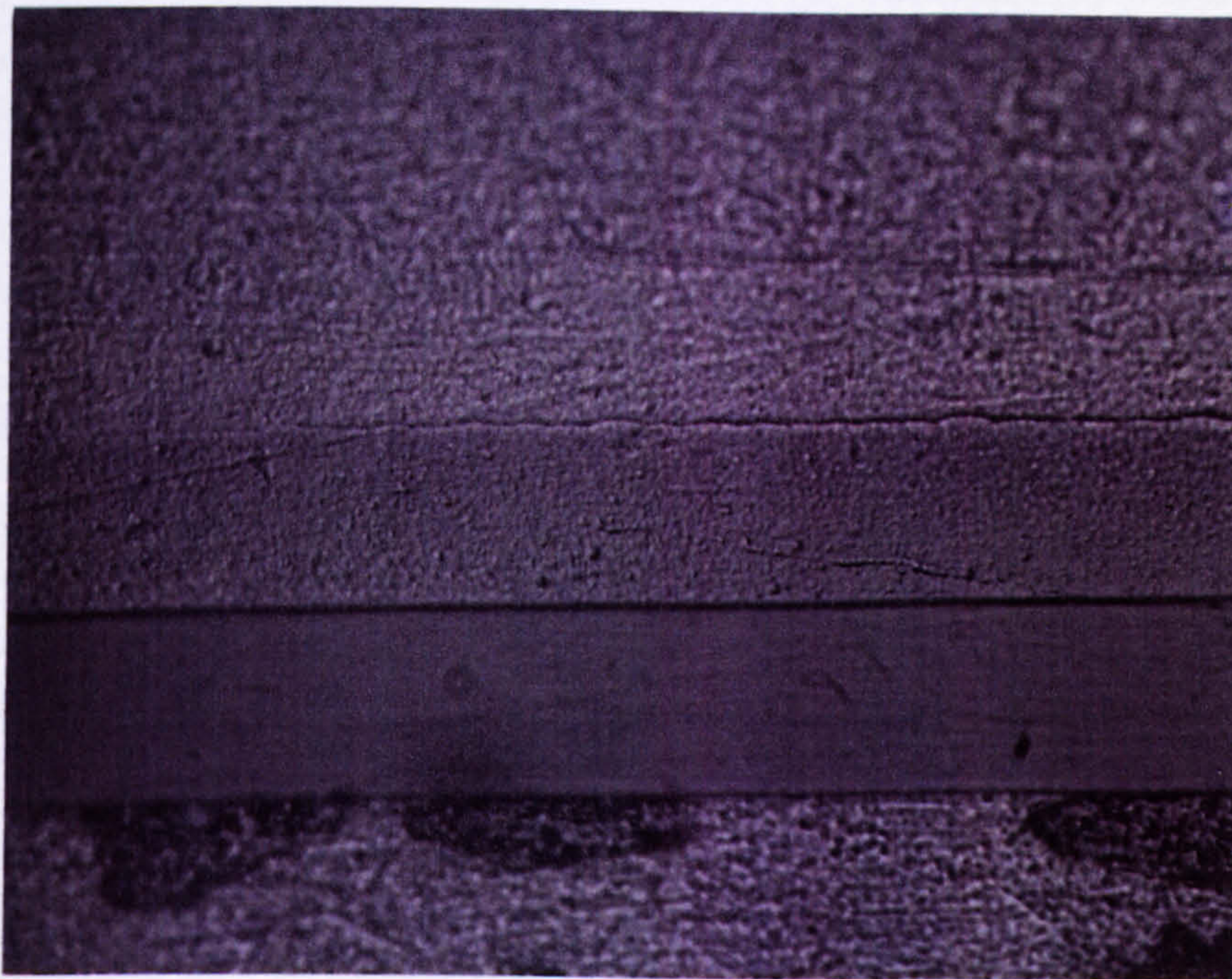
Photograph 14. SEM micrograph of a conventional deposit produced at a current density of 5.0 mA cm^{-2} . Deposit thickness = $18.0 \mu\text{m}$.



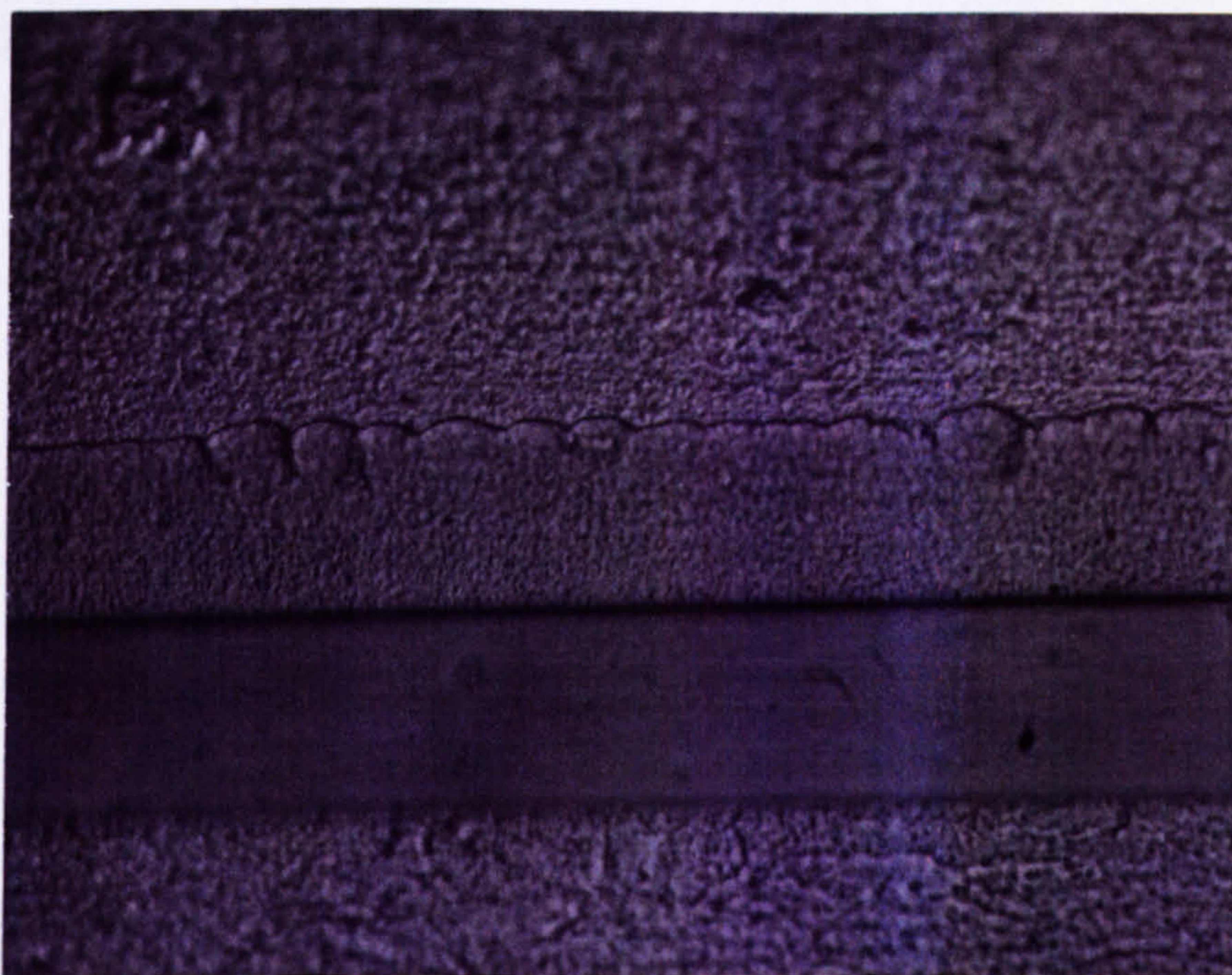
Photograph 15. Microsection of a pure gold deposit produced from the optimised citrate gold electrolyte. Current density = 2.0 A cm^{-2} . Re. = 12078. Temperature = 55°C . X 2000



Photograph 16. Microsection of a deposit produced from the optimised citrate gold electrolyte. Current density = 4.0 A cm^{-2} . Re. = 12078. Temperature = 55°C . X 2000



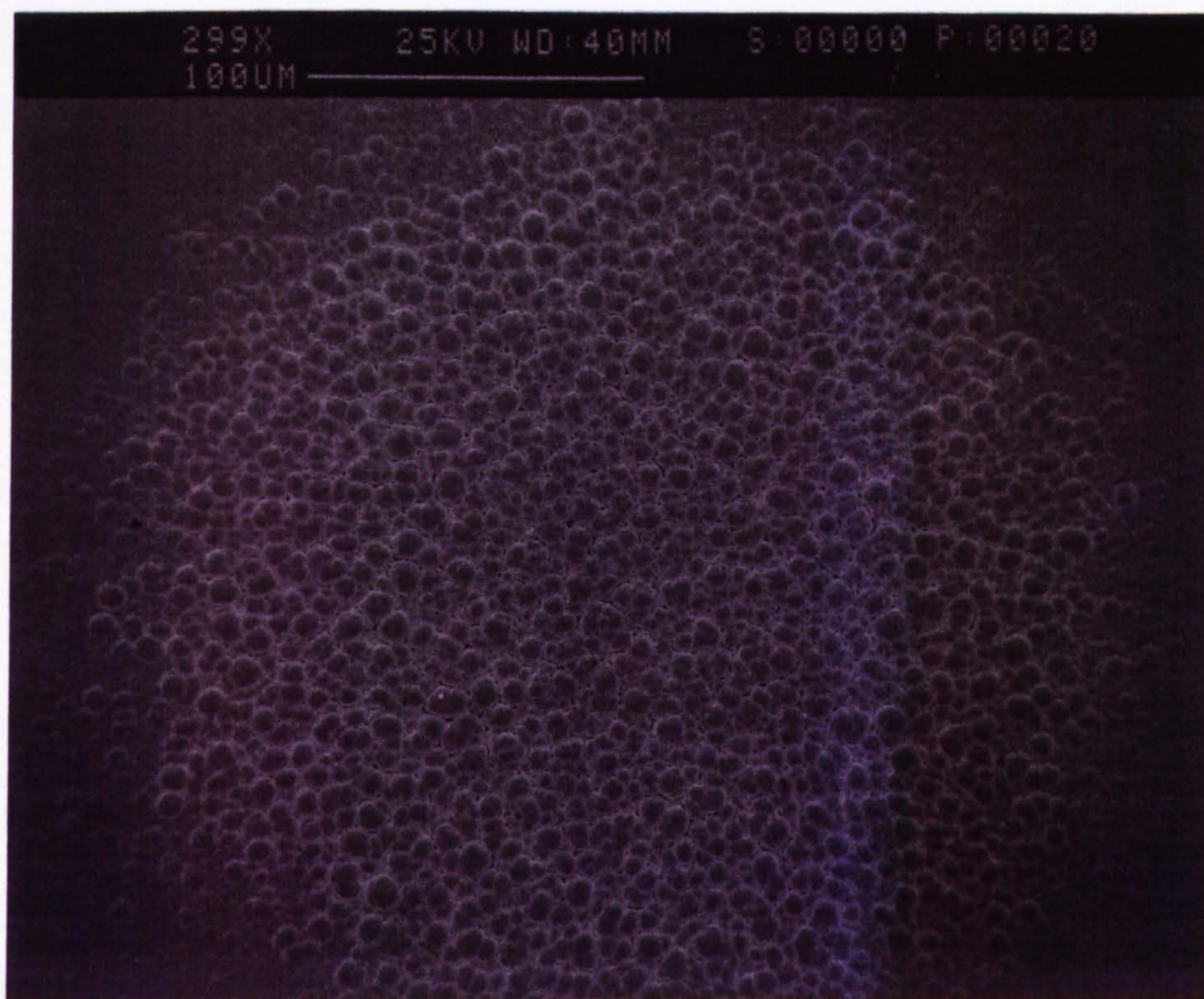
Photograph 17. Microsection of a deposit produced from the optimised citrate gold electrolyte. Current density = 6.0 A cm^{-2} . Re. = 12078. Temperature = 55°C . X 2000



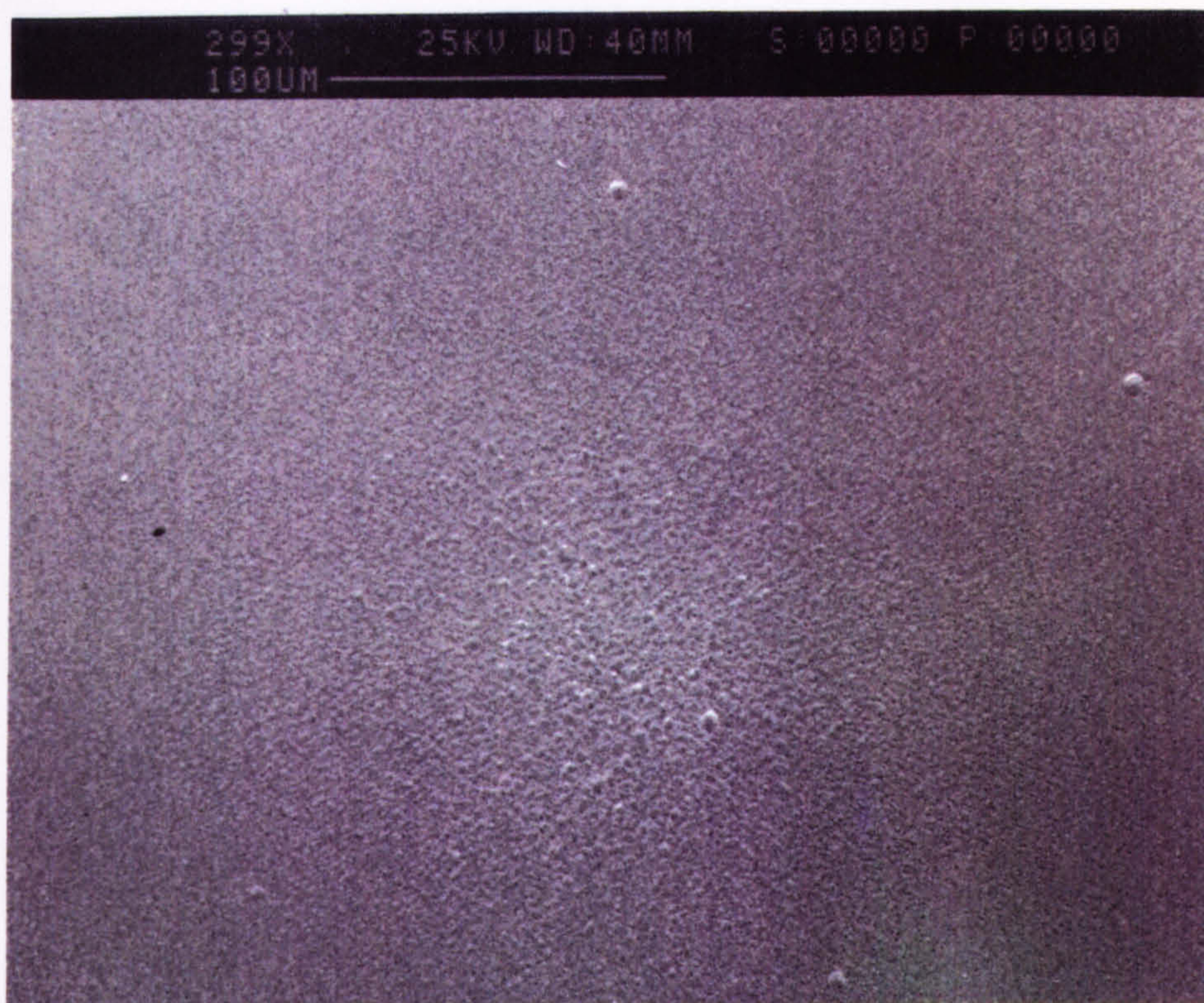
Photograph 18. Microsection of a deposit produced from the optimised citrate gold electrolyte. Current density = 7.0 A cm^{-2} . Re. = 12078. Temperature = 55°C . X 2000



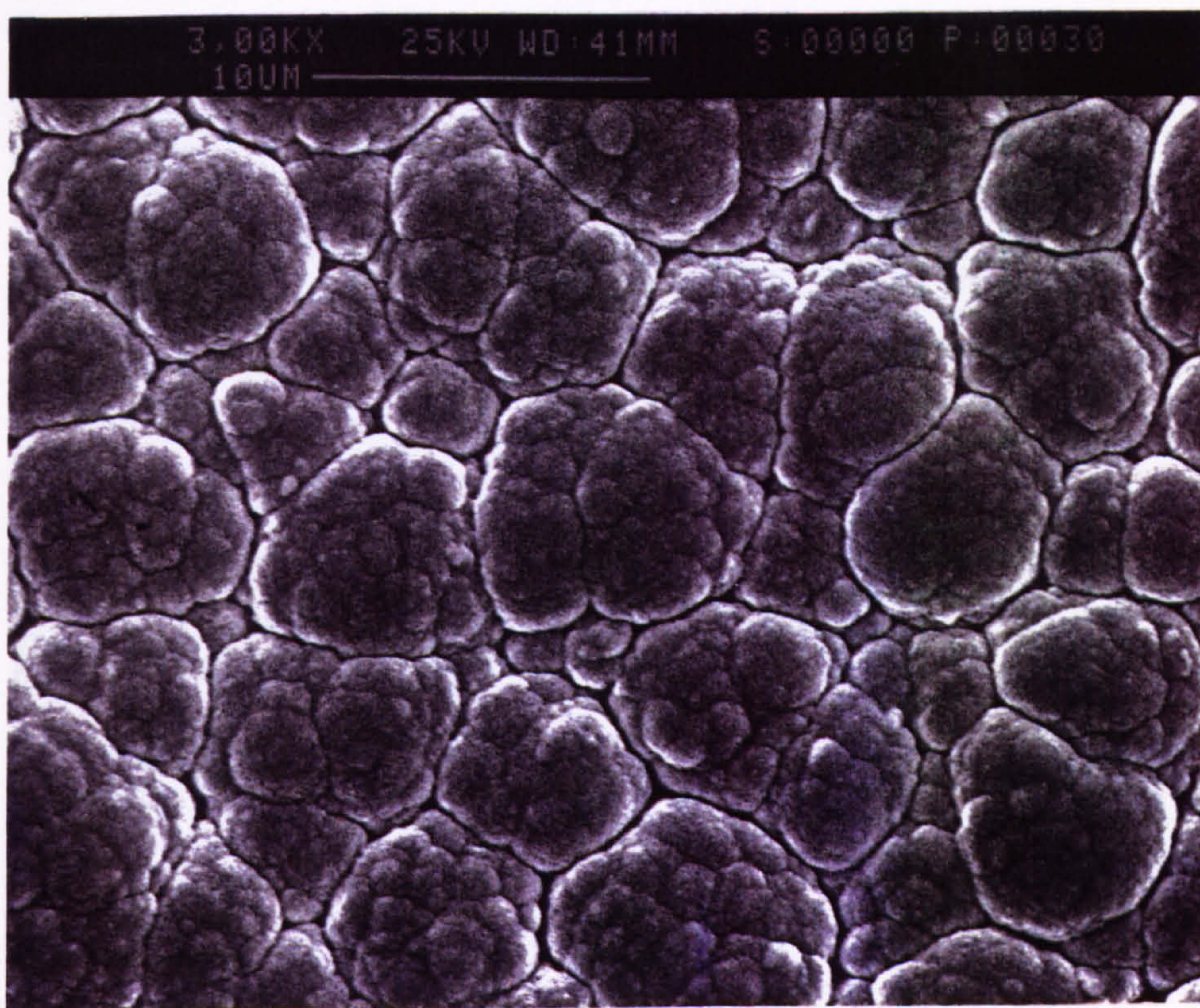
Photograph 19. The effects of electrolyte velocity. 0.28M citrate electrolyte. Current density = 4.75 A cm^{-2} . Temp. = 55°C . Re. = 1044.



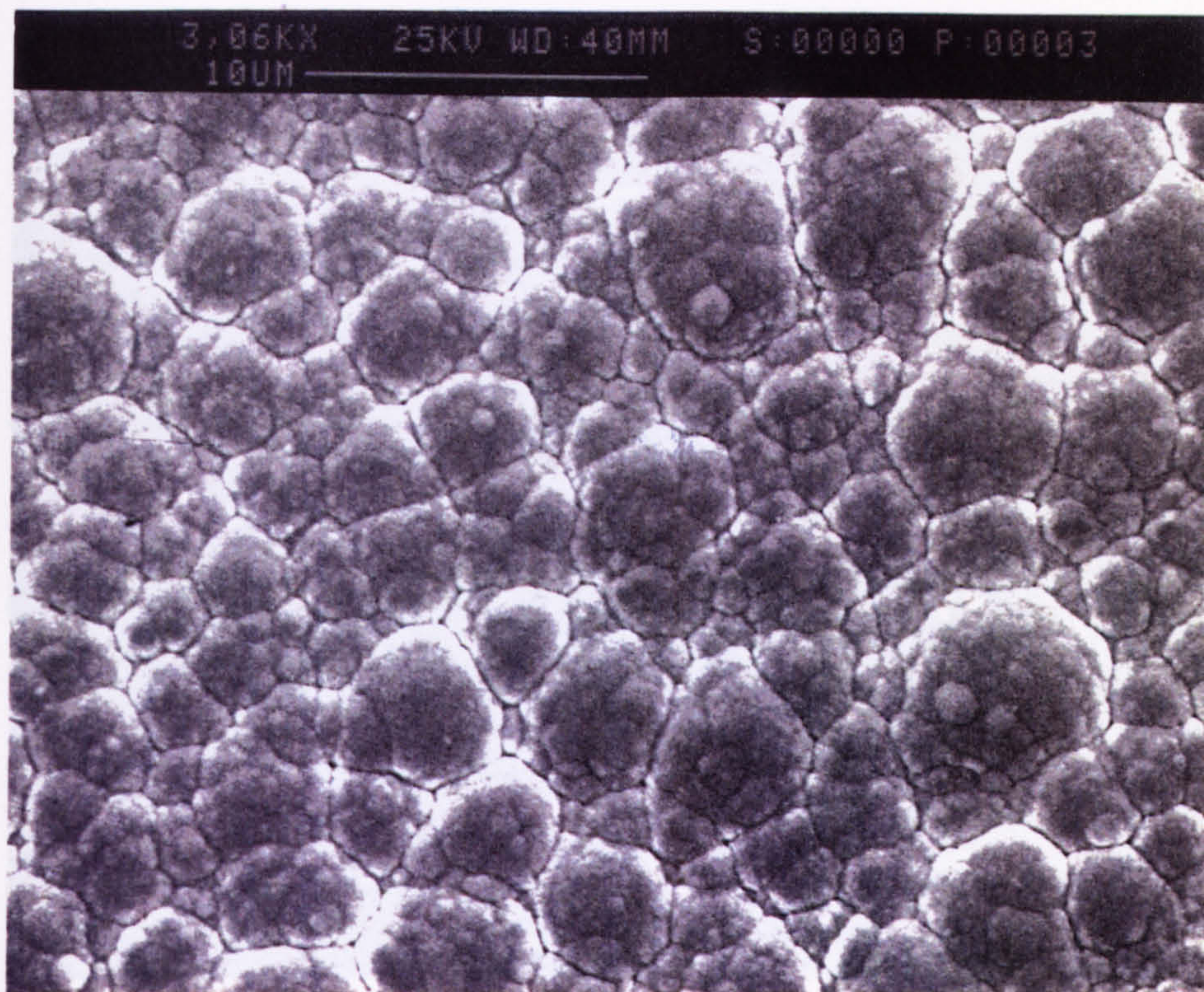
Photograph 20. The effects of electrolyte velocity. 0.28M citrate electrolyte. Current density = 4.75 A cm^{-2} . Temp. = 55°C . Re. = 5220.



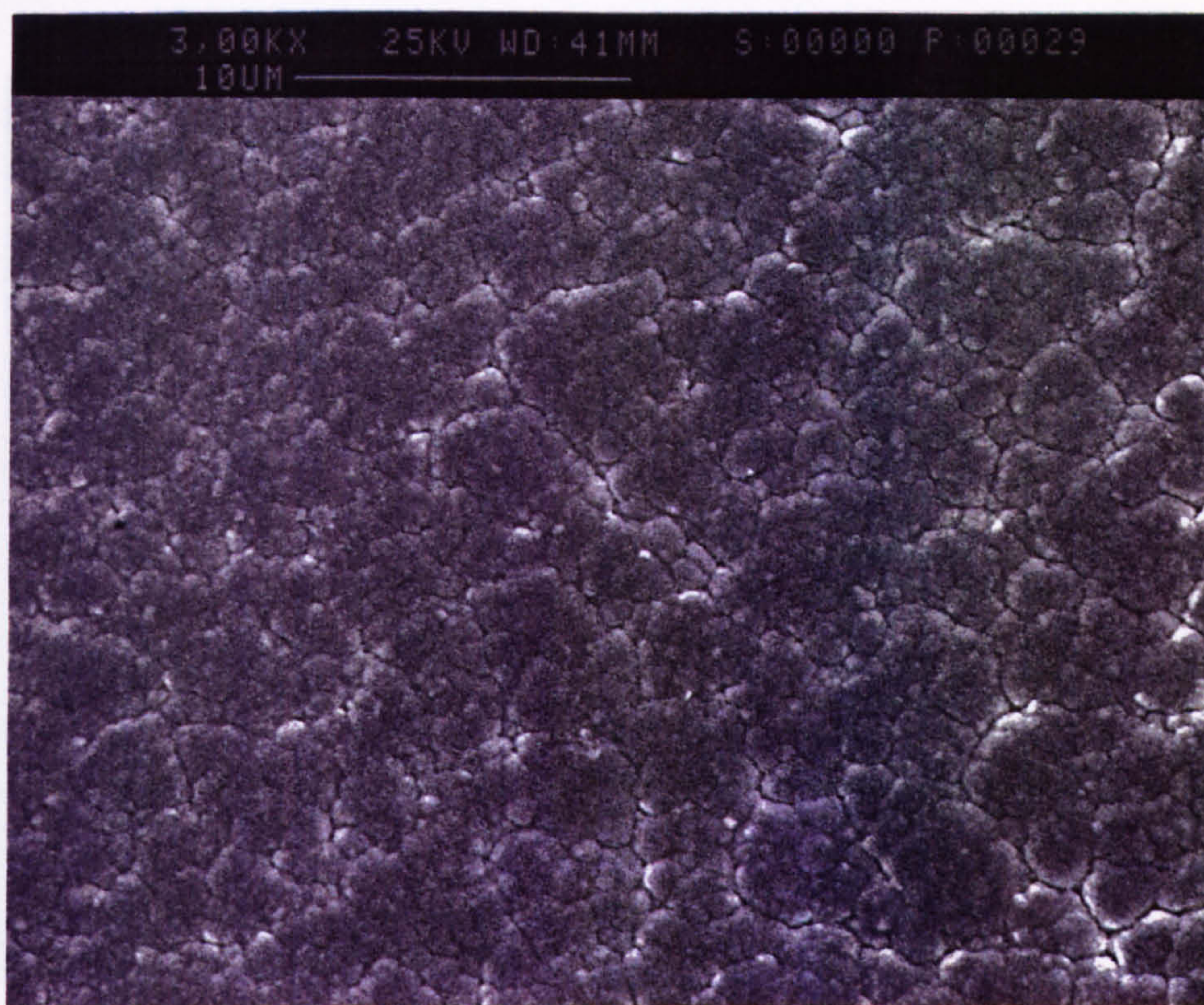
Photograph 21. The effects of electrolyte velocity. 0.28M citrate electrolyte. Current density = 4.75 A cm^{-2} . Temp. = 55°C . Re. = 9396.



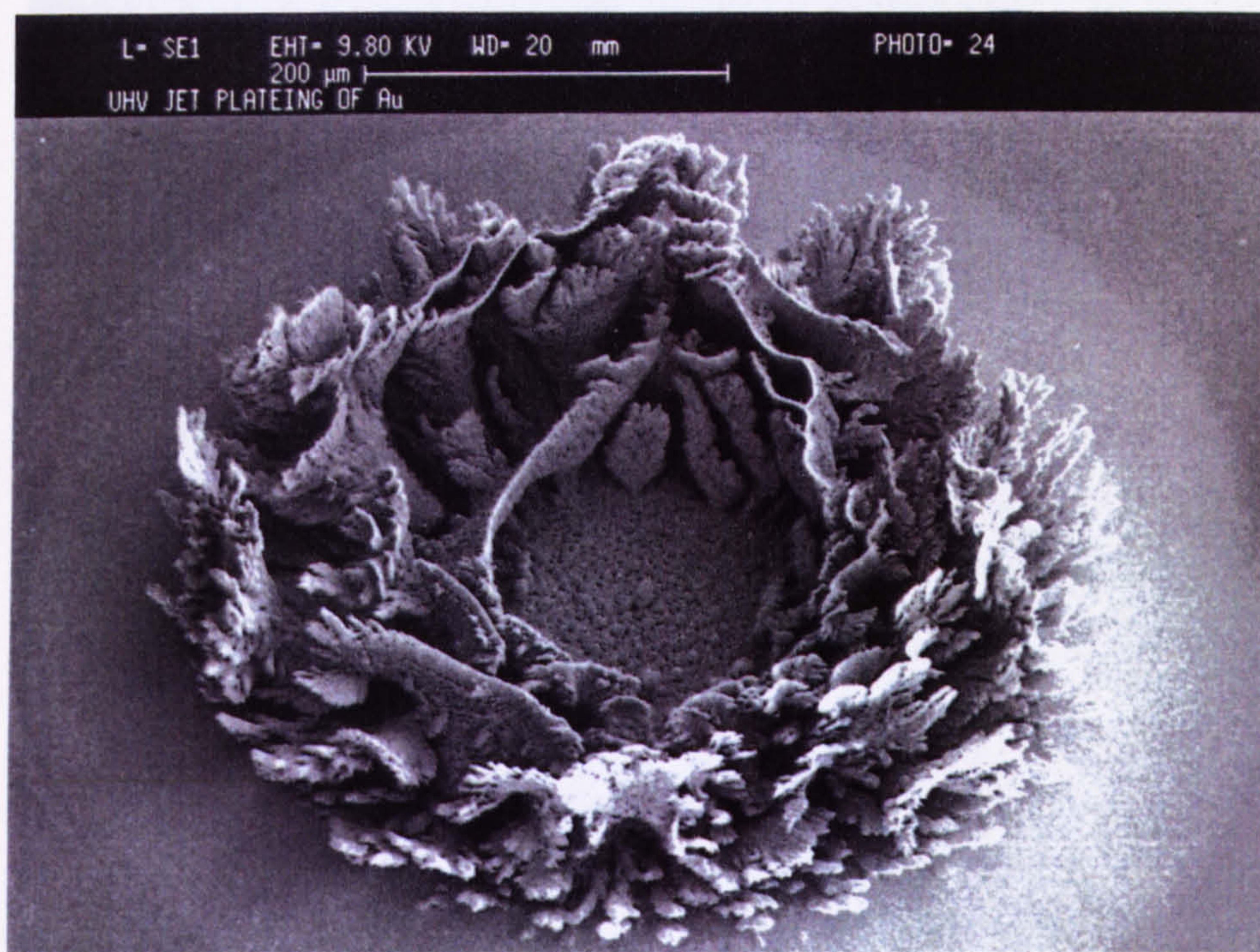
Photograph 22. The influence of electrolyte pH. 0.17M citrate gold. Current density = 5.0 A cm^{-2} . Temp. = 55°C . Re. = 12078. pH = 5.3.



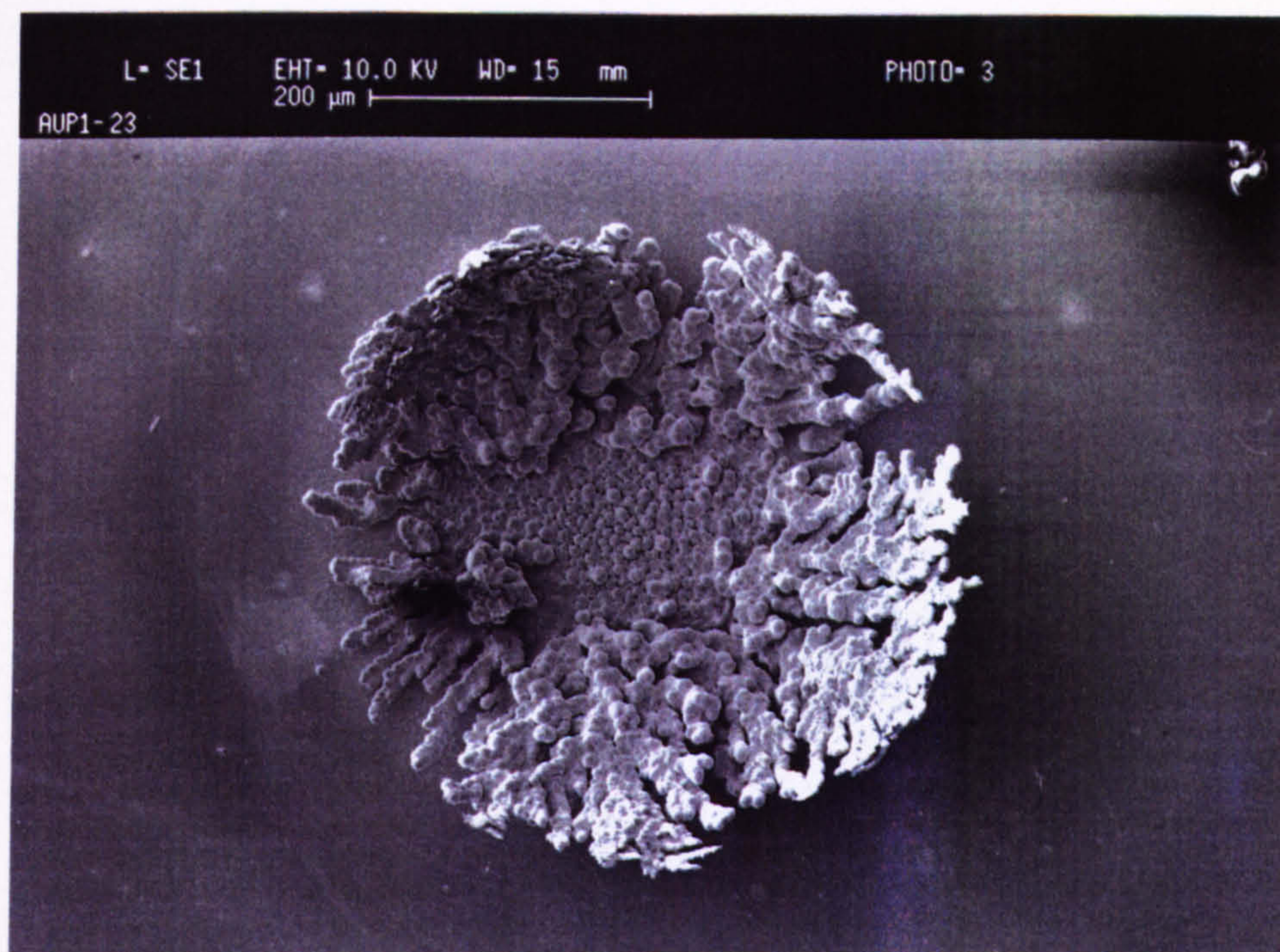
Photograph 23. The influence of electrolyte pH. 0.17M citrate gold. Current density = 5.0 A cm^{-2} . Temp. = 55°C . Re. = 12078. pH = 6.1.



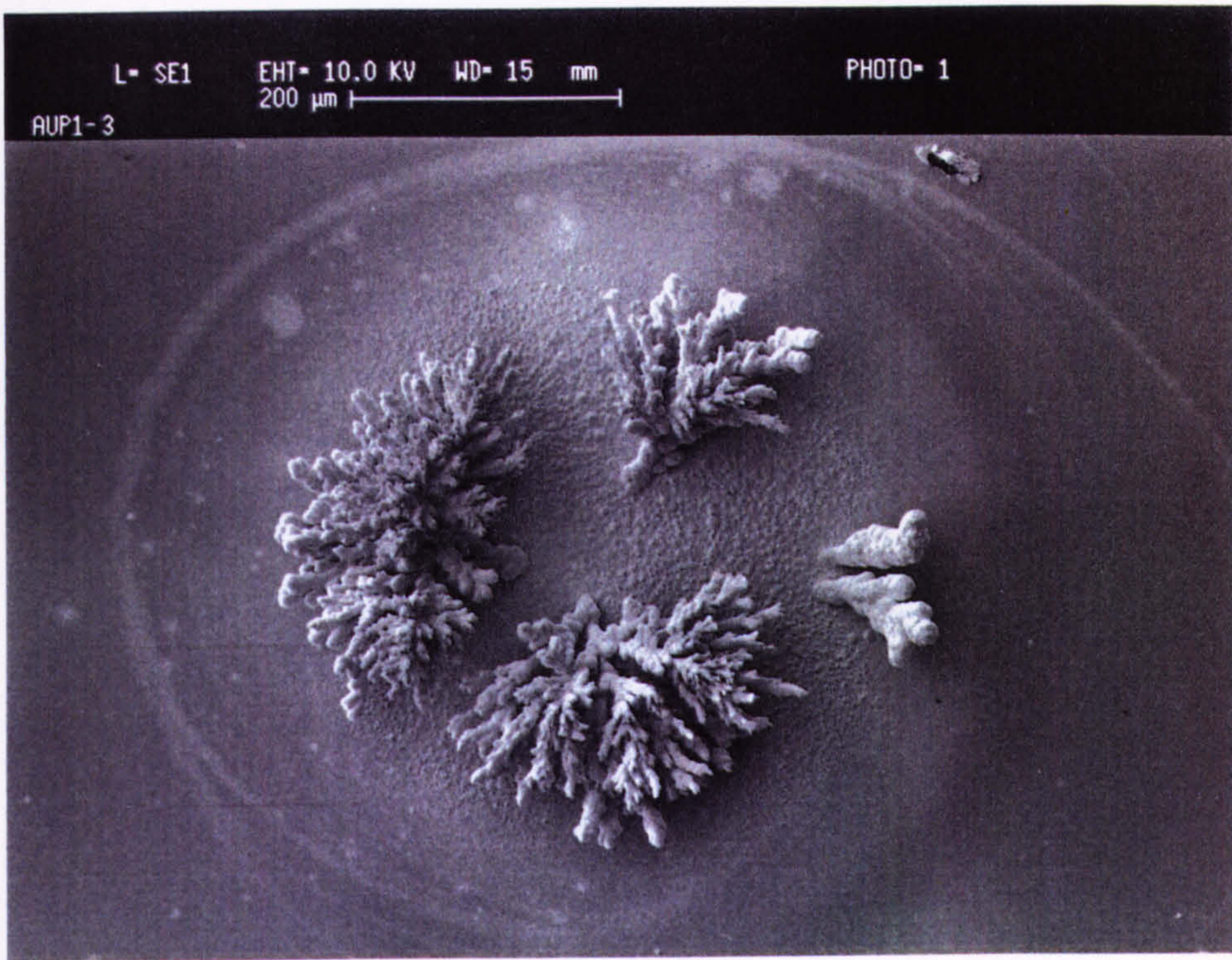
Photograph 24. The influence of electrolyte pH. 0.17M citrate gold. Current density = 5.0 A cm^{-2} . Temp. = 55°C . Re. = 12078. pH = 8.1.



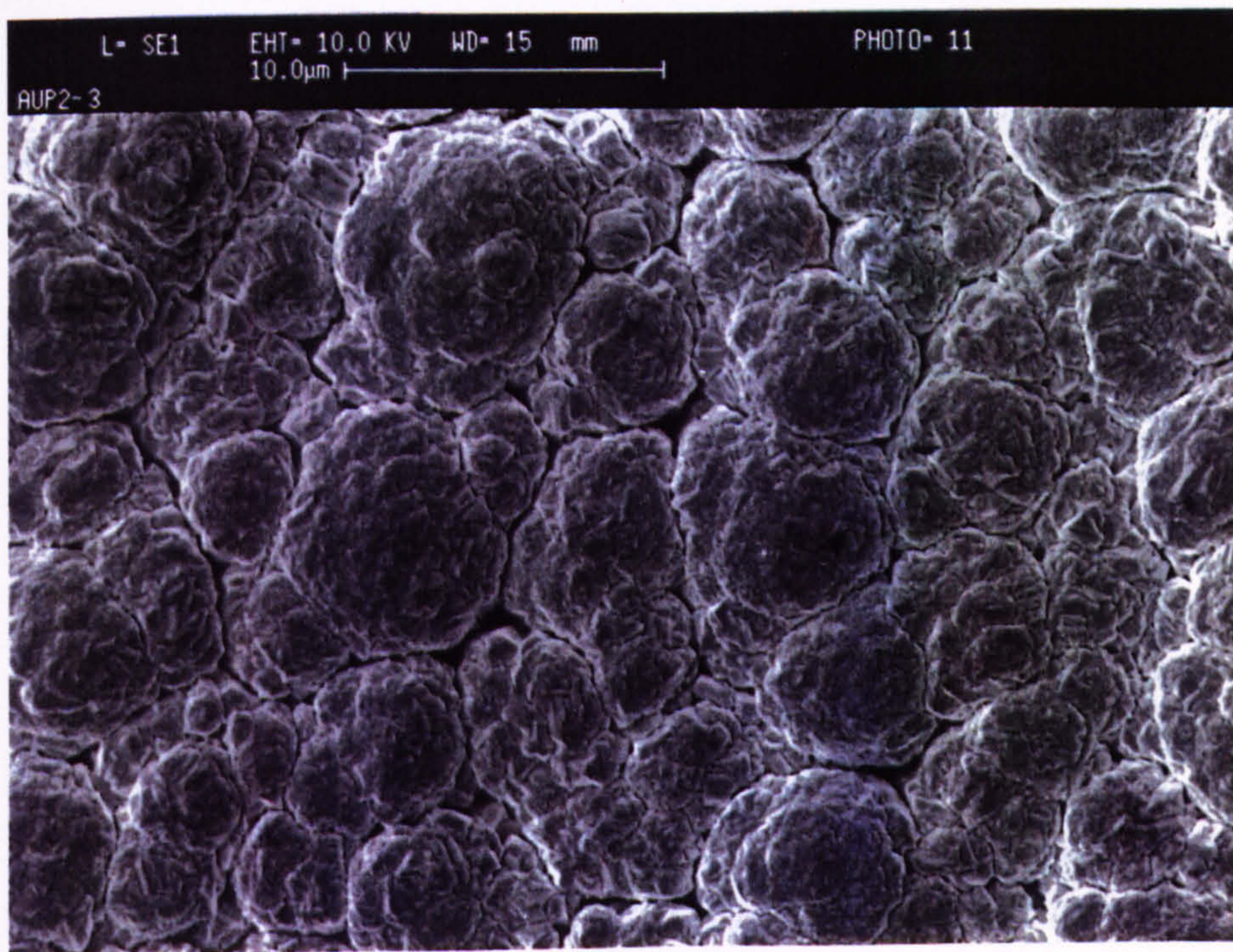
Photograph 25. A typical example of a "rose" type morphology produced using pulsed current in conjunction with HSSJE.



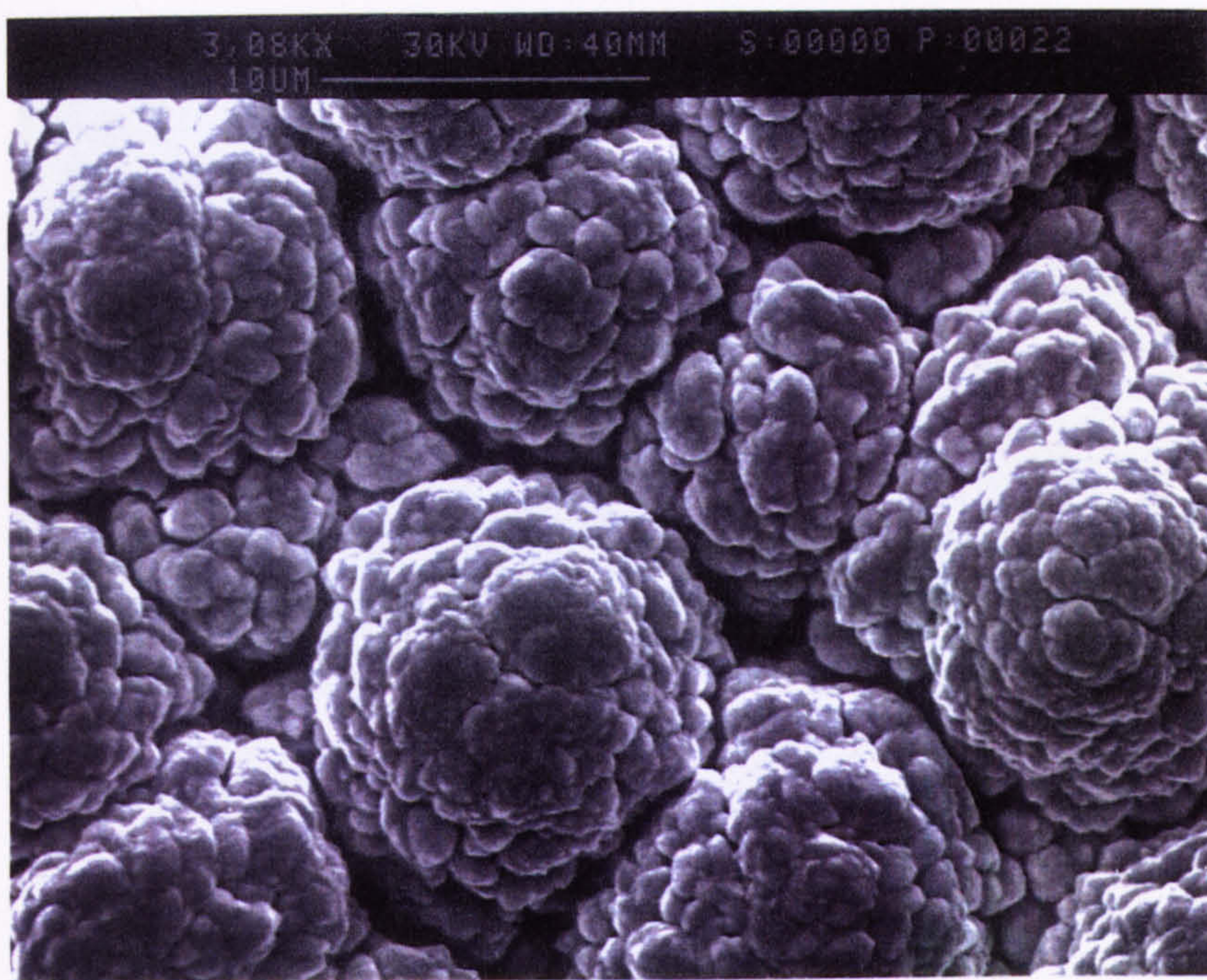
Photograph 26. A typical example of a "crown" type morphology produced using pulsed current in conjunction with HSSJE.



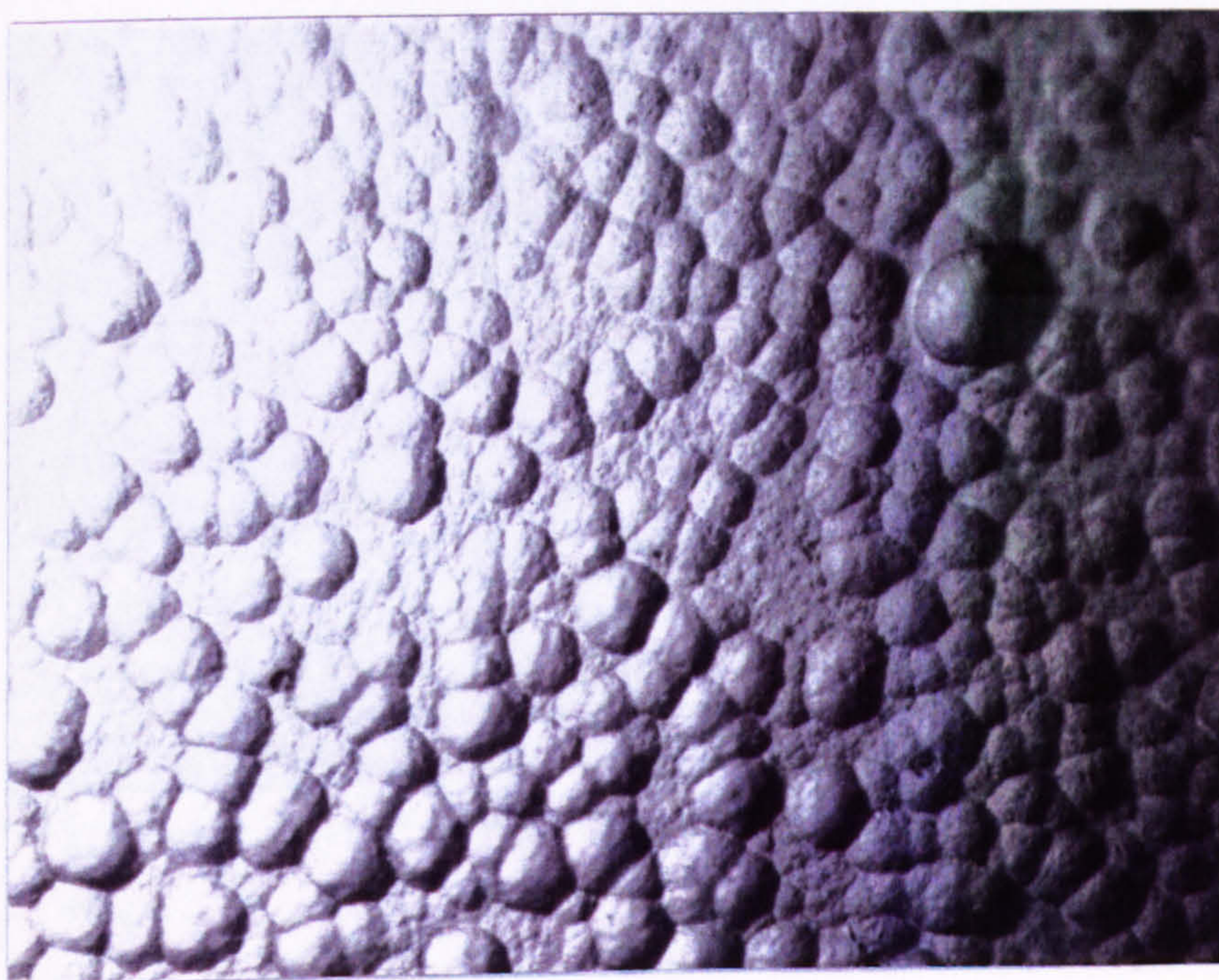
Photograph 27. A typical example of a "field oriented random" type morphology produced using pulsed current in conjunction with HSSJE.



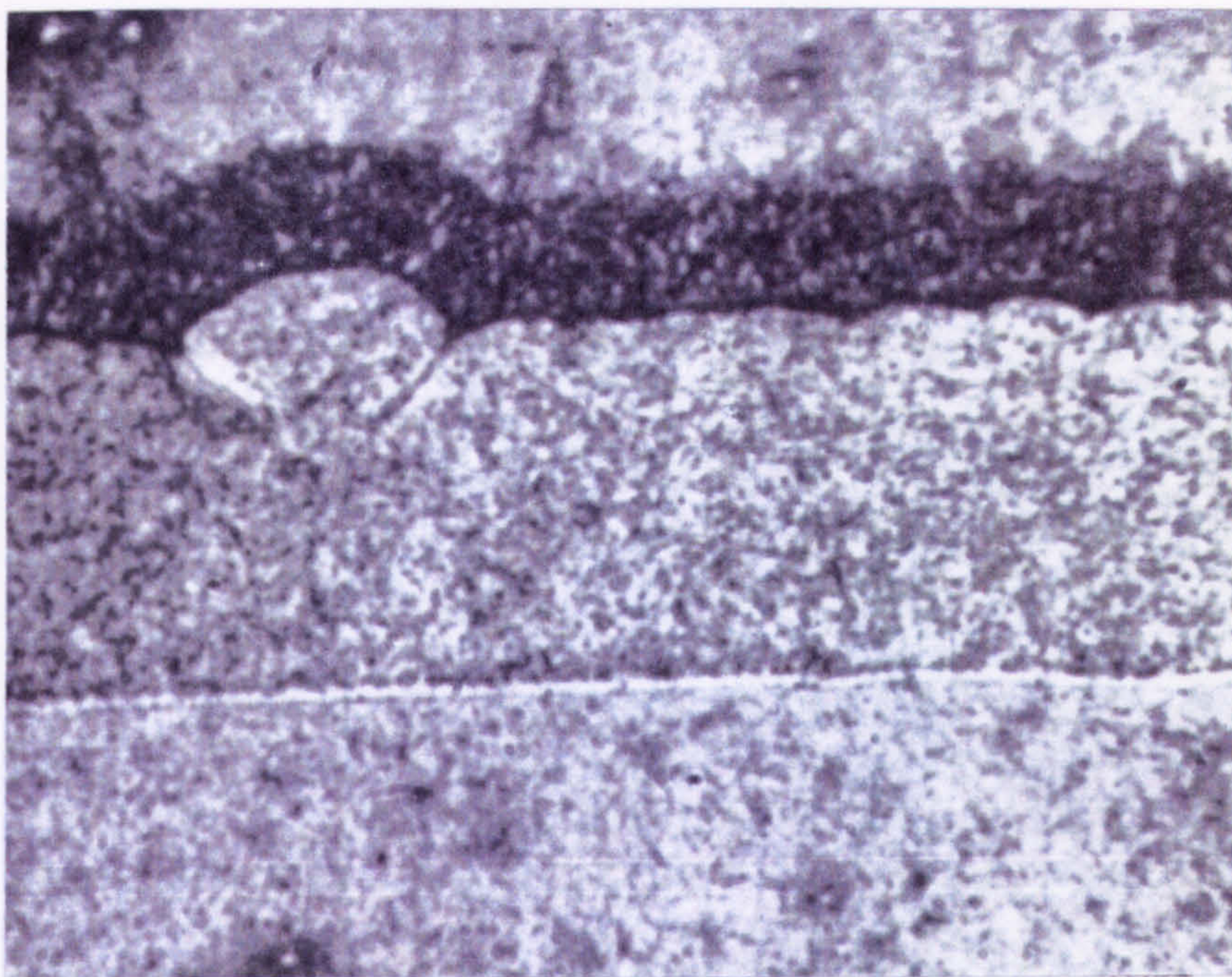
Photograph 28. A typical example of a "smooth" type morphology produced using pulsed current in conjunction with HSSJE.



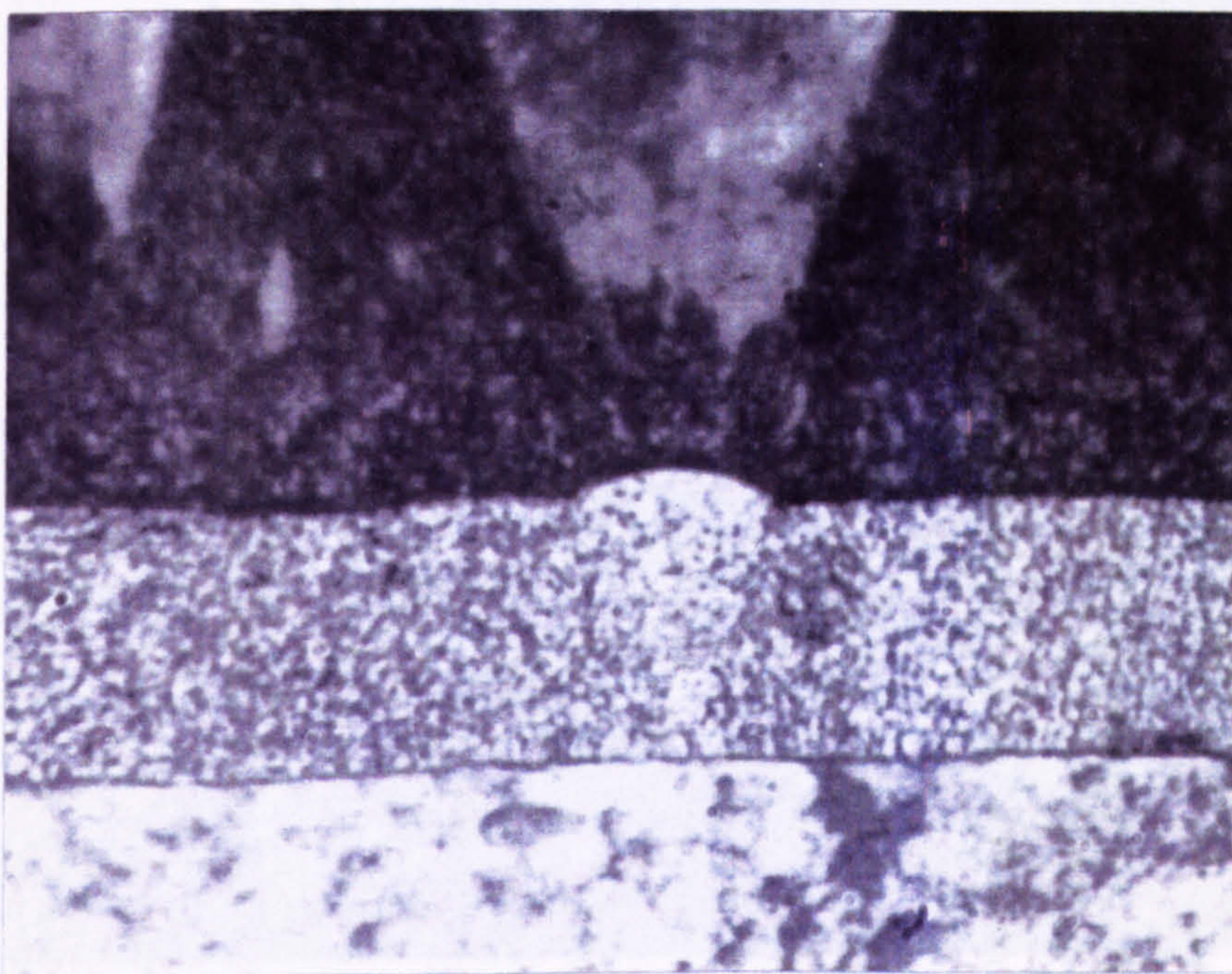
Photograph 29. A typical example of a "nodular" type morphology produced using pulsed current in conjunction with HSSJE.



Photograph 30. An optical micrograph of a $17.2\ \mu\text{m}$ gold deposit produced from a Ronoval N electrolyte containing $60\ \text{ml l}^{-1}$ "booster" but no nickel. Current density = $8.0\ \text{A cm}^{-2}$. Re. = 10800. X 2000



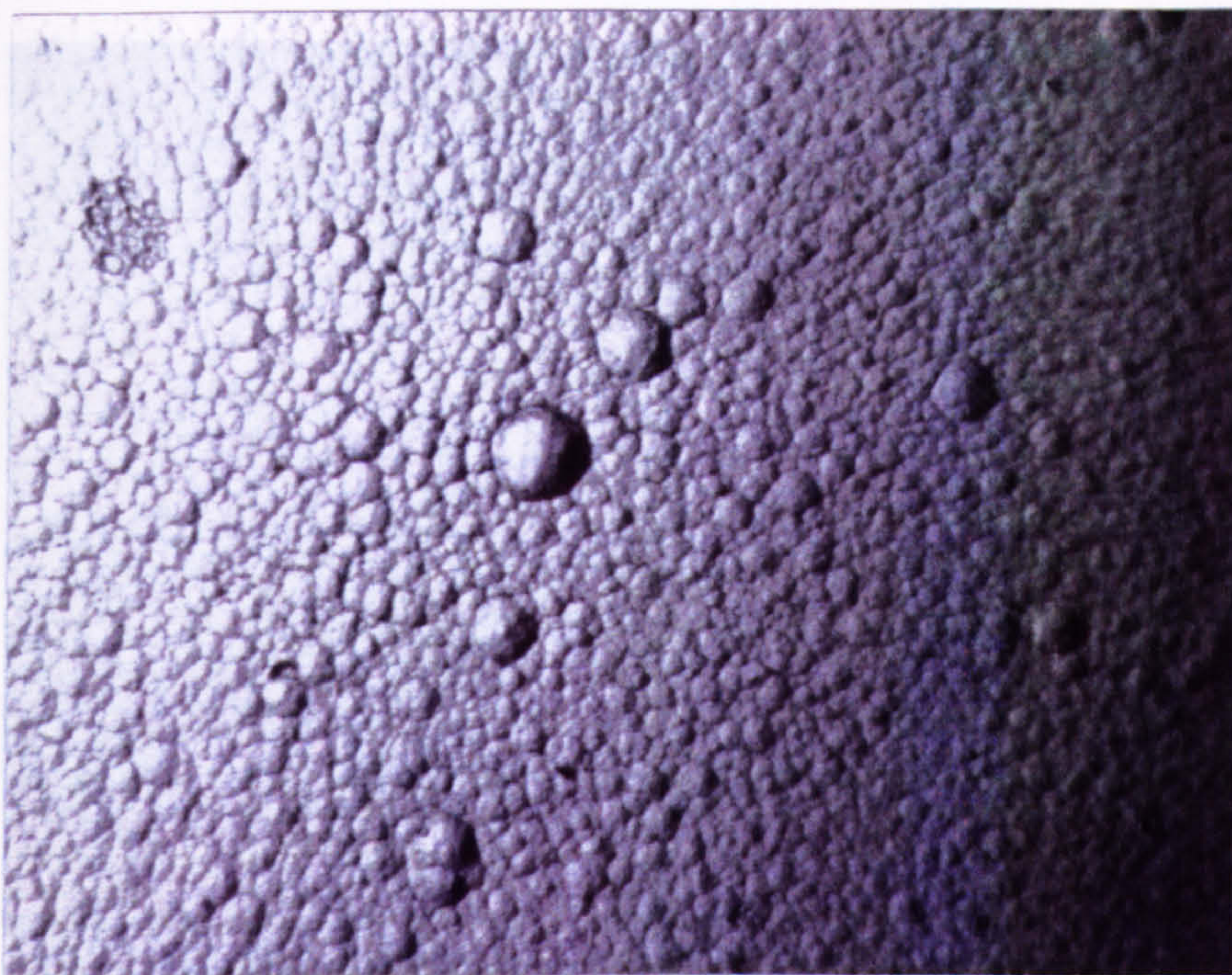
Photograph 31. A microsection of a gold deposit produced from a Ronoval N electrolyte containing 60 ml l⁻¹ "booster" but no nickel. Current density = 9.0 A cm⁻². Re. = 10800. X2000



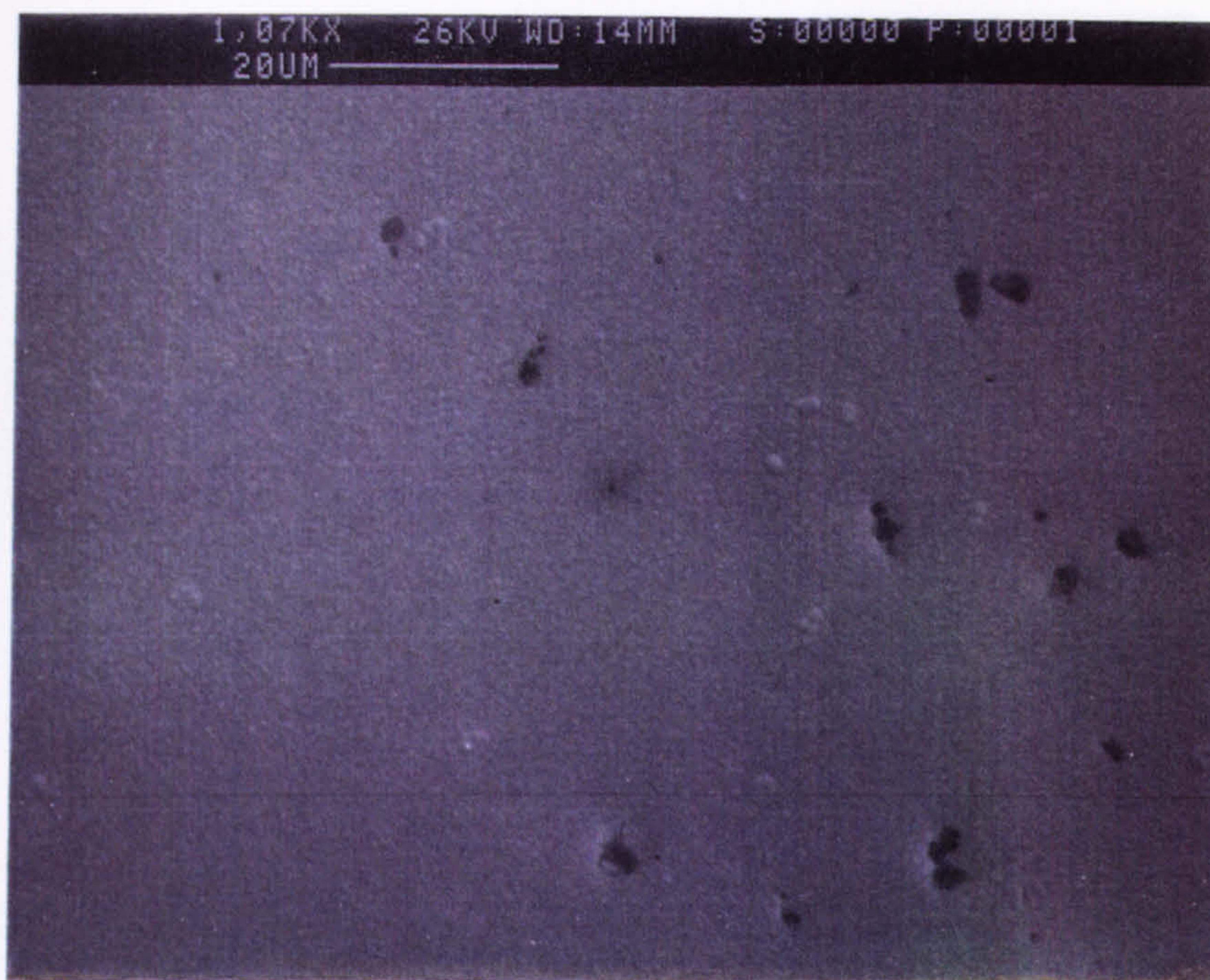
Photograph 32. A microsection of a gold deposit produced from a Ronoval N electrolyte containing 60 ml l⁻¹ "booster" and 3.0 g l⁻¹ nickel. Current density = 6.0 A cm⁻². Re. = 10800. X2000



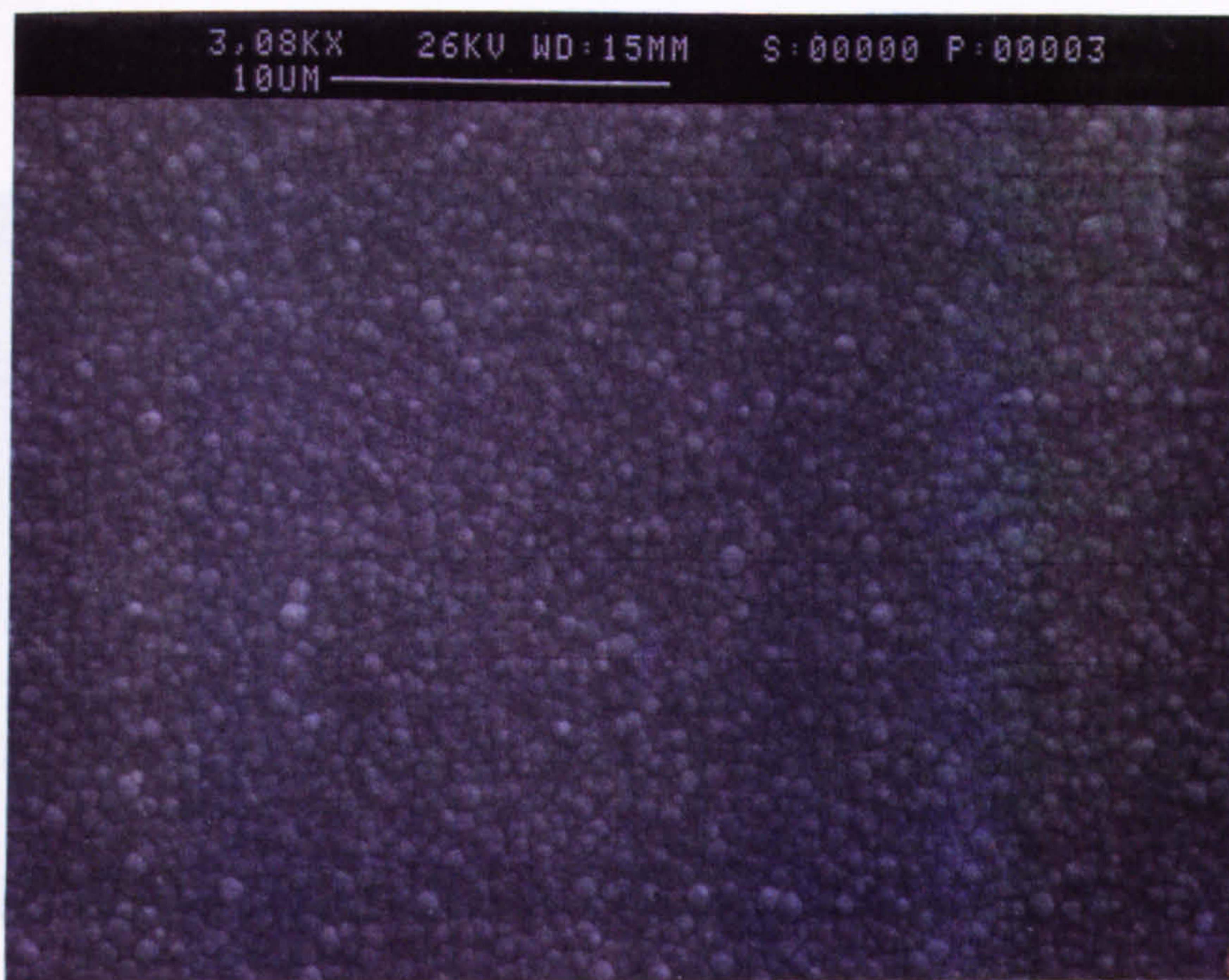
Photograph 33. An optical micrograph of a 17.6 μm gold/nickel alloy deposit produced from a Ronoval N electrolyte containing 60 ml l⁻¹ booster and 0.7 g l⁻¹ nickel. Current density = 8.0 A cm⁻². Re. = 10800. X 1000



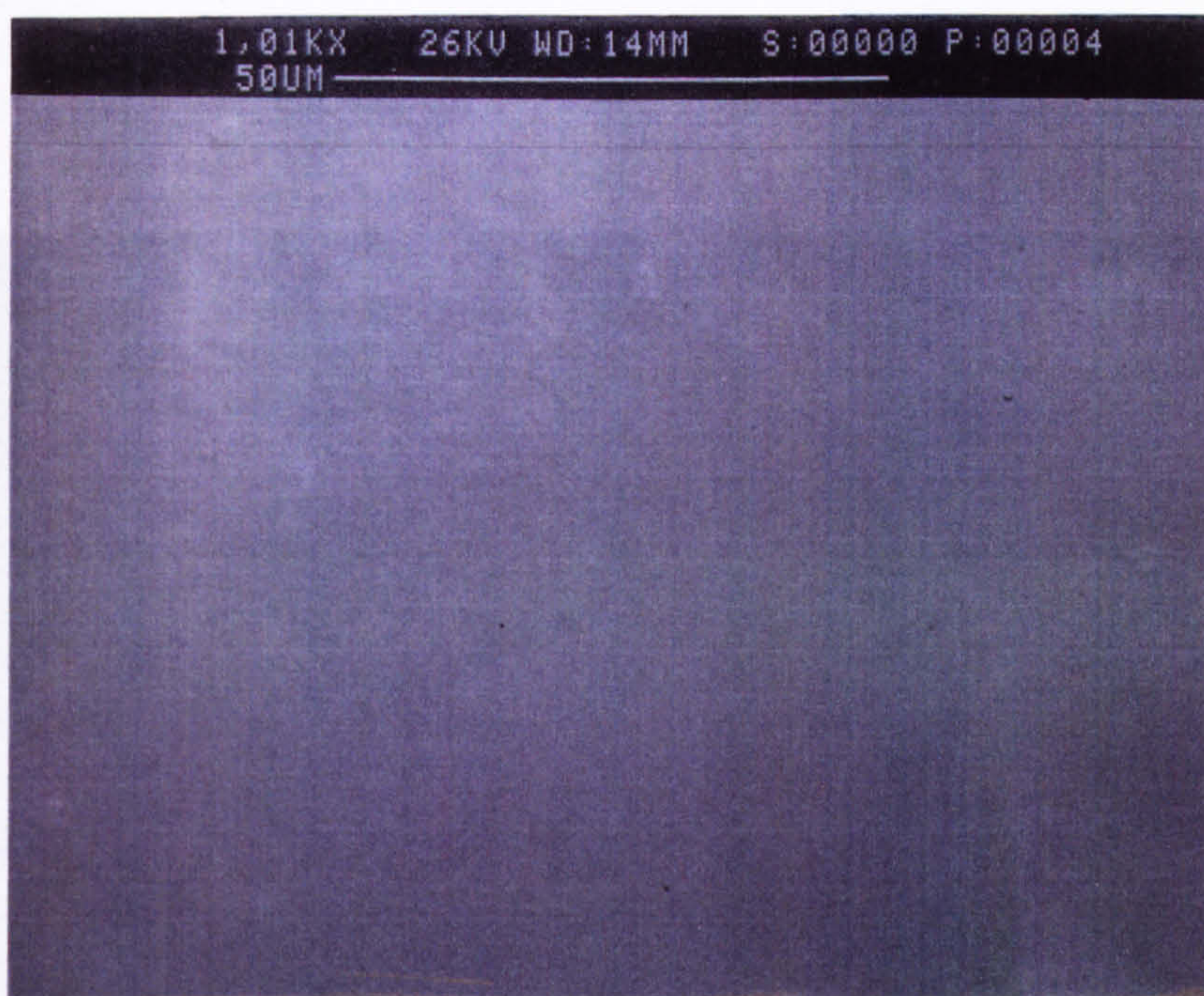
Photograph 34. An optical micrograph of a 17.9 μm gold/nickel alloy deposit produced from a Ronoval N electrolyte containing 60 ml l⁻¹ booster and 2.2 g l⁻¹ nickel. Current density = 8.0 A cm⁻². Re. = 10800. X 1000



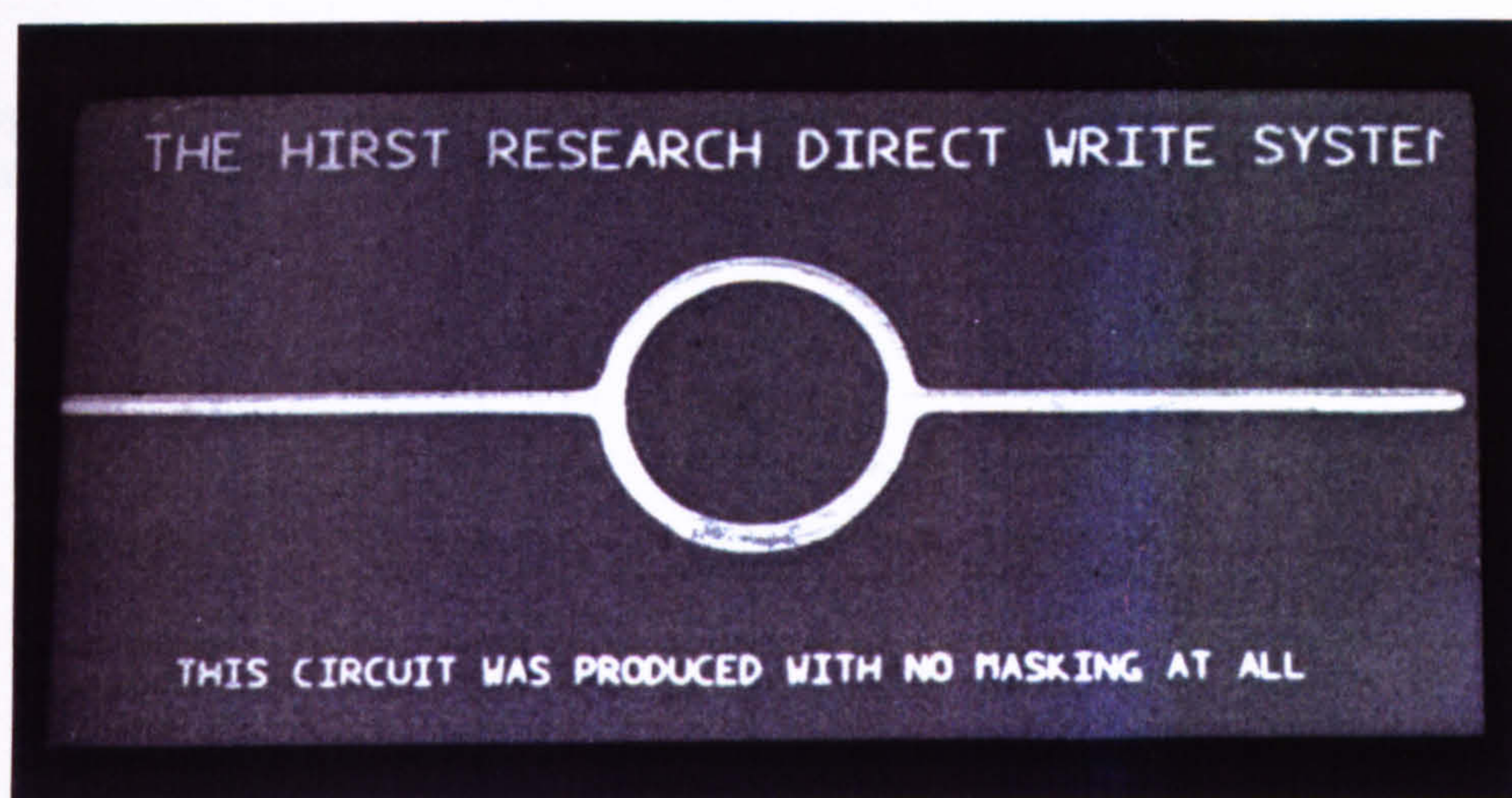
Photograph 35. SEM micrograph of a 2.5 μm gold/nickel alloy deposit produced from a Ronoval electrolyte containing 60 ml l^{-1} and 1.9 g l^{-1} nickel. Current density = 10.0 A cm^{-2} . Re. = 10800.



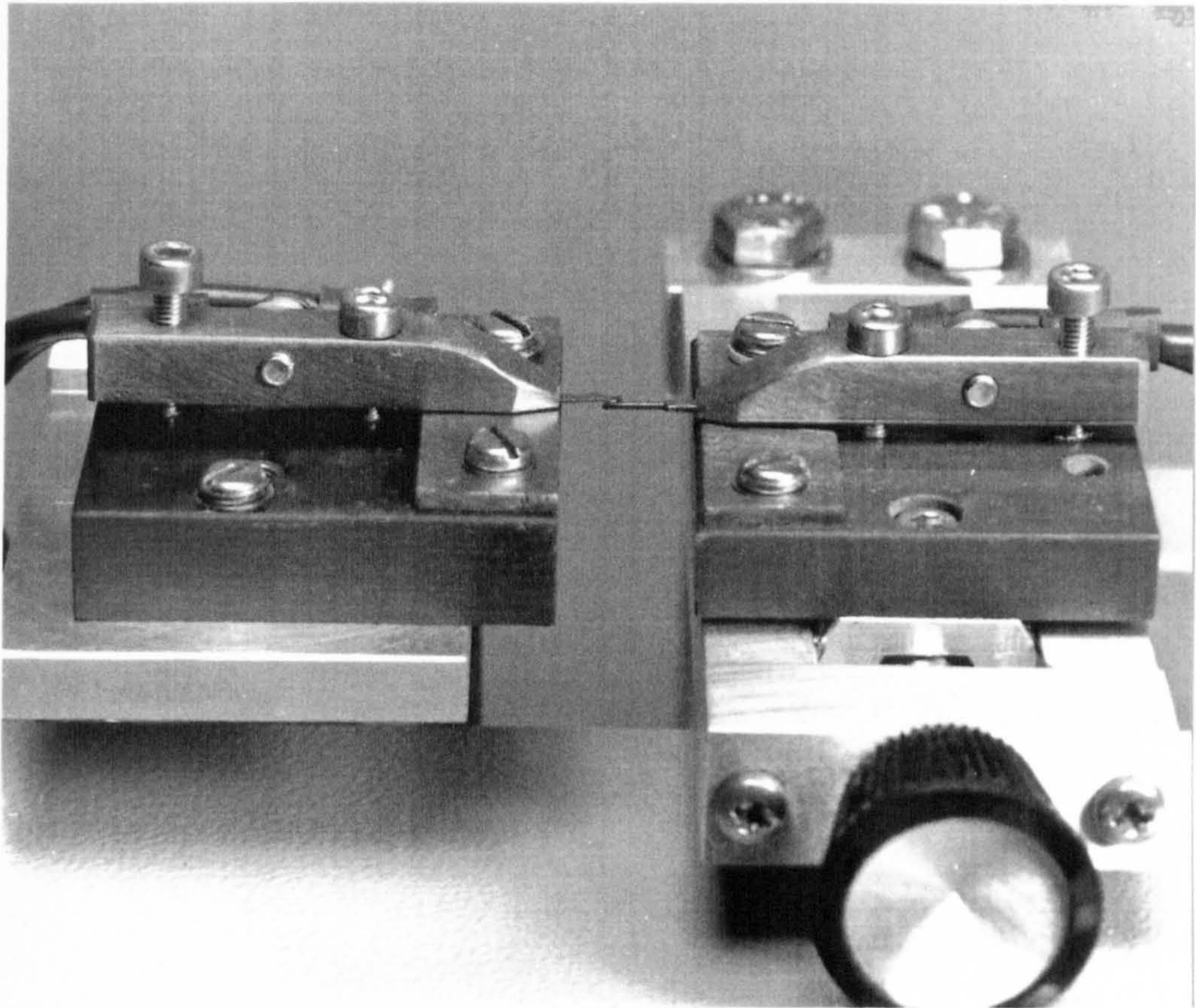
Photograph 36. SEM micrograph of a 2.5 μm gold/nickel alloy deposit produced from a Ronoval electrolyte containing 60 ml l^{-1} and 1.9 g l^{-1} nickel. Current density = 12.0 A cm^{-2} . Re. = 10800.



Photograph 37. SEM micrograph of a 2.5 μm gold/nickel alloy deposit produced from a Ronoval N electrolyte using conventional deposition conditions. Current density = 10 mA cm^{-2} . Temperature = 35°C.



Photograph 38. An example of a directly written ring oscillator produced by HSSJE with both a 400 μm and a 100 μm nozzle after removal of the metallised "seed" layer.



Photograph 39. The connector wear test configuration as used by the GEC Contact Tester showing an actual contact pair under test.

DATA TABLES

These tables list the most relevant data obtained during this study.

0.041M CITRATE GOLD ELECTROLYTE		
Gold (as potassium gold cyanide) Diammonium hydrogen citrate Citric acid Potassium hydroxide	8.2 g l ⁻¹ 45.0 g l ⁻¹ 15.0 g l ⁻¹ to pH 6.0	
Kinematic viscosity	25°C 40°C 55°C	0.0100203 cm ² sec ⁻¹ 0.0073904 cm ² sec ⁻¹ 0.0058590 cm ² sec ⁻¹
Conductivity	25°C 55°C	49.6 mS cm ⁻¹ 83.12 mS cm ⁻¹
0.28M CITRATE GOLD ELECTROLYTE		
Gold (as potassium gold cyanide) Diammonium hydrogen citrate Citric acid Potassium hydroxide	54.0 g l ⁻¹ 45.0 g l ⁻¹ 15.0 g l ⁻¹ to pH 6.0	
Kinematic viscosity	25°C 40°C 55°C	0.012284 cm ² sec ⁻¹ 0.009221 cm ² sec ⁻¹ 0.0076567 cm ² sec ⁻¹
Conductivity	25°C 55°C	55.3 mS cm ⁻¹ 97.6 mS cm ⁻¹
0.17M CITRATE GOLD ELECTROLYTE		
Gold (as potassium gold cyanide) Diammonium hydrogen citrate Citric acid Potassium hydroxide	33.5 g l ⁻¹ 45.0 g l ⁻¹ 15.0 g l ⁻¹ to pH 6.0	
Kinematic viscosity	25°C	0.005906 cm ² sec ⁻¹
Conductivity	55°C	92.3 mS cm ⁻¹
0.28M LOW CONDUCTIVITY CITRATE		
Gold (as potassium gold cyanide) Diammonium hydrogen citrate Citric acid Potassium hydroxide	54.0 g l ⁻¹ 1.0 g l ⁻¹ 1.0 g l ⁻¹ to pH 6.0	
Kinematic viscosity	55°C	0.04232 cm ² sec ⁻¹
Conductivity	55°C	48.8 mS cm ⁻¹
0.27M PHOSPHATE GOLD ELECTROLYTE		
Gold (as potassium gold cyanide) Di-potassium hydrogen phosphate Potassium di-hydrogen phosphate Potassium hydroxide	53.1 g l ⁻¹ 40.0 g l ⁻¹ 10.0 g l ⁻¹ to pH 7.1	
Kinematic viscosity	25°C 40°C 55°C	0.009164 cm ² sec ⁻¹ 0.006891 cm ² sec ⁻¹ 0.005426 cm ² sec ⁻¹
Conductivity	25°C 55°C	52.44 mS cm ⁻¹ 90.02 mS cm ⁻¹

TABLE 1. Composition and some properties of the pure gold electrolytes used in this study.

PURE GOLD DEPOSITED SPOTS. PLATING PARAMETER DATA

SAMPLE NO.	Au1		ELECTROLYTE		0.041M Citrate													
Temp. = 25 C		Nozzle velocity m/sec = 2		Nozzle area cm sq = 0.00126		Reynolds No. 796.4												
pH = 6.1		Nozzle size cm = 0.04		Viscosity cm sq/sec. = 0.01002														
Spot number	1	2	3	4	5	6	7	8	9	10	11	12	13	14	15	16	17	18
Current density A/cm sq	0.25	0.5	0.75	1	1.25	1.5	1.75	2	2.25	2.5	2.75	3	4	5	6			
Current applied mA	0.31	0.63	0.94	1.26	1.57	1.88	2.20	2.51	2.83	3.14	3.45	3.77	5.02	6.26	7.54			
Time secs	123	62.5	41.45	31.25	24.9	20.8	17.82	15.63	13.86	12.5	11.35	10.42	7.8	6.25	5.2			
Total coulombs	0.03862	0.03826	0.03806	0.03826	0.03806	0.03819	0.03817	0.03826	0.03817	0.03826	0.03820	0.03826	0.03819	0.03826	0.03819			
Thickness um	0.5	5.4	6.9	11.9	16.8	19.6	-											
Plating rate u/sec	0.0041	0.086	0.166	0.381	0.675	0.942	-											
Deposit quality	d	s	d	d	n	en	ene											

SAMPLE NO.	Au2		ELECTROLYTE		0.041M Citrate													
Temp. = 25 C		Nozzle velocity m/sec = 5		Nozzle area cm sq = 0.00126		Reynolds No. 1996												
pH = 6.1		Nozzle size cm = 0.04		Viscosity cm sq/sec. = 0.01002														
Spot number	1	2	3	4	5	6	7	8	9	10	11	12	13	14	15	16	17	18
Current density A/cm sq	0.25	0.5	0.75	1	1.25	1.5	1.75	2	2.25	2.5	2.75	3	4	5	6			
Current applied mA	0.31	0.63	0.94	1.26	1.57	1.88	2.20	2.51	2.83	3.14	3.45	3.77	5.02	6.26	7.54			
Time secs	123	62.5	41.45	31.25	24.9	20.8	17.82	15.63	13.86	12.5	11.35	10.42	7.8	6.25	5.2			
Total coulombs	0.03862	0.03826	0.03806	0.03826	0.03806	0.03819	0.03817	0.03826	0.03817	0.03826	0.03820	0.03826	0.03819	0.03826	0.03819			
Thickness um	0	4.6	8.6	10.6	12.6	16.1	17.4	19.3										
Plating rate u/sec	0	0.074	0.207	0.339	0.506	0.774	0.976	1.235										
Deposit quality	nd	s	d	d	n	n	en	ne	ene	ene	ene	ene	ene	ene	ene			

SAMPLE NO.	Au3		ELECTROLYTE		0.041M Citrate													
Temp. = 25 C		Nozzle velocity m/sec = 10		Nozzle area cm sq = 0.00126		Reynolds No. 3992												
pH = 6.1		Nozzle size cm = 0.04		Viscosity cm sq/sec. = 0.01002														
Spot number	1	2	3	4	5	6	7	8	9	10	11	12	13	14	15	16	17	18
Current density A/cm sq	0.25	0.5	0.75	1	1.25	1.5	1.75	2	2.25	2.5	2.75	3	4	5	6			
Current applied mA	0.31	0.63	0.94	1.26	1.57	1.88	2.20	2.51	2.83	3.14	3.45	3.77	5.02	6.26	7.54			
Time secs	123	62.5	41.45	31.25	24.9	20.8	17.82	15.63	13.86	12.5	11.35	10.42	7.8	6.25	5.2			
Total coulombs	0.03862	0.03826	0.03806	0.03826	0.03806	0.03819	0.03817	0.03826	0.03817	0.03826	0.03820	0.03826	0.03819	0.03826	0.03819			
Thickness um	0	3.3	7.5	9.9	8.9	12.6	14.4	15.4	15.6									
Plating rate u/sec	0	0.053	0.181	0.317	0.357	0.606	0.808	0.985	1.126									
Deposit quality	nd	s	s	s/d	d	d	n	en	en	ne/en	ne/en	ene	ene	ene	ene			

SAMPLE NO.	Au4		ELECTROLYTE		0.041M Citrate													
Temp. = 25 C		Nozzle velocity m/sec = 15		Nozzle area cm sq = 0.00126		Reynolds No. 5966												
pH = 6.1		Nozzle size cm = 0.04		Viscosity cm sq/sec. = 0.01002														
Spot number	1	2	3	4	5	6	7	8	9	10	11	12	13	14	15	16	17	18
Current density A/cm sq	0.25	0.5	0.75	1	1.25	1.5	1.75	2	2.25	2.5	2.75	3	4	5	6			
Current applied mA	0.31	0.63	0.94	1.26	1.57	1.88	2.20	2.51	2.83	3.14	3.45	3.77	5.02	6.26	7.54			
Time secs	123	62.5	41.45	31.25	24.9	20.8	17.82	15.63	13.86	12.5	11.35	10.42	7.8	6.25	5.2			
Total coulombs	0.03862	0.03826	0.03806	0.03826	0.03806	0.03819	0.03817	0.03826	0.03817	0.03826	0.03820	0.03826	0.03819	0.03826	0.03819			
Thickness um	0	2.5	6.3	8.3	10.6	11	13.6	14.9	15.6	16.5								
Plating rate u/sec	0	0.04	0.152	0.266	0.426	0.529	0.763	0.953	1.126	1.32								
Deposit quality	nd	s	s	s	d	d	d	n	n/en	en	ne	ene	ene	ene	ene			

DEPOSIT QUALITY KEY		s - smooth & bright	d - smooth & dull
Visual assessment only		sb - semi-bright	n - slight nodulation
		en - severe nodulation	ne - slight needle growth
		ene - severe needle growth	jc - jet core dendrite
		cr - cracks	nd - no viable deposit

TABLE 2

PURE GOLD DEPOSITED SPOTS. PLATING PARAMETER DATA

SAMPLE NO.	Au5		ELECTROLYTE		0.041M Citrate													
Temp. = 25 C		Nozzle velocity m/sec = 18		Nozzle area cm sq = 0.00126		Reynolds No. 7185												
pH = 6.1		Nozzle size cm = 0.04		Viscosity cm sq/sec = 0.01002														
Spot number	1	2	3	4	5	6	7	8	9	10	11	12	13	14	15	16	17	18
Current density A/cm sq	0.25	0.5	0.75	1	1.25	1.5	1.75	2	2.25	2.5	2.75	3	4	5	6	8		
Current applied mA	0.31	0.63	0.94	1.26	1.57	1.88	2.20	2.51	2.83	3.14	3.45	3.77	5.02	6.28	7.54	10.05		
Time secs	123	62.5	41.45	31.25	24.9	20.8	17.82	15.63	13.66	12.5	11.35	10.42	7.8	6.25	5.2	3.9		
Total coulombs	0.03862	0.03925	0.03806	0.03925	0.03808	0.03819	0.03817	0.03826	0.03817	0.03825	0.03820	0.03826	0.03819	0.03925	0.03819	0.03819		
Thickness um	0	2.2	4.9	8	10.3	12.3	13.7	15.9	16.1	16.9								
Plating rate u/sec	0	0.035	0.118	0.256	0.414	0.591	0.789	1.017	1.162	1.352								
Deposit quality	nd	s	s	s	s	dl	n	n	n	sn/ne	ne	ane	ane	ane	ane	ane		

SAMPLE NO.	Au6		ELECTROLYTE		0.041M Citrate													
Temp. = 40 C		Nozzle velocity m/sec = 2		Nozzle area cm sq = 0.00126		Reynolds No. 1082												
pH = 6.1		Nozzle size cm = 0.04		Viscosity cm sq/sec. = 0.00739														
Spot number	1	2	3	4	5	6	7	8	9	10	11	12	13	14	15	16	17	18
Current density A/cm sq	0.25	0.5	0.75	1	1.25	1.5	1.75	2	2.25	2.5	2.75	3	4	5	6	8		
Current applied mA	0.31	0.63	0.94	1.26	1.57	1.88	2.20	2.51	2.83	3.14	3.45	3.77	5.02	6.28	7.54	10.05		
Time secs	123	62.5	41.45	31.25	24.9	20.8	17.82	15.63	13.66	12.5	11.35	10.42	7.8	6.25	5.2	3.9		
Total coulombs	0.03862	0.03925	0.03806	0.03925	0.03808	0.03819	0.03817	0.03826	0.03817	0.03825	0.03820	0.03826	0.03819	0.03925	0.03819	0.03819		
Thickness um	0	4.2	4.4	7.4	10.4	10.3	14	15.7	17.4	22.3	21.1	20	20.7					
Plating rate u/sec	0	0.067	0.106	0.237	0.418	0.495	0.786	1.004	1.255	1.784	1.859	1.919	2.6538					
Deposit quality	nd	d	d/s	s	n	sn	sn	sn	sn	sn	sn	sn	sn	sn/ne	sn/ne	sn/ne		

SAMPLE NO.	Au7		ELECTROLYTE		0.041M Citrate													
Temp. = 40 C		Nozzle velocity m/sec = 5		Nozzle area cm sq = 0.00126		Reynolds No. 2706												
pH = 6.1		Nozzle size cm = 0.04		Viscosity cm sq/sec. = 0.00739														
Spot number	1	2	3	4	5	6	7	8	9	10	11	12	13	14	15	16	17	18
Current density A/cm sq	0.25	0.5	0.75	1	1.25	1.5	1.75	2	2.25	2.5	2.75	3	4	5	6	8		
Current applied mA	0.31	0.63	0.94	1.26	1.57	1.88	2.20	2.51	2.83	3.14	3.45	3.77	5.02	6.28	7.54	10.05		
Time secs	123	62.5	41.45	31.25	24.9	20.8	17.82	15.63	13.66	12.5	11.35	10.42	7.8	6.25	5.2	3.9		
Total coulombs	0.03862	0.03925	0.03806	0.03925	0.03808	0.03819	0.03817	0.03826	0.03817	0.03825	0.03820	0.03826	0.03819	0.03925	0.03819	0.03819		
Thickness um	0	2.9	6.4	8.2	10.4	11.7	14.9	16.6	17.4	18.7	18.8	17.9						
Plating rate u/sec	0	0.046	0.154	0.262	0.418	0.563	0.836	1.062	1.255	1.496	1.656	1.718						
Deposit quality	nd	d	d/s	s	d/s	n	sn	sn	sn	sn	sn	sn	sn	sn/ne	ne/jc	jc		

SAMPLE NO.	Au8		ELECTROLYTE		0.041M Citrate													
Temp. = 40 C		Nozzle velocity m/sec = 10		Nozzle area cm sq = 0.00126		Reynolds No. 5412												
pH = 6.1		Nozzle size cm = 0.04		Viscosity cm sq/sec = 0.00739														
Spot number	1	2	3	4	5	6	7	8	9	10	11	12	13	14	15	16	17	18
Current density A/cm sq	0.25	0.5	0.75	1	1.25	1.5	1.75	2	2.25	2.5	2.75	3	4	5	6	8		
Current applied mA	0.31	0.63	0.94	1.26	1.57	1.88	2.20	2.51	2.83	3.14	3.45	3.77	5.02	6.28	7.54	10.05	0.00	0.00
Time secs	123	62.5	41.45	31.25	24.9	20.8	17.82	15.63	13.66	12.5	11.35	10.42	7.8	6.25	5.2	3.9		
Total coulombs	0.03862	0.03925	0.03806	0.03825	0.03808	0.03819	0.03817	0.03826	0.03817	0.03825	0.03820	0.03826	0.03819	0.03925	0.03819	0.03819	0.00000	0.00000
Thickness um	0	2.4	5	7.1	8.5	9.4	12.8	14.3	14.2	16	16.1	16	15.3	16.2				
Plating rate u/sec	0	0.038	0.121	0.227	0.382	0.452	0.718	0.915	1.025	1.28	1.419	1.727	1.9615	2.592	0	0	EAR	EAR
Deposit quality	nd	d	d	s	s	s/d	n	sn	sn	sn	sn	sn	sn	sn	sn	ne		

DEPOSIT QUALITY KEY

Visual assessment only

s - smooth & bright d - smooth & dull
sb - semi-bright n - slight nodulation
sn - severe nodulation ne - slight needle growth
ane - severe needle growth jc - jet core dendrite
cr - cracks nd - no visible deposit

TABLE 3

PURE GOLD DEPOSITED SPOTS. PLATING PARAMETER DATA

SAMPLE NO.	Au9		ELECTROLYTE		0.041M Citrate													
Temp. = 40 C		Nozzle velocity m/sec = 15				Nozzle area cm sq = 0.00126				Reynolds No. 8119								
pH = 6.1		Nozzle size cm = 0.04				Viscosity cm sq/sec = 0.00739												
Spot number	1	2	3	4	5	6	7	8	9	10	11	12	13	14	15	16	17	18
Current density A/cm sq	0.25	0.5	0.75	1	1.25	1.5	1.75	2	2.25	2.5	2.75	3	4	5	6	8		
Current applied mA	0.31	0.63	0.94	1.26	1.57	1.88	2.20	2.51	2.83	3.14	3.45	3.77	5.02	6.28	7.54	10.05		
Time secs	123	62.5	41.45	31.25	24.9	20.8	17.82	15.63	13.66	12.5	11.35	10.42	7.8	6.25	5.2	3.9		
Total coulombs	0.03862	0.03926	0.03905	0.03926	0.03809	0.03919	0.03917	0.03926	0.03917	0.03926	0.03920	0.03926	0.03919	0.03926	0.03919	0.03919		
Thickness um	0	1.1	4.7	7.2	9.3	10.3	11.2	12.9	14.7	14.6	17.6	16.4	16.8	16.4				
Plating rate u/sec	0	0.018	0.113	0.23	0.373	0.495	0.629	0.825	1.061	1.168	1.551	1.574	2.1538	2.624				
Deposit quality	nd	d	d	s	s	s/d	d/n	sn	sn	sn	sn	sn	sn	sn	sn	ne		

SAMPLE NO.	Au10	ELECTROLYTE		0.041M Citrate														
Temp. = 40 C	Nozzle velocity m/sec = 18	Nozzle area cm sq = 0.00126		Reynolds No. 9742														
pH = 6.1	Nozzle size cm = 0.04	Viscosity cm sq/sec. = 0.00739																
Spot number	1	2	3	4	5	6	7	8	9	10	11	12	13	14	15	16	17	18
Current density A/cm sq	0.25	0.5	0.75	1	1.25	1.5	1.75	2	2.25	2.5	2.75	3	4	5	6	8		
Current applied mA	0.31	0.63	0.94	1.26	1.57	1.88	2.20	2.51	2.83	3.14	3.45	3.77	5.02	6.28	7.54	10.05		
Time secs	123	62.5	41.45	31.25	24.9	20.8	17.62	15.63	13.66	12.5	11.35	10.42	7.8	6.25	5.2	3.9		
Total coulombs	0.03862	0.03926	0.03905	0.03926	0.03809	0.03919	0.03917	0.03926	0.03917	0.03926	0.03920	0.03926	0.03919	0.03926	0.03919	0.03919		
Thickness um	0	1.3	4.6	8.7	8.9	9.5	10.4	12.1	14.2	15.4	16.2	16.3	16.2	14.8				
Plating rate u/sec	0	0.021	0.111	0.214	0.357	0.457	0.584	0.774	1.025	1.232	1.427	1.564	2.0769	2.368				
Deposit quality	nd	d	d	s	s	s	s/d	n	n	n	sn	sn	sn	sn	sn/ne	sn		

SAMPLE NO.	Au11		ELECTROLYTE		0.041M Citrate													
Temp. = 55 C	Nozzle velocity m/sec = 2		Nozzle area cm sq = 0.00126		Reynolds No. 1365													
pH = 6.1	Nozzle size cm = 0.04		Viscosity cm sq/sec. = 0.00698															
Spot number	1	2	3	4	5	6	7	8	9	10	11	12	13	14	15	16	17	18
Current density A/cm sq	0.25	0.5	0.75	1	1.25	1.5	1.75	2	2.25	2.5	2.75	3	4	5	6	8		
Current applied mA	0.31	0.63	0.94	1.26	1.57	1.88	2.20	2.51	2.83	3.14	3.45	3.77	5.02	6.28	7.54	10.05		
Time secs	123	62.5	41.45	31.25	24.9	20.8	17.62	15.63	13.66	12.5	11.35	10.42	7.8	6.25	5.2	3.9		
Total coulombs	0.03862	0.03926	0.03905	0.03926	0.03809	0.03919	0.03917	0.03926	0.03917	0.03926	0.03920	0.03926	0.03919	0.03926	0.03919	0.03919		
Thickness um	0	1.1	6	7.4	9	10.6	12.3	14	21	19								
Plating rate u/sec	0	0.018	0.145	0.237	0.361	0.51	0.69	0.896	1.515	1.52								
Deposit quality	nd	d	d	d	d	sb	sb	sn	sn	sn	sn	sn	sn	sn	sn	sn		

SAMPLE NO.	Au12		ELECTROLYTE		0.041M Citrate													
Temp. = 55 C	Nozzle velocity m/sec = 5		Nozzle area cm sq = 0.00126		Reynolds No. 3414													
pH = 6.1	Nozzle size cm = 0.04		Viscosity cm sq/sec = 0.00698															
Spot number	1	2	3	4	5	6	7	8	9	10	11	12	13	14	15	16	17	18
Current density A/cm sq	0.25	0.5	0.75	1	1.25	1.5	1.75	2	2.25	2.5	2.75	3	4	5	6	8		
Current applied mA	0.31	0.63	0.94	1.26	1.57	1.88	2.20	2.51	2.83	3.14	3.45	3.77	5.02	6.28	7.54	10.05		
Time secs	123	62.5	41.45	31.25	24.9	20.8	17.82	15.63	13.66	12.5	11.35	10.42	7.8	6.25	5.2	3.9		
Total coulombs	0.03862	0.03926	0.03905	0.03926	0.03909	0.03919	0.03917	0.03926	0.03917	0.03926	0.03920	0.03926	0.03919	0.03925	0.03919	0.03919		
Thickness um	0	5.2	7.1	7.4	9	10.3	11.7	13	16.5									
Plating rate u/sec	0	0.083	0.171	0.237	0.361	0.495	0.657	0.832	1.19									
Deposit quality	nd	d	d	d	d	d/s	s	sb	n	sn	sn	sn	sn	sn	sn	sn		

DEPOSIT QUALITY KEY

Visual assessment only

s - smooth & bright d - smooth & dull
sb - semi-bright n - slight nodulation
sn - severe nodulation ne - slight needle growth
sne - severe needle growth jc - jet core dendrite
cr - cracks nd - no visible deposit

TABLE 4

PURE GOLD DEPOSITED SPOTS. PLATING PARAMETER DATA

SAMPLE NO.	Au13			ELECTROLYTE			0.041M Citrate											
Temp. = 55 C		Nozzle velocity m/sec = 10				Nozzle area cm sq = 0.00126				Reynolds No. 6627								
pH = 6.1		Nozzle size cm = 0.04				Viscosity cm sq/sec. = 0.00566												
Spot number	1	2	3	4	5	6	7	8	9	10	11	12	13	14	15	16	17	18
Current density A/cm sq	0.25	0.5	0.75	1	1.25	1.5	1.75	2	2.25	2.5	2.75	3	4	5	6	8		
Current applied mA	0.31	0.63	0.94	1.26	1.57	1.88	2.20	2.51	2.83	3.14	3.45	3.77	5.02	6.28	7.54	10.05		
Time secs	123	62.5	41.45	31.25	24.9	20.8	17.82	15.63	13.86	12.5	11.35	10.42	7.8	6.25	5.2	3.9		
Total coulombs	0.03862	0.03925	0.03805	0.03825	0.03808	0.03819	0.03817	0.03826	0.03817	0.03825	0.03820	0.03825	0.03819	0.03925	0.03819	0.03819		
Thickness um	0	0.5	4.2	5.8	7.5	8.3	9.6	11.1	10.7	12.6	13.3	15.6	16.7	16.5	18.3	16.2		
Plating rate u/sec	0	0.008	0.101	0.186	0.301	0.399	0.539	0.71	0.772	1.008	1.172	1.497	2.141	2.64	3.519	4.154		
Deposit quality	nd	sb	d	d	d	d/s	s	s	sb/n	sn	sn	sn	sn	sn	sn	sn		

SAMPLE NO.	Au14			ELECTROLYTE			0.041M Citrate											
Temp. = 55 C		Nozzle velocity m/sec = 15		Nozzle area cm sq = 0.00126		Reynolds No. 10241												
pH = 6.1		Nozzle size cm = 0.04		Viscosity cm sq/sec = 0.00566														
Spot number	1	2	3	4	5	6	7	8	9	10	11	12	13	14	15	16	17	18
Current density A/cm sq	0.25	0.5	0.75	1	1.25	1.5	1.75	2	2.25	2.5	2.75	3	4	5	6	8		
Current applied mA	0.31	0.63	0.94	1.26	1.57	1.88	2.20	2.51	2.83	3.14	3.45	3.77	5.02	6.28	7.54	10.05		
Time secs	123	62.5	41.45	31.25	24.9	20.8	17.82	15.63	13.86	12.5	11.35	10.42	7.8	6.25	5.2	3.9		
Total coulombs	0.03862	0.03925	0.03805	0.03825	0.03808	0.03819	0.03817	0.03826	0.03817	0.03825	0.03820	0.03825	0.03819	0.03825	0.03819	0.03819		
Thickness um	0	0.3	3.2	5.3	7.1	8.1	9.9	10.9	11.7	12.5	13	13.7	17.1	17.6	16.7	17.1		
Plating rate u/sec	0	0.005	0.077	0.17	0.285	0.389	0.556	0.697	0.844	1	1.145	1.315	2.1923	2.816	3.596	4.385		
Deposit quality	nd	d	d	d	d	d	d/s	s	s	sb	n	sn	sn	sn	sn	sn		

SAMPLE NO.	Au15			ELECTROLYTE			0.041M Citrate											
Temp. = 55 C		Nozzle velocity m/sec = 18		Nozzle area cm sq = 0.00126		Reynolds No. 12289												
pH = 6.1		Nozzle size cm = 0.04		Viscosity cm sq/sec. = 0.00566														
Spot number	1	2	3	4	5	6	7	8	9	10	11	12	13	14	15	16	17	18
Current density A/cm sq	0.25	0.5	0.75	1	1.25	1.5	1.75	2	2.25	2.5	2.75	3	4	5	6	8		
Current applied mA	0.31	0.63	0.94	1.26	1.57	1.88	2.20	2.51	2.83	3.14	3.45	3.77	5.02	6.28	7.54	10.05		
Time secs	123	62.5	41.45	31.25	24.9	20.8	17.82	15.63	13.86	12.5	11.35	10.42	7.8	6.25	5.2	3.9		
Total coulombs	0.03062	0.03925	0.03805	0.03825	0.03808	0.03819	0.03817	0.03826	0.03817	0.03825	0.03820	0.03825	0.03819	0.03825	0.03819	0.03819		
Thickness um	0	0.4	2.4	5.4	7.1	8.4	10	11	11.9	12.4	13.3	14	16.8	17.8	15.4	16.6		
Plating rate u/sec	0	0.006	0.058	0.173	0.285	0.404	0.561	0.704	0.859	0.992	1.172	1.344	2.1538	2.848	2.962	4.256		
Deposit quality	nd	s	d	d	d	d	s	s	s	s/sb	n	sn	sn	sn	sn	sn		

SAMPLE NO.	Au16		ELECTROLYTE		0.26M Citrate														
Temp. = 25 C		Nozzle velocity m/sec = 2		Nozzle area cm sq = 0.00126		Reynolds No. 651.3													
pH = 6.1		Nozzle size cm = 0.04		Viscosity cm sq/sec = 0.01228															
Spot number	1	2	3	4	5	6	7	8	9	10	11	12	13	14	15	16	17	18	
Current density A/cm sq	0.25	0.75	1	2	3	3.25	3.5	3.75	4	4.25	4.5	4.75	5	5.5	6	6.5	7		
Current applied mA	0.31	0.94	1.26	2.51	3.77	4.08	4.40	4.71	5.02	5.34	5.65	5.97	6.28	6.91	7.54	8.16	8.79		
Time secs	123	41.45	31.25	15.63	10.42	9.6	8.9	8.3	7.8	7.4	6.9	6.57	6.25	5.68	5.21	4.61	4.46		
Total coulombs	0.03062	0.03906	0.03826	0.03826	0.03826	0.03819	0.03812	0.03809	0.03818	0.03850	0.03800	0.03820	0.03825	0.03824	0.03826	0.03827	0.03821		
Thickness um	0	10.6	Depos																
Plating rate u/sec	0	0.256																	
Deposit quality	nd	s	ne	ne	ne	ne/cr	ne	ne	ne	ne	ne	ne	ne	ne	ne	ne/jc			

DEPOSIT QUALITY KEY		e - smooth & bright	d - smooth & dull
		sb - semi-bright	n - slight nodulation
Visual assessment only		sn - severe nodulation	ne - slight needle growth
		ane - severe needle growth	jc - jet core dendrite
		cr - cracks	nd - no visible deposit

TABLE 5

PURE GOLD DEPOSITED SPOTS. PLATING PARAMETER DATA

SAMPLE NO.		Au17		ELECTROLYTE		0.28M Citrate												
Temp. = 25 C		Nozzle velocity m/sec = 5		Nozzle area cm sq = 0.00126		Reynolds No. 1628												
pH = 8.1		Nozzle size cm = 0.04		Viscosity cm sq/sec. = 0.01228														
Spot number	1	2	3	4	5	6	7	8	9	10	11	12	13	14	15	16	17	18
Current density A/cm sq	0.25	0.75	1	2	3	3.25	3.5	3.75	4	4.25	4.5	4.75	5	5.5	6	6.5	7	
Current applied mA	0.31	0.94	1.26	2.51	3.77	4.08	4.40	4.71	5.02	5.34	5.65	5.97	6.28	6.61	7.54	8.16	8.79	
Time secs	123	41.45	31.25	15.63	10.42	9.6	8.9	8.3	7.8	7.4	6.9	6.57	6.25	5.68	5.21	4.81	4.46	
Total coulombs	0.03862	0.03905	0.03925	0.03926	0.03926	0.03919	0.03912	0.03909	0.03919	0.03950	0.03900	0.03920	0.03925	0.03924	0.03926	0.03927	0.03921	
Thickness um	-	-	7.5	9.7	15.6	16.1	18.2	21.7	27.3									
Plating rate u/sec	0	0	0.24	0.621	1.497	1.677	2.045	2.614	3.5									
Deposit quality	s	s	s/ne	s/ne/c	s/ne/c	s/ne/c	ne/cr	ne/cr	sne	ne	ne	sne	sne/jc	sne/jc	sne/jc	sne/jc	sne/jc	

SAMPLE NO.		Au18		ELECTROLYTE		0.28M Citrate												
Temp. = 25 C		Nozzle velocity m/sec = 10		Nozzle area cm sq = 0.00126		Reynolds No. 3256												
pH = 8.1		Nozzle size cm = 0.04		Viscosity cm sq/sec. = 0.01228														
Spot number	1	2	3	4	5	6	7	8	9	10	11	12	13	14	15	16	17	18
Current density A/cm sq	0.25	0.75	1	2	3	3.25	3.5	3.75	4	4.25	4.5	4.75	5	5.5	6	6.5	7	
Current applied mA	0.31	0.94	1.26	2.51	3.77	4.08	4.40	4.71	5.02	5.34	5.65	5.97	6.28	6.61	7.54	8.16	8.79	
Time secs	123	41.45	31.25	15.63	10.42	9.6	8.9	8.3	7.8	7.4	6.9	6.57	6.25	5.68	5.21	4.81	4.46	
Total coulombs	0.03862	0.03905	0.03925	0.03926	0.03926	0.03919	0.03912	0.03909	0.03919	0.03950	0.03900	0.03920	0.03925	0.03924	0.03926	0.03927	0.03921	
Thickness um	-	5.4	5.7	11.7	14.1													
Plating rate u/sec	0	0.13	0.162	0.749	1.353													
Deposit quality	s	s	sb	sb/ne	sb/ne	ne	sne	sne	sne	sne	sne	sne/jc	sne	sne	sne	jc	jc	

SAMPLE NO.		Au19		ELECTROLYTE		0.28M Citrate												
Temp. = 25 C		Nozzle velocity m/sec = 16		Nozzle area cm sq = 0.00126		Reynolds No. 5661												
pH = 8.1		Nozzle size cm = 0.04		Viscosity cm sq/sec. = 0.01228														
Spot number	1	2	3	4	5	6	7	8	9	10	11	12	13	14	15	16	17	18
Current density A/cm sq	0.25	0.75	1	2	3	3.25	3.5	3.75	4	4.25	4.5	4.75	5	5.5	6	6.5	7	
Current applied mA	0.31	0.94	1.26	2.51	3.77	4.08	4.40	4.71	5.02	5.34	5.65	5.97	6.28	6.61	7.54	8.16	8.79	
Time secs	123	41.45	31.25	15.63	10.42	9.6	8.9	8.3	7.8	7.4	6.9	6.57	6.25	5.68	5.21	4.81	4.46	
Total coulombs	0.03862	0.03905	0.03925	0.03926	0.03926	0.03919	0.03912	0.03909	0.03919	0.03950	0.03900	0.03920	0.03925	0.03924	0.03926	0.03927	0.03921	
Thickness um	-	5.4	8.3	14.7														
Plating rate u/sec	0	0.13	0.266	0.94														
Deposit quality	sb	s	s/ne	sne	sne	sne	sne	sne	sne	sne	sne	sne	sne	sne	sne	sne	sne/jc	

SAMPLE NO.		Au20		ELECTROLYTE		0.28M Citrate												
Temp. = 40 C		Nozzle velocity m/sec = 2		Nozzle area cm sq = 0.00126		Reynolds No. 867.6												
pH = 8.1		Nozzle size cm = 0.04		Viscosity cm sq/sec. = 0.00822														
Spot number	1	2	3	4	5	6	7	8	9	10	11	12	13	14	15	16	17	18
Current density A/cm sq	0.25	0.75	1	2	3	3.25	3.5	3.75	4	4.25	4.5	4.75	5	5.5	6	6.5	7	
Current applied mA	0.31	0.94	1.26	2.51	3.77	4.08	4.40	4.71	5.02	5.34	5.65	5.97	6.28	6.61	7.54	8.16	8.79	
Time secs	123	41.45	31.25	15.63	10.42	9.6	8.9	8.3	7.8	7.4	6.9	6.57	6.25	5.68	5.21	4.81	4.46	
Total coulombs	0.03862	0.03905	0.03925	0.03926	0.03926	0.03919	0.03912	0.03909	0.03919	0.03950	0.03900	0.03920	0.03925	0.03924	0.03926	0.03927	0.03921	
Thickness um	-	7.1	9.8	17.2	18.8	20.4	20.7	21.8	24.5	22.5	24.9	22.7	25.5					
Plating rate u/sec	0	0.171	0.314	1.1	1.604	2.125	2.326	2.627	3.141	3.041	3.609	3.455	4.08					
Deposit quality	nd	s	s	sb	sb/ne	n	n	n	n/ne	n	n	sn	sn	sn/ne	jc	jc	jc	

DEPOSIT QUALITY KEY		s - smooth & bright	d - smooth & dull
Visual assessment only		sb - semi-bright	n - slight nodulation
		sn - severe nodulation	ne - slight needle growth
		sne - severe needle growth	jc - jet core dendrite
		cr - cracks	nd - no visible deposit

TABLE 6

PURE GOLD DEPOSITED SPOTS. PLATING PARAMETER DATA

SAMPLE NO.	Au21		ELECTROLYTE		0.26M Citrate													
Temp. =	40 C		Nozzle velocity m/sec	= 5		Nozzle area cm sq	= 0.00126		Reynolds No. 2169									
pH =	6.1		Nozzle size cm	= 0.04		Viscosity cm sq/sec	= 0.00822											
Spot number	1	2	3	4	5	6	7	8	9	10	11	12	13	14	15	16	17	18
Current density A/cm sq	0.25	0.75	1	2	3	3.25	3.5	3.75	4	4.25	4.5	4.75	5	5.5	6	6.5	7	8
Current applied mA	0.31	0.94	1.26	2.51	3.77	4.08	4.40	4.71	5.02	5.34	5.65	5.97	6.28	6.61	7.54	8.16	8.79	10.05
Time secs	123	41.45	31.25	15.63	10.42	9.6	8.9	8.3	7.8	7.4	6.9	6.57	6.25	5.68	5.21	4.81	4.46	3.9
Total coulombs	0.03862	0.03906	0.03926	0.03926	0.03926	0.03919	0.03912	0.03909	0.03919	0.03950	0.03900	0.03920	0.03925	0.03924	0.03926	0.03927	0.03921	0.03919
Thickness um	-	6.1	8.3	15.5	18.1	18.7	18.3	18.9	19.4	20								
Plating rate u/sec	0	0.147	0.268	0.992	1.737	1.948	2.056	2.277	2.487	2.703								
Deposit quality	nd	s	s	sb	n	sn	sn	sn	sn	sn/ne	sn/ne	sn/ne	sne	sne/jc	sne	sne	sne/jc	jc

SAMPLE NO.		Au22		ELECTROLYTE		0.25MCitrate												
Temp. = 40 C		Nozzle velocity m/sec = 10		Nozzle area cm sq = 0.00126		Reynolds No 4338												
pH = 6.1		Nozzle size cm = 0.04		Viscosity cm sq/sec = 0.00822														
Spot number	1	2	3	4	5	6	7	8	9	10	11	12	13	14	15	16	17	18
Current density A/cm sq	0.25	0.75	1	2	3	3.25	3.5	3.75	4	4.25	4.5	4.75	5	5.5	6	6.5	7	8
Current applied mA	0.31	0.94	1.26	2.51	3.77	4.08	4.40	4.71	5.02	5.34	5.65	5.97	6.28	6.61	7.54	8.16	8.79	10.05
Time secs	123	41.45	31.25	15.63	10.42	9.6	8.9	8.3	7.8	7.4	6.9	6.57	6.25	5.68	5.21	4.81	4.46	3.9
Total coulombs	0.03862	0.03905	0.03925	0.03926	0.03926	0.03919	0.03912	0.03909	0.03919	0.03950	0.03900	0.03920	0.03925	0.03924	0.03926	0.03927	0.03921	0.03919
Thickness um	-	4.9	7.3	14.7	15.9	16.2	16.7	16.7	17	17.5	18.1							
Plating rate u/sec	0	0.118	0.234	0.94	1.526	1.687	1.876	2.012	2.179	2.365	2.333							
Deposit quality	nd	s	s	s	s	sb	sb	sb/n	sb/n	n/ne	n/ne	n/ne	sn/ne	ne	sne	sne	sne	sne

SAMPLE NO.	Au23		ELECTROLYTE		0.26M Citrate													
Temp. =	40 C		Nozzle velocity m/sec =		18		Nozzle area cm sq =		0.00126		Reynolds No. 7808							
pH =	6.1		Nozzle size cm =		0.04		Viscosity cm sq/sec =		0.00822									
Spot number	1	2	3	4	5	6	7	8	9	10	11	12	13	14	15	16	17	18
Current density A/cm sq	0.25	0.75	1	2	3	3.25	3.5	3.75	4	4.25	4.5	4.75	5	5.5	6	6.5	7	8
Current applied mA	0.31	0.94	1.26	2.51	3.77	4.08	4.40	4.71	5.02	5.34	5.65	5.97	6.28	6.61	7.54	8.16	8.79	10.05
Time secs	123	41.45	31.25	15.63	10.42	9.6	8.9	8.3	7.8	7.4	6.9	6.57	6.25	5.68	5.21	4.81	4.46	3.9
Total coulombs	0.03862	0.03906	0.03926	0.03926	0.03926	0.03919	0.03912	0.03909	0.03919	0.03950	0.03900	0.03920	0.03925	0.03924	0.03926	0.03927	0.03921	0.03919
Thickness um	-	4.1	6.5	14	15.7	15.5	15.5	16.1	16.4	15.9								
Plating rate u/sec	0	0.099	0.208	0.896	1.507	1.615	1.742	1.94	2.103	2.149								
Deposit quality	nd	s	s	s	sb/ne	sb/ne	sb/ne	sb	sb/ne	ne	sne	sne	sne	sne	sne	sne	sne	sne

SAMPLE NO.	Au24		ELECTROLYTE		0.28M Citrate													
Temp. =	55 C		Nozzle velocity m/sec	= 2		Nozzle area cm sq	= 0.00126		Reynolds No		1045							
pH =	6.1		Nozzle size cm	= 0.04		Viscosity cm sq/sec	= 0.00788											
Spot number	1	2	3	4	5	6	7	8	9	10	11	12	13	14	15	16	17	18
Current density A/cm sq	0.25	0.75	1	2	3	3.25	3.5	3.75	4	4.25	4.5	4.75	5	5.5	6	6.5	7	8
Current applied mA	0.31	0.94	1.26	2.51	3.77	4.08	4.40	4.71	5.02	5.34	5.65	5.97	6.28	6.61	7.54	8.16	8.79	10.05
Time secs	123	41.45	31.25	15.63	10.42	9.6	8.9	8.3	7.8	7.4	6.9	6.57	6.25	5.68	5.21	4.81	4.46	3.9
Total coulombs	0.03862	0.03906	0.03926	0.03926	0.03926	0.03919	0.03912	0.03909	0.03919	0.03950	0.03900	0.03920	0.03925	0.03924	0.03926	0.03927	0.03921	0.03919
Thickness um	-	4.9	7.6	14.2	18.9	19.7	20.6	20.3	21.4	20.6	20.2							
Plating rate u/sec	0	0.118	0.243	0.909	1.814	2.052	2.315	2.446	2.744	2.784	2.928							
Deposit quality	nd	d	s	so	b	n	sn	sn	sn	sn/ne	sn/ne	jc	sn/sne	jc	jc	jc	jc	c

DEPOSIT QUALITY KEY	s - smooth & bright d - smooth & dull
Visual assessment only	sb - semi-bright n - slight nodulation
	sn - severe nodulation ne - slight needle growth
	sne - severe needle growth jc - jet core dendrite
	cr - cracks nd - no visible deposit

TABLE 7

PURE GOLD DEPOSITED SPOTS. PLATING PARAMETER DATA

SAMPLE NO.		Au25		ELECTROLYTE		0.26M Citrate												
Temp. = 55 C		Nozzle velocity m/sec = 5		Nozzle area cm sq = 0.00126		Reynolds No. 2612												
pH = 6.1		Nozzle size cm = 0.04		Viscosity cm sq/sec = 0.00766														
Spot number	1	2	3	4	5	6	7	8	9	10	11	12	13	14	15	16	17	18
Current density A/cm sq	0.25	0.75	1	2	3	3.25	3.5	3.75	4	4.25	4.5	4.75	5	5.5	6	6.5	7	8
Current applied mA	0.31	0.94	1.26	2.51	3.77	4.08	4.40	4.71	5.02	5.34	5.65	5.97	6.28	6.91	7.54	8.16	8.79	10.05
Time secs	123	41.45	31.25	15.63	10.42	9.6	8.9	8.3	7.8	7.4	6.9	6.57	6.25	5.68	5.21	4.81	4.46	3.9
Total coulombs	0.03862	0.03905	0.03925	0.03926	0.03926	0.03919	0.03912	0.03909	0.03919	0.03950	0.03900	0.03920	0.03925	0.03924	0.03926	0.03927	0.03921	0.03919
Thickness um	-	3.8	6.3	11.4	15.4	16.8	22.3	18.1	18.7	19.2	18.9	19.1	19.5					
Plating rate u/sec	0	0.092	0.202	0.729	1.478	1.75	2.506	2.181	2.397	2.595	2.739	2.907	3.12					
Deposit quality	nd	d	s	sb	s	s	n	n	sn	sn	sn	sn	sn	sn/ne	sn/c	jc	jc	jc

SAMPLE NO.		Au26		ELECTROLYTE		0.26M Citrate												
Temp. = 55 C		Nozzle velocity m/sec = 10		Nozzle area cm sq = 0.00126		Reynolds No 5224												
pH = 6.1		Nozzle size cm = 0.04		Viscosity cm sq/sec = 0.00766														
Spot number	1	2	3	4	5	6	7	8	9	10	11	12	13	14	15	16	17	18
Current density A cm sq	0.25	0.75	1	2	3	3.25	3.5	3.75	4	4.25	4.5	4.75	5	5.5	6	6.5	7	8
Current applied mA	0.31	0.94	1.26	2.51	3.77	4.08	4.40	4.71	5.02	5.34	5.65	5.97	6.28	6.91	7.54	8.16	8.79	10.05
Time secs	123	41.45	31.25	15.63	10.42	9.6	8.9	8.3	7.8	7.4	6.9	6.57	6.25	5.68	5.21	4.81	4.46	3.9
Total coulombs	0.03862	0.03905	0.03925	0.03926	0.03926	0.03919	0.03912	0.03909	0.03919	0.03950	0.03900	0.03920	0.03925	0.03924	0.03926	0.03927	0.03921	0.03919
Thickness um	-	2.9	5.5	10.8	15.8	17.1	17.2	17.3	17.7	18.7	18	19.2	19.4					
Plating rate u/sec	0	0.07	0.176	0.691	1.516	1.781	1.933	2.084	2.269	2.527	2.609	2.922	3.104					
Deposit quality	nd	d	sd	sd	s	s	s	s	n	n	n	sn	sn	sn	sn/ne	jc	jc	jc

SAMPLE NO.		Au27		ELECTROLYTE		0.25M Citrate												
Temp = 55 C		Nozzle velocity m/sec = 18		Nozzle area cm sq = 0.00126		Reynolds No 9404												
pH = 6.1		Nozzle size cm = 0.04		Viscosity cm sq/sec = 0.00766														
Spot number	1	2	3	4	5	6	7	8	9	10	11	12	13	14	15	16	17	18
Current density A/cm sq	0.25	0.75	1	2	3	3.25	3.5	3.75	4	4.25	4.5	4.75	5	5.5	6	6.5	7	8
Current applied mA	0.31	0.94	1.26	2.51	3.77	4.08	4.40	4.71	5.02	5.34	5.65	5.97	6.28	6.91	7.54	8.16	8.79	10.05
Time secs	123	41.45	31.25	15.63	10.42	9.6	8.9	8.3	7.8	7.4	6.9	6.57	6.25	5.68	5.21	4.81	4.46	3.9
Total coulombs	0.03862	0.03905	0.03925	0.03926	0.03926	0.03919	0.03912	0.03909	0.03919	0.03950	0.03900	0.03920	0.03925	0.03924	0.03926	0.03927	0.03921	0.03919
Thickness um	-	1.6	4.8	10.2	14.9	16	16.9	17.4	17.6	16.8	17.3	17.9	18.3	18.8	18.2	18.3		
Plating rate u/sec	0	0.039	0.154	0.653	1.43	1.667	1.899	2.096	2.256	2.27	2.507	2.725	2.928	3.31	3.493	3.805		
Deposit quality	nd	d	d	sd	s	s	s	s	s	s	s	s	sn	sn	sn	sn	sn	jc

SAMPLE NO.		Au28		ELECTROLYTE		0.27M Phosphate													
Temp = 25 C		Nozzle velocity m/sec = 2		Nozzle area cm sq = 0.00126		Reynolds No 273.2													
pH = 7.1		Nozzle size cm = 0.04		Viscosity cm sq/sec = 0.00816															
Spot number	1	2	3	4	5	6	7	8	9	10	11	12	13	14	15	16	17	18	
Current density A/cm sq	0.25	0.75	1	2	3	3.25	3.5	3.75	4	4.25	4.5	4.75	5	5.5	6	6.5	7	8	
Current applied mA	0.31	0.94	1.26	2.51	3.77	4.08	4.40	4.71	5.02	5.34	5.65	5.97	6.28	6.91	7.54	8.16	8.79	10.05	
Time secs	123	41.45	31.25	15.63	10.42	9.6	8.9	8.3	7.8	7.4	6.9	6.57	6.25	5.68	5.21	4.81	4.46	3.9	
Total coulombs	0.03862	0.03905	0.03925	0.03926	0.03926	0.03919	0.03912	0.03909	0.03919	0.03950	0.03900	0.03920	0.03925	0.03924	0.03926	0.03927	0.03921	0.03919	
Thickness um	No thic																		
Plating rate u/sec																			
Deposit quality	nd	d	s sd	sn	jc	jc	jc	jc	jc	jc	jc	jc	jc	jc	jc	jc	jc	jc	

DEPOSIT QUALITY KEY		s - smooth & bright	d - smooth & dull
		sb - semi-bright	n - slight nodulation
Visual assessment only		sn - severe nodulation	ne - slight needle growth
		sne - severe needle growth	jc - jet core dendrite
		cr - cracks	nd - no visible deposit

TABLE 8

PURE GOLD DEPOSITED SPOTS. PLATING PARAMETER DATA

SAMPLE NO.	Au29		ELECTROLYTE		0.27M Phosphate													
Temp. = 25 C		Nozzle velocity m/sec = 5				Nozzle area cm sq = 0.00126				Reynolds No. 2183								
pH = 7.1		Nozzle size cm = 0.04				Viscosity cm sq/sec. = 0.00916												
Spot number	1	2	3	4	5	6	7	8	9	10	11	12	13	14	15	16	17	18
Current density A/cm sq	0.25	0.5	1	2	3	3.25	3.5	3.75	4	4.25								
Current applied mA	0.31	0.63	1.26	2.51	3.77	4.08	4.40	4.71	5.02	5.34								
Time secs	123	41.45	31.25	15.63	10.42	9.6	8.9	8.3	7.8	7.4								
Total coulombs	0.03862	0.02603	0.03926	0.03926	0.03926	0.03919	0.03912	0.03909	0.03919	0.03950								
Thickness um	No thic																	
Plating rate u/sec																		
Deposit quality	nd	s	s	sn	sn/cr	sn/cr	sn/cr	cr	cr	cr								

SAMPLE NO.	Au30		ELECTROLYTE		0.27M Phosphate													
Temp. =	25 C		Nozzle velocity m/sec =		10		Nozzle area cm sq =		0.00126		Reynolds No. 4368							
pH =	7.1		Nozzle size cm =		0.04		Viscosity cm sq/sec =		0.00916									
Spot number	1	2	3	4	5	6	7	8	9	10	11	12	13	14	15	16	17	18
Current density A/cm sq	0.25	0.5	1	2	3	3.25	3.5	3.75	4	4.25								
Current applied mA	0.31	0.63	1.26	2.51	3.77	4.08	4.40	4.71	5.02	5.34								
Time secs	123	41.45	31.25	15.63	10.42	9.6	8.9	8.3	7.8	7.4								
Total coulombs	0.03862	0.02603	0.03925	0.03926	0.03926	0.03919	0.03912	0.03909	0.03919	0.03950								
Thickness um	No thic																	
Plating rate u/sec																		
Deposit quality	nd	s	s	sn	sn/cr	sn/cr	sn/cr	sn/cr	sn/cr	cr								

SAMPLE NO.		Au31		ELECTROLYTE		0.27M Phosphate												
Temp. = 25 C		Nozzle velocity m/sec = 18		Nozzle area cm sq = 0.00126		Reynolds No 7359												
pH = 7.1		Nozzle size cm = 0.04		Viscosity cm sq/sec = 0.00916														
Spot number	1	2	3	4	5	6	7	8	9	10	11	12	13	14	15	16	17	18
Current density A cm sq	0.25	0.5	1	2	3	3.25	3.5	3.75	4	4.25	4.5							
Current applied mA	0.31	0.63	1.26	2.51	3.77	4.08	4.40	4.71	5.02	5.34	5.65							
Time secs	123	41.45	31.25	15.63	10.42	9.6	8.9	8.3	7.8	7.4	6.9							
Total coulombs	0.03862	0.02603	0.03925	0.03926	0.03926	0.03919	0.03912	0.03909	0.03919	0.03950	0.03900							
Thickness um	No thic																	
Plating rate u sec																		
Deposit quality	nd	sb	sn	sne	sne	sne	sne	sne	sne	sne/cr	cr							

SAMPLE NO.		Au32		ELECTROLYTE		0.27M Phosphate													
Temp. = 40 C		Nozzle velocity m/sec = 2		Nozzle area cm sq = 0.00126		Reynolds No. 1181													
pH = 7.1		Nozzle size cm = 0.04		Viscosity cm sq/sec = 0.00888															
Spot number	1	2	3	4	5	6	7	8	9	10	11	12	13	14	15	16	17	18	
Current density A/cm sq	0.25	0.75	1	2	3	3.25	3.5	3.75	4	4.25	4.5	4.75	5	5.5	6				
Current applied mA	0.31	0.94	1.26	2.51	3.77	4.08	4.40	4.71	5.02	5.34	5.65	5.97	6.28	6.91	7.54				
Time secs	123	41.45	31.25	15.63	10.42	9.6	8.9	8.3	7.8	7.4	6.9	6.57	6.25	5.68	5.21				
Total coulombs	0.03862	0.07906	0.07925	0.07926	0.07926	0.07919	0.07912	0.07909	0.07919	0.07950	0.07900	0.07920	0.07925	0.07924	0.07926				
Thickness um	-	6.6	10.2	18.6															
Plating rate u/sec	0	0.159	0.326	1.19															
Deposit quality	nd	s	s	sb/n	ne	sne	sne	sne	sn/sne	sn/sne	sn/sne	sn/cr	cr	cr	cr				

DEPOSIT QUALITY KEY

Visual assessment
only

s - smooth & bright d - smooth & dull
sb - semi-bright n - slight nodulation
sn - severe nodulation ne - slight needle growth
sne - severe needle growth cr - jet core denrite
cr - cracks nd - no visible deposit

TABLE 9

PURE GOLD DEPOSITED SPOTS. PLATING PARAMETER DATA

SAMPLE NO.	Au33		ELECTROLYTE		0.27M Phosphate													
Temp. = 40 C		Nozzle velocity m/sec = 5		Nozzle area cm sq = 0.00128		Reynolds No. 2902												
pH = 7.1		Nozzle size cm = 0.04		Viscosity cm sq/sec = 0.00888														
Spot number	1	2	3	4	5	6	7	8	9	10	11	12	13	14	15	16	17	18
Current density A/cm sq	0.25	0.75	1	2	3	3.25	3.5	3.75	4	4.25	4.5	4.75						
Current applied mA	0.31	0.94	1.26	2.51	3.77	4.08	4.40	4.71	5.02	5.34	5.65	5.97						
Time secs.	123	41.45	31.25	15.63	10.42	9.6	8.9	8.3	7.8	7.4	6.9	6.57						
Total coulombs	0.03882	0.03906	0.03925	0.03928	0.03928	0.03919	0.03912	0.03908	0.03919	0.03950	0.03900	0.03920						
Thickness um	-	5	8.4	16.4	20													
Plating rate u/sec	0	0.121	0.269	1.049	1.919													
Deposit quality	nd	s	s	s	sb/n	sn	sn/ne	sn/ne	sn/ne	sn/ne	sn/ne	sn/ne						

SAMPLE NO.	Au34		ELECTROLYTE		0.27M Phosphate													
Temp. = 40 C		Nozzle velocity m/sec = 10		Nozzle area cm sq = 0.00128		Reynolds No. 5805												
pH = 7.1		Nozzle size cm = 0.04		Viscosity cm sq/sec = 0.00888														
Spot number	1	2	3	4	5	6	7	8	9	10	11	12	13	14	15	16	17	18
Current density A/cm sq	0.25	0.75	1	2	3	3.25	3.5	3.75	4	4.25	4.5	4.75	5	5.5				
Current applied mA	0.31	0.94	1.26	2.51	3.77	4.08	4.40	4.71	5.02	5.34	5.65	5.97	6.28	6.91				
Time secs.	123	41.45	31.25	15.63	10.42	9.6	8.9	8.3	7.8	7.4	6.9	6.57	6.25	5.68				
Total coulombs	0.03882	0.03906	0.03925	0.03928	0.03928	0.03919	0.03912	0.03908	0.03919	0.03950	0.03900	0.03920	0.03925	0.03924				
Thickness um	-	4.6	7.7	16	17.4													
Plating rate u/sec	0	0.111	0.246	1.024	1.87													
Deposit quality	nd	s	s	s	n/ne	sn/ne	sn/ne	sn/ne	sn/ne	sn/ne	sn/ne	sn/ne	sn/ne	jc				

SAMPLE NO.	Au35		ELECTROLYTE		0.27M Phosphate													
Temp. = 40 C		Nozzle velocity m/sec = 18		Nozzle area cm sq = 0.00128		Reynolds No. 10448												
pH = 7.1		Nozzle size cm = 0.04		Viscosity cm sq/sec = 0.00888														
Spot number	1	2	3	4	5	6	7	8	9	10	11	12	13	14	15	16	17	18
Current density A/cm sq	0.25	0.75	1	2	3	3.25	3.5	3.75	4	4.25	4.5	4.75	5	5.5	6	6.5	7	8
Current applied mA	0.31	0.94	1.26	2.51	3.77	4.08	4.40	4.71	5.02	5.34	5.65	5.97	6.28	6.91	7.54	8.16	8.79	10.05
Time secs.	123	41.45	31.25	15.63	10.42	9.6	8.9	8.3	7.8	7.4	6.9	6.57	6.25	5.68	5.21	4.81	4.46	3.9
Total coulombs	0.03882	0.03906	0.03925	0.03928	0.03928	0.03919	0.03912	0.03908	0.03919	0.03950	0.03900	0.03920	0.03925	0.03924	0.03926	0.03927	0.03921	0.03919
Thickness um	-	4.3	7.3	15.6	17.6	17.4												
Plating rate u/sec	0	0.104	0.234	1.011	1.669	1.813												
Deposit quality	nd	s	s	s	s	s/ne	ne	ne	sn	sn/cr	sn/cr	sn/cr	sn	sn	sn	sn	sn	sn

SAMPLE NO.	Au36		ELECTROLYTE		0.27M Phosphate													
Temp. = 55 C		Nozzle velocity m/sec = 2		Nozzle area cm sq = 0.00128		Reynolds No. 1474												
pH = 7.1		Nozzle size cm = 0.04		Viscosity cm sq/sec = 0.00543														
Spot number	1	2	3	4	5	6	7	8	9	10	11	12	13	14	15	16	17	18
Current density A/cm sq	0.25	0.75	1	2	3	3.25	3.5	3.75	4	4.25	4.5	4.75	5	5.5				
Current applied mA	0.31	0.94	1.26	2.51	3.77	4.08	4.40	4.71	5.02	5.34	5.65	5.97	6.28	6.91				
Time secs.	123	41.45	31.25	15.63	10.42	9.6	8.9	8.3	7.8	7.4	6.9	6.57	6.25	5.68				
Total coulombs	0.03882	0.03906	0.03925	0.03928	0.03928	0.03919	0.03912	0.03908	0.03919	0.03950	0.03900	0.03920	0.03925	0.03924				
Thickness um	-	5.2	8.1	14.9	20	20.5												
Plating rate u/sec	0	0.125	0.259	0.953	1.919	2.135												
Deposit quality	nd	d	sb	sb	n	n	sn	sn	-	sn/ne	sn/ne	sn/cr	sn/cr	jc				

DEPOSIT QUALITY KEY		s - smooth & bnght	d - smooth & dull
Visual assessment only		sb - semi-bnght	n - slight nodulation
		sn - severe nodulation	ne - slight needle growth
		sn - severe needle growth	jc - jet core dendrite
		cr - cracks	nd - no visible deposit

TABLE 10

PURE GOLD DEPOSITED SPOTS. PLATING PARAMETER DATA

SAMPLE NO.	Au37		ELECTROLYTE		0.27M Phosphate													
Temp. = 55 C		Nozzle velocity m/sec = 5		Nozzle area cm sq = 0.00126		Reynolds No. 3686												
pH = 7.1		Nozzle size cm = 0.04		Viscosity cm sq/sec = 0.00543														
Spot number	1	2	3	4	5	6	7	8	9	10	11	12	13	14	15	16	17	18
Current density A/cm sq	0.25	0.75	1	2	3	3.25	3.5	3.75	4	4.25	4.5	4.75	5	5.5	6	6.5	7	8
Current applied mA	0.31	0.94	1.26	2.51	3.77	4.08	4.40	4.71	5.02	5.34	5.65	5.97	6.28	6.91	7.54	8.16	8.79	10.05
Time secs	123	41.45	31.25	15.63	10.42	9.6	8.9	8.3	7.8	7.4	6.9	6.57	6.25	5.68	5.21	4.81	4.46	3.9
Total coulombs	0.03862	0.03906	0.03925	0.03926	0.03926	0.03919	0.03912	0.03909	0.03919	0.03950	0.03900	0.03920	0.03925	0.03924	0.03926	0.03927	0.03921	0.03919
Thickness um	-	3.1	6.3	12.4	16.8	18.4	17.9	19.1	19.2	19.6								
Plating rate u/sec	-	0.075	0.202	0.793	1.612	1.917	2.011	2.301	2.462	2.649								
Deposit quality	nd	d	d	sb	s	s/n	n	n	n	n	ane	ne	ane	ane	jc	jc	jc	jc

SAMPLE NO.		Au38		ELECTROLYTE		0.27M Phosphate												
Temp. = 55 C		Nozzle velocity m/sec = 10		Nozzle area cm sq = 0.00126		Reynolds No. 7372												
pH = 7.1		Nozzle size cm = 0.04		Viscosity cm sq/sec. = 0.00543														
Spot number	1	2	3	4	5	6	7	8	9	10	11	12	13	14	15	16	17	18
Current density A/cm sq	0.25	0.75	1	2	3	3.25	3.5	3.75	4	4.25	4.5	4.75	5	5.5	6	6.5	7	8
Current applied mA	0.31	0.94	1.26	2.51	3.77	4.08	4.40	4.71	5.02	5.34	5.65	5.97	6.28	6.91	7.54	8.16	8.79	10.05
Time secs	123	41.45	31.25	15.63	10.42	9.6	8.9	8.3	7.8	7.4	6.9	6.57	6.25	5.68	5.21	4.81	4.46	3.9
Total coulombs	0.03862	0.03906	0.03925	0.03926	0.03926	0.03919	0.03912	0.03909	0.03919	0.03950	0.03900	0.03920	0.03925	0.03924	0.03926	0.03927	0.03921	0.03919
Thickness um	-	3.4	5.8	12	15.6	16.6	17.9	18.2	18									
Plating rate u/sec		0.082	0.186	0.768	1.497	1.729	2.011	2.193	2.308									
Deposit quality	nd	d	d	sb	s	s	s/n	n	n	n	ane	ane	-	jc	jc	jc	jc	jc

SAMPLE NO.	Au39		ELECTROLYTE		0.27M Phosphate													
Temp. = 55 C	Nozzle velocity m/sec = 18		Nozzle area cm sq = 0.00126		Reynolds No. 1399													
pH = 7.1	Nozzle size cm = 0.04		Viscosity cm sq/sec = 0.00543															
Spot number	1	2	3	4	5	6	7	8	9	10	11	12	13	14	15	16	17	18
Current density A/cm sq	0.25	0.75	1	2	3	3.25	3.5	3.75	4	4.25	4.5	4.75	5	5.5	6	6.5	7	8
Current applied mA	0.31	0.94	1.26	2.51	3.77	4.08	4.40	4.71	5.02	5.34	5.65	5.97	6.28	6.91	7.54	8.16	8.79	10.05
Time secs	123	41.45	31.25	15.63	10.42	9.6	8.9	8.3	7.8	7.4	6.9	6.57	6.25	5.68	5.21	4.81	4.46	3.9
Total coulombs	0.03862	0.03906	0.03925	0.03926	0.03926	0.03919	0.03919	0.03909	0.03919	0.03950	0.03900	0.03920	0.03925	0.03924	0.03926	0.03927	0.03921	0.03919
Thickness um	-	1.7	4.4	11.3	15	16.1	16.1	16.5	17.9	18.3	18.2	18.7	18.9					
Plating rate u/sec		0.041	0.141	0.723	1.44	1.677	2.034	2.229	2.295	2.473	2.636	2.646	3.024					
Deposit quality	nd	d	d	s	s	s	s	s	s/n	s/n	s/n	n	n	n/ne	ne	ne/jc	jc	ane

SAMPLE NO.	Au 40		ELECTROLYTE		0.27M Phosphate Sample to evaluate the influence of dissolved oxygen													
Temp. =	40	Nozzle velocity m/sec =		10	Nozzle area cm sq =		0.00126								Reynolds No. 7372			
pH =	7.1	Nozzle size cm =		0.04	Viscosity cm sq/sec. =		0.00543											
Spot number	1	2	3	4	5	6	7	8	9	10	11	12	13	14	15	16	17	18
Current density A/cm sq	0.25	0.25	0.25	0.25														
Current applied mA	0.31	0.31	0.31	0.31														
Time secs	123	123	123	123														
Total coulombs	0.03862	0.03862	0.03862	0.03862														
Thickness um	-	-	-	-														
Plating rate u/sec																		
N2 purge time mins		25	40	55														
Deposit quality																		

DEPOSIT QUALITY KEY	s - smooth & bright d - smooth & dull
Visual assessment only	sb - semi-bright n - slight nodulation
	sn - severe nodulation ne - slight needle growth
	ane - severe needle growth jc - jet core dendrite
	cr - cracks nd - no viable deposit

TABLE 11

PURE GOLD DEPOSITED SPOTS. PLATING PARAMETER DATA

SAMPLE NO.	Au41		ELECTROLYTE		0.27M Phosphate		Sample de-aerated with nitrogen 40 mins											
Temp. =		40	Velocity m/sec		= 10		Nozzle area cm sq		= 0.00128		Reynolds No. 5805							
pH =		7.1	Nozzle size cm		= 0.04		Viscosity cm sq/sec.		= 0.00888									
Spot number	1	2	3	4	5	6	7	8	9	10	11	12	13	14	15	16	17	18
Current density A/cm sq	0.25	0.75	1	2	3	3.25	3.5	3.75	4	4.25	4.5	4.75	5	5.5				
Current applied mA	0.31	0.94	1.26	2.51	3.77	4.08	4.40	4.71	5.02	5.34	5.65	5.97	6.28	6.61	0.00	0.00	0.00	0.00
Time secs	123	41.45	31.25	15.63	10.42	9.6	8.9	8.3	7.8	7.4	6.9	6.57	6.25	5.68				
Total coulombs	0.03862	0.03805	0.03825	0.03826	0.03826	0.03819	0.03812	0.03809	0.03819	0.03850	0.03800	0.03820	0.03825	0.03824	0.00001	0.00000	0.00000	0.00000
Thickness um																		
Plating rate u/sec	0	0	0	0	0	0	0	0	0	0	0	0	0	0				
Deposit quality	d	s	s	sn	sn	sn	sn	ne	ne	ne	ne	ne	ne	ne				

SAMPLE NO.	Au42		ELECTROLYTE		0.27M Phosphate		Sample de-aerated with nitrogen 40 mins											
Temp. =		55	Velocity m/sec		= 18		Nozzle area cm sq		= 0.00128		Reynolds No. 13269							
pH =		7.1	Nozzle size cm		= 0.04		Viscosity cm sq/sec.		= 0.00843									
Spot number	1	2	3	4	5	6	7	8	9	10	11	12	13	14	15	16	17	18
Current density A/cm sq	0.25	0.75	1	2	3	3.25	3.5	3.75	4	4.25	4.5	4.75	5	5.5	6	6.5	7	8
Current applied mA	0.31	0.94	1.26	2.51	3.77	4.08	4.40	4.71	5.02	5.34	5.65	5.97	6.28	6.61	7.54	8.16	8.79	10.05
Time secs	123	41.45	31.25	15.63	10.42	9.6	8.9	8.3	7.8	7.4	6.9	6.57	6.25	5.68	5.21	4.81	4.46	3.9
Total coulombs	0.03862	0.03805	0.03825	0.03826	0.03826	0.03819	0.03812	0.03809	0.03819	0.03850	0.03800	0.03820	0.03825	0.03824	0.03826	0.03827	0.03821	0.03819
Thickness um																		
Plating rate u/sec	0	0	0	0	0	0	0	0	0	0	0	0	0	0	0	0	0	0
Deposit quality	-	d	d	s	s	s	s	s	s	s	s	n	n	sn	sn/ne	ne	jc	jc

SAMPLE NO.	Au43		ELECTROLYTE		0.27M Phosphate		Sample de-aerated with nitrogen 40 mins											
Temp. =		40	Velocity m/sec		= 18		Nozzle area cm sq		= 0.00128		Reynolds No. 10448							
pH =		7.1	Nozzle size cm		= 0.04		Viscosity cm sq/sec		= 0.00888									
Spot number	1	2	3	4	5	6	7	8	9	10	11	12	13	14	15	16	17	18
Current density A/cm sq	0.25	0.75	1	2	3	3.25	3.5	3.75	4	4.25	4.5	4.75	5	5.5	6	6.5	7	8
Current applied mA	0.31	0.94	1.26	2.51	3.77	4.08	4.40	4.71	5.02	5.34	5.65	5.97	6.28	6.61	7.54	8.16	8.79	10.05
Time secs	123	41.45	31.25	15.63	10.42	9.6	8.9	8.3	7.8	7.4	6.9	6.57	6.25	5.68	5.21	4.81	4.46	3.9
Total coulombs	0.03862	0.03805	0.03825	0.03826	0.03826	0.03819	0.03812	0.03809	0.03819	0.03850	0.03800	0.03820	0.03825	0.03824	0.03826	0.03827	0.03821	0.03819
Thickness um																		
Plating rate u/sec	0	0	0	0	0	0	0	0	0	0	0	0	0	0	0	0	0	0
Deposit quality	d	s	s	s	ne	ne	ne	ne	ne	ne	ne	ne	ne	ne	ne/jc	ne/jc	ne/jc	ne/jc

SAMPLE NO.	Au44a		ELECTROLYTE		0.27M Phosphate		Sample de-aerated with nitrogen 40 mins											
Temp. =		40	Velocity m/sec		= 10		Nozzle area cm sq		= 0.00128		Reynolds No. 5805							
pH =		7.1	Nozzle size cm		= 0.04		Viscosity cm sq/sec.		= 0.00888									
Spot number	1	2	3	4	5	6	7	8	9	10	11	12	13	14	15	16	17	18
Current density A/cm sq	0.25	0.75	1	2	3	3.25	3.5	3.75	4	4.25	4.5	4.75	5	5.5	6	6.5	7	8
Current applied mA	0.31	0.94	1.26	2.51	3.77	4.08	4.40	4.71	5.02	5.34	5.65	5.97	6.28	6.61	7.54	8.16	8.79	10.05
Time secs	123	41.45	31.25	15.63	10.42	9.6	8.9	8.3	7.8	7.4	6.9	6.57	6.25	5.68	5.21	4.81	4.46	3.9
Total coulombs	0.03862	0.03805	0.03825	0.03826	0.03826	0.03819	0.03812	0.03809	0.03819	0.03850	0.03800	0.03820	0.03825	0.03824	0.03826	0.03827	0.03821	0.03819
Thickness um	0.3	7.4	9.2	15.1	19													
Plating rate u/sec	0.0024	0.179	0.294	0.966	1.823	0	0	0	0	0	0	0	0	0	0	0	0	0
Deposit quality	d	s	s	s	n	ne/cr	ne/cr	sn/ne	sn/ne	sn/ne	sn/ne	sn/ne	ne/jc	ne/jc	ne/jc	jc	jc	jc

DEPOSIT QUALITY KEY		s - smooth & bright	d - smooth & dull
Visual assessment only		sb - semi-bright	n - slight nodulation
		sn - severe nodulation	ne - slight needle growth
		ane - severe needle growth	jc - jet core dendrite
		cr - cracks	nd - no visible deposit

TABLE 12

PURE GOLD DEPOSITED SPOTS. PLATING PARAMETER DATA

SAMPLE NO.	Au44b		ELECTROLYTE		0.27M Phosphate		Sample aerated for 40 mins											
Temp. =	10		Velocity m/sec	= 10		Nozzle area cm sq	= 0.00126		Reynolds No. 5805									
pH =	7.1		Nozzle size cm	= 0.04		Viscosity cm sq/sec	= 0.00888											
Spot number	1	2	3	4	5	6	7	8	9	10	11	12	13	14	15	16	17	18
Current density A/cm sq	0.25	0.75	1	2	3	3.25	3.5	3.75	4	4.25	4.5	4.75	5	5.5	6	6.5	7	8
Current applied mA	0.31	0.94	1.26	2.51	3.77	4.08	4.40	4.71	5.02	5.34	5.65	5.97	6.28	6.91	7.54	8.16	8.79	10.05
Time secs	123	41.45	31.25	15.83	10.42	9.6	8.9	8.3	7.8	7.4	6.9	6.57	6.25	5.68	5.21	4.81	4.46	3.9
Total coulombs	0.03862	0.03806	0.03825	0.03826	0.03826	0.03819	0.03812	0.03809	0.03819	0.03850	0.03800	0.03820	0.03825	0.03824	0.03826	0.03827	0.03821	0.03818
Thickness um	-	5.2	8.1	15.5	17.9													
Plating rate u/sec		0.125	0.259	0.992	1.718													
Deposit quality	nd	s	s	s	ne	ne	sn/ne	sn/ne	sn/ne	sn/ne	sn/ne	sn/jc	sn/jc	sn/jc	jc	jc	jc	sn/jc

SAMPLE NO.	Au46		ELECTROLYTE		0.27M Phosphate		Effect of nozzle distance See Figure 18											
Temp. =	40		Velocity m/sec	= 18		Nozzle area cm sq	= 0.00126		Reynolds No. 10448									
pH =	7.1		Nozzle size cm	= 0.04		Viscosity cm sq/sec.	= 0.00888											
Spot number	1	2	3	4	5	6	7	8	9	10	11	12	13	14	15	16	17	18
Current density A/cm sq	3	3	3	3	3	3	3	3	3	3								
Current applied mA	3.78	3.77	3.77	3.77	3.77	3.77	3.77	3.77	3.77	3.77								
Time secs	9.6	9.6	9.6	9.6	9.6	9.6	9.6	9.6	9.6	9.6								
Total coulombs	0.03627	0.03617	0.03617	0.03617	0.03617	0.03617	0.03617	0.03617	0.03617	0.03617								
Thickness um	17.4	15.2	15.2	14.6	14.9	14.5	14.6	14.6	13.6	13.7								
Noz. distance mm	0.25	0.5	1	1.25	1.5	1.75	2	2.25	3	3.5								
H/d	0.625	1.25	2.5	3.125	3.75	4.375	5	5.625	7.5	8.75								

SAMPLE NO.	Au47		ELECTROLYTE		0.27M Phosphate		Effect of increasing time See Figure 61											
Temp. =	40		Velocity m/sec	= 18		Nozzle area cm sq	= 0.00126		Reynolds No. 10448									
pH =	7.1		Nozzle size cm	= 0.04		Viscosity cm sq/sec.	= 0.00888											
Spot number	1	2	3	4	5	6	7	8	9	10	11	12	13	14	15	16	17	18
Current density A/cm sq	3	3	3	3	3	3	3	3	3									
Current applied mA	3.77	3.77	3.77	3.77	3.77	3.77	3.77	3.77	3.77									
Time secs	0.5	1	2	4	8	12	15	20	30									
Total coulombs	0.00188	0.00377	0.00754	0.01507	0.03014	0.04522	0.06783	0.07536	0.11304									
Thickness um	0.8	1.5	3.3	6.6	12.7	19.3	22.4	30.8	-									
Plating rate u/sec	1.6	1.5	1.65	1.7	1.588	1.608	1.493	1.54	-									
Deposit quality																		

SAMPLE NO.	Au48		ELECTROLYTE		0.27M Phosphate		Effect of increasing time											
Temp. =	40		Velocity m/sec	= 18		Nozzle area cm sq	= 0.00126		Reynolds No. 10448									
pH =	7.1		Nozzle size cm	= 0.04		Viscosity cm sq/sec	= 0.00888											
Spot number	1	2	3	4	5	6	7	8	9	10	11	12	13	14	15	16	17	18
Current density A/cm sq	2.5	2.5	2.5	2.5	2.5	2.5	2.5	2.5	2.5									
Current applied mA	3.14	3.14	3.14	3.14	3.14	3.14	3.14	3.14	3.14									
Time secs	0.5	1	2	4	8	12	15	20	30									
Total coulombs	0.00157	0.00314	0.00628	0.01256	0.02512	0.03768	0.04710	0.06280	0.09420									
Thickness um	0.7	1.4	2.8	5	9.6	15.3	19.1	26.4	40.8									
Plating rate u/sec	1.4	1.4	1.3	1.25	1.2	1.275	1.273	1.32	1.36									
Deposit quality																		

DEPOSIT QUALITY KEY	s - smooth & bright d - smooth & dull
Visual assessment only	sb - semi-bright n - slight nodulation
	sn - severe nodulation ne - slight needle growth
	ane - severe needle growth jc - jet core dendrite
	cr - cracks nd - no visible deposit

TABLE 13

PURE GOLD DEPOSITED SPOTS. PLATING PARAMETER DATA

SAMPLE NO.	Au49		ELECTROLYTE		0.25M Citrate		The effect of pH											
Temp. = 55		Velocity m/sec = 18		Nozzle area cm sq = 0.00126		Reynolds No. 9399												
pH = 5.3		Nozzle size cm = 0.04		Viscosity cm sq/sec = 0.00766														
Spot number	1	2	3	4	5	6	7	8	9	10	11	12	13	14	15	16	17	18
Current density A/cm sq	0.25	0.75	1	2	3	3.25	3.5	3.75	4	4.25	4.5	4.75	5	5.5	6	6.5	7	8
Current applied mA	0.31	0.94	1.26	2.51	3.77	4.08	4.40	4.71	5.02	5.34	5.65	5.97	6.28	6.91	7.54	8.16	8.79	10.05
Time secs	123	41.45	31.25	15.63	10.42	9.6	8.9	8.3	7.8	7.4	6.9	6.57	6.25	5.68	5.21	4.81	4.46	3.9
Total coulombs	0.03862	0.03905	0.03925	0.03926	0.03926	0.03919	0.03912	0.03909	0.03919	0.03950	0.03900	0.03920	0.03925	0.03924	0.03926	0.03927	0.03921	0.03919
Thickness um	-	1.4	4.1	9	16.2	16.7	17.4	17.6	18.1	18.8	18.5	19.6	19.4					
Plating rate u/sec	0	0.034	0.131	0.576	1.555	1.74	1.955	2.12	2.321	2.541	2.681	2.983	3.104	0	0	0	0	0
Deposit quality	nd	d	d	s	s	s	s	n	n	n	sn	sn	sn	jc	jc	jc	jc	jc

SAMPLE NO.	Au50	ELECTROLYTE						0.26M Citrate		The effect of pH								
Temp. = 55		Velocity m/sec = 18						Nozzle area cm sq = 0.00126				Reynolds No. 9399						
pH = 8		Nozzle size cm = 0.04						Viscosity cm sq/sec = 0.00766										
Spot number	1	2	3	4	5	6	7	8	9	10	11	12	13	14	15	16	17	18
Current density A/cm sq	0.25	0.75	1	2	3	3.25	3.5	3.75	4	4.25	4.5	4.75	5	5.5	6	6.5	7	8
Current applied mA	0.31	0.94	1.26	2.51	3.77	4.08	4.40	4.71	5.02	5.34	5.65	5.97	6.28	6.91	7.54	8.16	8.79	10.05
Time secs	123	41.45	31.25	15.63	10.42	9.6	8.9	8.3	7.8	7.4	6.9	6.57	6.25	5.68	5.21	4.81	4.46	3.9
Total coulombs	0.03862	0.03905	0.03925	0.03926	0.03926	0.03919	0.03912	0.03909	0.03919	0.03950	0.03900	0.03920	0.03925	0.03924	0.03926	0.03927	0.03921	0.03919
Thickness um	-	1	3.6	11.8	15.9	16.4	16.5	16.8	16.9	17.3								
Plating rate u/sec	0	0.024	0.115	0.755	1.526	1.708	1.854	2.024	2.167	2.338	0	0	0	0	0	0	0	0
Deposit quality	nd	d	d	s	s	s	s	s	s	n/ne	n/ne	sn	sn	sn/jc	jc	jc	jc	jc

SAMPLE NO.	Au51		ELECTROLYTE		0.17M Citrate		Effect of pH											
Temp =	55	Velocity m/sec	=	18	Nozzle area cm sq	=	0.00126	Reynolds No. 9399										
pH =	6	Nozzle size cm	=	0.04	Viscosity cm sq/sec	=	0.00766											
Spot number	1	2	3	4	5	6	7	8	9	10	11	12	13	14	15	16	17	18
Current density A/cm sq	0.25	0.75	1	2	3	3.25	3.5	3.75	4	4.25	4.5	4.75	5	5.5	6	6.5	7	8
Current applied mA	0.31	0.94	1.26	2.51	3.77	4.08	4.40	4.71	5.02	5.34	5.65	5.97	6.28	6.91	7.54	8.16	8.79	10.05
Time secs	123	41.45	31.25	15.63	10.42	9.6	8.9	8.3	7.8	7.4	6.9	6.57	6.25	5.68	5.21	4.81	4.46	3.9
Total coulombs	0.03862	0.03905	0.03925	0.03926	0.03926	0.03919	0.03912	0.03909	0.03919	0.03950	0.03900	0.03920	0.03925	0.03924	0.03926	0.03927	0.03921	0.03919
Thickness um	-	1.9	4.7	10.3	13.2	13.2	14.3	14.6	15.4	16	16.2	16.4	16.1	16.6	17.3	18.1	17.5	18.7
Plating rate u/sec	0	0.046	0.15	0.659	1.267	1.375	1.607	1.759	1.974	2.162	2.348	2.496	2.576	2.923	3.321	3.763	3.924	4.795
Deposit quality	-	d	d	s	s	s	s	s	s	s	s	s	sn	n	n	n	n	sn

SAMPLE NO.	Au52		ELECTROLYTE		0.17M Citrate													
Temp =	55	Velocity m/sec	=	18	Nozzle area cm sq	=	0.00126	Reynolds No. 12183										
pH =	8	Nozzle size cm	=	0.04	Viscosity cm sq/sec	=	0.00691											
Spot number	1	2	3	4	5	6	7	8	9	10	11	12	13	14	15	16	17	18
Current density A cm sq	0.25	0.75	1	2	3	3.25	3.5	3.75	4	4.25	4.5	4.75	5	5.5	6	6.5	7	8
Current applied mA	0.31	0.94	1.26	2.51	3.77	4.08	4.40	4.71	5.02	5.34	5.65	5.97	6.28	6.91	7.54	8.16	8.79	10.05
Time secs	123	41.45	31.25	15.63	10.42	9.6	8.9	8.3	7.8	7.4	6.9	6.57	6.25	5.68	5.21	4.81	4.46	3.9
Total coulombs	0.03862	0.03905	0.03925	0.03926	0.03926	0.03919	0.03912	0.03909	0.03919	0.03950	0.03900	0.03920	0.03925	0.03924	0.03926	0.03927	0.03921	0.03919
Thickness um	-	1.3	4.4	9.6	12.4	12.6	13.8	13.9	14.9	14.3	15	15.4	16	16.5	16.9	17.1	17.9	18.2
Plating rate u/sec	0	0.031	0.141	0.614	1.19	1.333	1.551	1.675	1.91	1.932	2.174	2.344	2.56	2.905	3.244	3.555	4.013	4.667
Deposit quality	nd	d	d	s	s	s	s	s	s	s	s	s	s	s	s	n	n	n

DEPOSIT QUALITY KEY		s - smooth & bright	d - smooth & dull
Visual assessment only		sb - semi-bright	n - slight nodulation
		sn - severe nodulation	ne - slight needle growth
		sn - severe needle growth	jc - jet core dendrite
		cr - cracks	nd - no visible deposit

TABLE 14

PURE GOLD DEPOSITED SPOTS. PLATING PARAMETER DATA

SAMPLE NO.		Au53		ELECTROLYTE		0.28M Citrate (Low conductivity)													
Temp. = 55		Velocity m/sec = 18		Nozzle area cm sq = 0.00126		Reynolds No. 17013													
pH = 8.1		Nozzle size cm = 0.04		Viscosity cm sq/sec = 0.00423															
Spot number	1	2	3	4	5	6	7	8	9	10	11	12	13	14	15	16	17	18	
Current density A/cm sq	0.25	0.75	1	2	3	3.25	3.5	3.75	4	4.25	4.5	4.75	5	5.5	6	6.5	7	8	
Current applied mA	0.31	0.94	1.26	2.51	3.77	4.08	4.40	4.71	5.02	5.34	5.65	5.97	6.28	6.91	7.54	8.16	8.79	10.05	
Time secs	123	41.45	31.25	15.63	10.42	9.6	8.9	8.3	7.8	7.4	6.9	6.57	6.25	5.68	5.21	4.81	4.46	3.9	
Total coulombs	0.03882	0.03805	0.03825	0.03824	0.03824	0.03819	0.03812	0.03808	0.03818	0.03840	0.03800	0.03820	0.03825	0.03824	0.03824	0.03827	0.03821	0.03819	
Thickness um	-	9.2	11	15.2	18.3	18.7	18.4	19.1	19.9	20.5	20.8	21.5	21.4	22.1	23.7	23.9	24.3	25.5	
Plating rate u/sec		0.222	0.352	0.972	1.756	1.946	2.067	2.301	2.551	2.77	3.014	3.272	3.424	3.891	4.549	4.969	5.448	6.536	
Deposit quality	nd	d	s	s	s	s	sn	sn	sn	sn	sn	sn	sn	sn	sn	sn	sn	sn	

SAMPLE NO.		Au54a		ELECTROLYTE		0.17M Citrate												
Temp. = 55		Velocity m/sec = 19.1		Nozzle area cm sq = 0.00008		Reynolds No. 3232												
pH = 8.1		Nozzle size cm = 0.01		Viscosity cm sq/sec = 0.00581														
Spot number	1	2	3	4	5	6	7	8	9	10	11	12	13	14	15	16	17	18
Current density A/cm sq	0.25	0.75	1	2	3	3.25	3.5	3.75	4	4.25	4.5	4.75	5	5.5	6	6.5	7	8
Current applied mA	0.02	0.06	0.06	0.16	0.24	0.26	0.27	0.29	0.31	0.33	0.35	0.37	0.39	0.43	0.47	0.51	0.55	0.63
Time secs	123	41.45	31.25	15.63	10.42	9.6	8.9	8.3	7.8	7.4	6.9	6.57	6.25	5.68	5.21	4.81	4.46	3.9
Total coulombs	0.00241	0.00244	0.00245	0.00245	0.00245	0.00245	0.00245	0.00244	0.00245	0.00247	0.00244	0.00245	0.00245	0.00245	0.00245	0.00245	0.00245	0.00245
Thickness um									0.79	1.35	1.64			2.49		3.2		3.72
Plating rate u/sec									0.095	0.173	0.222			0.3984		0.614		0.834
Deposit quality	s	s	s	s	s	s	s	s	s	s	s	s	s	s	s	s	s	s

SAMPLE NO.		Au54b		ELECTROLYTE		0.17M Citrate												
Temp. = 55		Velocity m/sec = 19.1		Nozzle area cm sq = 0.00008		Reynolds No. 3232												
pH = 8.1		Nozzle size cm = 0.01		Viscosity cm sq/sec = 0.00581														
Spot number	1	2	3	4	5	6	7	8	9	10	11	12	13	14	15	16	17	18
Current density A/cm sq	9	10	11	12	13	14	15	20										
Current applied mA	0.71	0.79	0.86	0.94	1.02	1.10	1.16	1.57										
Time secs	3.45	3.125	2.84	2.6	2.405	2.23	2.08	1.56										
Total coulombs	0.00245	0.00247	0.00244	0.00244	0.00245	0.00245	0.00245	0.00245										
Thickness um			6.16															
Plating rate u/sec			2.169															
Deposit quality	s	s	s	s	s	s	s	ne										

SAMPLE NO.		Au55		ELECTROLYTE		0.17M Citrate												
Temp. = 55		Velocity m/sec		= 18		Nozzle area cm sq		= 0.00229		Reynolds No. 16447								
pH = 8.1		Nozzle size cm		= 0.054		Viscosity cm sq/sec		= 0.00581										
Spot number	1	2	3	4	5	6	7	8	9	10	11	12	13	14	15	16	17	18
Current density A/cm sq	0.25	0.75	1	2	3	3.25	3.5	3.75	4	4.25	4.5	4.75	5	5.5	6	6.5	7	8
Current applied mA	0.57	1.72	2.29	4.58	6.87	7.44	8.01	8.58	9.16	9.73	10.30	10.87	11.45	12.59	13.73	14.86	16.02	16.31
Time secs	123	41.45	31.25	15.63	10.42	9.6	8.9	8.3	7.8	7.4	6.9	6.57	6.25	5.68	5.21	4.81	4.46	3.9
Total coulombs	0.07039	0.07116	0.07153	0.07156	0.07156	0.07142	0.07130	0.07125	0.07142	0.07199	0.07108	0.07144	0.07153	0.07151	0.07156	0.07157	0.07146	0.07142
Thickness um	-	4.4	7.2	13.1	15.9	16.5	16.5	16.7	17.6	17.7	17.5	17.9	17.6	18.4	19.4	19.3	19.4	21.5
Plating rate u/sec		0.106	0.23	0.838	1.526	1.719	1.854	2.012	2.256	2.392	2.536	2.725	2.816	3.239	3.724	4.012	4.35	5.513
Deposit quality	nd	d	d	d	s	s	s	s	s	s	s	s	s	s	n	n	n	n

DEPOSIT QUALITY KEY		s - smooth & bright	d - smooth & dull
Visual assessment only		sb - semi-bright	n - slight nodulation
		sn - severe nodulation	ne - slight needle growth
		sne - severe needle growth	jc - jet core dendrite
		cr - cracks	nd - no visible deposit

TABLE 15

Pulse plating samples

Sample Number Aup1

General conditions for sample:				Electrolyte 0.17M Cltrate Au			
Temp =	55.00	Schmidt No =	351.55				
pH =	8.10	Viscosity cm sq/sec =	0.005006				
Nozzle Velocity M/sec =	20.00	Nozzle Area sq cm =	0.00126				
Nozzle Size cm =	0.04	Reynolds No =	13545.00				

Spot Number	1	2	3	4	5	6	7	8	9	10	11	12	13	14	15	16	17	18
Peak current applied mA	150.72	75.36	37.68	15.07	150.72	75.36	37.68	15.07	150.72	75.36	37.68	15.07	150.72	75.36	37.68	15.07	150.72	75.36
Total Coulombs	0.03937	0.03937	0.03937	0.03937	0.03937	0.03937	0.03937	0.03937	0.03937	0.03937	0.03937	0.03937	0.03937	0.03937	0.03937	0.03937	0.03937	0.03937
Peak Current Density A/cm sq	120	60	30	12	120	60	30	12	120	60	30	12	120	60	30	12	120	60
On-time msec	0.10	0.10	0.10	0.10	0.14	0.14	0.14	0.14	0.20	0.20	0.20	0.20	0.50	0.50	0.50	0.50	1.00	1.00
Off-time msec	1.90	0.90	0.40	0.10	2.66	1.26	0.56	0.14	3.80	1.80	0.80	0.20	9.50	4.50	2.00	0.50	19.00	9.00
Duty Cycle %	5.00	10.00	20.00	50.00	5.00	10.00	20.00	50.00	5.00	10.00	20.00	50.00	5.00	10.00	20.00	50.00	5.00	10.00
Frequency Hz	500.00	1000.00	2000.00	5000.00	357.14	714.29	1428.57	3571.43	250.00	500.00	1000.00	2500.00	100.00	200.00	400.00	1000.00	50.00	100.00
Aver Current Density A/cm sq	6.00	6.00	6.00	6.00	6.00	6.00	6.00	6.00	6.00	6.00	6.00	6.00	6.00	6.00	6.00	6.00	6.00	6.00
Total time secs	5.22	5.22	5.22	5.22	5.22	5.22	5.22	5.22	5.22	5.22	5.22	5.22	5.22	5.22	5.22	5.22	5.22	5.22
Thickness um	0.00	0.00	0.00	18.00	0.00	0.00	0.00	17.80	0.00	0.00	0.00	17.68	0.00	0.00	0.00	17.65	0.00	0.00
Deposition Rate um/sec	0.00	0.00	0.00	3.45	0.00	0.00	0.00	3.41	0.00	0.00	0.00	3.38	0.00	0.00	0.00	3.38	0.00	0.00
Width mm	-	-	-	1.29	-	-	-	1.27	-	-	-	1.34	-	-	-	1.33	-	-
Deposit Quality	rose	rose	fa/ dendritic	slightly nodular	rose	rose	fa/ crown	nodular	rose	fa/rose crown	fa/ crown	nodular	rose	fa/rose crown	fa/ crown	very nodular	rose	fa/ crown
Thickness 'a'	0.00	0.00	0.00	16.40	-	-	-	16.70	-	-	-	15.77	-	-	-	16.20	-	-
Thickness 'b'	-	-	-	9.00	-	-	-	10.00	-	-	-	8.60	-	-	-	9.26	-	-
Thickness 'c'	-	-	-	2.70	-	-	-	3.10	-	-	-	2.46	-	-	-	2.62	-	-
Thickness 'd'	-	-	-	0.50	-	-	-	0.60	-	-	-	0.50	-	-	-	0.54	-	-
Thickness 'e'	-	-	-	0.15	-	-	-	0.19	-	-	-	0.17	-	-	-	0.18	-	-
Thickness 'f'	-	-	-	-	-	-	-	-	-	-	-	-	-	-	-	-	-	-
Thickness 'g'	-	-	-	-	-	-	-	-	-	-	-	-	-	-	-	0.07	-	-

Spot Number	19	20	21	22	23	24	25	26	27	28	29	30	31	32	33	34	35	36
Peak current applied mA	0.00	0.00	0.00	0.00	0.00	0.00	0.00	75.36	37.68	15.07	150.72	75.36	37.68	15.07	150.72	75.36	37.68	15.07
Total Coulombs	0.03937	0.03937	0.03937	0.03937	0.03937	0.03937	0.03937	0.03937	0.03937	0.03937	0.03937	0.03937	0.03937	0.03937	0.03937	0.03937	0.03937	0.03937
Peak Current Density A/cm sq	30	12	120	60	30	12	120	60	30	12	120	60	30	12	120	60	30	12
On-time msec	1.00	1.00	2.00	2.00	2.00	2.00	5.00	5.00	5.00	5.00	10.00	10.00	10.00	10.00	20.00	20.00	20.00	20.00
Off-time msec	4.00	1.00	38.00	18.00	8.00	2.00	95.00	45.00	20.00	5.00	190.00	90.00	40.00	10.00	380.00	180.00	80.00	20.00
Duty Cycle %	20.00	50.00	5.00	10.00	20.00	50.00	5.00	10.00	20.00	50.00	5.00	10.00	20.00	50.00	5.00	10.00	20.00	50.00
Frequency Hz	200.00	500.00	25.00	50.00	100.00	250.00	10.00	-	-	-	-	-	-	-	-	-	-	-
Aver Current Density A/cm sq	6.00	6.00	6.00	6.00	6.00	6.00	6.00	6.00	6.00	6.00	6.00	6.00	6.00	6.00	6.00	6.00	6.00	6.00
Total time secs	5.22	5.22	5.22	5.22	5.22	5.22	5.22	5.22	5.22	5.22	5.22	5.22	5.22	5.22	5.22	5.22	5.22	5.22
Thickness um	0.00	18.90	0.00	0.00	0.00	19.20	0.00	0.00	0.00	20.04	-	0.00	0.00	17.60	-	0.00	0.00	0.00
Deposition Rate um/sec	0.00	3.62	0.00	0.00	0.00	3.68	0.00	0.00	0.00	3.80	-	0.00	0.00	3.37	-	0.00	0.00	0.00
Width mm	-	1.33	-	-	-	1.26	-	-	-	1.24	-	-	-	1.37	-	-	-	-
Deposit Quality	fa/ crown	very nodular	rose	fa/ random	fa/ crown	very nodular	rose	rose	rose	slightly nodular	-	fa	fa/ dendritic	slightly nodular	-	slight rose	v slight fa	sl nod + needles
Thickness 'a'	0.00	18.90	0.00	0.00	0.00	19.20	0.00	0.00	0.00	20.40	-	0.00	0.00	17.60	-	0.00	0.00	0.00
Thickness 'b'	-	17.20	-	-	-	17.30	-	-	-	18.30	-	-	-	14.30	-	-	-	-
Thickness 'c'	-	6.90	-	-	-	10.70	-	-	-	10.40	-	-	-	6.20	-	-	-	-
Thickness 'd'	-	2.70	-	-	-	3.00	-	-	-	3.30	-	-	-	2.30	-	-	-	-
Thickness 'e'	-	0.60	-	-	-	0.60	-	-	-	0.73	-	-	-	0.60	-	-	-	-
Thickness 'f'	-	0.20	-	-	-	0.16	-	-	-	0.20	-	-	-	0.18	-	-	-	-
Thickness 'g'	-	0.10	-	-	-	0.05	-	-	-	-	-	-	-	-	-	-	-	-

Pulse plating samples

Sample Number Aup2

General conditions for sample:					Electrolyte 0.17M Citrate Au				
Temp. =	55.00	Schmidt No. =	351.55						
pH =	8.10	Viscosity cm sq/sec. =	0.005906						
Nozzle Velocity M/sec. =	20.00	Nozzle Area sq cm =	0.00128						
Nozzle Size cm =	0.04	Reynolds No. =	13545.00						

Spot Number	1	2	3	4	5	6	7	8	9	10	11	12	13	14	15	16	17	18
Peak current applied mA	25.12	16.64	15.07	12.56	10.77	8.37	25.12	16.64	15.07	12.56	10.77	8.37	25.12	16.64	15.07	12.56	10.77	8.37
Total Coulombs	0.03937	0.03937	0.03937	0.03937	0.03937	0.03937	0.03937	0.03937	0.03937	0.03937	0.03937	0.03937	0.03937	0.03937	0.03937	0.03937	0.03937	0.03937
Peak Current Density A/cm sq	20.00	15.00	12.00	10.00	8.57	6.67	20.00	15.00	12.00	10.00	8.57	6.67	20.00	15.00	12.00	10.00	8.57	6.67
On-time msec.	0.10	0.10	0.10	0.10	0.10	0.10	1.00	1.00	1.00	1.00	1.00	1.00	10.00	10.00	10.00	10.00	10.00	10.00
Off-time msec.	0.23	0.15	0.10	0.07	0.04	0.01	2.33	1.50	1.00	0.67	0.43	0.11	23.33	15.00	10.00	6.67	4.29	1.11
Duty Cycle %	30.00	40.00	50.00	60.00	70.00	90.00	30.00	40.00	50.00	60.00	70.00	90.00	30.00	40.00	50.00	60.00	70.00	90.00
Frequency Hz	3000.00	4000.00	5000.00	6000.00	7000.00	9000.00	300.00	400.00	500.00	600.00	700.00	900.00	30.00	40.00	50.00	60.00	70.00	90.00
Aver. Current Density A/cm sq	6.00	6.00	6.00	6.00	6.00	6.00	6.00	6.00	6.00	6.00	6.00	6.00	6.00	6.00	6.00	6.00	6.00	6.00
Total time sec.	5.22	5.22	5.22	5.22	5.22	5.22	5.22	5.22	5.22	5.22	5.22	5.22	5.22	5.22	5.22	5.22	5.22	5.22
Thickness um	17.50	16.20	16.90	16.00	14.60	0.00	0.00	16.90	16.10	19.60	16.00	16.50	-	-	-	21.00	21.20	19.00
Deposition Rate um/sec.	3.35	3.46	3.62	3.45	2.83	0.00	0.00	3.62	3.46	3.75	3.45	3.54	0.00	0.00	0.00	4.02	4.06	3.64
Width mm	1.16	1.42	1.45	1.06	1.52	0.00	0.00	1.26	1.26	1.22	1.35	1.32	-	-	-	1.16	1.19	1.31
Deposit Quality	dull smooth	dull smooth	smooth	smooth	semi-bright	incorrect	to/crown	smooth	very nodular	very nodular	very nodular	slightly nodular	to/needle	to/needle	very nodular	very nodular	very nodular	slightly nodular
Thickness 'a'	17.50	16.20	16.90	16.00	14.60	0.00	0.00	16.90	16.10	19.60	16.00	16.50	0.00	0.00	0.00	21.00	21.20	19.00
Thickness 'b'	16.90	17.50	16.10	15.90	13.00	-	-	17.20	17.20	16.60	16.50	15.60	-	-	-	20.00	17.50	16.10
Thickness 'c'	10.80	10.20	8.00	9.50	6.20	-	-	8.70	9.90	9.20	9.10	8.50	-	-	-	10.30	9.70	8.90
Thickness 'd'	3.30	3.30	2.80	3.00	2.50	-	-	2.60	3.20	2.90	3.10	3.40	-	-	-	3.10	3.10	3.10
Thickness 'e'	0.50	0.7	0.60	0.70	0.90	-	-	0.60	0.90	0.70	0.80	1.00	-	-	-	0.60	0.90	0.90
Thickness 'f'	0.15	0.20	0.20	0.20	0.20	-	-	0.20	0.20	0.30	0.32	0.26	-	-	-	0.20	0.20	0.20
Thickness 'g'	-	0.10	0.08	0.12	0.10	-	-	0.09	0.06	0.13	0.07	0.10	-	-	-	0.05	0.04	0.08

TABLE 17

Pulse plating samples

Sample Number Aup3

General conditions for sample:				Electrolyte 0.17M Citrate Au			
Temp =	55.00	Schmitt No =	35155	Viscosity cm sq/sec =	0.005406		
pH =	8.10	Nozzle Area sq cm =	0.00126	Reynolds No =	13545.00		
Nozzle Velocity M/sec =	20.00						
Nozzle Size cm =	0.04						

Spot Number	1	2	3	4	5	6	7	8	9	10	11	12	13	14	15
Peak current applied mA	29.31	21.98	17.58	14.65	12.56	9.77	29.31	21.98	17.58	14.65	12.56	9.77	14.65	12.56	9.77
Total Coulombs	0.03937	0.03937	0.03937	0.03937	0.03937	0.03937	0.03937	0.03937	0.03937	0.03937	0.03937	0.03937	0.03937	0.03937	0.03937
Peak Current Density A/cm sq	23.33	17.50	14.00	11.67	10.00	7.78	23.33	17.50	14.00	11.67	10.00	7.78	11.67	10.00	7.78
On time msec	0.10	0.10	0.10	0.10	0.10	0.10	1.00	1.00	1.00	1.00	1.00	1.00	1.00	1.00	1.00
Off time msec	0.23	0.15	0.10	0.07	0.04	0.01	2.33	1.50	1.00	0.67	0.43	0.11	0.67	0.43	0.11
Duty Cycle %	30.00	40.00	50.00	60.00	70.00	90.00	30.00	40.00	50.00	60.00	70.00	90.00	60.00	70.00	90.00
Frequency Hz	3000.00	4000.00	5000.00	6000.00	7000.00	9000.00	3000.00	4000.00	5000.00	6000.00	7000.00	9000.00	6000.00	7000.00	9000.00
Aver Current Density A/cm sq	7.00	7.00	7.00	7.00	7.00	7.00	7.00	7.00	7.00	7.00	7.00	7.00	7.00	7.00	7.00
Total time sec	4.48	4.48	4.48	4.48	4.48	4.48	4.48	4.48	4.48	4.48	4.48	4.48	4.48	4.48	4.48
Thickness um	0.00	18.10	18.60	18.80	18.10	x	0.00	0.00	18.00	19.80	19.58	20.30	-	20.60	20.60
Deposition Rate um/sec	0.00	4.04	4.15	4.20	4.04	x	0.00	0.00	4.02	4.42	4.37	4.53	0.00	4.60	4.60
Width mm	-	1.22	1.20	1.23	1.24	x	-	-	1.16	1.20	1.27	1.23	-	1.23	1.23
Deposit Quality	slight nodular	slight nodular	slight nodular	nodular	central nodular	x	crown	rose	nodular	nodular	slight nodular	v slight nodular	needle	slight nodular	slight nodular
Thickness 'a'	0.00	18.10	18.60	18.80	18.10	x	0.00	0.00	18.00	19.80	19.56	20.30	0.00	20.60	20.60
Thickness 'b'	-	17.40	17.90	15.90	15.30	x	-	-	16.40	17.60	17.60	16.90	-	16.40	17.40
Thickness 'c'	-	10.30	9.20	9.60	9.40	x	-	-	9.20	10.50	10.40	10.20	-	10.10	10.70
Thickness 'd'	-	2.90	2.80	3.10	3.20	x	-	-	3.00	3.50	3.50	3.20	-	3.50	3.70
Thickness 'e'	-	0.50	0.50	0.70	0.80	x	-	-	0.60	0.70	0.90	1.00	-	1.00	1.00
Thickness 'f'	-	0.13	0.14	0.15	0.20	x	-	-	0.13	0.20	0.20	0.20	-	0.30	0.20
Thickness 'g'	-	-	0.06	0.03	0.05	x	-	-	0.02	0.20	0.04	0.06	-	0.08	-

Spot Number	16	17	18	19	20	21	22	23	24	25	26	27	28	29	30
Peak current applied mA	33.49	25.12	20.10	16.75	14.35	11.16	33.49	25.12	20.10	16.75	14.35	11.16	16.75	14.35	11.16
Total Coulombs	0.03937	0.03937	0.03937	0.03937	0.03937	0.03937	0.03937	0.03937	0.03937	0.03937	0.03937	0.03937	0.03937	0.03937	0.03937
Peak Current Density A/cm sq	26.67	20.00	16.00	13.33	11.43	8.89	26.67	20.00	16.00	13.33	11.43	8.89	13.33	11.43	8.89
On time msec	0.10	0.10	0.10	0.10	0.10	0.10	1.00	1.00	1.00	1.00	1.00	1.00	1.00	1.00	1.00
Off time msec	0.23	0.15	0.10	0.07	0.04	0.01	2.33	1.50	1.00	0.67	0.43	0.11	0.67	0.43	0.11
Duty Cycle %	30.00	40.00	50.00	60.00	70.00	90.00	30.00	40.00	50.00	60.00	70.00	90.00	60.00	70.00	90.00
Frequency Hz	3000.00	4000.00	5000.00	6000.00	7000.00	9000.00	3000.00	4000.00	5000.00	6000.00	7000.00	9000.00	6000.00	7000.00	9000.00
Aver Current Density A/cm sq	8.00	8.00	8.00	8.00	8.00	8.00	8.00	8.00	8.00	8.00	8.00	8.00	8.00	8.00	8.00
Total time sec	3.92	3.92	3.92	3.92	3.92	3.92	3.92	3.92	3.92	3.92	3.92	3.92	3.92	3.92	3.92
Thickness um	0.00	18.00	18.60	19.70	16.50	0.00	0.00	0.00	0.00	20.40	22.80	0.00	0.00	0.00	22.40
Deposition Rate um/sec	0.00	4.59	4.75	5.03	4.21	0.00	0.00	0.00	0.00	5.21	5.82	0.00	0.00	0.00	5.72
Width mm	-	1.07	1.13	1.20	1.20	-	-	-	-	1.16	1.16	-	-	-	1.17
Deposit Quality	rose/ crown	smooth	nodular	nodular	nodular	nodular	fof crown	slight crown	fof crown	nodular	nodular/ needle	not possible	needle	nodular/ needle	nodular
Thickness 'a'	0.00	18.00	18.60	19.70	16.50	0.00	0.00	0.00	0.00	20.40	22.80	0.00	0.00	0.00	22.40
Thickness 'b'	-	16.30	17.20	16.10	14.10	-	-	-	-	19.30	20.60	-	-	-	20.10
Thickness 'c'	-	10.10	11.00	10.60	8.80	-	-	-	-	10.40	13.50	-	-	-	10.90
Thickness 'd'	-	3.20	3.80	3.50	2.90	-	-	-	-	3.60	4.20	-	-	-	3.70
Thickness 'e'	-	0.60	0.90	0.90	0.70	-	-	-	-	0.90	1.10	-	-	-	1.00
Thickness 'f'	-	0.07	0.10	0.20	0.15	-	-	-	-	0.20	0.20	-	-	-	0.20
Thickness 'g'	-	-	-	-	-	-	-	-	-	-	-	-	-	-	-

TABLE 18A

Pulse plating samples Sample Number Aup4

General conditions for sample:										Electrolyte 0.17M Citrate Au									
Temp =		55		Schmidt No =		35155													
pH =		8.1		Viscosity cm eq/sec =		0.005908													
Nozzle Velocity M/sec =		20		Nozzle Area sq cm =		0.00128													
Nozzle Size cm =		0.04		Reynolds No =		13545													

Spot Number	1	2	3	4	5	6	7	8	9	10	11	12	13	14	15	16	17	18	19	20
Peak current applied mA	75.36	37.68	25.12	18.84	87.92	43.98	29.30667	21.98	100.48	50.24	33.49333	25.12	113.04	56.52	37.68	28.28	125.6	62.8	41.86667	31.4
Total Coulombs	0.03937	0.03937	0.03937	0.03937	0.03937	0.03937	0.03937	0.03937	0.03937	0.03937	0.03937	0.03937	0.03937	0.03937	0.03937	0.03937	0.03937	0.03937	0.03937	0.03937
Peak Current Density A/cm sq	60	30	20	15	70	35	23.33333	17.5	60	40	26.66667	20	90	45	30	22.5	100	50	33.33333	25
On-time msec	0.02	0.02	0.02	0.02	0.02	0.02	0.02	0.02	0.02	0.02	0.02	0.02	0.02	0.02	0.02	0.02	0.02	0.02	0.02	0.02
Off-time msec	0.180	0.080	0.047	0.030	0.180	0.080	0.047	0.030	0.180	0.080	0.047	0.030	0.180	0.080	0.047	0.030	0.180	0.080	0.047	0.030
Duty Cycle %	10	20	30	40	10	20	30	40	10	20	30	40	10	20	30	40	10	20	30	40
Frequency Hz	5000	10000	15000	20000	5000	10000	15000	20000	5000	10000	15000	20000	5000	10000	15000	20000	5000	10000	15000	20000
Aver Current Density A/cm sq	6	6	6	6	7	7	7	7	8	8	8	8	9	9	9	9	10	10	10	10
Total time sec	5.224257	5.224257	5.224257	5.224257	4.477934	4.477934	4.477934	4.477934	3.918193	3.918193	3.918193	3.918193	3.462638	3.462638	3.462638	3.462638	3.134554	3.134554	3.134554	3.134554
Thickness um	0	0	18.6	20.9	0	17.3	19.3	20.2	0	0	17.5	0	0	0	19.3	0	0	9.2	0	0
Deposition Rate um/sec	0	3.560315	3.875164	4.000598	0	3.863308	4.310023	4.511008	0	0	4.466345	0	0	0	5.541458	0	0	2.935027	0	0
Width mm	-	1.08	1.17	1.18	-	1.06	1.12	1.12	-	-	1.1	-	-	-	1.11	-	-	0.99	-	-
Deposit Quality	rose	smooth	smooth	slight nodular	rose	slight nodular	slight nodular	slight nodular	rose/fo	smooth/anne fo	smooth	smooth/anne need	rose	slight rose	smooth	slight needle	-	smooth	slight needle	severe needle
Thickness a	0	18.6	19.2	20.9	0	17.3	19.3	20.2	0	0	17.5	0	0	0	19.3	0	0	9.2	0	0
Thickness b	-	18	18.6	19	-	15.9	17	17.3	-	-	17.2	-	-	-	16.3	-	-	9.2	-	-
Thickness c	-	11.2	8.6	11.1	-	10.8	9.8	9.1	-	-	11.4	-	-	-	10.4	-	-	8.6	-	-
Thickness d	-	2.9	3	3.7	-	2.8	2.5	2.5	-	-	3.1	-	-	-	2.7	-	-	1.4	-	-
Thickness e	-	0.3	0.5	0.84	-	0.3	0.5	0.5	-	-	0.5	-	-	-	0.4	-	-	0.1	-	-
Thickness f	-	0.05	0.12	0.14	-	0.04	0.07	0.1	-	-	0.09	-	-	-	-	-	-	-	-	-
Thickness g	-	-	0.01	0.02	-	-	-	-	-	-	-	-	-	-	-	-	-	-	-	-

TABLE 18B

Sample	C.D. mA cm ⁻²	Ni Dep. %	Ni Soln g l ⁻¹	Hard. kg mm ⁻²	Ni At %	Boos. ml l ⁻¹	Thickn. um	
RNC 3	3	0.31	1.7	201.5	1.03	60	12	Conventional Ronoval N
RNC 7	7	0.276	1.7	204	0.92	60	16	
RNC10	10	0.266	1.7	196.9	0.89	60	13.7	
RNC15	15	0.23	1.7	192.6	0.77	60	13	
RNC20	20	0.19	1.7	176.1	0.63	60	12.6	
RNC40	40	0.175	1.7	131	0.56	60	14.7	
MRN 3	3	0.41	1.5	159.3	1.37	0	13	Conventional Auronal MRN
MRN 7	7	0.35	1.5	164.7	1.17	0	13.3	
MRN10	10	0.28	1.5	166.5	0.93	0	15.8	
MRN15	15	0.24	1.5	155.3	0.8	0	13.6	
MRN20	20	0.27	1.5	200.7	0.9	0	11.2	
MRN40	40	0.2	1.5	210	0.67	0	16.6	
XAUP 1	1	0	0	94.9	0	0		Conventional Pure Gold
XAUP 3	3	0	0	96.8	0	0		
XAUP 5	5	0	0	100.1	0	0		
XAUP 7	7	0	0	95.2	0	0		
XAUP10	10	0	0	83.8	0	0		
XAUP20	20	0	0	50.8	0	0		
	A cm ⁻²							
RNX5	5	0.259	3	123.6		60	20	Jet plated samples
RNX6	7	0.21	3	143.2		60	16	
RNX7	9	0.182	3	169.7		60	17.6	
RNX8	16	0.13	3			60	20	
RNX 9	3	0	0	152.6	0	80	14.2	Jet plated samples
RNX10	5	0	0	148.3	0	80	14.9	
RNX11	7	0	0	154	0	80	14.2	
RNX12	9	0	0	159.5	0	80	13.4	
RNX13	16	0	0		0	80	15	
RNX14	3	0	0	200.1	0	60	15.8	Jet plated samples
RNX15	5	0	0	205.2	0	60	17.6	
RNX16	7	0	0	203.6	0	60	16.2	
RNX17	9	0	0	212.6	0	60	16	
RNX18	16	0	0		0	60	17.9	
RNX19	3	0.24	1.9	127	0.801	60	17.3	Jet plated samples
RNX20	5	0.158	1.9	132	0.528	60	16.7	
RNX21	7	0.13	1.9	150	0.435	60	17.6	
RNX22	9	0.11	1.9	170	0.368	60	14.9	
RNX23	16	0.079	1.9		0.265	60	16.1	
RNX24	1	0	0	143.3	0	0	2.3	Jet plated samples
RNX25	2	0	0	163.9	0	0	6.6	
RNX26	4	0	0	196.9	0	0	17.5	
RNX27	6	0	0	203.5	0	0	30	
RNX28	8	0	0		0	0		

TABLE 19

ALLOY GOLD DEPOSITED SPOTS. PLATING PARAMETER DATA

SAMPLE NO.	RN1 & 2		ELECTROLYTE		Renoval N		NICKEL IN ELECTROLYTE g/l =		-		BOOSTER ml/l =		60					
Temp. =		55		Velocity m/sec		=		20		Nozzle area cm sq		=		0.00126		Reynolds No. 10624		
pH =		4.6		Nozzle size cm		=		0.04		Viscosity cm sq/sec.		=		0.00753				
Spot number	1	2	3	4	5	6	7	8	9	10	11	12	13	14	15	16	17	18
Current density A/cm sq	0.25	0.75	1	3	3	4	5	6	7	8	9	10	11	12	13	14	15	16
Current applied mA	0.31	0.94	1.26	3.77	3.77	5.02	6.26	7.54	8.79	10.05	11.30	12.56	13.82	15.07	16.33	17.58	18.84	20.10
Time secs	246	82.9	62.5	31.26	20.84	15.6	12.5	10.42	8.92	7.8	6.9	6.24	5.66	5.21	4.61	4.46	4.16	3.9
Total coulombs	0.07724	0.07809	0.07850	0.11779	0.07853	0.07837	0.07850	0.07853	0.07842	0.07837	0.07800	0.07837	0.07847	0.07853	0.07854	0.07842	0.07837	0.07837
Thickness um	0.5	2.6	2.6	13.8	17.4	18	18.2	17.6	17.3	17.2	16.8	16.3	16.1	16.7	15.4			14.9
Plating rate um/sec	0.002	0.031	0.042	0.441	0.835	1.154	1.456	1.689	1.939	2.205	2.435	2.612	2.8345	3.205	3.202			3.821
Nickel in deposit %																		
Hardness kg/mm2					200.1		205.2		203.6		212.6							

SAMPLE NO.	RN3		ELECTROLYTE		Renoval N		NICKEL IN ELECTROLYTE g/l =		0.5		BOOSTER ml/l =		80					
Temp. =		55		Velocity m/sec		=		20		Nozzle area cm sq		=		0.00126		Reynolds No. 10624		
pH =		4.6		Nozzle size cm		=		0.04		Viscosity cm sq/sec.		=		0.00753				
Spot number	1	2	3	4	5	6	7	8	9	10	11	12	13	14	15	16	17	18
Current density A/cm sq	0.25	0.75	1	3	3	4	5	6	7	8	9	10	11	12	13	14	15	16
Current applied mA	0.31	0.94	1.26	3.77	3.77	5.02	6.26	7.54	8.79	10.05	11.30	12.56	13.82	15.07	16.33	17.58	18.84	20.10
Time secs	246	82.9	62.5	31.26	20.84	15.6	12.5	10.42	8.92	7.8	6.9	6.24	5.66	5.21	4.61	4.46	4.16	3.9
Total coulombs	0.07724	0.07809	0.07850	0.11779	0.07853	0.07837	0.07850	0.07853	0.07842	0.07837	0.07800	0.07837	0.07847	0.07853	0.07854	0.07842	0.07837	0.07837
Thickness um																		
Plating rate um/sec																		
Nickel in deposit %		0.075		0.04		0.033		0.025				0.016						0.01
Hardness kg/mm2			162.3		164.2		174		183.2									

SAMPLE NO.	RN4		ELECTROLYTE		Renoval N		NICKEL IN ELECTROLYTE g/l =		0.72		BOOSTER ml/l =		60					
Temp. =		55		Velocity m/sec		= 20		Nozzle area cm sq		= 0.00126		Reynolds No. 10624						
pH =		4.6		Nozzle size cm		= 0.04		Viscosity cm sq/sec		= 0.00753								
Spot number	1	2	3	4	5	6	7	8	9	10	11	12	13	14	15	16	17	18
Current density A/cm sq	0.25	0.75	1	3	3	4	5	6	7	8	9	10	11	12	13	14	15	16
Current applied mA	0.31	0.94	1.26	3.77	3.77	5.02	6.26	7.54	8.79	10.05	11.30	12.56	13.82	15.07	16.33	17.58	18.84	20.10
Time secs	246	82.9	62.5	31.26	20.84	15.6	12.5	10.42	8.92	7.8	6.9	6.24	5.66	5.21	4.61	4.46	4.16	3.9
Total coulombs	0.07724	0.07809	0.07850	0.11779	0.07853	0.07837	0.07850	0.07853	0.07842	0.07837	0.07800	0.07837	0.07847	0.07853	0.07854	0.07842	0.07837	0.07837
Thickness um																		
Plating rate um/sec																		
Nickel in deposit %				0.11		0.088		0.059		0.047				0.034				0.038
Hardness kg/mm2					146.2		150.8		160.8		164.5							

SAMPLE NO.	RN5		ELECTROLYTE		Renoval N		NICKEL IN ELECTROLYTE g/l =		0.72		BOOSTER ml/l =		60					
Temp. =	55		Velocity m/sec		= 20		Nozzle area cm sq		= 0.00126		Reynolds No. 10624							
pH =	4.6		Nozzle size cm		= 0.04		Viscosity cm sq/sec		= 0.00753									
Spot number	1	2	3	4	5	6	7	8	9	10	11	12	13	14	15	16	17	18
Current density A/cm sq	0.25	0.75	1	3	3	4	5	6	7	8	9	10	11	12	13	14	15	16
Current applied mA	0.31	0.94	1.26	3.77	3.77	5.02	6.26	7.54	8.79	10.05	11.30	12.56	13.82	15.07	16.33	17.58	18.84	20.10
Time secs	246	82.9	62.5	31.26	20.84	15.6	12.5	10.42	8.92	7.8	6.9	6.24	5.66	5.21	4.61	4.46	4.16	3.9
Total coulombs	0.07724	0.07809	0.07850	0.11779	0.07853	0.07837	0.07850	0.07853	0.07842	0.07837	0.07800	0.07837	0.07847	0.07853	0.07854	0.07842	0.07837	0.07837
Thickness um																		
Plating rate um/sec																		
Nickel in deposit %				0.13		0.129		0.114		0.082				0.055				0.047
Hardness kg/mm2					137.4		146		155.8		173.4							

TABLE 20

ALLOY GOLD DEPOSITED SPOTS. PLATING PARAMETER DATA

SAMPLE NO.	RN6		ELECTROLYTE		Ronoval N		NICKEL IN ELECTROLYTE g/l =		1.5		BOOSTER ml/l =		60					
Temp. = 55		Velocity m/sec = 20		Nozzle area cm sq = 0.00126		Reynolds No. 10624												
pH = 4.6		Nozzle size cm = 0.04		Viscosity cm sq/sec = 0.00753														
Spot number	1	2	3	4	5	6	7	8	9	10	11	12	13	14	15	16	17	18
Current density A/cm sq	0.25	0.75	1	3	3	4	5	6	7	8	9	10	11	12	13	14	15	16
Current applied mA	0.31	0.94	1.26	3.77	3.77	5.02	6.28	7.54	8.79	10.05	11.30	12.56	13.82	15.07	16.33	17.58	18.84	20.10
Time secs	246	82.9	62.5	31.26	20.84	15.6	12.5	10.42	8.92	7.8	6.9	6.24	5.66	5.21	4.81	4.46	4.16	3.9
Total coulombs	0.07724	0.07809	0.07850	0.11779	0.07853	0.07837	0.07850	0.07853	0.07842	0.07837	0.07800	0.07837	0.07847	0.07853	0.07854	0.07842	0.07837	0.07837
Thickness um				13.7			19			18.1	17.6	17.3	16.8					
Plating rate um/sec				0.436			1.52			2.321	2.551	2.772	2.9577					15.5
Nickel in deposit %				0.25		0.168		0.135		0.106				0.079				0.081
Hardness kg/mm2					128.9		140.6		150.5		175.6							

SAMPLE NO.		RN7		ELECTROLYTE		Ronoval N		NICKEL IN ELECTROLYTE g/l =		2.2		BOOSTER ml/l =		60				
Temp. = 55		Velocity m/sec = 20		Nozzle area cm sq = 0.00126		Reynolds No. 10624												
pH = 4.6		Nozzle size cm = 0.04		Viscosity cm sq/sec = 0.00753														
Spot number	1	2	3	4	5	6	7	8	9	10	11	12	13	14	15	16	17	18
Current density A/cm sq	0.25	0.75	1	3	3	4	5	6	7	8	9	10	11	12	13	14	15	16
Current applied mA	0.31	0.94	1.26	3.77	3.77	5.02	6.28	7.54	8.79	10.05	11.30	12.56	13.82	15.07	16.33	17.58	18.84	20.10
Time secs	246	82.9	62.5	31.26	20.84	15.6	12.5	10.42	8.92	7.6	6.9	6.24	5.66	5.21	4.81	4.46	4.16	3.9
Total coulombs	0.07724	0.07809	0.07850	0.11779	0.07853	0.07837	0.07850	0.07853	0.07842	0.07837	0.07800	0.07837	0.07847	0.07853	0.07854	0.07842	0.07837	0.07837
Thickness um		0.6	2.1	13.1	16.5	19.4	19.2	18.6	18.3	17.9	17.5	17.4	16.9	16.3	16.2	16.3	15.9	16.2
Plating rate um/sec		0.007	0.034	0.419	0.888	1.244	1.536	1.804	2.052	2.295	2.536	2.766	2.9754	3.129	3.368	3.655	3.822	4.154
Nickel in deposit %		0.308		0.19		0.167		0.126				0.098						0.092
Hardness kg/mm2			125.5		136.1		148		168.6									

SAMPLE NO.	RN8	ELECTROLYTE		Ronoval N	NICKEL IN ELECTROLYTE g/l =		2.5 BOOSTER ml/l =		60									
Temp. = 55		Velocity m/sec = 20		Nozzle area cm sq = 0.00126		Reynolds No. 10624												
pH = 4.6		Nozzle size cm = 0.04		Viscosity cm sq/sec = 0.00753														
Spot number	1	2	3	4	5	6	7	8	9	10	11	12	13	14	15	16	17	18
Current density A/cm sq	0.25	0.75	1	3	3	4	5	6	7	8	9	10	11	12	13	14	15	16
Current applied mA	0.31	0.94	1.26	3.77	3.77	5.02	6.28	7.54	8.79	10.05	11.30	12.56	13.82	15.07	16.33	17.58	18.84	20.10
Time secs	246	82.9	62.5	31.26	20.84	15.6	12.5	10.42	8.92	7.6	6.9	6.24	5.66	5.21	4.81	4.46	4.16	3.9
Total coulombs	0.07724	0.07809	0.07850	0.11779	0.07853	0.07837	0.07850	0.07853	0.07842	0.07837	0.07800	0.07837	0.07847	0.07853	0.07854	0.07842	0.07837	0.07837
Thickness um			1.6	11.9	17.6	19.3	19.2	18.6	18.2	17.6		16.8	17.1	16.7	16.4	15.8	15.6	15.9
Plating rate um/sec			0.026	0.381	0.845	1.237	1.536	1.804	2.04	2.256		2.692	3.0106	3.205	3.41	3.543	3.75	4.077
Nickel in deposit %				0.31		0.236		0.174		0.147				0.131				0.087
Hardness kg/mm2					115.9		133.5		149.5		176.1							

SAMPLE NO.	RN9	ELECTROLYTE		Ronoval N	NICKEL IN ELECTROLYTE g/l =		3	BOOSTER ml/l =		60								
Temp. =	55	Velocity m/sec		=	20	Nozzle area cm sq		=	0.00126	Reynolds No. 10624								
pH =	4.6	Nozzle size cm		=	0.04	Viscosity cm sq/sec		=	0.00753									
Spot number	1	2	3	4	5	6	7	8	9	10	11	12	13	14	15	16	17	18
Current density A/cm sq	0.25	0.75	1	3	3	4	5	6	7	8	9	10	11	12	13	14	15	16
Current applied mA	0.31	0.94	1.26	3.77	3.77	5.02	6.28	7.54	8.79	10.05	11.30	12.56	13.82	15.07	16.33	17.58	18.84	20.10
Time secs	246	82.9	62.5	31.26	20.84	15.6	12.5	10.42	8.92	7.6	6.9	6.24	5.66	5.21	4.81	4.46	4.16	3.9
Total coulombs	0.07724	0.07809	0.07850	0.11779	0.07853	0.07837	0.07850	0.07853	0.07842	0.07837	0.07800	0.07837	0.07847	0.07853	0.07854	0.07842	0.07837	0.07837
Thickness um			2	11.6	17.6	19.4	19.2	19	18.7	18.1	17.7	17.5	17					15.9
Plating rate um/sec			0.032	0.377	0.845	1.244	1.536	1.823	2.096	2.321	2.565	2.804	2.993					4.077
Nickel in deposit %				0.44		0.31		0.241		0.178				0.158				0.129
Hardness kg/mm2					106.3		123.6		143.2		169.7							

TABLE 21

ALLOY GOLD DEPOSITED SPOTS. PLATING PARAMETER DATA

SAMPLE NO.	RN10			ELECTROLYTE	Ronoval N			NICKEL IN ELECTROLYTE g/l	= 0			BOOSTER ml/l	= 80					
Temp. =	55			Velocity m/sec	= 20			Nozzle area cm sq	= 0.00128			Reynolds No. 10624						
pH =	4.8			Nozzle size cm	= 0.04			Viscosity cm sq/sec	= 0.00753									
Spot number	1	2	3	4	5	6	7	8	9	10	11	12	13	14	15	16	17	18
Current density A/cm sq	0.25	0.75	1	3	3	4	5	6	7	8	9	10	11	12	13	14	15	16
Current applied mA	0.31	0.94	1.26	3.77	3.77	5.02	6.28	7.54	8.79	10.05	11.30	12.56	13.82	15.07	16.33	17.58	18.84	20.10
Time secs	246	82.8	62.5	31.26	20.84	15.6	12.5	10.42	8.92	7.8	6.9	6.24	5.68	5.21	4.81	4.46	4.16	3.9
Total coulombs	0.07724	0.07809	0.07850	0.11779	0.07853	0.07837	0.07850	0.07853	0.07842	0.07837	0.07800	0.07837	0.07847	0.07853	0.07854	0.07842	0.07837	0.07837
Thickness um			5.3	13	14.4	14.2	13.8	13.4	13.2	13.1	13.5	12.7	12.5	12.2	12.1	11.8	11.4	11.5
Plating rate u/sec	0	0	0.085	0.416	0.691	0.91	1.104	1.286	1.46	1.679	1.957	2.035	2.2007	2.342	2.516	2.646	2.74	15.5
Nickel in deposit %																		
Hardness kg/mm2					152.8		148.3		154		159.5							

TABLE 22

SAMPLE	C.D.	D_{111} Å (111)	D_{222} Å (111)	D_{222} Å (222)	$\langle \epsilon^2 \rangle$ (111)	α (111)	Ni g dm ⁻³	Booster cm ³ dm ⁻³	Hardness kg mm ⁻¹
Pure Au Conv.	3.0 mA/cm ²	2352	744	540	0.000035	n/d	0	0	101
Pure Au Conv.	7.0 mA/cm ²	2321	860	551	0.000035	n/d	0	0	102.4
Pure Au Jetted	2.0 A/cm ²	324	326	198	0.00011	0.007	0	0	163.9
Pure Au Jetted	4.0 A/m ²	350	349	206	0.00015	n/d	0	0	198.9
Pure Au Jetted	6.0 A/cm ²	335	327	215	0.000115	n/d	0	0	203.5
Pure Au Jetted	8.0 A/cm ²	328	304	205	0.000135	n/d	0	0	204.1
Ronoval N Conv.	10.0 mA/cm ²	261	104	128	0.00015	n/d	1.7	60	198
Ronoval N Conv.	40.0 mA/cm ²	254	107	128	0.000135	n/d	1.7	60	130
Ronoval N Jetted	3.0 A/cm ²	324	340	209	0.000115	0.021	0	60	200.1
Ronoval N Jetted	9.0 A/cm ²	289	307	189	0.00013	0.022	0	60	212.2
Ronoval N Jetted	3.0 A/cm ²	191	182	104	0.00017	poor peak resolution	1.9	60	127
Ronoval N Jetted	9.0 A/cm ²	200	201	128	0.00015	0.027	1.9	60	170

TABLE 23. Crystallite size, RMS strain and stacking fault probabilities for some samples for the (111) planes only. Note n/d = not detectable.

ELECTROLYTE	MAX.USEFUL C.D.	MAX. DEP. RATE
0.041M citrate gold	3.0 A cm ⁻²	1.7 μm sec ⁻¹
0.17M citrate gold pH 6.0	5.5 A cm ⁻²	2.9 μm sec ⁻¹
0.17M citrate gold pH 8.1	6.0 A cm ⁻²	3.4 μm sec ⁻¹
0.28M citrate gold pH 6.0	5.0 A cm ⁻²	2.9 μm sec ⁻¹
0.27M phosphate gold pH 7.1	3.75 A cm ⁻²	2.2 μm sec ⁻¹

TABLE 24. The maximum useful current densities and deposition rates for the pure gold electrolytes studied.

ELECTROLYTE	MAX. PLATING RATE	MAX. C.D.
Ronovel CM	1.6 μm sec ⁻¹ .	5.0 A cm ⁻²
Ronovel N	2.0 μm sec ⁻¹ .	6.7 A cm ⁻²
Auruna 7000	2.3 μm sec ⁻¹ .	10.0 A cm ⁻²

TABLE 25. The maximum useful current densities and deposition rates obtained during the initial study of the alloy gold electrolytes.

Reynolds number		1893	5252	7538
Limiting C.D.		0.367	0.47	0.591
Sherwood number		953	1220	1535
Alkire & Chin	$Sh = 21.03Re^{0.448}$	618	976	1148
Chin & Hsueh	$Sh = 0.9Re^{-5}Sc^{.33}(H/d)^{-0.09}$	461	768	923
Chin & Tsang	$Sh = 1.51Re^{-5}Sc^{.33}(H/d)^{-0.054}$ (Laminar flow)	774	-	-
	$Sh = 1.12Re^{-5}Sc^{.33}(H/d)^{-0.057}$ (Turbulent flow)	-	956	1145
Diffusion coefficient	$5.7 \times 10^{-5} \text{ cm}^2\text{sec}^{-1}$			
Viscosity 0.014M Cu	$0.010879 \text{ cm}^2\text{sec}^{-1}$			

TABLE 26. Limiting current density and Sherwood number data obtained using the 0.041M copper electrolyte, together with calculated values using models derived by other authors.

Reynolds No.		3355	6710	13545	10600
$i_L(\text{SCPV}) \text{ A cm}^{-2} \text{ (pure)}$		4.41(-8%)		9.97(+10%)	
$i_L(\text{SVPA}) \text{ A cm}^{-2} \text{ (pure)}$			6.3(-3%)		
$i_L(\text{SCPV}) \text{ A cm}^{-2} \text{ (R.N. no ni)}$					5.1(+8%)
$i_L(\text{SCPV}) \text{ A cm}^{-2} \text{ (R.N. + ni)}$					5.03(+6%)
$i_L(\text{correlated})$	$Sh = 21.03Re^{0.448}$	4.78	6.52	8.94	4.71

TABLE 27. Limiting current density data for the 0.17M citrate gold and the Ronoval N, together with calculated values based on the Alkire & Chin model. Percentage values represent the deviation from the model.

ADDENDUM

Published papers related to this work

**TEXT BOUND INTO
THE SPINE**

High Speed Selective Jet Electrodeposition

C Bocking

GEC-Marconi,
Hirst Research Centre,
East Lane, Wembley,
Middlesex, HA9 7PP

SUMMARY — High speed selective jet electrodeposition is a process whereby electrodeposits may be produced in a selective manner without the need for masking. The principle is that a non-submersed, free standing electrolyte jet impinges onto a substrate and deposition occurs within the impingement region, with little or no deposition occurring in the surrounding areas. The deposition of copper from an acid sulphate electrolyte has been examined and deposit structure and quality has been related to the prevailing hydrodynamic conditions of deposition. The selectivity or resolution of the process has been examined. Further work has been carried out using an acid citrate gold electrolyte and some initial results are presented, and also relating deposit structure and quality with the hydrodynamic conditions of deposition. Examples of applications are discussed.

INTRODUCTION

High Speed Selective Jet Electrodeposition (HSSJE) is a process whereby electrodeposits may be produced in a selective manner without the need for masking. The principle is that a non-submersed, free standing electrolyte jet impinges at a high velocity onto a substrate and with the application of an electric current, deposition occurs within the impingement region and the immediately surrounding region. Due to the resistive nature of the electrolyte and the properties of the hydrodynamic flow surrounding the impingement region, the spread of the deposit is limited. Whilst Selective Jet Deposition is not a new technique, the principle being patented by NASA¹ in 1974, there has not been a significant commercial exploitation of the process. The NASA patent refers to feeding an electrolyte at high pressure through a jet nozzle onto the surface to be selectively plated. An image of the pattern to be plated was scanned using a video scanner in a raster fashion in the same way as an electron beam is scanned on a television screen to obtain pattern defining signals. The nozzle was scanned in the same way and the pattern defining signals controlled the amplitude of the plating voltage. Thus, in regions where plating was required, the voltage was modulated to give the plating current. In this way, the pattern was built up in a similar way to a dot matrix printer.

A forced flow selective plating system was described by R. Haynes *et al*² in 1978 and Dorey *et al* used a modified version to gold plate connectors³ in order to evaluate thermocompression bonding characteristics of the deposits produced. The maximum flow rate used was 39 cm/sec and current densities of up to 1.3 A/cm². With a nozzle diameter of 0.5 cm, the flow under these circumstances is laminar. However, deposit quality deteriorated at current densities in the region of 0.86 A/cm² by nodule formation. It was claimed that nodular deposits did not necessarily reduce bondability.

Safranek⁴ describes jet plating systems in commercial operation but these all involve a non-conducting mask. The selective plating of connectors in some commercial plants is currently carried out using jet deposition on a step and repeat basis using masks and electrolyte velocities of up to 2m/sec.

There have been a number of papers and monographs that describe the hydro-

dynamic behaviour of a free standing jet of fluid^{5,6,7,8,9}. These deal mainly with mathematical models together with experimental verification of the fluid flow from a free standing jet. Nakoryakov⁶ describes the mass transfer in all regions of the jet and impingement region together with the hydrodynamic characteristics of the jet. The system used for verification of their calculations was an alkaline ferri-ferrocyanide solution. As well as developing a mathematical model of the free standing jet system, Alkire *et al*¹⁰ related this model to the ferri/ferrocyanide system and to the deposition of copper from an acid sulphate system, both with and without the addition of a more noble ferric/ferrous redox couple. The measurements that they made on the mass transfer characteristics in the jet impingement region agreed well with the work of Chin *et al*¹¹ who measured the mass transfer characteristics of a submerged jet. The Alkire/Chen model included a prediction of the selectivity of the process. Selectivity may be described as the ratio of reactant production in the impingement region to the reactant production in the surrounding region, which is known as the wall jet region. Whilst the theoretical model was able to accurately predict the selectivity for the redox system, it was not as accurate for the acid copper deposition reaction¹². No mention was made of the morphology of the deposits produced.

There are a number of commercial systems that utilise high speed jet deposition both with and without masking but information on the maskless system is comparatively rare. This is presumably due to commercial confidentiality reasons. Gold deposition using small bore jets (1mm to 0.25 mm diameter) was examined by Bocking¹³. He examined the morphology of the deposits produced and related these to the electrolyte velocity. The current efficiency of the process was also assessed. Also described was a "direct write" facility whereby the jet could be moved in relation to the substrate by means of a computer controlled X-Y table thus producing tracks.

This work is designed to examine the selective plating of small areas using a nozzle diameter of 400 µm. It is part of a BRITE* collaborative project on the improvement in the control and attainment of high speed electrodeposition processes. It is not the purpose of this paper to verify

the relationship between the mathematical models put forward by the aforementioned authors and experimental observations, but is an initial examination of the relationship between the deposition conditions and the size, shape and topography of the deposits produced. An acid sulphate copper, a citrate based cyanide gold electrolyte and a phosphate based cyanide gold electrolyte have been examined. The structures and dimensions of the deposits have been examined and related to the prevailing hydrodynamic conditions. The selectivity of the process is also described. This initial phase of the project was designed to establish the basic principles of the system using an acid copper system and was followed by the optimisation of the gold electrolyte for maximum deposition rates using a DC controlled current.

EXPERIMENTAL

Figure 1 shows a schematic diagram of the Jet Plating system together with the control equipment. The jet consisted of a platinum tube sealed into a lead-soda glass tube. The pump was a diaphragm type dosing pump capable of delivering up to 70 l/hour. Delivery rates could be adjusted with a reproducibility of better than 2%. The output from the pump was fitted to the jet via a precision flowmeter and a pressure transducer. Also fitted to the pump outlet was a pulsation damper to maintain a constant pressure during use and a pressure relief valve. The maximum safe continuous working pressure of the pump was 7 Bar and the relief valve was set to 8.25 Bar.

The jet was fitted to a computer controlled X-Y table. This allowed a number of electrodeposited spots to be produced on a single substrate by a step and repeat process. A computer was used with a

control program developed "in-house". The computer program could also take plot files from computer aided design packages (CAD) and convert them to output files for the X-Y table, allowing very elaborate designs to be directly written by electro-deposition.

The jet was connected to the positive terminal of the controlled current power supply and acted as the anode. Due to the resistive nature of the thin electrolyte jet, the power supply was custom built and was capable of delivering up to 350 mA at a voltage of up to 57V, with a resolution of 0.01 mA. During deposition, the cell voltage was monitored using a chart recorder. The plating current could be preset via a short circuit switch prior to each deposit spot produced. The current was monitored using a calibrated digital multimeter.

The electrolyte flow rate was calibrated for each different electrolyte used. The pump output was controlled by both a numerical handwheel that set the length of the diaphragm stroke and a thyristor motor speed controller. Calibration consisted of measuring the volume of electrolyte discharged and allowed an accurate setting of the flowmeter for differing handwheel and motor speed settings. The output pressure was then related to the discharge and a calibration curve drawn.

The electrolytes were prepared using Analar grade reagents dissolved in double de-ionised water. After preparation, the solutions were carbon treated for 2 hours and filtered twice. The electrolytes were then analysed using X-ray spectroscopy to establish the metal ion concentrations. For each electrolyte, the viscosity was measured using an Ostwald Viscometer in accordance with BS 188 (1977) at the relevant operating temperatures. The density of each electrolyte was also measured using a density bottle at the relevant temperatures.

COPPER DEPOSITION

The copper electrolytes used were 0.8M, 0.20M and 0.08M with 0.51M sulphuric acid in each case. Electrodeposited copper spots were produced from these electrolytes

using various electrolyte velocities and current densities. Each sample group of spots was plated onto OFHC copper strips. The strips were prepared by polishing to a mirror finish and then cleaning in a proprietary soak cleaner for 3 minutes using ultrasonic agitation. This was followed by cathodic cleaning in a cyanide based cold cleaner for 1 minute. Immediately before use, the substrates were given a bright dip to lightly etch the surface and finally given a further 1 minute in the cathodic cleaner. The substrates were then thoroughly rinsed in de-ionised water and carefully dried.

Trial deposits produced from the 0.8M electrolyte were plated over a range of between 0.25 and 50 A/cm² in order to identify the useful current density (C.D.) range using a total charge of 0.017 Coulombs per spot. The nominal thickness of these spots was calculated to be 5 µm. Subsequent deposits from this electrolyte were produced using a total charge of 0.068 C per spot, giving a calculated thickness of 20 µm. Deposits produced from the 0.08 M and the 0.2 M solutions were plated over a current density range of between 0.25 and 3.0 A/cm² as very poor quality spots occurred above this maximum. A total charge of 0.068 Coulombs was used for these deposits, giving a calculated thickness of 20 µm, assuming a cylindrical deposit growth. In addition, a series of spots were prepared at a constant current density and velocity but with increasing time to establish how the deposit structure varied with increasing thickness.

All deposits were produced at a temperature of 25°C. The jet to substrate distance was maintained at 0.5mm. Electrolyte velocities ranged from 2m/sec up to 18 m/sec. These related to Re. values ranging from 546 up to 6970. Thickness measurement of the spots was carried out using a Sloan Dektak 3030 Surface Profilometer. This gave a profile across the centre of each spot. As deposited spots produced by selective jetting show a broad gaussian profile¹³, with the maximum thickness at the spot centre the average thickness at the centre of the spot was recorded. All thicknesses and plating rates mentioned in this paper are based on the thickness at this position. The surface morphology was examined using both Scanning Microscopy as well as optical microscopy.

The structures of some of the thicker deposits were examined using standard microsection techniques. In samples that showed a significant porosity, the percentage gross porosity was calculated using data obtained from an Optimax video contrast system. The resultant percentages were subtracted from the thicknesses measured and the corrected thicknesses were recorded.

GOLD DEPOSITION

Table 1 shows the basic formulations of the electrolytes used in these trials. The viscosities of the electrolytes were measured at the chosen deposition temperatures 25°C, 40°C and 55°C ± 0.2°C using a calibrated U-tube viscometer. The conductivities of the electrolytes were also measured at the temperatures stated. Gold spots were produced on polished, nickel plated substrates with a 0.1 µm gold flash (to prevent immersion deposits). The spots were pro-

*BRITE project R11B-0304, in partnership with Centro Sviluppo Materiali of Italy and Loughborough University of Technology.

Figure 1. Schematic of jet plating unit

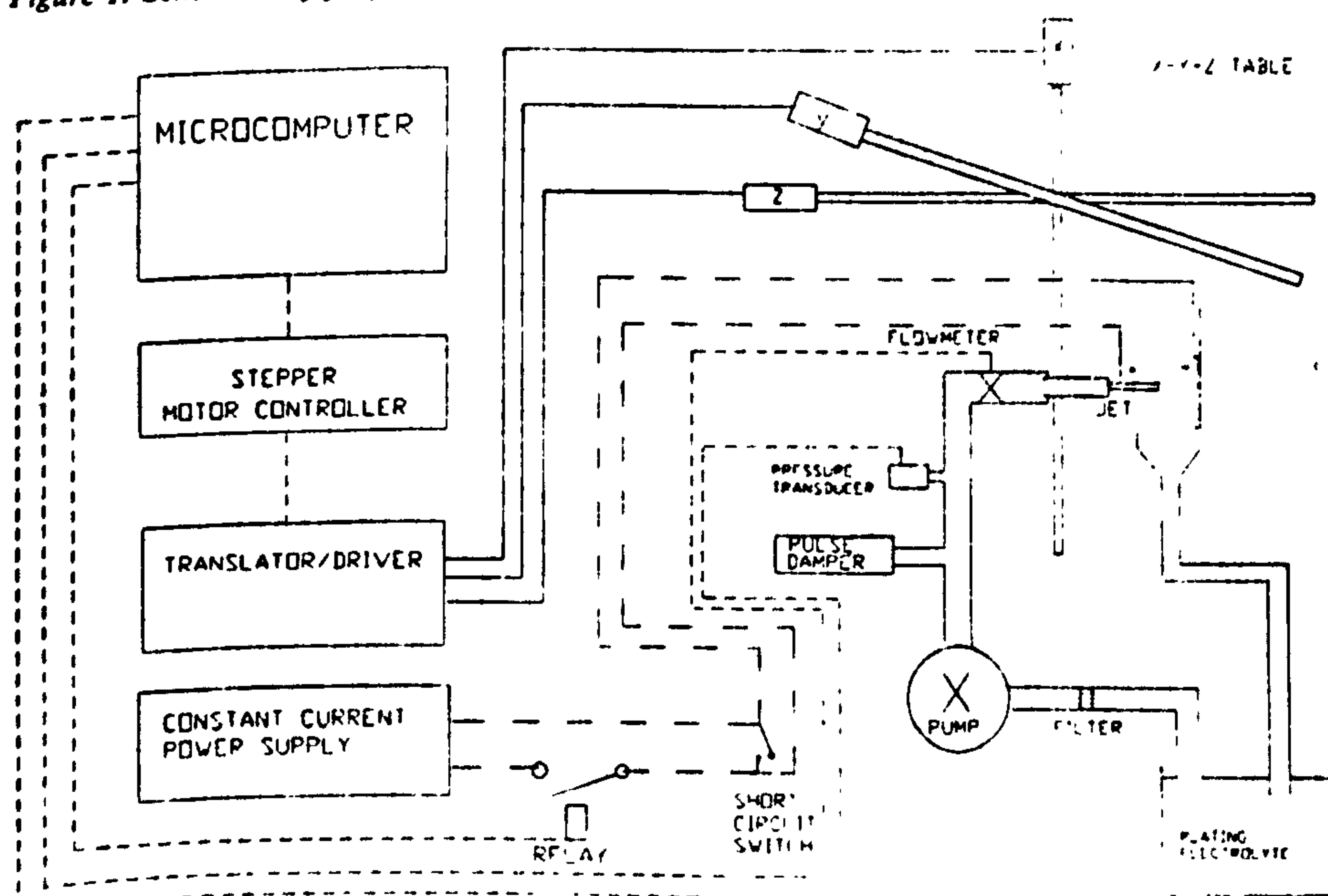


Table 1. Gold electrolytes used.

(1) gold (as potassium gold cyanide)	8.2 g/l (0.041M)
Diammonium hydrogen citrate	45.0 g/l
Citric acid	15.0 g/l
Potassium hydroxide to pH 6.0	
(2) Gold (as potassium gold cyanide)	54.0 g/l (0.28M)
Diammonium hydrogen citrate	45.0 g/l
Citric acid	15.0 g/l
Potassium hydroxide to pH 6.0	
(3) Gold (as gold potassium cyanide)	53.5 g/l (0.27M)
Di-potassium hydrogen phosphate	40.0 g/l
Potassium di-hydrogen phosphate	10.0 g/l
Potassium hydroxide to pH 7.0	
(4) Gold (as potassium gold cyanide)	33.5 g/l (0.17M)
Diammonium hydrogen citrate	45.0 g/l
Citric acid	15.0 g/l
Potassium hydroxide to pH 6.0	
(5) Gold (as potassium gold cyanide)	54.0 g/l (0.28M)
Diammonium hydrogen citrate	1.0 g/l
Citric acid	1.0 g/l
Potassium hydroxide to pH 6.0	

duced using current densities between 0.25 A/cm² and 20 A/cm². The time of deposition was adjusted to supply a total of 0.03938 ± 0.00008 coulombs per spot. Up to 18 spots were deposited onto a single substrate. Each series of spots were produced using electrolyte temperatures of 25°C, 40°C and 55°C. The electrolyte velocities used were 2m/sec, 5 m/sec, 10 m/sec and 18 m/sec. Another series of spots was prepared at a constant current density and velocity but with a varying jet to substrate distance.

Using the optimum conditions for the phosphate electrolyte, the effects of dissolved oxygen were examined by preparing a series of spots with the electrolyte de-aerated by bubbling nitrogen through it for 30 minutes prior to plating.

A further 2 series of spots using the optimum velocity and temperature were prepared from the citrate electrolyte but at a pH of 5.3 and 8.1 to examine the effect of pH.

Scanning electron micrographs were taken of selected spots showing the topography of the deposits.

Because the total mass of each spot was in the region of 8 × 10⁻⁵ g, the current efficiency could not be measured on the samples produced above. It was necessary to prepare either a single spot plated for a considerably greater time or a series of identical spots on a single substrate. In order to minimise substrate effects, glass slides were sputtered with 0.04 µm of chromium followed by 0.1 µm of gold. The

efficiency could then be measured using the weigh, plate, weigh method.

RESULTS AND DISCUSSION

Examination of the spots showed a significant similarity of the structures and behaviour of deposition. For both metals, the deposits that were produced were circular in shape and exhibited an essentially gaussian profile. The overall diameter of the deposits were about twice the diameter of the nozzle but this varied depending on the conditions of deposition with a distinct increase in deposit diameter at current densities below 1.0A/cm². However, it is convenient to examine both metals separately.

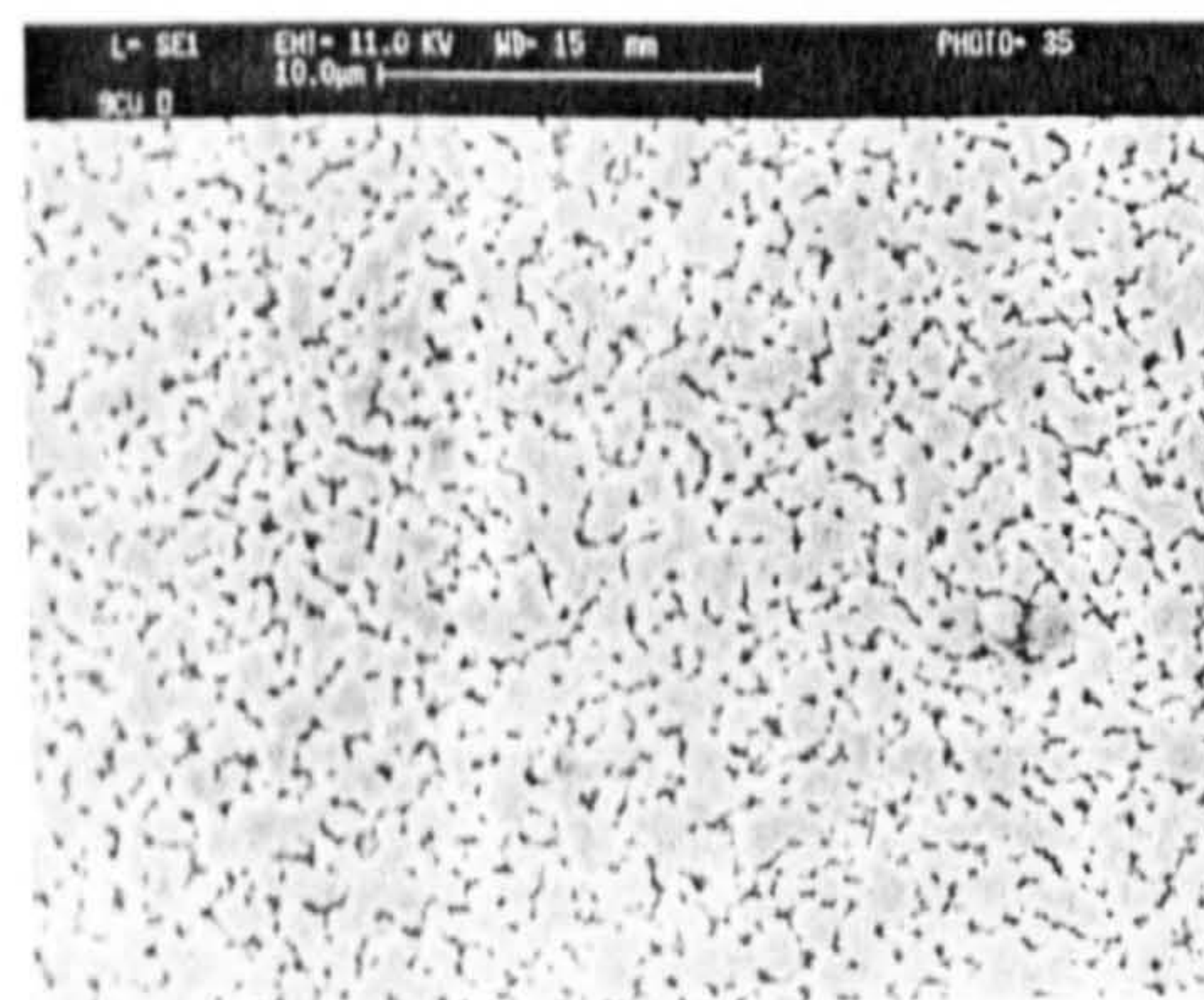
COPPER DEPOSITS

The Effect of Current Density

The effect of increasing the current density can be summarised by looking at the deposit structures. In general, for all the electrolytes, the deposits produced showed the following structures as the C.D. was increased.

- Smooth, equiaxed crystallites (Figure 2)
- Columnar structures with a large number of nucleation sites. (Figure 3)
- Coarse, nodular structures with a lower number of nucleation sites. (Figure 4)
- Coarse, nodular structures with evident 3 dimensional nucleation, but few nucleation sites. Evident secondary dendrites. (Figure 5)
- Powdery, dendritic structures. (Figure 6)

Figure 2. (a) Microsection of a copper deposit, X 1000. (b) Surface Morphology of the same deposit. 0.8M copper, C.D. 2.0 A/cm², Re. 1365.



In some cases, it can be seen that the deposit has experienced some light etching, probably from the wash of the electrolyte

Figure 3. (a) Microsection of a copper deposit, X 1000. (b) Surface Morphology of the same deposit. 0.8M copper, C.D. 3.0 A/cm², Re. 1365.

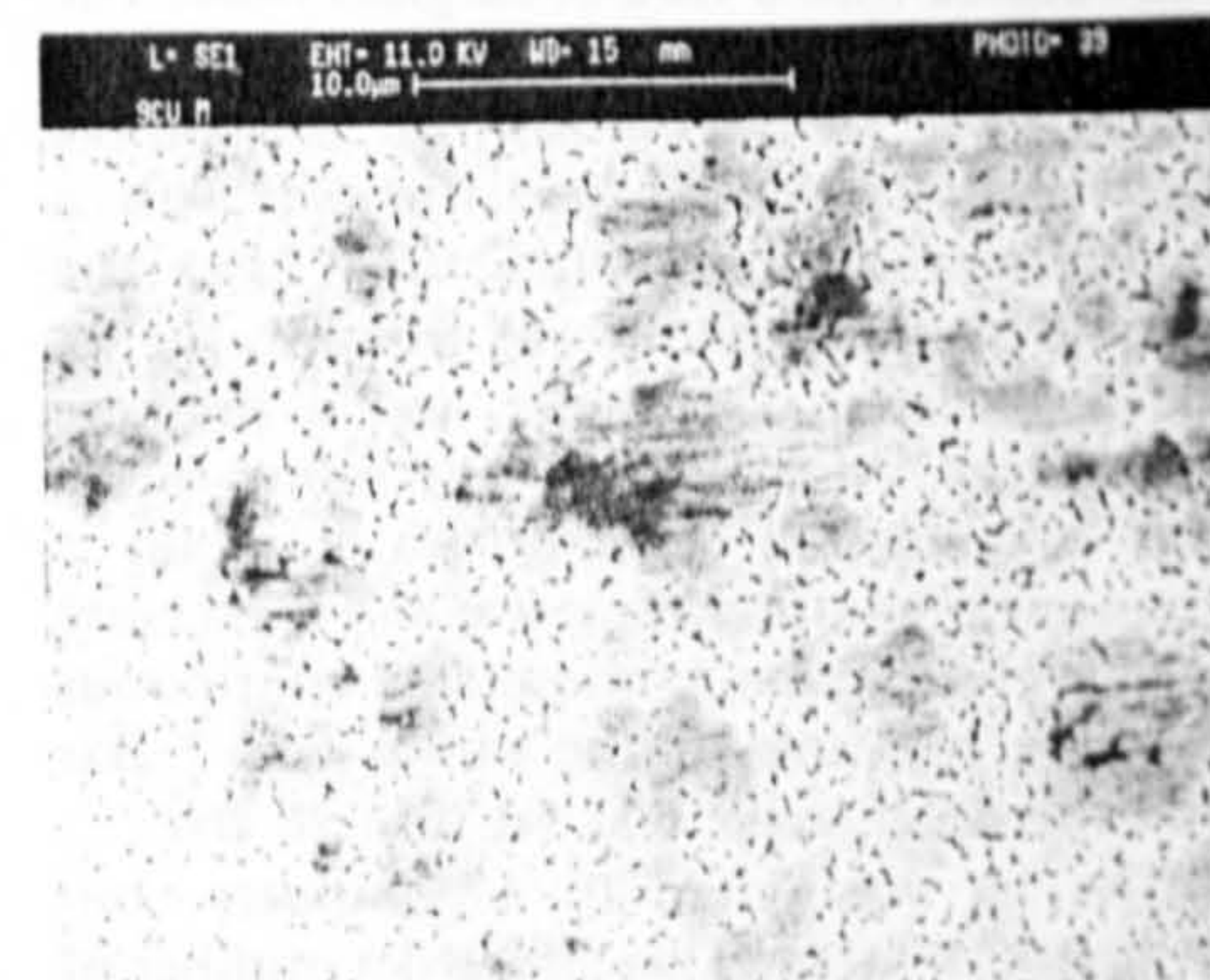
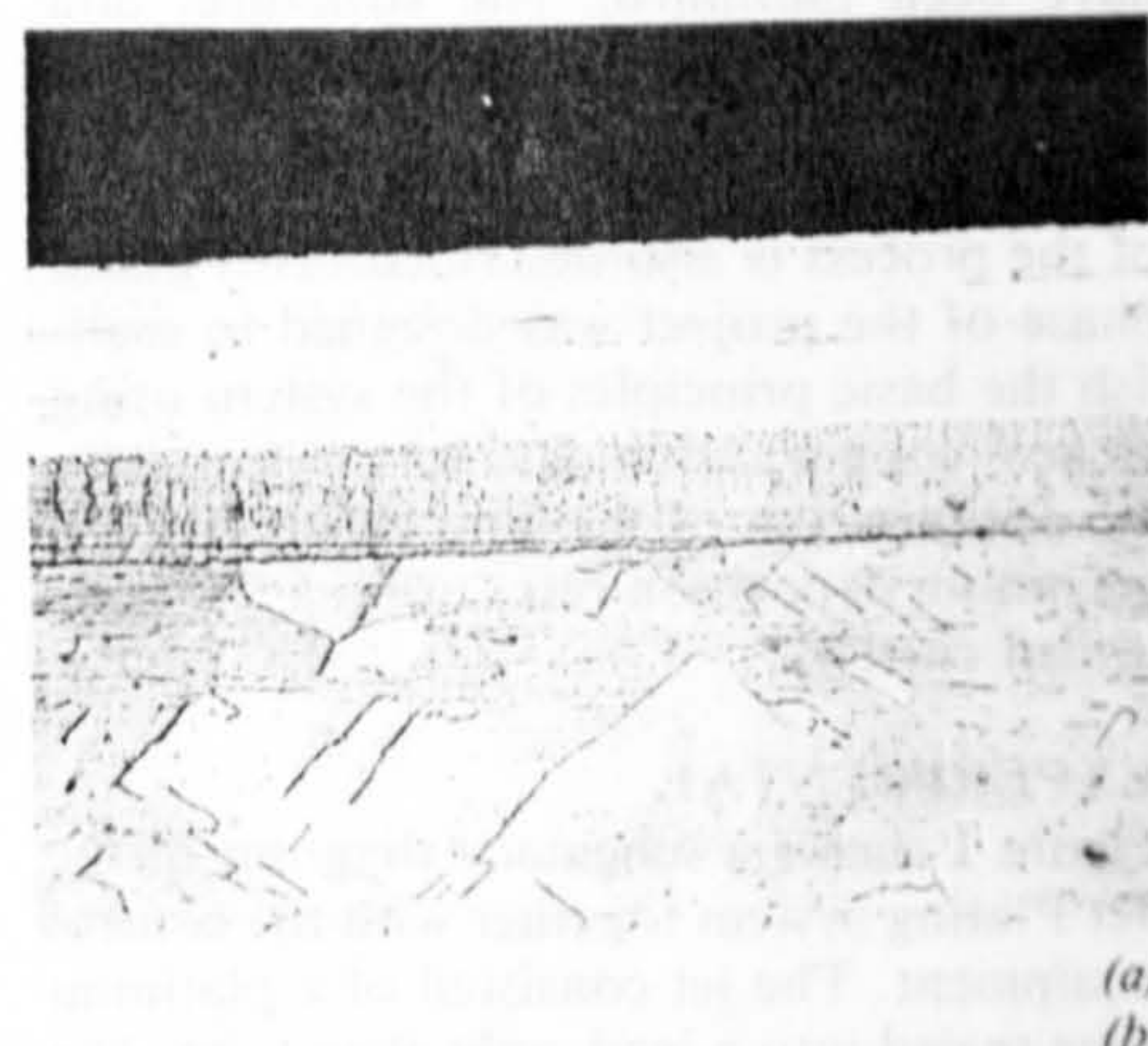
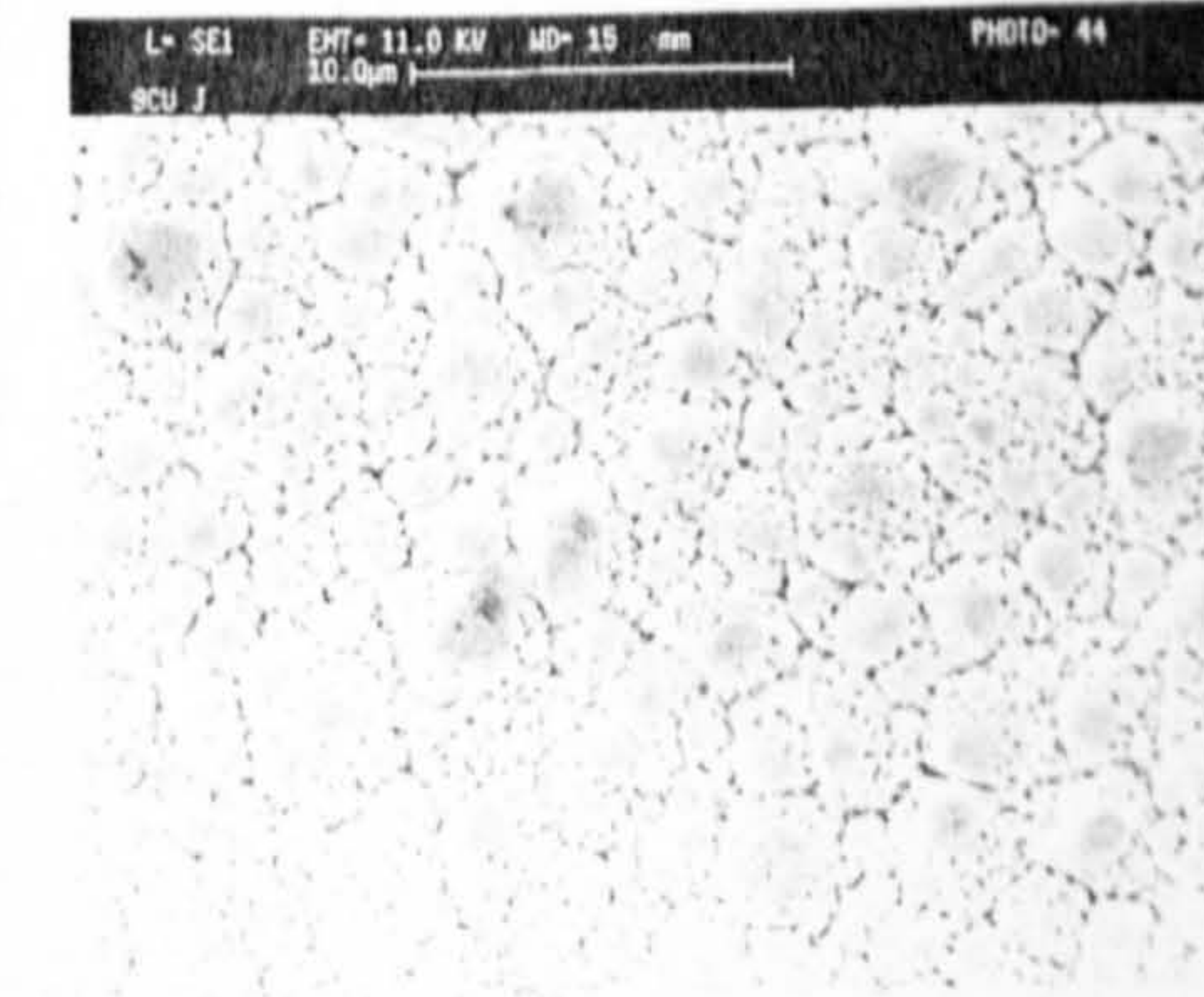


Figure 4. (a) Microsection of a copper deposit, X 1000. (b) Surface Morphology of the same deposit. 0.8M copper, C.D. 7.6 A/cm², Re. 1365.



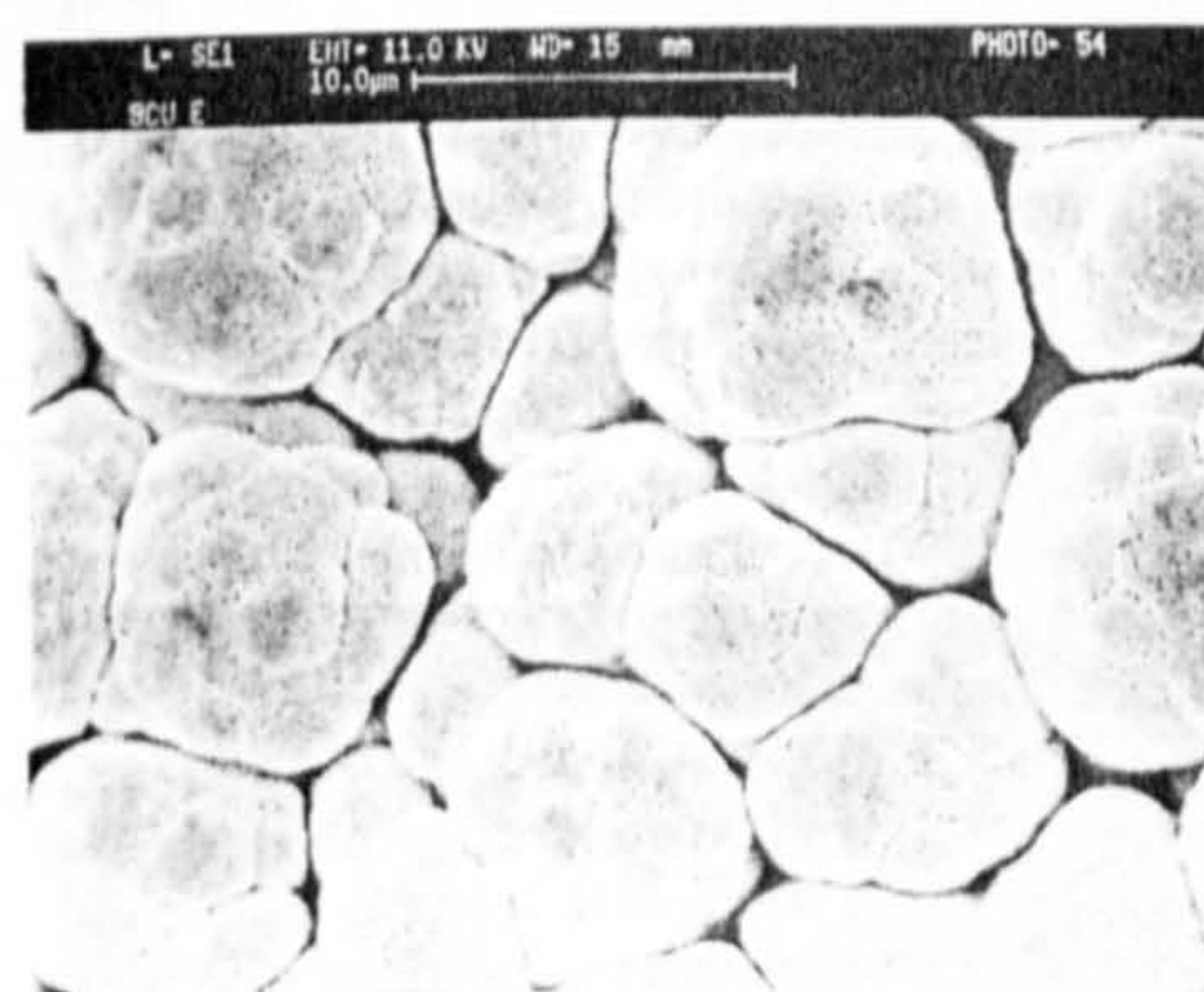
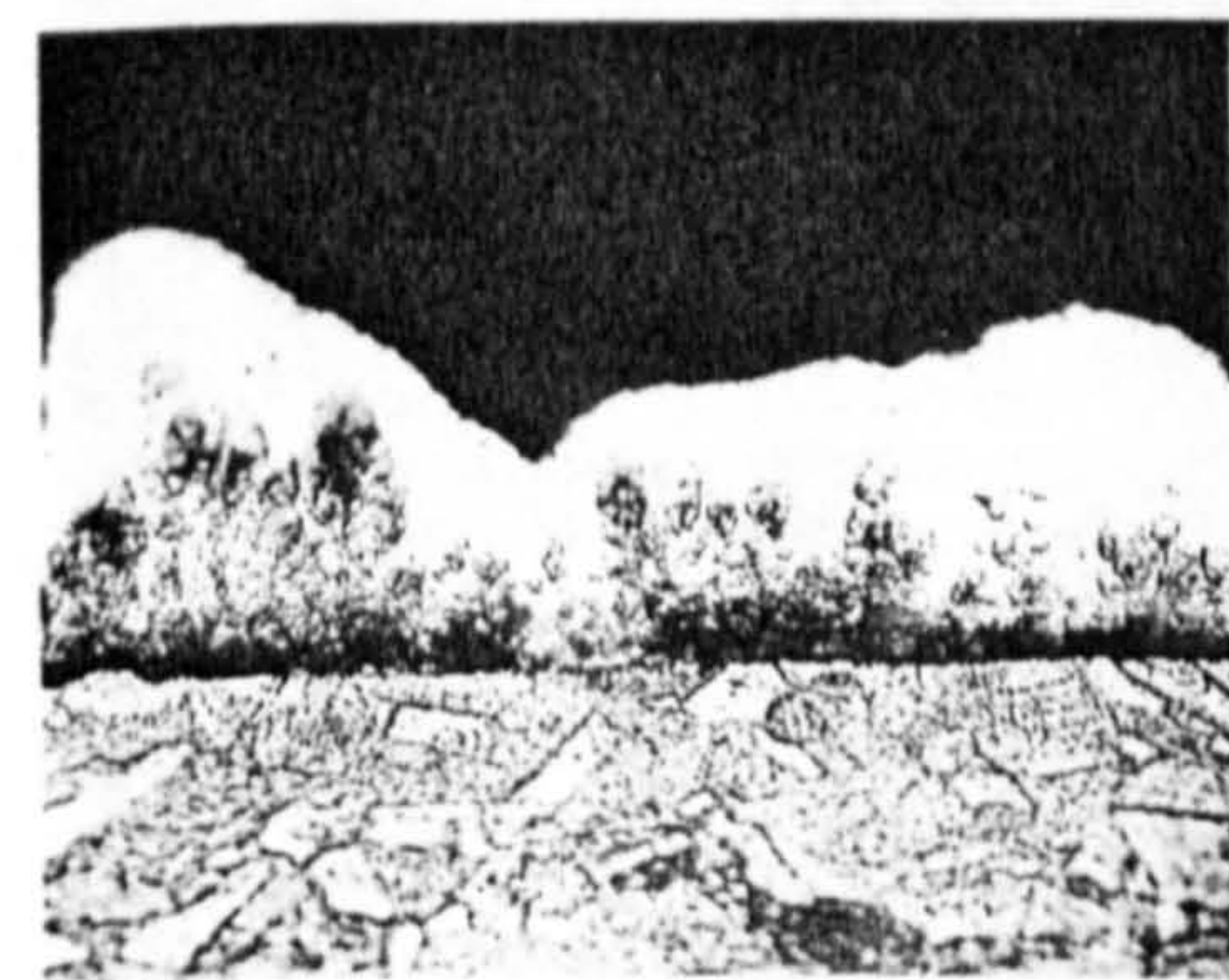


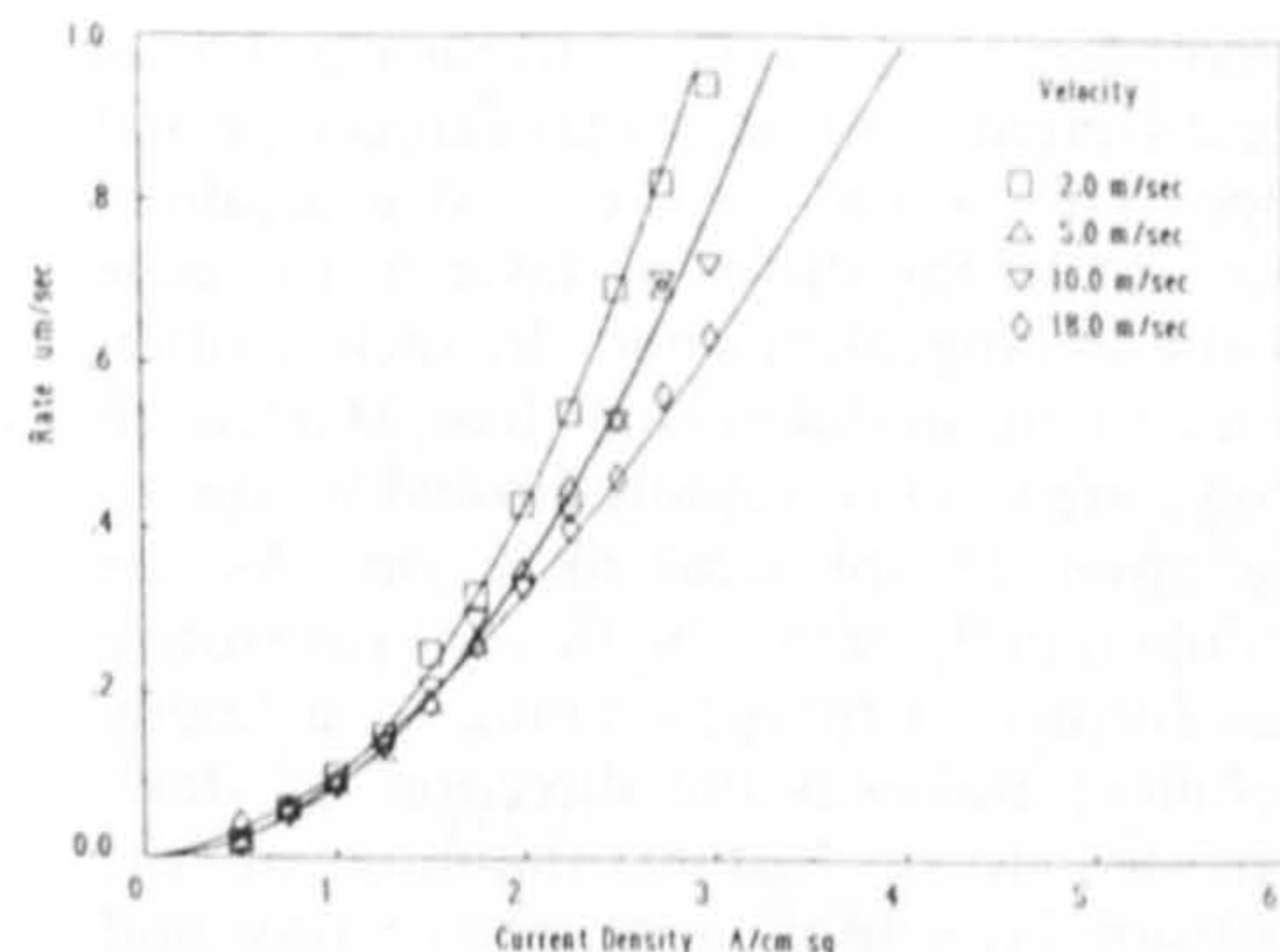
Figure 5. (a) Microsection of a copper deposit, $\times 1000$. (b) Surface Morphology of the same deposit. 0.8M copper, C.D. 15.4 A/cm², Re. 1365.

Figure 6. Microsection of a copper deposit, $\times 1000$. 0.8M copper, C.D. 50.0 A/cm², Re. 1365.

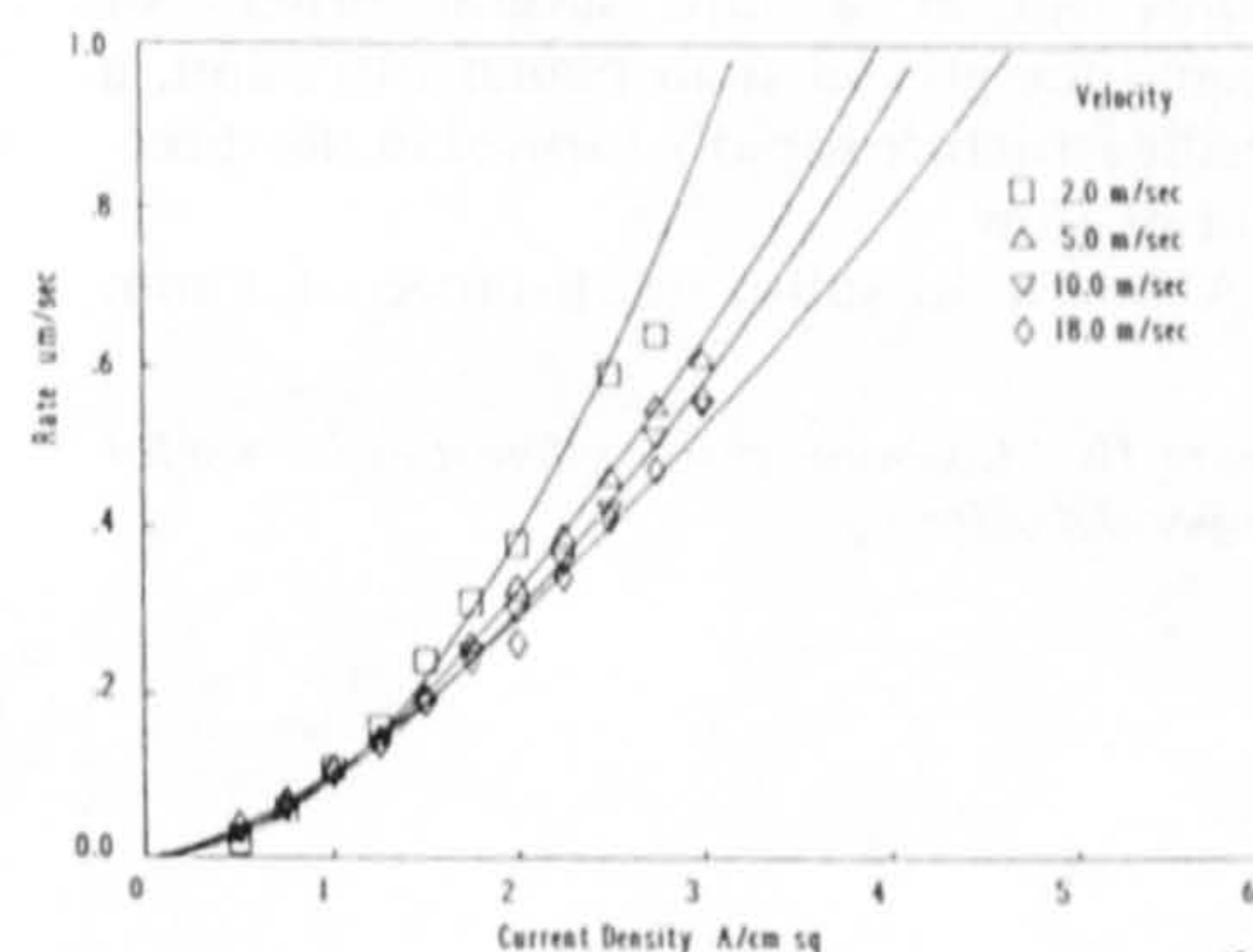


jet while other spots were being plated.

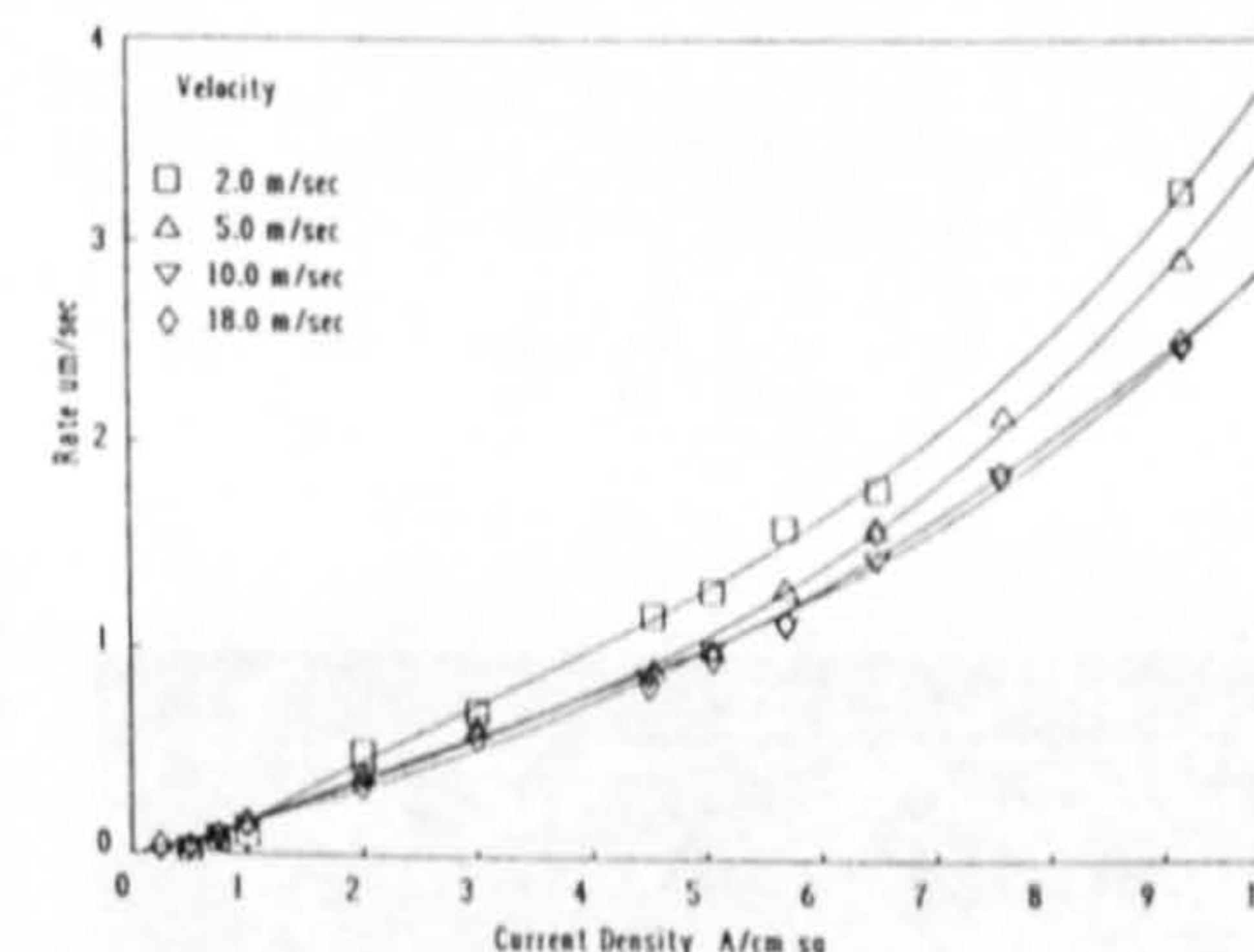
Figures 7(a), (b) and (c) show the relationship between the plating rate and current density for each electrolyte. As the number of coulombs used per spot was constant, it would be expected that the plating rate would remain constant over the current density range. It can be seen that at low current densities, the plating rate is low and increases with increasing C.D. There could be several reasons for this behaviour. At low current densities, the deposit may appear to be thin as the spread of the spot may be greater i.e. the selectivity may be poor. There may be another reduction reaction such as hydrogen evolution or oxygen reduction occurring. As the efficiency of the copper deposition process is usually 100% at low current densities, then hydrogen evolution is unlikely to be the cause. The influence of oxygen reduction



(a)



(b)



(c)

Figure 7. (a) Plating rate vs current density 0.08M copper. (b) Plating rate vs current density 0.204M copper. (c) Plating rate vs current density 0.8M copper.

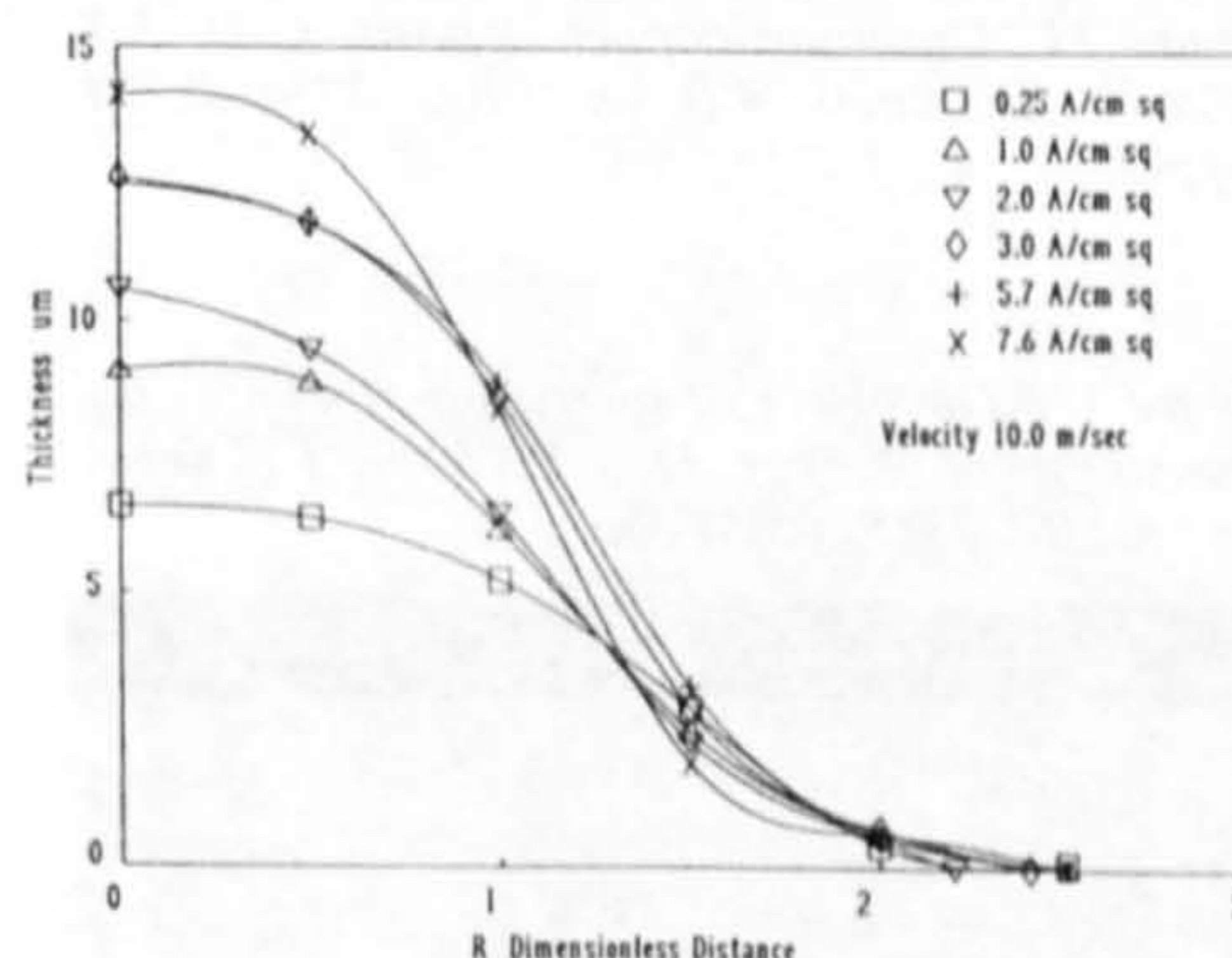


Figure 8. The effect of current density on selectivity 0.8M copper.

was not examined for the copper system but has been examined for the gold system. Figure 8 shows a plot of the selectivity of spots at different current densities. R is a

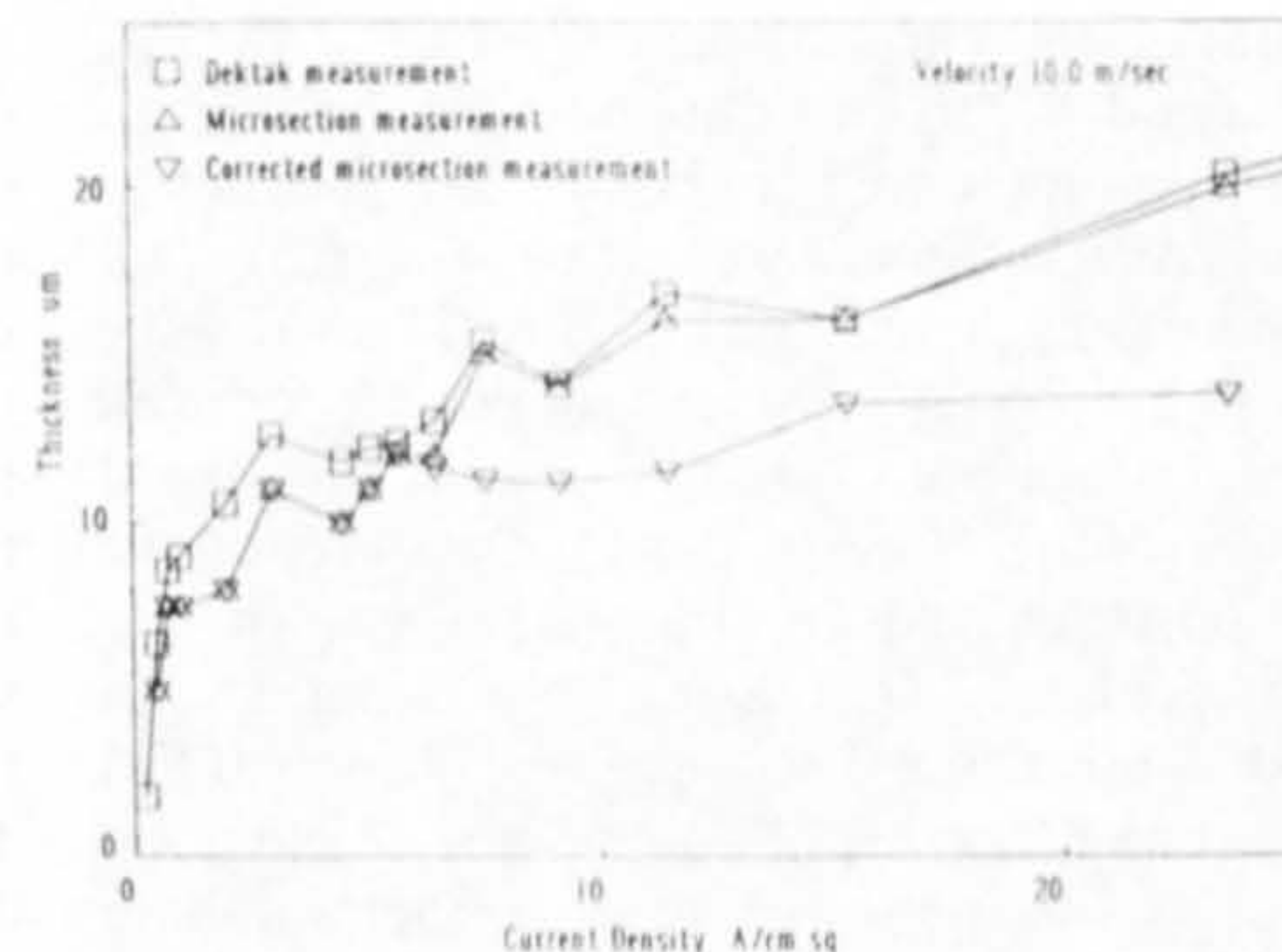


Figure 9. Thickness vs current density 0.8M copper.

dimensionless distance and is the ratio of nozzle radius to radial distance from the centre of the jet. It can be seen that there was no significant effect of current density on selectivity with the exception of the deposit produced at 7.6 A/cm². This profile indicates that the deposit was tending towards greater selectivity. At this current density, the deposit became more nodular and field orientated and the apparent plating rate became greater within the region of the electric field i.e. within the electrolyte jet. However, this behaviour has been seen with gold deposition and is discussed below.

Figure 9 compares the Dektak thickness measurements with microsection. It can be seen that there is a reasonable correlation. From the microsections, it can be seen that C.D.'s above 5 A/cm² the deposit begins to exhibit porosity due to the reduction in nucleation sites and growth, but not merging, of nodules from these sites. By measuring the percentage gross porosity, the distorting effect to the thickness vs C.D. curve could be reduced. The porosity was measured within the microsections using an Optimax Video Contrast Image Analyser. The porosity was separated from the deposit using image contrast and the proportion of porosity to metal presented as a percentage. The thickness measured was then reduced by this percentage to give the resultant curve in Figure 9. It can be seen that the slope of this curve is considerably reduced and is closer to that expected for deposits produced with a constant number of coulombs. This porosity explains the tendency for the deposit thickness to appear to increase as the current density was increased past the optimum C.D.

The Effect of Metal Concentration

The metal ion content of the electrolyte has a significant influence on the deposits. Low metal ion concentrations gave rise to low maximum useable current densities above which a dendritic, powdery structure formed, with pronounced 3D nucleation. At higher metal ion concentrations, higher useable current densities were obtained. The deposits deteriorated above these values by nodule formation that became increasingly incoherent. Figure 10 shows a plot of the maximum current densities that allowed coherent deposits to be obtained for different values of Re. The deposit thicknesses were approximately 5 μ m. This

maximum current density was, however, dependent on the thickness of the deposit with an increased coherence being obtained at greater thicknesses. (See The Effect of Increasing Thickness) Figure 11 shows the topography of a 4 μm deposit produced under optimum conditions for the 0.8M electrolyte. Note the surface etching of the deposit caused by the backwash of the electrolyte. Increasing the metal ion concentration to values greater than 0.8M increased the likelihood of nozzle clogging during idle periods due to copper sulphate crystal formation.

The Effect of Electrolyte Velocity

An increase in the flow rate, increased the current density at which loose powdery deposits formed. However, only with the 0.8M electrolyte did the velocity significantly increase the current density at which deposits of good quality were produced. It can be seen from Figure 10 that the 0.8M electrolyte shows a measured maxima at $Re = 2730$ and then falls with increasing Re . A similar behaviour is seen with gold and will be discussed later. Examination of Figures 7(a), (b) and (c) show that the slope of the plating rate/C.D. curve is reduced with increasing velocity. It is likely that the deposits were becoming more compact and less porous as the velocity was increased as this effect was less noticeable as the metal content was increased.

The Effect of Increasing Thickness

Figures 12, 13 and 14 show the effect of increasing thickness of the deposit. The current density chosen was in excess of that conducive to coherent deposits at a thickness of 4 μm . At low thicknesses ($< 3 \mu\text{m}$) the deposit consisted of small nodules, largely unconnected, of about 2 μm in diameter. At a thickness of 12 μm certain nodules had grown and engulfed others, leading to a more coherent structure. The nodule size had increased to approximately 6 μm . At a thickness of 62 μm , the nodule size had increased to 25 μm .

GOLD DEPOSITS

The Effect of Nozzle Distance

It was noticed that a nozzle to substrate distance of 0.5 mm led, particularly at low velocities, to the nozzle being engulfed in the electrolyte wash and thus behaving as a submerged jet. This did not occur with copper and is probably due to differences in surface tension between the electrolytes. It was therefore necessary to use a greater nozzle to substrate distance. In order to establish how this would influence the growth pattern of the deposit, a series of spots were produced at differing distances over the range 0.25 mm up to 3.5 mm at 0.25 mm intervals. A current density of 3.0 A/cm^2 and a velocity of 18 m/sec was used at a temperature of 40°C using electrolyte [3]. It was found that at distances greater than 1.75 mm, radial needle structures started to form as in Figure 15. This was due to the outer part of the electrolyte jet slowing down due to viscose drag as it passed through the air. The greater the distance, the greater the drag. When the jet impinged on the substrate, the lower velocity at the edge of the impingement

region led to increased turbulence due to the differential velocity between centre and edge. This would have caused a localised thinning of the diffusion layer at the edge of the impingement zone. In such a situation, small nodules that had started to grow, grew more rapidly probably due to the onset of spherical diffusion. As the nodule rapidly grew, the flow of electrolyte was further disrupted leading to a highly turbulent wake in the direction of flow. This led to a further thinning of the diffusion layer in the direction of flow and growth was enhanced in that direction. As spherical diffusion takes place at a small radius tip at a rate several orders of magnitude greater than planar diffusion, a needle structure rapidly formed in the direction of flow.

A nozzle to substrate distance of 1 mm

Figure 10. Maximum current densities for useful copper deposits.

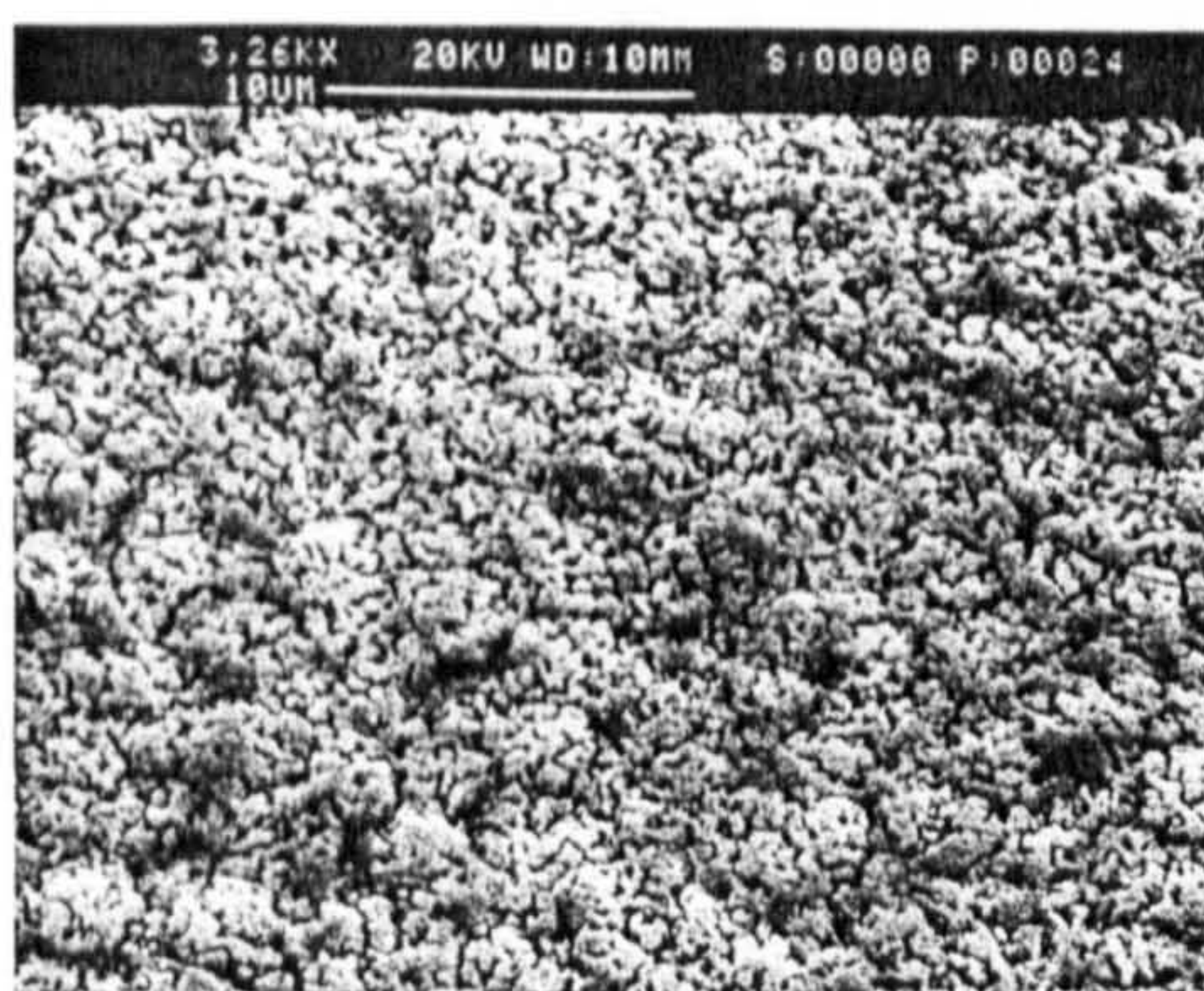
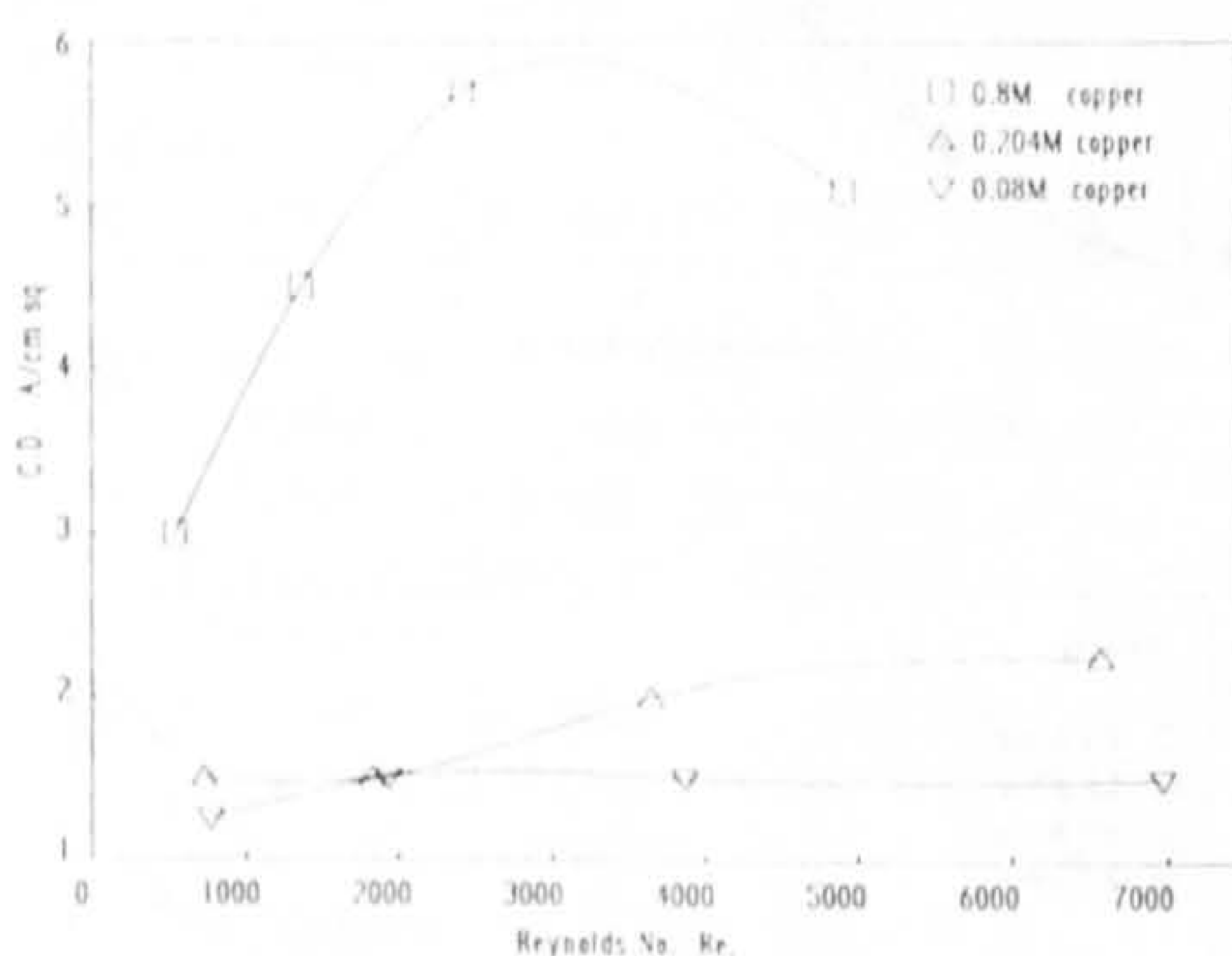
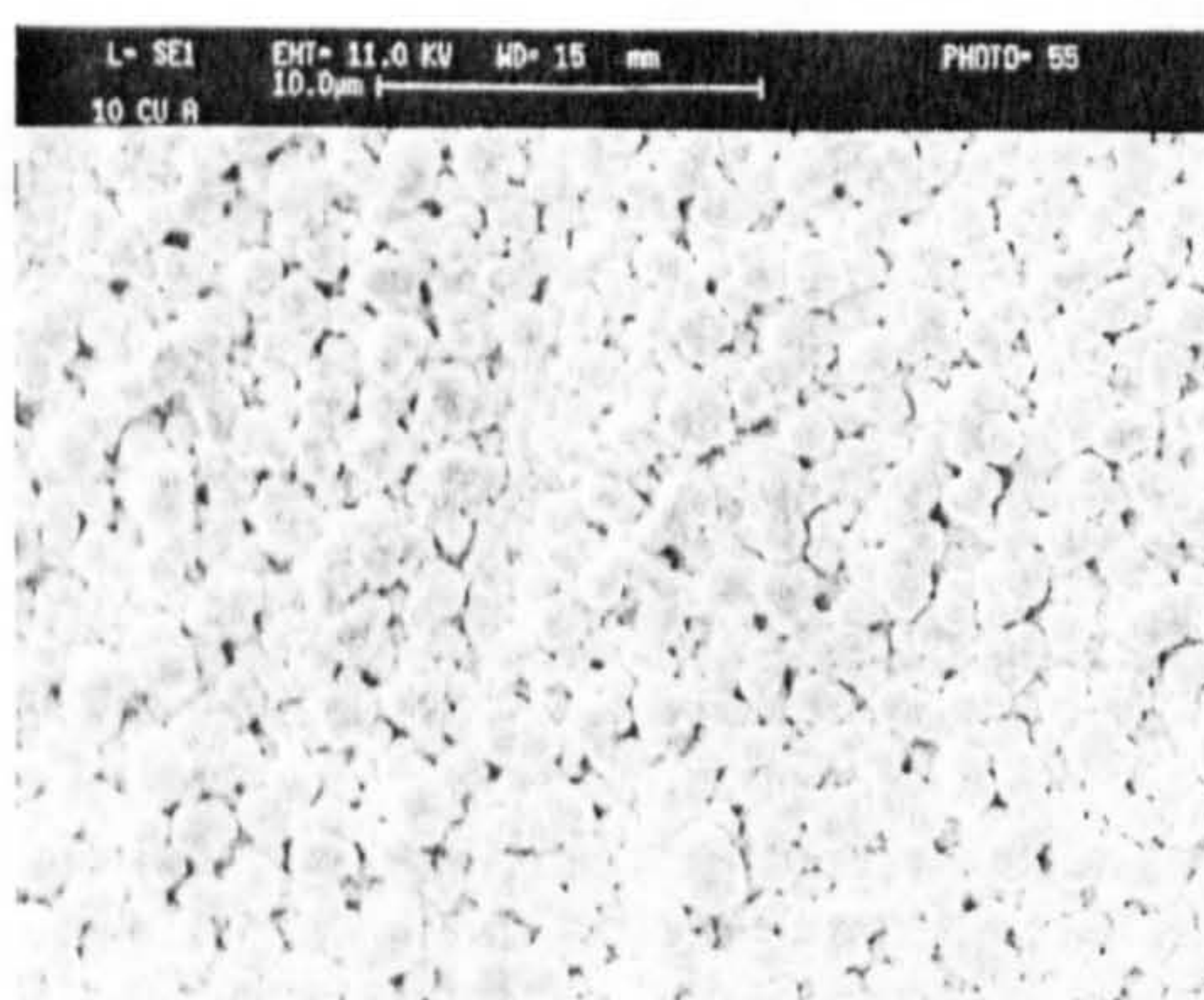


Figure 11. Optimum copper deposit. C.D. 5.7 A/cm^2 , Thickness 4.0 μm , $Re = 2730$ 0.8M copper.

Figure 12. The effect of increasing thickness on deposit morphology. C.D. 5.7 A/cm^2 , Thickness 2.3 μm , $Re = 1365$, 0.8M copper.



was found to be acceptable for the bulk of this work as there were no difficulties with the nozzle being engulfed by the electrolyte wash and the influence of the surrounding air is minimal at nozzle to substrate distances of about 2D where D is the nozzle diameter.

The Effect of Current Density

The effect of current density on deposit thickness is very similar to that of copper. Low current densities ($< 1 \text{A}/\text{cm}^2$) gave rise to thin deposits. A current density of 0.25 A/cm^2 showed virtually no deposition within the impingement region although a "halo" with a diameter of 0.4 mm was observed surrounding it. It was not possible to identify the presence of any deposit by thickness measurement using the Dektak. At first, it was thought that there was a

Figure 13. The effect of increasing thickness on deposit morphology. C.D. 5.7 A/cm^2 , Thickness 12.1 μm , $Re = 1365$, 0.8M copper.

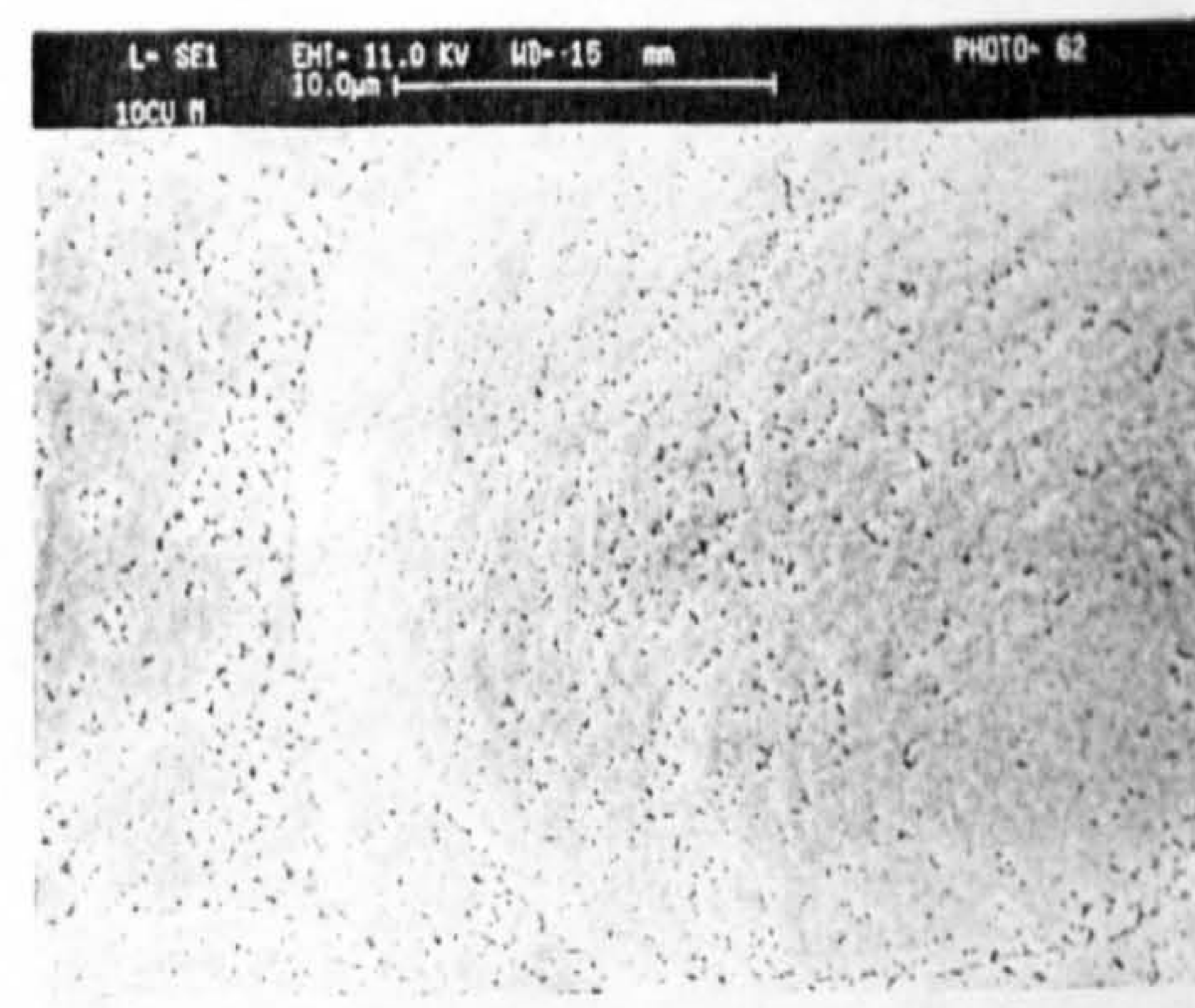
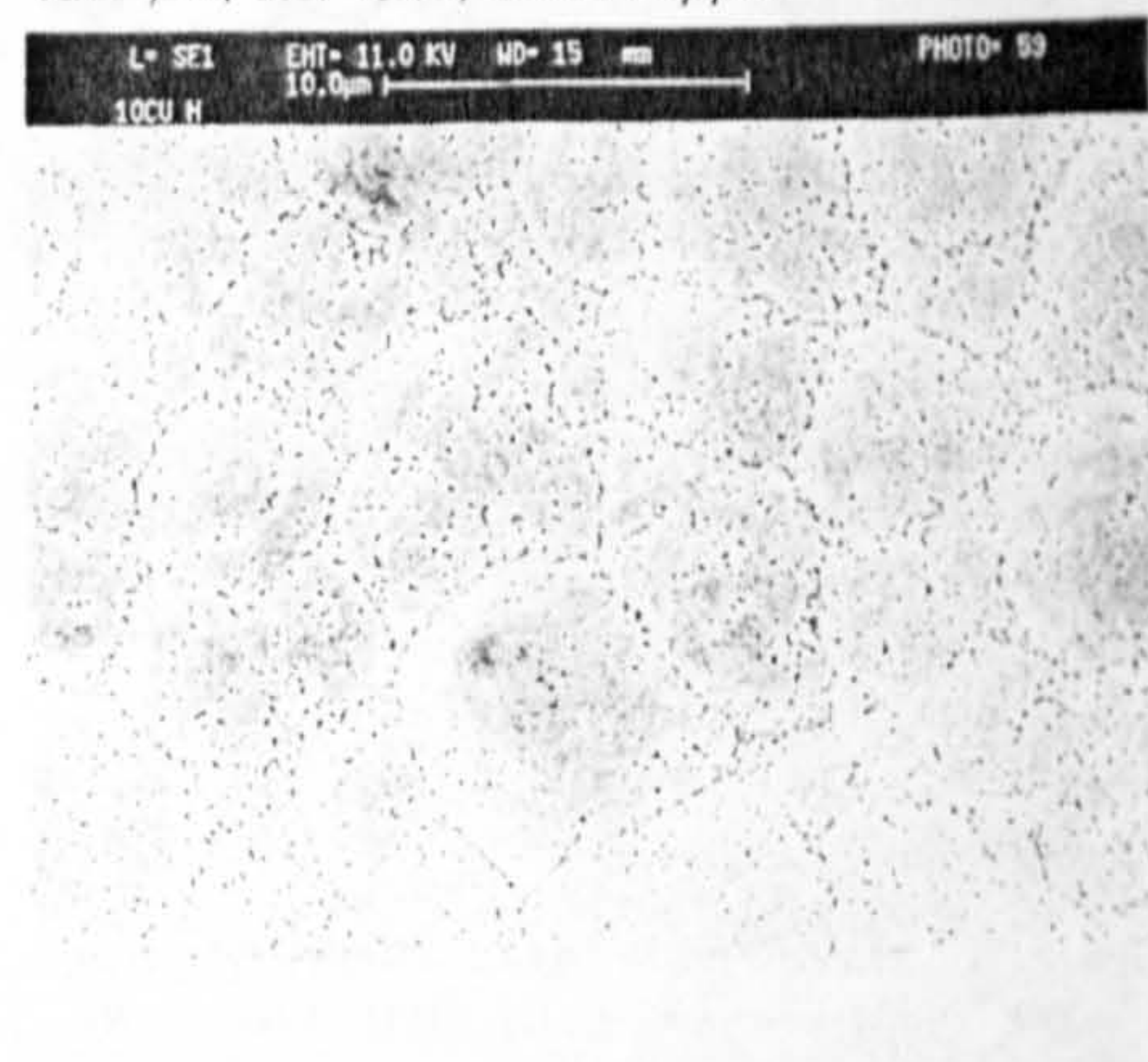
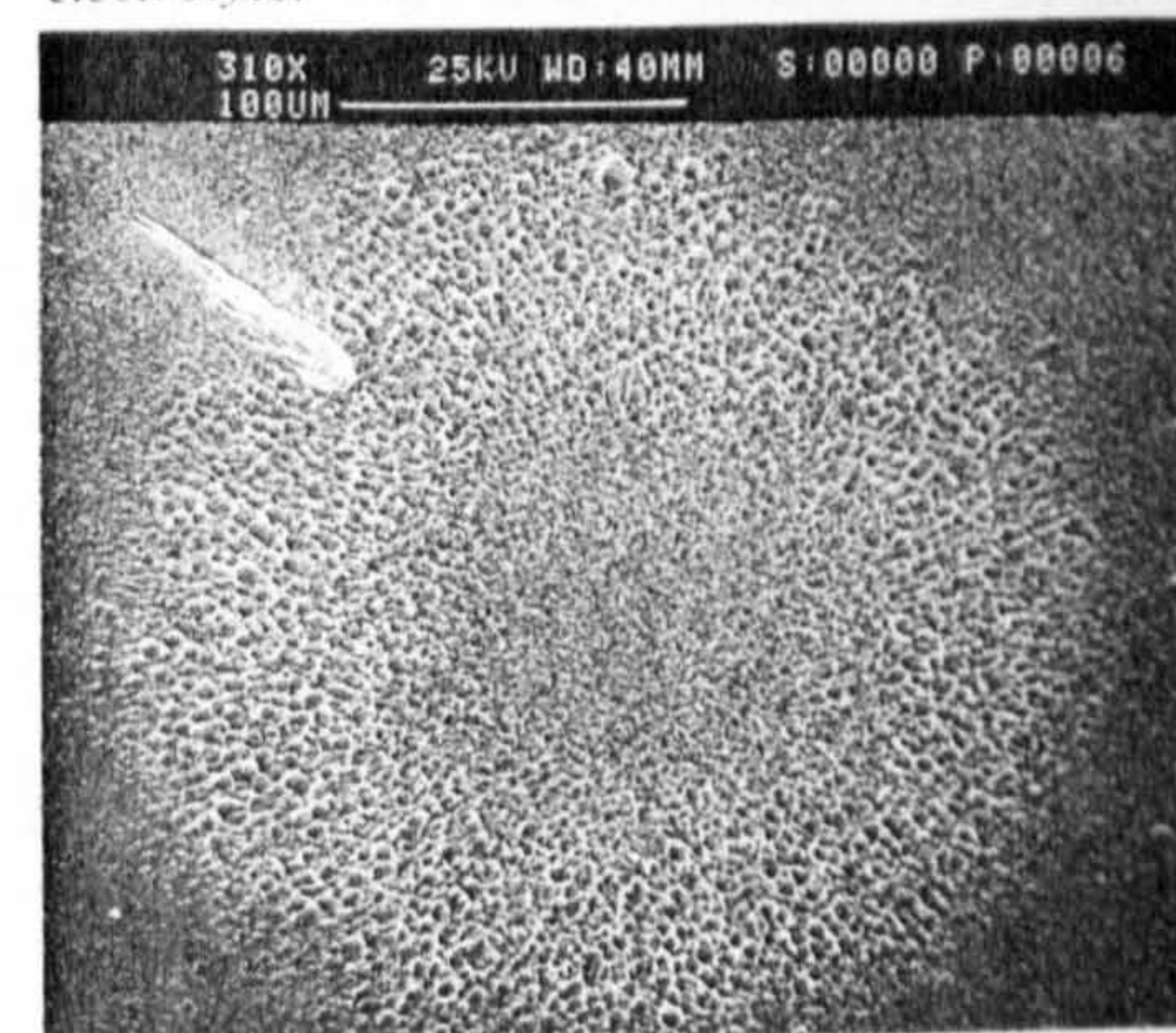


Figure 14. The effect of increasing thickness on deposit morphology. C.D. 5.7 A/cm^2 , Thickness 62.0 μm , $Re = 1365$, 0.8M copper.

Figure 15. Typical needle type structures that formed when the nozzle to substrate distance was increased above 1.75 mm. 0.27M gold phosphate electrolyte.



competing reaction such as hydrogen evolution or oxygen reduction. The effect of oxygen reduction was established by de-aerating the electrolyte by bubbling nitrogen through it for 30 minutes prior to deposition. It was found that deposits produced from de-aerated solutions did produce a measurable deposit of $0.3 \mu\text{m}$ at a C.D. of 0.25 A/cm^2 . In addition, an increase in deposit thickness of approximately 10% was seen up to a C.D. of 1.0 A/cm^2 after which no further increase was seen.

In order to establish what was happening, a number of deposits were produced on sputtered glass substrates. Deposits up to a current density of 7.0 A/cm^2 were produced using a total number of coulombs of 0.576 and the efficiency of the process was measured by the weigh, plate, weigh method. The efficiencies are shown in Figure 16. It was possible to measure the total spread of the deposit optically. The sputtered gold/chrome layer was thin enough to transmit a strong light beam. However, where deposition had occurred, the light was extinguished and this point was used to identify the edge of the deposit. The diameters of the spots were measured using an eyepiece micrometer attached to a low power microscope. Figure 17 shows how the true diameters varied with current density. It is evident that at low current densities, the deposit spreads over a greater distance but the efficiency is low. At higher current densities, the efficiency is increased to about 70% and the total spread of the deposit coincides with that as measured by the Dektak.

The cathode efficiency behaviour of the electrolytes is similar to that seen under conventional deposition conditions, with low efficiencies being observed at low current densities and increasing as the current density is increased¹⁴. This would be expected as the E° (rest potential) value of gold is about -0.61 V . At a pH of 6.0, the E° value of hydrogen is about -0.3 V . Therefore, at low overpotentials, a significant quantity of hydrogen will be co-deposited, reducing as the overpotential is increased. In addition, it has been shown that the reduction of oxygen also occurs at low current densities¹⁴. It would appear that a similar behaviour occurred under jetting conditions.

The structure of the deposit is significantly affected by current density. At current densities above 0.25 A/cm^2 , the deposits changed from smooth and dull to semi-bright and then to bright as the C.D. increased. This was followed by either a nodular structure or needle growth and finally above 6.0 A/cm^2 the growth pattern became dendritic with a pronounced dendritic field orientated growth. However, in the case of electrolyte [4] no dendritic growth was seen. It should be remembered that the deposit thickness also increased with increasing current density and this would have had an influence on the deposit structure and appearance. (See the Effect of Increasing Thickness).

The effect of current density on selectivity can be seen in Figure 18. It can be seen that at low current densities, the selectivity is poor. As the C.D. is increased,

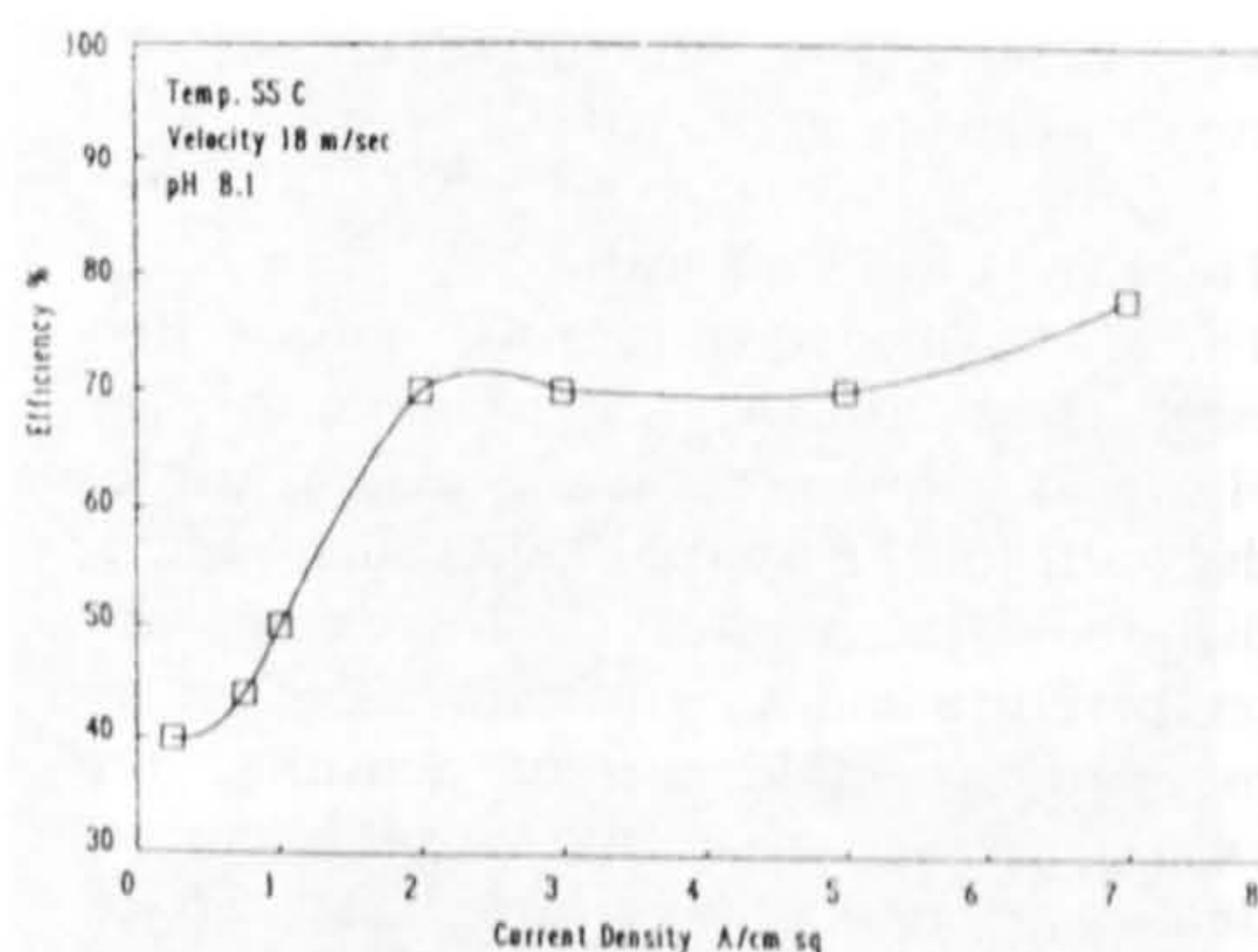


Figure 16. Current efficiency vs current density 0.17M citrate gold.

Figure 17. Current density vs deposit width — maximum spread of spots.

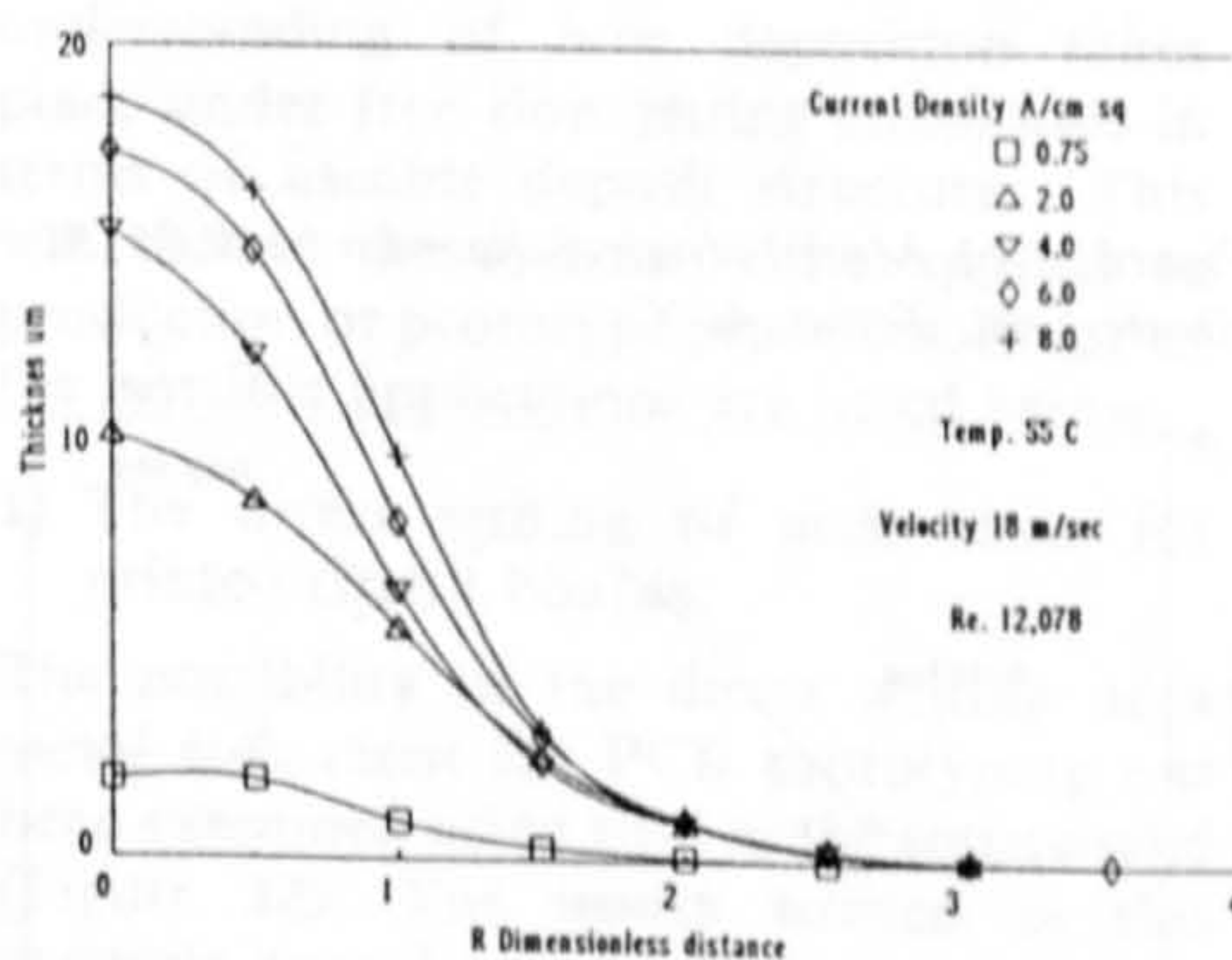
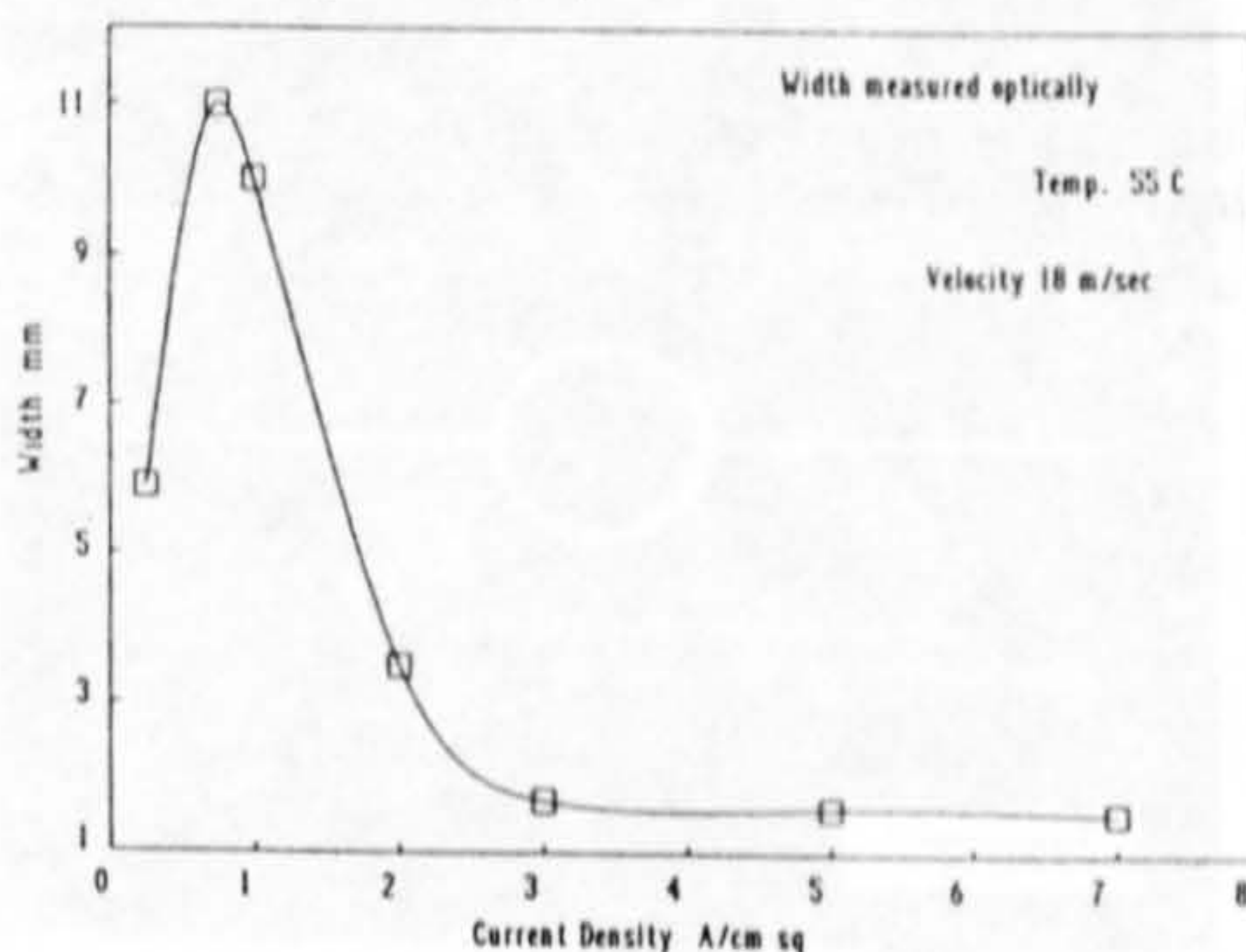


Figure 18. The effect of current density on selectivity 0.17M citrate gold.

the selectivity improves.

The Effect of Gold Concentration

As the gold content was increased, so the maximum useful current density and plating rate increased. However, a maximum was reached at 0.17M where increasing the concentration led to a slight reduction in the useful current density and plating rate. The maximum plating rate obtained from the 0.17M electrolyte at pH 8.1 was $3.4 \mu\text{m/sec}$ at a current density of 6.0 A/cm^2 . This was the highest plating rate obtained in this series of experiments. The structure of this deposit can be seen in Figure 19. It can be seen that the jetted deposit exhibits a much less angular structure than the conventional deposit.

At a concentration of 0.28M, the maximum plating rate was $2.9 \mu\text{m/sec}$ at a current density of 5.0 A/cm^2 . This effect



Figure 19. The morphology of the gold deposit produced at the greatest plating rate. 0.17M gold (citrate electrolyte). Temp. 55°C C.D. 6.0 A/cm^2 , Re. 12,078, plating rate $3.4 \mu\text{m/sec}$, pH 8.1.

Figure 20. Current density vs plating rate for different gold concentrations, citrate electrolyte.

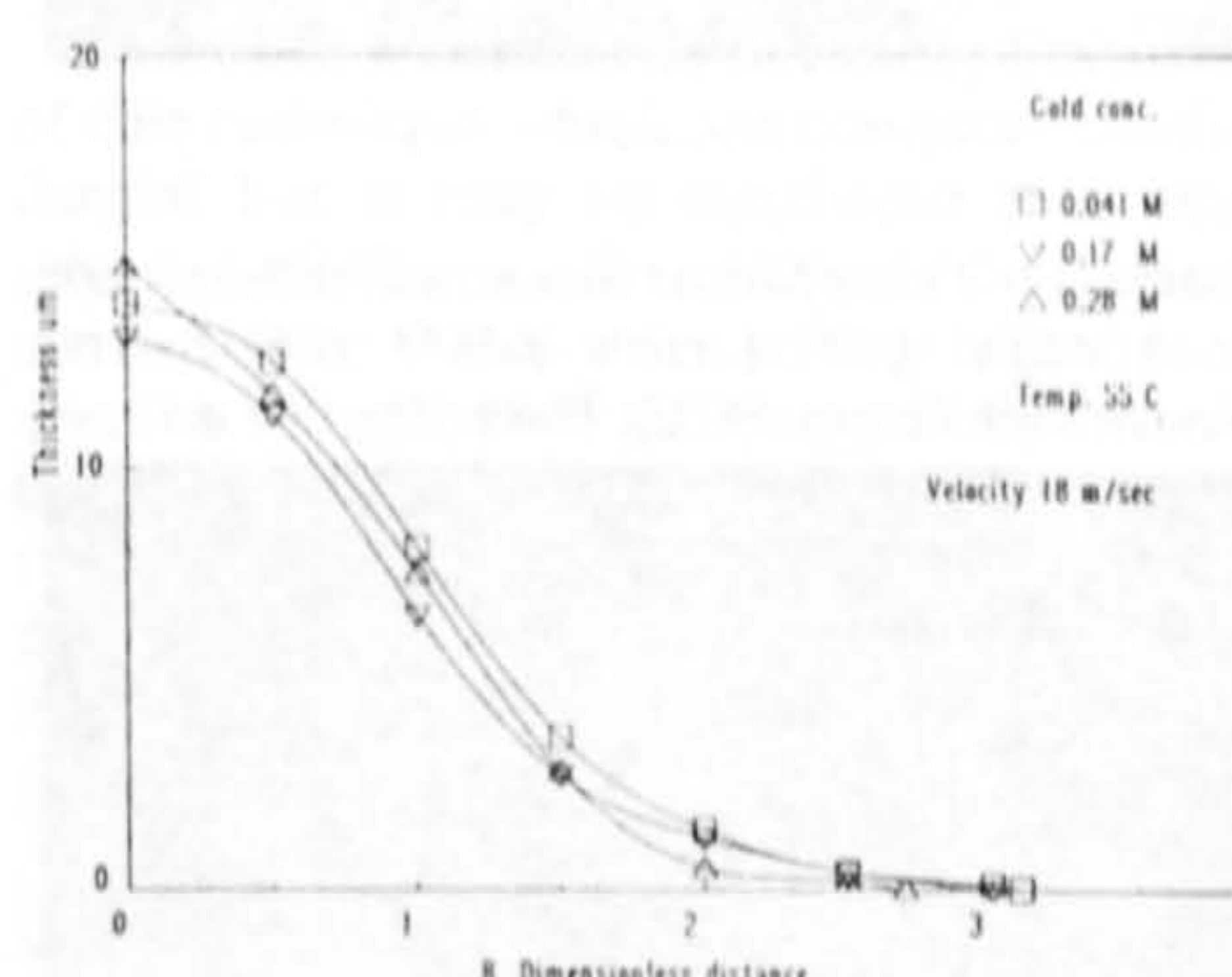
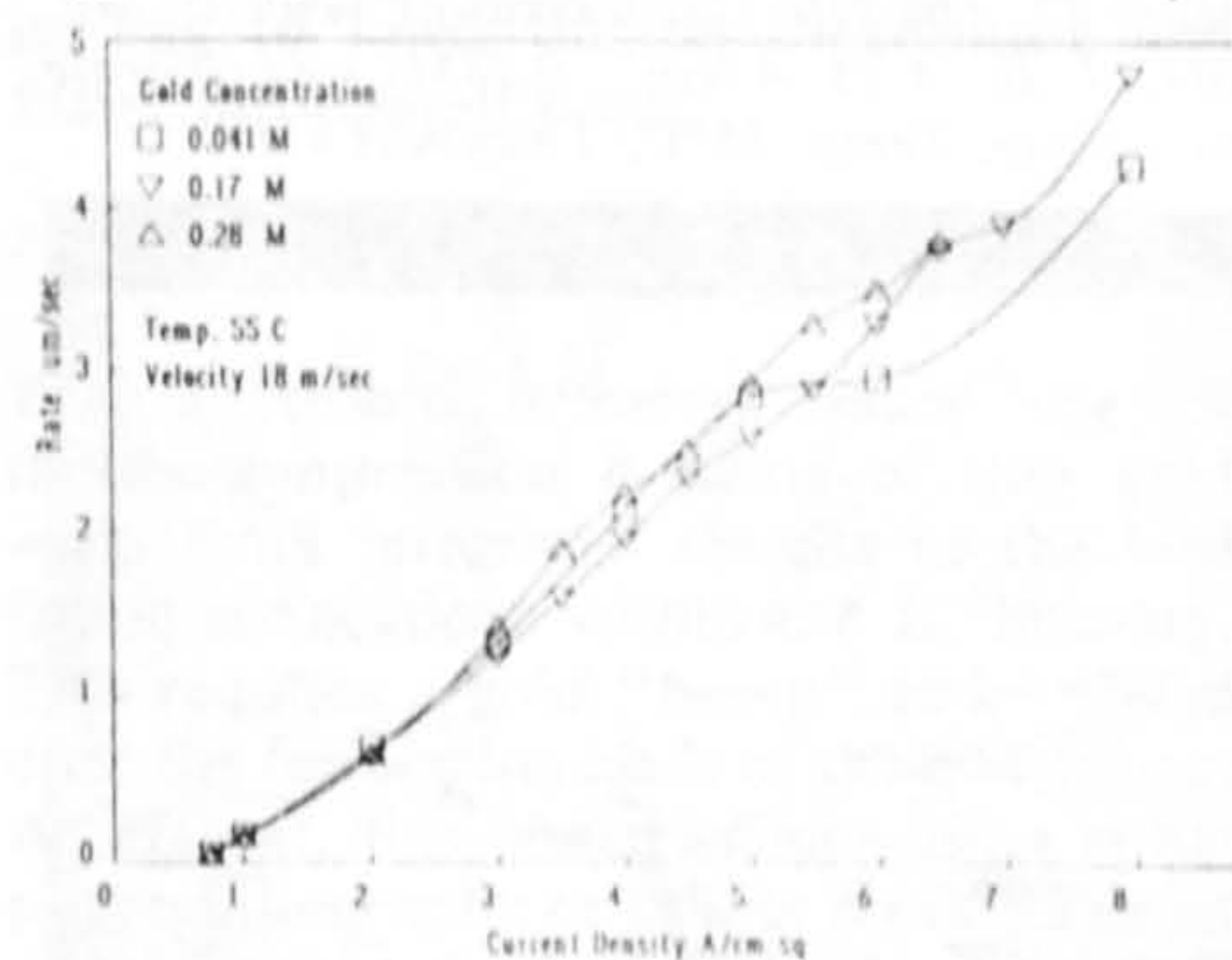


Figure 21. The effect of concentration on selectivity, citrate gold.

was also seen in copper deposition. The reason for this is that higher metal ion concentrations allow individual nodules to grow larger. This effect is also enhanced by greater velocities. This indicates that the mechanism and rate of nodule growth is diffusion controlled.

Figure 20 shows the plating rates for the different concentrations of gold over the C.D. range used. It can be seen that at the lower current densities, the plating rates are coincident but above 3.0 A/cm^2 , the curves no longer coincide, with lower concentration electrolytes showing an apparently greater plating rate. This was due to the fact that at high current densities, the density of the deposit fell as the deposit quality deteriorated due to an increase in voids. It can be seen that the curves for the 0.041M and 0.28M electrolytes show a significant deviation at the high

C.D. end of the curve and this corresponds with poor deposits. The 0.17M electrolyte curve, whose deposit quality remained reasonably good over the range shown, maintained an almost linear relationship.

Figure 21 shows the effect of concentration on the selectivity. It can be seen that the selectivity is not significantly affected by gold concentration.

The Effect of Electrolyte Velocity

Like the copper system, as the velocity is increased, so the deposit became smoother and less nodular for a particular current density and temperature. This effect can be seen in Figures 22, 23 and 24. Because of the number of spots produced, it was possible to construct some simple morphological diagrams relating structure to Re. and C.D. These are shown in Figures 25 (a), (b) and (c). It can be seen that as the Re.

was increased, so the maximum useable current density increased.

The Effect of Temperature

The effect of temperature was not precisely established for the same values of Re. However, some general conclusions can be drawn from the morphological diagrams at different temperatures. Increasing the temperature had a significant effect on the maximum useable current densities. For example, the maximum useful current density at a temperature of 25°C and an Re. = 6000 was 2.0 A/cm² for the 0.28M electrolyte. At 40°C this increased to 3.8 A/cm² and at 55°C to 4.0 A/cm². The most noticeable effect was on the deposits that had a poor structure. The 0.28M electrolyte produced deposits with a transition point from smooth to needle type deposits at 25°C but at 55°C the transition was to a

nodular structure. A similar effect was seen with the other electrolytes. Needle type structures were only seen at low Re. values at 55°C.

The Effect of pH

It was found that deposit structures improved at a pH of 8.1 for both the 0.28M and the 0.17M electrolytes. This allowed a greater plating rate to be used. Figures 26, 27 and 28 show deposits from the 0.28M electrolyte at pH 5.3, 6.1 and 8.1 respectively. An increased plating rate at the higher pH value would be expected as the E° value for hydrogen (-0.5V) shifted closer to the deposition potential for gold.

The Effect of Conductivity

Electrolyte [5] was developed so that a low conductivity solution could be tested. The conductivity was about half that of the

Figure 22. The effect of increasing velocity. Re. 1044, C.D. 4.75 A/cm², 0.28M gold (citrate electrolyte), Temp. 55°C, Thickness n/m.



Figure 25(a). Morphological diagram for 0.041M citrate gold, Temp. 25°C.

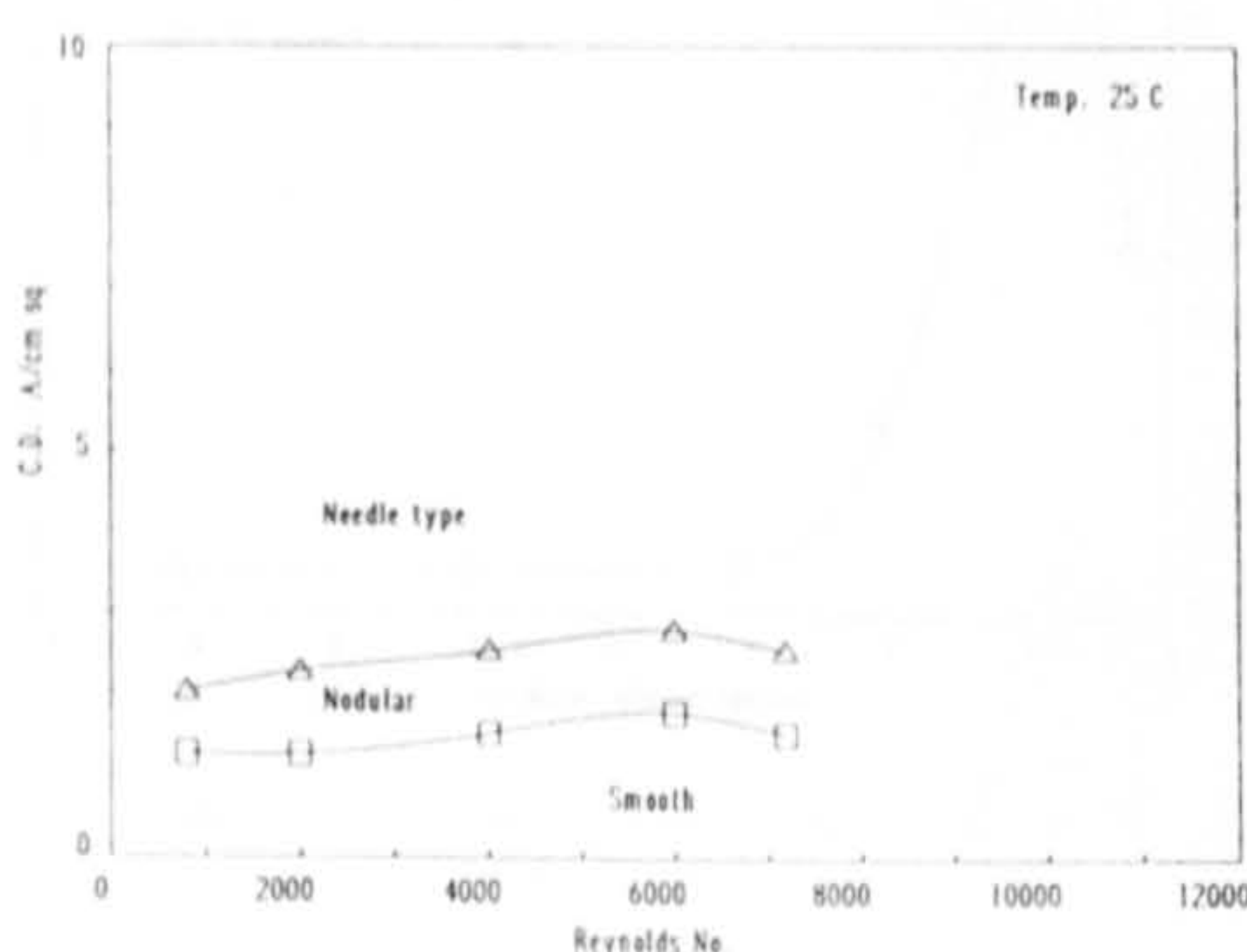


Figure 26. The effect of pH. 0.28M gold (citrate electrolyte), pH 5.3 C.D. 5.0 A/cm², Re. 9396, Temp. 55°C, Thickness 19.4 μm.

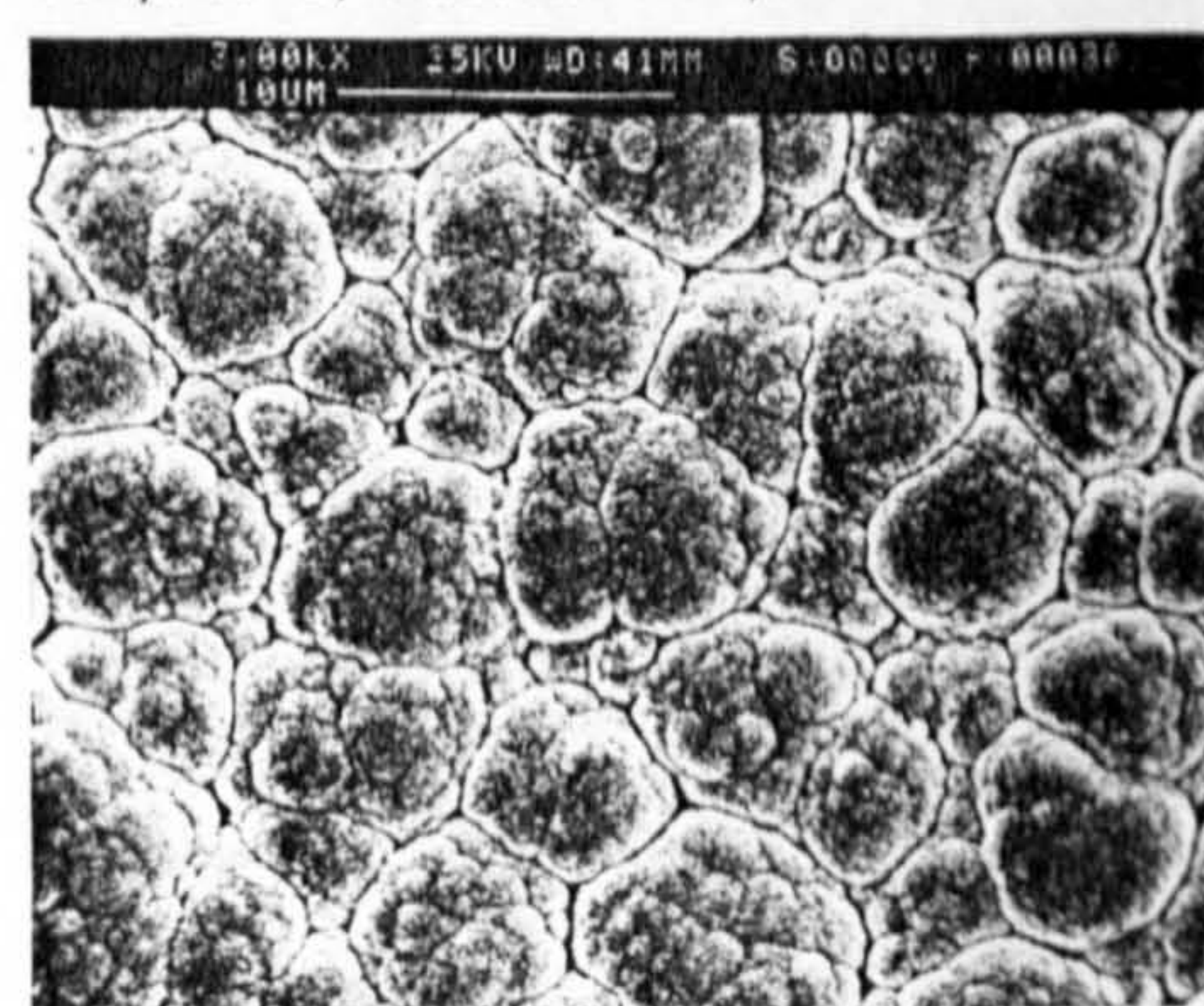


Figure 23. The effect of increasing velocity. Re. 2610, C.D. 4.75 A/cm², 0.28M gold (citrate electrolyte) Temp. 55°C, Thickness 19.1 μm.

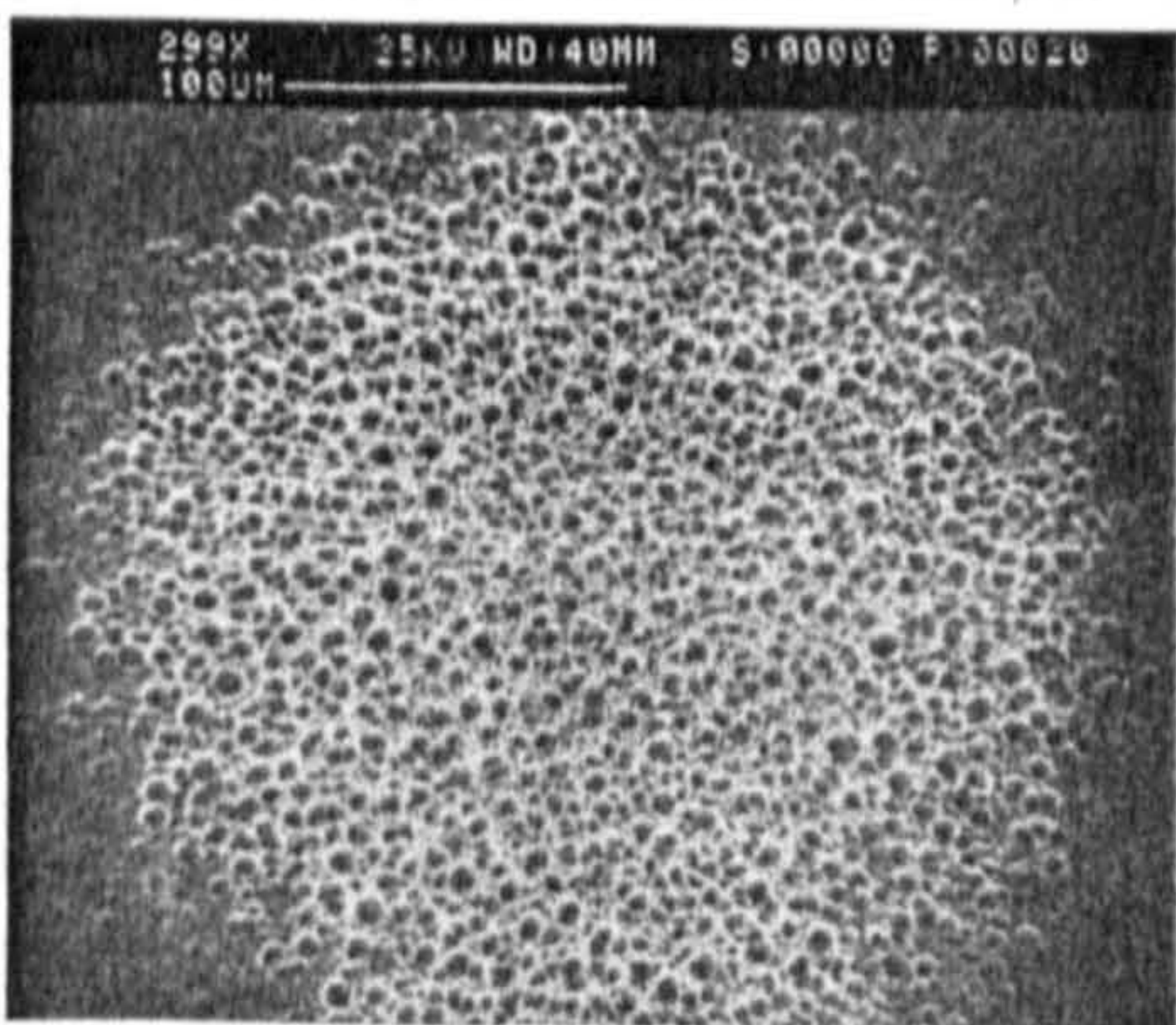


Figure 25(b). Morphological diagram for 0.041M citrate gold, Temp. 40°C.

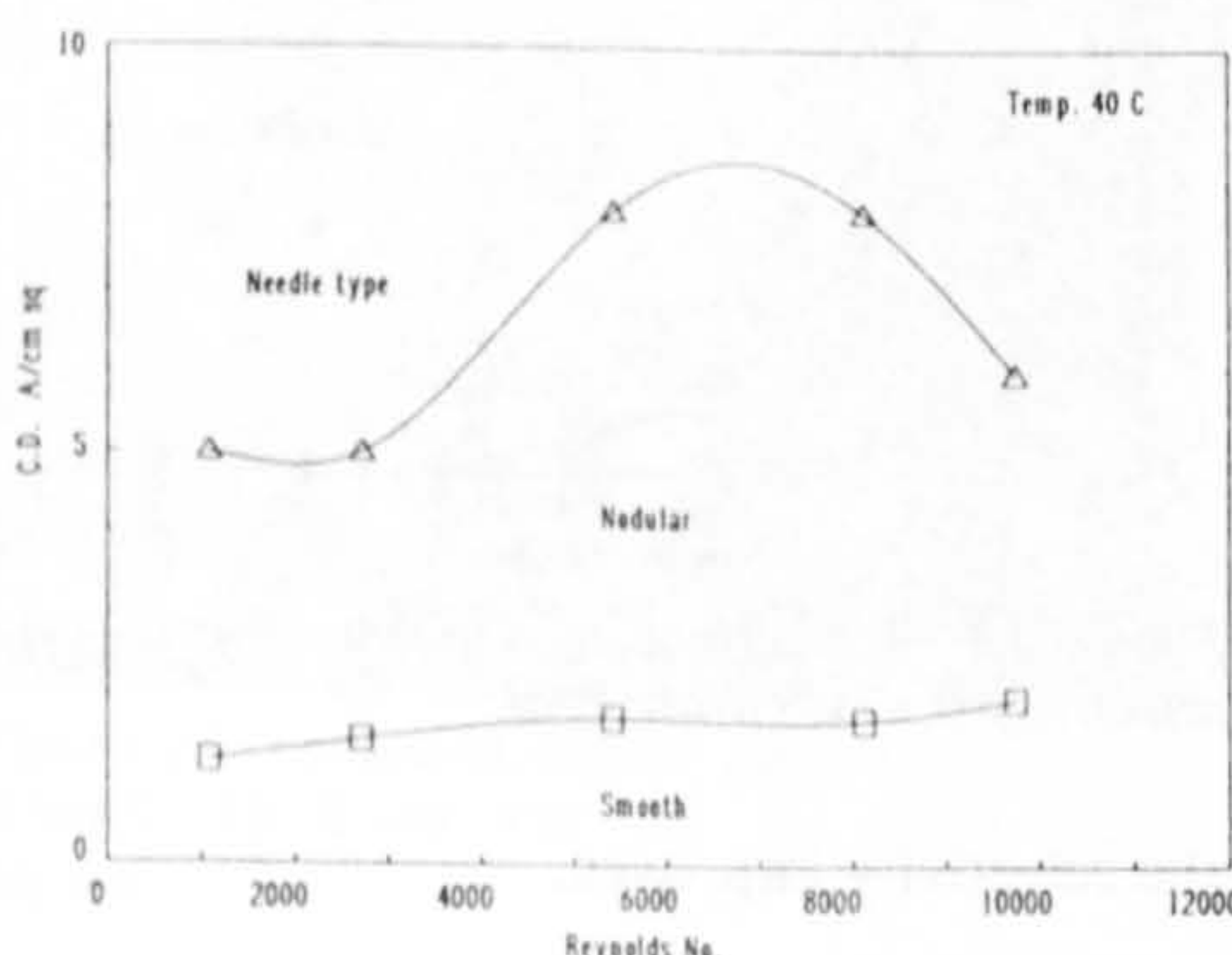


Figure 27. The effect of pH. 0.28M gold (citrate electrolyte), pH 6.1 C.D. 5.0 A/cm², Re. 9396, Temp. 55°C, Thickness 18.3 μm.

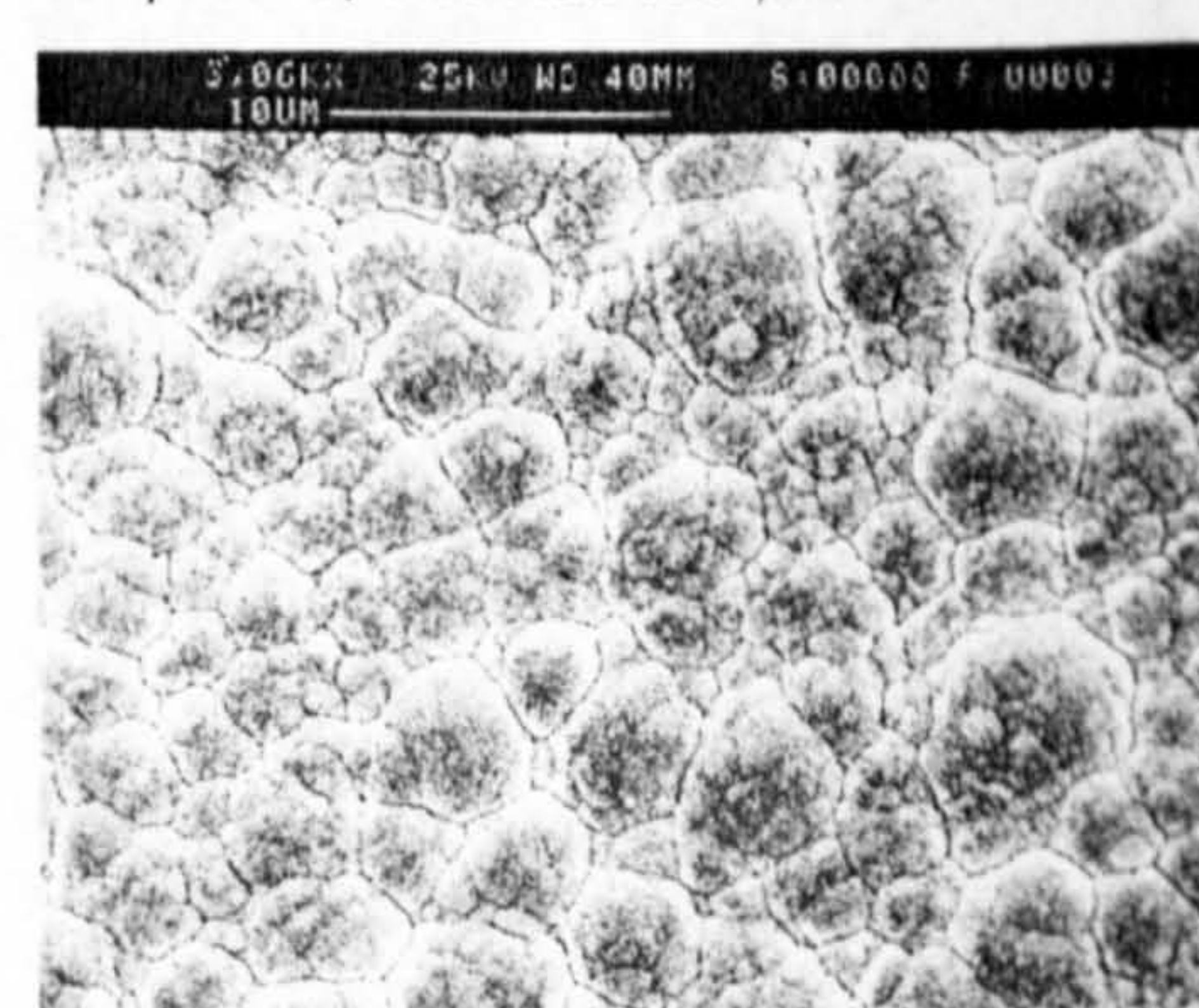


Figure 24. The effect of increasing velocity. Re. 9396, C.D. 4.75 A/cm², 0.28M gold (citrate electrolyte) Temp. 55°C, Thickness 17.9 μm.

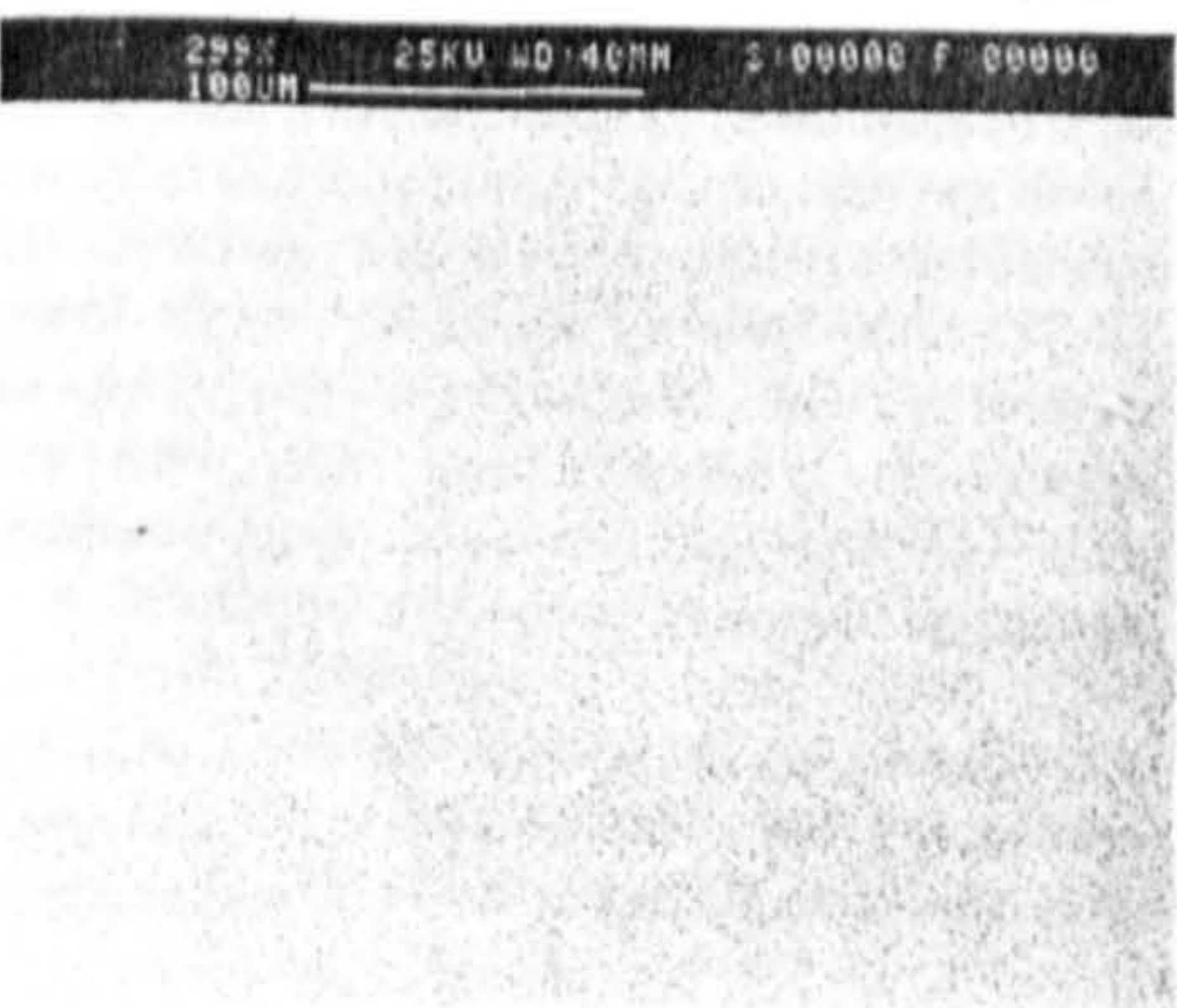


Figure 25(c). Morphological diagram for 0.041M citrate gold, Temp. 55°C.

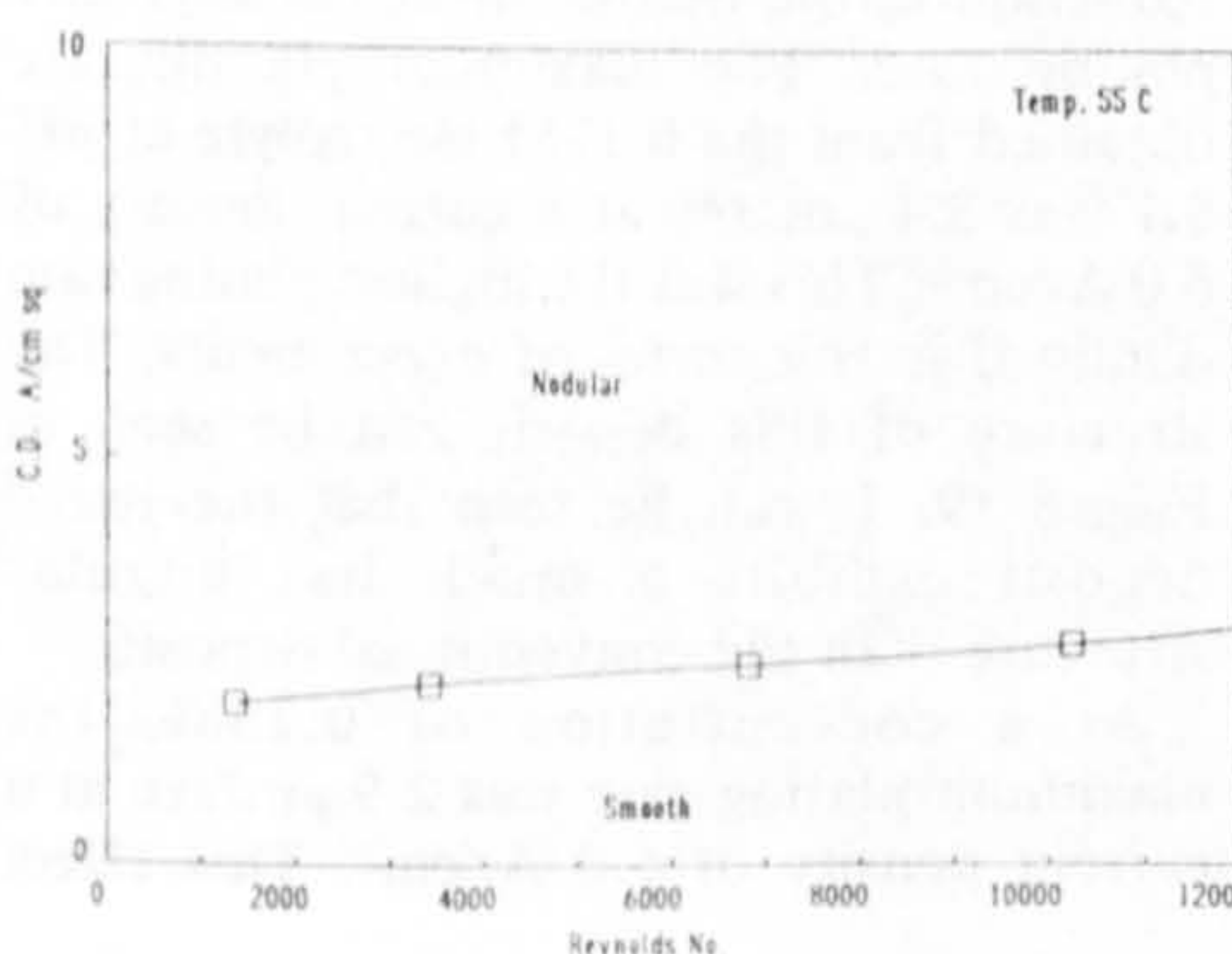


Figure 28. The effect of pH. 0.28M gold (citrate electrolyte), pH 8.1 C.D. 5.0 A/cm², Re. 9396, Temp. 55°C, Thickness 18.0 μm.

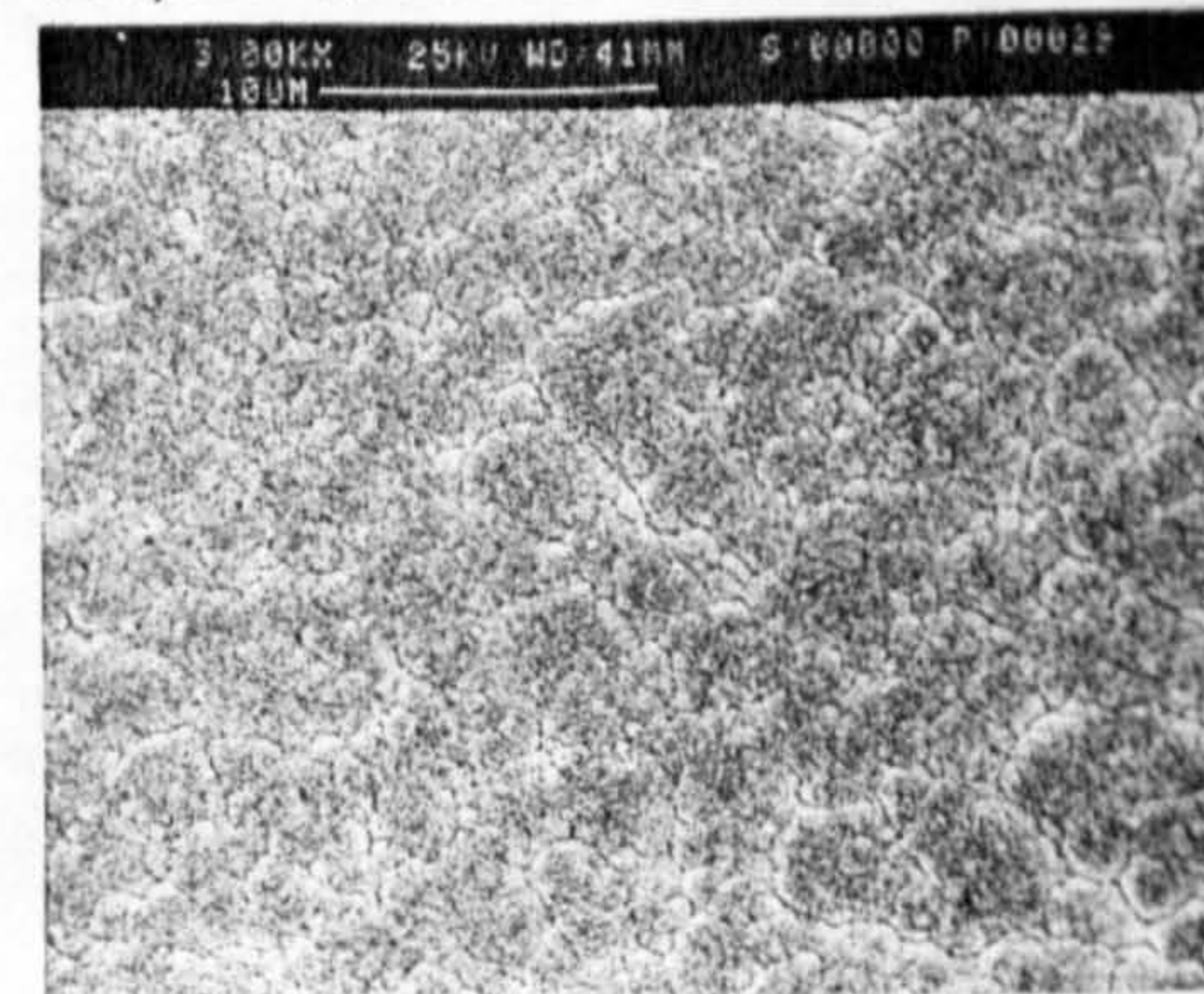




Figure 29. A gold deposit from a citrate electrolyte produced under conventional conditions. C.D. 5.0 mA/cm², 0.06M gold, Thickness 18 μm.

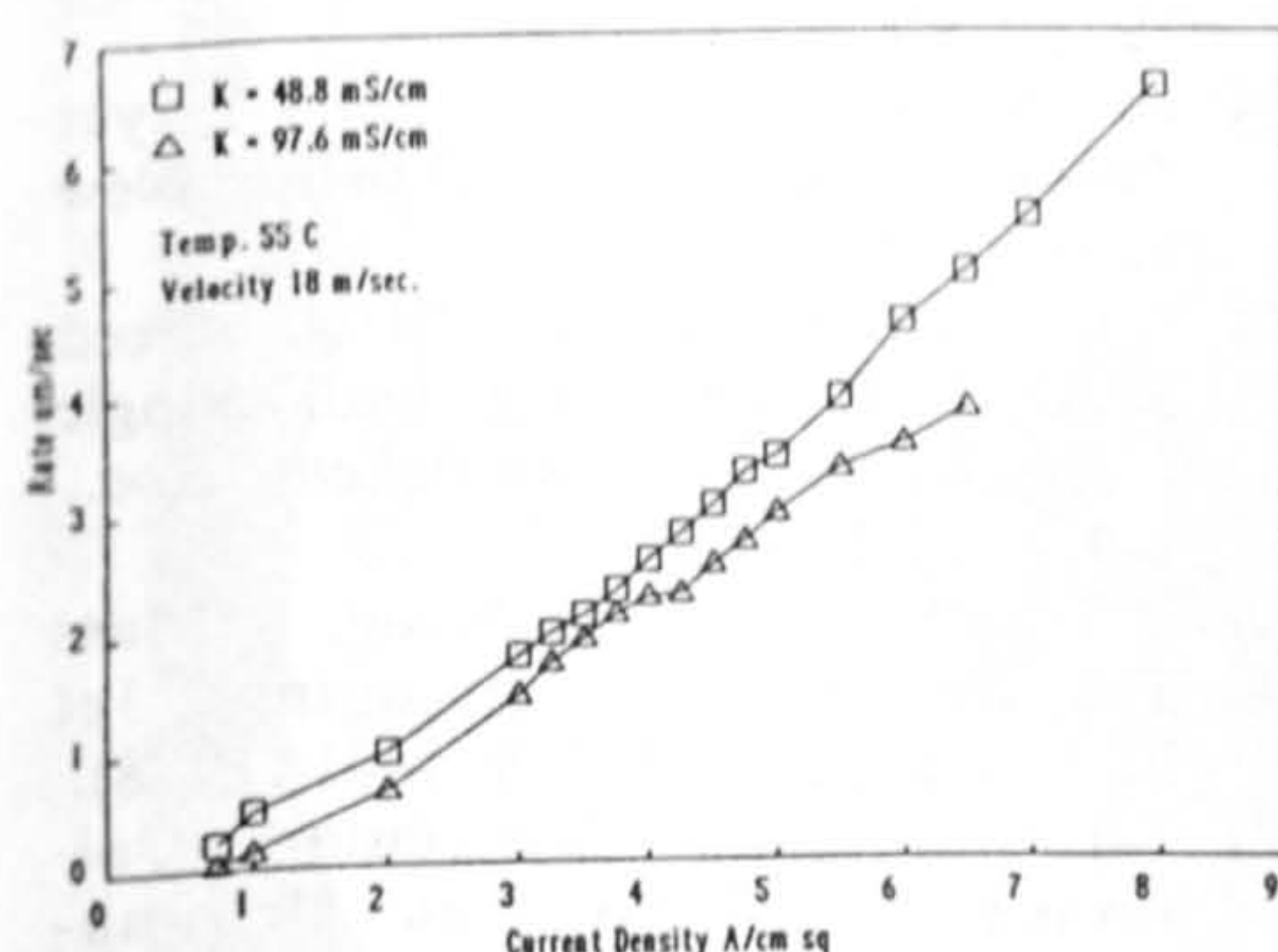


Figure 30. The effect of conductivity on plating rate, 0.28M citrate gold.

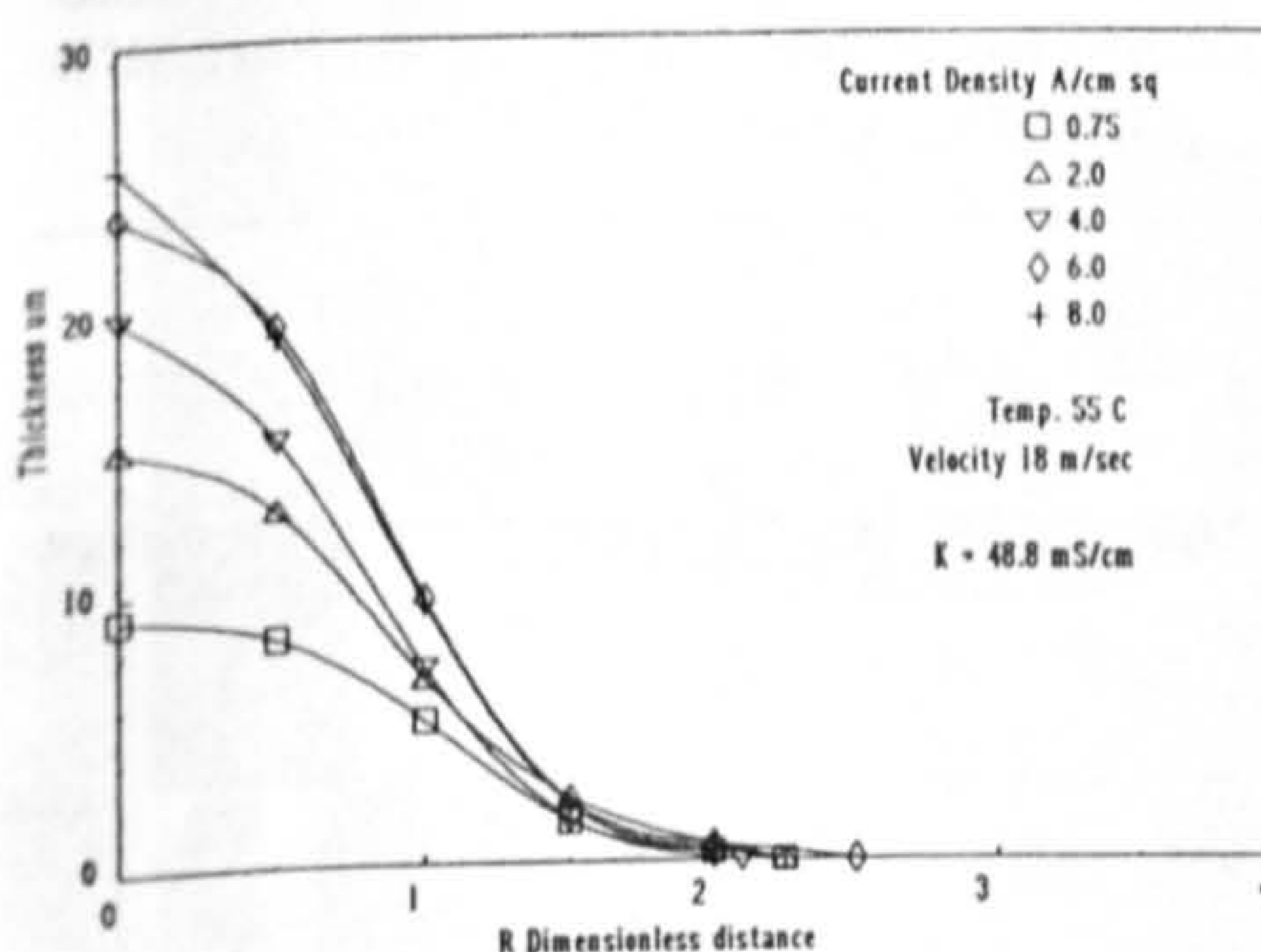


Figure 31. The effect of current density on selectivity. Low conductivity electrolyte.

other electrolytes. Figure 30 shows a comparison between the apparent plating rate of the low conductivity electrolyte and the 0.28M citrate gold. It can be seen that the low conductivity electrolyte exhibited a much greater apparent plating rate. Examination of Figure 31 reveals that the selectivity is much better with the low conductivity electrolyte and this explains the greater plating rate. This electrolyte gave the best selectivity of all the electrolytes tested, with a maximum R of 2.5. However, the deposit structure was not as good as the higher conductivity electrolyte, with large incoherent nodules occurring at current densities as low as 3.75 A/cm². At this current density, a plating rate of 2.3 μm/sec was achieved.

APPLICATIONS

The purpose of this work is to achieve a full

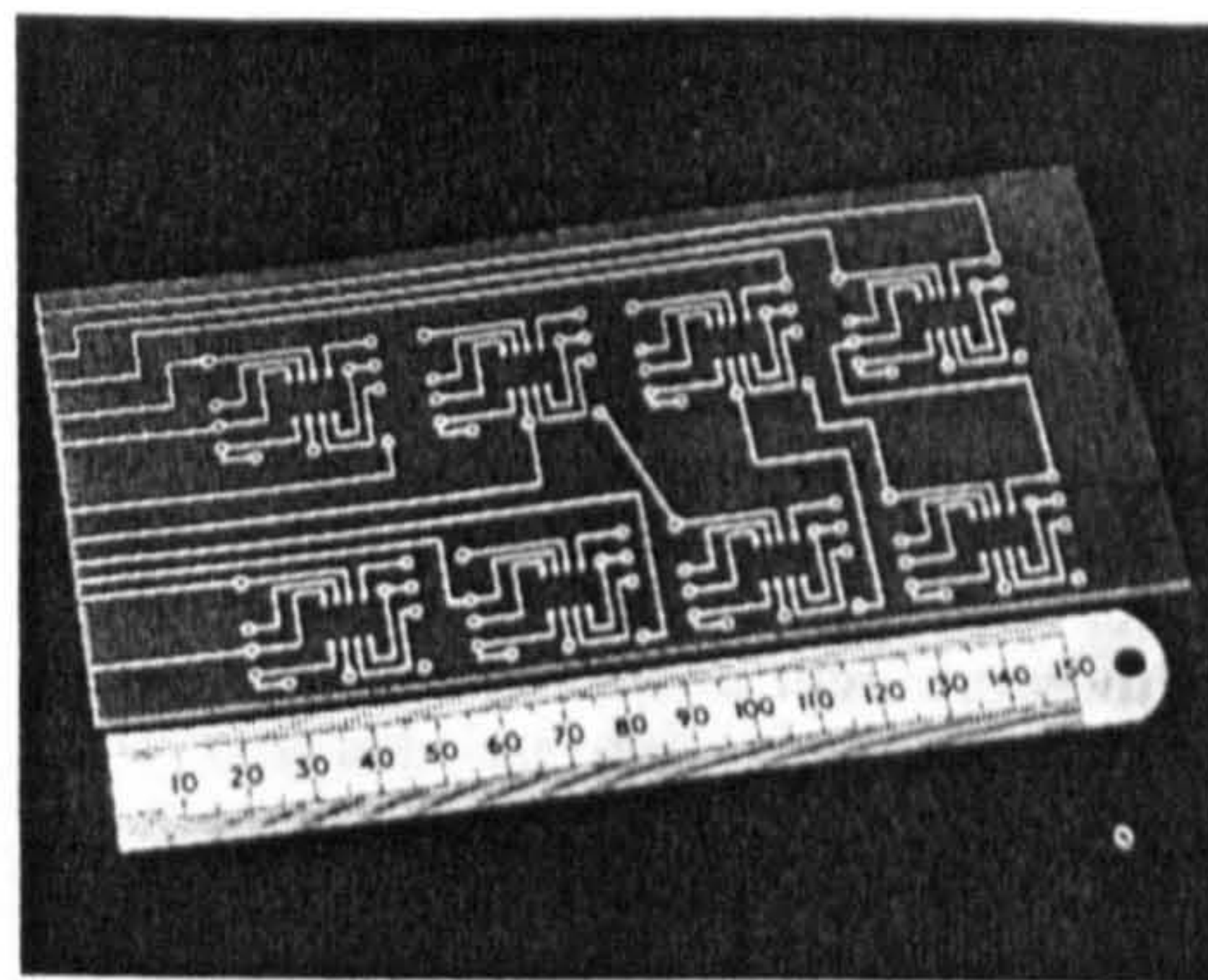


Figure 32. A printed circuit board produced by direct writing on a gold etch resist.

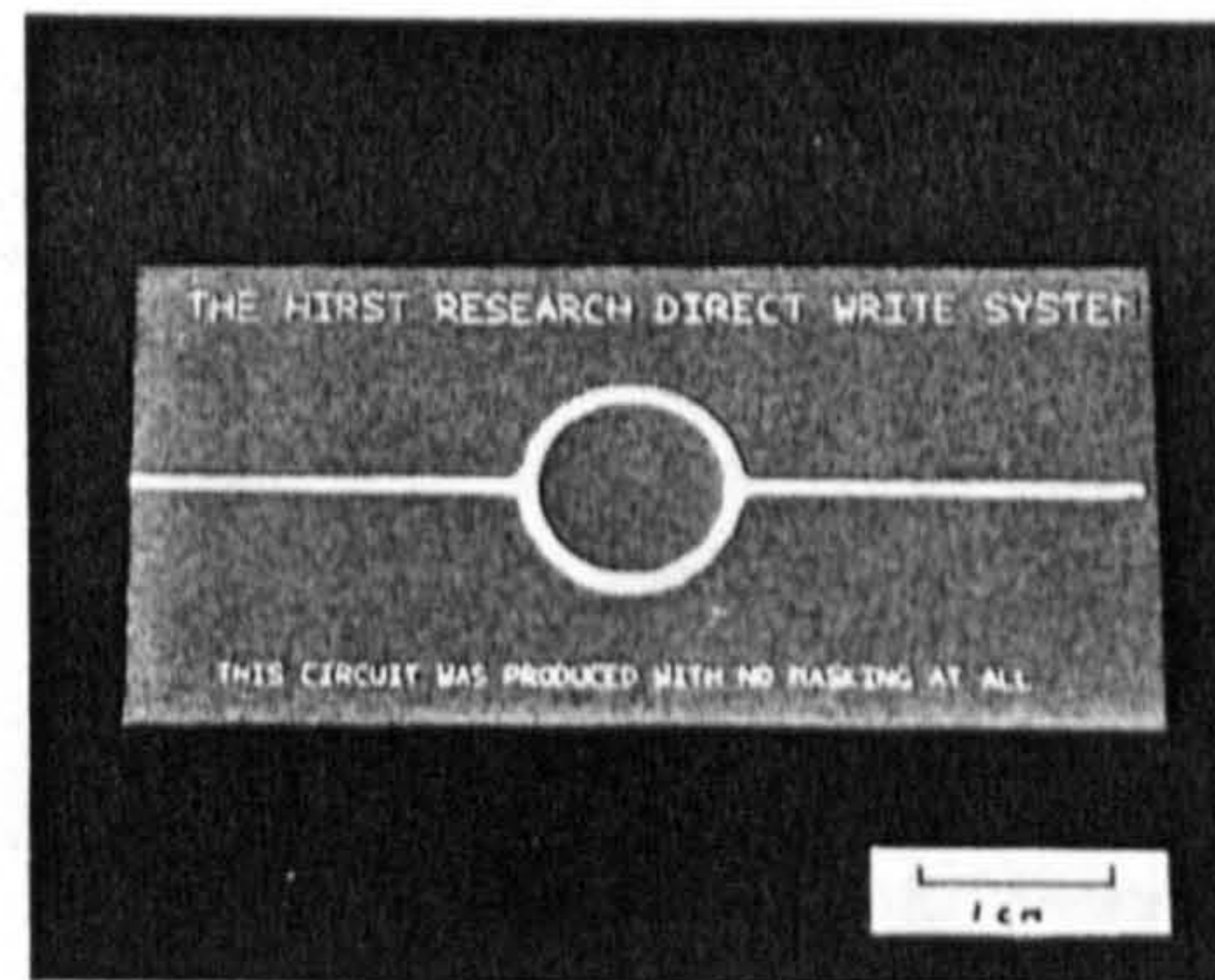


Figure 33. A ring oscillator microwave circuit produced by direct writing.

understanding of how deposition takes place under free flow jetting conditions in terms of useable deposit structures. This will enable the system to be applied to production or prototype processes. Some of the possible applications are listed below.

- 1) The direct writing of etch resist for printed circuit boards.

The possibility of the direct writing of a metal etch resist for PCB prototyping has been examined using gold as the resist metal (Figure 32). The tracks written in this example were 3.6 μm thick and written at a linear velocity of 1.0 mm/sec. Examination of the tracks revealed a very good edge definition even when using a ferric chloride etch. Whilst this process may not lend itself to high volume production work, it is very suitable for prototyping low volume circuit boards direct from a CAD design. Eventually, it is intended to develop a high speed tin electrolyte as an etch resist material.

- 2) The direct writing of Microwave Integrated Circuit Substrates

Microwave Integrated Circuit Substrates are used throughout the telecommunications industry for the mounting of active devices such as amplifiers etc. These are usually made from sintered alumina, quartz or PTFE composites. The circuits are produced by metallising the substrate by sputtering and the tracks are produced in the conventional way by gold electro-deposition, either by the additive or subtractive method. Either way, expensive

photo-lithographic techniques are required. By using direct writing, the latter process is not required as the gold may be directly written onto the metallised substrate from the CAD design. Figure 33 shows a simple ring oscillator circuit produced by direct writing.

- 3) The selective plating of reel-to-reel components.

Large volumes of strip or pressed strip components such as connectors and lead frames are currently produced either by controlled depth immersion or by jet deposition with the components held between rubber masks. The direct write system will enable such components to be produced at very high production rates on a continuous basis without the need for expensive masks as the spread of the deposit is self limiting. The size of the plant and the quantity of electrolyte required will be significantly reduced leading to lower capital expenditure and faster throughput times.

- 4) Bump plating of TAB lands

The electronic industry makes use of thermocompression bonding of thin gold wires from integrated circuits to the lead frame connections within the IC housing. This requires a gold "bump" to be plated onto the connecting leads of the lead frame. At present, this is carried out using either photo-lithography or rubber masks. The jet plating process will allow the production of these "bumps" without the need for masking.

There are a number of other applications of this technique which are company confidential but it may be concluded that any selective plating requirement may be carried out with the direct write jetting technique, even on complicated geometry components and with any metal or alloy, provided that a suitable electrolyte formulation can be produced that allows high speed deposition and is not chemically aggressive to either the substrate or the deposit produced.

CONCLUSIONS

It has been shown that the behaviour of both a simple salt copper sulphate electrolyte and a complexed salt gold electrolyte, behave in a similar way when deposited under high speed jetting conditions. However, the copper electrolyte exhibits a slight chemical attack on the deposits produced by the electrolyte wash.

The factors that influence the maximum useful current densities and thus the maximum plating rates that produce high quality deposits are:

- a) The electrolyte temperature — the higher the temperature, the greater the plating rate. This parameter had the greatest influence on the gold system, presumably because of the reduction in thickness of the diffusion layer. It has yet to be established whether copper electrolytes exhibit a similar temperature dependence.
- b) The electrolyte velocity — the greater the velocity (of Re), the higher the plating rate that can be achieved.

c) The metal ion concentration — increased metal ion concentrations lead to higher plating rates but only up to a certain value. Above this value, no improvement or a reduction in useful plating rates is observed.

Gold deposits are also influenced by the pH of the electrolyte, the most suitable pH was found to be 8.1. A further increase in pH was not tested as alkaline electrolytes are generally unacceptable for electronic applications.

For both systems, the deposit structure undergoes considerable changes in morphology as the current density is increased up to a point where the structure deteriorates due to isolated nodule formation.

The selectivity of the process was not significantly affected by the above parameters with the exception of the current density. Low current densities ($<1.0\text{A}/\text{cm}^2$) show a greater spread of the deposit, although the thickness of the deposit outside the impingement region is very low. As the current density is increased, selectivity is not significantly affected. However, as the current density is increased past the point at which deterioration of the deposit occurs, the growth of the deposit is increasingly influenced by the electric field within the jet and thus growth is limited to within the jet stream.

The selectivity is most influenced by the conductivity of the electrolyte. This is due to the fact that the electrolyte within the wall jet region is extremely thin and therefore has a high electrical resistance. By reducing the conductivity, the wall jet region becomes more resistive and therefore the degree of lateral deposition is reduced.

Maximum plating rates have been established for both systems. For the copper

system, at 25°C , the maximum plating rate was found to be $1.6\text{ }\mu\text{m}/\text{second}$ at a current density of $6.5\text{ A}/\text{cm}^2$ using a 0.8M copper concentration. The measured Reynolds number was 2730. The maximum plating rate for gold using electrolyte [4] at a pH of 8.1 and a temperature of 55°C was found to be $3.4\text{ }\mu\text{m}/\text{second}$. The measured Reynolds number was 12,078.

This work represents the initial results obtained from a longer term study of the High Speed Selective Jet Electrodeposition process. Further analysis of the results and examination of the samples produced is continuing and will be presented at a later date. Work will continue on the enhancement of the plating rates for the gold and other metal and alloy systems.

ACKNOWLEDGEMENTS

The author wishes to thank Mr Ian Gunter, of the Metallurgy Group, Hirst Research Centre, for his invaluable assistance in the design of the control equipment and the computer programming that made this work possible. Thanks also go to staff of the Materials and Components Assessment Laboratory, Hirst Research Centre and the Electron Microscopy Unit of the Loughborough University of Technology for producing the SEM micrographs presented here.

REFERENCES

- 1) US Patent No. 3,810,829, May 1974, James C. Fletcher, NASA.
- 2) R. Haynes, K. Ramachandran & D.J. Fineberg, "The Technique of Fluid Flow Masking Selective Plating", *The Western Electric Engineer*, **22**, 61, (1978).

- 3) J.K. Dorey II, R. Haynes, R.E. Sinitski & R.E. Woods, "Thermocompression Bonding Using High Speed Selective Gold Plating", *Plat. & Surf. Fin.* **67**, 81, (1980).
- 4) W.H. Safranek, "High Speed Electroplating", *Ibid*, **69**, 48 (1982).
- 5) E.J. Watson, "The Radial Spread of a Liquid Over a Horizontal Plane", *J. Fluid Mech.* **20**, 3, 481.
- 6) V.E. Nakoryakov, G.G. Pokusaev & E.N. Troyan, "Impingement of an Axisymmetric Liquid Jet on a Barrier", *Int. J. Heat Mass Transfer*, **21**, 1175 (1978).
- 7) I. Tani, "Water Jump in the Boundary Layer", *J. Phys. Soc. Jpn.*, **4**, 212 (1948).
- 8) T. Tanaka & E. Tanaka, "Experimental Study of a Radial Turbulent Jet", *Bull. JSME*, **19**, 133, 792 (1976).
- 9) H. Schlichting, "Boundary-Layer Theory", 4th ed. McGraw-Hill, New York (1960).
- 10) R.C. Alkire & T-J. Chen, "High Speed Selective Electroplating with Single Circular Jets", *J. Electrochem. Soc.*, **129**, 11, 2424 (1982).
- 11) D-T. Chin & C-H Tsang, "Mass Transfer to an Impinging Jet Electrode", *Ibid.* **125**, 9, 1461 (1978).
- 12) T-J Chen, Ph.D. Dissertation, University of Illinois at Urbana-Champaign, IL (1981).
- 13) C.C. Bocking, "Laser Enhanced and High Speed Jet Selective Deposition" *Trans. IMF*, 1988, **66**, 50.
- 14) R.T. Page, "A Review of Gold Electroplating Solutions — Part 4". *Met. Fin. J.* **20**, 229, 4 (1974).

Edelmetalle–
Moderne Technologien
und Anwendungen

east-report 1991

erstu

european
academy
of surface
technology

schwäbisch gmünd

Hrsg. ZOG Zentrum für Oberflächentechnik
Schwäbisch Gmünd e.V.
Eugen G. Leuze Verlag, Saulgau/Württ.

Best Copy
Available

The High Speed Selective Jet Electrodeposition of Gold

By C. Bocking, F.I.M.F., Wembley, Middlesex (England)

Selektive elektrolytische Strahl-Hochgeschwindigkeitsabscheidung von Gold

Die selektive elektrolytische Strahl-Hochgeschwindigkeitsabscheidung ist ein Verfahren, bei dem eine selektive Abscheidung ohne Abdeckung erfolgt. Das Prinzip besteht darin, daß ein freier Strahl des Elektrolyten mit hoher Geschwindigkeit auf das Substrat aufprallt und dabei ein elektrischer Strom fließt. Durch die elektrochemischen und hydrodynamischen Eigenschaften wird Metall nur an der Aufprallstelle des Strahls und in deren Umgebung abgeschieden. Auf diese Weise wird eine Ausbreitung des Metallüberzugs begrenzt. Ist eine geeignete Anordnung vorhanden, kann der Strahl computerkontrolliert so geführt werden, daß unmittelbar Leiterbahnen und -punkte u. a. gezeichnet werden. Im Aufsatz werden die Faktoren diskutiert, die auf die Abscheidung der Goldschicht Einfluß haben, wie diese aufwächst und wie ihre Ausmaße gesteuert werden können. Ebenso werden Faktoren diskutiert, die die Abscheidungsgeschwindigkeit beeinflussen. Mögliche Anwendungsgebiete werden aufgezeigt.

High speed selective jet electrodeposition is a process whereby metals may be deposited in a selective manner without the need for masking. The principle is that a free standing jet of electrolyte impinges on a substrate at a high velocity and an electric current is passed. Due to both electrochemical and hydrodynamic properties of the jet, metal is deposited only within the impingement region and the immediately surrounding region. In this way, the spread of the deposit is limited. By use of suitable engineering, the jet can be moved under computer control allowing the direct writing of tracks, spots etc. This paper discusses the factors that govern the way in which a gold deposit produced in this way grows and how the dimensions of the deposit may be controlled. The paper also discusses the factors that control the rate of deposition and possible applications of the technique.

Introduction

High Speed Selective Jet Electrodeposition (HSSJE) is a process in which metal may be deposited selectively without the need for masking. The principle of the process is that a free standing, non-submersed jet of electrolyte flowing at a high velocity impinges onto a substrate. The application of a suitable voltage between the substrate (cathode) and the nozzle (anode) causes metal to be deposited within the impingement region and the immediately surrounding region. Due to the properties of the hydrodynamic flow sur-

rounding the impingement region, the electrolyte forms an extremely thin radial layer as it flows away. Because this layer, termed the wall jet region [1], is so thin, the electrical resistance of the electrolyte is comparatively high. This means that under certain conditions, deposition is limited to the impingement region, with little deposition occurring within the highly resistive wall jet region. In this way selectivity is achieved. *Figure 1* shows a schematic view of the electrolyte flow. Due to high electrolyte velocity, high current densities can be applied and therefore high plating rates can be achieved.

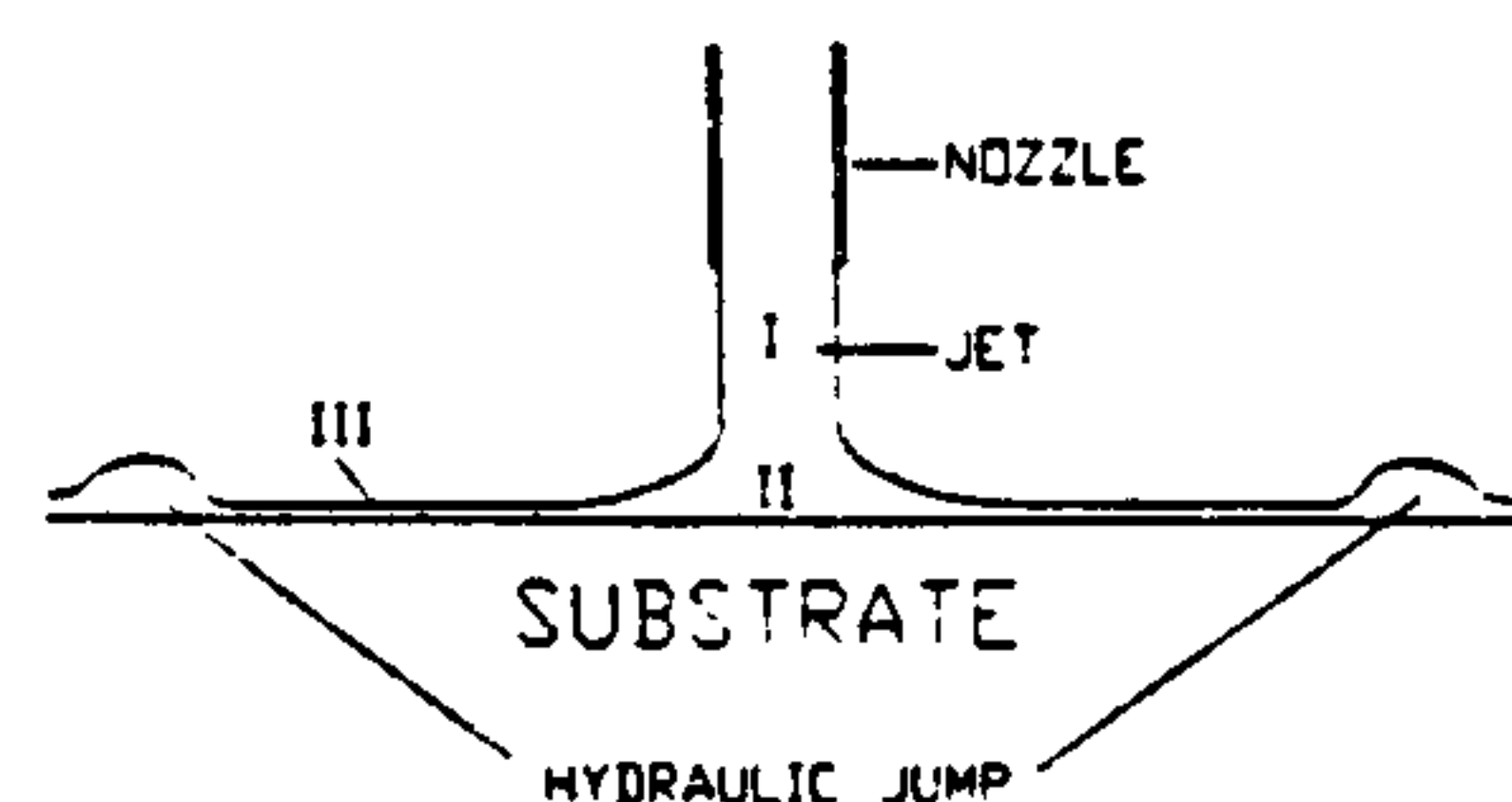


Fig.1: A schematic diagram of the non-submerged jet
Zone I Free jet; Zone II Impingement zone; Zone III: Wall jet

Selective Jet Deposition is not a new process, with the principle being patented by NASA [2] in 1974. This patent described a forced electrolyte flow system in which the nozzle was scanned across the substrate and current applied at appropriate times in accordance with a control pattern. In this way, a plated pattern could be written, much in the same way as a picture is formed on a dot-matrix printer. The process described here however uses a "direct write" system more like the way a plotter produces an image.

Since 1974, there has been comparatively little information published on the subject of HSSJE, possibly due to commercial confidentiality reasons. *Haynes et al* [3] described a forced flow jet plating system in 1978 and *Dorey et al* [4] used a modified version of this equipment to gold plate connectors for the evaluation of the thermocompression bonding characteristics of the deposits. The maximum flow rate used was 39 cm/sec. and current densities of up to 1.3 A/cm². They found that the deposit quality deteriorated at

current densities in the region of 0.86 A/cm^2 by nodule formation. However, it was claimed that nodular deposits did not detract from bondability. There have been a number of papers published attempting to correlate mathematical models of jet plating systems with experimental results [5,6,7,8]. However, little work has been published on the morphological characteristics of deposits produced in this way.

Bocking [9] described selective pure gold deposition using both laser enhanced jet deposition and HSSJE using small bore nozzles (1 mm to 0.25 mm). He examined the morphology of the deposits produced and related these to the electrolyte velocity. The current efficiency of deposition was also described. He went on to show a "direct write" facility whereby the jet could be moved in relation to the substrate by means of a computer controlled X-Y table, producing plated tracks and lines.

The selective deposition of both copper and gold deposits has been described in depth by Bocking [10] focusing on the relationship between deposition and deposit morphology.

This paper describes pure gold desposition using HSSJE. The morphologies of deposits produced are briefly described. The way in which these deposits grow is discussed and the factors that control the dimensions of the deposits are given.

Previous Studies

Previous work by the author [10] had enabled the relationship between the conditions of deposition and the deposit morphologies to be established. It will be helpful to summarise the results of this previous study in order to provide a starting point for the results of this work.

It was found that the deposits produced had a gaussian profile. This shape can be seen in Figure 2 which shows a typical selectivity plot of deposits produced under different conditions. Selectivity is a measure of the deposit thickness within the impingement zone compared with the thickness produced in the wall jet region. The dimensionless distance, R , is the ratio of the radial distance from the centre of the impingement region to the radius of the nozzle. By plotting the thickness against the dimensionless distance, the selectivity under different deposition conditions can be compared irrespective of nozzle size. A dimensionless distance of 1 indicates the end of the impingement region and the start of the wall jet region.

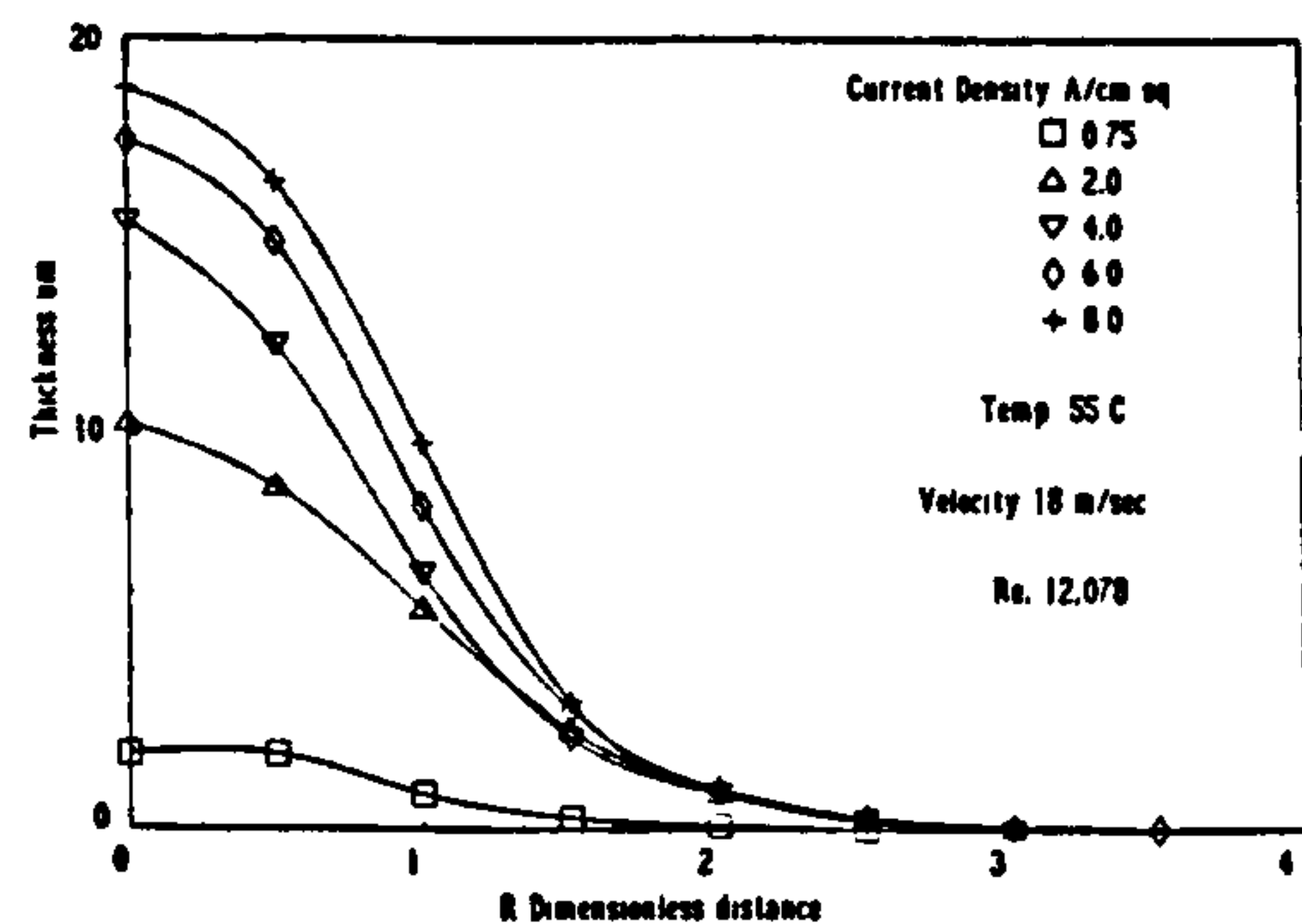


Fig.2: The effect on current density on selectivity, 0.17M citrate gold



Fig.3: Gold deposit produced at maximum usable current density and plating rate
C.D. = 6 A/cm^2 ; 3.4 μm/sec ; pH = 8.1; Temp. = 55°C ; 0.17M citrate gold electrolyte; Re = 12078; Thickness = 18 μm



Fig.4: Gold deposit produced from a citrate gold electrolyte by conventional deposition
C.D. = 5 A/cm^2 ; 0.06M gold; Thickness = 18 μm

Where thickness measurements are quoted, these refer to the thickness at the centre of the impingement region. Unless otherwise stated, the nozzle diameter used was 0.4 mm. Current densities quoted are based on the surface area of the impingement region only i.e. on the surface area of the cross section of the jet. The spots were all produced using a total charge of 0.03938 ± 0.00008 coulombs each. The maximum plating rate that produced acceptable deposits was $3.4 \mu\text{m/sec}$. at a current density of 6.0 A/cm^2 using a 0.17M citrate gold electrolyte at pH 8.1. Figure 3 shows an example of a gold deposit produced under the above conditions. For comparison, a conventional gold deposit of the same thickness is shown in Figure 4.

1. The effect of current density, temperature and Reynolds Number

The structure and spread of the deposit is significantly affected by the current density. At low current densities ($< 1.0 \text{ A/cm}^2$) the deposits were found to have a poor selectivity and low thickness. Deposits were up to 11 mm in diameter but had thickness in the region of about $1 \mu\text{m}$ or less within the impingement region, reducing to less than $0.1 \mu\text{m}$ in the wall jet region. This thickness reduction appears to be asymptotic. At higher current densities, ($> 2.0 \text{ A/cm}^2$) the selectivity was improved with a diameter of between 1.1 and 1.2 mm, depending on the precise conditions. Thicknesses were in the region of $18 \mu\text{m}$, again depending on the precise conditions used. Figure 5 shows the effect of current density on the current efficiency. At low current densities the efficiency is low (approx 40%) but increases to about 70% with increasing current density. Neither temperature or flow rate had much effect on the selectivity.

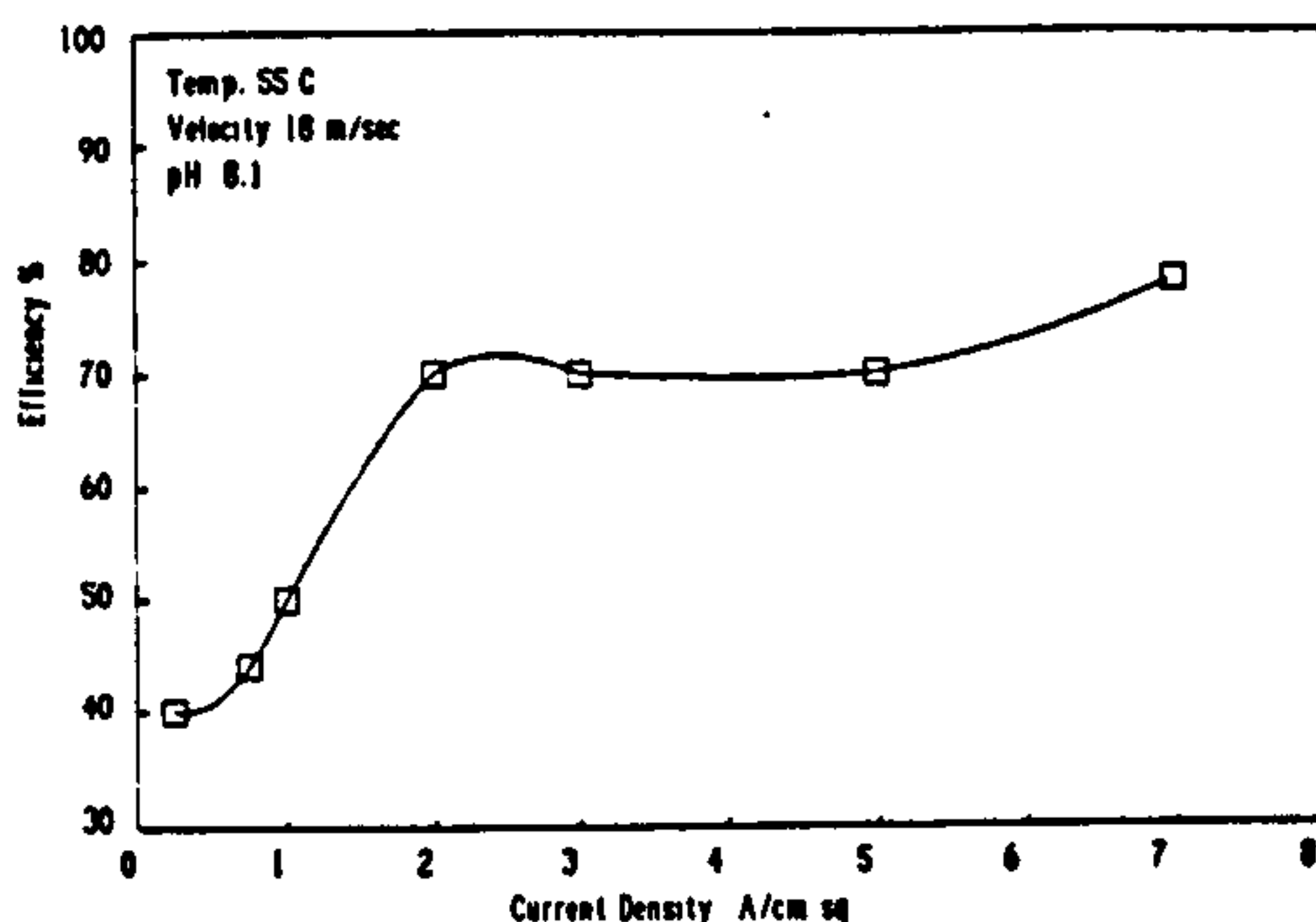


Fig.5: Current efficiency vs current density; 0.17M citrate gold

Figures 6 to 8 show morphological diagrams for the 0.28M citrate gold system. These relate current density to Reynolds Number, (dV/v) a dimensionless measure of electrolyte flow, where d = the nozzle diameter in cm, V = the electrolyte velocity in cm/sec and v = the kinematic viscosity in cm^2/sec . It can be seen that the structure of the deposit is

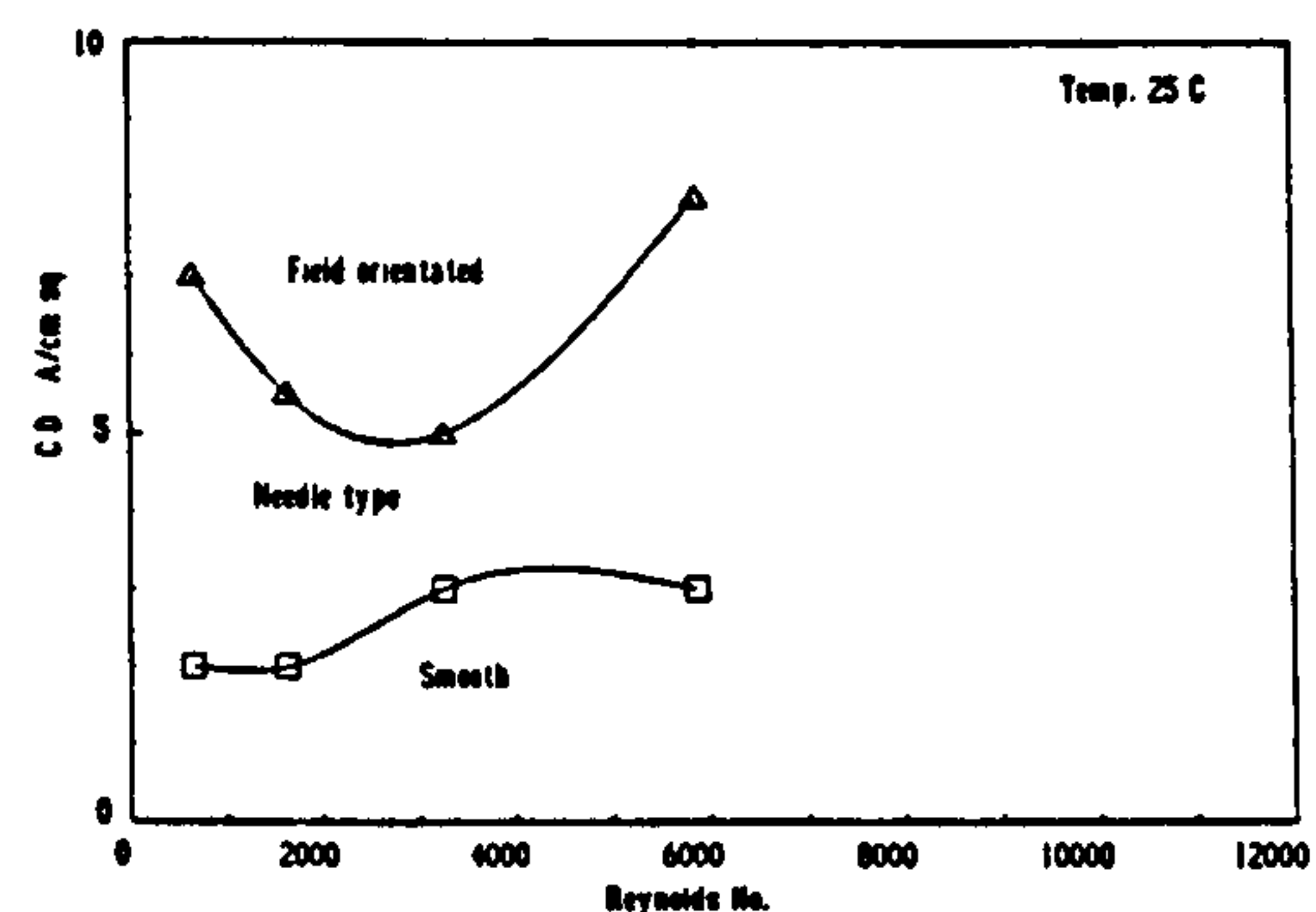


Fig.6: Morphological diagram for 0.28M citrate gold. Temperature 25°C

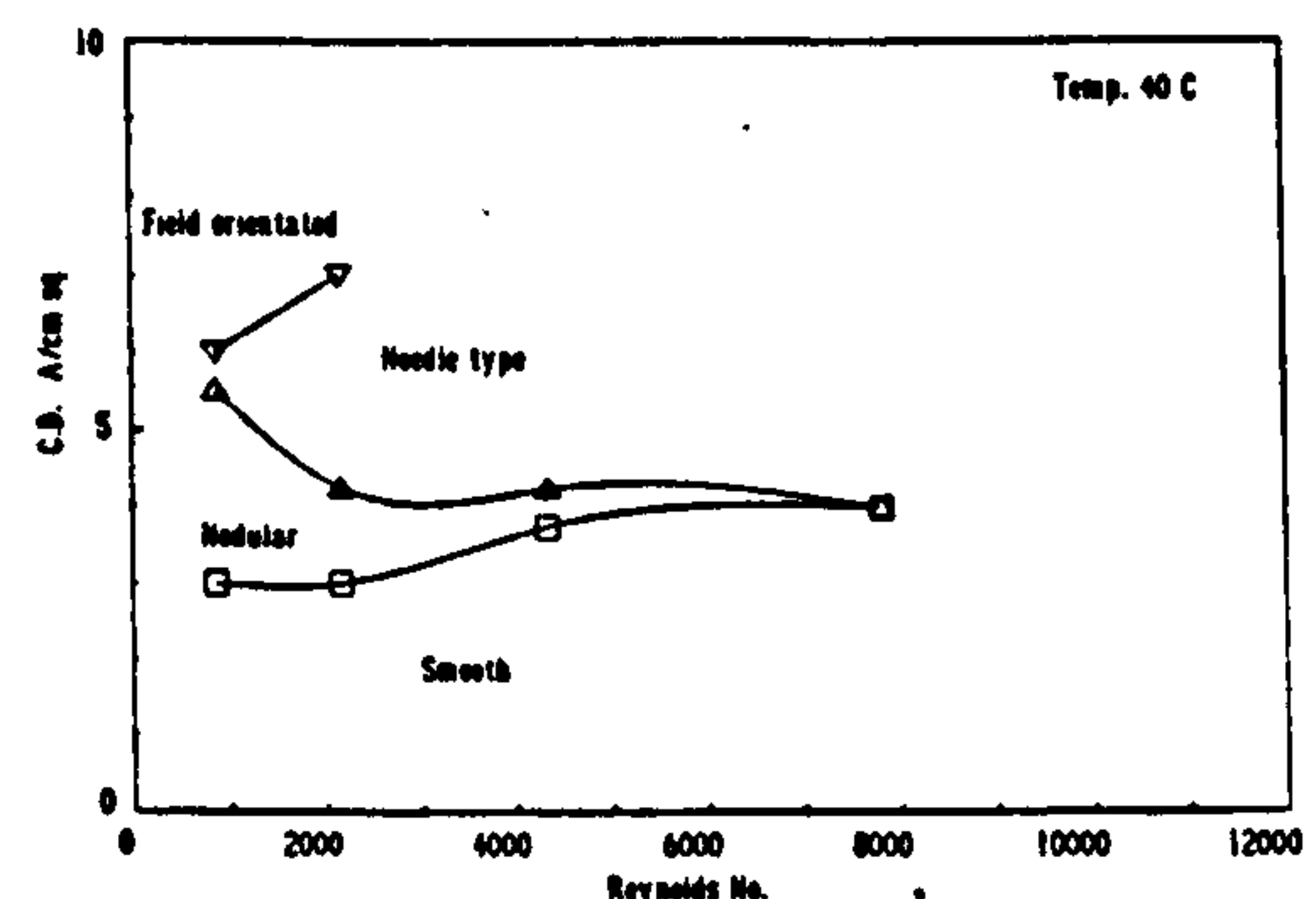


Fig.7: Morphological diagram for 0.28M citrate gold. Temperature 40°C

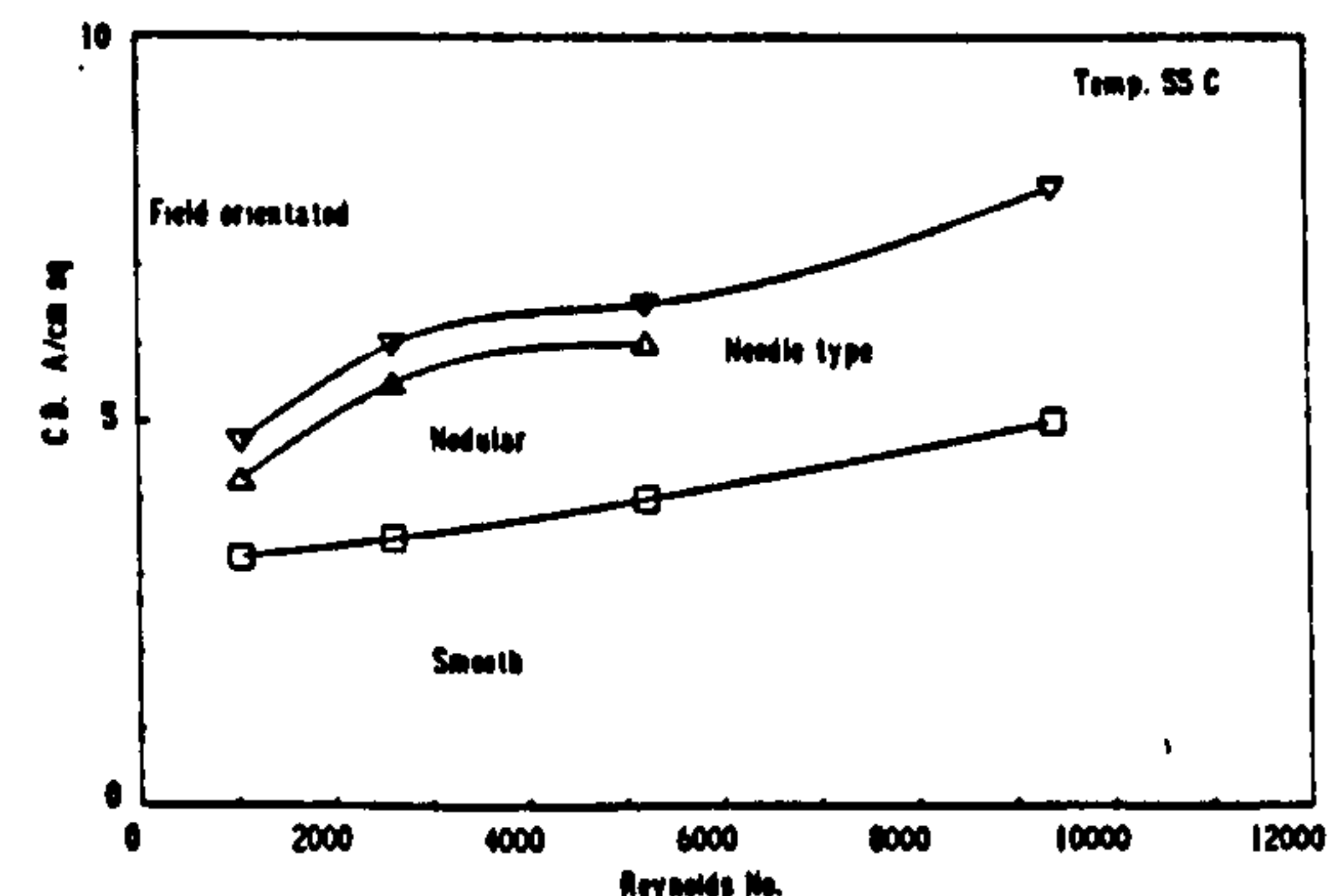


Fig.8: Morphological diagram for 0.28M citrate gold; Temperature 55°C

very dependent on the current density, temperature and flow rate. High flow rates and temperatures allow high current densities that still enable smooth, pore free deposits to be produced. However, it was noticed that at very high flow rates or Reynolds Number, the maximum current density was slightly reduced.

2. The effect of gold concentration

It was found that increasing the gold concentration of the electrolyte increased the maximum current density and thus the plating rate at which smooth deposits could be produced. However, at concentrations much above 0.17M, the maximum current density and plating rate was reduced slightly. Selectivity was not significantly affected by the gold concentration.

3. The effect of conductivity

Electrolyte conductivity influenced both the selectivity and the structure. Reducing the conductivity by half improved the selectivity such that the deposit diameters were in the region of 0.9 mm. However, the deposit structure deteriorated at much lower current densities and a maximum plating rate of only $2.9 \mu\text{m}/\text{sec}$ could be achieved.

4. The effect of pH

The effect of pH was studied over the range 5.3 to 8.1. It was found that at the higher pH, slightly higher plating rates could be

achieved with a small improvement in deposit structure.

5. The effect of nozzle to substrate distance

For most of the experiments, the nozzle to substrate distance was maintained at 1 mm. However, decreasing this distance improved the selectivity slightly. Increasing the distance had little effect on selectivity but the morphology of the deposit altered. The deposit became more nodular towards the wall jet region and random needles appeared oriented in the flow direction.

For any particular set of conditions, it was found that the overall deposit width was reproducible to better than $\pm 1.8\%$.

In order to establish a means of improving the deposition rate further, it was necessary to have, at least, an empirical understanding of the way in which the deposit grew and more importantly, the reasons for the deterioration of the deposit when higher plating rates than the current optimum were attempted. Part of this work attempts to establish an empirical mechanism of growth and deterioration of gold deposits.

Experimental

A complete description of the equipment used has been given in a previous paper [10]. However, a schematic diagram of jet plating system is shown in Figure 9. The nozzle con-

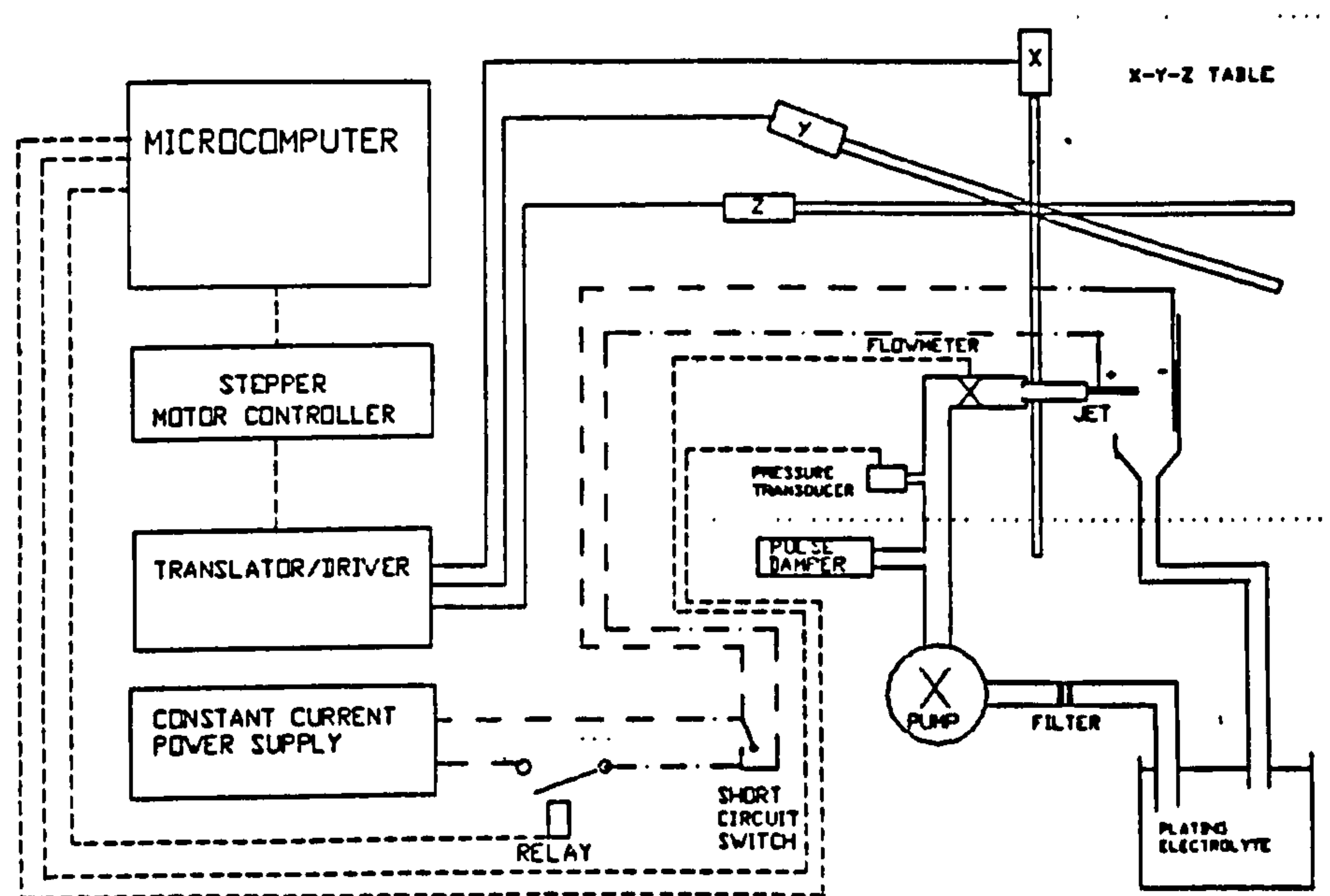


Fig.9: Schematic of jet plating unit

sisted of a 400 μm platinum tube sealed into a lead-soda glass tube. The nozzle was fitted to a computer controlled X-Y table. This allowed electrodeposited spots to be produced on a single substrate on a step and repeat basis. The computer also controlled the magnitude of the currents and times of deposition, allowing a large number of deposits to be produced under different conditions automatically. The control program also enabled computer aided design (CAD) plot files to control the X-Y table allowing complex designs to be directly written by electrodeposition.

The deposits were produced either on polished, nickel plated substrates with a 0.1 μm gold flash (to prevent immersion deposits) or onto glass substrates sputtered with chromium/gold conducting layers.

A series of deposited spots were produced at current densities of 6, 7 and 10 A/cm^2 for different times, between 0.05 seconds and 10 seconds, on the sputtered glass substrates with Reynolds numbers of between 3355 and 12078. This gave a representation of the growth mode of the deposits with respect to time. The electrolyte formulation used for the current work is given in Table 1.

The thicknesses and profiles of the electrodeposited spots were measured using a *Sloan Dektak 3030 Surface Profilometer*. The crystallographic orientation was measured by X-ray diffraction. Examination of the deposits was carried out by means of optical microscopy and Scanning Electron Microscopy.

Polarisation measurements were carried out using a *Wenking HP72 potentiostat* and a pulse generator. The working electrode was a 400 μm diameter copper wire embedded in an epoxy block so that only the end face of the wire was exposed. Adjacent to this was a

platinum wire, 200 μm in diameter also embedded and separated from the working electrode by a distance of 100 μm . This acted as the reference electrode. Prior to measurements, both the working electrode and the reference electrode were polished and pre-plated with gold at current density of 5 mA/cm^2 for 2 minutes. Whilst this type of reference electrode was not ideal due to its poor reversibility in the system under study, it was justified by the necessity to use a small diameter, flush mounted reference so that the flow patterns were not disrupted.

Polarisation curves were produced by sampled current pulse voltammetry at different electrolyte velocities. Because the deposit growth was so rapid at these high current densities, conventional steady state polarisation techniques could not be used. It was found that a steady state condition could be achieved within 20 to 40 milliseconds under jetting conditions. A series of potential pulses of 40 milliseconds duration were applied and the current measured at the end of each pulse. The substrate was re-polished and re-plated prior to each measurement. Prior to the application of the pulse, a pre-electrolysis for 30 seconds at 0.3 volts vs the gold reference electrode (GRE) was applied.

Results

Deposit Morphology

Figures 10a to 10e show a typical range of structures produced by the jetting process. Lower flow rates and temperatures also affected the type of structure but they all followed a typical pattern. At low current densities ($< 1.0 \text{ A}/\text{cm}^2$) the deposits were of a plate-like structure as in Figure 10a. As the current density was increased, the deposits adopted a closed, pore free structure with few surface features. Higher current densities

Table 1: Electrolyte formulations

[1]	Gold (as potassium gold cyanide)		54.0 g/l (0.28M)
	Diammonium hydrogen citrate		45.0 g/l
	Citric acid		15.0 g/l
	Potassium hydroxide		to pH 6.0
	Kinematic viscosity	25°C	0.012284 cm^2/sec
		40°C	0.009221 cm^2/sec
		55°C	0.0076567 cm^2/sec
[2]	Gold (as potassium gold cyanide)		33.5 g/l (0.17M)
	Diammonium hydrogen citrate		45.0 g/l
	Citric acid		15.0 g/l
	Potassium hydroxide		to pH 8.1
	Kinematic viscosity	55°C	0.005906 cm^2/sec

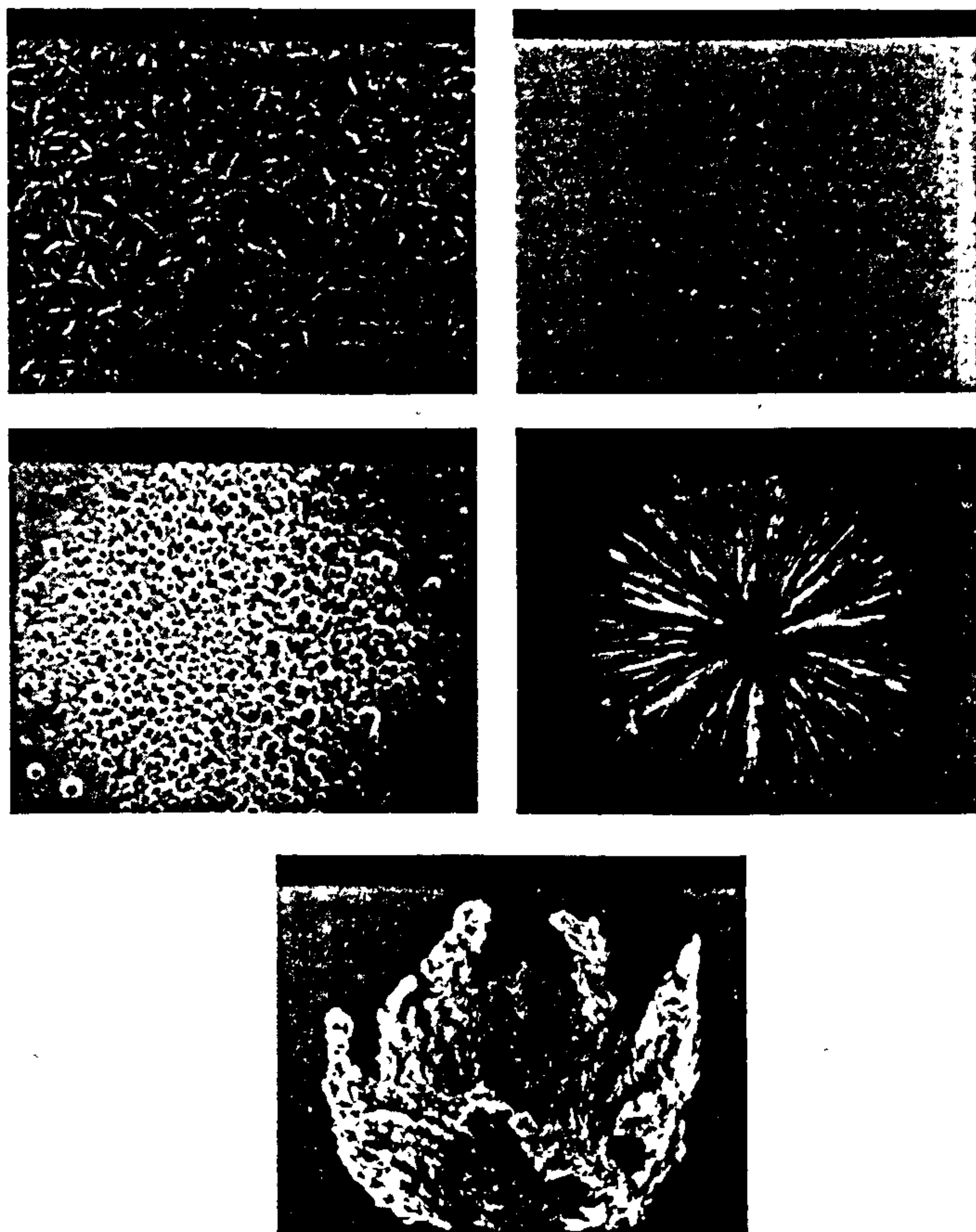


Fig.10: A typical range of structures produced in ascending order of current density. Whilst the deposits were produced under different sets of conditions, they present the growth changes as the current density is increased for any single set of conditions

produced a surface with smooth hemispherical mounds of low amplitude. As the current density was increased further, the deposits showed an enhanced growth at certain sites as some of the rounded structures grew faster than their neighbours creating a cauliflower like appearance. Increasing the current density further, or reducing the flow rate caused these nodules to act as precursors for the growth of needle like structures that grew in the direction of flow, particularly towards the edge of the impingement zone. Still further increase in current density led to growth of dendritic structures in the direction of the electric field along the wall of the electrolyte jet. Lowering the temperature caused an increased rate of nodule and needle formation at lower current densities.

The series of deposits produced with increasing time show this pattern of growth develop. *Figures 11a to 11d and 12a to 12f* show typical deposits produced at 7.0 A/cm^2 and 10 A/cm^2 for increasing deposition times. Both samples show that certain sites produced faster growing nodules. Depending on the current density, these then developed into either needle like structures in the radial flow direction or field oriented dendrites in the direction of the jet in the case of the higher current density. The lower current density samples simply produced larger nodules that eventually became powdery and non-adherent. At low temperatures, dendritic growth was less field oriented and adopted a finer, filamentary structure as in *Figure 13*.

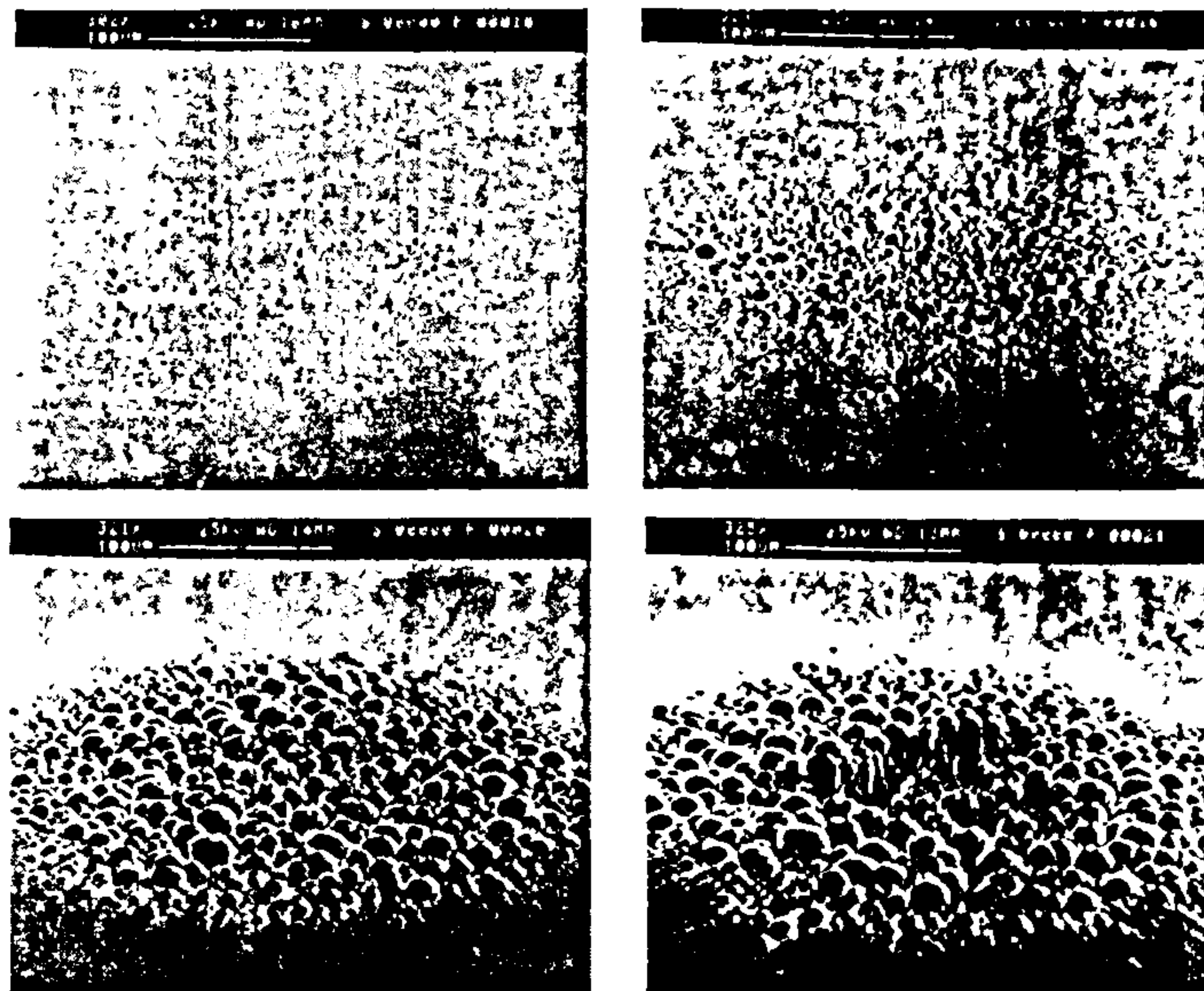


Fig.11: The growth of deposit with increasing time
C.D. = 7 A/cm²; Re. = 3335; (a) 1.5 secs. (b) 3.0 secs (c) 3.5 secs.; (d) 5.0 secs.; 0.17M citrate gold

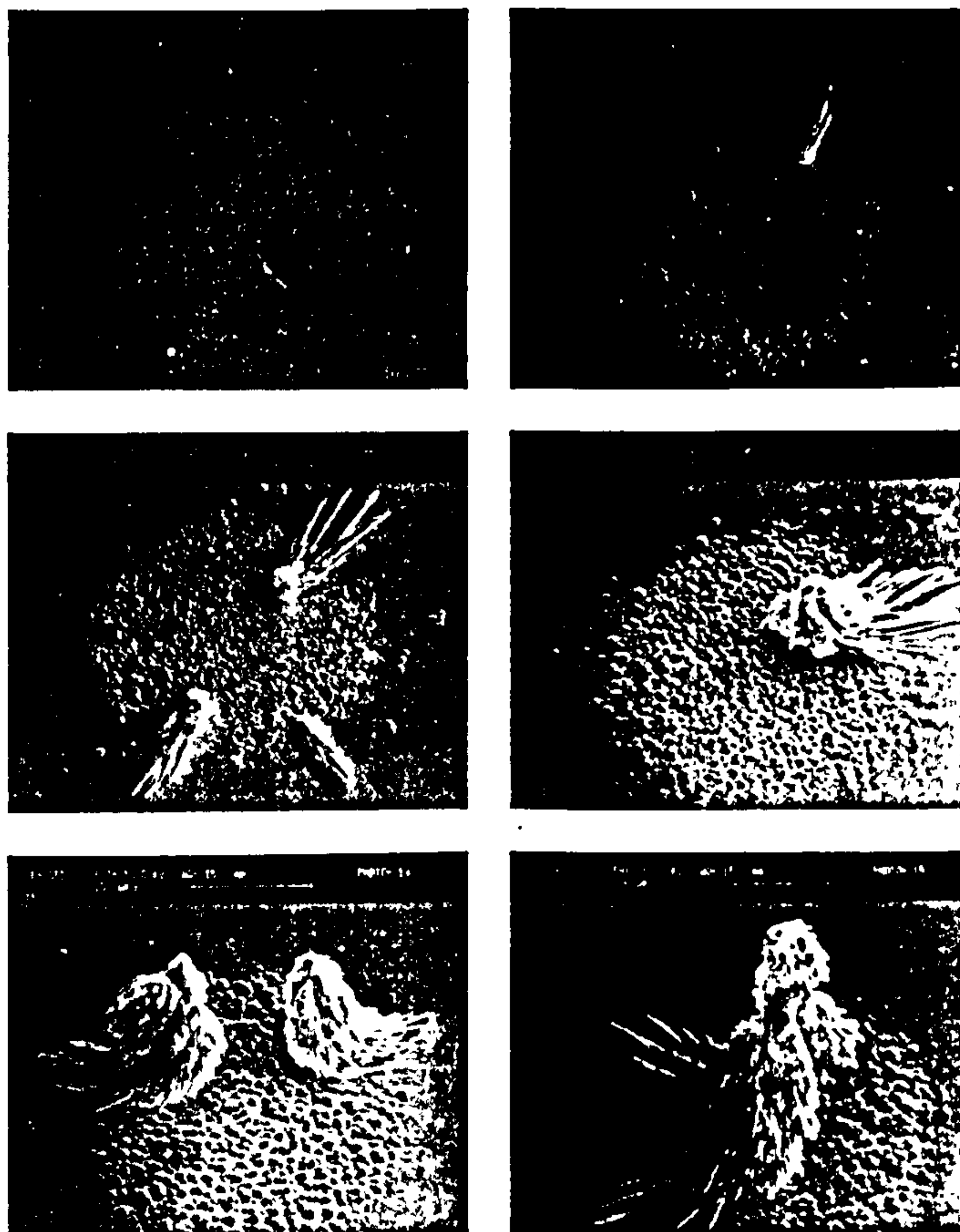


Fig.12: The growth of the deposit with increasing time
C.D. = 10 A/cm²; Re. = 12078; (a) 0.6 secs. (b) 1.5 secs. (c) 2.0 secs. (d) 3.5 secs. (e) 6.0 secs.; (f) 8.0 secs. 0.17M citrate gold

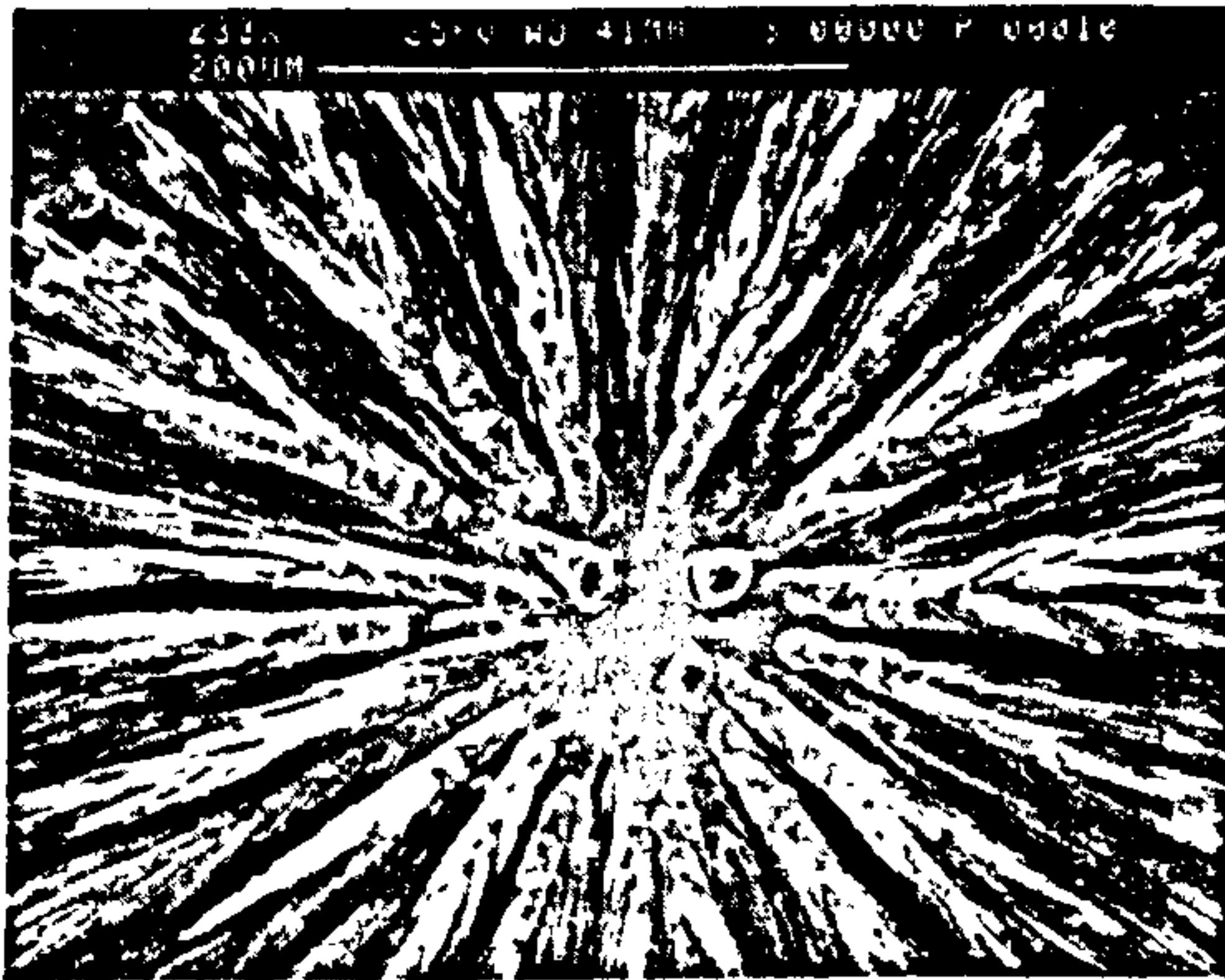


Fig.13: Deposit produced at low temperature
 C.D. = 4.75 A/cm²; Re. = 5686; 0.28M citrate gold electrolyte

Polarisation Studies

Figure 14 shows the polarisation curves for a 0.17M citrate gold at velocities of 2, 10 and 20 m/second. It can be seen that at a velocity of 20 m/second, up to a current density of 2 A/cm², deposition proceeds under activation control. The Tafel slope is -355 mV/dec. Above this value, mixed activation and diffusion control occurs. No clearly defined limiting current is observed. This could be due to the fact that hydrogen evolution competed with gold deposition and the limiting current plateau was hidden or that mass transfer within the jet was so high. However, it can be seen that the deposit began to deteriorate in the mixed control region. This applied to the other velocities except that deterioration occurred at lower current densities.

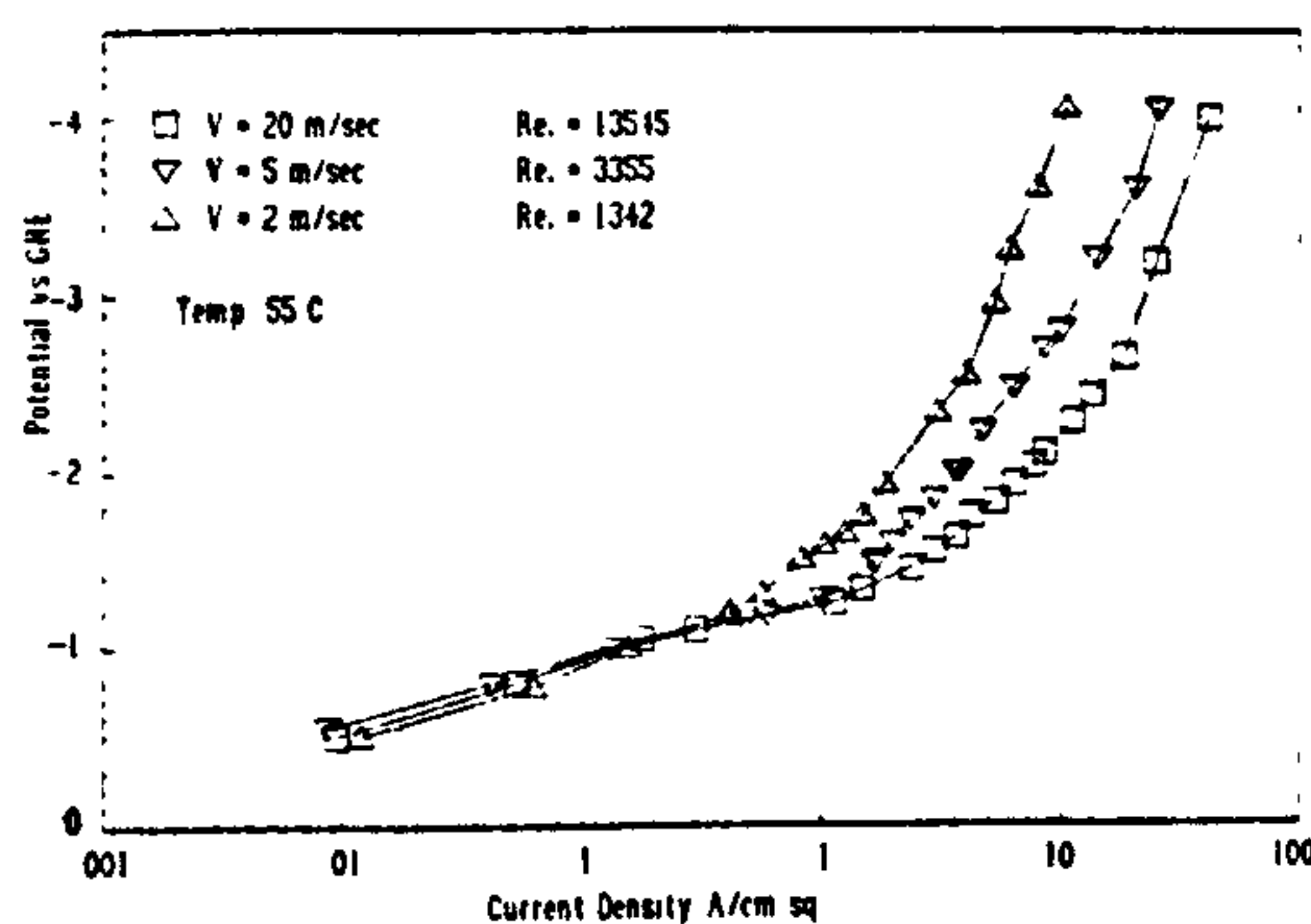


Fig.14: Polarisation curves for a 0.17M citrate gold,
 Temp. = 55°C

X-ray diffraction Studies

X-ray diffraction studies showed that over the current density range of between 0.75 to 7.0 A/cm² and a Re. of 12078, there was no

evidence of preferred orientation of the deposit. Under these conditions, no needles or dendrites were produced. Figure 15 shows a typical diffraction pattern. Deposits produced at higher current densities showed evidence of a decreasing grain size with increasing current density, the maximum grain size occurring at a current density of 0.75 A/cm².

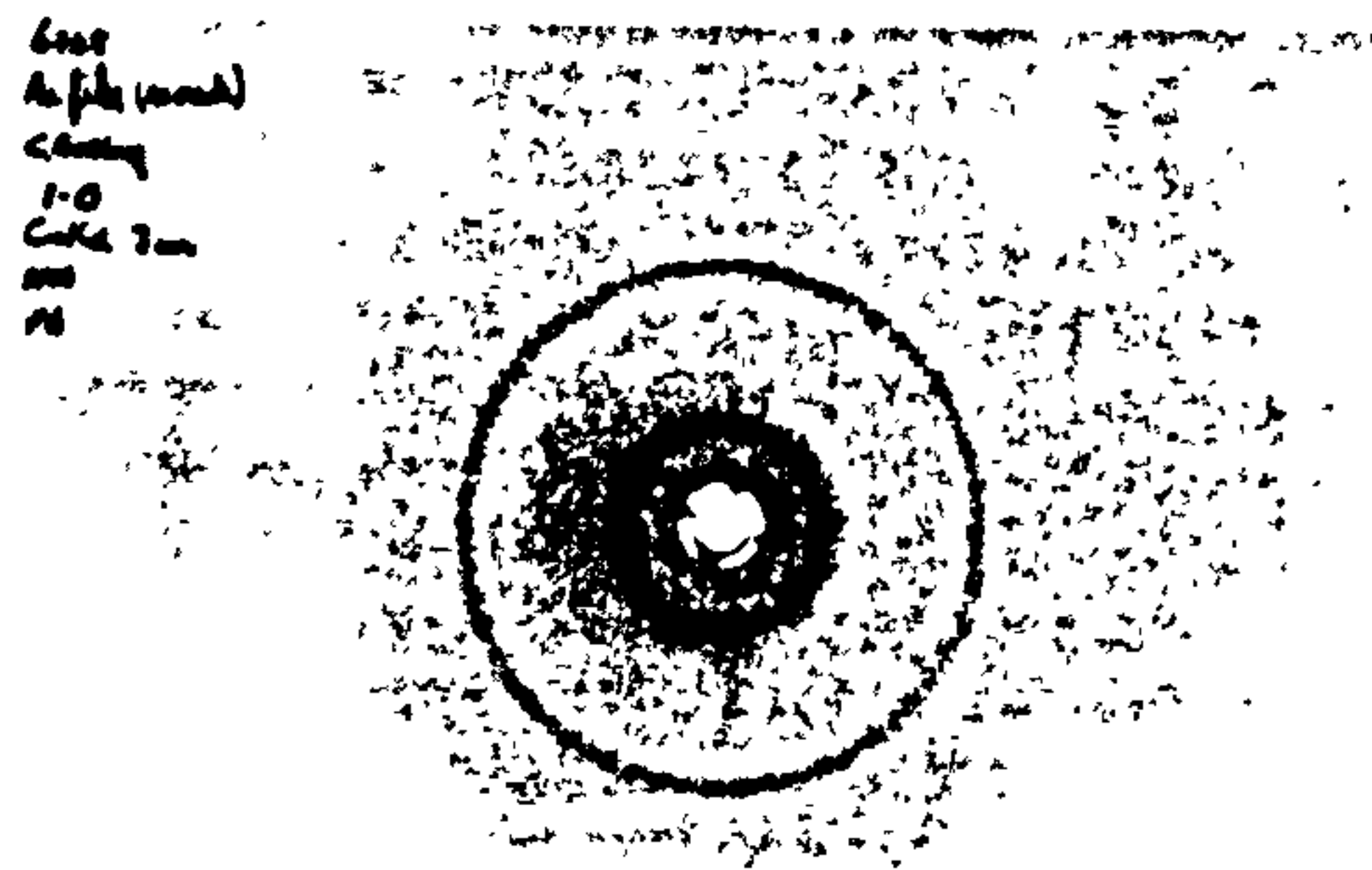


Fig.15: A typical x-ray diffraction pattern produced
 by jet electrodeposited spots
 C.D. = 1 A/cm²

Discussion

Based on the evidence obtained to date, a mechanism of growth and deterioration of the deposits could be postulated. It is beyond the scope of this paper to develop a rigorous mathematical model of the growth mechanisms involved. However, a possible mechanism could be empirically developed. At low current densities (< 1.0 A/cm²) the mechanism of growth was similar to conventional gold. Because the deposit spread was so great at these low current densities (up to 11mm diameter) it is reasonable to assume that the true current density was much lower than that based on the impingement zone area. This was confirmed by the marked similarity to conventional deposits of gold of similar thickness that have been published previously. It is likely that the spread observed here was due to the long time periods used to pass the required number of coulombs (up to 140 seconds). This allowed a build up of deposit beyond the impingement zone. However, it must be remembered that this surrounding deposit was extremely thin (< 0.1 μm). It can also be seen from the efficiency measurements that secondary reactions such as oxygen reduction and hydrogen evolution were occurring.

As the current density was increased above 1.0 A/cm², all of the deposition occurred wi-

thin a region of 3 times the jet diameter, the actual spread depending on the prevailing conditions of deposition. Most of the deposition occurred within the impingement zone. The deposits produced at these higher current densities showed a slight hemispherical surface texture. It can be seen from *Figure 14* showing the polarisation curves that in the case of the curve corresponding to a Reynolds number, Re , of 13545 that deposition assumed mixed activation-diffusion control at a current density of about 2.0 A/cm^2 . Lower Re values showed this transition at lower current densities.

The structure of these deposits also indicated that the mode of growth was by 3D nucleation. It can clearly be seen in *Figures 11c* and *11d* that fresh nucleation occurred on existing grains forming a cauliflower-type structure. This type of nucleation generally occurs at high overpotentials in the region of mixed activation/diffusion control. The polarisation curves show that relatively high overpotentials are required to achieve the current densities applied and that deposition is occurring under mixed control.

X-ray diffraction studies showed that there was no evidence of preferred orientation in the samples examined. However, these samples did not include any deposits exhibiting needles or dendrites, which have a strong preferred orientation. It is well known that certain crystallographic planes tend to grow faster than others. Inspection of *Figures 11a* to *11d* showed that some nodules grew faster than others. It can be seen in *Figure 11a* that nodulation was particularly prevalent in the region of surface imperfections such as scratches etc. This is not surprising as these sites presented the lowest energy requirements for nucleation and subsequent growth. It was at these sites that growth occurred most rapidly, at least in the initial stages. Above a critical ratio of flow rate to current density, the growth of these nodules was accelerated, especially those towards the edge of the impingement zone. To understand the reason for this, it is necessary to understand the behaviour of the flow and the diffusion layer during deposition under these conditions.

The hydrodynamics of an impinging free jet on a surface normal to the flow has been described by several authors [1, 11, 12, 13]. In brief, when the jet hits the surface, the flow decelerates rapidly in the axial direction and accelerates in the radial direction forming the wall jet. This gives rise to a region where a viscous boundary layer of constant, but low,

thickness occurs in the centre of the impingement zone. This is known as the stagnation region as axial flow is negligible. Dawson [14] has estimated the transition between the stagnation zone and the wall jet to be $x/d = 4$, where x = radial distance from the centre of the jet and d = the jet diameter. In the present case, this transition occurred at $r = 50 \mu\text{m}$. Beyond this region, the boundary layer thickness increased until it obtained the thickness of the wall jet. At this point, the hydraulic jump [12] occurred.

The behaviour of the diffusion layer is complex under these circumstances. Although a measure of the thickness of the diffusion layer cannot be made directly, as the value of the limiting current density, i_L , could not be obtained, a maximum value can be estimated approximately from the polarisation curve. At a Reynolds number, Re , of 13545, high quality deposits are obtained up to a current density in the region of 6.0 A/cm^2 . It is known that deposits produced above the limiting current are dendritic or powdery and non-adherent. Therefore, if a value of 7.0 A/cm^2 is taken arbitrarily as the limiting current, the thickness of the diffusion layer can be found from a derivation of Ficks first law of diffusion;

$$\delta = \frac{nFDC_b}{i_L}$$

where n = valency of Au, F = the Faraday constant, D = the diffusion coefficient in cm^2/sec , C_b = the bulk concentration of Au in mol/cm^3 and i_L = the limiting current density in A/cm^2 and δ = the diffusion layer thickness in cm. The effect of migration has been ignored but as the gold is in the form of an anion, the net effect would be negative. For the purposes of this approximation, the diffusion coefficient of $1.68 \times 10^{-5} \text{ cm}^2/\text{sec}$ at 60°C as given by Cheh, has been used. This value was evaluated from a citrate type gold electrolyte with a gold concentration of 0.007M . It is known that an increase in concentration decreases the value of D but this is relatively small and will be ignored in this instance. Values of D for the concentration of gold being used are being estimated at present. Under the conditions specified, the maximum diffusion layer thickness would be $4 \mu\text{m}$. However, this value is likely to be high because of the arbitrary choice of the limiting current value and the high value of D . Realistically, a diffusion layer thickness of closer to $2 \mu\text{m}$ is more likely.

Whilst a fast growing nodule exists within the diffusion layer, its growth will be controlled by planar diffusion. Its growth will be enhanced slightly by the fact that its local

current density will be higher than the surrounding deposit. If the nodule penetrates the bulk diffusion layer, a local diffusion layer will develop around it. If the radius of the nodule is much less than the thickness of the local diffusion layer, then a regime of spherical diffusion will take over. As spherical diffusion occurs at several orders of magnitude faster than planar diffusion, then the growth of the nodule will be accelerated even further. As the nodule grows, the field intensity will increase and the local current density will increase, accelerating growth even further. On penetrating the static hydrodynamic boundary layer, the nodule will disrupt the flow, causing a local increase in turbulence in its wake. This will lead to a further increase in diffusion in the direction of the flow. In this way, a structure such as that seen in *Figure 10d* will develop. Examination of the structures shown in *Figures 12b, c and d* showed that some nodules exceeded a height of $3\ \mu\text{m}$ whilst others have enhanced growth to the point of needle formation.

If the current density is sufficiently high, then as a fast growing nodule penetrates the diffusion layer, the deposit will grow in the direction of the electric field and thus will grow in the axial direction of the jet along the jet wall as well as the radial direction. Such growths are dendritic in nature and the structure assumes a crown-like appearance as in *Figure 10e*. Current densities higher than those that produce this latter structure lead to a second type of field oriented growth where the dendrite or dendrites grow within the central core region of the jet. Whilst the main growth front will be towards the nozzle, semi-radial needles will grow in the direction of the flow towards the surface for the same reasons as described above. This will give rise to a structure as seen in *Figure 12f*. This behaviour arises when a radial needle grows adjacent to and above the stagnation region and into the flowing central core of the jet. Residual radial needles can be observed adjacent to these field orientated growths. In many of the examples shown, it will be noted that in the stagnation region, there is no flow directional growth apparent. The radius of this region is about $50\ \mu\text{m}$ and supports the claim of Dawson of the dimension of the transition between the stagnation region and the wall jet as mentioned previously.

Temperature and metal ion concentration also influence the morphology as they both influence the diffusion coefficient and thus the limiting current density. Small differences in morphology have been recognised at lower

temperatures and concentrations but these are not important for the empirical model described here.

With an understanding of the way in which the deposit deteriorates, ways of increasing the usable current densities and therefore plating rates may be investigated.

Applications

High Speed Selective Jet Electrodeposition has numerous potential applications. It can be applied to any situation where selective deposition is an important requirement. Some possible applications are described below.

1) The direct writing of Microwave Integrated Circuit Substrates (MICS).

MICS are used extensively throughout the telecommunications and defence industries for mounting active devices such as amplifiers, delay lines etc. These can be made from sintered alumina, quartz or PTFE composites. The substrates are metallised using sputtering or electroless plating and circuit tracks are produced either by the additive or subtractive routes using photolithographic methods. These processes are expensive. However, by using the direct writing facility, the circuits can be written without the need for masking directly from the CAD designs. The thin seed layers can then be removed by etching with virtually no attack on the written gold layer. *Figure 16* shows a simple ring oscillator produced by direct writing.

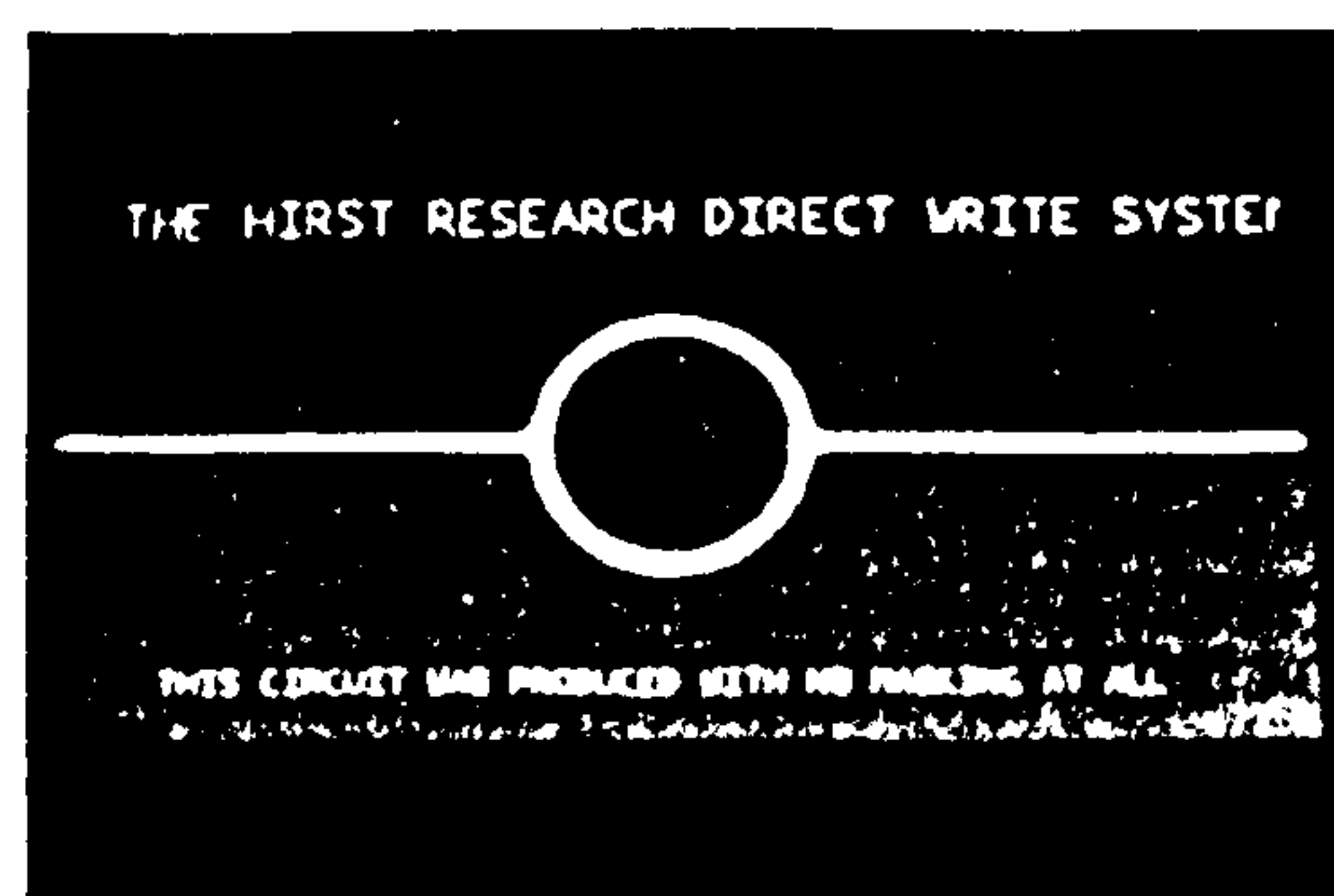


Fig.16: An example of a directly written microwave ring oscillator on an alumina substrate

2) The selective plating of reel to reel components.

Large quantities of strip or pressed strip components such as connectors and lead frames are currently being produced either by controlled depth immersion or by submersed jet deposition with the reel being held between

either fixed or moveable rubber masks. The direct write system will enable such components to be produced at very high production rates without the need for the rubber masks. The size of the plant required and the volume of electrolyte will be considerably reduced, thus reducing the capital expenditure and reducing throughput times. Hard gold is used in the majority of reel-to-reel processing and work to develop hard gold solutions suitable for jet plating is currently being undertaken.

3) Bump plating.

Tape Automated Bonding is a technique that is acquiring importance in the electronics industry. The process consists of the production of lead frames on a metallised plastic strip, similar to a 35 mm photographic film. In order to connect the integrated circuits to the lead frames, ultrasonic bonding of gold or aluminium wires is used. To facilitate this, a gold bump is required at the end of each lead. There are a number of difficulties in using a photoresist technique for this. However, selective jetting can overcome many of these problems.

4) The direct writing of etch resist for printed circuit boards.

Printed circuit boards have been directly written using gold as an etch resist. *Figure 17* shows an example of this method. No masking was used. This technique can be used for small prototype boards where turn-round times can be extremely short. The process can take CAD designs and write the resist pattern in a matter of minutes, the time depending on the complexity and size of the board. The example shown took 15 minutes to produce and 5 minutes to etch. Edge definition is good and undercut is minimal. By the use of multiple jets, many circuits can be written simultaneously allowing the process to be used for small to medium sized batches.

The process is not limited to gold. Other metals have been examined and work is continuing on processes directly relevant to the electronics industry. It may be concluded that this process offers a significant step forward in selective plating due to its high speed and

cost savings in the elimination of masking processes, relatively low capital cost and simplicity of operation.

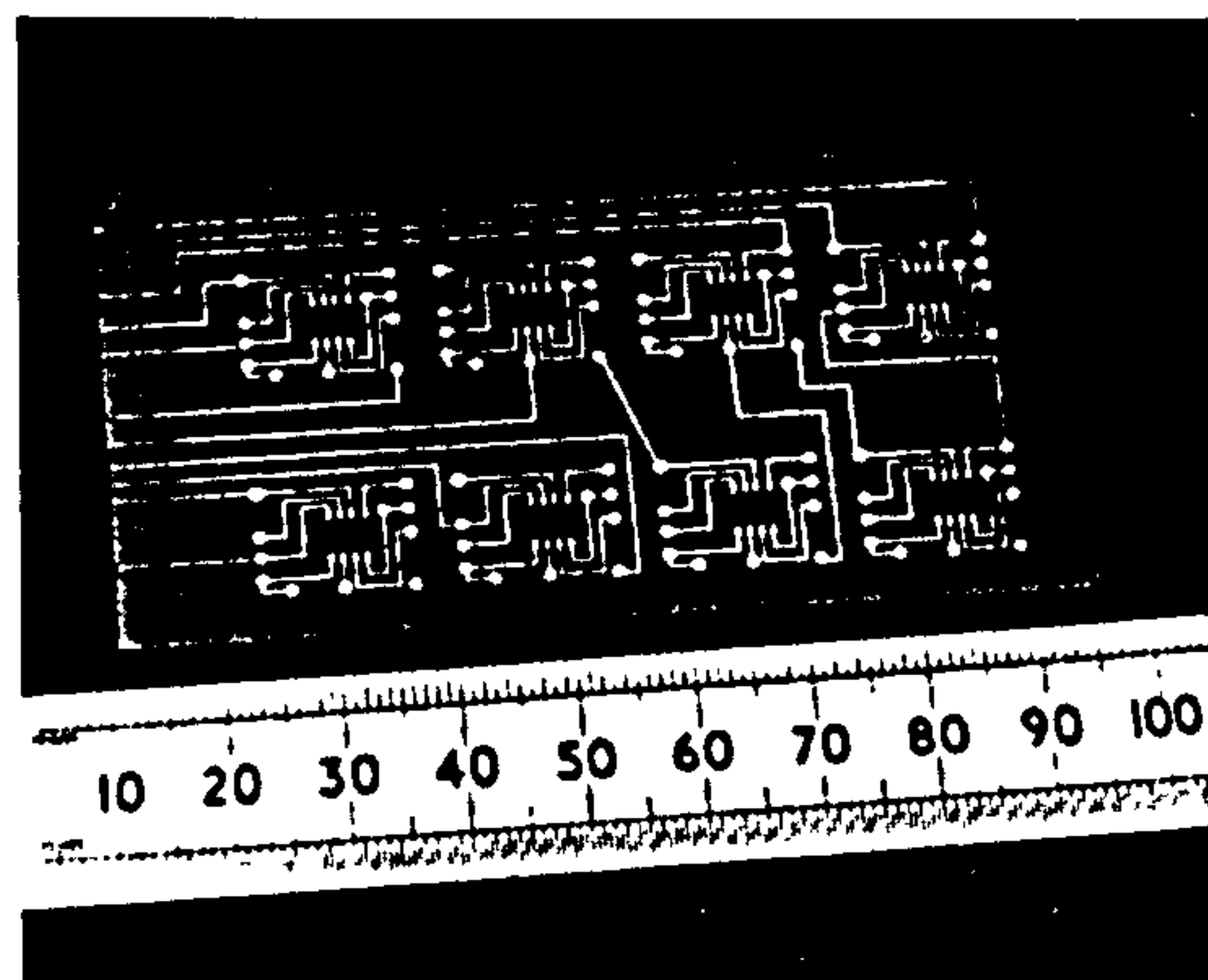


Fig.17: An example of a directly written etch resist pattern for a printed circuit board after etching with a copper cladding

Acknowledgements

The author wishes to thank Mr Ian Gunter of the Metallurgy Group, Hirst Research Centre, for his invaluable assistance in the design of the control equipment and the computer programming that made this work possible. Thanks also go to staff of the Materials and Components Assessment Laboratory, Hirst Research Centre and the Electron Microscopy Unit of the Loughborough University of Technology for producing the SEM micrographs presented here.

This work is part of a BRITE/EURAM project No. RI1B-0304, in partnership with Centro Sviluppo Materiali of Italy and Loughborough University of Technology and thanks go to them for their agreement to publish this paper.

The Author also wishes to thank Dr D. Gabe and Mr I. Christie for their helpful comments.

References

- [1] M.B. Glauert, *J. Fluid Mech.* 1, 625 (1956)
- [2] US Patent No. 3,810,829, May 1974, James Fletcher, NASA
- [3] R. Haynes, K. Ramachandran & D.J. Fineberg, *The Western Electric Engineer*, 22, 61, (1978)
- [4] J. K. Dorey II, R. Haynes, R.E. Sinitski and R.E. Woods, *Plat. & Surf. Fin.* 67, 81 (May 1980)
- [5] R.C. Alkire & T.J. Chen, *J. Electrochem. Soc.* 129, 11, 2424, (1982)
- [6] K.-L. Hsueh & D.-T. Chin, *Ibid.* 133, 1, 75, (1986)
- [7] D.-T. Chin & C.-H. Tsang, *Ibid.* 125, 9, 1461, (1978)
- [8] R. Alkire & J.-B. Ju, *Ibid.* 134, 2, 294, (1987)
- [9] C.C. Bocking, *Trans. IMF*, 66, 50, (1988)
- [10] C.C. Bocking, *Proceedings of the 59th Intl. Conf. On Surf. Fin. Torquay*, 2, 51, (1991)
- [11] E.J. Watson, *J. Fluid Mech.*, 20, 3, 481, (1964)
- [12] H. Schlichting, "Boundary Layer Theory", 4th ed., McGraw-Hill, New York (1960)
- [13] V.E. Nakoryakov, B.G. Pokusaev & E.N. Troyan, *Int. J. Heat Mass Transfer*, 21, 1175, (1978)
- [14] D.A. Dawson & O. Trass, *Can. J. Chem. Engng.* 44, 121, (1966)

HIGH SPEED SELECTIVE JET ELECTRODEPOSITION OF GOLD AND COPPER

C. BOCKING

High Speed Selective Jet Electrodeposition (HSSJE) is a process by which metals may be electrodeposited in a spatially selective manner without the need for masking. This paper discusses the principles that underlie HSSJE and the factors that influence the rates of deposition, selectivity and deposit quality for both copper and gold. Also presented is an empirical model of how the hydrodynamic and electrochemical factors influence growth mechanisms and limit deposition rates. Potential applications of the process are also discussed.

NOMENCLATURE

B	Proportionality constant of Fick's first law
c	Concentration of ionic species of interest (mol/cm ³)
c_b	Concentration of ionic species of interest in the bulk electrolyte (mol/cm ³)
c_0	Concentration of ionic species of interest at the surface (mol/cm ³)
D	Diffusion coefficient (cm ² /s)
d	Jet diameter (cm)
F	Faraday constant
i	Current density (A/cm ²)
i_L	Limiting current density (A/cm ²)
J_D	Diffusion flux (mol/s/cm ²)
n	Number of electrons in electrode reaction
R	Universal gas constant
R_d	Dimensionless spread parameter, y/r'
Re	Reynolds number
r	Stagnation zone radius (cm)
r'	Nozzle radius (cm)
T	Temperature (K)
x	Distance from electrode (cm)
y	Radial distance from the centre of the impingement zone (cm)
y_d	Radial edge of deposit (cm)
δ	Diffusion layer thickness (cm)
ν	Kinematic viscosity (cm ² /s)

1. INTRODUCTION

Electrodeposition, otherwise known as electroplating, is a process involving the coating of a material with a layer of metal. It is a widely used method of modifying the surface characteristics of a material in order to confer specific surface properties. These properties include corrosion and wear resistance, electrical conductivity, or simply an improved appearance. The technology is applied throughout the engineering and electronics industries as well as for decorative purposes. The principle of electrodeposition is simple. The workpiece is made the cathodic electrode in an electrolyte containing, amongst other things, ions of the metal to be deposited. This is achieved by connecting it to the 'negative' terminal of a low voltage DC supply. The circuit is completed by means of a second electrode, the anode, connected to the 'positive' terminal of the supply. The anode is usually made of the same metal as that to be deposited although an inert material can be used. By the application of a suitable voltage from the supply, the metal ions adjacent to the cathode surface are electrochemically reduced to the metal thereby producing an electrodeposit. Oxidation reactions occur at the anode.

The rate of deposition is controlled by both the magnitude of current per unit area, or the current density (C.D.) and the time of deposition. However, there is a limit to this rate, as it is a function of the electrochemical characteristics of the electrolyte and of the prevailing hydrodynamic conditions during electrodeposition. The upper limit is set by the maximum rate of mass transfer of metal ions to the surface of the cathode. In the region of this limit, the deposit becomes powdery and poorly adherent. There is obviously a commercial advantage in maximizing the rate of deposition and, for many applications, a significant amount of research has been carried out to this end. Generally, high rates of deposition can be realized only under conditions of vigorous agitation or high flow rates of the electrolyte. This assists in the transport of the metal ions to the surface. For many processes, the maximum rate of deposition for acceptable quality coatings is around 0.5 to 1.0 $\mu\text{m/s}$.

It is not always desirable to deposit a metal over the entire surface of a component. In particular, in the

electronics industry, gold is frequently used because of its inert character as well as its high electrical conductivity and low contact resistance. However, it is an expensive metal and in order to reduce costs, it is often restricted to where it is needed. This is normally achieved by masking those regions where the deposit is not required. There are numerous ways of doing this including photo-resists, chemically resistant lacquers, or pre-formed masks made from neoprene or silicone rubber. Each method has its advantages and disadvantages, but they tend to be expensive. They can also involve complicated engineering practices particularly for continuous, automatic plating processes such as the reel-to-reel plating of connector components. Such practices are termed selective plating.

High Speed Selective Jet Electrodeposition (HSSJE) is a process in which metal may be deposited selectively at a fast rate without the need for masking. The work described in this article aims to establish an understanding of the factors which control the morphology and structure of deposits of gold and copper produced using this technique. These metals were chosen as they are widely used throughout the electronics industry. They are also representative of the two main classes of electrolyte used in electrodeposition. These are simple salt electrolytes, in the case of copper, and complexed salt electrolytes in the case of gold. The work is part of a BRITE/EURAM project (number RI1B-0304) entitled 'Improvement in the Control and Attainment of High Speed Electrodeposition Processes'. The partners in the project are Centro Sviluppo Materiali (CSM) of Italy and Loughborough University of Technology.

2. FUNDAMENTAL CONCEPTS

In HSSJE, a free-standing, non-submersed jet of electrolyte flowing at a high velocity impinges onto a substrate. The application of a suitable voltage between the substrate (cathode) and the nozzle (anode) causes metal to be deposited within the impingement region and the immediately surrounding region. Fig. 1 shows a schematic view of the electrolyte flow. The properties of the hydrodynamic flow surrounding the impingement region are such that the

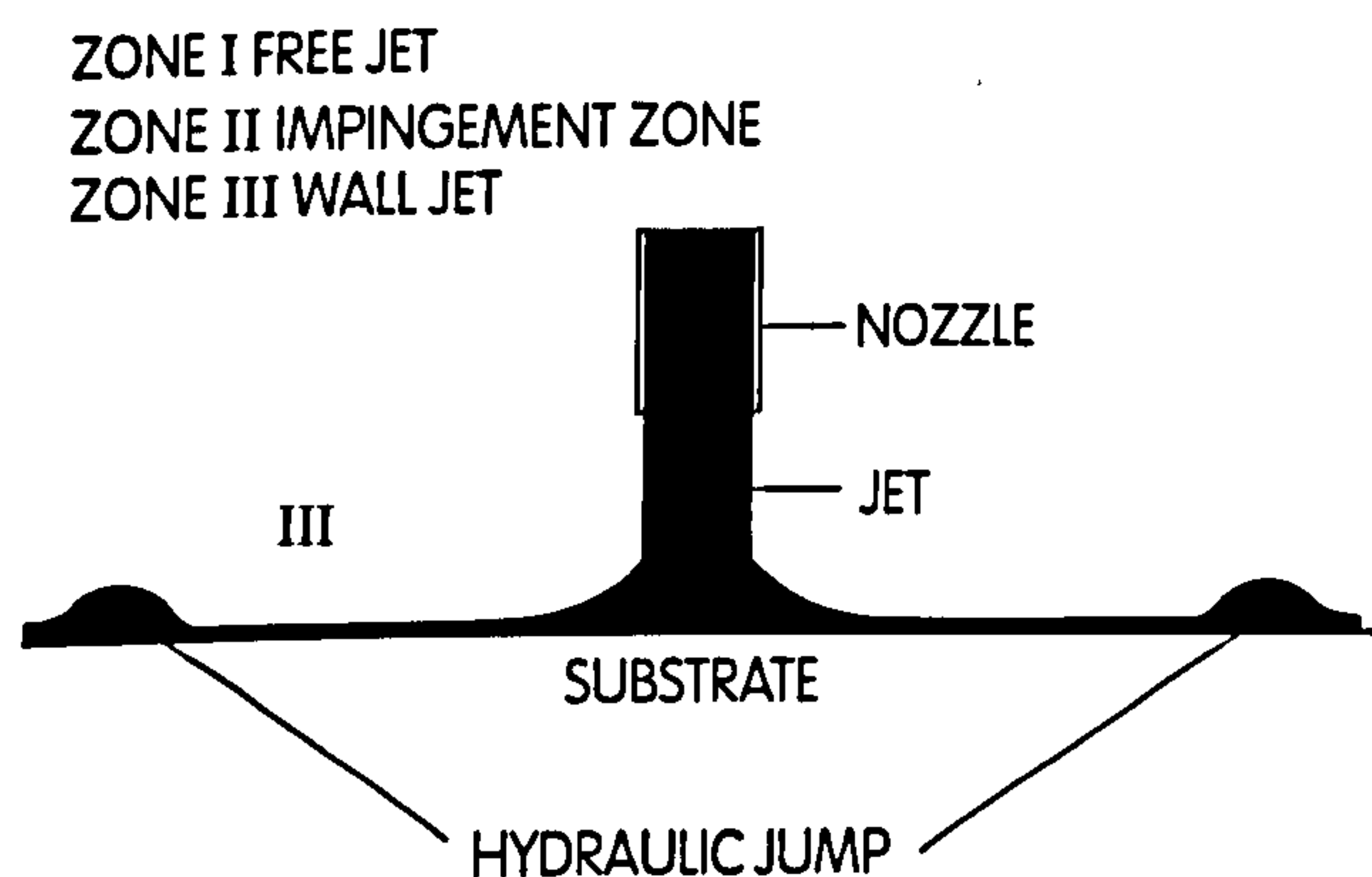


Fig. 1. Schematic diagram of the electrolyte flow from an impinging jet

electrolyte forms an extremely thin radial layer as it flows away. Because this layer, termed the wall jet region⁽¹⁾, is so thin, the electrical resistance of the electrolyte is comparatively high. This means that under certain conditions, deposition is limited to the impingement region, with little or no deposition occurring within the highly resistive wall jet region. In this way, the desired selectivity is achieved. In order to understand how high rates of deposition can be obtained, it is necessary to establish the mechanisms that control the mass transport of metal ions to the surface.

2.1. Mass transport and the diffusion layer

For a metal to be deposited from an electrolyte, metal ions need to be present at the surface to accept electrons and become incorporated into the growing surface. During deposition, metal ions are discharged at the interface. These are replaced by metal ions reaching the surface from the body of the electrolyte by means of hydrodynamic flow, migration and diffusion. Hydrodynamic flow results from the movement of the bulk electrolyte by stirring or forced flow. Migration occurs as the result of the electric field acting on the charged ions. For example, Cu^{2+} ions having a positive charge will migrate under the influence of the electric field to the cathode. However, a complexed anion such as the cyanoaurate anion, $\text{Au}(\text{CN})_2^-$ (the metal ion species in gold plating electrolytes) will migrate to the anode. The influence of migration can be affected by the quantity of other charged species in the electrolyte that do not take part in the electrode reaction, as each charged species is responsible for carrying a portion of the current. In the presence of a large excess of charge carriers other than the electroactive species of interest, the influence of migration on each individual electroactive ion is minimized. Most plating electrolytes contain these excess charge carriers.

Diffusion occurs because a concentration gradient has been set up. Ions outside the interface region will tend to diffuse to the lower concentration region near the surface, under the influence of the concentration gradient. The region over which this directional diffusion occurs is known as the diffusion layer. The thickness of the diffusion layer is very dependent on the prevailing hydrodynamic conditions within the bulk of the electrolyte, namely the flow. In unstirred solutions, the diffusion layer thickness can reach typically $50\mu\text{m}$, whereas under conditions of high electrolyte flow, it can be as low as $2.0\mu\text{m}$. The diffusion flux, J_D , is related to the current density and it can be found using Fick's law of diffusion. If migration is ignored, because of the presence of an excess of other charge carriers, then

$$\frac{i}{nF} = J_D = -D \left(\frac{dc}{dx} \right)_{x=0} \quad (1)$$

This can be put in terms of the concentration at the interface as

$$\frac{i}{nF} = J_D = -D \frac{(c_b - c_0)}{\delta} \quad (2)$$

Solving for i gives

$$i = -nFD \frac{(c_b - c_0)}{\delta} \quad (3)$$

If the current density is raised sufficiently, diffusion will not be able to re-supply the metal ions and the concentration at the interface will drop to zero. This represents the limit of current density that can be applied under any set of hydrodynamic conditions, as given by eqn. (4).

$$i_L = -\frac{nFDc_b}{\delta} \quad (4)$$

Any further increase in current density will result in a secondary electrode reaction such as hydrogen evolution. Also, the diffusion coefficient is temperature dependent, as can be seen from

$$J = -D \frac{dc}{dx} = -BRT \frac{dc}{dx} \quad (5)$$

where B is a constant.

It can be seen from eqn. (4) that the magnitude of the limiting current density is controlled by the thickness of the diffusion layer, the concentration of metal ions and the temperature. There is a certain limit to the metal ion concentration that can be used. This is dictated by the solubility of that particular species in the electrolyte. However, the thickness of the diffusion layer is dependent on the degree of agitation of the bulk electrolyte.

It follows that for high speed electrodeposition, high metal ion concentrations in conjunction with high rates of agitation and high temperatures would appear to give the highest rates of deposition.

Despite the fact that the limiting current density determines the maximum deposition rate for a particular set of conditions, it has been found by a number of workers⁽²⁻⁴⁾ that the deposit quality begins to deteriorate at some value below i_L . This deterioration is apparent from the formation of either dendritic growth or nodular powdery deposits. It is important, therefore, to ascertain the fraction of the limiting current density at which deposits begin to deteriorate rather than the limiting current density itself.

There is a further factor that limits the maximum deposition rate. For many electrodeposition reactions, not all the current is used for depositing the metal. Some of the current is expended in reducing hydrogen ions, which are plentiful in aqueous electrolytes, to form hydrogen gas. There are a number of reasons for this, but these are beyond the scope of this paper. However, the tendency for this side reaction to occur increases with increasing current density because of the resulting reduction in the surface concentration of metal ions. The current efficiency of the reaction is a measure of this secondary reaction and can be defined as the fraction of the current used for metal deposition, given as a percentage. This is a further reason for maintaining as high a surface metal ion concentration as possible by means of agitation.

2.2. The relationship between overpotential and current density

Much information about the behaviour of an electrochemical system can be gained by observing the relationship between overpotential and current density. The overpotential is the extra voltage required in order to drive an electrochemical reaction and allow current to flow. This relationship is best shown in the form of a polarization curve, where the current density is plotted on a log scale against the overpotential. Fig. 2 shows such a curve. These curves are produced by applying incremental potential steps to the cathode (known as the working electrode). The potential of the working electrode is controlled by means of a potentiostat. This is a feedback device that maintains the applied overpotential to the working electrode with reference to a third electrode known as the reference. For each value of applied overpotential, the current flowing is measured. From this, the current density can be obtained.

It is beyond the scope of this paper to derive the mathematical relationship between the overpotential and current density. However, some aspects of a polarization curve will be mentioned.

The linear part is known as the Tafel region and represents the overpotential range in which the kinetics of the electrode reaction control the overall rate of reaction. This is often referred to as activation control. Beyond the Tafel region, mass transfer begins to affect the rate of reaction and the rate is controlled by both activation and diffusion. Eventually, as the limiting current density is reached, the rate is controlled purely by mass transfer. Beyond this point, providing secondary reactions are absent (for example, hydrogen evolution), the current remains constant with increasing overpotential and this is known as the limiting current plateau. Under conditions of vigorous agitation, however, this plateau does not always appear because of the very high rates of mass transfer.

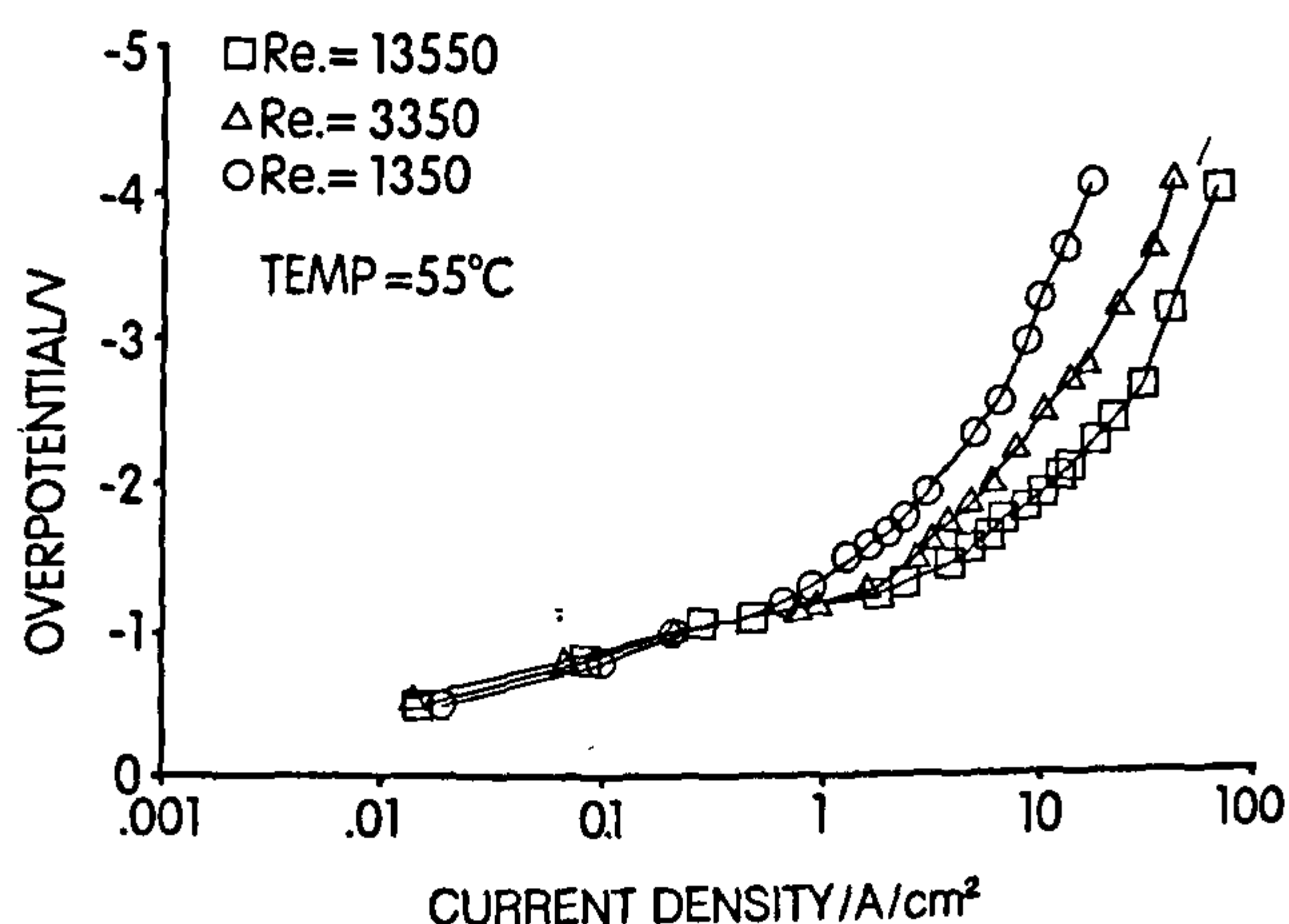


Fig. 2. Polarization curves of the 0.17 M gold electrolyte at various values of Reynolds number. Overpotential measured with respect to the gold reference electrode

3. BACKGROUND

Selective jet deposition is not a new process, with the principle having been patented by NASA⁽⁵⁾ in 1974. This patent described a forced electrolyte flow system in which the nozzle was scanned across the substrate and current applied at appropriate times in accordance with a control pattern. In this way, a plated pattern could be written, much in the same way as a picture is formed on a dot-matrix printer. The process as subsequently described, however, uses a 'direct write' system in the manner that a plotter produces an image.

Since that time, there has been comparatively little information published on the subject of HSSJE, presumably for reasons of commercial confidentiality. Haynes *et al.*⁽⁶⁾ described a forced flow jet plating system in 1978 and Dorey *et al.*⁽⁷⁾ used a modified version of this equipment to gold plate connectors for the evaluation of the thermocompression bonding characteristics of the deposits. The maximum flow velocity used was 39 cm/s and the current densities were up to 1.3 A/cm². In this work, it was found that the deposit quality deteriorated at current densities in the region of 0.86 A/cm² because of nodule formation. However, it was claimed that nodular deposits did not detract from bondability. There have been several papers published that attempt to correlate mathematical models

of jet plating systems with experimental results⁽⁸⁻¹¹⁾. However, little work has been published on the morphological characteristics of deposits produced in this way.

Bocking⁽¹²⁾ has described selective pure gold deposition using both laser-enhanced jet deposition and HSSJE using small bore nozzles (1mm to 0.25mm). He examined the morphology of the deposits produced and related these to the electrolyte velocity. The current efficiency of deposition was also described. He went on to show a 'direct write' facility whereby the jet could be moved in relation to the substrate by means of a computer controlled X-Y table, producing plated tracks and lines.

The selective deposition of both copper and gold deposits has been described in depth by Bocking⁽¹³⁾, relating deposition conditions to deposit morphology.

4. EXPERIMENTAL DETAILS

Fig. 3 shows a schematic diagram of the equipment used in this study. A platinum tube nozzle with a diameter of 400 μ m was sealed into a lead/soda glass tube. This was connected to the pump outlet and was mounted onto the X-Y table. The table was driven by two stepper motors in half-step mode allowing increments of 2.5 μ m/step. The controlled current

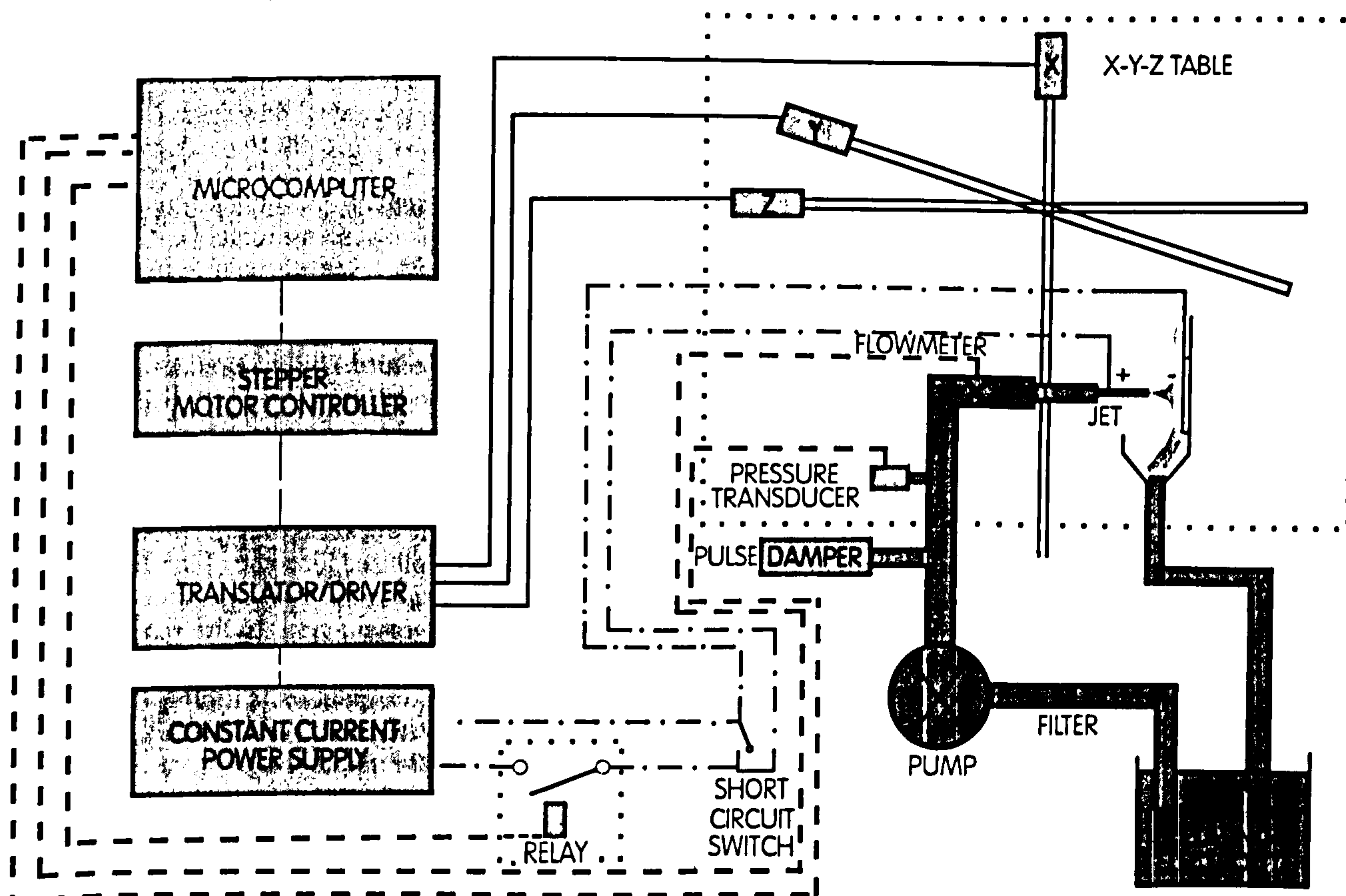


Fig. 3. Schematic diagram of the experimental jet plating unit

power supply, with a resolution of 0.01 mA, provided the plating current. The motion of the X-Y table, the magnitude of the plating current and its duration were controlled by the computer. This allowed a number of deposit spots to be generated on a step-and-repeat basis. The facility was amenable to computer aided design (CAD) control, thus permitting complex designs to be directly written by electrodeposition. To explore the operational limits of the process, deposit spots were produced over a wide range of current densities, metal ion concentrations, temperatures and electrolyte velocities. In all cases, a constant total charge was used. A more graphic description of the equipment and experimental detail is given in reference (13).

The thicknesses and profiles of the electrodeposited spots were measured using a Sloan Dektak 3030 Surface Profilometer. The crystallographic orientation was determined using X-ray diffraction. Examination of the deposits was carried out using both optical microscopy and scanning electron microscopy (SEM). Some samples were also examined by standard micro-section techniques. Polarization measurements were carried out on one of the gold electrolytes using a Wenking HP72 potentiostat and a pulse generator. The working electrode was a 400 μm diameter copper wire embedded in an epoxy block so that only the end face of the wire was exposed. Adjacent to this was a platinum wire, 200 μm in diameter also embedded and separated from the working electrode by a distance of 100 μm . This acted as the reference electrode. Prior to measurements, both the working electrode and the reference electrode were polished and pre-plated with gold at a current density of 5 mA/cm² for 2 minutes. Whilst this type of reference electrode was not ideal because of its poor reversibility in the system under study, it was justified by the need to use a small diameter, flush-mounted reference so that the flow patterns were not disrupted.

Polarization curves were produced using 'sampled current pulse voltammetry' at different electrolyte velocities, as described below. Because the deposit growth was so rapid at these high current densities, conventional steady-state polarization techniques could not be used. It was found that a steady state condition could be achieved after between 20 and 40 ms under jetting conditions. A series of increasing potential pulses of 40 ms duration was applied and the current measured at the end of each pulse. The substrate was re-polished and re-plated before each measurement. Prior to the application of each pulse, a pre-electrolysis for 30 s at 0.3 V with respect to the gold reference electrode (GRE) was applied.

The electrolytes used, together with some of their relevant physical details, are given in table 1. It should be noted that the copper electrolytes represent a class known as simple salt systems because the metal ion is in the form of a cation, Cu²⁺. The gold, on the other hand, is typical of a complexed metal ion system, being present in the form of an anion, Au(CN)₂⁻.

Table 1
Details of electrolytes used

1. Gold electrolytes			
Parameter	sample [1]	sample [2]	sample [3]
Gold (g/litre) (as potassium gold cyanide)	54.0 (0.28 M)	33.5 (0.17 M)	54.0 (0.28 M)
Diammonium hydrogen citrate (g/litre)	45.0	45.0	1.0
Citric acid (g/litre)	15.0	15.0	1.0
Potassium hydroxide	to pH 6.0	to pH 6.0 (initially)	to pH 6.0
Kinematic viscosity (cm ² /s)	0.012284 (25°C) 0.009221 (40°C) 0.0076567 (55°C)	0.005906 (55°C)	
Conductivity (mS/cm)	55.3 (25°C) 97.6 (55°C)	88.2 (55°C)	28.2 (25°C) 48.8 (55°C)

2. Copper electrolytes	
Copper (as copper sulphate)	0.08 M 0.204 M 0.8 M
Sulphuric acid	0.51 M (for all copper concs.)

5. RESULTS

5.1. Criteria for assessment

It was found that the deposit spots exhibited a gaussian profile with maximum thickness at the centre of the spot. Where thickness measurements are quoted, these refer to the thickness at the centre of the spot. Current densities quoted are based on the surface area of the impingement zone, in other words, the surface area of the nozzle aperture. Deposition rates are based on the thickness of the centre of the spot divided by the time of deposition and are given in $\mu\text{m/s}$.

The selectivity of the process has been established by means of distribution plots. Because the deposits were symmetrical, the thickness over the profile of half of the spot has been plotted for some of the deposits as a function of the ratio of the radial distance from the centre of the impingement zone to the radius of the nozzle. This gives a dimensionless spread parameter, R_d . This method of presentation is useful when comparing different nozzle sizes. A value of $R_d = 1$ signifies the edge of the impingement zone and if no deposition occurs past this position, complete selectivity has been achieved. Any deposition beyond this point is a measure of the reduction of selectivity.

The electrolyte jet exit velocity, measured in m/s, is not an accurate means of comparing different electrolytes. This is because of the differences in viscosity

between them, which gives rise to different shear frictional forces and it does not describe the true flow conditions. In order to make satisfactory comparisons, the dimensionless Reynolds number (Re) is used. The Reynolds number takes into account the kinematic viscosity of the electrolyte and is defined as dV/ν , where d = the nozzle diameter in cm, V = the electrolyte velocity in cm/s and ν = the kinematic viscosity in cm^2/s .

5.2. The influence of deposition conditions

5.2.1. The effect of current density

Both the copper and gold electrolytes exhibited a similar behaviour as current density was increased, all other conditions remaining constant. At low current densities ($< 1.0 \text{ A/cm}^2$) deposits were thin compared to the higher current density samples and showed a poor selectivity with R_d values approaching 27. However, the thickness of the gold beyond the impingement zone was negligible (about $0.1 \mu\text{m}$). Increasing the current density above this value led to improved selectivity with an R_d value of 3. The morphology of the deposit was also significantly affected by the current density. The actual current densities at which morphological changes occurred depended on the prevailing conditions of temperature, electrolyte velocity and metal ion concentration but the following general pattern was observed. At current densities below 1.0 A/cm^2 , deposits were similar in appearance to those produced by conventional electrodeposition. Increasing the current density led, initially, to a very smooth structure with few surface features. A further increase in current density produced small, hemispherical features. As the current density was increased still further, a nodular structure formed. Finally, a wide variety of dendritic structures was formed, ranging from radial needles to dendritic columns.

The way in which current efficiency varied with increasing current density for a given flow condition was also measured and can be seen in fig. 4

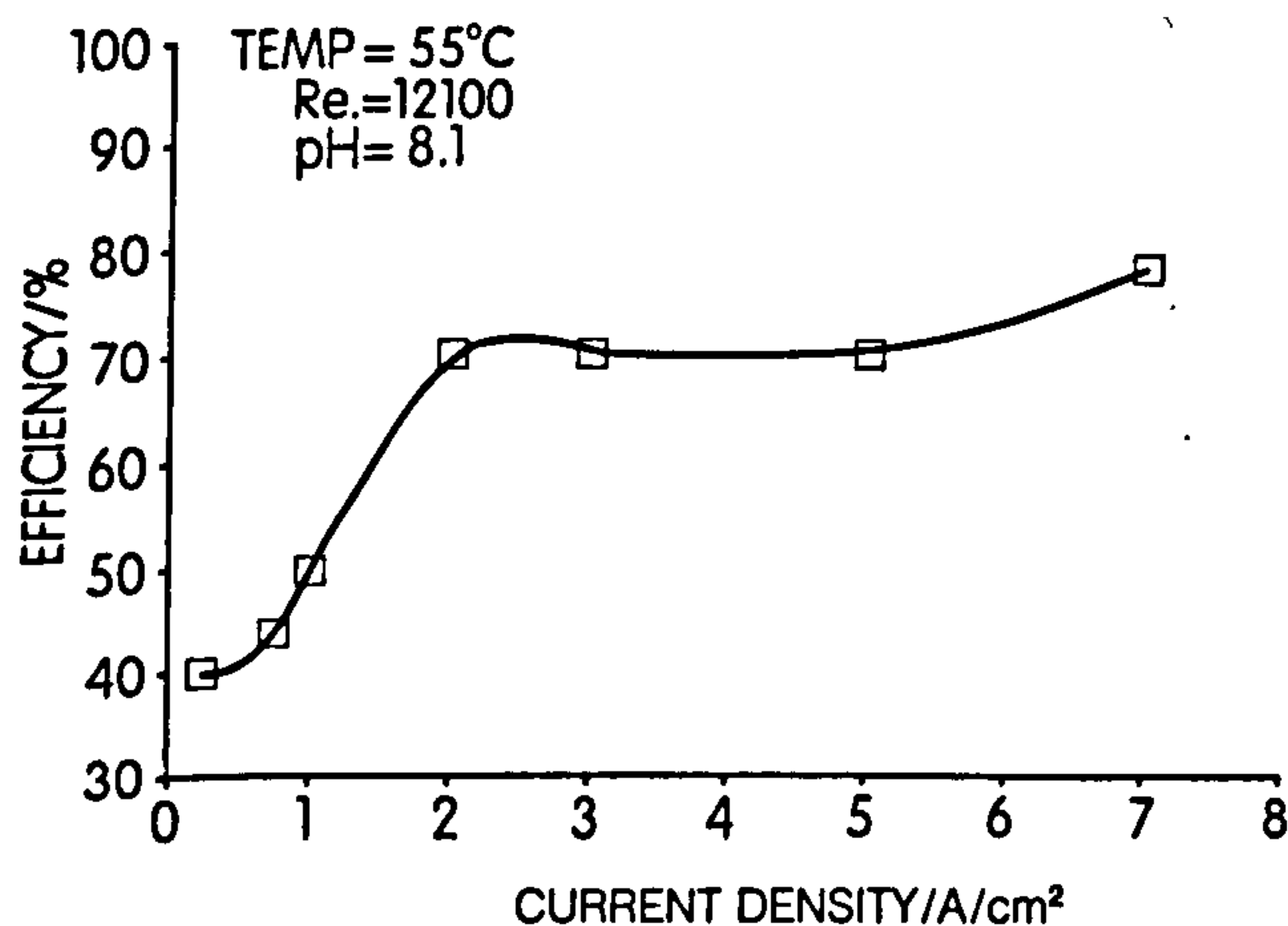


Fig. 4. Current efficiency vs current density, 0.17M gold

5.2.2. The effect of metal ion concentration

It was found that increasing the metal ion concentration of the electrolytes increased the maximum current density and thus the plating rate at which smooth deposits could be produced. However, above a certain value of concentration, the maximum current density and maximum plating rate were reduced slightly. This can be seen in fig. 5 which shows a plot of the maximum useful current densities against Reynolds number for different metal ion concentrations of copper. Similar effects were observed for gold, particularly at a temperature of 25°C . Selectivity was not significantly affected by the metal ion concentration.

5.2.3. The effect of electrolyte velocity

The velocity of the electrolyte, or more precisely, its Reynolds number, has a significant effect on the morphology of the deposits produced. Figs. 6 to 8 show a series of simple morphological diagrams for the 0.28M gold system. These relate the Reynolds number to the current density and show the range of morphological structures observed. Other gold concentrations showed differing morphological habits but the general trends were similar. Increasing the velocity allowed a

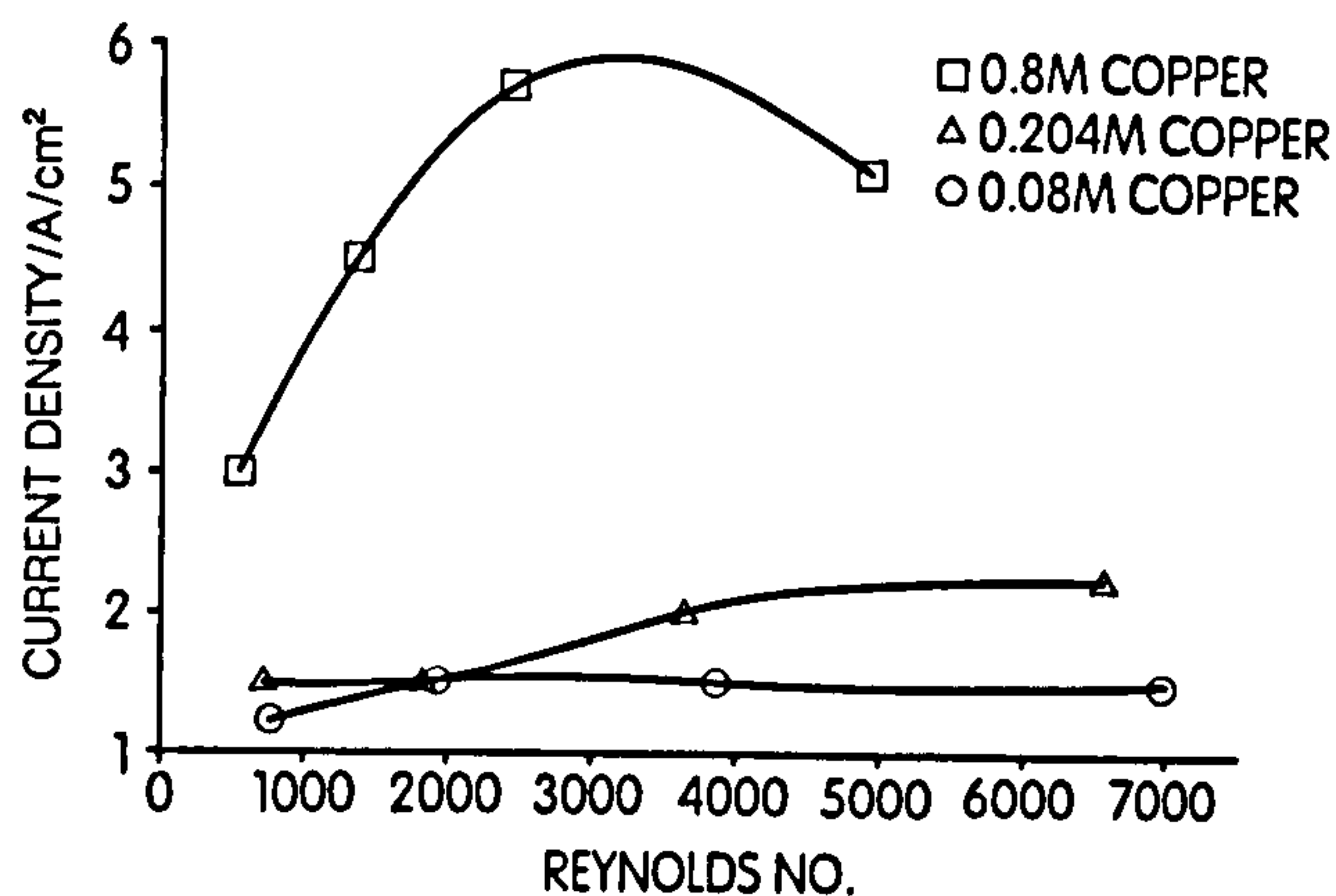


Fig. 5. Maximum current densities for acceptable deposits from various copper concentrations, as a function of Reynolds number

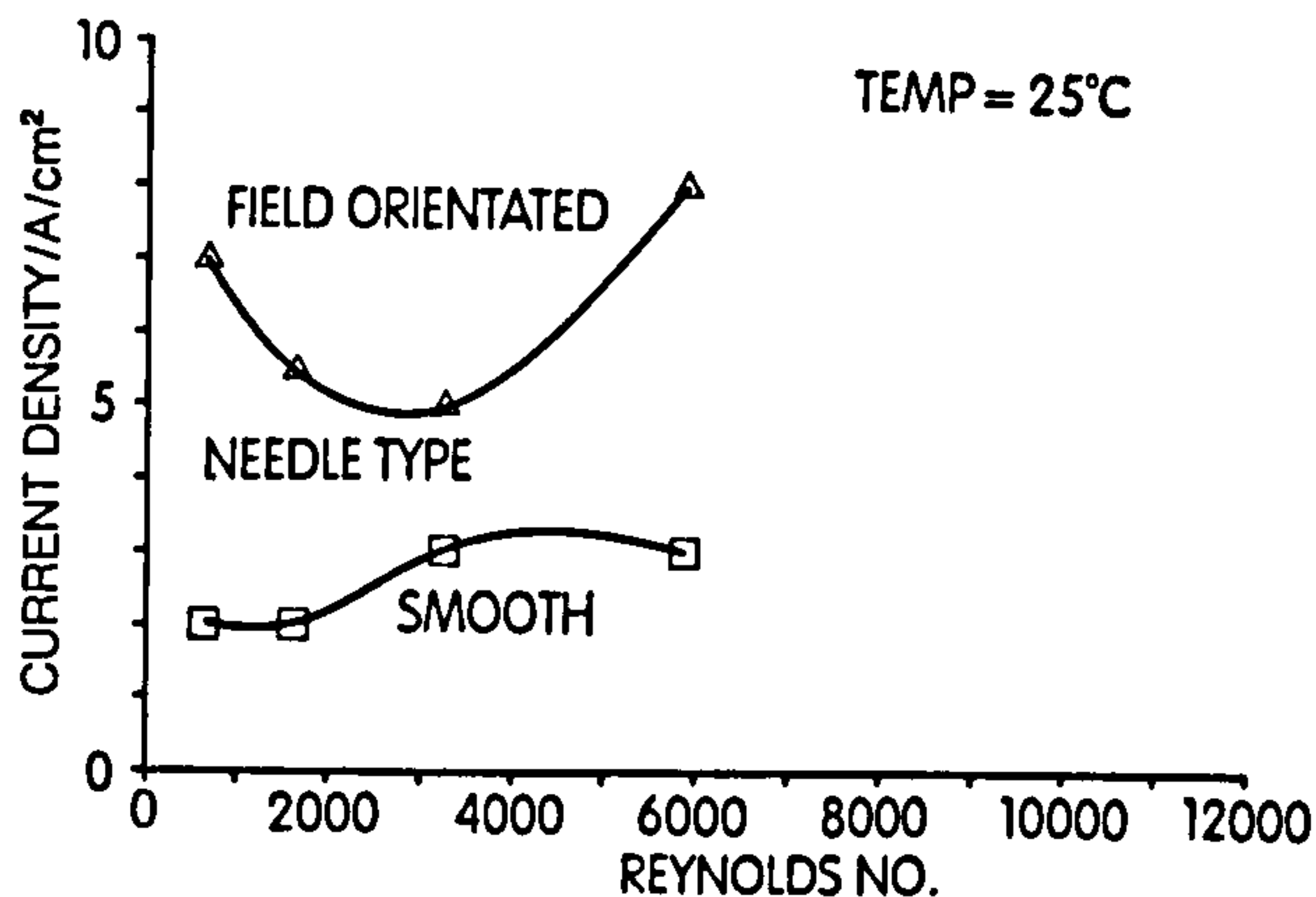


Fig. 6. Morphological diagram of the deposits produced from the 0.28M gold electrolyte at 25°C as a function of deposition conditions (current density, C.D. and Reynolds number)

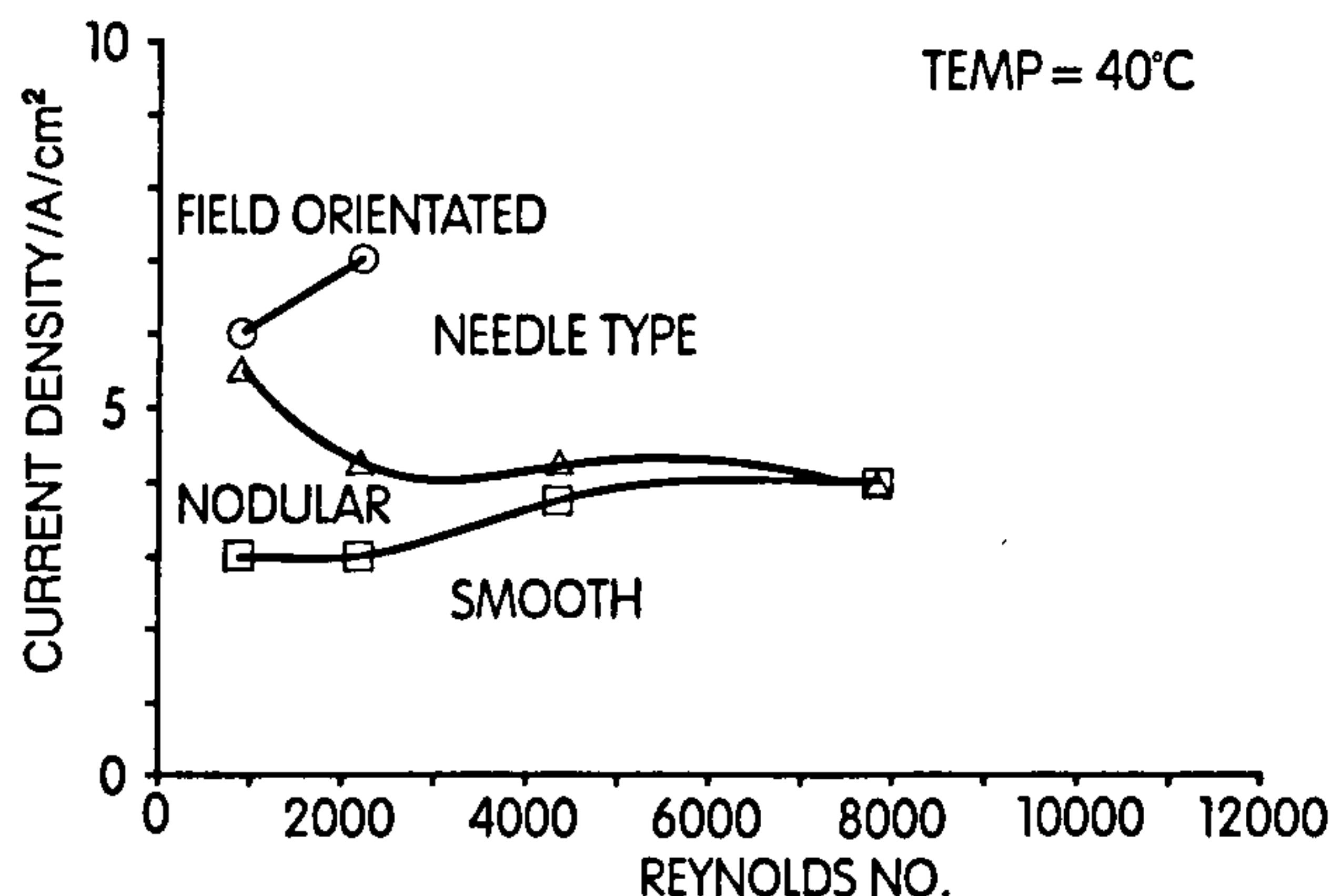


Fig. 7. Morphological diagram of the deposits produced from the 0.28M gold electrolyte at 40°C as a function of deposition conditions

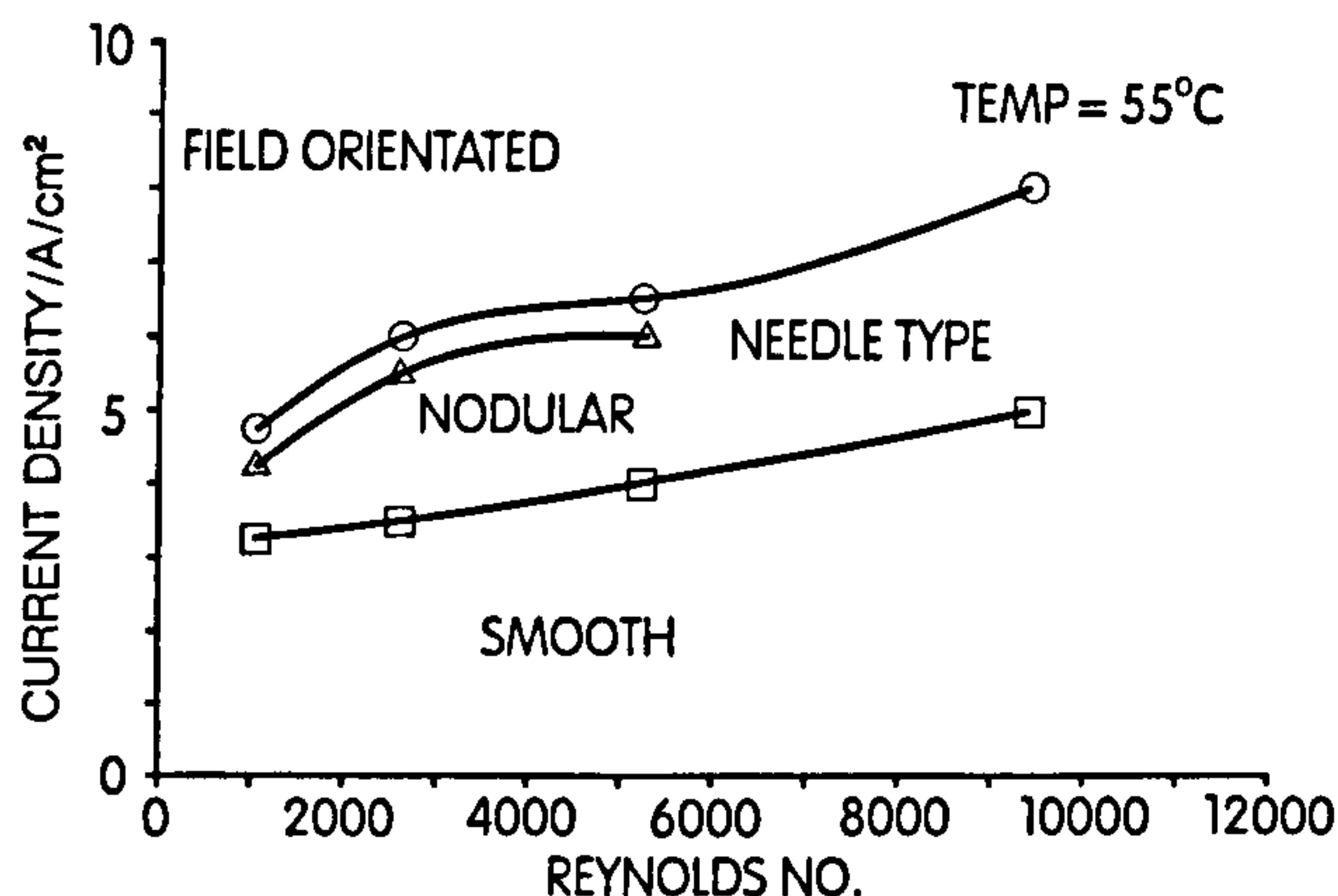


Fig. 8. Morphological diagram of the deposits produced from the 0.28M gold electrolyte at 55°C as a function of deposition conditions

greater current density and thus a higher deposition rate to be used. There is little influence on selectivity by the electrolyte velocity.

5.2.4. The effect of electrolyte temperature

The effect of temperature has not been evaluated as yet for the copper system. The gold system has not been directly evaluated but the overall effect of temperature can be seen from the morphological diagrams. Temperature has a very marked effect on both the maximum usable current density and the deposit structure beyond this maximum. For a temperature increase of 30°C, the maximum current density is doubled. The effect of electrolyte temperature on selectivity has yet to be established.

5.2.5. The effect of nozzle to substrate distance

The effect of the nozzle to substrate distance was established using the 0.17M gold electrolyte only. For most of the experiments with the gold electrolytes, the nozzle to substrate distance was maintained at 1mm. However, decreasing this distance improved the

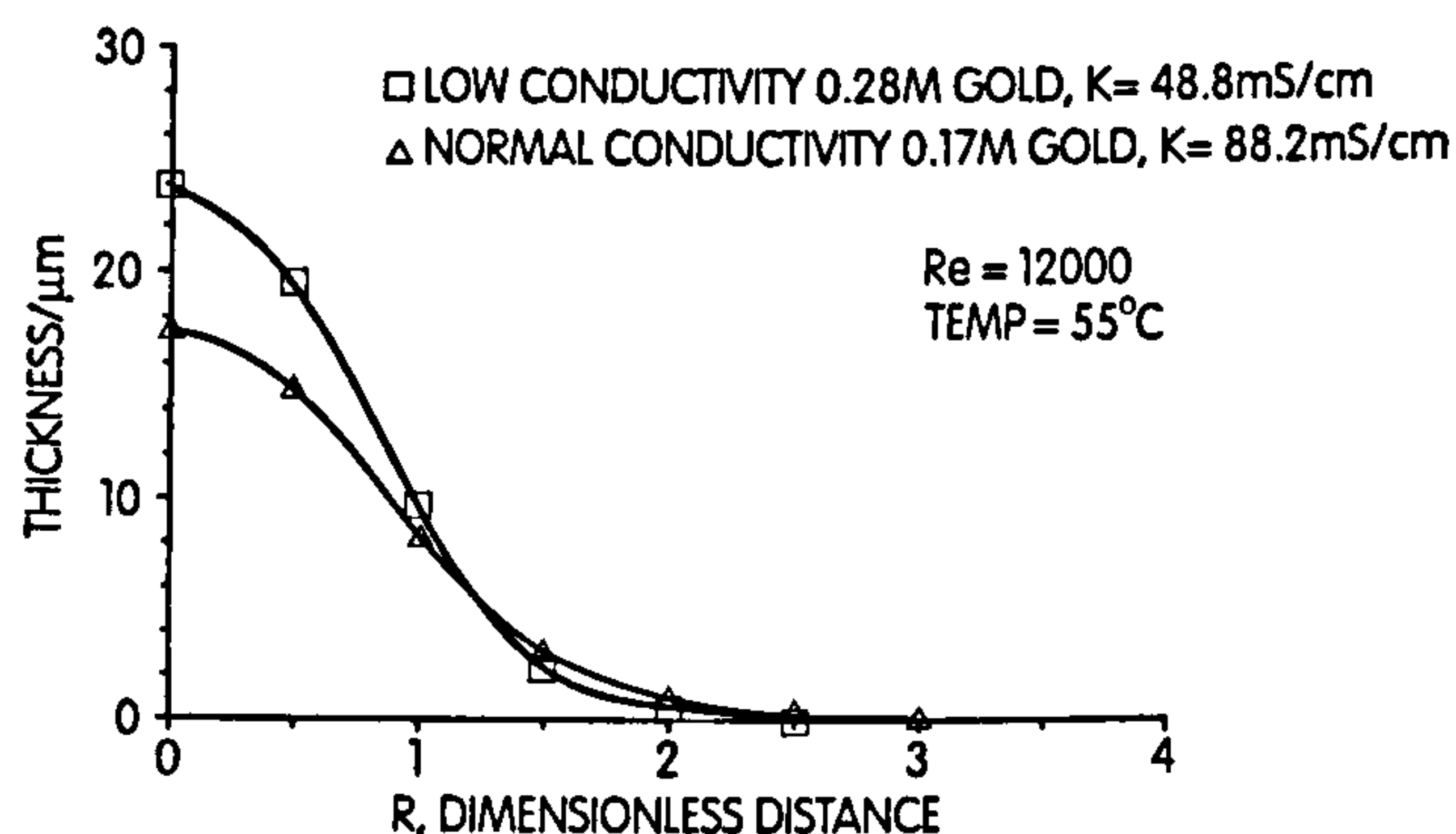


Fig. 9. Typical selectivity plot of the low conductivity and the 0.17M gold electrolytes

selectivity slightly. Increasing the distance had little effect on selectivity but the morphology of the deposit altered. The deposit became more nodular towards the wall-jet region and some needles were observed, oriented in the flow direction.

5.2.6. The effect of electrolyte conductivity

The influence of the electrolyte conductivity was established only with a gold electrolyte. Conductivity influenced both the selectivity and the structure. Reducing the conductivity by half improved the selectivity, with $R_d = 2.5$, as can be seen in fig. 9. However, the deposit structure deteriorated at much lower current densities and a maximum plating rate of only 2.9 μm/s could be achieved.

5.2.7. The effect of electrolyte pH

It was not possible to adjust the pH of the copper electrolytes as this would have significantly altered the composition of the electrolyte. The effect of pH was studied using the gold system over the range 5.3 to 8.1. It was found that at the higher pH, slightly higher plating rates could be achieved with a small improvement in deposit structure. No significant influence of pH on selectivity has yet been established.

5.2.8. Optimum conditions obtained to date

It was found that the maximum useful current density for copper was 6.5 A/cm² giving a deposition rate of 1.6 μm/s at 25°C using a 0.8M metal ion content and a Reynolds number of 2750. A typical deposit is shown in fig. 10. It can be seen that there is a significant degree of surface etching of the sample, which was caused by exposure of the deposit to the wash of the rapidly flowing electrolyte. The degree of etching is dependent on the length of exposure, with approximately 1 μm of the deposit being removed in 1 hour. However, there is a tendency for enhanced etching to occur at the boundaries of the individual growth sites. This can lead to an increase in gross porosity, particularly for thin deposits. Selectivity plots for copper showed that for the conditions above, an R value of 2.5 was obtained.

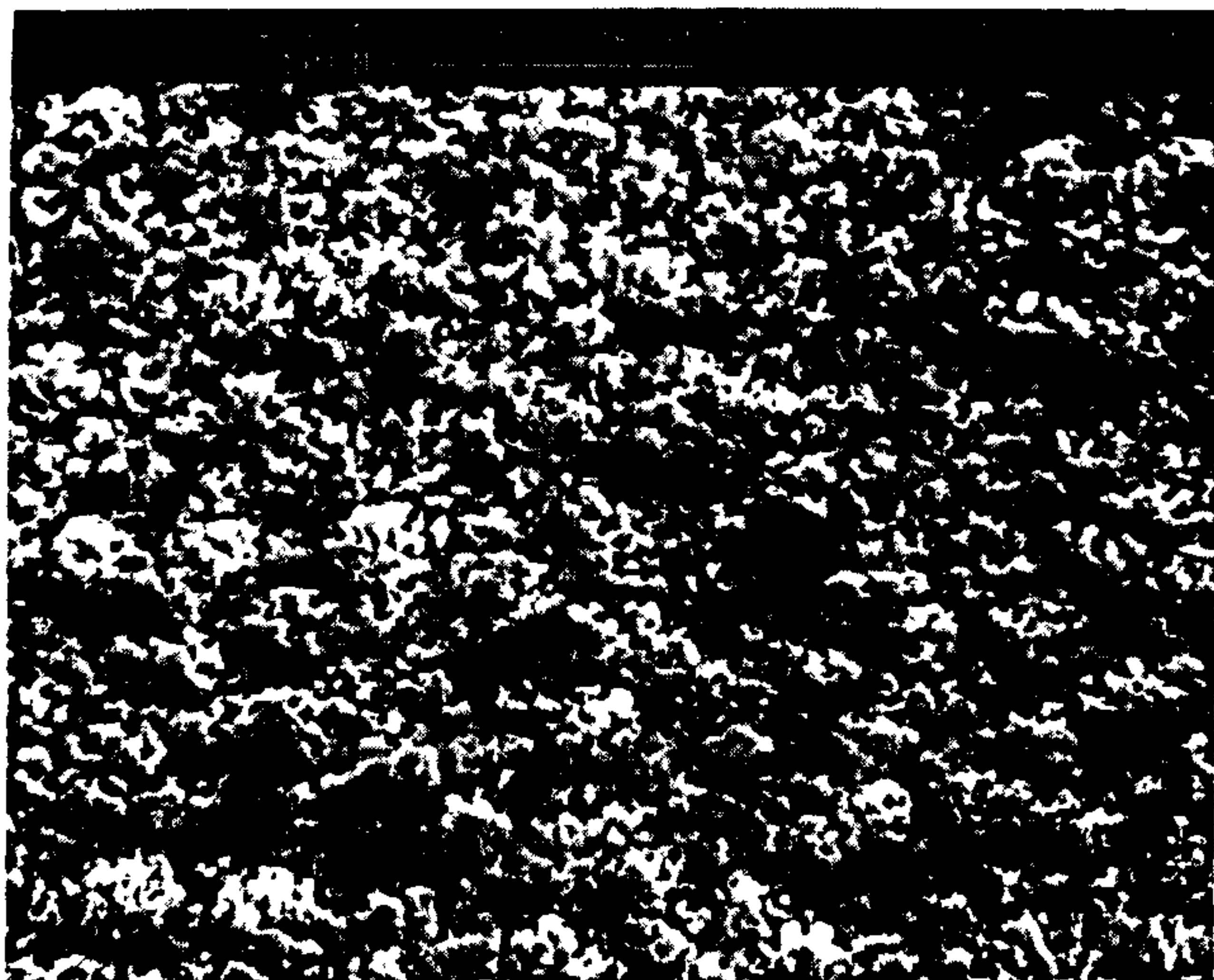


Fig. 10. A typical copper deposit produced at the maximum plating rate of $1.6 \mu\text{m/s}$. Current density = 5.7 A/cm^2 , $Re = 2750$, copper = 0.8 M , thickness = $4.0 \mu\text{m}$.

In the case of gold, electrolyte [2] (see table 1) gave the best performance. The maximum useful current density was 6.0 A/cm^2 giving a plating rate of $3.4 \mu\text{m/s}$ at a temperature of 55°C and a pH of 8.1. Fig. 11 shows an example of a deposit produced under these conditions. This can be compared with fig. 12 which shows a deposit of gold of the same thickness deposited conventionally. Selectivity plots showed that an R_d value of 3.0 was achieved.

5.3. Polarization studies

Fig. 2 shows the polarization curves for a 0.17 M citrate gold for Reynolds number values of 13550, 3350 and 1350. This shows a plot of the overpotential against the current density. It can be seen that at a Reynolds number of 13550 and with a current density of up to 2.0 A/cm^2 , deposition proceeded under activation control. The Tafel slope was -355 mV/decade . Above this value, mixed activation and diffusion control occurred. No clearly-defined limiting current was observed. This was because hydrogen evolution competed with gold deposition and the limiting current plateau was hidden. However, it can be seen that the deposit began to deteriorate in the mixed control region at a current density of 6.0 A/cm^2 . This also applied to the other velocities except that deterioration occurred at lower current densities.

5.4. X-Ray diffraction studies

X-ray diffraction studies of the gold deposits showed that over the current density range of between 0.75 to 7.0 A/cm^2 and a Reynolds number of 12100, there was no evidence of preferred orientation of the deposit. Deposits produced at higher current densities showed evidence of a decrease in crystallite size with increasing current density.



Fig. 11. A typical gold deposit produced at the maximum plating rate of $3.4 \mu\text{m/sec}$. Current density = 6.0 A/cm^2 , $Re = 12100$, gold = 0.17 M , pH = 8.1, thickness = $18.0 \mu\text{m}$.

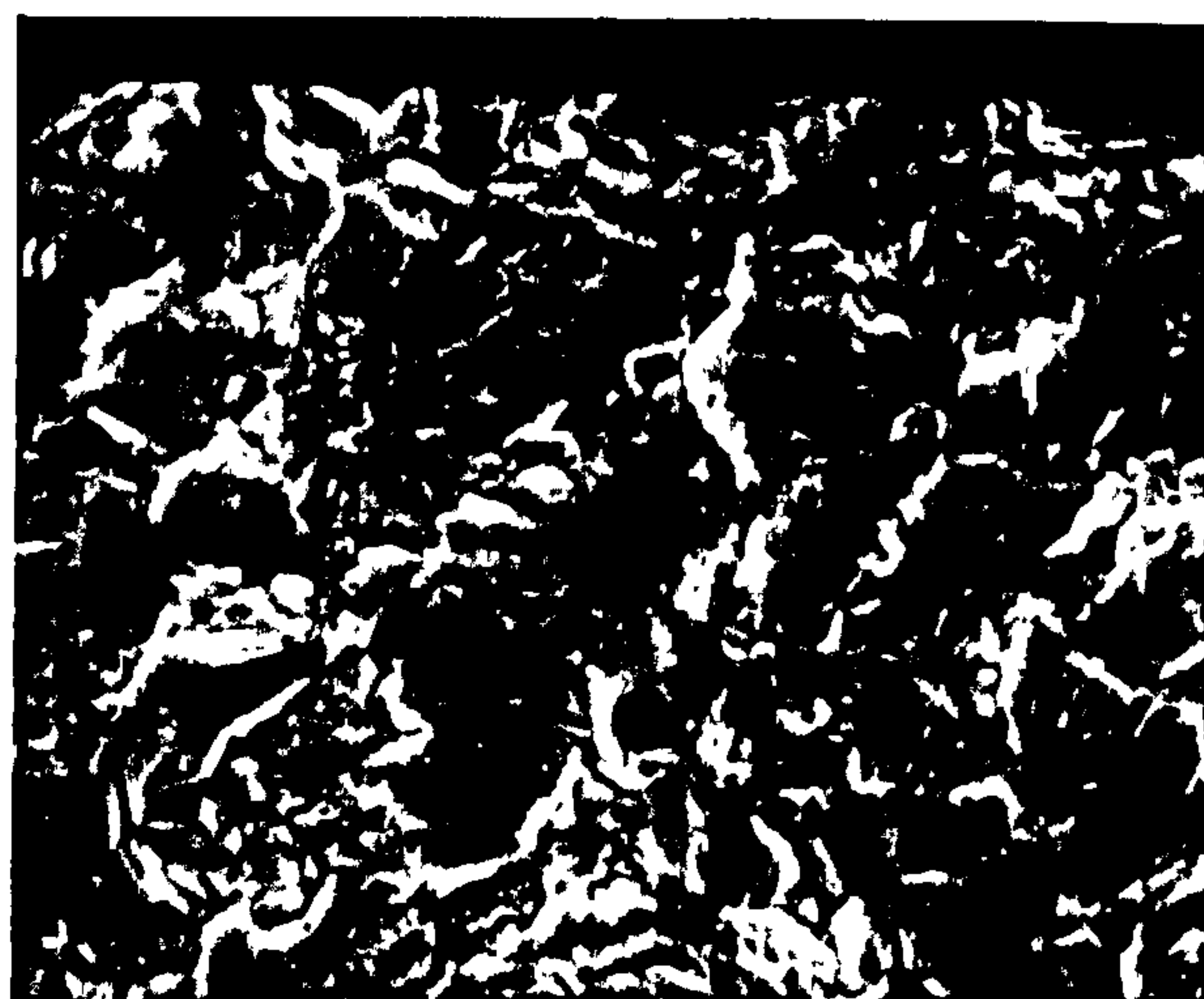


Fig. 12. A gold deposit produced from a citrate electrolyte under conventional conditions. Current density = 5.0 mA/cm^2 , gold = 0.06 M , thickness = $18.0 \mu\text{m}$.

6. MECHANISMS OF DEPOSIT GROWTH

6.1. Morphological aspects

Both the copper and gold systems exhibited a similar morphological behaviour. Whilst lower flow rates and temperatures affected some morphological details, deposit structures generally followed a typical pattern. At low current densities ($< 1.0 \text{ A/cm}^2$) the deposits assumed a plate-like structure. As the current density was increased, the deposits adopted a closed, pore-free structure with few surface features. Higher current densities produced a surface with smooth hemispherical mounds of low amplitude. As the current density was increased further, the deposits showed an enhanced growth at certain sites as some of the

rounded structures grew faster than their neighbours, creating a cauliflower-like appearance. Increasing the current density further, or reducing the flow rate, caused these nodules to act as precursors for the formation of needle-like structures that grew in the direction of flow, particularly towards the edge of the impingement zone. A further increase in current density led to growth of dendritic structures in the direction of the electric field along the wall of the electrolyte jet. Lowering the temperature caused an increased rate of nodule and needle formation at lower current densities.

Figs. 13a to 13f show typical gold deposits produced at 10 A/cm^2 for increasing deposition times. These show that certain sites produced faster growing nodules. These then developed into needle-like structures in the radial flow direction. As the needles grew, they developed in the axial direction in the form of field-oriented dendrites. At a current density of 8.0 A/cm^2 there was no field-oriented growth and samples exhibited an increase in radial needle formation. At 7.0 A/cm^2 , increasing times simply produced larger nodules that eventually became powdery and non-adherent. At low temperatures, dendritic growth was less field oriented and produced a finer, filamentary structure.

6.2. Proposed mechanisms for the growth structures

Based on the empirical evidence obtained to date, possible mechanisms for the observed growth of the deposits can be deduced. At low current densities ($< 1.0\text{ A/cm}^2$) the mechanism of growth was similar to that for conventional gold. Because the deposit spread was so great at these low current densities (up to 11 mm diameter) it is reasonable to assume that the true current density was much lower than that based on the impingement zone area. This was confirmed by the marked similarity to conventional deposits of gold of similar thickness that have been published previously. It is likely that the spread observed here was a consequence of the long time periods used to pass the required number of coulombs (up to 140 s). This allowed a build up of deposit well beyond the impingement zone. However, it must be remembered that this surrounding deposit was extremely thin ($< 0.1\text{ }\mu\text{m}$). It can also be seen from the efficiency measurements that secondary reactions such as oxygen reduction and hydrogen evolution were occurring.

As the current density was increased above 1.0 A/cm^2 , all of the deposition occurred within a region of 3 times the jet diameter, the actual spread depending on the prevailing conditions of deposition. Most of the deposition occurred within the impingement zone. The deposits produced at these higher current densities showed a slightly hemispherical surface texture. It can be seen from the polarization curves in fig. 2 that, in the case of the curve corresponding to a Reynolds number of 13550, deposition assumed mixed activation-diffusion control at a current density of about 2.0 A/cm^2 . Lower Reynolds number values produced this transition at lower current densities.

The structure of both gold and copper deposits produced at current densities above 6.0 A/cm^2 indicated that the mode of growth was by 3D nucleation. Fresh nucleation occurred on existing grains forming a cauliflower-type structure. This type of nucleation generally occurs at high overpotentials in the region of mixed activation/diffusion control. The polarization curves show that relatively high overpotentials are required to achieve the current densities applied and that deposition is controlled by mixed mechanisms.

X-ray diffraction studies could not provide any evidence of preferred orientation in the samples examined. However, these samples did not include any deposits containing needles or dendrites, which have a strong, preferred orientation. During electro-crystallization, growth occurs faster in certain crystallographic directions than in others. Because of this, certain areas of the deposit grew faster, providing sites for subsequent needle or dendritic growth.

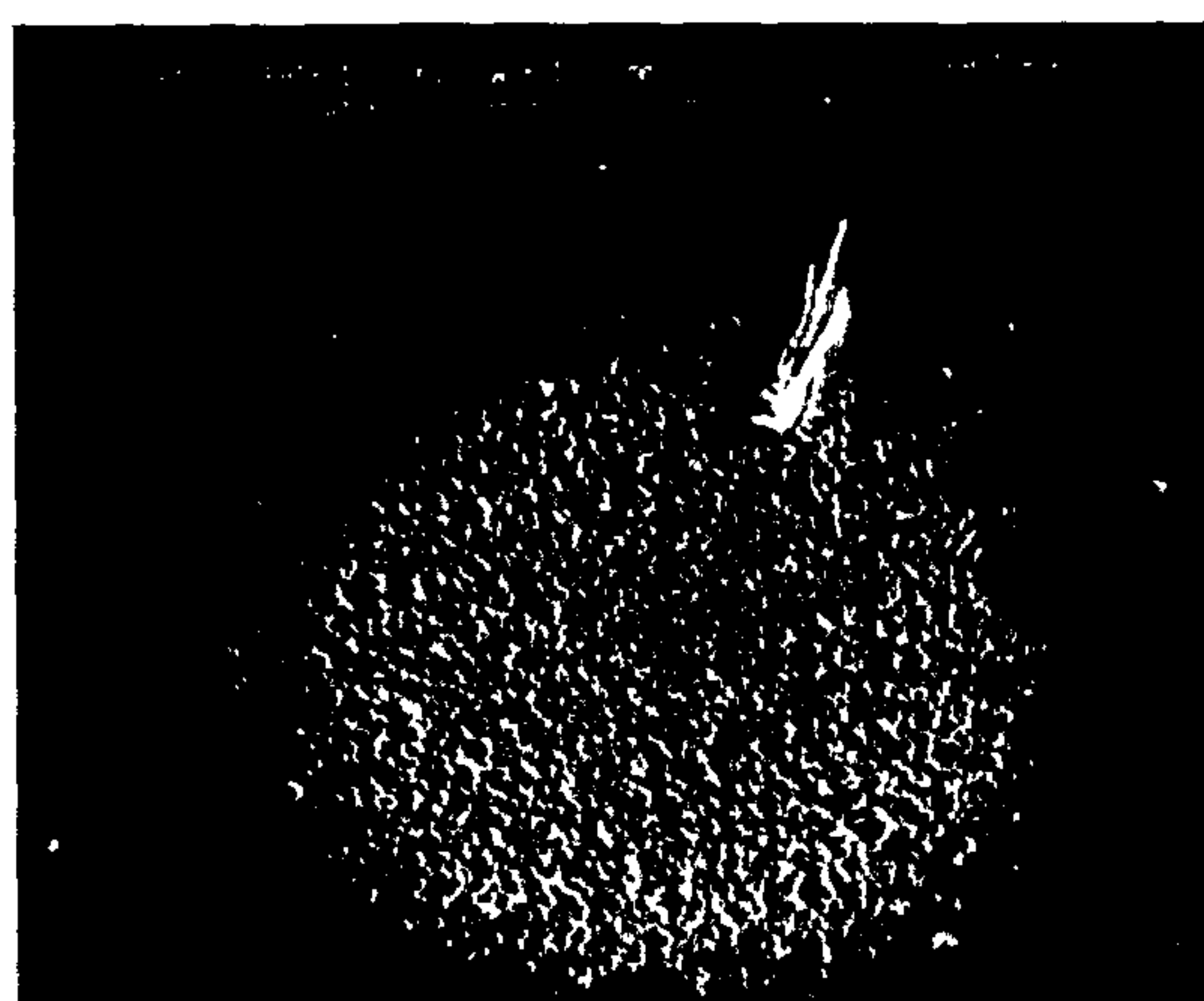
It was also observed that nodulation was particularly prevalent in the region of surface imperfections such as scratches etc. This is not surprising as these sites presented the lowest energy requirements for nucleation and subsequent growth. It was at these sites that growth occurred most rapidly, at least in the initial stages. Above a critical ratio of flow rate to current density, the growth of these nodules was accelerated, especially those towards the edge of the impingement zone. To understand the reason for this, it is necessary to examine the behaviour of the flow and the diffusion layer during deposition under these conditions.

The hydrodynamics of an impinging free jet on a surface normal to the flow has been described by several authors^(1, 14-16). In brief, when the jet hits the surface, the flow decelerates rapidly in the axial direction and accelerates in the radial direction forming the wall jet. This gives rise to a region where a viscous boundary layer of constant, but low, thickness occurs in the centre of the impingement zone. This is known as the stagnation region as axial flow is negligible. Dawson⁽¹⁷⁾ has estimated the transition between the stagnation zone and the wall jet to be $y/d = 4$, where y = radial distance from the centre of the jet and d = the jet diameter. In the present case, this transition occurred at $r = 50\text{ }\mu\text{m}$. Beyond this region, the boundary layer thickness increased until it reached the thickness of the wall jet. At this point, a hydraulic jump⁽¹⁵⁾ occurred in order to conserve the electrolyte momentum.

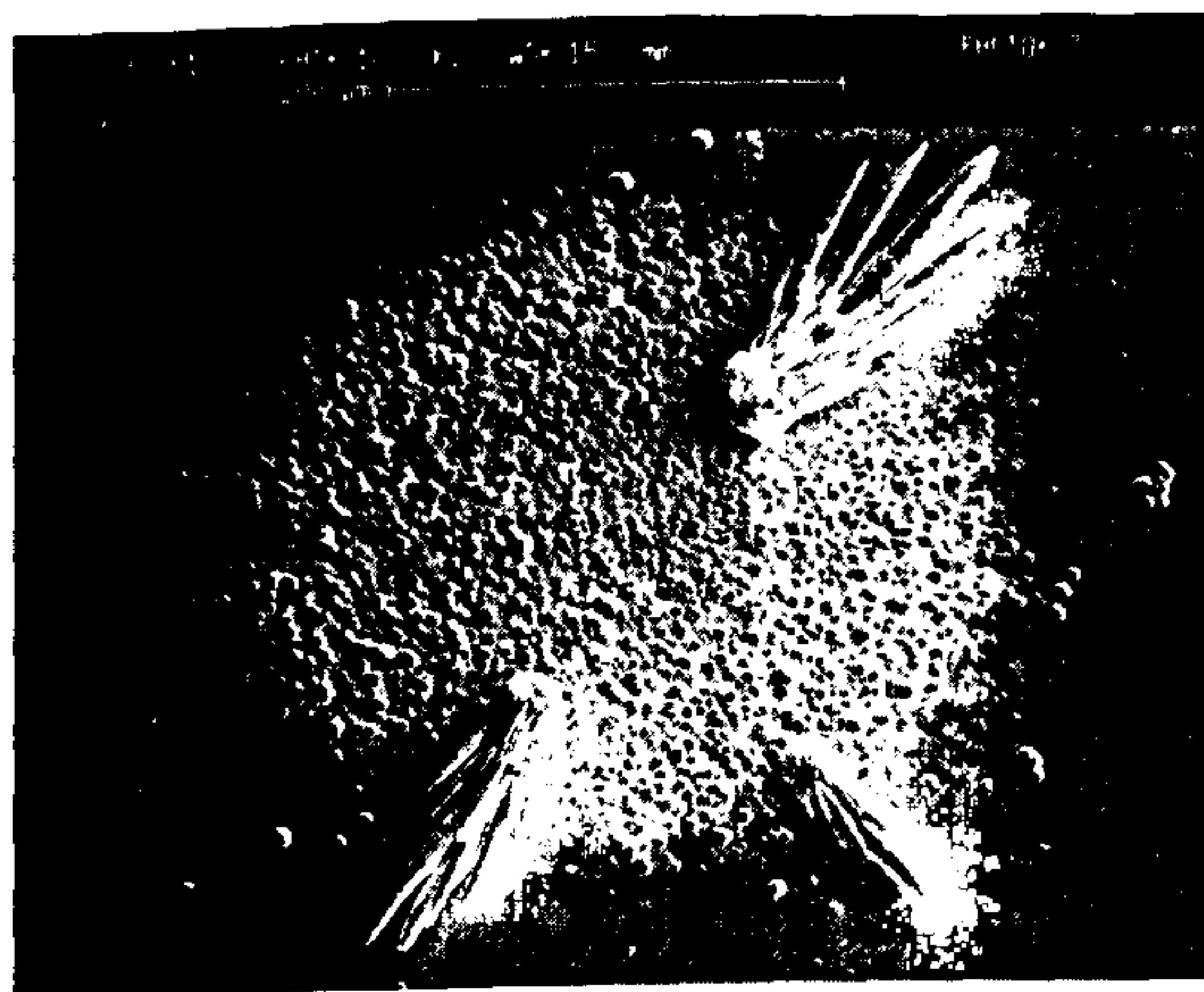
The behaviour of the diffusion layer is complex under these circumstances. Although the thickness of the diffusion layer cannot be measured directly, as the value of the limiting current density (i_L) cannot be measured, a maximum value can be estimated approximately from the polarization curve. At a Reynolds number, of 13550, high quality deposits are obtained up to a current density in the region of 6.0 A/cm^2 . It was found that deposits produced above this value were nodular or dendritic. Therefore, if a value of 7.0 A/cm^2 is taken arbitrarily as the limiting current density, the thickness of the diffusion layer can be calculated from eqn. (4). The effect of migration has again been ignored, but as the gold is anionic, the net effect would be negative. For the purposes of this



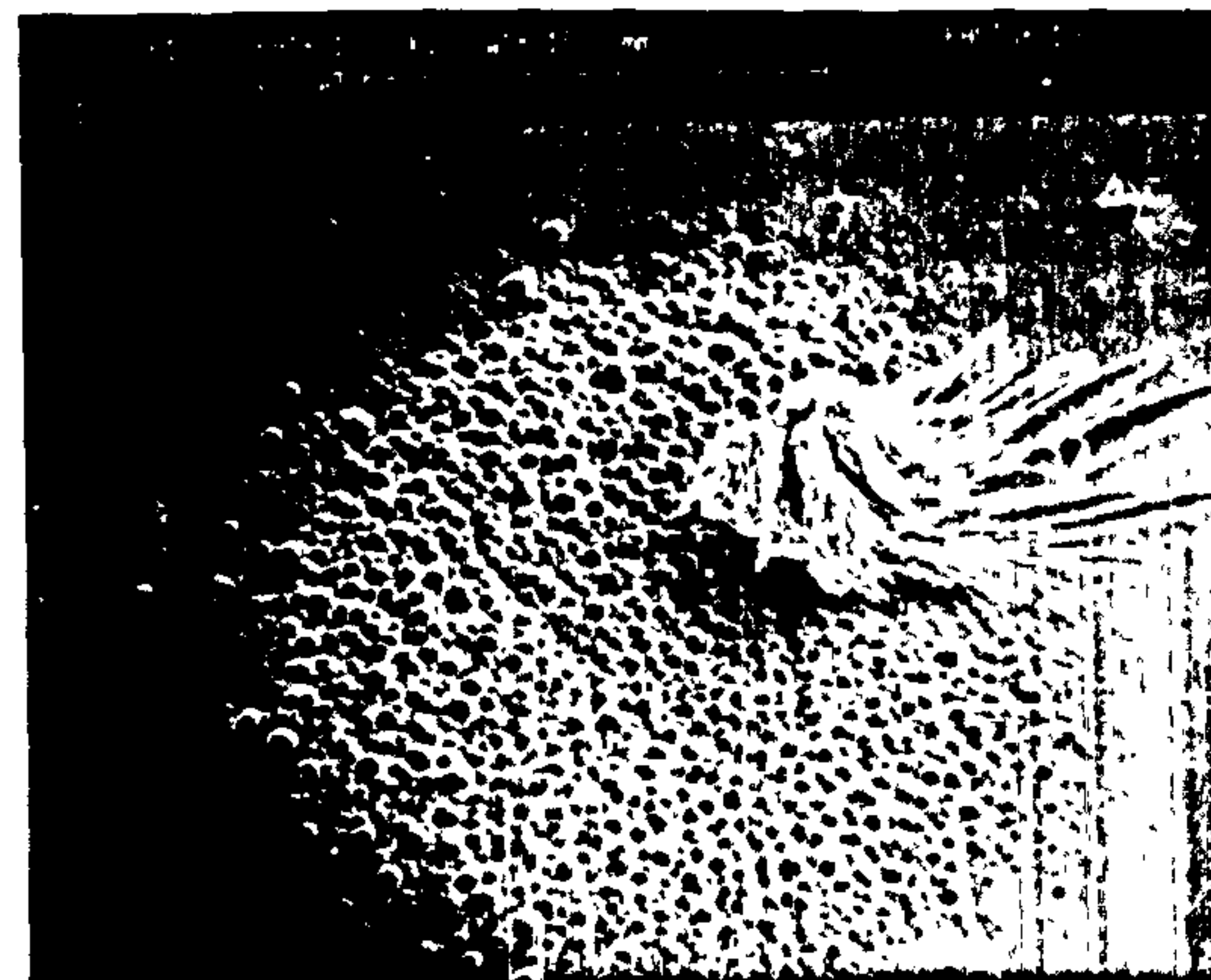
a)



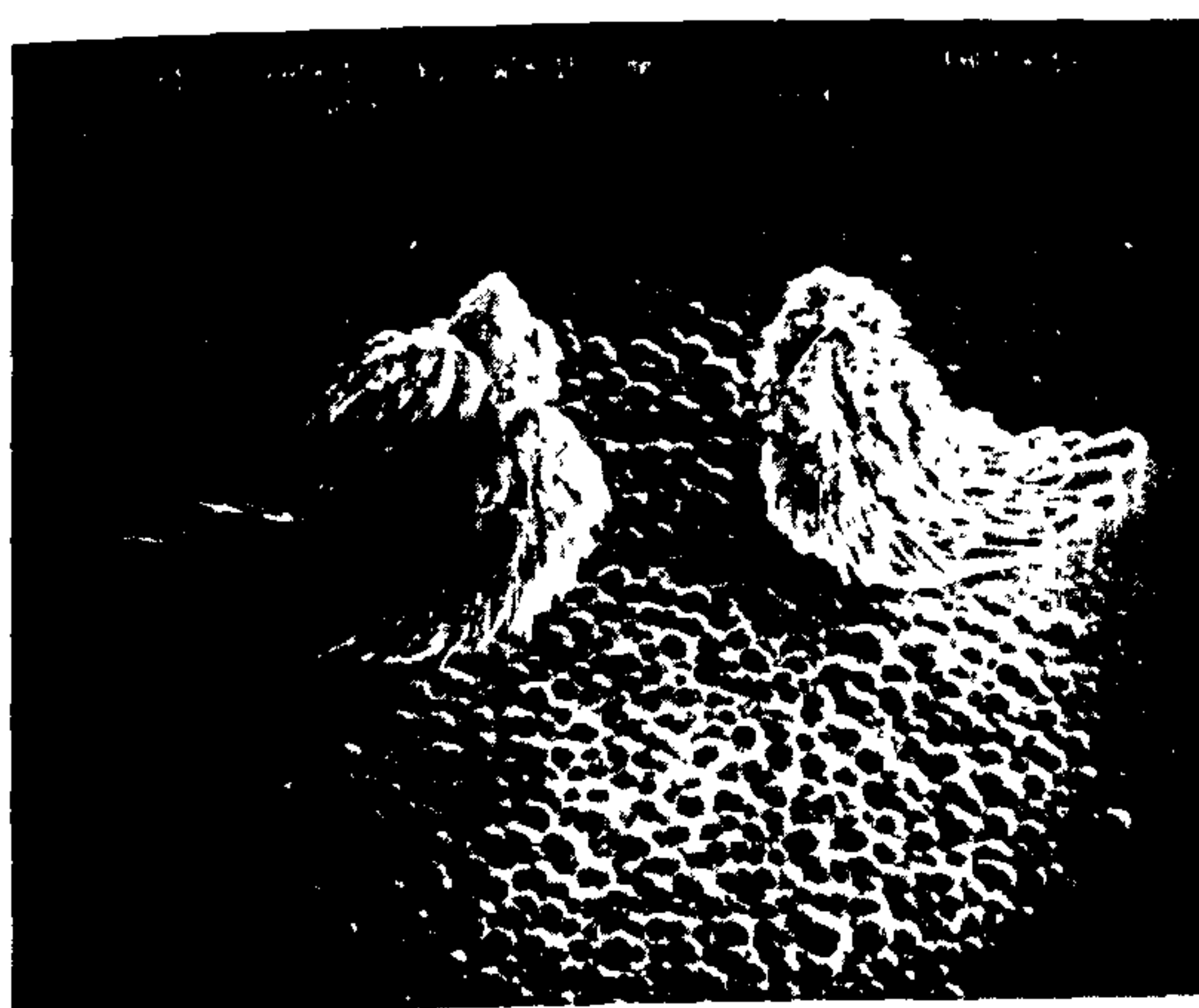
b)



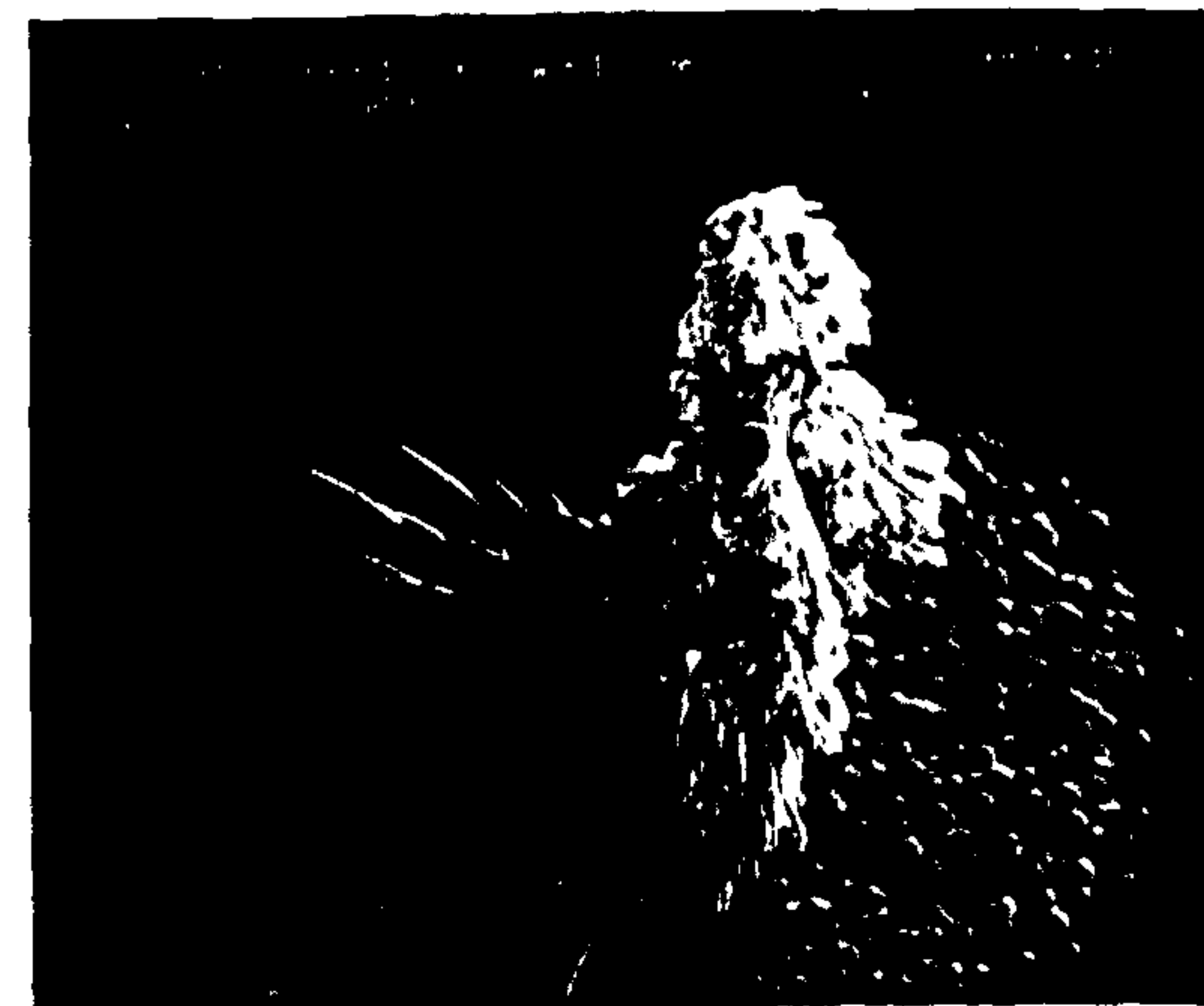
c)



d)



e)



f)

Fig. 13. The growth of the deposit with increasing time. Current density = 10.0 A/cm^2 , $Re = 12100$, gold = 0.17 M .
a) 0.6 s b) 1.5 s c) 2.0 s d) 3.5 s e) 6.0 s f) 8.0 s

calculation, the diffusion coefficient D of $1.68 \times 10^{-5} \text{ cm}^2/\text{s}$ at 60°C as given by Cheh⁽¹⁸⁾, has been used. This value was derived from a citrate type gold electrolyte with a gold concentration of 0.007M . It is known that an increase in concentration decreases the value of D but this decrease is relatively small and will be ignored in this instance. More accurate values of D for the concentration of gold being used are being estimated at the present time. Under the conditions specified, the maximum diffusion layer thickness is calculated to be $4\mu\text{m}$. However, this value is likely to be high because of the arbitrary choice of the limiting current density value and the high value of D . A diffusion layer thickness of closer to $2\mu\text{m}$ is more realistic.

Whilst a fast growing nodule is confined to the diffusion layer, its growth will be controlled by planar diffusion. Its growth will be enhanced by the fact that its local current density will be higher than that of the surrounding deposit. If the nodule penetrates the bulk diffusion layer, a local diffusion layer will develop around it. If the radius of the nodule is much less than the thickness of the local diffusion layer, then spherical diffusion will take over as the dominant mass transfer mechanism. As spherical diffusion occurs at a rate which is several orders of magnitude faster than planar diffusion, then the growth of the nodule will be accelerated even further. As the nodule grows, the field intensity will increase and the local current density will increase, accelerating growth even further. On penetrating the static hydrodynamic boundary layer, the nodule will disrupt the flow, causing a local increase in turbulence in its wake. This will lead to a further increase in diffusion in the direction of the flow. In this way, a structure such as that seen in fig. 14 will develop.

If the current density is sufficiently high, when a fast growing nodule penetrates the diffusion layer, the deposit will grow in the direction of the electric field and thus will grow in the axial direction of the jet along the jet wall as well as in the radial direction. Such growths are dendritic in nature and the structure assumes a crown-like appearance, as in fig. 15. Current densities higher than those that produce this structure

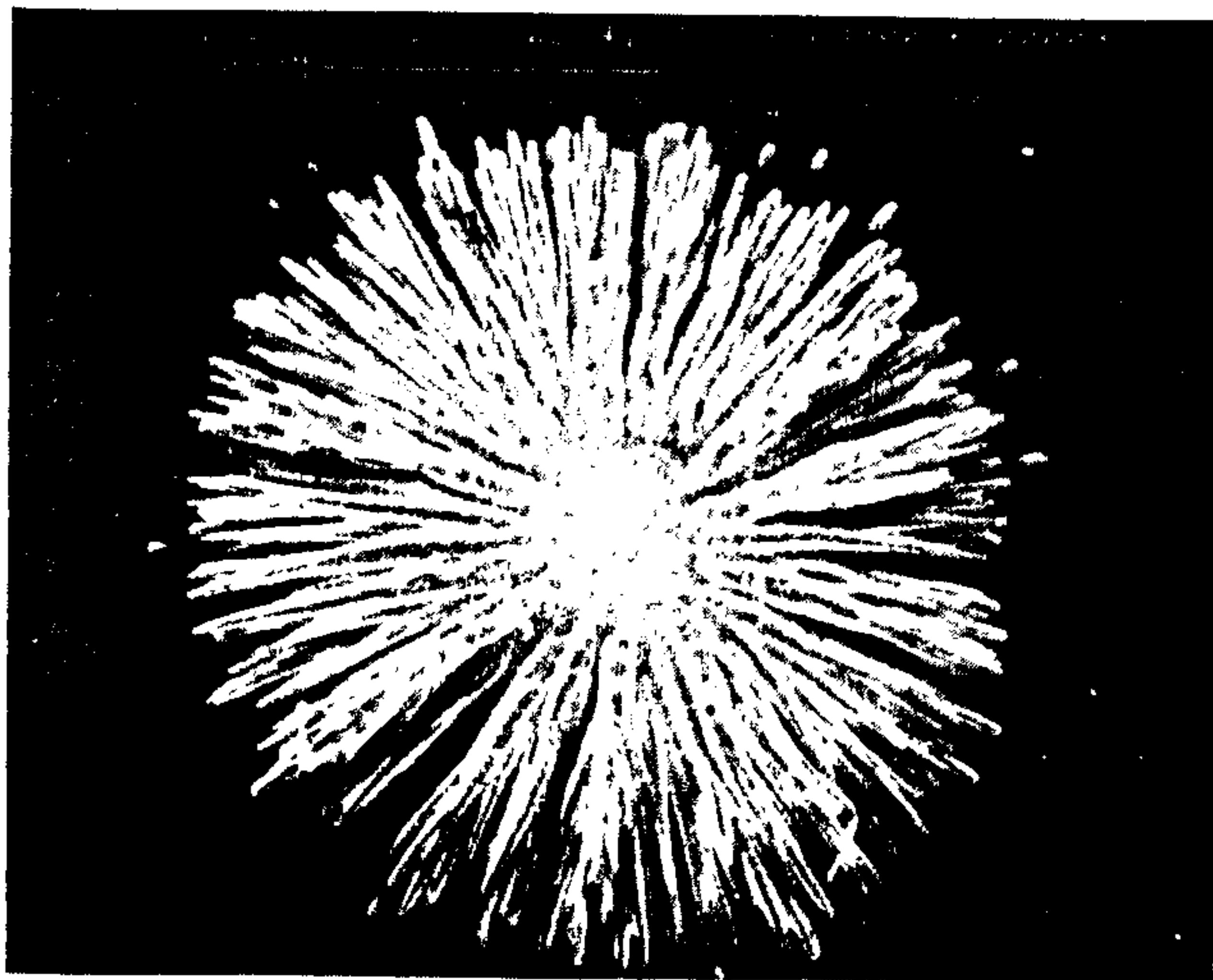


Fig. 14. A typical radial needle structure

lead to a second type of field-oriented growth, where the dendrite or dendrites grow within the central core region of the jet. While the main growth front is towards the nozzle, semi-radial needles grow in the direction of the flow towards the surface for the same reasons as described above. This gives rise to a structure shown in fig. 13f and, ultimately, a structure such as that shown in fig. 16 and on the front cover of this issue. This behaviour arises when a radial needle grows adjacent to, and above, the stagnation region and into the flowing central core of the jet. Residual radial

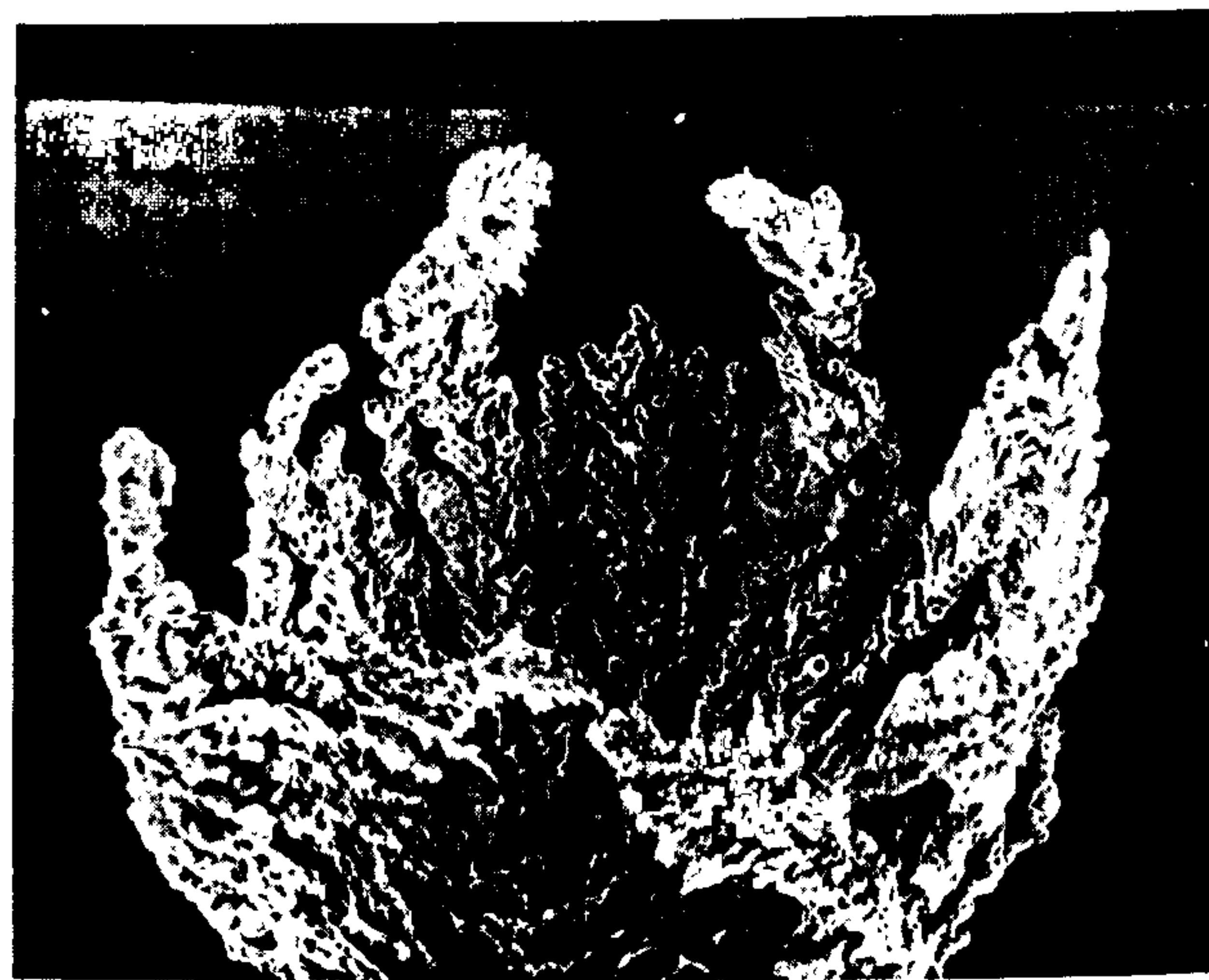


Fig. 15. A typical field-orientated dendritic 'crown' structure



Fig. 16. A typical jet core dendritic structure

needles can be observed adjacent to these field-orientated growths. In many of the examples shown, it will be noted that, in the stagnation region, there is no flow-directional growth apparent. The radius of this region is about $50\mu\text{m}$ and supports the claim of Dawson⁽¹⁷⁾ mentioned earlier.

Temperature and metal ion concentration also affect the morphology as they both influence the diffusion coefficient and thus the limiting current density. Small differences in morphology have been recognized at lower temperatures and concentrations, but these are caused by differences in the ratio of the diffusion and boundary layer thicknesses.

7. APPLICATIONS OF HSSJE

High speed selective jet electrodeposition has numerous potential applications. It can be applied to any situation where selective deposition is an important requirement. The following examples are being addressed but, at this stage, a full evaluation of both the mechanical and electrical properties of the various examples has not been completed.

7.1. The direct writing of microwave integrated circuit substrates (MICS)

MICS are used extensively throughout the telecommunications and defence industries for mounting active devices such as amplifiers, delay lines etc. The substrates can be made from sintered alumina, quartz or PTFE composites. These are metallized using sputtering or electroless plating methods and circuit tracks are produced either by additive or subtractive photolithography. These methods are expensive.

However, by using the direct writing facility provided by HSSJE, the circuits might be written, without the need for masking, directly from the CAD designs. A sputtered or electroless plated layer is still required in order to make the insulator conductive. After the direct writing process, these thin metallized layers can then be removed by etching with virtually no attack on the written gold layer. Initial evaluations of the microwave propagation properties of such tracks are encouraging. Fig. 17 shows a simple ring oscillator produced by direct writing.

7.2. The selective plating of reel-to-reel components

Large quantities of strip or pressed strip components such as connectors and lead frames are currently being produced either by controlled-depth immersion or by submersed jet deposition, with the reel being held between either fixed or movable rubber masks. The direct-write system might enable such components to be produced at very high production rates without the need for the rubber masks. The size of the plant required and the volume of electrolyte could be considerably reduced, thus reducing the capital expenditure and throughput times. Hard gold is used in the majority of reel-to-reel processing and work on the hard gold system is currently being undertaken in this project.

7.3. Bump plating

Tape automated bonding (TAB) is a technique that is important in the electronics industry. The process involves the production of lead frames on a metallized plastic strip, similar to a 35 mm photographic film. In order to connect the integrated circuits to the lead frames, ultrasonic bonding of gold or aluminium wires is used. To facilitate this, a gold bump is required at the end of each lead. There are several difficulties in using a photoresist technique for this. However, selective jetting may be able to overcome many of these problems.

7.4. The direct writing of etch resist for printed circuit boards

Printed circuit boards have been directly written using gold as an etch resist. Fig. 18 shows an example of this method. No masking was used. This technique could be used for small prototype boards where extremely short turn-round times are desirable. The process can take CAD designs and write the resist pattern in a matter of minutes, the time depending on the complexity and size of the board. The example shown took 15 minutes to produce and 5 minutes to

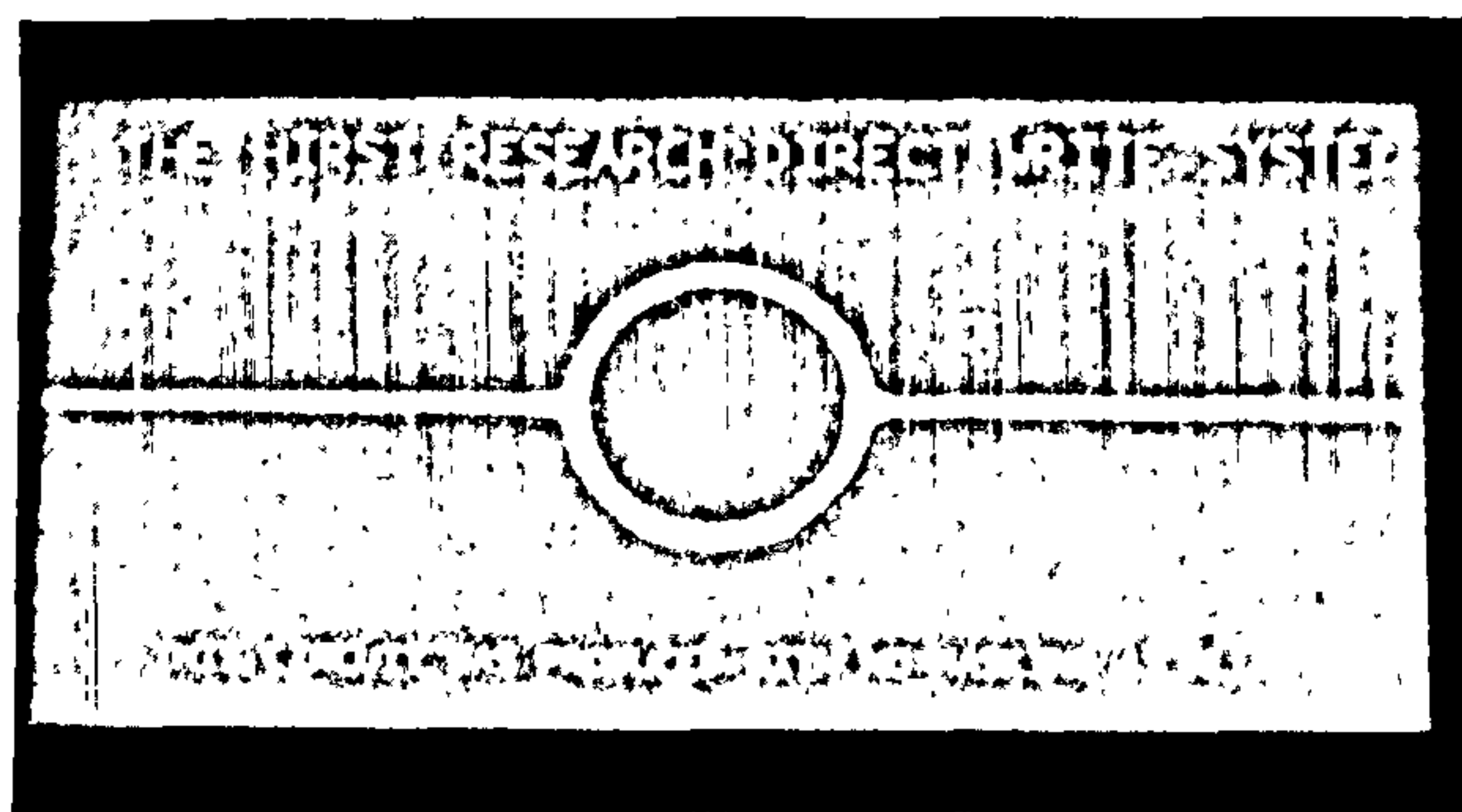


Fig. 17. A ring oscillator microwave circuit demonstrator produced by direct writing

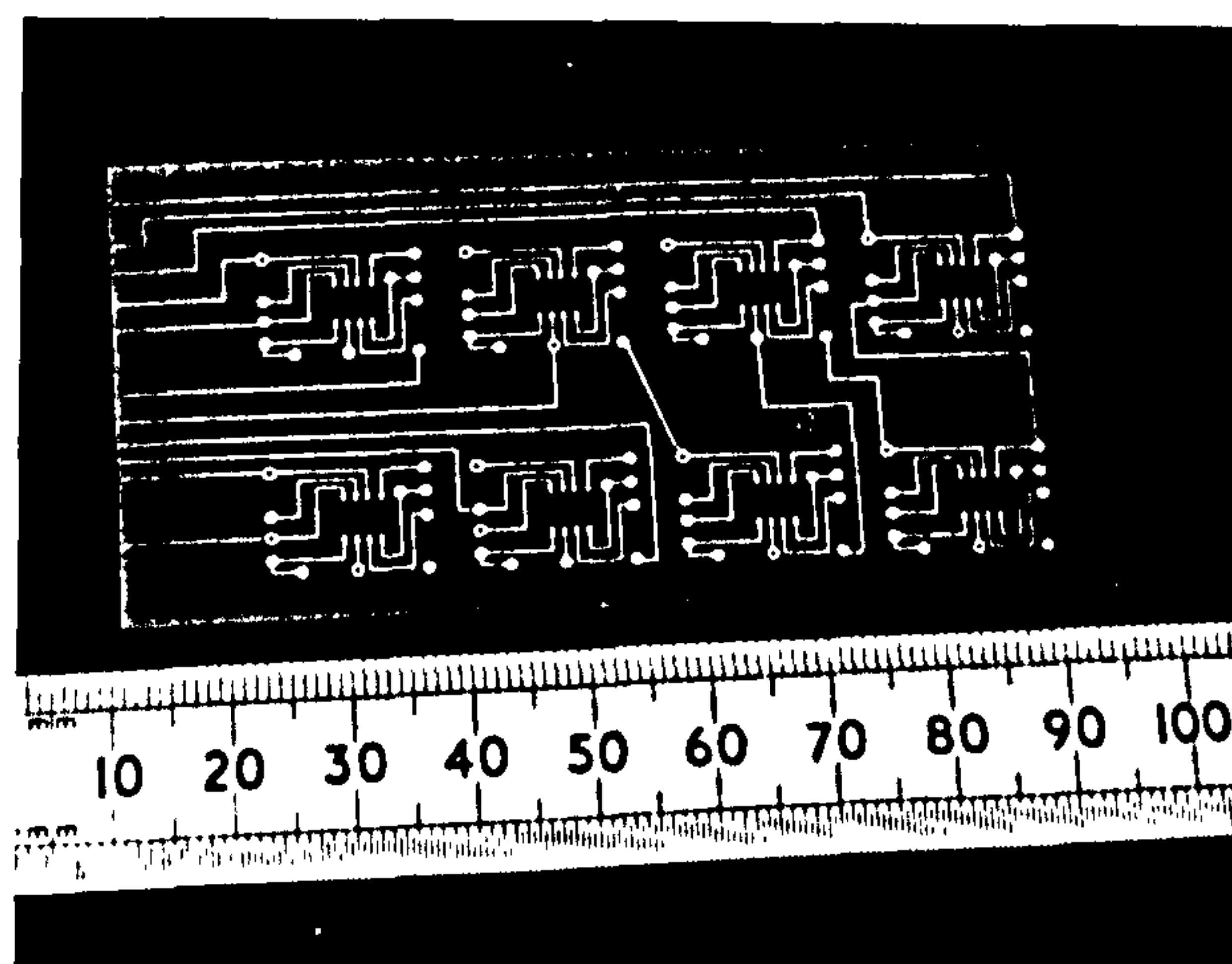


Fig. 18. An example of a directly written etch resist pattern for a printed circuit board after etching the copper cladding

etch the unwanted copper clad layer. Edge definition is good and undercut is minimal. By the use of multiple jets, many circuits could be written simultaneously, allowing the process to be used for small to medium sized batches.

There are many other applications of the process which are company confidential. The process is not limited to gold. Other metals have been examined and work is continuing on processes directly relevant to the electronics industry. It may be concluded that this process may offer a significant step forward in selective plating because of its high speed and cost savings in the elimination of masking processes, relatively low capital cost and simplicity of operation.

8. SUMMARY

It has been shown that, by means of a high velocity jet of electrolyte impinging on a substrate, gold and copper deposits can be produced at high deposition rates, some two to four times the maximum for conventional methods. For pure gold, deposition rates of up to $3.5\mu\text{m/s}$ have been obtained. For copper deposits, deposition rates of up to $1.6\mu\text{m/s}$ were obtained. However, the electrolyte currently used tends to etch the surface after the deposit has formed.

The relationships between deposition conditions and deposit structure and selectivity have been established. Mechanisms for the growth and degradation, based on empirical observations of the gold system, have been proposed. It is hoped that an understanding of these mechanisms will assist in achieving higher plating rates.

Some potential applications have been described and some demonstration samples have been produced using the HSSJE in combination with a CAD/CAM system. These processes will be developed further to establish a facility that will enable selective electrodeposition to be carried out on a faster, cheaper and less labour intensive basis.

ACKNOWLEDGEMENTS

The author wishes to thank Mr I. Gunter of the Metallurgy Group, Hirst Research Centre, for his invaluable assistance in the design of the control equipment and the computer programming that made this work possible. Other staff of the Materials and Components Assessment Laboratory, Hirst Research Centre and Mr F. Page of the Electron Microscopy Unit of the Loughborough University of Technology are acknowledged for producing the SEM micrographs presented here.

This work is part of a BRITE/EURAM project, No. RI1B-0304, in partnership with Centro Sviluppo Materiali of Italy and Loughborough University of Technology and they are thanked for their agreement to publish this paper.

The author also wishes to thank Dr D. Gabe, Mr I. Christie and Dr B. Cameron for their helpful comments.

REFERENCES

- 1 GLAUERT, M.B., 'The Wall Jet', *J. Fluid Mech.* **1**, p. 625, 1956.
- 2 ROBINSON, D.J. and GABE, D.R., 'High Speed Electrodeposition of Copper from Conventional Sulphate Electrolytes', *Trans. Inst. Met. Fin.*, **48**, p. 35, 1970.
- 3 GABE, D.R. and WALSH, F.C., 'Enhanced mass transfer at the rotating cylinder electrode. I. Characterization of a smooth cylinder and roughness development in solutions of constant concentration', *J. Appl. Electrochem.*, **14**, p. 555, 1984.
- 4 BARKEY, D.P., MULLER R.H. and TOBIAS, C. W., 'Roughness Development in Metal Electrodeposition. 1 Experimental Results', *J. Electrochem. Soc.* **136**, 8, p. 2199, 1989.
- 5 US Patent No. 3810829, James C. Fletcher, NASA, May 1974.
- 6 HAYNES, R., RAMACHANDRAN, K. and FINEBERG, D.J., 'The technique of fluid flow masking selective plating. Part 1 - Development of the technique', *The Western Electric Engineer*, **22**, p. 61, April 1978.
- 7 DOREY II, J.K., HAYNES, R., SINITSKI, R.E. and WOODS, R.E., 'High-speed gold plating from dilute electrolytes', *Plat. and Surf. Fin.* **67**, p. 81 May 1980.
- 8 ALKIRE, R.C. and CHEN, T.J., 'High speed selective electroplating with single circular jets', *J. Electrochem. Soc.* **129**, 11, p. 2424, 1982.
- 9 HSUEH, K.L. and CHIN, D.T., 'Mass transfer to cylindrical surface from an unsubmerged impinging jet', *J. Electrochem. Soc.* **133**, 1, p. 75, 1986.
- 10 CHIN, D.T. and TSANG, C.H., 'Mass transfer to an impinging jet electrode', *Ibid*, **125**, No.9, p. 1461, 1978.
- 11 ALKIRE, R. and JU, J.B., 'High speed selective electroplating with impinging two dimensional slot jet flow', *Ibid*, **134**, 2, p. 294, 1987.
- 12 BOCKING, C.C., 'Laser enhanced and high speed jet electrodeposition', *Trans. Inst. Met. Fin.*, **66**, p. 50, 1988.
- 13 BOCKING, C.C., 'High speed selective jet electrodeposition', *Proc. 59th Intl. Conf. on Surf. Fin.* **2**, p. 51, April 1991.
- 14 WATSON, E.J., 'The radial spread of a liquid jet over a horizontal plane', *J. Fluid Mech.*, **20**, 3, p. 481, 1964.
- 15 SCHLICHTING, H., 'Boundary Layer Theory', 4th ed., McGraw-Hill, New York, 1960.
- 16 NAKORYAKOV, V.E., POKUSAEV, B.G. and TROYAN, E.N., 'Impingement of an axisymmetric liquid jet on a barrier', *Int. J. Heat Mass Transfer*, **21**, p. 1175, 1978.
- 17 DAWSON, D.A. and TRASS, O., *Can. J. Chem. Engng*, **44**, p. 121, 1966.
- 18 CHEH, H.Y. and SARD, R., 'Electrochemical and Structural Aspects of Gold Electrodeposition from Dilute Solutions by Direct Current', *J. Electrochem. Soc.* **118**, 11, p. 1737, 1971.

The Use of High Speed Selective Jet Electrodeposition of Gold for the Plating of Connectors

C. Bocking and
Dr. B. Cameron

GEC-Marconi Hirst Research Centre,
Wembley, UK.

SUMMARY — High speed selective jet electrodeposition (HSSJE) is a process by which electrodeposits can be produced at very high deposition rates, selectively, without the need for masking. Previous papers by Bocking have described the principles of the process. This paper describes the adaptation of a commercially available hard gold electrolyte to the process. Deposition rates of up to $2.5 \mu\text{m}/\text{second}$ were found to be possible under jetting conditions. The properties of the deposits produced under high speed jet conditions have been defined and compared to conventionally produced deposits of the same type. A prototype reel-to-reel plating unit based on the principles of HSSJE has been built which, due to the compactness of the nozzle unit and jet cleaning process, is a fraction of the size of more conventional reel-to-reel plating units. Whilst the results of long term trials are not yet available, some initial results of the performance of connectors plated with this unit are presented.

INTRODUCTION

Most electrical devices interconnect with other devices and the outside world by means of the ubiquitous electrical connector. Vast quantities of connectors are produced throughout the world, many are very low cost particularly in the Far East. The satisfactory performance of a connector is crucial to the overall reliability of any piece of electrical equipment. It has to have a low contact resistance, good corrosion resistance and good wear resistance. This latter property is necessary because connectors are frequently mated and unmated during the course of the equipment lifetime. Many specifications require a connector to remain functional through up to 500 insertion/withdrawal cycles. In order to achieve such a performance, they are usually electroplated with gold, alloyed with small quantities ($\approx 0.1\text{--}0.3\%$) of cobalt or nickel. This increases the hardness whilst maintaining a satisfactory contact resistance. Despite competition from the Far East, Europe maintains a healthy production record in connector production. It is estimated that in 1990, 6,869 kg of gold was plated onto connectors in Europe alone¹. The gold plating on a connector constitutes a significant part of the manufacturing cost. As a consequence, there has been a trend to reduce the quantity of gold used either by reducing the thickness or by limiting its application to the functional region by means of selective plating or both. This paper describes a further advance in the selective plating of connectors. The method requires no masking and can deposit suitable gold alloys at much higher speeds than have been achieved previously.

A BRIEF HISTORY OF THE SELECTIVE PLATING OF CONNECTORS

Early high reliability connectors were plated all over with gold. It soon became clear that by limiting the required thickness of gold to the functional contact area, great cost savings could be made. In fact, by the use of selective plating of gold, tonnes of the precious metal have been saved. Non-functional areas were given a much thinner coating to provide a degree of tarnish and corrosion resistance. One of the earliest and still commonly used methods is the use of controlled depth immersion, which is a relative simple selective plating technique. The continuous strip is fed vertically into a plating electrolyte at a controlled depth. The immersed region therefore gets plated whilst the remainder does not. The solution level is maintained by means of a weir at each end of the plating tank. The electrolyte is pumped into the tank from a reservoir to provide a rapid flow past the work allowing high current densities to be used. Hain *et al*² described the advantages of the system as being simple and versatile but listed as disadvantages surface turbulence and capillary action which reduce the selectivity. As a consequence, the feed-through rates have to be low. Also, as many components such as connectors require plating on one face only, and as the whole of the immersed component is plated, there is a considerable wastage of gold.

The use of selective plating of continuous strip became popular in the early '70s. In 1975, Heiestad³ described a variety of selective strip plating equipment

Paper received 5 October 1993

that he was involved in developing. These included anode geometry control (shielding), stationary mask striping, tip plating, moving mask stripe plating and mask spot plating.

Stripe plating is a process in which a stripe of metal or metals is plated onto a continuous strip of metal ribbon. The strip could then be punched and formed into the connector. The stationary mask method made use of a rubber lipped longitudinal slot placed with the plating cell. The moving strip was passed over this slot and was tensioned against it to obtain a solution seal. The electrolyte was pumped at high velocity through the slot and onto the strip. In this way, stripes of 2mm width with a tolerance of ± 0.13 mm could be achieved. Current densities of up to 600 mA/cm² were used for gold plating.

The moving mask stripe plating was achieved by means of synchronising the mask and the strip as it was moved through the plating bath. A split ring and rubber belt combination was used for the mask. However, its plating speed was limited by poor anode positioning and current densities of between 50 and 100 mA/cm² were used. The process did have the advantage of allowing the plating of pre-punched strip lead frames.

Mask spot plating was achieved by using a wheel mask constructed from G10 fibreglass with appropriate holes for delineating the deposit. This had problems with speed and registration but showed the principle of operation very well.

Strip speeds for the various processes were described by Heiestad and range from 6ft/min, for intermittent wheel spot platers, up to 36 ft/min for the continuous processing stripe plating of lead frames, both receiving 50 μ m of gold.

At the same time, Texas Instruments⁴ reported the use of a spot plater for plating nickel gold onto continuous contact strip. A Teflon mask incorporating a platinised tantalum mesh anode was used. No mention was made of whether the mask was stationary or moving or of the strip speed used.

Menzies⁵ described reel-to-reel plating in 1978. The two techniques mentioned are controlled depth immersion and stripe plating, similar to that described previously. At the same time, Rherig⁶ described a step and repeat spot plating unit for the plating of lead frame bond pads in which the spot plating was carried out using a mask that opened and closed in a clamshell manner. The mask was constructed from silicone rubber.

Hain and Rudolf² reviewed selective plating techniques. These included controlled depth immersion, fixed masks and moving masks as well as fluid flow masking. They commented on the various advantages and limitations of the methods, noting that fixed mask systems can create problems of distortion and slow strip speeds due to friction between the mask and the strip.

In 1982, Turner⁷ described the latest techniques for the selective plating of connectors with gold. He described how high agitation rates and high metal ion concentrations enabled high processing speeds to

be achieved. Current densities in the gold bath were in the region of 250 mA/cm². He claimed that a combination of dielectric masking and fluid flow masking (jetting in air) was the most successful technique for high speed continuous strip plating. Details of how this was obtained are not given in this reference.

A more recent review of the selective plating of precious metals for connectors has been given by Wingenfeld⁸. He stated that the moving mask system in conjunction with jetting of the electrolyte is the most widely used selective plating system. A wide range of configurations were described for many connector set types brush. He also described the use of techniques for connectors, making use of either a moving brush or a stationary brush. The moving brush consists of a cylinder, wrapped in an absorbent material, partially dipped into the electrolyte. The cylinder, which is made from platinised titanium, is used as the anode. This slowly rotates and the connector strip passes along the cylinder with only the area requiring plating in contact with it. In this way, selective plating is achieved. Plating rates of up to 6 μ m/min. of gold can be achieved with this method. This technique is becoming less popular as connector sizes become smaller, the area of contact reduces and the required degree of selectivity can no longer be achieved. It has been replaced by the stationary brush. The brush is a V shaped hollow platinised titanium block covered with an absorbent material. The angle of the V is such that the point has a contact area of about 0.8 mm. The electrolyte is pumped at low pressure into the block. A series of holes allows the material to become wetted by the electrolyte by capillary action. The components are then passed along the V of the block and where they touch, electrolyte gently oozes out at a slow but constant rate. The block is mounted onto an adjustment platform that allows the position and the angle of tilt of the block to be set. By tilting the block, larger areas may be plated. Plating rates of between 5–6 μ m/min. are obtained with this method.

Whilst all these methods can satisfactorily produce selectively plated connectors, they do have disadvantages. Generally, the plant takes up a considerable floor-space, is of a complex construction particularly in the case of the moving mask system or is relatively slow as with brush plating. The high speed selective jet electrodeposition method described in this paper addresses these problems. The plant required is relatively small and inexpensive, of a simple design and there is no requirement for masking. In addition, the jet velocity is such that significantly higher deposition rates can be achieved, allowing a high throughput of strip.

THE PRINCIPLES OF HIGH SPEED SELECTIVE JET ELECTRODEPOSITION.

High Speed Selective Jet Electrodeposition (HSSJE) is a process in which metal may be deposited selectively without the need

for masking. The principle of the process is that a free standing, non-submersed jet of electrolyte flowing at a high velocity impinges onto a substrate. The application of a suitable voltage between the substrate (cathode) and the nozzle (anode) causes metal to be deposited within the impingement and the immediately surrounding region. Due to the properties of the hydrodynamic flow surrounding the impingement regions, the electrolyte forms an extremely thin radial layer as it flows away. Because this layer, termed the wall jet region, is so thin, the electrical resistance of the electrolyte is comparatively high. This means that under certain conditions, deposition is limited to the impingement region, with little deposition occurring within the highly resistive wall jet. In this way selectivity is achieved. Figure 1 shows a schematic view of the electrolyte flow. Due to the high electrolyte velocity, high current densities can be applied and therefore high plating rates can be realised.

Selective Jet Deposition is not a new process, with the principle being patented by NASA⁹ in 1974. This patent described a forced electrolyte flow system in which the nozzle was scanned across the substrate and current applied at appropriate times in accordance with a control pattern. In this way, a plated pattern could be written, much in the same way as a picture is formed on a dot-matrix printer. The process described here however uses a "direct write" system more like the way a plotter produces an image.

Since 1974, there has been comparatively little information published on the subject of HSSJE, possibly due to commercial confidentiality reasons. Haynes et al¹⁰ described a forced flow jet plating system in 1978 and Dorey et al¹¹ used a modified version of this equipment to gold plate connectors for the evaluation of the thermocompression bonding characteristics of the deposits. The maximum flow rate used was 39 cm/sec and current densities of up to 1.3 A/cm². They found that the deposit quality deteriorated at current densities in the region of 0.86 A/cm² by nodule formation. However, it was claimed that nodular deposits did not detract from bondability. There have been a number of papers published attempting to correlate mathematical models of jet plating systems with experimental results^{12,13,14,15}. However, little work has been published on the morphological characteristics of deposits produced in this way.

Bocking¹⁶ described selective pure gold deposition using both laser enhanced jet deposition and HSSJE using small bore nozzles (1mm to 0.25mm). He examined the morphology of the deposits produced and related these to the electrolyte velocity. The current efficiency of deposition was also described. He went on to show a "direct write" facility whereby the jet could be moved in relation to the substrate by means of a computer controlled X-Y table, producing plated tracks and lines.

The selective deposition of both copper and pure gold deposits has been described

in depth by Bocking^{17,18} focusing on the relationship between deposition conditions and deposit morphology. He found that deposition rates for high quality pure gold deposits could be as high as 3.4 $\mu\text{m}/\text{second}$ at a current density of 6.0 A/cm^2 . The conditions required in order to achieve these rates can be summarised as follows. A high metal ion concentration is required, together with a rapid electrolyte velocity. However, there exists a limit to both. For any particular value of either parameter, an increase in one or the other beyond a certain value leads to a deterioration of the deposit, effectively lowering the deposition rate that can be achieved. An empirical description of the processes involved is given in Reference 18. A third requirement is a high electrolyte temperature.

HARD GOLD ALLOY DEPOSITION USING HSSJE

Whilst it has been shown that it is possible to deposit pure gold at very high deposition rates, there has been no literature describing the composition, properties and

quality of gold alloy deposits at deposition rates in excess of about 0.5 $\mu\text{m}/\text{second}$. The work on pure gold deposition has now been extended to gold alloys and some results of these studies are discussed here. It has been found that gold alloy deposits of good morphological appearance and functional quality can be achieved at deposition rates of up to 3.0 $\mu\text{m}/\text{second}$. A commercially available electrolyte was chosen for this work, the Ronoval N (Supplied by LeaRonol). This electrolyte normally produces gold/nickel alloy deposits with deposit nickel values of about 0.15% at current densities up to 1.0 A/cm^2 and deposition rates of up to 0.25 $\mu\text{m}/\text{second}$. It was designed for the more conventional "high speed" jet plating systems described earlier. As part of its composition, a current density extender, referred to as a "Booster" has been included. This additive is composed primarily of an aqueous solution of nicotinamide. For the purposes of these experiments, the gold concentration was increased to 20g/l to allow the higher current densities to be used with HSSJE.

The deposits from this electrolyte produced under high speed selective jet conditions were examined for the following; (i) nickel concentration in the deposit, (ii) hardness, (iii) structure and morphology and (iv) wear resistance. They were also compared with deposits produced by more conventional routes.

Experimental Method

The experimental techniques used have been described in detail elsewhere^{17,18}. However, a brief description of the methodology used will be given. Deposits of gold/nickel alloy were produced over a range of current densities using a constant number of coulombs ($0.07876 \pm 0.0001 \text{ C}$) for each set of conditions varied. For analytical and structural studies, the total number of coulombs passed should have produced deposits of 20 μm thickness. For examination of the topography of the deposits more akin to normal production thicknesses, 2.5 μm deposits were produced, again using a constant but lower number of coulombs for the series ($0.010944 \pm 0.000025 \text{ C}$). A 400 μm

- ZONE I Free jet
- ZONE II Impingement zone
- ZONE III Wall jet

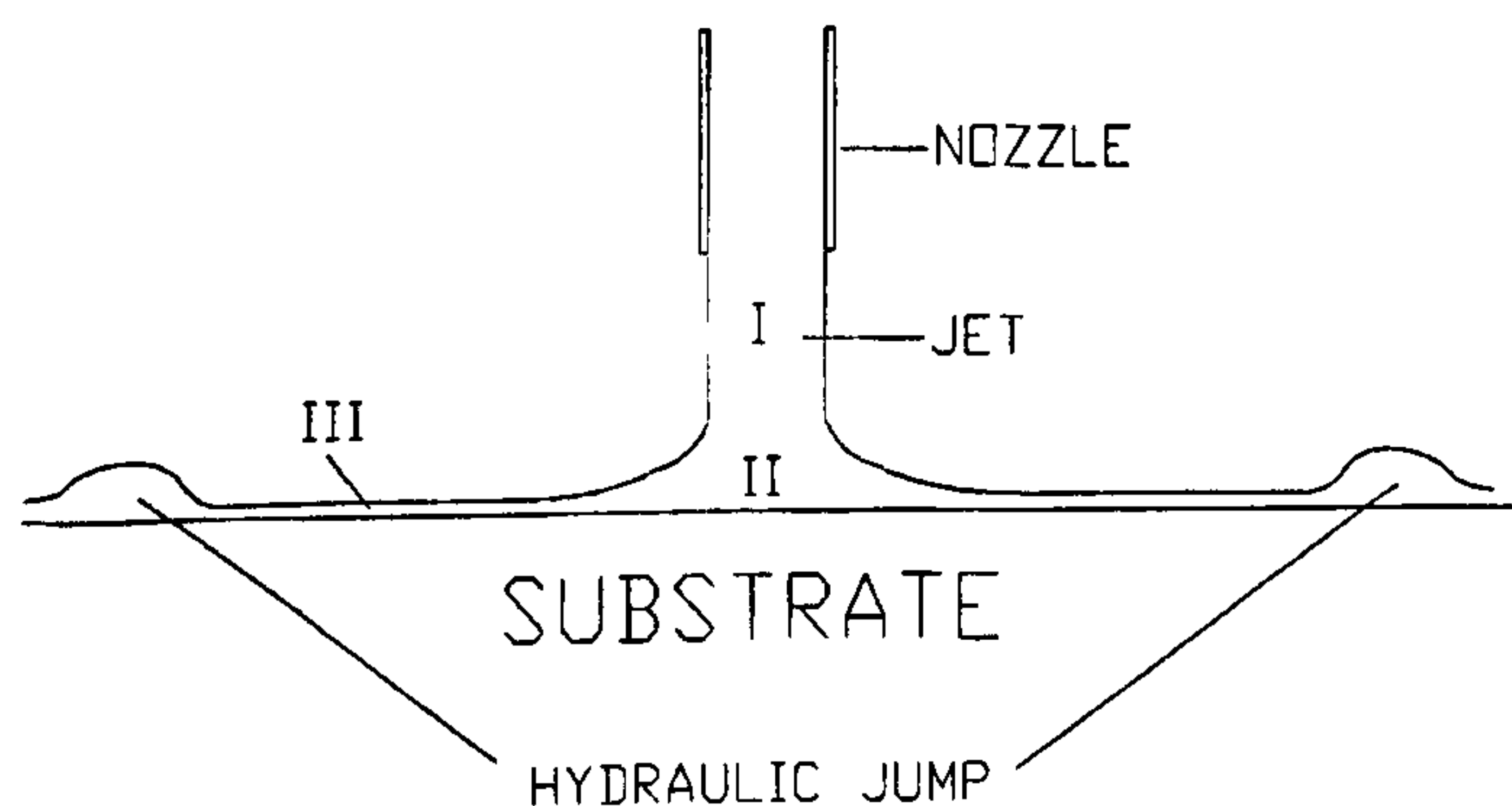


Figure 1. Schematic of the electrolyte jet interaction with the substrate.

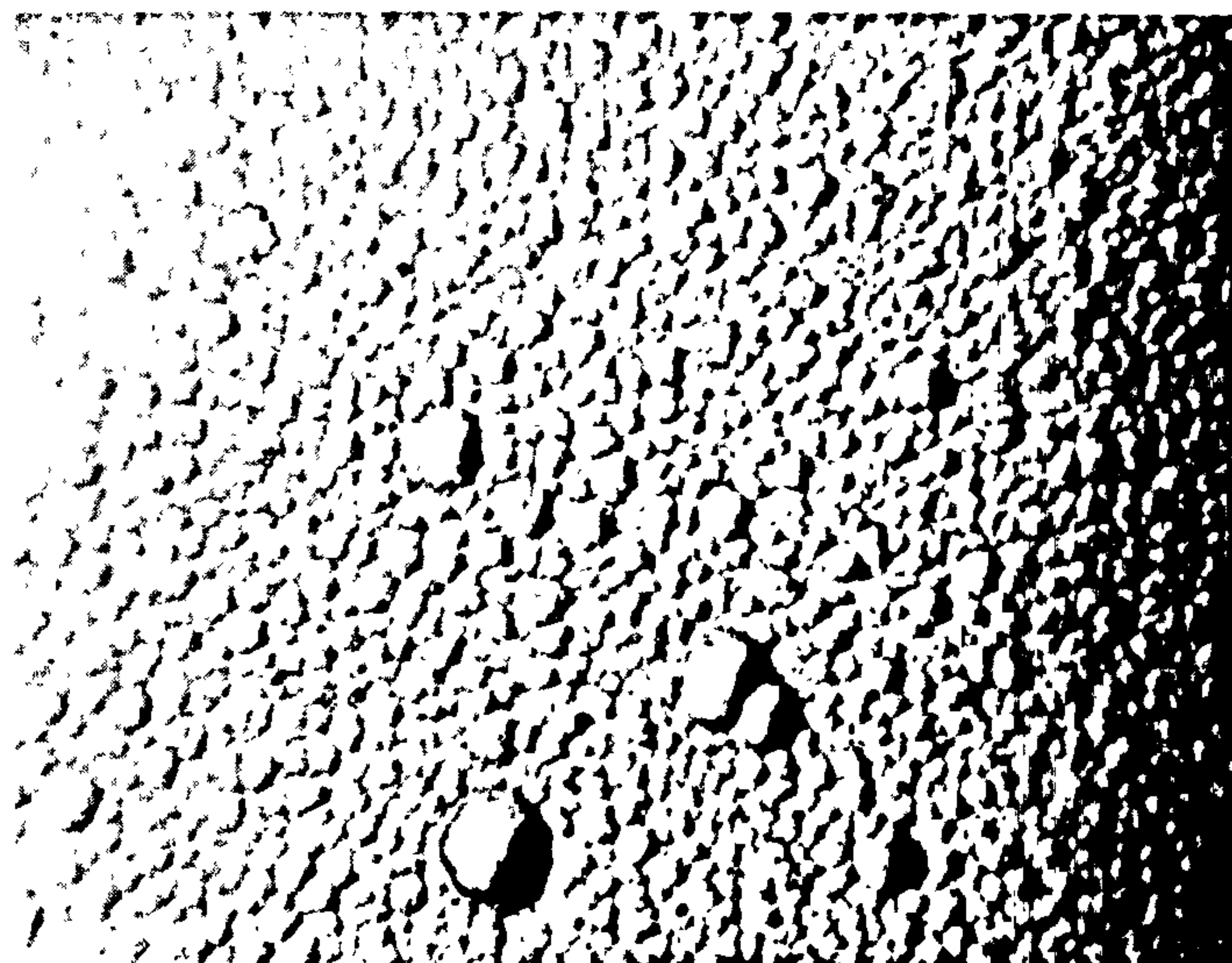


Figure 3. Optical micrograph of a jet deposit from the Ronoval N electrolyte. Current density = 9.0 A/cm^2 , Ni in electrolyte = 2.2 g/l, deposit thickness = 17.5 μm . X1000.

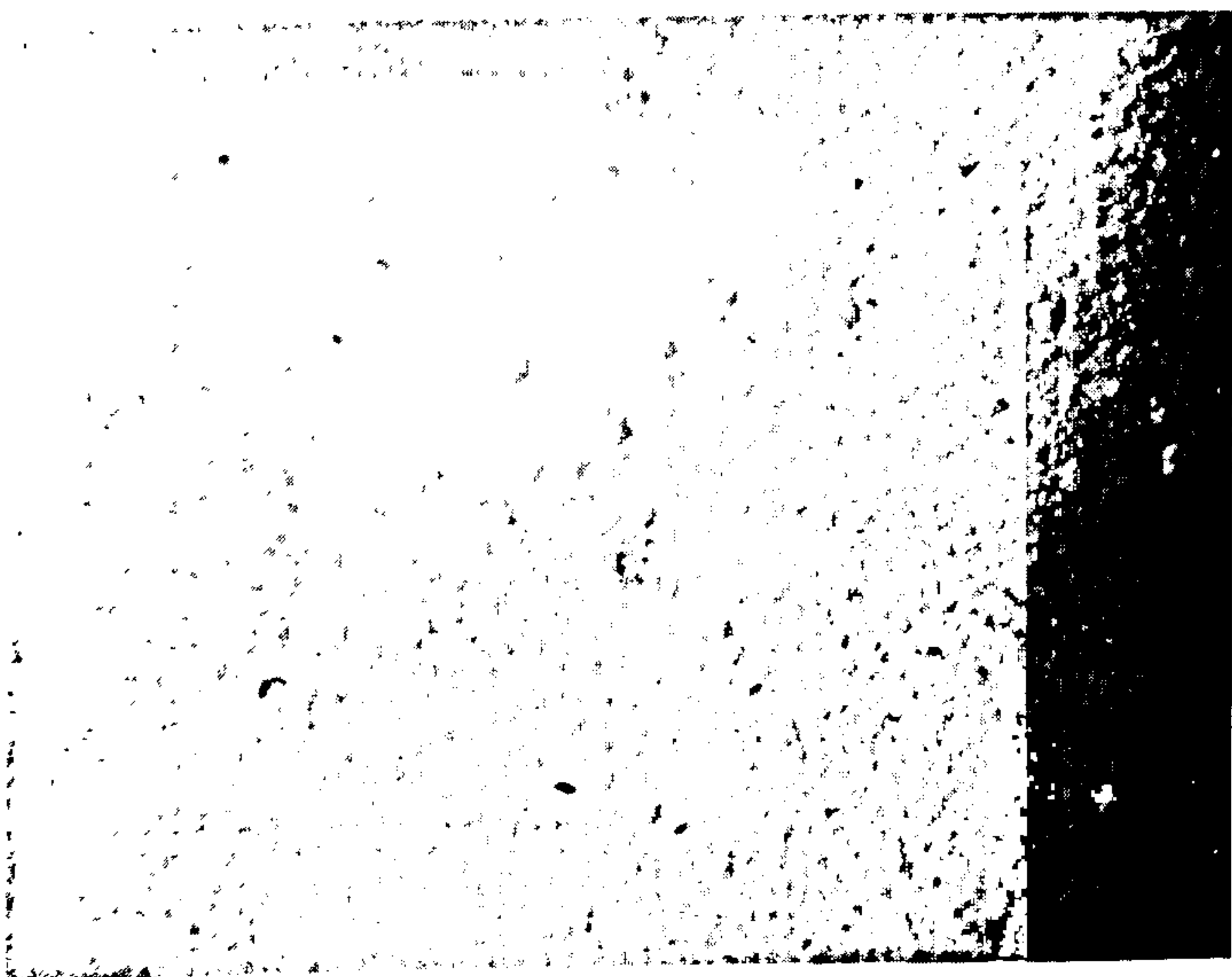


Figure 2. Optical micrograph of a jet deposit from the Ronoval N Electrolyte. Current density = 6.0 A/cm^2 , Ni in electrolyte = 2.2 g/l, deposit thickness = 17 μm . X1000.

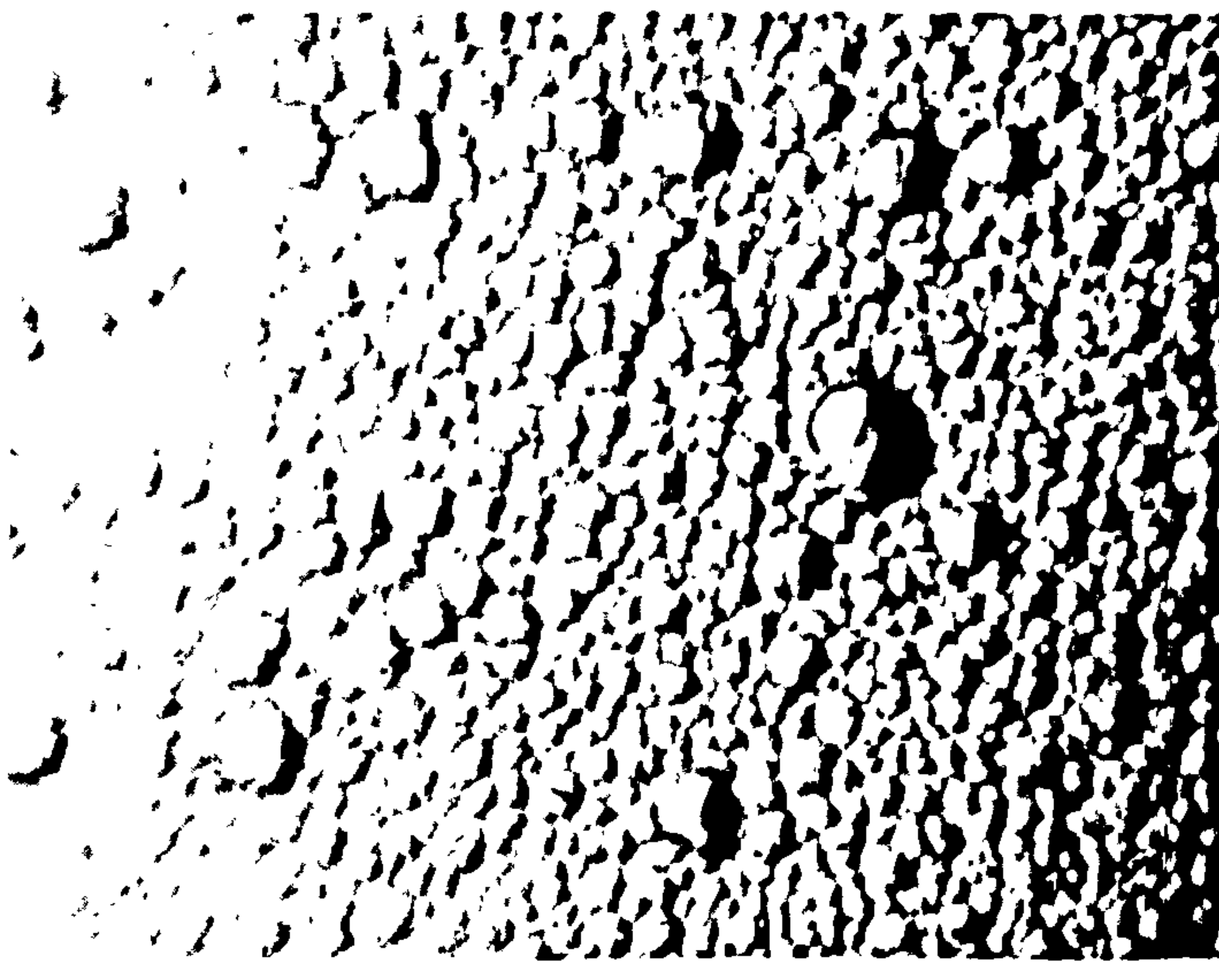


Figure 4. Optical micrograph of a jet deposit from the Ronoval N electrolyte. Current density = 10.0 A/cm^2 , Ni in electrolyte = 2.2 g/l, deposit thickness = 17.4 μm . X1000.

nozzle was used with a nozzle to substrate distance of 1mm. For this work, an electrolyte velocity equivalent to a Reynolds Number, Re, of 10600 was used. This was based on the results obtained from the pure gold studies. The concentration of nickel in the electrolyte was varied between 0 and 3.0 g/l. The temperature was maintained at $55^{\circ}\text{C} \pm 2^{\circ}\text{C}$. The thickness of the deposit spots was measured using a Dektak II Surface Profilometer. The nickel in the deposit was analysed using X-ray Fluorescence spectroscopy (XRF) on arrays of 90 identically produced deposit spots. Hardness measurements were carried out using a Matzusawa microhardness tester fitted with a Vickers Pyramidal diamond. A load of 25g was used. The measurements were carried out directly on the as-plated surface, ensuring that the deposit thickness was in excess of $16\text{ }\mu\text{m}$. Topographical examination was by accomplished using Scanning Electron Microscopy as well as optical microscopy.

After establishing the optimum nickel

concentration in the electrolyte, more detailed studies were carried out using this optimised solution. The cathodic current efficiency was measured using a weigh-plate-weigh method. A total of 90 deposit spots were plated onto a weighed substrate under identical conditions. The substrate was then re-weighed and the efficiency calculated in the usual way. Deposit structure was examined using both microsection methods and X-Ray Diffraction (XRD). The XRD was performed on a Siemens S5000 X-Ray Diffractometer on arrays of 25 identically produced deposit spots.

Wear Measurement Method

Wear measurements were carried out using the GEC Contact Tester CTII. This is an instrument designed to allow the measurement of contact resistance against an adjustable contact force both prior to, during and after a pre-determined number of insertion/withdrawal cycles. Actual pairs of contacts are used rather than the pin and disc configuration which is commonly used; the test geometry is thus

much more representative of the actual wear situation. The individual contact halves are clamped between gold plated jaws, one on each half of the test stage as in Figure 18. One half of the test stage can be moved in a reciprocating manner. The other half of the test stage is provided with X-Y control for alignment of the contact halves. The Z adjustment controls the contact force between the pair. The instrument gives a true four point measurement of resistance by determining the voltage drop across the contact pair when a current of 25 milliamps is passed through the mated contacts. The force measurement system uses a stiff, bridge strain gauged load cell beam. Measurements were made at two loads, 55g and 100g. Contact resistance measurements were made after the initial set-up and then after 50, 100 and 200 insertion/withdrawals. The insertion/withdrawal rate was 40 cycles per minute. A number of contact pairs were measured at each condition and the contact resistance values presented are an average for each set of conditions.

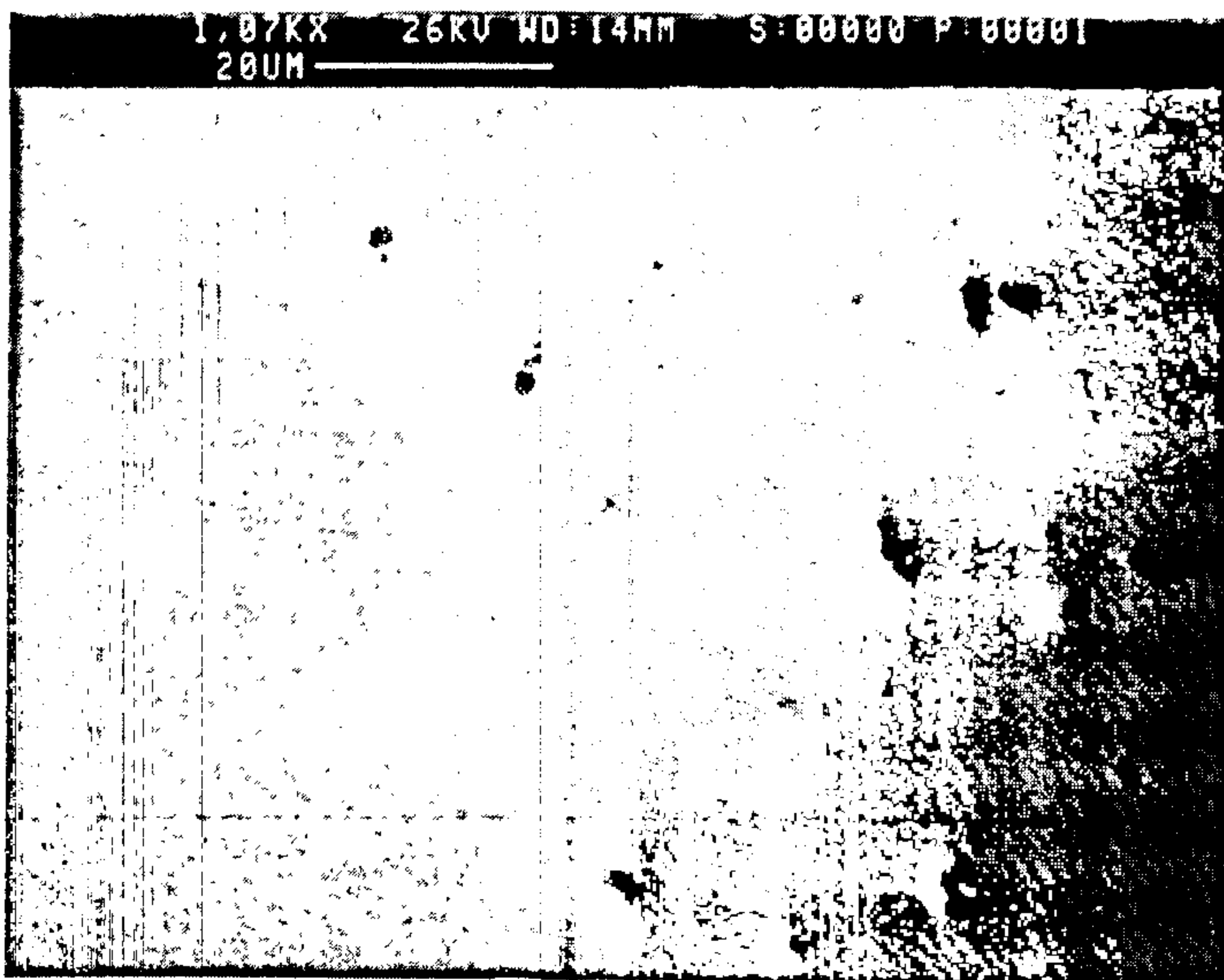


Figure 5. SEM micrograph of a $2.5\text{ }\mu\text{m}$ gold/nickel deposit spot produced by jetting at a current density of 10.0 A/cm^2 with a nickel in electrolyte concentration of 1.9 g/l .

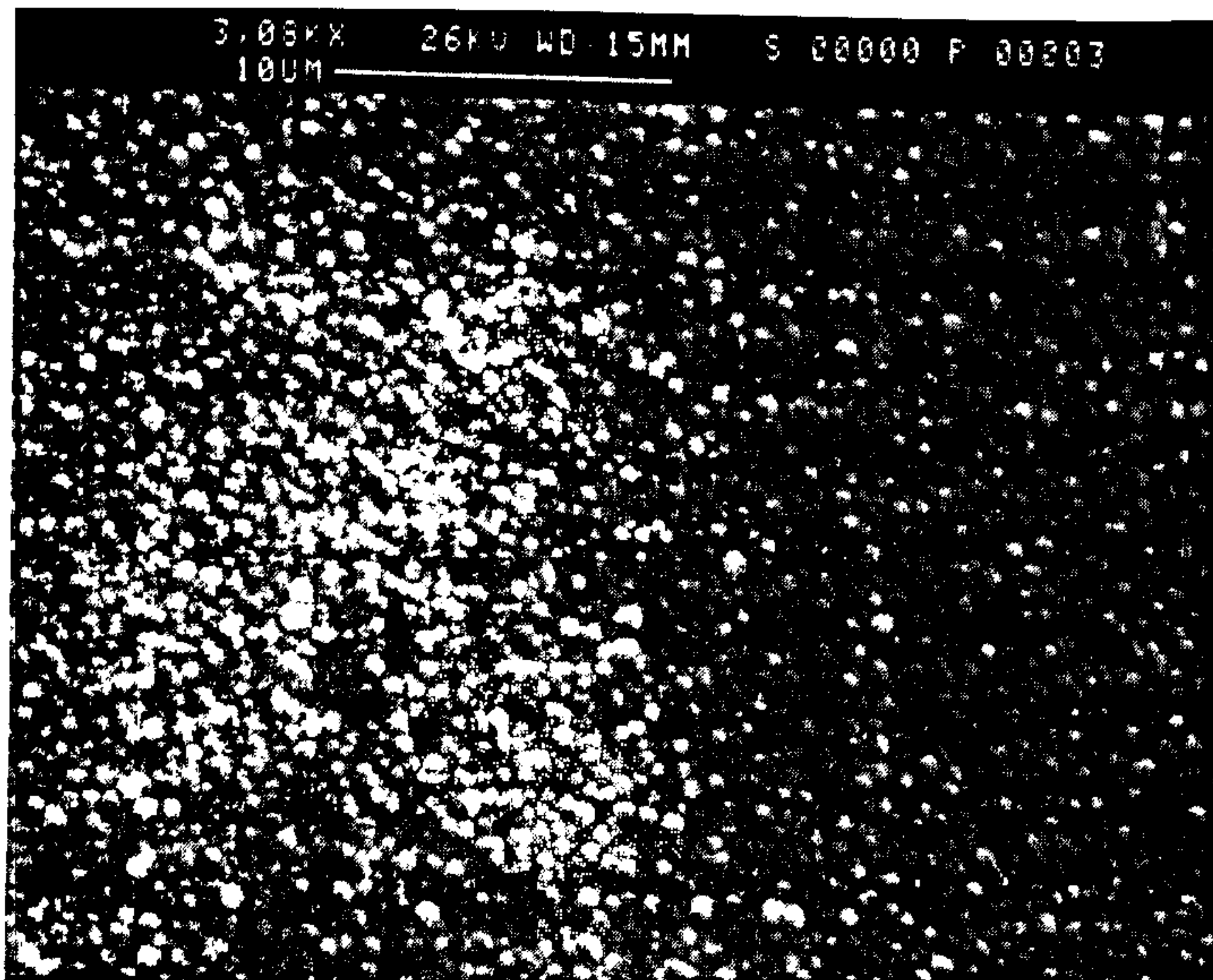


Figure 6. SEM micrograph of a $2.5\text{ }\mu\text{m}$ gold/nickel deposit produced by jetting at a current density of 12.0 A/cm^2 with a nickel in electrolyte concentration of 1.9 g/l .

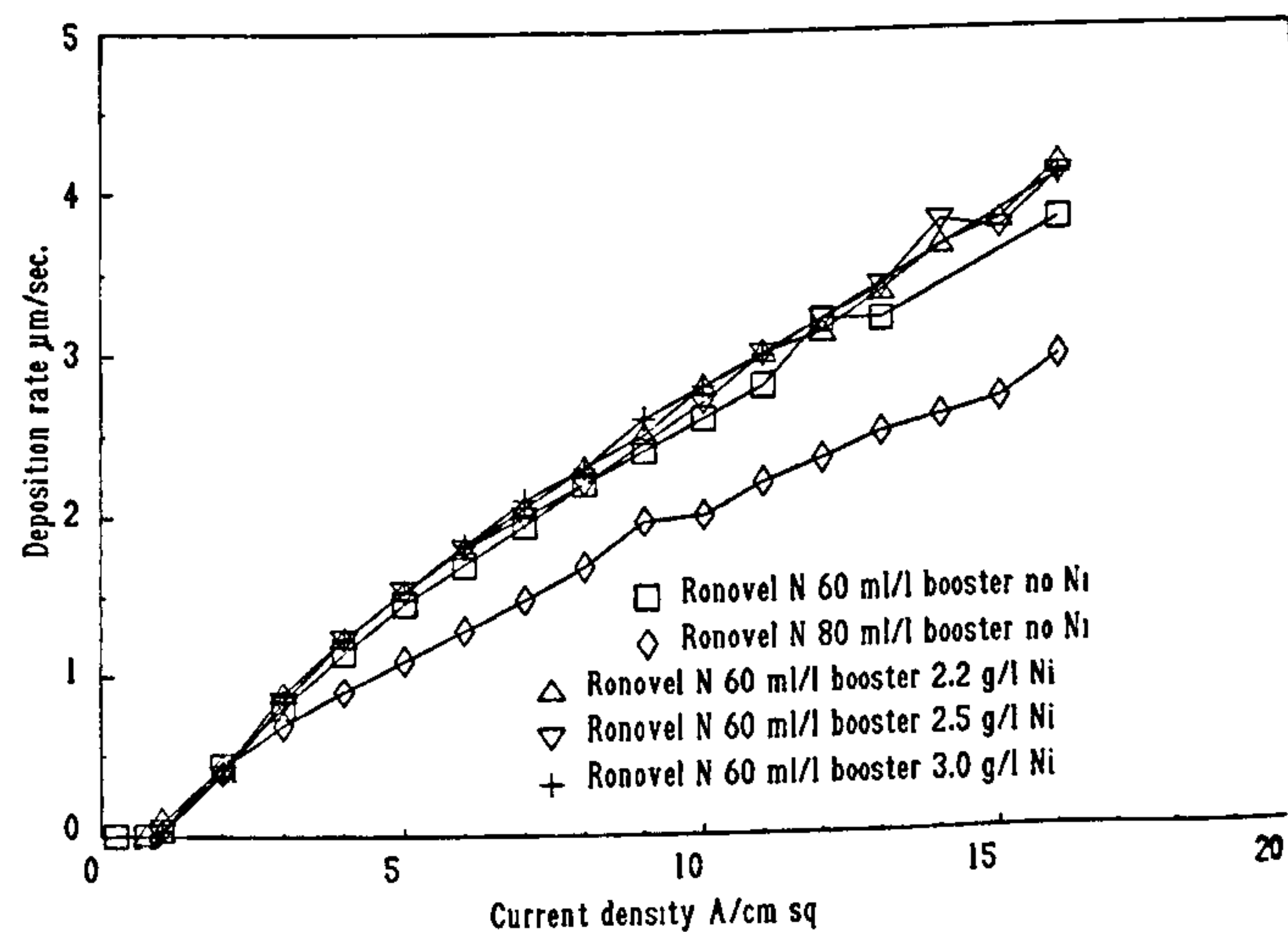


Figure 7. Current density vs deposition rate for various concentrations of nickel and booster in the Ronovel N electrolyte.

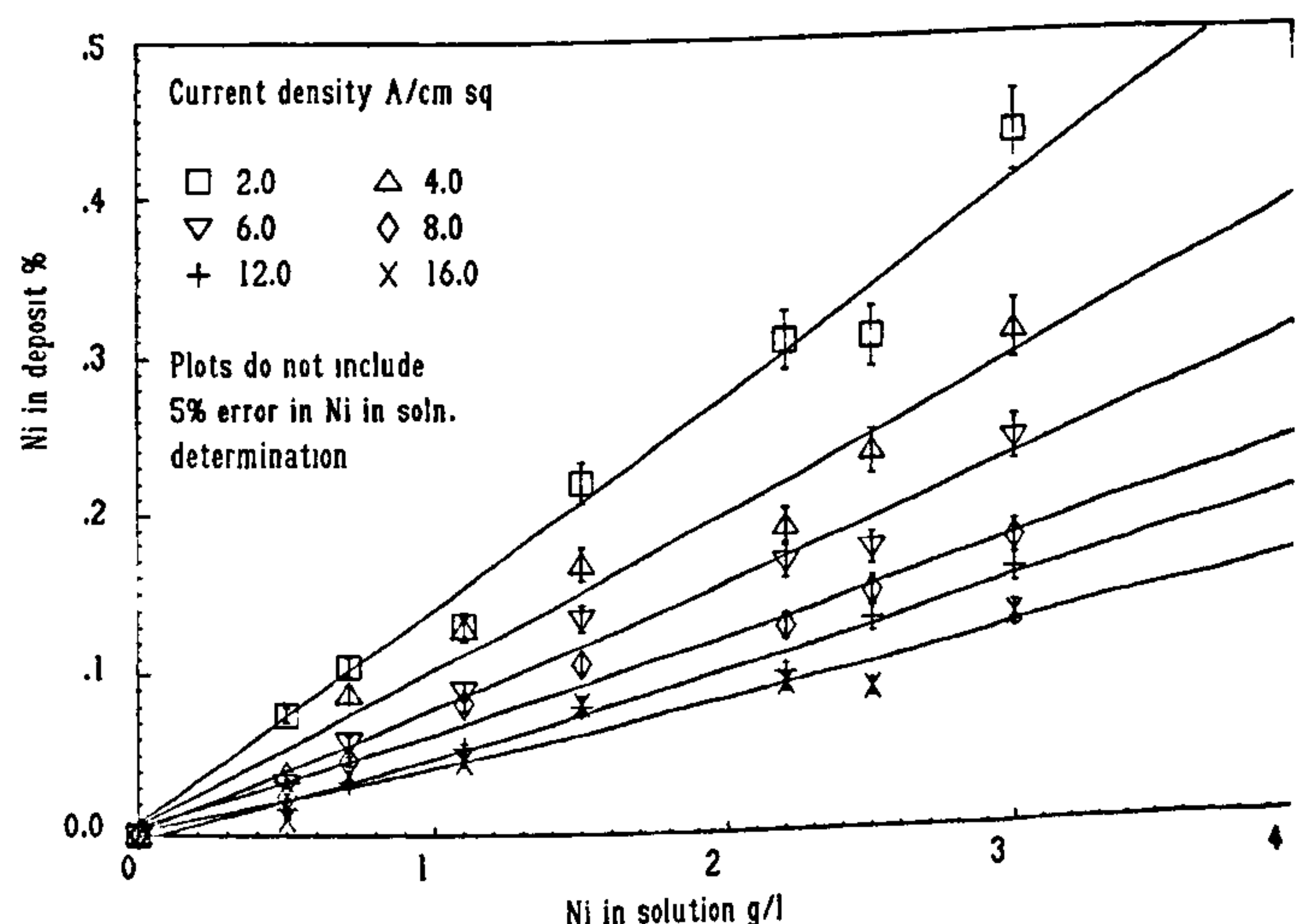


Figure 7. The relationship between the nickel in solution and the nickel in the deposit for different applied current densities.

The tests were carried out using male and female connectors plated with both HSSJE and conventional deposits, with thicknesses of 0.5 and 1.0 μm . The jetted samples were prepared at a current density of 5 A/cm^2 , using a Ronoval N electrolyte containing 1.9 g/l nickel whilst the samples prepared under conventional plating conditions were plated at 15 mA/cm^2 . The nickel concentration of this electrolyte was 1.7g/l. For simplicity, the deposits were produced directly onto the copper substrates with no intermediate layer of nickel. Both male and female connectors were microsectioned to show the distribution of gold over the mating surfaces. It was found that the deposit thickness was constant over the desired area of contact.

After testing, the wear scars were examined using scanning electron microscopy with an energy dispersive X-ray analysis facility. Copper X-ray maps with accompanying micrographs were produced of the contact regions to determine the extent of the penetration of the gold layer.

Deposit topography and appearance

The deposit spots were found to be similar in profile to those of pure gold, ie a broad

symmetrical Gaussian shape. Examination of samples produced using the greater number of coulombs revealed that between 0.25 A/cm^2 and 2.0 A/cm^2 , there was a significant spread of the deposit beyond the impingement zone similar to that observed with pure gold deposits. This spread reached up to 9 mm at a current density of 0.75 A/cm^2 . As these deposits were sub-micron in thickness, little relevant topographical information could be obtained. Between a current density of 2.0 A/cm^2 and 9.0 A/cm^2 , the deposits were much greater in thickness ($> 16\mu\text{m}$). The deposit spread over this current density range was found to be a constant 1.2mm. It could be seen that the deposits were generally smooth and bright although small hemispherical mounds were present at the surface, increasing in size and prominence with increasing current density. At and beyond 9.0 A/cm^2 , it was clear that the surface no longer exhibited mounds but was distinctly nodular. This trend was apparent irrespective of the quantity of nickel in deposit. Figures 2, 3, and 4, show some typical examples. However, examination of deposits having a thickness of $\approx 2.5 \mu\text{m}$ showed few surface features up to a current density of 10.0 A/cm^2 . Above this

value, numerous small nodules were quite evident. This trend can be seen in Figures 5 and 6. Figure 5 is comparable to a conventional deposit produced from the Ronoval N electrolyte.

Deposition Rates

Figure 7 shows typical deposition rates vs current density for different concentrations of nickel in the electrolyte. The nickel concentration did not appear to influence the deposition rate. From the above observations, it would appear that for deposit thicknesses of 2.5 μm or less, a maximum deposition rate of 2.8–3.0 $\mu\text{m}/\text{second}$ could be achieved whilst maintaining a similar topography to that of conventionally deposited gold alloys.

The relationship between the nickel in the electrolyte and nickel in the deposit

Figure 8 shows the relationship between the nickel in the deposit and the nickel in solution over a range of current densities. It can be seen that there is a linear relationship between these parameters for all current densities and concentrations examined. This would indicate that the nickel in the deposit could be easily controlled by means of relatively simple

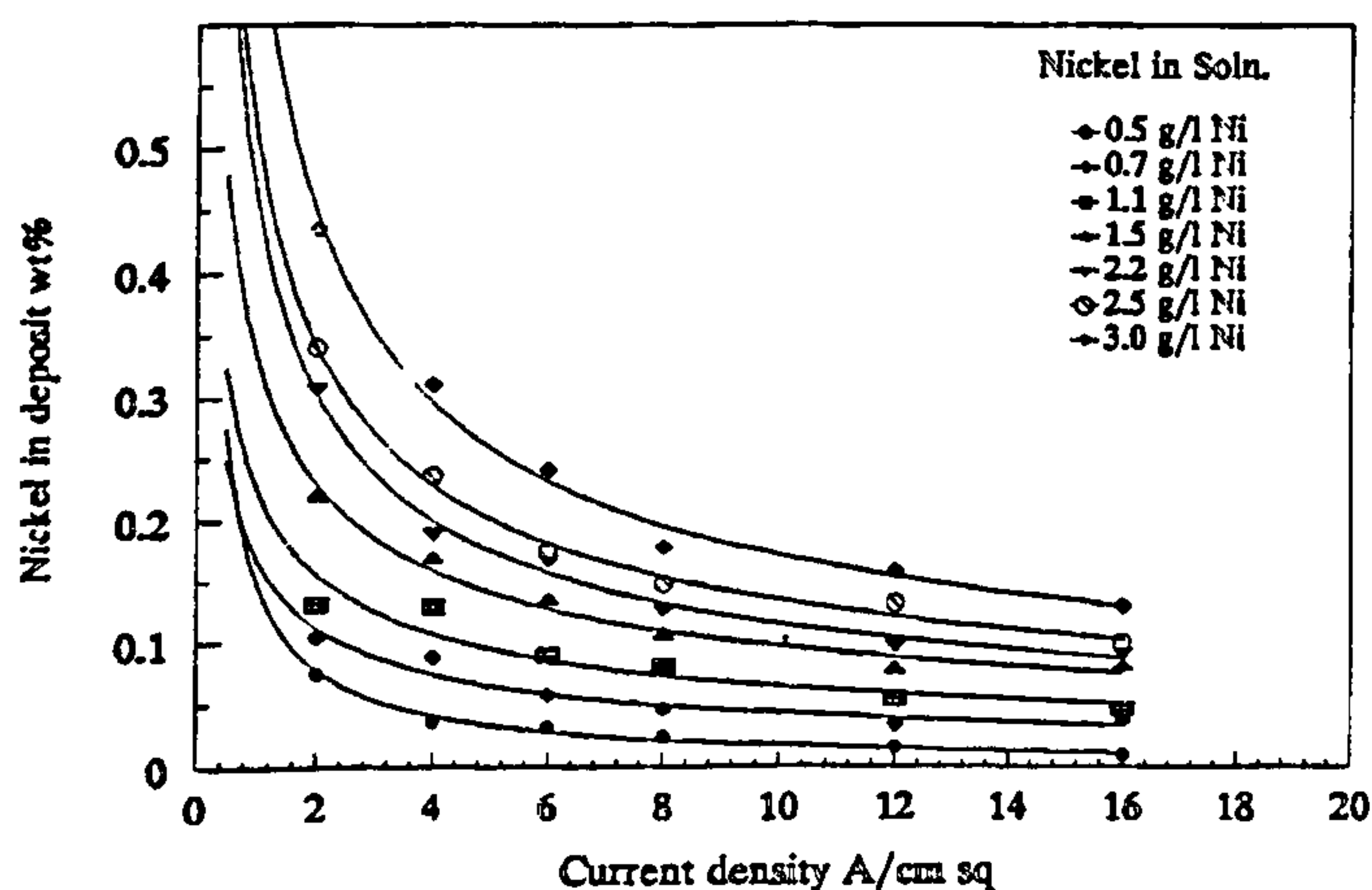


Figure 9. The relationship between the nickel in the deposit and the applied current density for different concentrations of nickel in the electrolyte.

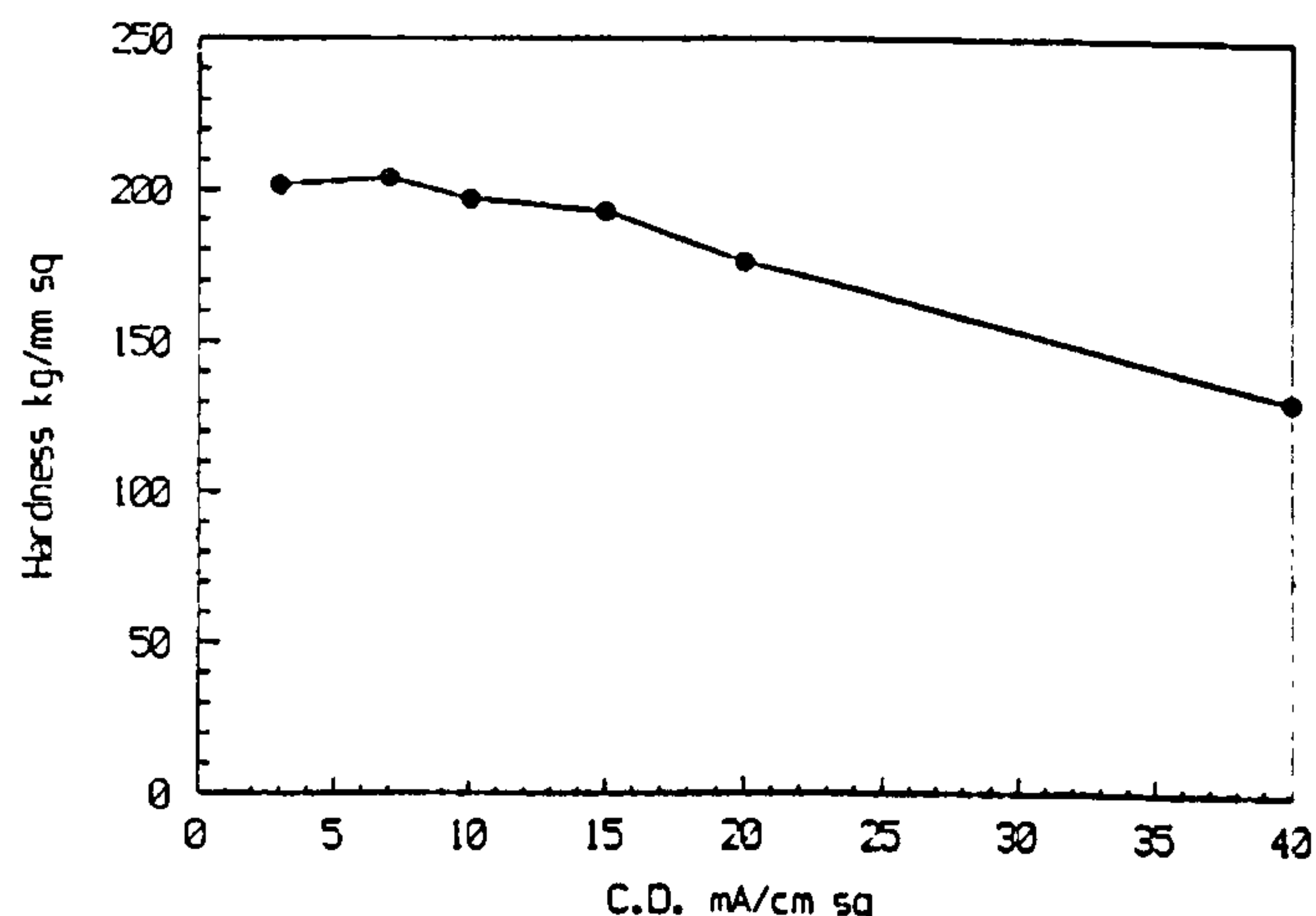


Figure 11. The relationship between the hardness and current density for a conventional deposit from a Ronoval N electrolyte.

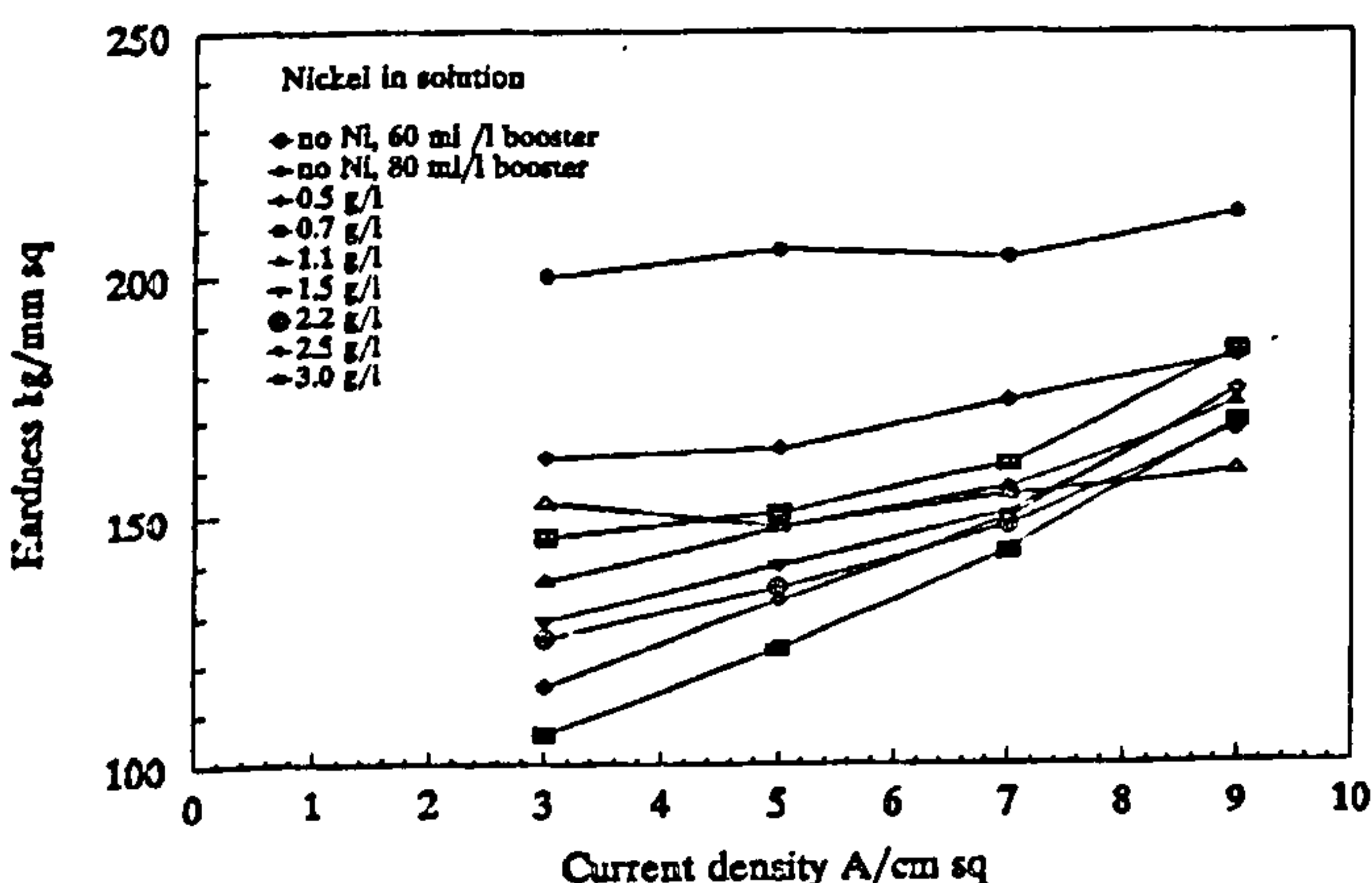


Figure 10. Deposit hardness vs current density for different concentrations of nickel in the electrolyte.



Figure 12. A microsection of a jet deposited gold/nickel alloy. Current density = 6.0 A/cm^2 , Ni in electrolyte = 2.2 g/l, Ni in deposit = 0.17%. X2000.

analytical controls of the nickel in the electrolyte and the applied current density (See the next Section).

The relationship between nickel in the deposit and the current density

Figure 9 shows a graph of the nickel in the deposit and the applied current density for different values of nickel in the electrolyte. A geometric regression has been applied as providing the best fit for the data. It is quite evident that for any value of nickel in the solution, the nickel concentration decreases with increasing applied current density. At a current density of 2.0 A/cm², the nickel in the deposit is about double that present at 9.0 A/cm².

Hardness of the deposits

Hardness measurements revealed significant differences in the influence of nickel additions between conventional and jet deposits. Ordinarily, the addition of nickel to a gold electrolyte causes an increase in the hardness of the deposit. However, examination of Figure 10 shows the opposite trend. The basic electrolyte with no nickel produced deposits with a hardness in the region of 200 kg/mm².

With the addition of nickel, this hardness was reduced to an extent, dependent on the concentration of nickel in the deposit, down to a value of 110 kg/mm². Conventional hard gold deposits exhibit a hardness in the range of 130 to 200 kg/mm². By choosing the appropriate nickel concentration in the electrolyte and current density, deposit hardnesses similar to conventional deposits could easily be achieved. For comparison purposes, Figure 11 shows the hardness vs current density for a conventional deposit from a Ronoval N electrolyte.

Structure of the deposits

Etched microsection of deposit spots showed very few features, indicating that the deposit was fine grained. A typical example is shown in Figure 12. At current densities in excess of 9.0 A/cm², at which modulation occurred, fan shaped structures associated with surface nodules could be seen in the microsections. Macroporosity was clearly associated with these structures as can be seen in Figure 13.

The crystal structure of the deposits obtained using HSSJE were compared with conventionally produced (vat plated)

deposits from the Ronoval N electrolyte. Figure 14 shows the relationship between the preferred orientation and the current density for the conventional Ronoval N deposit. The preferred orientation is shown in terms of the intensity of the individual parallel planes as a percentage of the sum of the intensities. The parallel lines indicate the calculated relative intensities of a randomly orientated gold specimen. It is quite clear that a very strong (111) texture is present over the recommended current density range. This (111) texture has been found in other hard alloy gold samples²² within the normal operating current density range of the studied electrolyte and is partially responsible for the properties of such deposits. In addition, the role of the nicotinamide has been shown to extend the current density range of the nickel hardened alloy gold by maintaining the (111) texture¹⁹. Figure 15 shows the relationship between the preferred orientation and current density for samples produced using HSSJE. It is quite clear that a strong (111) texture is present up to a current density of 9.0 A/cm² above which the deposit tends towards a more random

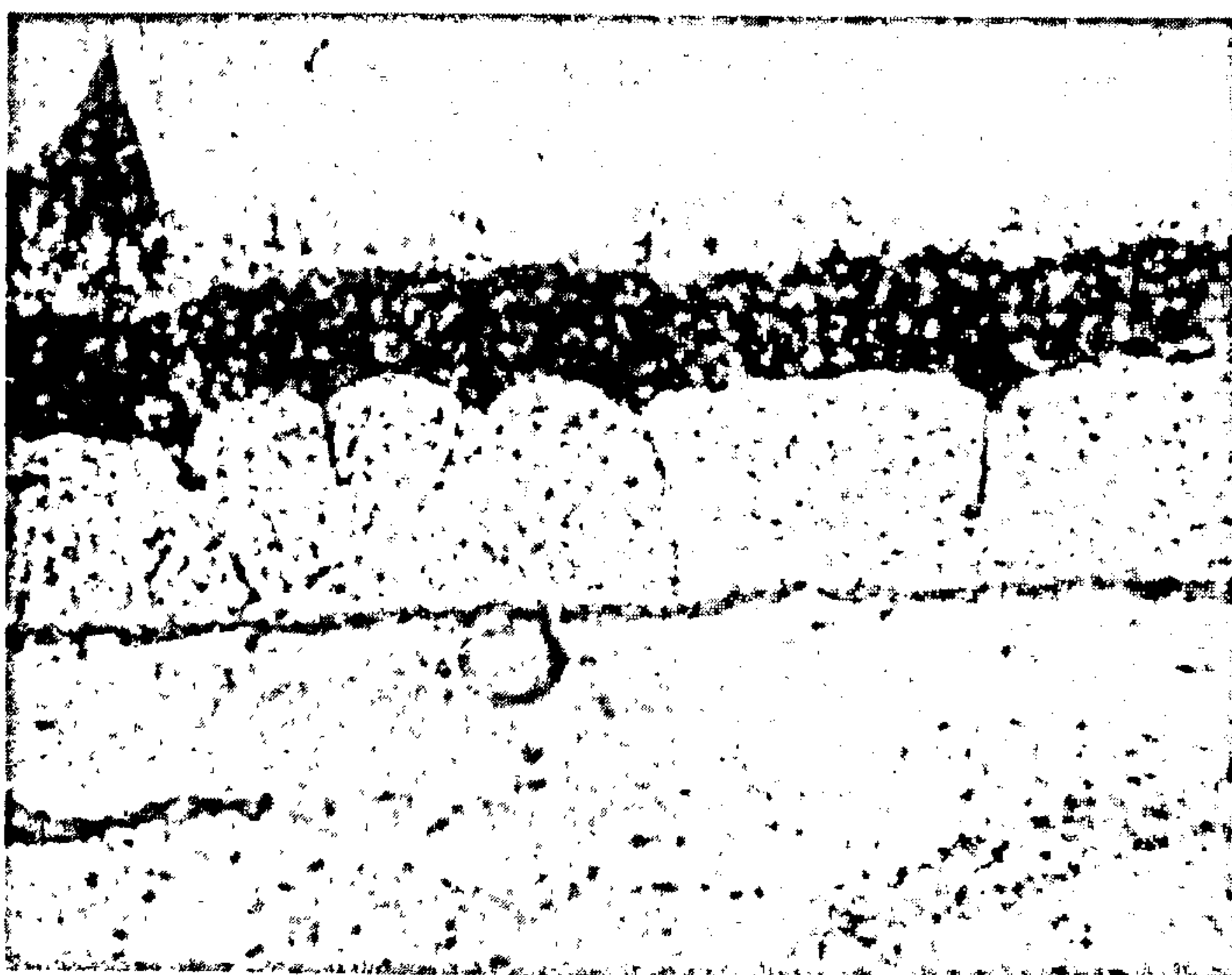


Figure 13. A microsection of a jet deposited gold/nickel alloy. Current density = 12.0 A/cm², Ni in electrolyte = 2.2 g/l, Ni in deposit = 0.098%. X2000.

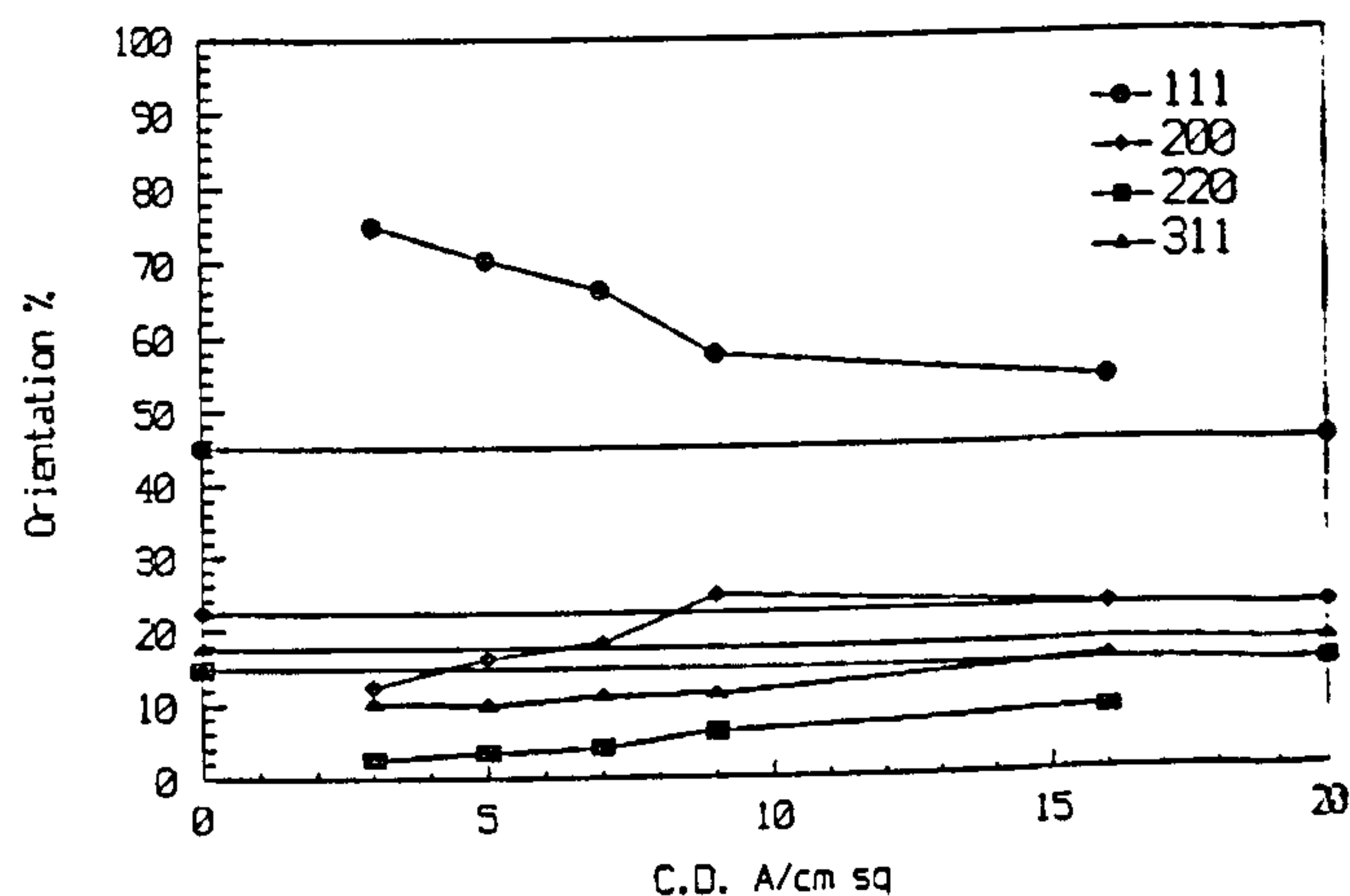


Figure 15. The relationship between preferred orientation and current density for jet deposits from the Ronoval N electrolyte.

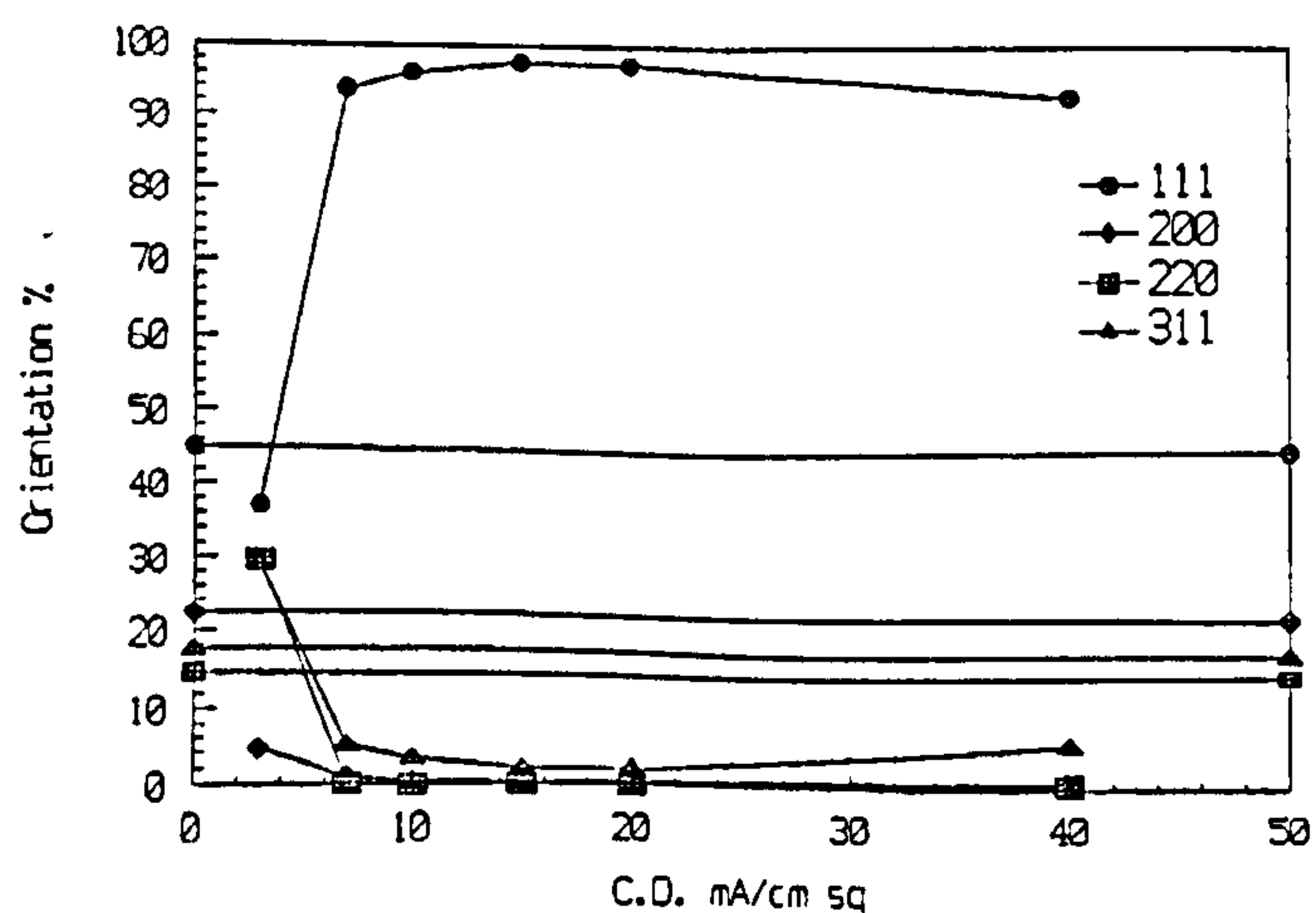


Figure 14. The relationship between preferred orientation and current density for deposits from a conventional Ronoval N electrolyte. The orientation is expressed for each reflection as a percentage of the total reflection intensity of the major planes.

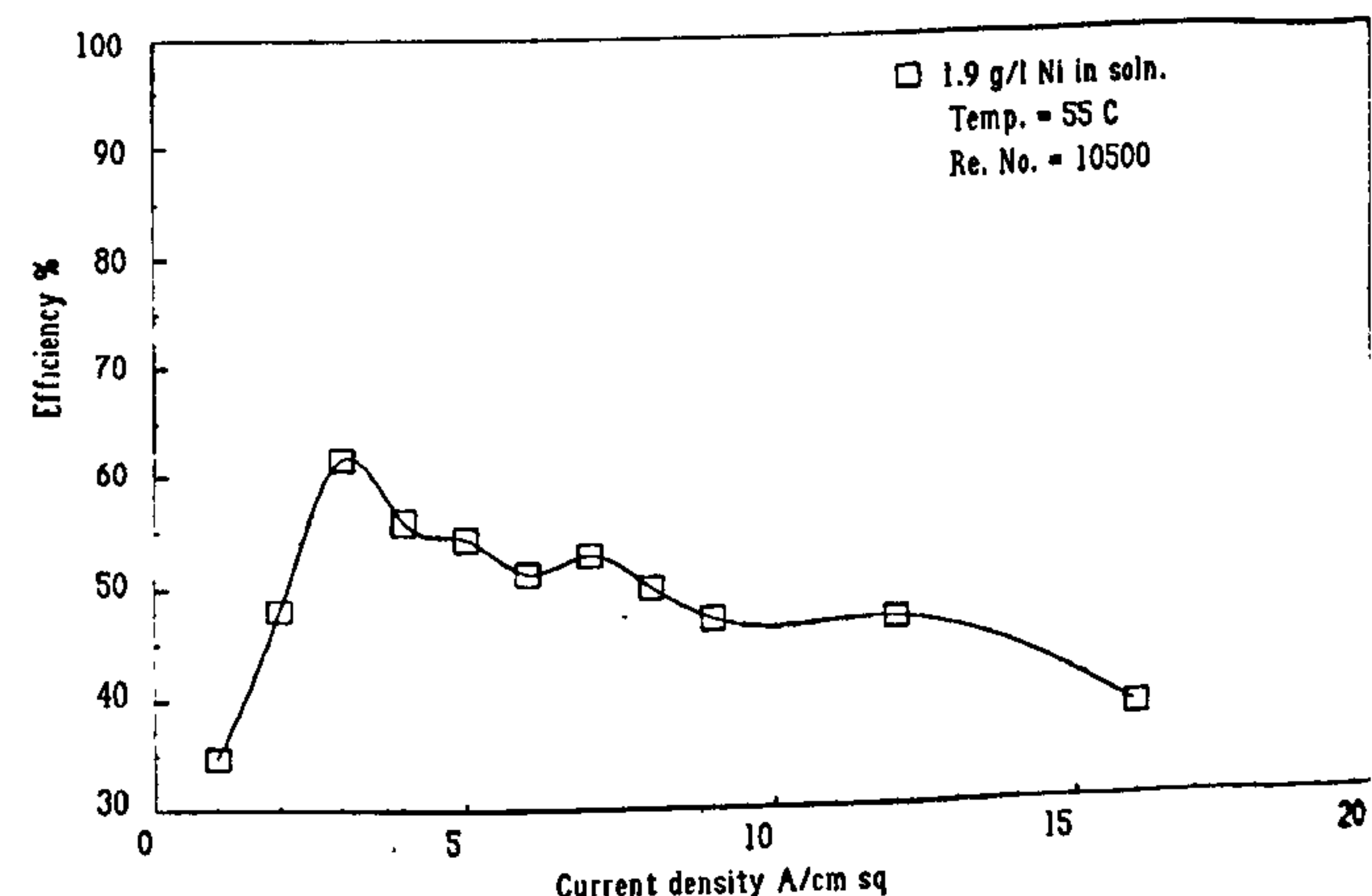


Figure 16. The relationship between the current efficiency and current density for the Ronoval N electrolyte using HSSJE.

structure. However, the texture is not as pronounced as in the case of the conventional Ronoval N deposits although quite comparable with other nickel brightened hard gold.

The cathode current efficiency

Figure 16 shows the cathode current efficiency for the Ronoval N electrolyte under HSSJE conditions. This is similar to that of a pure gold electrolyte, with low current densities exhibiting very low efficiencies. However, with the Ronoval N, the efficiency falls after reaching a peak whereas in the case of pure gold, it remains constant. In the current density range of practical use, the efficiency is quite acceptable, in the region of 50%.

Wear characteristics of HSSJE samples

Figure 17 shows how the contact resistance varies with the number of insertion/withdrawal cycles under different contact loads for both jetted and conventional deposits. In all cases, the contact resistance fell from the initial value during testing. In the case of the jetted samples, higher contact loads

gave rise to lower contact resistances. The conventional deposits only showed this effect with the 1.0 μm deposit. The overall contact resistance for both types of deposit was within generally accepted limits.

Figures 19 to 22 show micrographs and X-ray maps of typical wear scars on both male and female contacts. Figure 19 shows a 0.5 μm jetted deposit after 200 cycles at a load of 55 g. It can be seen that there is little apparent wear and no penetration through the gold to the copper. This may be compared with Figure 20 which shows a 0.5 μm conventional deposit tested under the same conditions. It is clear that significantly more wear has occurred on this sample with the gold evidently being penetrated.

Figure 21 shows a 1.0 μm jetted deposit after 200 cycles at a load of 100g. Severe wear, apparently abrasive in nature and penetrating the coating, can be observed. By comparison, Figure 22 shows a similar deposit produced under conventional conditions and tested under the same conditions. It is clear that significantly less wear has occurred although some penetration of the deposit is visible.

Examination of these connector pairs after 50 cycles showed that no wear had occurred at this stage.

DISCUSSION

It has been shown that some of the physical properties of hard gold deposits produced by HSSJE are similar to deposits produced by more conventional routes. Hardnesses have been found to be of the same order for each method and there are structural similarities. However, there are differences between the wear characteristics of the two types of deposit. It appears that the jetted deposits are superior at low loads (55g) and small thicknesses ($\approx 0.5 \mu\text{m}$) but inferior at greater thicknesses.

Reference to Figure 9 allows the estimation of the nickel content of the deposit for the jetted samples. At the current density used, 5.0 A/cm², a nickel content of $\approx 0.18\%$ would be expected. The nickel content of the conventional deposit has been determined to be 0.23%. Both values are within expected levels for such deposits and are unlikely to explain the

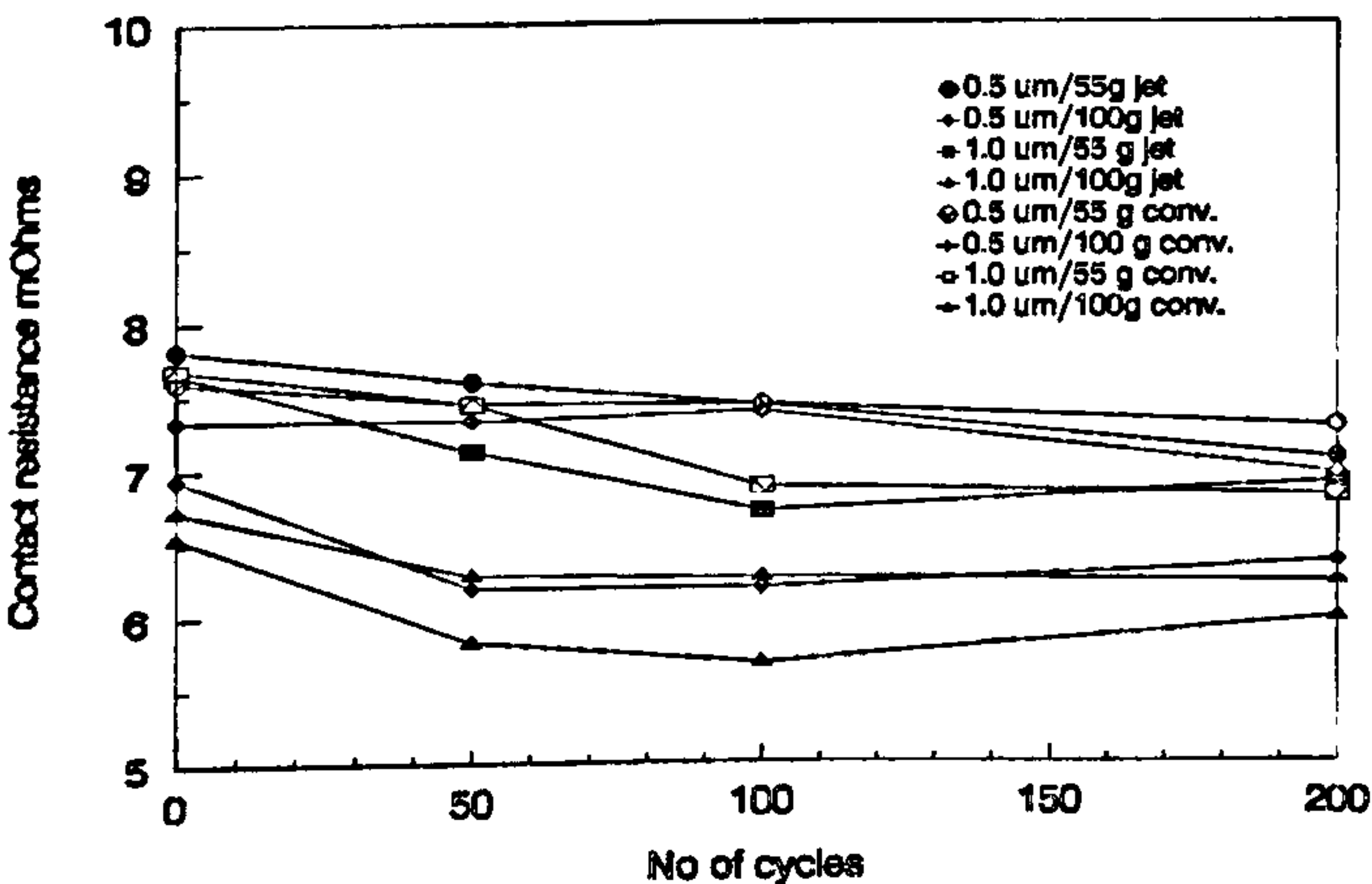


Figure 17. The variation of contact resistance with the number of insertion/withdrawal cycles for both jetted and conventional deposits under different load conditions.

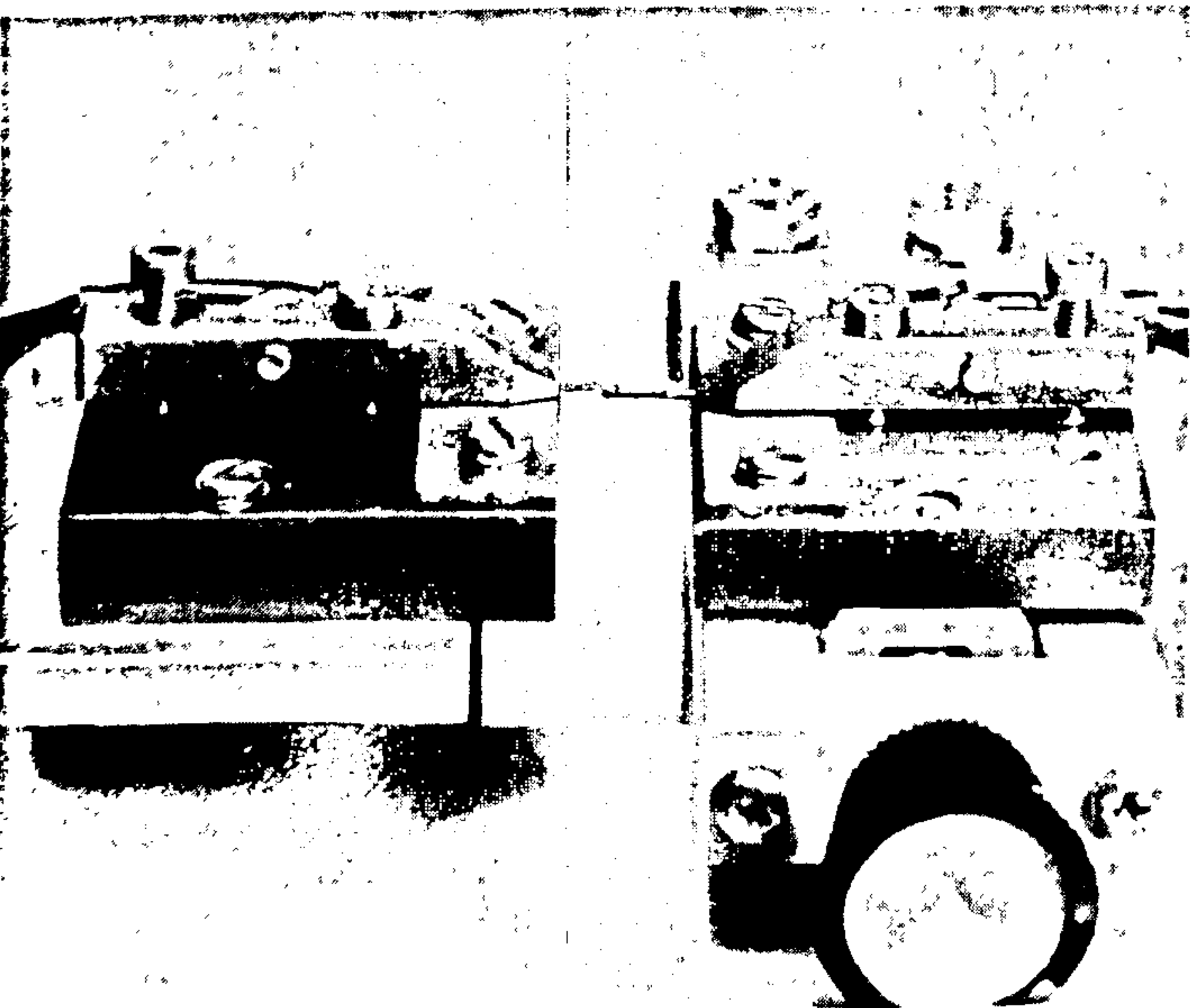


Figure 18. The connector wear test configuration as used by the GEC Contact Tester showing an actual contact pair under test.

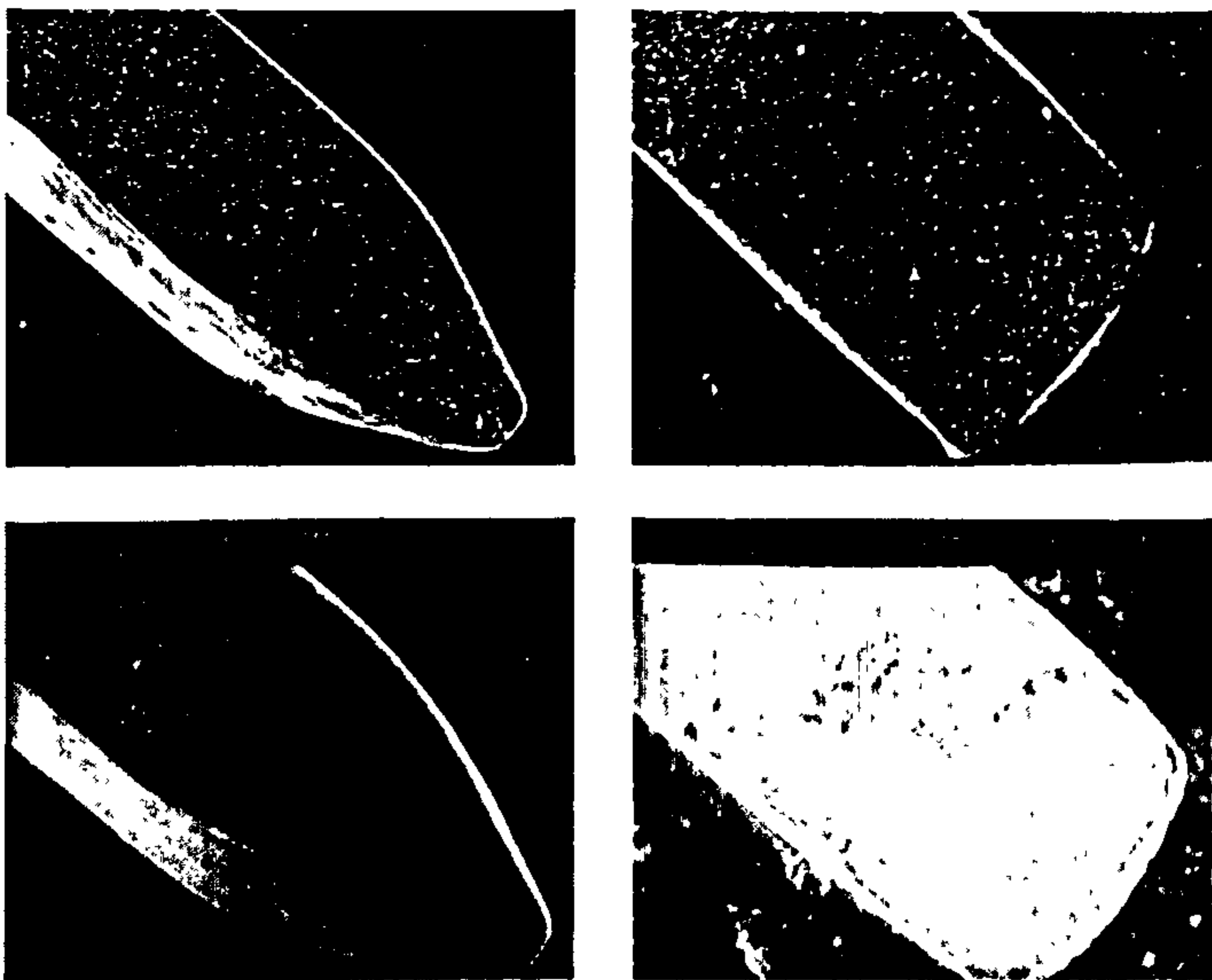


Figure 19. SEM micrographs and Cu radiation X-ray maps of a contact pair, jet plated with 0.5 μm gold/nickel alloy after wear testing for 200 cycles under a load of 55g.

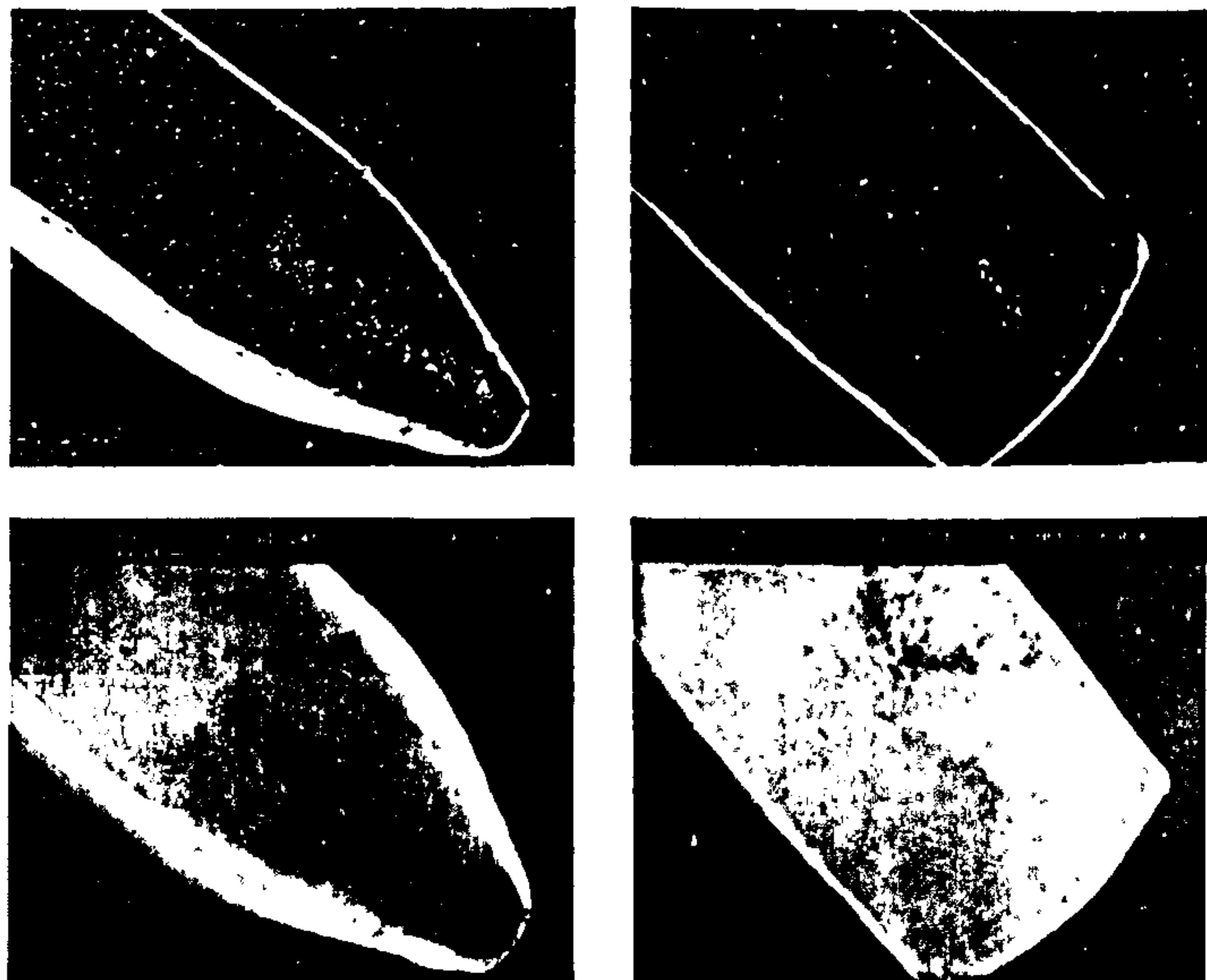


Figure 20. SEM micrographs and Cu radiation X-ray maps of a contact pair, conventionally plated with 0.5 μm gold/nickel alloy after wear testing for 200 cycles under a load of 55g.

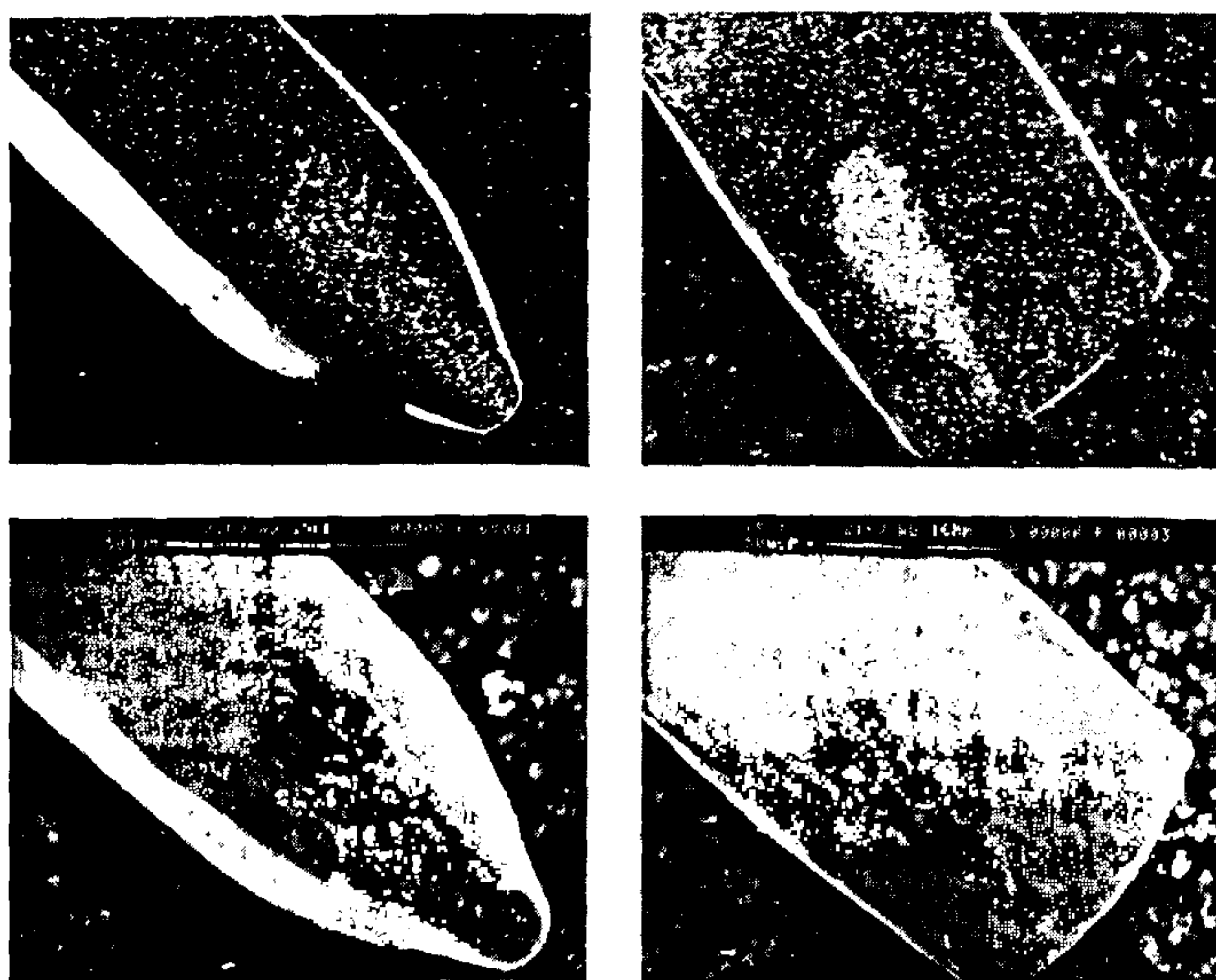


Figure 21. SEM micrographs and Cu radiation X-ray maps of a contact pair, jet plated with 1.0 μm gold/nickel alloy after wear testing for 200 cycles under a load of 100g.

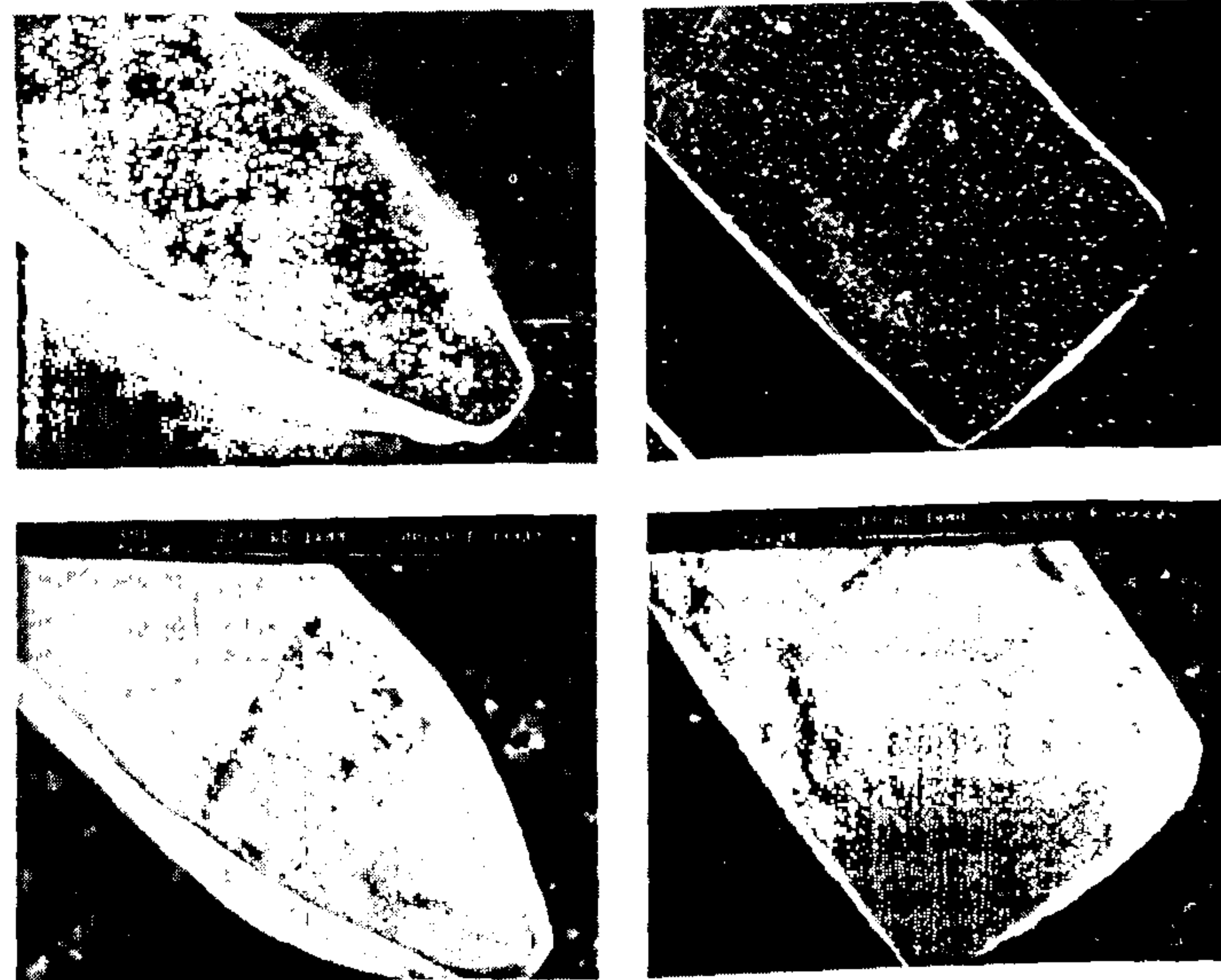


Figure 22. SEM micrographs and Cu radiation X-ray maps of a contact pair, conventionally plated with 1.0 μm gold/nickel alloy after wear testing for 200 cycles under a load of 100g.

differences in wear behaviour. By analogy with the cobalt electrolyte, it is not the absolute alloy concentration that influences wear characteristics but the proportion present in the form of a metal ion complex²⁰. If this holds true for the gold/nickel system, the proportion of complex may not be the same in each case and may explain, at least in part, the difference in wear behaviour.

The micro-hardness of the jetted deposit may be estimated from Figure 10. Under the conditions used, a hardness of 140 kg/mm² could be expected. In the case of the conventional deposit, the hardness has been measured on an 18 μm sample and found to be 192 kg/mm². It has been suggested by Antler²¹ that good wear resistance requires both high hardness and low ductility. This difference in hardness between the two samples may explain the poorer wear resistance of the thicker jetted samples. The thin deposits may behave differently due to the influence of the substrate on the physical properties. It is known that at low thicknesses, deposit characteristics are largely controlled by the influence of the substrate, particularly in terms of internal stress, which may be more significant than the deposition parameters.

The results presented here were for jetted samples produced at an intermediate, but still high, current density (5.0 A/cm²). As Figure 10 shows, the hardness increased with increasing current density and at the maximum useable current density of 10.0 A/cm², deposits of a hardness in the region of 180 kg/mm² can be produced.

CONCLUSION

It has been shown that the use of HSSJE with a modified Ronoval N electrolyte allows high quality gold deposits with similar properties to those obtained under conventional deposition conditions. The deposits exhibit strong structural similarities as well as hardnesses. The wear characteristics differ from those of conventional deposits when applied to real connectors under simulated conditions of

use. The results indicate that deposit hardness may be a significant factor in the wear properties of plated deposits. Jetted deposits of higher hardness are easily achievable and will be the subject of future work.

Deposition rates in the region of 3.0 $\mu\text{m}/\text{second}$ are realisable and because of the self limiting nature of the HSSJE process, a high degree of selectivity can be obtained without the need for masking. As a consequence, connectors can be produced at a faster throughput than is currently obtainable, on a reel-to-reel unit that is a fraction of the size of conventional units. In addition, because there is no need for masking, the engineering complexity of such plant can be greatly reduced. A prototype plant is being constructed for large scale trials. To give some idea of the size reduction, this plant can be operated with a strip speed of up to 20 m/minute and with a footprint comparable to a large office desk.

Whilst the use of HSSJE of gold alloys has been shown to potentially reduce the cost of plant and processing, work still has to be undertaken on both improved wear characteristics and the production of nickel coatings using the technique.

ACKNOWLEDGMENTS

This work was carried out as part of a BRITE Project No. RIIB-0304, "Improvement in the Control and Attainment of High Speed Deposition Processes" in partnership with CSM (Roma) and Loughborough University of Technology. The authors wish to thank the EEC and their partners for their kind agreement to publication. In addition, thanks go to the staff of the Materials Science Laboratory of the Hirst Research Centre for their assistance in producing the SEM micrographs, the XRD data and the analytical results.

REFERENCES

1. "The consumption of gold products by the West European Electronics and Electrical Industries, third quarter and whole year, 1991", C.G. Wedgewood

Consultancy Service, London, December, 1991.

2. W.R. Hain and L.W. Rudolf, *Western Electric Eng.*, 1978, April, 91.
3. D. Heiestad, '8th Annual Connector Symposium', Cherry Hill, N.J. Electronic Computer Study Group, 337, 1975.
4. "Texas Instruments uses spot plating of gold to cut costs of keyboards". *Plating & Surf. Finish.*, 1975, 62(9), 846.
5. G. Menzies, *Electronic Prod.* 1978, May, 38.
6. D.L. Rehrig, *Western Electric Eng.*, 1978, April, 48.
7. D.R. Turner, *Thin Solid Films*, 1982, 95, 1443.
8. P. Wingenfeld, *Proc Connectors* 91, 1991, 91.
9. J.C. Fletcher, NASA, U.S. Patent No. 3810829, 1974 May.
10. R. Haynes, K Ramachandran and D.J. Fineberg, *Western Electric Eng.* 1978, April, 22, 61.
11. J.K. Dorey II, R. Haynes, R.E. Sinitski and R.E. Woods, *Plating & Surf. Finish.*, 1980, May, 67, 81.
12. D-T. Chin and C-H. Tsang, *J. Electrochem. Soc.*, 1978, 125(9), 1461.
13. A.A. Sonin, *J. Electrochem. Soc.* 1983, 130(7), 1501.
14. D-T. Chin and M Agarwal, *ibid*, 1991, 138(9), 2643.
15. R.C. Alkire and T-J. Chen, *ibid*, 1982, 129(11), 2424.
16. C.C. Bocking, *Trans. IMF.*, 1988, 66, 50.
17. C.C. Bocking, *Proc. 59th Intl. Conf. On Surf. Fin.* 1991, April, 2, 51.
18. C.C. Bocking, East Report, Eugen G. Leuze Verlag, Saulgau, 1992.
19. C.C. Bocking and C. Dineen, To be published.
20. R. DeDoncker and J. Vanhumbeek, *Trans. IMF.*, 1985, 62, 59.
21. M Antler, *IEEE Trans. Components, Hybrids & Man. Tech.*, CHMT-4, 1981, 1, 15.
22. M.DeBonte, J.P. Celis, J.R. Roos and J. Vanhumbeek, EAST Report, Eugen G. Leuze Verlag, Saulgau, 1992.

THE INSTITUTE OF METAL FINISHING

Paper to be presented at the Annual Technical Conference
at NEC, Birmingham 28-30 March 1994

Advance Copy

Copyright Reserved

**THE STRUCTURE OF GOLD AND GOLD ALLOYS PRODUCED USING HIGH
SPEED SELECTIVE JET ELECTRODEPOSITION.**

C. BOCKING GradIMF,FIMF *GEC Hirst Research Centre Elstree Way, Borehamwood*
C. DINEEN MSc,BSc *GEC Hirst Research Centre Elstree Way, Borehamwood*

ABSTRACT

Modern reel-to-reel plating facilities apply selective deposits of gold and gold alloys during the production of pressed copper and copper alloy or nickel-iron alloy strip components. These components are fabricated into electrical connectors or semi-conductor lead frames. Selectivity is usually achieved by the use of some form of dielectric masking. Recent developments have shown that such components may be plated with gold or gold alloys at deposition rates of up to 3.5 microns per second, selectively and without the need for masking. This paper discusses the microstructure of such deposits from studies using X-Ray diffraction and other physical testing methods and compares them with those produced under conventional deposition conditions.

1 INTRODUCTION

High Speed Selective Jet Electrodeposition (HSSJE) is a process by which electrodeposits can be produced at very high deposition rates, selectively, without the need for masking. In HSSJE, a jet of electrolyte is pumped at high velocity from a small nozzle ($< 1\text{mm}$) through an air gap onto the substrate whilst applying a suitable electrical potential. The nozzle is made anodic whilst the substrate is the cathode. Metal is deposited in the impingement region and its immediate surroundings. The spread of the deposit is limited because the electrolyte forms a very thin radial layer as it flows away from the impingement region. This radial layer is highly electrically resistive in comparison to the jet and therefore most of the metal is deposited in the impingement region. Bocking^{1,2,3} has described in detail the electrodeposition of copper and pure gold using this method. More recently, Bocking and Cameron⁴ have described the electrodeposition of nickel alloyed hard gold. Such deposits are widely used for the selective electrodeposition of electrical connectors. They presented details of the hardness and wear characteristics of the deposits produced. They also described the results of some initial studies of the crystal structure of these deposits. It was established that whilst there were many similarities between HSSJE deposits and those produced by more conventional methods, there were some differences in the wear behaviour.

This paper describes the results of the examination of both pure and nickel alloyed hard gold deposits produced by HSSJE using X-ray diffraction techniques (XRD) and compares these with those produced by more conventional methods. Possible reasons for the differences in the wear behaviour are suggested.

2 BACKGROUND

References 1-3 give a complete background to experimental studies on the HSSJE of both pure gold and copper deposits. However, some necessary information on the mechanisms of deposition and the types of deposit will be given here. When electrodeposition is carried out using HSSJE, a deposit spot is produced in the jet impingement region. The spot thickness profile is approximately Gaussian with over 85% of deposition occurring within the impingement region. The maximum deposit thickness is obtained at the jet centre line. Figure 1 shows the profile over one half of a typical deposit and is presented as thickness against R , where R is defined as the ratio of the radial distance from the centre line to the nozzle radius.

It was found that by using a citrate based electrolyte containing 0.17M gold, pure gold deposition rates at the jet centre line as high as $3.4 \mu\text{m sec}^{-1}$ at a current density of 6.0 A cm^{-2} could be achieved whilst maintaining a high quality deposit. In order to attain these deposition rates, a high electrolyte velocity was required. Most of the work in these studies was carried out using a 0.4mm diameter nozzle and the highest deposition rates were obtained with jet velocities of 18 m sec^{-1} . This was equivalent to a Reynolds Number, $Re = 12000^*$. It has also been shown⁴ that gold alloy deposits can also be produced at deposition rates of up to $3.0 \mu\text{m sec}^{-1}$ at current densities of up to 9.0 A cm^{-2} .

3 EXPERIMENTAL

Samples of HSSJE pure gold deposits were prepared using the 0.17M electrolyte developed in the previous studies. For the gold alloy deposition, it was decided to use a proprietary electrolyte.

A number of proprietary electrolytes designed for high speed gold alloy electrodeposition are currently available. A preliminary study of deposition rates and deposit morphologies obtained using a number of these proprietary electrolytes indicated that Ronovel N (supplied by Lea Ronal) exhibited the most promising performance. It was found that a gold metal concentration of 20 g dm^{-3} (0.1M) gave the highest deposition rates in conjunction with HSSJE, up to $3.0 \mu\text{m sec}^{-1}$. All subsequent studies were carried out with this electrolyte. The basic Ronovel N electrolyte contains as part of its formulation an additive referred to as "booster". This additive is claimed to extend the current density range of the electrolyte. Three electrolytes were prepared, one with no nickel, but containing booster, the other two containing booster and 1.9 g dm^{-3} and 3.0 g dm^{-3} of added nickel respectively.

Glass substrates, $1.5 \times 1.5 \text{ cm}$, metallised using sputtered coatings of chromium followed by gold (400 \AA and 1000 \AA respectively) were used for this study. Samples of HSSJE gold alloy deposits for XRD examination were prepared over a current density range of between 3.0 and 16.0 A cm^{-2} with differing quantities of nickel and/or addition agent (booster) in the deposit. In the case of HSSJE pure gold, samples were produced over a current density range of between 1.0 and 8.0 A cm^{-2} . The samples consisted of an array of 25 identically produced spots plated onto the substrates. Prior to XRD examination, the chromium/gold layers not

*The Reynolds Number is a dimensionless term that expresses fluid motion, taking into account the nozzle diameter and the electrolyte viscosity. It is defined as $Re = Ud/\nu$ where U = velocity in cm sec^{-1} , d = nozzle diameter in cm and ν = the electrolyte viscosity in $\text{cm}^2 \text{ sec}^{-1}$.

covered by the deposited spots were stripped using commercially available stripping solutions. As the metallised layers were extremely thin, the stripping operation left the HSSJE spots virtually unaffected. The centre-line thickness of the spots in the array was maintained above $15.0\ \mu\text{m}$ and confirmed by measurement using a Dektak Surface Profilometer after the XRD examination had taken place.

For comparison, a series of control samples were prepared for XRD examination by conventional vat deposition methods. One set were produced from a Ronovel N electrolyte containing $1.7\ \text{g dm}^{-3}$ nickel over the current density range $3.0 - 40\ \text{mA cm}^{-2}$. A further set of samples were produced over the same current density range from an Auronal MRN bath also containing $1.7\ \text{g dm}^{-3}$ nickel, which is identical to the Ronovel N but contains no booster. These samples were used to study the influence of the booster. Pure gold samples were produced from a typical acid citrate electrolyte containing 0.06M gold, over a current density range of 1.0 to $20\ \text{mA cm}^{-2}$. These deposits covered the same total surface area of the substrate as that covered by the jet plated spot array.

The X-ray diffraction data was acquired using an Siemens D5000 X-ray Powder Diffractometer (Bragg-Brentano geometry) equipped with a diffracted beam monochromator ((Cuk α)). Measurements of diffracted intensity were carried out over the 2θ range 30° to 90° . Corrections to the angular positions and breadth of the diffraction peaks derived from the samples, required to compensate for various instrumental and physical effects were applied. To determine these corrections, each sample was dusted with a fine layer of powdered silicon (@ $1\ \mu\text{m}$ in size). The positions and Full Widths at Half Maximum (FWHM) intensity of the silicon peaks which bracketed those from the gold were used to calculate the appropriate corrections to position and width. Using the precisely known lattice parameter of silicon it was possible to interpolate a correction to the position of the gold peaks and thus calculate an accurate value for the lattice parameter for each line. The correction for line broadening was made by assuming Gaussian models for the observed profiles, instrumental and corrected diffraction profiles.

Data was derived from an analysis of the position, intensity and FWHM of the first five diffraction peaks recorded from the gold deposits. In the Bragg - Brentano geometry, the diffraction pattern originates only from those crystallographic planes which are essentially parallel to the surface of the sample. The 111, 200, 220 and 311 reflections are therefore derived from quite separate and distinct crystallites within the deposit. Only the 111 and 222 reflections are derived from the same crystallites. Considerable care therefore needs to be exercised in interpreting data from samples which do not exhibit a true crystallographic random orientation.

covered by the deposited spots were stripped using commercially available stripping solutions. As the metallised layers were extremely thin, the stripping operation left the HSSJE spots virtually unaffected. The centre-line thickness of the spots in the array was maintained above $15.0\ \mu\text{m}$ and confirmed by measurement using a Dektak Surface Profilometer after the XRD examination had taken place.

For comparison, a series of control samples were prepared for XRD examination by conventional vat deposition methods. One set were produced from a Ronovel N electrolyte containing $1.7\ \text{g dm}^{-3}$ nickel over the current density range $3.0 - 40\ \text{mA cm}^{-2}$. A further set of samples were produced over the same current density range from an Auronal MRN bath also containing $1.7\ \text{g dm}^{-3}$ nickel, which is identical to the Ronovel N but contains no booster. These samples were used to study the influence of the booster. Pure gold samples were produced from a typical acid citrate electrolyte containing 0.06M gold, over a current density range of 1.0 to $20\ \text{mA cm}^{-2}$. These deposits covered the same total surface area of the substrate as that covered by the jet plated spot array.

The X-ray diffraction data was acquired using an Siemens D5000 X-ray Powder Diffractometer (Bragg-Brentano geometry) equipped with a diffracted beam monochromator ($\text{CuK}\alpha$). Measurements of diffracted intensity were carried out over the 2θ range 30° to 90° . Corrections to the angular positions and breadth of the diffraction peaks derived from the samples, required to compensate for various instrumental and physical effects were applied. To determine these corrections, each sample was dusted with a fine layer of powdered silicon ($@\ 1\ \mu\text{m}$ in size). The positions and Full Widths at Half Maximum (FWHM) intensity of the silicon peaks which bracketed those from the gold were used to calculate the appropriate corrections to position and width. Using the precisely known lattice parameter of silicon it was possible to interpolate a correction to the position of the gold peaks and thus calculate an accurate value for the lattice parameter for each line. The correction for line broadening was made by assuming Gaussian models for the observed profiles, instrumental and corrected diffraction profiles.

Data was derived from an analysis of the position, intensity and FWHM of the first five diffraction peaks recorded from the gold deposits. In the Bragg - Brentano geometry, the diffraction pattern originates only from those crystallographic planes which are essentially parallel to the surface of the sample. The 111, 200, 220 and 311 reflections are therefore derived from quite separate and distinct crystallites within the deposit. Only the 111 and 222 reflections are derived from the same crystallites. Considerable care therefore needs to be exercised in interpreting data from samples which do not exhibit a true crystallographic random orientation.

Lattice parameters were calculated from the angular positions of the first five lines (111, 200, 220, 311 and 222) in the diffraction pattern from each of the samples.

In order to demonstrate the difference in preferred orientation between the samples the intensities of the first four lines of the X-ray diffraction pattern are expressed as a percentage of the sum of the intensities of these lines. The relevant intensities for a randomly oriented sample were also calculated and these are shown as horizontal lines in the Figures. This form of presentation permits a rapid graphical means of assessing and demonstrating the differences in preferred orientation between samples.

For the purposes of this paper, crystallite size will be defined as a single, coherent diffracting region. This is not always the same as the true crystallite size, D , as will be explained below, but is used for convenience. The full width at half maximum intensity of the $K\alpha_1$ line corrected for instrumental broadening was used to calculate the crystallite size using the Scherrer equation.

$$B = \frac{(0.9\lambda)}{(t \cos \theta)}$$

where B = the broadening of the diffraction line measured at its half width maximum intensity (radians), t = diameter of the crystal particle λ = radiation wavelength and θ = angular position in degrees.

It was noted that the crystallite size values calculated from the broadening of the 111 reflections using the Scherrer equation were significantly greater than the values derived from the 222 reflections. The crystallite sizes calculated for the two planes should be the same; that they are not, suggests that the Scherrer model employed, which attributes all the intrinsic line broadening to crystallite size effects, is an over-simplification. On the basis of this information samples were selected for a more detailed analysis in order to separate the contribution to the observed line broadening from crystallite size and strain (RMS) effects. This was undertaken using the method of Warren and Averbach⁵. The successful application of this type of analysis requires as many unique orders of reflection as possible. However, for an FCC metal examined using copper radiation, the number of accessible reflections with multiple orders is just 2, the

111 (222) and the 200 (400). In this study, line overlap problems combined with low peak intensities ruled out the use of the h00 reflections so that only the 111 and the 222 peaks were used for the analysis.

In order to accomplish the analysis a better defined instrumental line broadening standard was required. This was achieved by producing a pure gold powder and annealing it to the point where no further improvement in the resolution of the $k\alpha_1$ and $k\alpha_2$ lines could be achieved. It is particularly difficult to obtain a suitable gold powder commercially and anneal it in this way due to its tendency for grain growth and sintering. Therefore, a powder was specifically produced*. The observed diffraction lines were corrected for instrumental broadening by dividing the Fourier Transform of the diffraction lines derived from the sample by the Fourier Transform of the appropriate line from the standard as described by Stokes⁶. It was found necessary to subtract the signal derived from the blank glass substrates from that of the samples prior to calculating the transform, in order to obtain a level base line required for an accurate analysis.

The full application of this analysis yields the mean column length ($n_0 a_3$) and its distribution and the RMS strain and its distribution. The apparent cell size is a_3 and n_0 , the number of cells in the average column length, is determined by a linear extrapolation of the real part of the Fourier Transform of the (000) reflection.

The cell size (a_3) is determined by the angular range over which the diffraction profile is analysed and is given by:-

$$l - 1/2 = 2a_3/\lambda \sin(\theta)$$

$$l = 2a_3/\lambda \sin(\theta)$$

$$l + 1/2 = 2a_3/\lambda \sin(\theta)$$

*A 50 g dm⁻³ solution of gold chloride was produced by dissolving pure gold powder in aqua-regia and evaporating to near dryness. Concentrated hydrochloric acid was added and re-evaporated until all oxides of nitrogen were removed. The solution was then adjusted to the correct concentration using de-ionised water. It was necessary to produce gold grains with a size in the region of 10 μ m with a well ordered structure. This meant they had to be nucleated and grown very slowly. It had been shown that such a structure could be achieved by reducing the gold chloride using acetone at room temperature. A 100 ml sample of the gold chloride was placed on a magnetic stirrer at a temperature of 35°C and 30 ml of acetone was added. Stirring was continued for a period of 5 hours after which the sample was cooled to ambient and allowed to stand for a period 3 days. At the end of this period, a layer of gold powder was seen at the bottom of the beaker that had merged to form a thin film. A piece of this film was cleaned in de-ionised water and mounted on a glass slide so that the X-ray diffraction pattern from the film could be recorded. The resolution of the $k\alpha$ doublet was determined for the first five lines in the X-ray diffraction pattern from the film. The film was then subjected to a number of annealing operations at 350°C until no further improvement resolution of the doublets was obtained. The total time of annealing to obtain this condition was 5 hours.

where Θ_1 and Θ_2 are the start and end of the diffraction profile, Θ_0 is the position of the peak, λ is the wavelength of the radiation employed and l is a reflection order as in hkl . In order to simplify the subsequent calculations, it is convenient to choose scan ranges so that a_s is the same for all reflections used in the analysis. In this study, a cell size of $2.4 \times d_{111}$ was used.

Close and careful examination of the diffraction patterns from these samples showed both the 111 and 222 diffraction peaks overlapped with their nearest neighbours, the 200 and 311 peaks respectively. This was also true for the specially prepared reference gold sample used to determine instrumental broadening. In the present study, data was collected over an angular range of $\pm 10^\circ$, centred about the 111/200 and 311/222 lines.

In order to obtain adequate representation of the diffraction profiles in the "tails" of the peaks (where most of the crystallite size and strain information is contained) a variety of mathematical functions were fitted to the experimental data and the parameters for the best fits used to calculate model diffraction profiles. Pearson 7, Split Pearson 7 and three different pseudo Voigt (mixed Cauchy and Gaussian) type functions were employed in the modelling.

The modelled 111 and 222 diffraction profiles were calculated at 1024 data points over an angular range of 16° and 20° respectively. Fourier transforms were calculated using an FFT routine. The instrumental contribution to the diffraction data was removed by dividing the FT of the samples by the FT derived from the precipitated and annealed gold powder described above. The Fourier coefficients of the 000 reflection were calculated using the extrapolation procedures described by Warren and Averbach⁵. This method enables the individual contributions of crystallite size and strain to line broadening to be evaluated. The contribution to broadening from crystallite size (column length) is independent of the order of reflection whilst that from strain is dependent on the order of reflection. Because of this, the two contributions may be resolved. The mean crystallite sizes were calculated by extrapolating the linear region of the real part of the 000 transform to obtain n_0 . The mean column lengths (crystallite size) and RMS strains are listed in Table 1.

In addition to crystallite size and RMS strain, layer sequence faults on the 111 plane may also contribute to line broadening. The contribution of stacking and twin faults to line broadening may be identified once the strain and size contributions have been established. The effective crystallite size, D_{eff} comprises for the (111) plane

$$1 / D_{\text{eff}} = 1 / D + (1.5\alpha + \beta) * \sqrt{3} / 4 a$$

where D is the true crystallite size, α is the stacking fault probability, β is the twin fault probability and a is the lattice parameter. The stacking fault probability may be established by measuring any relative shift between the 111 and the 200 peaks. The probability may then be calculated. Twin fault probabilities may be calculated from any asymmetry of the diffraction peaks that have been reconstructed from the inverse Fourier transform produced during the Warren and Averbach analysis. However, it was not possible to accurately calculate the twin fault probabilities because the deposit was highly oriented in the 111 direction. Twin fault probabilities are usually calculated for the 100 (200) reflections. Due to the high degree of texture, the 200 signal was very weak and could not be used for the analysis. Table 1 also includes the stacking fault probabilities where these were significant.

Metallurgical Microsection was carried out on a number of samples in order to observe any resolvable microstructures. The gold deposit was etched using a proprietary gold stripper dissolved in an alcohol/water mixture.

4 RESULTS

The results of the XRD analysis are presented in Figures 2 to 9 and Table 1. As would have been expected, there were considerable differences between the pure and alloy gold deposits so each will be presented separately.

4.1 Pure gold deposits

Figure 2 shows the lattice parameters and orientation of the major first and second order reflections for a deposit produced under conventional conditions. The normal operating current density range for this electrolyte was between 3 and 7 mA cm⁻².

Analysis of the data from Figure 2(a) showed that all planes generally exhibited the same lattice parameter, although a slight increase was observed with increasing current density. The average lattice parameter of 4.077 was close to that of pure gold, which is generally accepted as being 4.0786 Å at 25°C. It is thought that the single point of the 220 plane that deviates from this is due to experimental error.

It was noted that, on calculating the crystallite size using the Scherrer method, a significant variation was observed, depending on the reflection. This was particularly evident at the higher current densities. An analysis of this is difficult as the line broadening observed has been assumed to be purely due to crystallite size and ignores the existence of strains and faults that may also contribute. Analysis of the 111 reflection using the Warren and Averbach method indicated that such an assumption was invalid as the crystallite size was found to be considerably greater (See Table 1). The actual crystallite size after correcting for strain was in the region of 0.23 μm . No evidence of faulting was observed.

Figure 2(b) shows the degree of preferred orientation of the deposit. It can be seen that by comparison with the expected ratios of the various planes (parallel lines) that there is a distinct 311 texture over the normal current density range of 1-7 mA cm^{-2} . Above this, the deposit tends towards a more random orientation.

The RMS strain of the conventional deposits was independent of current density over the range analysed and was comparatively low, calculated to be $\langle e^2 \rangle = 0.000035$.

The above measurements of a conventional deposit were necessary to compare and contrast with those produced under jetting conditions. Whilst a direct comparison cannot be made due to the orders of magnitude difference in the current densities applied, in terms of the morphological characteristics ie the structural changes that occurred with increasing current density, a comparison was considered to be valid. Figure 3 shows similar graphs for samples produced from the 0.17M citrate gold using a Re. No. of 12,000. The maximum current density under which useful deposits could be produced was found to be 6.0 A cm^{-2} . The lattice parameter of each of the crystallites was slightly smaller than the bulk value, with an average value in the region of 4.075 \AA . However, at current densities below 2.0 A cm^{-2} , the lattice parameter exhibited a smaller size.

The crystallite size of the jetted sample calculated using the Scherrer equation was in the region of 200 \AA for all but the 111 plane which showed a size of around 300 \AA . It must be remembered that this method of estimating the crystallite size assumes all line broadening is attributable to grain size. The fact that the 222 planes were not the same as the 111 planes indicate that this assumption was incorrect. Further analysis of the line broadening revealed that this difference was due to residual strain, which over the current density range measured averaged $\langle e^2 \rangle = 0.0001275$. There was no evidence of either twin or stacking faults, except for a very low probability of $\alpha = 0.007$ at a low current density. The crystallite size of the 111 plane as determined by the Warren and Averbach method was found to be between 320 to 350 \AA .

The preferred orientation of the jetted sample was found to be strongly 220 above a current density of 2.0 A cm^{-2} . Below this value, a 111 orientation predominated.

The RMS strain observed in these samples given in Table 1 was nearly an order of magnitude greater than for deposits produced under conventional conditions. There was, however, no clear relationship with current density.

Polished and etched micro-sections of jetted samples can be seen in Figures 12 and 13. These showed that there were few structural features apparent at current densities below 6.0 A cm^{-2} . Above this value, fan shaped, cell-like structures could be observed. These cells became apparent after a thickness of about $8 \mu\text{m}$ had been achieved. Figure 13 shows examples of these cells. Below $8 \mu\text{m}$, the cell structure was integral with the rest of the deposit but as the thickness increased, the cell "wall" exhibited a discontinuity. Extrapolation of the wall line showed a coinciding point close to the substrate surface. Topographically, these cells appear as nodules, increasing in size with increasing current density as well as deposit thickness. These structures clearly resemble the "rounded mounds" described by Nakahara⁷ who studied the structure and morphology of gold alloy deposits. He concluded that such structures formed as a result of an inhibition process that forced a small crystallite size to be produced as well as forming the rounded mound structure.

4.2 Alloy gold deposits

Figure 4 shows the data obtained from deposits produced conventionally using a Ronovel N electrolyte, whilst Figure 5 shows that obtained from the Auronal MRN. In addition to the XRD data, the deposit hardness is shown.

The effect of the booster can be clearly established under conventional deposition conditions by comparing Figures 4 and 5. Figure 5(b) shows that in the case of the Auronal MRN, a distinct 111 texture is formed between 10 and 15 mA cm^{-2} , the normal operating range of this electrolyte. Indeed, below this range, the deposit appearance was matt. Above this range, the deposit showed signs of "burning" at the edges of the sample. Figure 4(b) shows that with the addition of the booster, the 111 texture was predominant above 5 mA cm^{-2} , with the apparent suppression of other growth directions. Pure gold, as has been seen earlier, possessed a distinct 311 texture under conventional deposition conditions. It would appear, therefore, that a 111 texture is one of the necessary conditions for the effective performance of a nickel hardened alloy gold. Hardness measurements showed that the deposits with the booster were

15% harder than those without, up to a current density of 15 mA cm⁻². It can also be seen that the booster reduced the effective lattice parameter compared to those deposits produced in its absence.

The lattice parameter of the conventional deposits without booster exhibited a mean lattice parameter ~ 0.27% less than that of annealed gold and remained essentially constant with current density. The values for all the planes were comparable within the overall accuracy of measurement. The lattice parameter of the conventional deposit containing booster was also lower than that of annealed gold, the mean value being ~0.33% less than that of pure gold and showed a small increasing linear dependence on current density. However the 220 planes were significantly larger and were comparable to those of the electrolyte without booster.

In both cases, the crystallite size of the 111 planes as determined by the Scherrer equation was greater than for the other measured planes. The calculated value for the 111 reflection was ~350 Å for deposits produced at the lower current densities, decreasing to ~200 Å with increased current density. The crystallite sizes calculated for the other planes measured were typically in the region of 100 Å. In the case of the samples produced from the electrolyte containing booster, closer analysis using the Warren and Averbach analysis revealed that a significant RMS strain contributed to this difference as can be seen from Table 1. In addition, a slight asymmetry of the reconstructed peaks suggested that some twin faulting was present but as explained earlier, no accurate measurements of their magnitude could be made.

Figures 6 and 7 show the data calculated from samples produced by jetting from electrolytes containing 60 cm³ dm⁻³ and 80 cm³ dm⁻³ booster respectively but no nickel. Figures 6(b) and 7(b) show the preferred orientation. It can be seen that with increasing current density, the 111 component of orientation rises rapidly to around 60% at the expense of the 220 component. The contributions from the 200 and 311 remained fairly constant and close to their values expected in a random sample. This is consistent with a 111 texture.

Figures 6(a) and 7(a) show the influence of the booster on the lattice parameter. There is a general trend of a reduction in the lattice parameter for all planes with increasing current density. It will be noted that the 200 plane exhibited a significantly smaller lattice parameter than the other planes. This would suggest that a distortion of the lattice was being created due to the incorporation of the booster (or breakdown product of it) within the 100 (200) planes.

As was observed in the previous samples, the 111 planes exhibited a larger apparent crystallite size than the others as determined using the Scherrer equation. For both concentrations of booster, the 111 plane was found to be in the region of 300 Å whilst that of the other measured planes was in the region of 150 Å. This may be attributed to both stacking faults as well as residual strain as can be seen from Table 1.

Figures 8 and 9 show the influence of nickel under jetting conditions. The addition of nickel to the electrolyte appeared to reinforce the effects of the booster with a greater degree of 111 texture being seen at current densities below 9.0 A cm⁻². Above this current density, the deposit tended towards a more random orientation unlike those samples containing booster alone.

The presence of nickel reduced the lattice parameter of most of the planes examined to below 4.07 Å at low current densities, increasing to slightly above 4.07 Å. This latter value was about the same as that for the samples containing booster alone. Examination of Figures 8(a) and 9(a) revealed that the lattice parameter of the 200 plane fell with increasing current density, similar to that of the samples with booster alone. With relatively large concentrations of nickel in the electrolyte, the 311 and the 220 also exhibited reductions in the lattice parameter, particularly at high current densities.

The crystallite size of the 111 planes as determined by the Scherrer equation was in the region of 200 Å whilst that of the other planes was in the region of 100 Å. Again, further analysis revealed that both stacking faults and RMS strain contributed to this difference.

To summarise, both the booster and the nickel induced a 111 preferred orientation but it was clear that the booster exhibited the greater influence over a wide current density range. The evidence provided by the measurement of the lattice parameter indicated that the presence of both booster and nickel reduced these values to below the pure gold value, probably due to incorporation of the additives within the lattice. Indeed, the evidence indicated that certain planes incorporated a larger proportion of these materials. The true grain size for the 111 plane, after correction for residual strain and stacking faults, indicated that for all the jetted samples, a small crystallite size in the region of 200 to 300 Å was produced. The nickel had a slight influence in reducing the crystallite size further under jetting conditions. However, under conventional deposition conditions, it appeared to be the main cause of the reduction of crystallite size.

Figure 10 shows the effect of current density and nickel in the electrolyte on the hardness of the jetted deposits. It can be clearly seen that a decrease in the current density as well as an increase in the nickel in the electrolyte reduced the hardness. This is unusual as under conventional deposition conditions, it is generally accepted that increasing the nickel in the electrolyte leads to an increase in the hardness. Figure 11 shows the relationship between the hardness and the nickel in the deposit for different concentrations of nickel in the electrolyte. It is evident that the quantity of nickel incorporated in the deposit is not the only factor governing the hardness but is also a function of the nickel concentration within the electrolyte.

Figure 14 shows a microsection of a typical alloy gold deposit produced using HSSJE. As in the case of a pure gold jetted deposit, fan-like cells leading to a rounded mound structure can be seen. No other internal structural features could be resolved using optical microscopy.

5 DISCUSSION

5.1 Pure gold deposits

Some of the more important physical and structural properties of pure gold deposits produced using HSSJE have been examined during the course of this experimental work. These properties have been compared to deposits produced under more conventional deposition conditions. Conventional pure gold deposits from a citrate electrolyte exhibit a crystallite size of around $0.2\ \mu\text{m}$ (after accounting for strain and faulting) for the 111 planes and have hardness values of around $100\ \text{kg mm}^{-2}$. These deposits exhibit a 311 preferred orientation. Such a texture has been observed by other workers.^{1,9} It was not possible to obtain data on the 311 crystallites as higher orders of reflection could not be obtained with this experimental method. However, examination of the lattice parameters would suggest that no stacking faults were present as they are all the same size. These samples exhibited the lowest RMS strain for the 111 planes of all the samples examined over the current density range analysed.

When deposits are produced from the same electrolyte using HSSJE, both the structure and morphology are significantly altered. This results from both intrinsic changes in the deposit structure due to the deposition conditions as well as the interaction with the electrolyte flow. The intrinsic changes result from the very high rates of deposition. The crystallite size is considerably reduced to a value in the region of $200\ \text{\AA}$, a tenfold reduction. Such a reduction is the most likely cause of the increase in the deposit hardness, increasing to a value of up to

200 kg mm⁻², the hardness showing an increase with increasing current density. Despite the high hardness observed with this type of gold deposit, it has been shown² that good thermocompression bonding properties were retained. The surface appearance of jetted deposits is smooth and featureless, gradually developing smooth rounded mounds with increasing current density. This rounded mound morphology is similar to that developed in the case of alloyed golds.

A 220 preferred orientation develops which, as has been suggested by Lin et al¹⁰, in their study of the effects of additives on gold deposits, may be caused by adsorbed species. A slight reduction in the lattice parameter is observed, which may be due to the incorporations of small quantities of foreign species. This would not be surprising at such high rates of deposition as the speed at which growth takes place can easily bury surface adsorbed species within the deposit. The evidence suggests that the reduction in the crystallite size during HSSJE is a result of inhibition of crystallite growth as a result of some adsorption effect. It has been shown by Eisenmann¹¹ that during gold deposition, growth proceeds via an adsorbed AuCN species and CN⁻ is produced from the reaction. It is known that CN⁻ can strongly adsorb onto gold surfaces and it is likely that this species is responsible for the crystallite growth mechanism observed here. It is important to note that for both the conventional and jetted pure gold deposits, the lattice parameter of each of the measured planes was consistent for each deposition method. This would suggest that the crystallite structure was fairly well ordered. No structural faults were detected, except for a very low probability at low current densities. This means that $D_{eff} = D$ and the true crystallite size is as shown in Table 1.

5.2 Alloy gold deposits

In the case of the alloy gold, conventional deposits produced from the Ronovel N electrolyte exhibited RMS strains higher than the equivalent pure gold samples. However, no evidence of stacking faults was seen from studies of relative peak shifts. There was a slight asymmetry of the peaks. Unfortunately, the twin fault probability cannot be calculated from the 111 peak. Therefore, whilst it is known that twin faults existed within the deposit, their contribution could not be measured. It is therefore most likely that in this case $D_{eff} < D$. It is possible that a significant contribution to broadening is due to twin faulting. Nakahara⁷ has studied transition metal hardened gold deposits produced under conventional deposition conditions, using the Transmission Electron Microscope (TEM) and observed similar topographic features as in this study, with the deposit surface exhibiting "rounded mounds" or small nodules. It

was found that the rounded mounds observed exhibited a strong 111 orientation with a crystallite size of between 200 and 300 Å. It was concluded that such a structure formed as a result of inhibition of lateral growth by adsorbed species, presumably transition metal complexes. The same inhibiting molecules adsorbed on the top surface of the growing planes and caused continuous nucleation leading to the small crystallite size and high hardness. A high number of twins were observed within the structure. It is evident that gold nickel alloy deposits produced conventionally shared a number of morphological features with both jetted pure and alloy gold deposits but some significant differences were observed in the microstructure.

In the case of the jetted samples, similar values of D_{eff} were observed for the conventional Ronovel N and jetted deposits containing only booster. The presence of nickel however led to a reduction of ~25% in this value. There appeared to be no direct dependence of D_{eff} on current density. It is generally accepted that increasing the current density in simple electrolyte systems leads to a reduction in crystallite size. These results would suggest that in the case of the conventional deposits, an inhibition process as envisaged by Nakahara was operative. The fact that a similar crystallite size was observed under jetting conditions suggests that inhibition processes were also responsible for the small crystallite size and not an influence of increased current density. The exact nature of this process is unclear and difficult to identify as there are a number of possible inhibiting species. These include AuCN, CN^- , booster and transition metal cyanide complexes. It is most likely that there is an equilibrium between the adsorbates which alters depending on the prevailing concentration and deposition conditions. The structural properties are therefore altered, depending on the nature of the inhibiting species incorporated within the deposit.

One of the most significant differences in physical properties between the conventionally produced gold alloy deposits and those produced by jetting is the influence of nickel additions. Conventionally produced pure gold deposits exhibit a hardness in the region of 100 kg mm⁻², whilst jetted pure gold deposits manifest a hardness in the region of 200 kg mm⁻² as do those produced from electrolytes containing booster. When nickel was added to a conventional electrolyte as in the case of the Auroral MRN, the hardness increased from 100 kg mm⁻² to between 150 and 200 kg mm⁻². Similar hardness values were observed when nickel was added to the Ronovel N electrolyte containing only booster. In the case of the electrolyte containing only nickel, there was a tendency for an increasing deposit hardness with increasing current density. In the case of the electrolyte containing booster and nickel, the opposite trend was seen. The hardness of the nickel containing deposit produced using HSSJE, is reduced pro-

portional to the quantity of *nickel added to the electrolyte*, from 200 kg mm⁻² down to as low as 110 kg mm⁻². There is no direct evidence to explain this behaviour as the jetted samples containing booster both with and without nickel exhibited similar structures in terms of RMS strain and stacking faults. The main difference was the reduction in the crystallite size in the case of the nickel containing sample. This alone was insufficient to account for the change in hardness as no current density dependence was seen in terms of the crystallite size. However, a linearly increasing current density dependence was observed in the lattice parameters. The nickel in the deposit reduces with increasing current density and there is an empirical linear relationship for alloys whose individual component structures are similar between the lattice parameter and the atomic percent of an alloy constituent (Vegards Law) This would imply that some of the nickel was being incorporated within the lattice in the form of metal atoms. It is known that when transition metals are added to a gold electrolyte, conventionally produced deposits incorporate the majority of the transition metal in the form of a cyano- complex. A change in the way in which the transition metal interacts with the deposit is the most likely explanation of the reduction in hardness observed. It is clear from Figures 10 and 11 that the change in the hardness is a function of the nickel in the electrolyte and not that in the deposit. This tends to confirm the inhibition mechanism as the main influence on the hardness changes observed.

It is further suggested that the change in the inhibition process is responsible for the change in the wear characteristics observed in the study by Bocking and Cameron.⁴ They found that jetted deposits showed some reduction in the wear resistance particularly with thicker coatings. There was also evidence that the wear mechanism was abrasive in nature. Such abrasive wear is not observed in gold alloy deposits produced from properly controlled electrolytes under conventional deposition conditions. DeDoncker and Vanhumbeek¹² have suggested that in the case of gold cobalt alloys, the wear behaviour is strongly related to the proportion of cobalt present as metal to that present as a cobalt ion complex, with high values of the latter being required for good wear resistance. If the cobalt concentration in the electrolyte was too high, the incorporation of the complex within the deposit was suppressed leading to too high a value of metallic cobalt in the deposit. Such deposits exhibit abrasive wear behaviour. In addition, Antler¹³ has found that in order to obtain good wear resistance, the deposit must have a low ductility as well as a high hardness. Such a combination would not be expected from a deposit in which the alloying constituent was present purely in the metallic phase. Nakahara⁷ has suggested that it is the inhibition due to the nickel complex and its incorporation into the deposit that is responsible for the crystallographic structure observed in gold nickel alloys. It would seem to follow, therefore, that due to the high rates of deposition achieved

in HSSJE, the inhibition process is changed, with much less of the nickel complex being incorporated into the deposit but as metal within the gold lattice. This would explain the reduction in the wear resistance observed by Bocking and Cameron.

6 CONCLUSION

It has been shown that the use of HSSJE can significantly alter the micro-structure of both pure and alloy gold deposits. Pure gold deposits become much harder, proportional to the applied current density. However, despite there being a reduction in crystallite size and an increase in RMS strain, no direct dependence on current density could be observed in the micro-structure. HSSJE causes a change in the texture, from a 311 for conventional deposits to a 220 under jetting conditions. Such a change in preferred orientation usually results from the use of organic additives that inhibit the electrocrystallisation process. Gold alloy deposits showed the greatest change compared to those produced conventionally. Whilst the texture remained generally a 111 preferred orientation for both methods of deposition, the micro-structure was altered considerably. It was found that although the morphology and crystallite size was similar for both, being in the region of 200 to 300Å and the nickel in the deposit was similar, the microstructure exhibited significant changes. Under conditions of HSSJE, a high stacking fault probability was observed which was not seen in deposits produced conventionally. It is thought that this change comes about as a result of a change in the surface adsorption/inhibition process resulting from deposition at very high current densities. As a result, less nickel, in the form of a cyano complex, is incorporated into the deposit. This would explain the reduction in the wear resistance of jetted deposits as the incorporation of the non-metallic inhibitor is responsible for the good wear characteristics of conventional deposits of this type. On the basis of the evidence presented in this and previous work on HSSJE, that whilst pure gold deposits were found to be harder and possess a finer grain structure, physical properties such as thermocompression bonding characteristics were not significantly affected. However, significant differences were observed in the structure of the nickel gold alloys that appeared to influence some of their physical properties. Indeed, under the test conditions given in the previous study,⁴ wear resistance of HSSJE deposits was reduced. This does not necessarily mean that the process cannot be applied to the gold plating of connectors. What will be required, however, is a greater understanding of the mechanisms by which the nickel and nickelo-cyanide complex is incorporated within the deposit and the factors that control the ratio of metal to complex within the deposit.

REFERENCES

1. C.C. Bocking, *Trans. Inst. Met. Fin.*, **66**, 50, 1988
2. C.C. Bocking, *Proc. 59th Intl. Conf. On Surf. Fin.* **2**, 51, April 1991
3. C.C. Bocking, *East Report*, Eugen G. Leuze Verlag, Saulgau, 1992
4. C.C. Bocking & B.P. Cameron, *Trans. Inst. Metal Fin.*, **72**, 1, 33, 1994
5. B.E. Warren & B.L. Averbach, *Journ. Appl. Phys.*, **21**, 595, 1950; **23**, 497, 1952
6. A.R. Stokes, *Proc. Phys. Soc. (London)*, **B61**, 382, 1948
7. S. Nakahara, *Journ. Cryst. Growth*, **75**, 212, 1986
8. M. Antler, *IEEE Trans. Components, Hybrids & Man. Tech.*, CHMT-4, **1**, 15, 1981
9. S.E. Craig Jr, R.E. Harr, J. Henry and P. Turner, *J. Electrochem. Soc.*, **117**, 1450, 1970
10. K-L. Lin, W-C. Liu, M.H.M. Lin & Y.W. Hu, *J. Electrochem. Soc.*, **138**, 3276, 1991
11. E.T. Eisenman, *J. Electrochem. Soc.*, **125**, 717, 1978
12. R. DeDoncker & J. Vanhumbeek, *Trans. Inst. Met. Fin.*, **62**, 59, 1985
13. M. Antler, *IEEE Trans. Components, Hybrids & Man. Tech.*, CHMT-4, **1**, 15, 1981

ACKNOWLEDGEMENTS

This work was carried out as part of a BRITE-EURAM project No RI1B-0304-C(A) "Improvement in the Control and Attainment of High Speed Electrodeposition Processes". The Authors wish to thank the European Commission, partners Centro Sviluppo Materiali and Loughborough University for their kind permission to publish this work.

SAMPLE	C.D.	D_{111} Å	D_{222} Å	D_{333} Å	$\langle \epsilon^2 \rangle$ (111)	α (111)	Ni g dm ⁻³	Booster cm ³ dm ⁻³	Hardness kg mm ⁻²
Pure Au Conv.	3.0 mA/cm ²	2352	744	540	0.000035	n/d	0	0	101
Pure Au Conv.	7.0 mA/cm ²	2321	860	551	0.000035	n/d	0	0	102.4
Pure Au Jetted	2.0 A/cm ²	324	326	198	0.00011	0.007	0	0	163.9
Pure Au Jetted	4.0 A/m ²	350	349	206	0.00015	n/d	0	0	198.9
Pure Au Jetted	6.0 A/cm ²	335	327	215	0.000115	n/d	0	0	203.5
Pure Au Jetted	8.0 A/cm ²	328	304	205	0.000135	n/d	0	0	204.1
Ronoval N Conv.	10.0 mA/cm ²	261	104	128	0.00015	n/d	1.7	60	198
Ronoval N Conv.	40.0 mA/cm ²	254	107	128	0.000135	n/d	1.7	60	130
Ronoval N Jetted	3.0 A/cm ²	324	340	209	0.000115	0.021	0	60	200.1
Ronoval N Jetted	9.0 A/cm ²	289	307	189	0.00013	0.022	0	60	212.2
Ronoval N Jetted	3.0 A/cm ²	191	182	104	0.00017	poor peak resolution	1.9	60	127
Ronoval N Jetted	9.0 A/cm ²	200	201	128	0.00015	0.027	1.9	60	170

TABLE 1. Crystallite size, RMS strain and stacking fault probabilities for some samples for the (111) planes only. Note n/d = not detectable, n/m = not measurable.

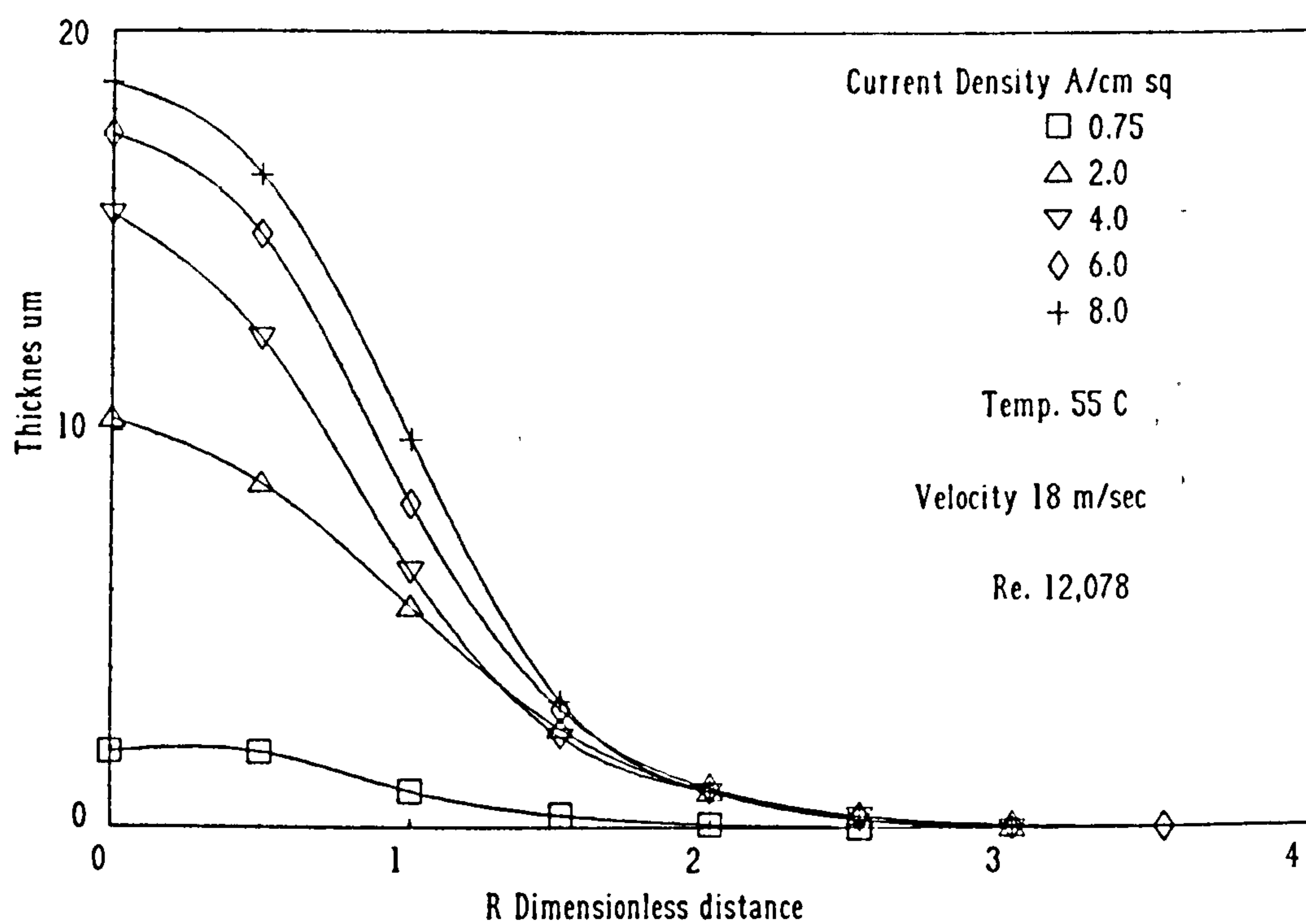


Figure 1. A typical selectivity plot showing selectivity as a function of the current density.

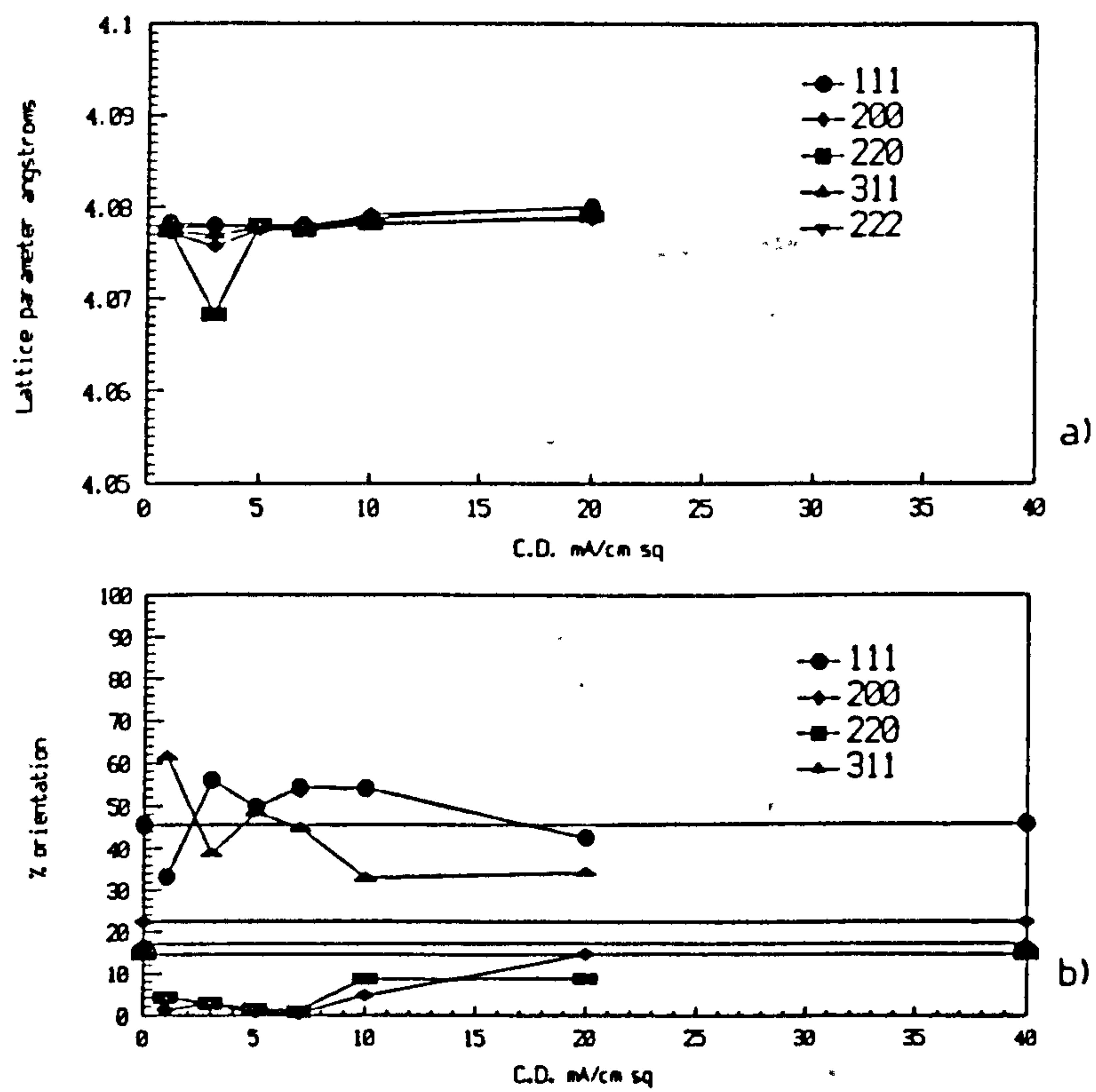


Figure 2. (a) Lattice parameter and (b) preferred orientation data for conventionally produced pure gold deposits.

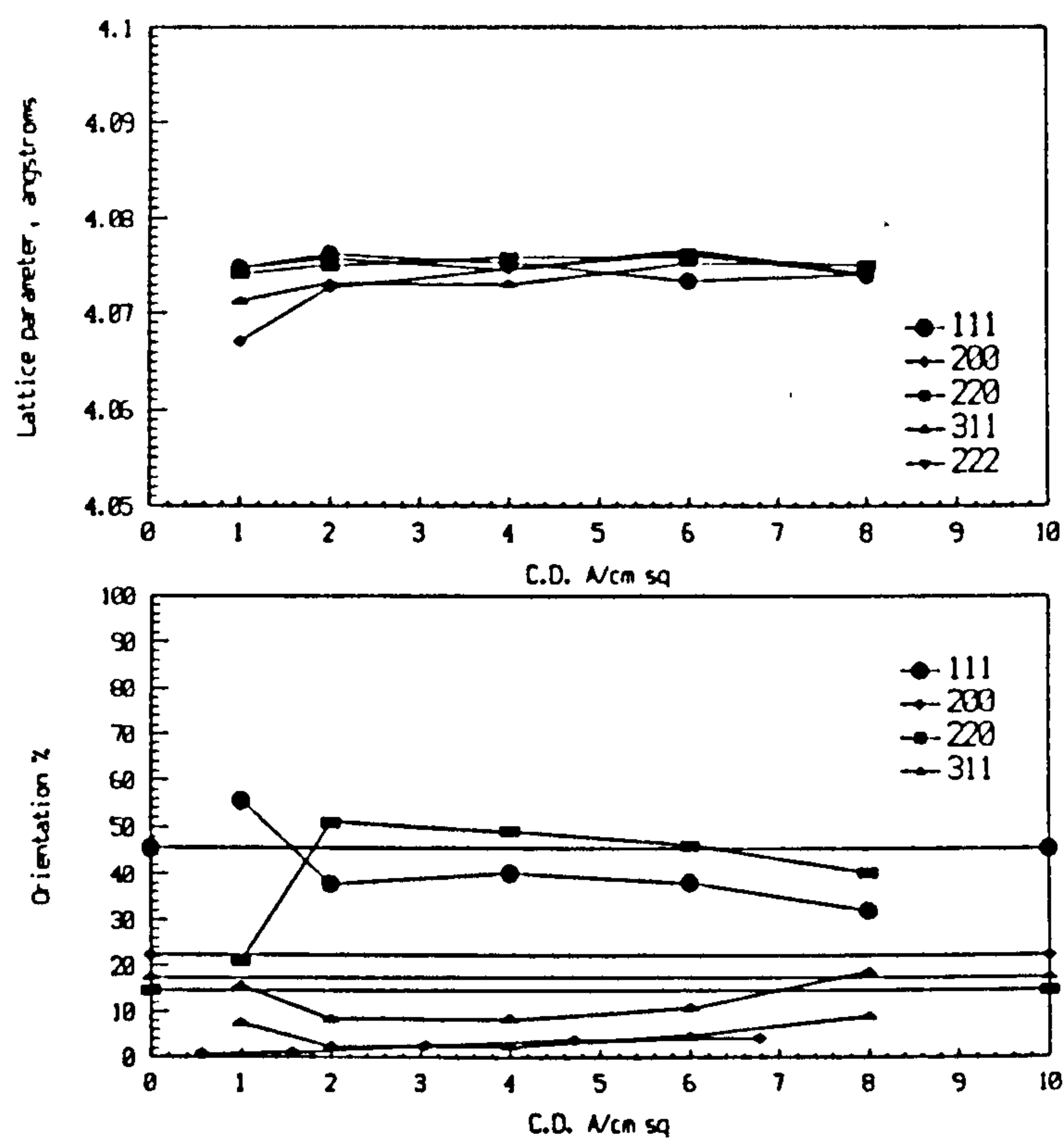


Figure 3. (a) Lattice parameter and (b) preferred orientation data for HSSJE pure gold deposits.

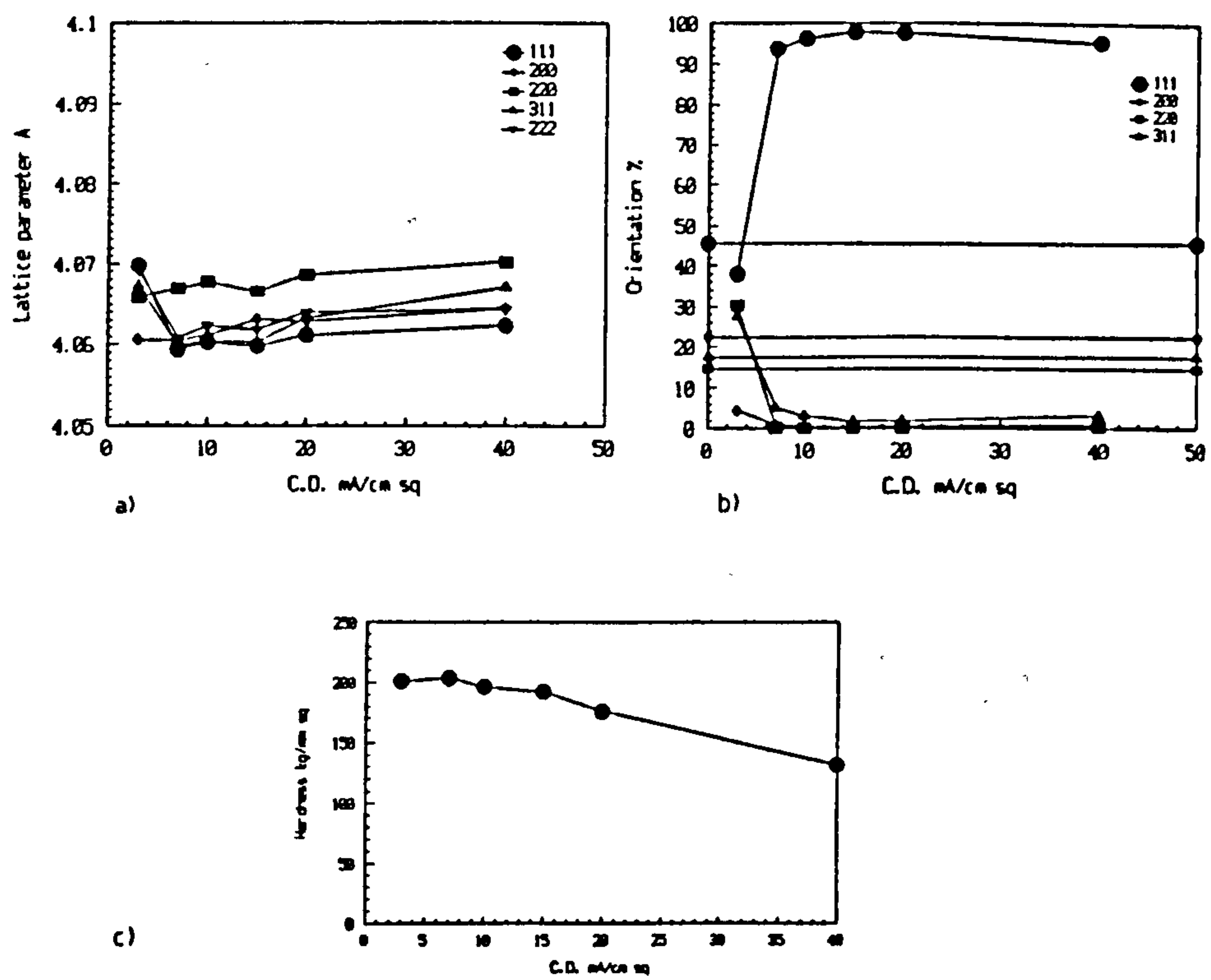


Figure 4. (a) Lattice parameter (b) preferred orientation and (c) hardness data for Ronovel N deposits produced conventionally.

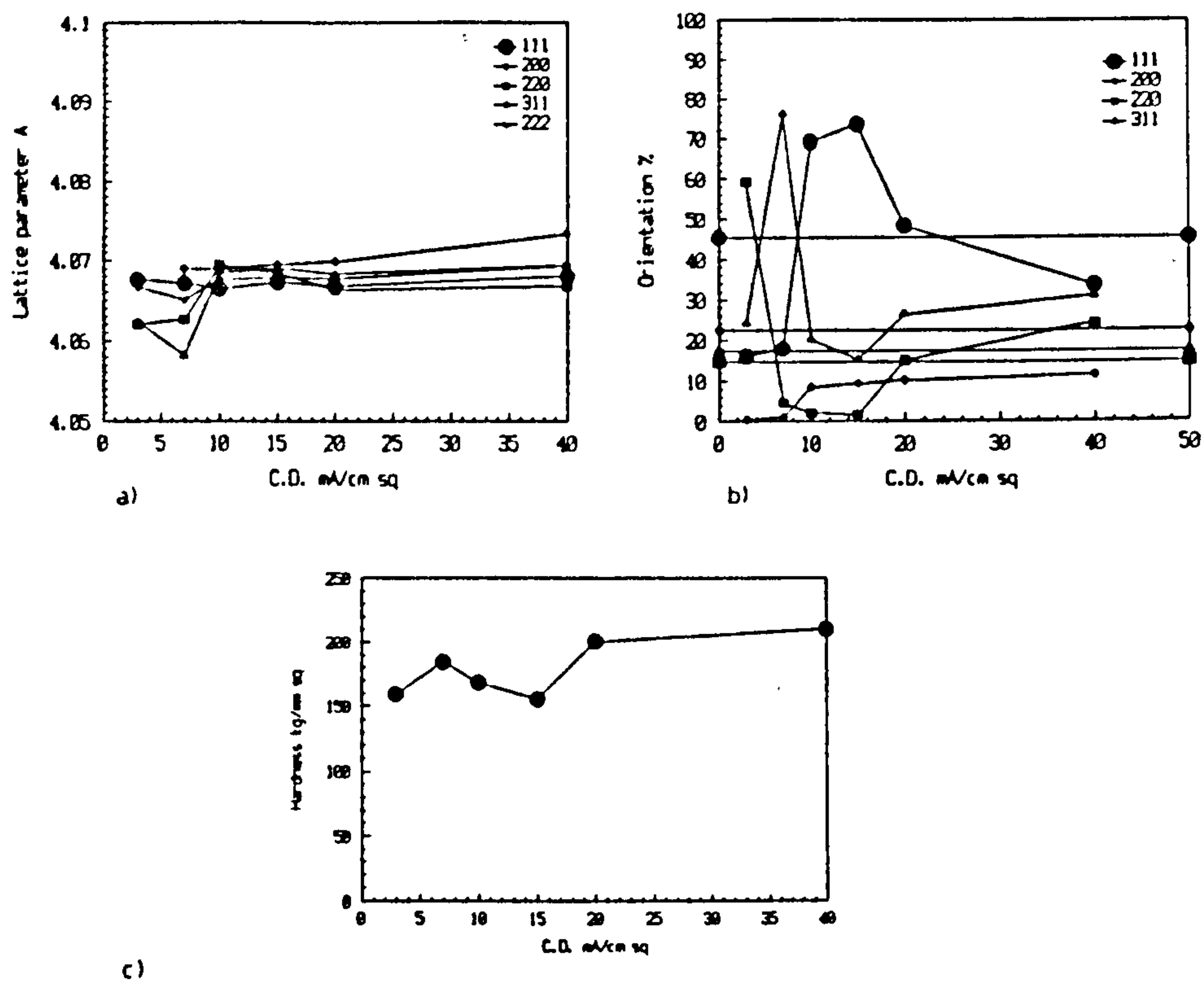


Figure 5. (a) Lattice parameter (b) preferred orientation and (c) hardness data for Auroral MRN deposits produced conventionally.

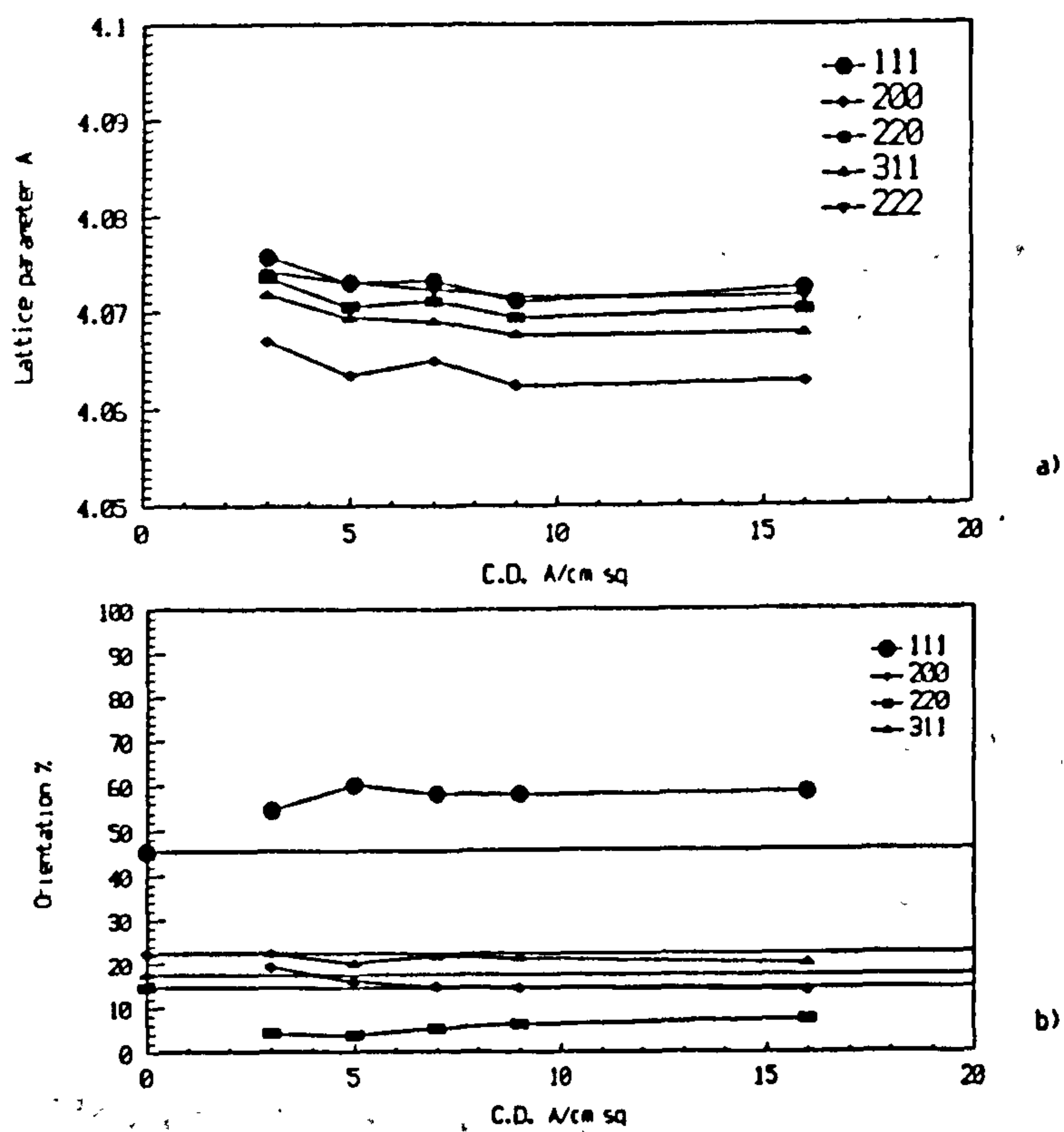


Figure 6. (a) Lattice parameter and (b) preferred orientation data for HSSJE Ronovel N deposits produced from an electrolyte containing $60 \text{ cm}^3 \text{ dm}^{-3}$ booster but no nickel.

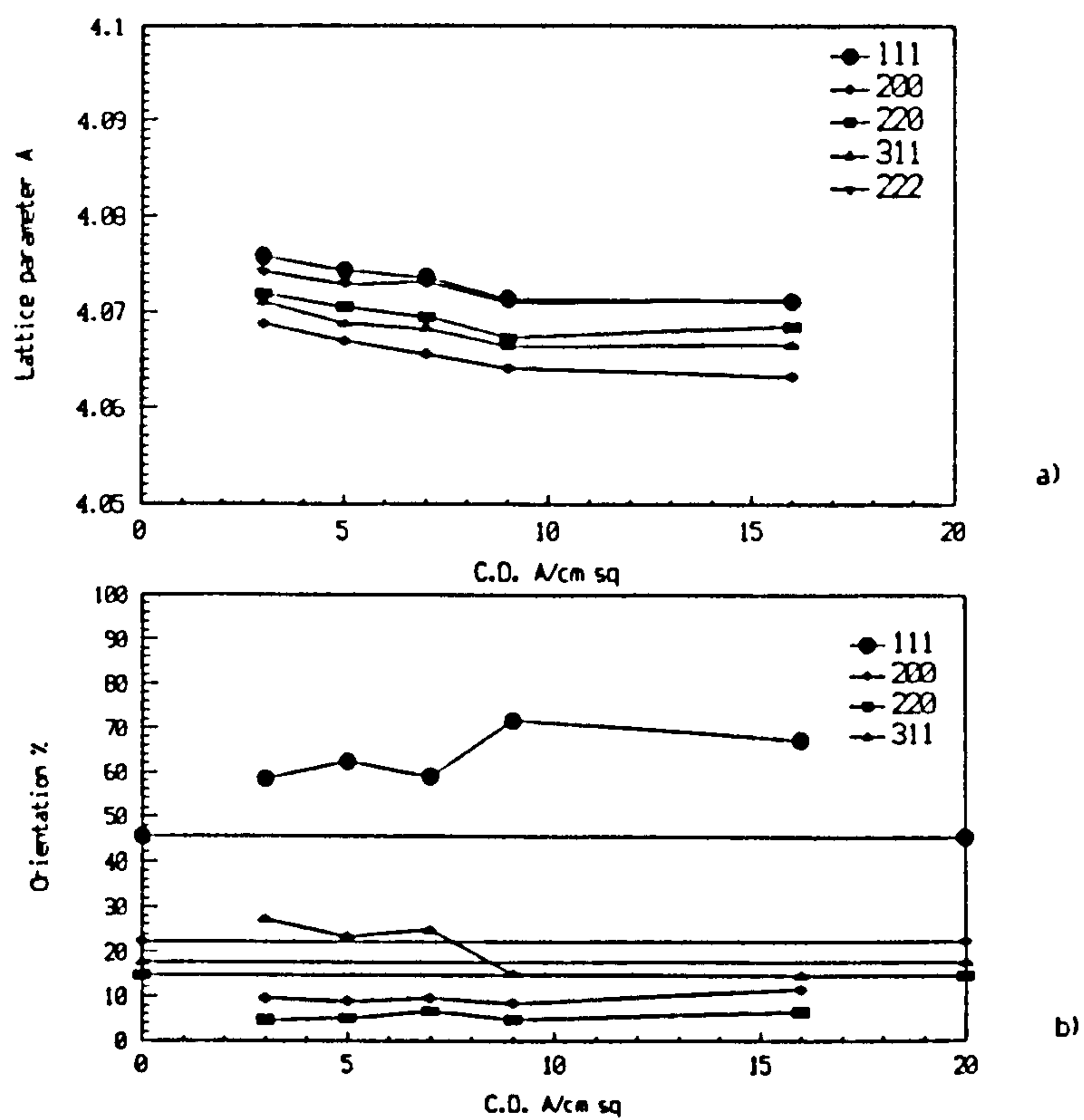


Figure 7. (a) Lattice parameter and (b) preferred orientation data for HSSJE Ronovel N deposits produced from an electrolyte containing $80 \text{ cm}^3 \text{ dm}^{-3}$ booster but no nickel.

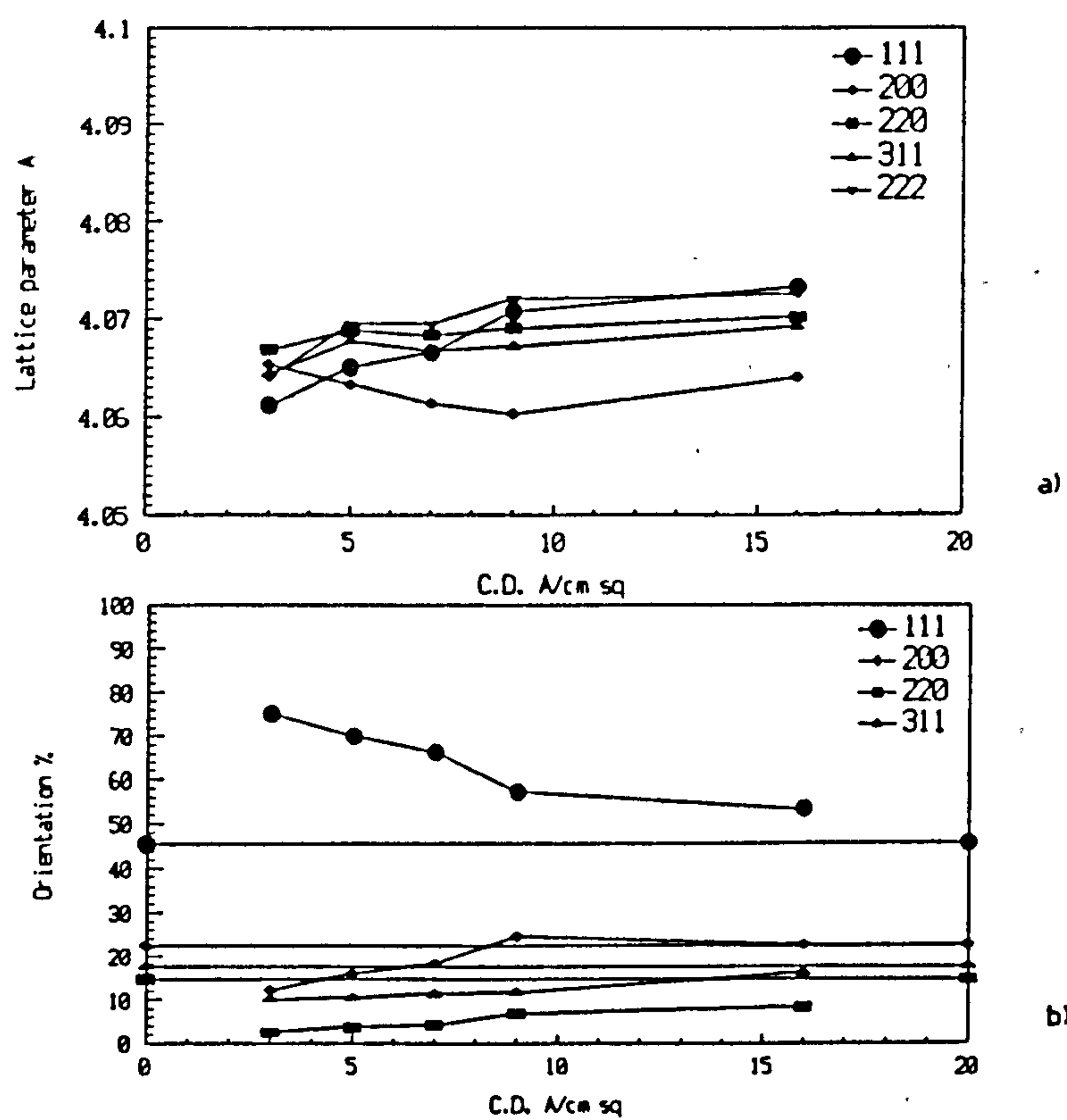


Figure 8. (a) Lattice parameter and (b) preferred orientation data for HSSJE Ronovel N deposits produced from an electrolyte containing $60 \text{ cm}^3 \text{ dm}^{-3}$ booster and 1.9 g dm^{-3} nickel.

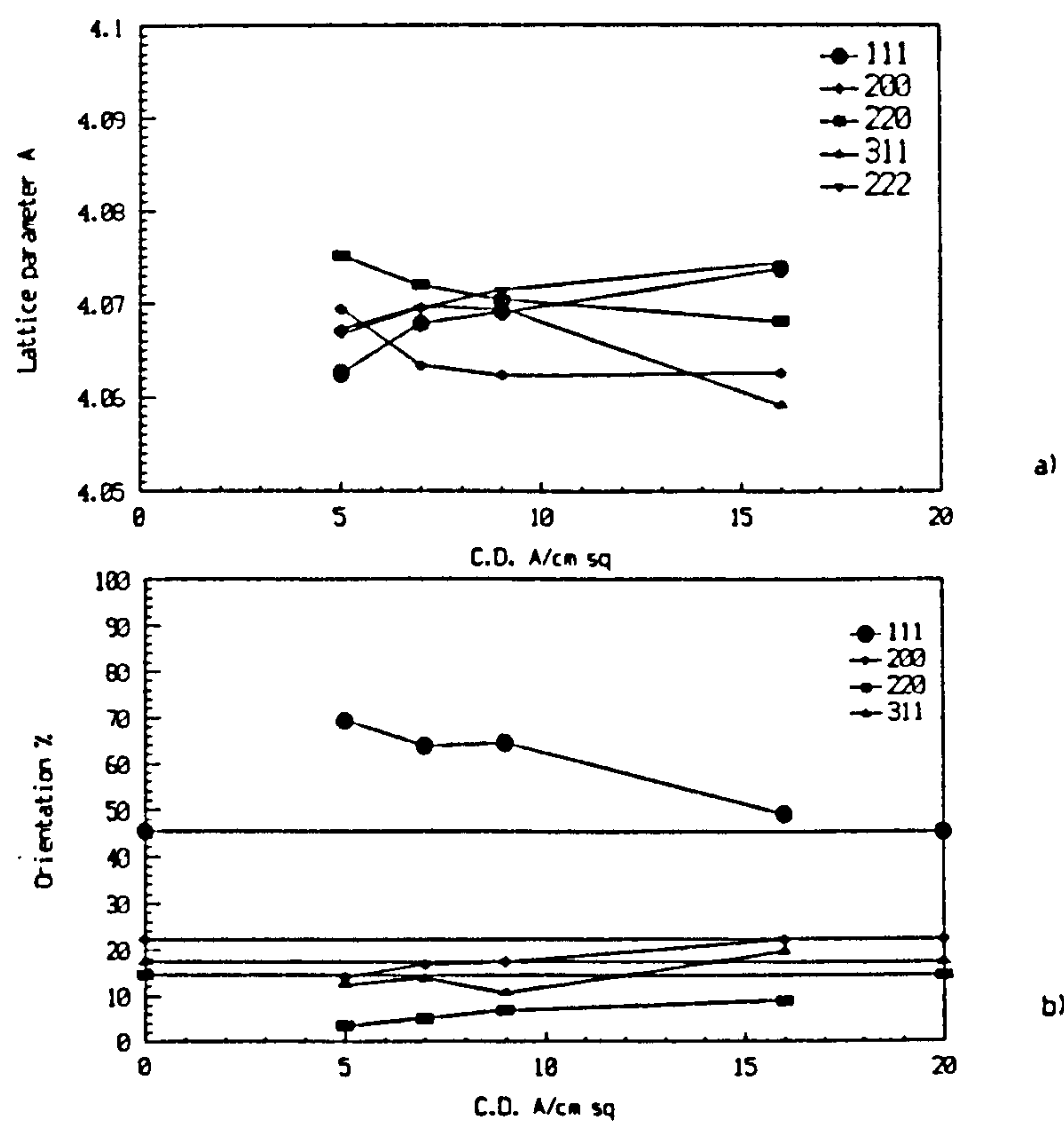


Figure 9. (a) Lattice parameter and (b) preferred orientation data for HSSJE Ronovel N deposits produced from an electrolyte containing $60 \text{ cm}^3 \text{ dm}^{-3}$ booster and 3.0 g dm^{-3} nickel.

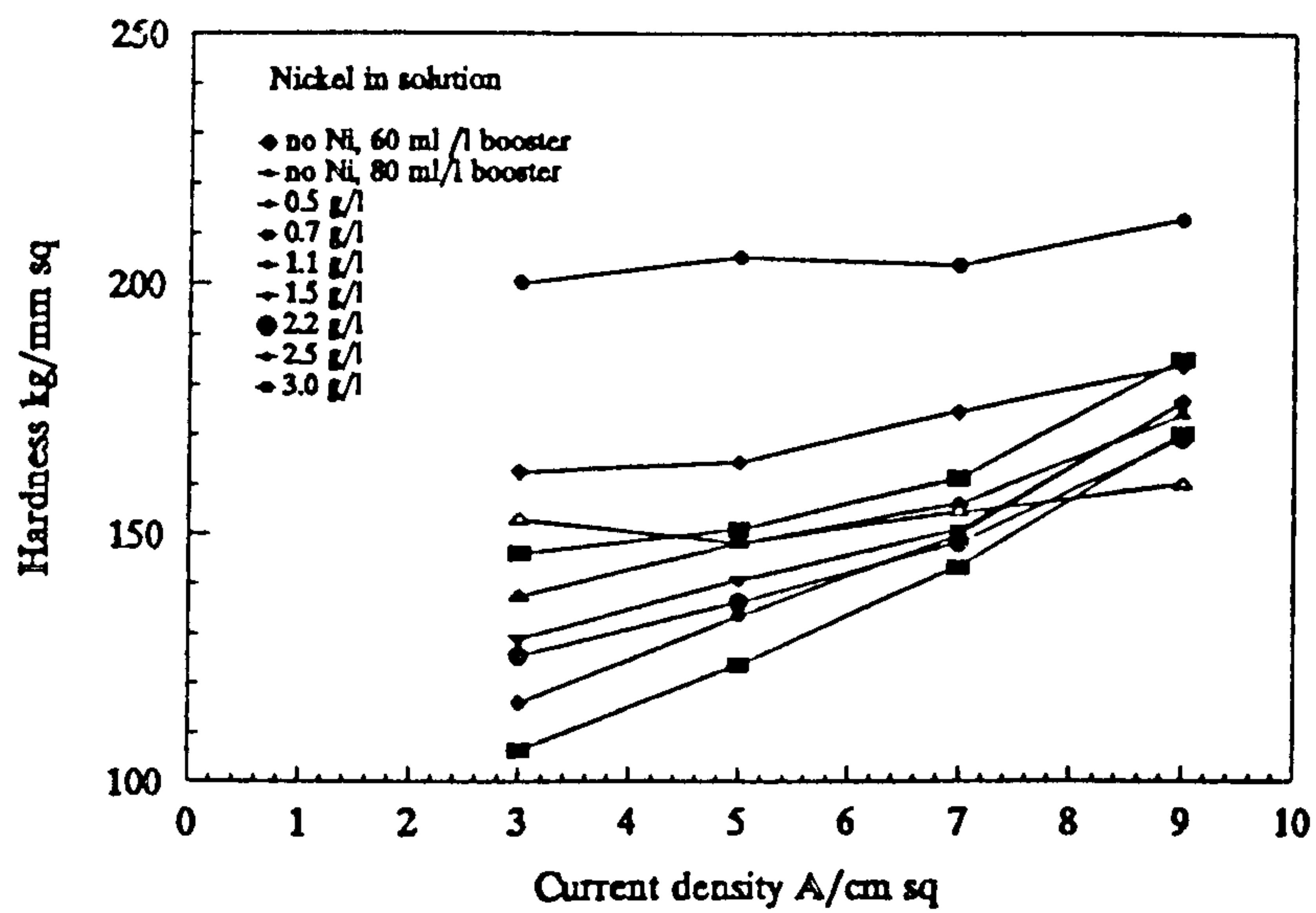
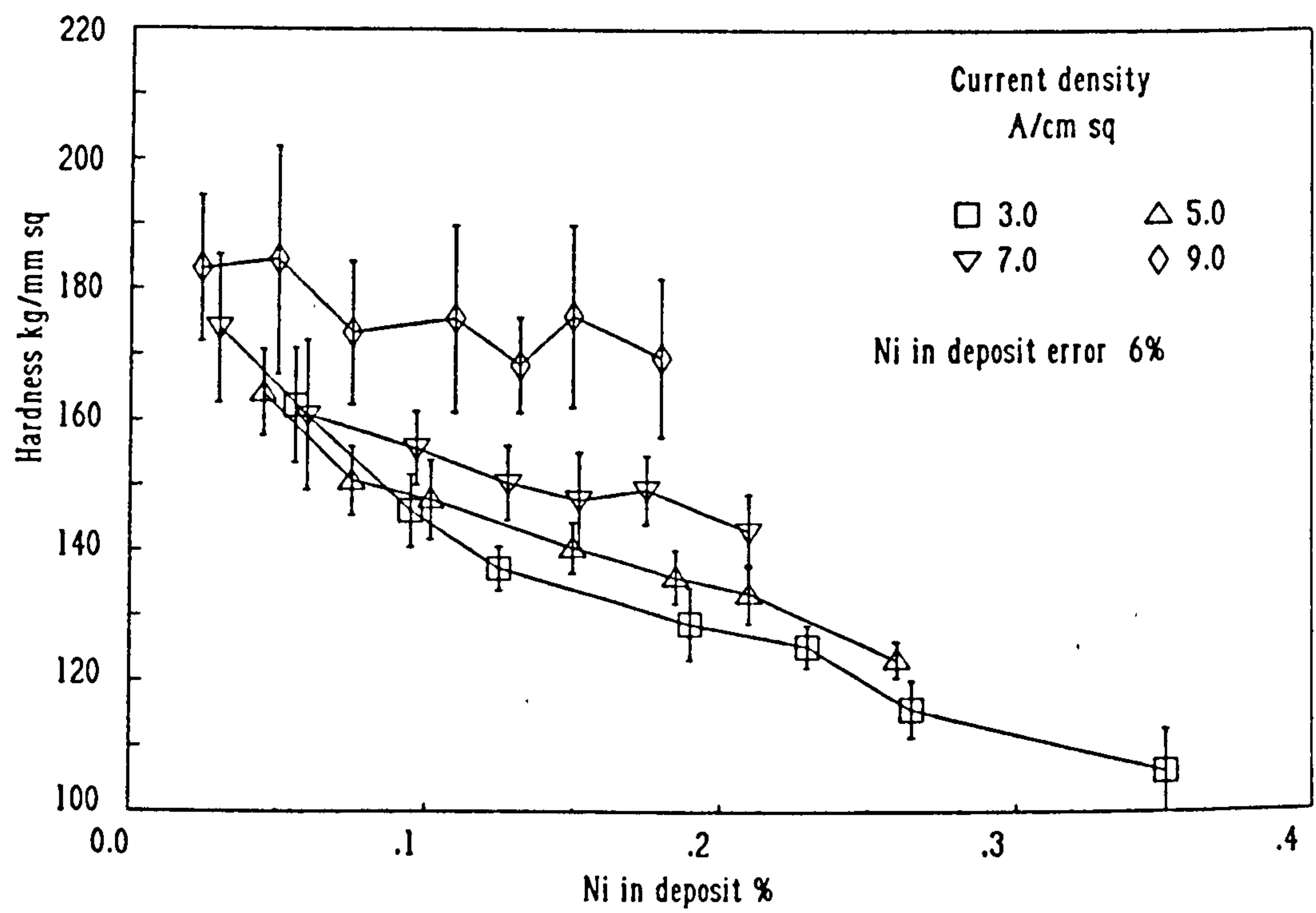


Figure 10. The effect of current density and nickel in the electrolyte on the hardness of gold nickel alloy deposits produced by HSSJE.



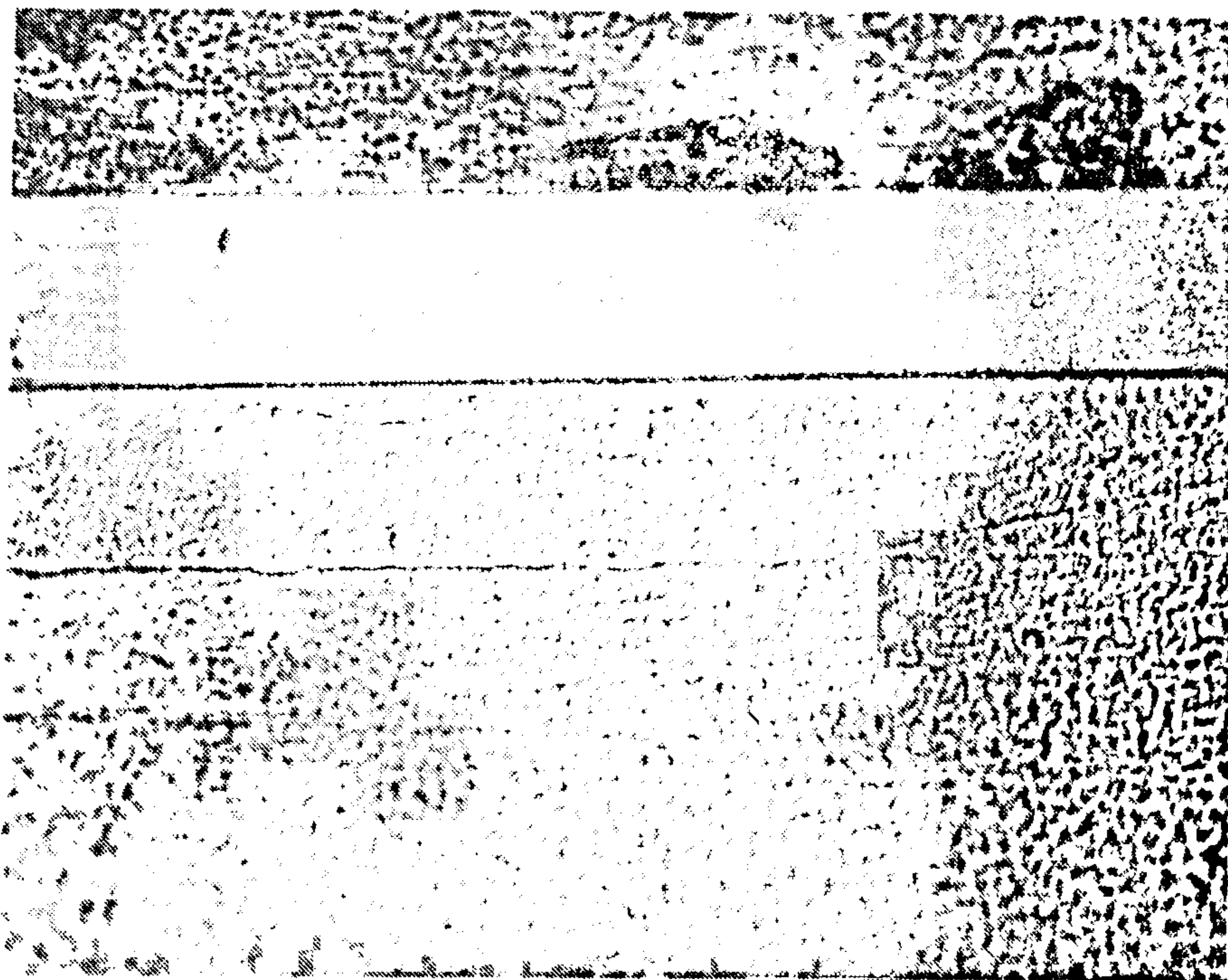


Figure 12. A microsection of a pure gold deposit produced using HSSJE. Current density = 6.0 A cm^{-2} , Re. = 12000, Temp. = 55°C . X 1000.

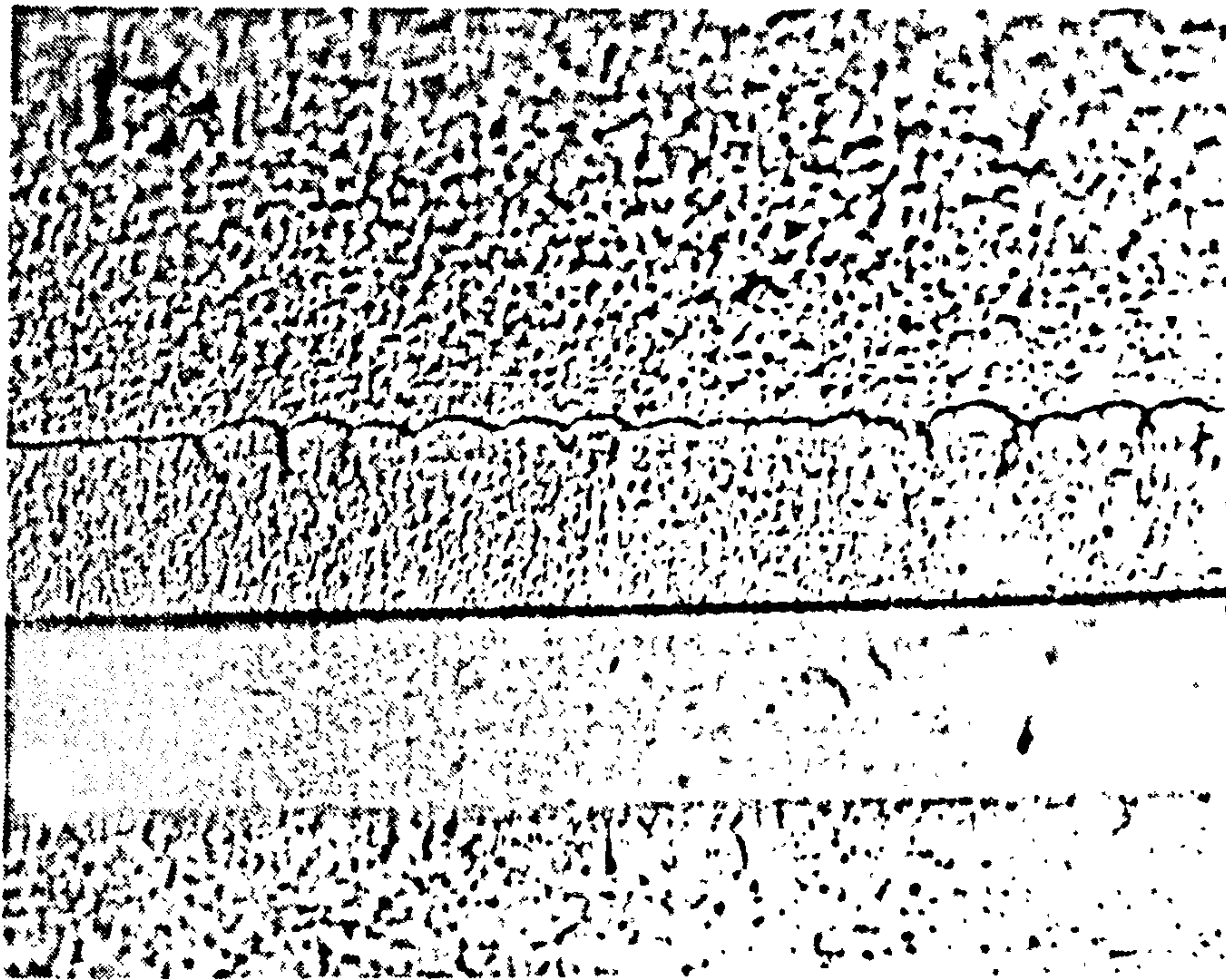


Figure 13. A microsection of a pure gold deposit produced using HSSJE. Current density = 7.0 A cm^{-2} , $Re. = 12000$, Temp. = 55°C . X 1000.

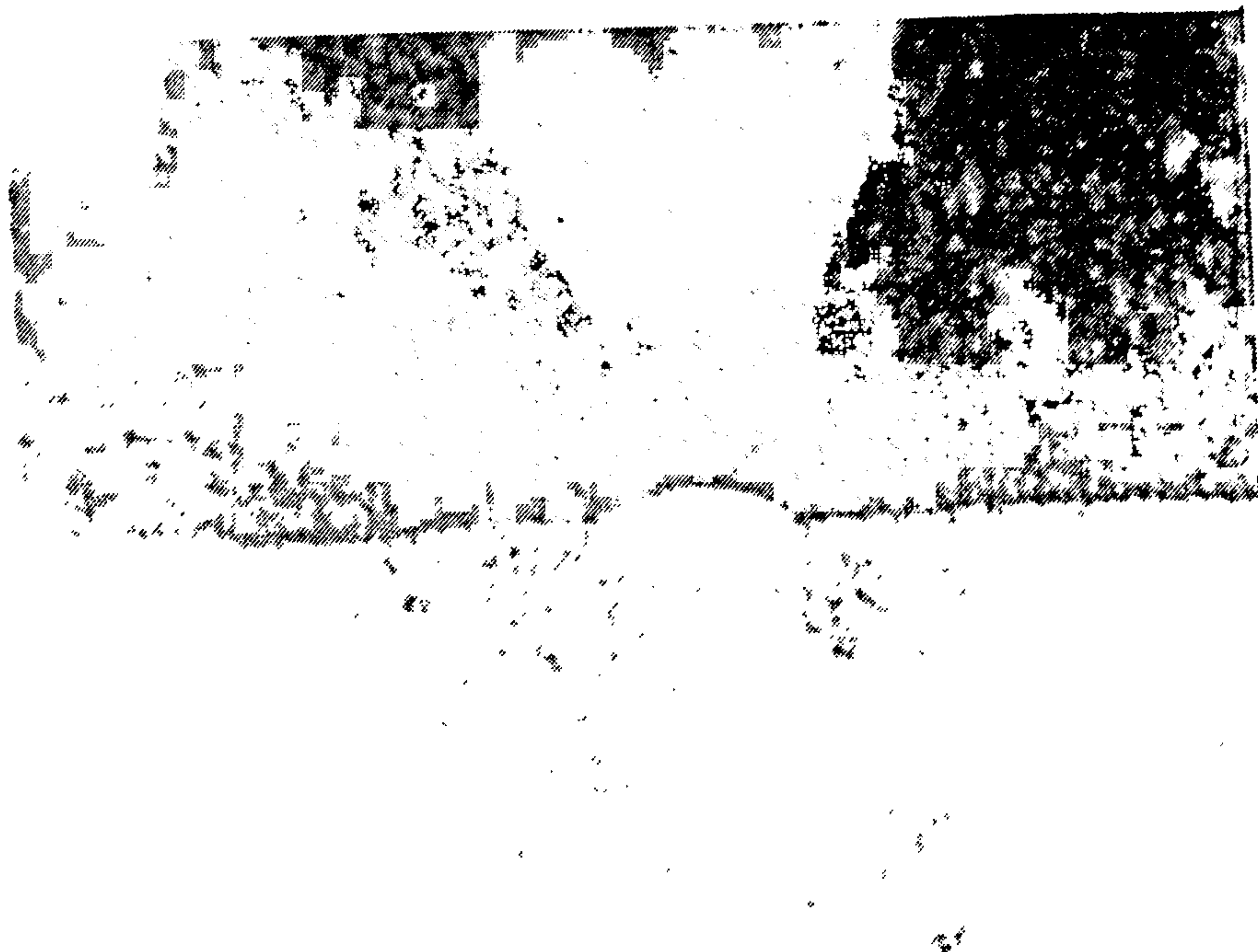


Figure 14. A microsection of a nickel/gold alloy deposit produced using HSSJE. Current density = 6.0 A cm^{-2} , $Re. = 10600$, Temp. = 55°C . Nickel in the electrolyte = 3.0 g dm^{-3} . X 1000.